PROCEEDINGS
of
SYMPOSIUM
on
ENGINEERING PROBLEMS OF FUSION RESEARCH

April 8-11, 1969

LOS ALAMOS SCIENTIFIC LABORATORY
of the
University of California
LOS ALAMOS • NEW MEXICO

UNITED STATES
ATOMIC ENERGY COMMISSION
CONTRACT W-7405-ENG. 36

This report expresses the opinions of the author or authors and does not necessarily reflect the opinions or views of the Los Alamos Scientific Laboratory.

Printed in the United States of America. Available from
Clearinghouse for Federal Scientific and Technical Information
National Bureau of Standards, U. S. Department of Commerce
Springfield, Virginia 22151
Price: Printed Copy $3.00; Microfiche $0.65

LA-4250
UC-20, CONTROLLED
THERMONUCLEAR RESEARCH
TID-4500

PROCEEDINGS

of

SYMPOSIUM

on

ENGINEERING PROBLEMS OF FUSION RESEARCH

held at the

LOS ALAMOS SCIENTIFIC LABORATORY

of the

UNIVERSITY OF CALIFORNIA

Los Alamos, New Mexico

April 8-11, 1969

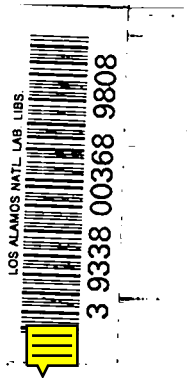

Distributed: January 1970

FOREWORD

This Symposium on the Engineering Problems of Fusion Research held at Los Alamos April 8 - 11, 1969, was the third United States Symposium. The papers represent a wide spectrum of engineering disciplines but all focused directly on fusion engineering. An equally important function of this Symposium was to provide direct personal contact between the engineers working in the various U. S. fusion laboratories. The Steering Committee believes that this personal contact is essential for the growth of fusion engineering. The papers contained in these Proceedings represent the ideas of the author without technical editing.

The Steering Committee is grateful to the Atomic Energy Commission and the Los Alamos Scientific Laboratory which sponsored the Symposium, and to Dr. N. E. Bradbury, Director of the Laboratory, and Dr. R. F. Taschek, Division Leader of the Physics Division. We are particularly grateful to Mrs. Harriett Sass who worked tirelessly during the planning phase of the Symposium and also organized the Proceedings for publication. Furthermore, we would like to recognize the valuable services of the Laboratory Public Relations group under R. Y. Porton. Special thanks also go to Mrs. Barbara Ray, Mrs. Sue Wooten, and Tom C. Langhorst.

The next Symposium is planned for the fall of 1970 at the Naval Research Laboratory in Washington, D. C.

E. L. Kemp, LASL, Chairman
T. H. Batzer, LRL
W. F. Gauster, ORNL
W. C. Gough, AEC, Washington
R. G. Mills, PPL
H. W. VanNess, LRL
M. P. Young, NRL

WELCOMING ADDRESS

by

N. E. Bradbury, Director
Los Alamos Scientific Laboratory

It is my pleasure to welcome you here this morning for this conference. I am amazed at its depth and length, and am also very pleased. First, it is quite clear that the problems which are faced by all of us in the Sherwood business are not entirely separate to each laboratory. They cut across all laboratory activities to the extent that we can save dollars or earn dollars by learning what other people have done, what problems they have solved, to that extent they can learn what we have solved -- all of us profit. It is a tragedy to have to reinvent things at different places or invent them in parallel. Secondly, I can be very sure that the questions you are facing today -- engineering design, engineering detail -- are merely the embryos of problems which you will be facing in some number of years. I won't hazard a guess as to how many. In some number of years you will have to face these problems for a real, power-producing fusion demonstration, so you might as well get to work on them now. They are hard enough today, but I suspect they will be tougher. Anyway, it is a very great pleasure to have this meeting here. I have taken a quick look over its agenda. I am impressed, as I said, with its length and detail, the breadth of its problems, and I wish you every success in dealing with it. I hope your time is both pleasant and constructive. Thank you for coming.

Opening Remarks

by

R. F. Taschek, Division Leader
Physics Division, LASL

I just want to extend a welcome from the Physics Division, in particular from the Sherwood or Controlled Thermonuclear Research people, and tell you that if you have problems of any kind, the Division office is quite close by and you can readily find access to it through Ed or any one of the local people. I think I can only perhaps reiterate some of the things Dr. Bradbury mentioned about engineering and technology in this particular field. I have had the impression that nearly all activities that end up in an applied form at some time or other go through sort of an evolution. That obviously is an oversimplified term -- if it is a physics type of application, it begins with physics; it then goes through a stage which is a combination of physics and technology and then goes into technology, and I am not attempting to distinguish between technology and engineering as long as they are intermingled so intensely nowadays that one doesn't know precisely where one begins and the other ends. In any case, I think right now the CTR activities are probably in this intermediate phase of physics and technology. Certainly the physics problems haven't been solved, and as Dr. Bradbury mentioned, one is only just beginning to get into the technology that one might foresee some years hence. This is quite an exciting time to be in the field because almost all people in the field and many out are pretty much convinced by now that the CTR program won't die and there will indeed be a true application. I think that the status of the technology is indicated in part by your program. At present it involves such very sophisticated things as use of superconductors, levitated systems, intense magnetic fields, and so on. It seems to me that if you compare what you might look forward to ten years from now in this field, that there even now exists no other technology either in nuclear reactor systems or nuclear weapons or rocket propulsion that is likely to contain more than a fraction of the difficult technological materials, engineering, and similar problems that this field is likely to have. It is therefore, good to be in on the beginning of it to see, and guide also, the directions in which you are heading at this particular time and in which you are really mapping out the future; so I leave you to start the real business of this meeting. Thank you.

SYMPOSIUM ON ENGINEERING PROBLEMS OF FUSION RESEARCH

LOS ALAMOS SCIENTIFIC LABORATORY

UNIVERSITY OF CALIFORNIA
Los Alamos, New Mexico
April 8 - 11, 1969

PROGRAM

Tuesday, April 8, 9:30 a.m.

Welcoming Address: N. E. Bradbury, Director
Los Alamos Scientific Laboratory

Opening Remarks: R. F. Taschek

RING CONDUCTOR EXPERIMENTS

Chairman, R. G. Mills, Princeton University

A1 HOOP LEVATOR DESIGN FOR A PLASMA OCTUPOLE, Neil Lien and Igor Sviatoslavsky, University of Wisconsin

A2 MAGNETIC PROPERTIES OF THE ORNL LEVITATED TOROIDAL QUADRUPOLE, M. Roberts, I. Alexeff, W. L. Stirling, and W. Halchin, Oak Ridge National Laboratory

A3 MECHANICAL DESIGN OF A QUADRUPOLE INJECTION EXPERIMENT, R. W. Kewish, Jr., R. S. Dike, J. E. Hammel, and A. R. Sherwood, Los Alamos Scientific Laboratory

A4 THE PRINCETON SPHERATOR, P. Bonanos, U. R. Christensen, D. H. Mullaney, Princeton University

A5 COILS FOR THE SUPERCONDUCTING LEVITRON, Clyde E. Taylor and Thomas J. Duffy, Lawrence Radiation Laboratory, Livermore

A6 THE PRINCETON FLOATING MULTIPOLE MACHINE, J. File, Princeton University

Tuesday, April 8, 2:00 p.m.

SYSTEMS AND DATA ACQUISITION

Chairman, John Philpott, Culham Laboratory

B1 THE PROBLEM OF CONTROL OF THERMONUCLEAR REACTORS, R. G. Mills, Princeton University

B2 PRESENT AND FUTURE 2X DATA SYSTEMS, George E. Vogtlin, Lawrence Radiation Laboratory, Livermore

B3 THE DATA ACQUISITION SYSTEM FOR THE SCYLLAC DEVICE, R. F. Gribble, D. Brown, J. Lillberg, G. A. Sawyer, and D. M. Weldon, Los Alamos Scientific Laboratory

B4 DATA ACQUISITION FOR THOMPSON SCATTERING EXPERIMENT ON CHALICE, Wayne E. Carr, Stevens Institute of Technology

B5 THE IMP FACILITY AT OAK RIDGE NATIONAL LABORATORY, R. J. Colchin, J. L. Dunlap, R. S. Edwards, D. P. Hammond, L. A. Massengill, T. F. Rayburn, R. G. Reinhardt, and E. R. Wells, Oak Ridge National Laboratory

B6 NEW ASTRON ACCELERATOR AND MAIN CHAMBER, Charles A. Hurley, Lawrence Radiation Laboratory, Livermore

B7 TECHNOLOGICAL PROBLEMS ASSOCIATED WITH THE ADDITION OF A HARD CORE TO THE PHAROS 2 MJ θ-PINCH, M. P. Young, U. S. Naval Research Laboratory, Washington, D. C.

B8 SOME REMARKS ON THE ENGINEERING PROBLEMS ENCOUNTERED IN THE CHALICE EXPERIMENT, G. J. Yevick, R. Harvey, W. Carr, and J. Karol, Stevens Institute of Technology

Wednesday, April 9, 9:00 a.m.
(Parallel session)

COMPONENTS AND TECHNOLOGY

Chairman, K. E. Wakefield, Princeton University

CI-1 CAPACITOR DEVELOPMENT FOR SCYLLAC, Grenfell P. Boicourt, Los Alamos Scientific Laboratory

CI-2 THE DEVELOPMENT OF RELIABLE, HIGH-VOLTAGE, LOW-INDUCTANCE COAXIAL CABLE FOR SCYLLAC, G. P. Boicourt and E. L. Kemp, Los Alamos Scientific Laboratory

CI-3 THE DESIGN AND DEVELOPMENT OF CABLE CARTRIDGES FOR SCYLLAC, K. W. Hanks and G. P. Boicourt, Los Alamos Scientific Laboratory

CI-4 AN INERT-FLUID COOLED AND MAGNETICALLY SHIELDED LOW-POWER KLYSTRON MILLIMETER SOURCE, W. P. Ernst, Princeton University

CI-5 EXTENSION OF THE ASTRON ACCELERATOR TO 8 MEV, Kenneth A. Saunders, Lawrence Radiation Laboratory, Livermore

CI-6 ANALYSIS OF FLUX REVERSAL IN TAPE CORES, S. D. Winter and R. W. Kuenning, Lawrence Radiation Laboratory, Livermore

CI-7 EXPERIMENTAL STUDY OF 50-50 Ni-Fe TAPE-WOUND MAGNETIC CORES FOR THE ASTRON ACCELERATOR, Gary G. Berg, Lawrence Radiation Laboratory, Livermore

CONTROL AND INSTRUMENTATION

Chairman, John Last, Culham Laboratory

CII-1 DIGITAL CONTROL OF A RESEARCH DEVICE, E. D. Simon, S. P. Durritt, M. Pelovitz, Princeton University

CII-2 PROGRAMMING CONSIDERATIONS OF THE PRINCETON FLOATING MULTIPOLE CONTROL SYSTEM, M. Pelovitz, S. P. Durritt, and E. D. Simon, Princeton University

CII-3 DESIGN AND TESTING OF SERVO STABILIZING SYSTEMS FOR LEVITATED SUPERCONDUCTING RINGS, P. A. Thompson, G. V. Sheffield, and F. H. Tenney, Princeton University

CII-4 REDESIGNED CONTROLS FOR THE ASTRON MAGNETIC FIELD USING OPERATIONAL AMPLIFIERS, Jerry W. Robinson, Lawrence Radiation Laboratory, Livermore

CII-5 A COMPUTER CONTROLLED ELECTRONIC SEQUENCE TIMER, S. Schweitzer, Princeton University

CII-6 DIAGNOSTIC DRIVES AND CONTROLS, V. S. Foote, Jr., Princeton University

CII-7 PROBE POSITIONING MECHANISMS, R. S. Christie, Princeton University

Wednesday, April 9, 2:00 p.m.
(Parallel session)

VACUUM AND UNIQUE DEVICES

Chairman, T. H. Batzer, LRL

Thursday, April 10, 9:00 a.m.

POWER SUPPLIES AND POWER TECHNOLOGY

Chairman, Hugh W. Van Ness, LRL

E1 A HIGH PERFORMANCE, PROGRAMMABLE 25-KV, 2-A POWER SUPPLY, A. F. Waugh, Lawrence Radiation Laboratory, Livermore

E2 PRECISE REGULATION OF A 500 KW D.C. GENERATOR WITH A 2500 AMPERE SERIES-PASS TRANSISTOR BANK, John McLeod and John L. Rand, Los Alamos Scientific Laboratory

E3 VARIABLE-VOLTAGE, DIRECT-CURRENT POWER SUPPLIES FOR ENERGIZING CRYOGENICALLY COOLED AND SUPERCONDUCTIVE ELECTROMAGNETS, J. C. Laurence, E. H. Meyn, and R. J. Jirberg, NASA, Lewis Research Center, Cleveland

E4 HIGH POWER TECHNOLOGY ASSOCIATED WITH DENSE PLASMA FOCUS RESEARCH, K. D. Ware, J. P. Carpenter, P. J. Bottoms, A. H. Williams, and J. W. Mather, Los Alamos Scientific Laboratory

E5 IMPEDANCE MATCHING THE PLASMA FOCUS DEVICE, J. P. Carpenter, K. D. Ware, P. J. Bottoms, A. H. Williams, and J. W. Mather, Los Alamos Scientific Laboratory

E6 AN INTERCHANGEABLE THETA-PINCH PLASMA FOCUS MACHINE, Charles P. Wolfe, National Center for Atmospheric Research, Boulder

E7 APPLICATION OF THE NET-1 NETWORK ANALYSIS PROGRAM TO DISTRIBUTED CIRCUITS, Grenfell P. Boicourt, Los Alamos Scientific Laboratory

E8 HIGH CURRENT COAXIAL DC BUS SYSTEMS, C. W. Bushnell, Princeton University

E9 HIGH-CURRENT JOINT TECHNIQUES, R. S. Dike and W. H. Borkenhagen, Los Alamos Scientific Laboratory

Thursday, April 10, 2:00 p.m.

SCYLLAC

Chairman, E. L. Kemp, LASL

F1 THE FINAL DESIGN OF SCYLLAC, Edwin L. Kemp, Los Alamos Scientific Laboratory

Tour of Sherwood Facilities

Friday, April 11, 9:00 a.m.

MAGNETIC FIELDS AND COILS

Chairman, W. F. Gauster, ORNL

G1 THE STABILITY OF MULTIFILAMENT SUPERCONDUCTORS, Carl D. Henning, Lawrence Radiation Laboratory, Livermore

G2 BASEBALL COIL FORM GEOMETRY AND FABRICATION, Manuel O. Calderon, Lawrence Radiation Laboratory, Livermore

G3 CRYOGENIC ASPECTS OF BASEBALL II, Robert L. Nelson, Lawrence Radiation Laboratory, Livermore

G4 MAGNETIC FIELD AND FORCE BY FINITE ELEMENT TECHNIQUES, Anthony R. Chargin and Carl D. Henning, Lawrence Radiation Laboratory, Livermore

G5 SUPERCONDUCTOR EVALUATION TESTS FOR IMP, D. L. Coffey and W. F. Gauster, Oak Ridge National Laboratory

G6 WINDING TECHNIQUES FOR SUPERCONDUCTING MAGNETS, R. L. Brown, Oak Ridge National Laboratory

G7 HIGH-FIELD CRYOGENIC MAGNETS WITH PURE ALUMINUM CONDUCTORS, Gerald F. Brown, NASA, Lewis Research Center, Cleveland

G8 A STUDY OF TOROIDAL AXISYMMETRIC MAGNETIC FIELD SYSTEMS INCLUDING THE EFFECTS OF FIELD DIFFUSION INTO THE RESISTIVE BOUNDARIES, J. Philpott, Culham Laboratory, England

Friday, April 11, 2:00 p.m.

Chairman, D. A. Baker, LASL

G9 DESIGN AND CONSTRUCTION OF AN IMPROVED $\ell = 3$ STABILIZING SYSTEM FOR THE MODEL C STELLERATOR, J. B. Joyce and G. V. Sheffield, Princeton University

G10 FABRICATION TECHNIQUES FOR RECENT COMPLEX MAGNET SYSTEMS, Arthur R. Harvey, Lawrence Radiation Laboratory, Livermore

G11 MINIMUM-B CONFIGURATION IN THE INTEREM FACILITY, R. C. Davis, J. N. Luton, Jr., O. D. Matlock, and W. L. Wright, Oak Ridge National Laboratory

Conference Summary

HOOP LEVATOR DESIGN FOR A PLASMA OCTUPOLE

Neil C. Lien and Igor N. Sviatoslavsky

Physical Sciences Laboratory, The University of Wisconsin
Stoughton, Wisconsin

ABSTRACT

Plasma confinement time in a multipole device is limited to a large extent by the supports which hold up the hoops during an experiment. For this reason, the new University of Wisconsin Octupole is designed with removable supports which leave the hoops suspended freely in a magnetic field when the device is electrically pulsed. The levator mechanism is designed to operate in a 10^{-8} torr vacuum and support a 335 pound load on the end of a ball-socketed probe which follows a path such that the ball moves in a vertical straight line. The available room to mount and operate is small to obtain the stroke lengths of 4-1/2 in. and 6-1/4 in. which are required. High strength and light weight materials are used to minimize inertia effects. A bellows seal at the pivot point of the mechanism eliminates the need for sliding seals. The actuator is an electrically pulsed, pneumatic device designed to withdraw the probe support in 20 milliseconds, hold it withdrawn for 20 milliseconds, then partially reinsert it in 20 milliseconds to catch the hoop and absorb its energy of fall, and then return it to its original position. The actuator is pulsed by a three-way pilot-operated solenoid valve connecting it alternately to a high pressure and a low pressure pneumatic source. An intermediate pressure is used to give the initial thrust for removing the probe. Check valves and volume chambers are used to provide damping cushions and the means for probe location at the instant when the hoop is caught. Forces are directly transmitted through a ball-socketed connecting link from the levator to the actuator and through rigidly mounted body and end caps to the vacuum tank. An adjustable dummy piston rod guide determines the stroke and hoop elevation. Test results indicate the desired requirements are met.

Plasma confinement time in a multipole device is limited by the presence of supports which hold up the conducting hoops that in turn provide the magnetic field. The Wisconsin Levitated Octupole, Figure 1, is designed to withdraw the hoop supports during the time the experiment is electrically pulsed for plasma injection and confinement and later reinsert them to catch the falling hoops. The device for removing the supports is called a levator. Each outer hoop, weighing 1,680 pounds, has five levators and each inner hoop, weighing 935 pounds, has three levators. The levators have the following design requirements:

1. Simple, dependable and economic.
2. Time sequence.
   a. Hoop supports withdrawn in 30 ms or less.
   b. Hoop supports remain withdrawn 20 ms or more.
   c. Hoop supports partially reinstated in 20 ms or less.
   d. Reproducibility to within $\pm$ 1 ms.
3. The kinetic energy of the hoop fall to be absorbed at any elevation without bounce.
4. Probe steady state adjustment capability:
   a. $\pm$ 0.4 in. in the vertical direction.
   b. $\pm$ 0.25 in. in the radial direction.
   c. 0.125 in. eccentrically.
5. Probe tip motion to be in a vertical straight line, to make it capable of catching the hoop at any elevation. Probe stroke 4-1/2 in. upper, 6-1/4 in. lower. When withdrawn the probe tip should be outside ψ critical the last MHD stable flux surface.

6. The probe to be electrically insulated from the remaining mechanism, and a lead provided for connecting to instruments outside the vacuum chamber.

7. Probe load design criteria:

   a. Normal vertical loading, 335 lbs.
   b. Emergency vertical loading, 1000 lbs.
   c. Radial loading, ± 250 lbs.
   d. Tangential loading capable of deflecting probe 0.125 in. ~ 50 lbs.

8. The probe housing to be part of a 10^{-8} torr vacuum system with a metal bellows vacuum seal suitable for angular motion. One seal to be used for attachment of the housing to the vacuum chamber.

9. All valves, restrictors and volume chambers to be an integral part of the actuator. Actuator body and end caps to be rigidly mounted to the vacuum chamber wall with all porting accomplished from below.

10. Connecting link to be ball socketed at piston and probe driving arm to allow for angular displacement. Both sockets to be accessible for greasing.

11. Assembly of unit to be accomplished within a 5 in. radial distance.

12. All materials to be non-magnetic.

The support mechanism, Figure 2, was designed to be assembled and to work within the limited space boundaries. The mounting to the vacuum chamber is accomplished with one "O" ring seal. The hoop is supported in a socket on the ball end of a probe extending into the vacuum chamber through a small hole in the wall. This probe constitutes one bar of a four bar linkage geometrically proportioned such that the center of the ball end travels in a vertical straight line within the angular displacement of its supporting bars. The actuator is attached to the end of one bar called a drive arm. The angular displacement of this arm is sealed across the vacuum barrier by a bellows. Using a bellows in this manner greatly reduces the force and velocity propagation between convolutions and substantially increases its life. The pivot bearings are of a teflon-lead compound impregnated into a spherized bronze interlayer backed by a bronze sleeve. These bearings are capable of operating in a 10^{-9} torr vacuum without lubrication. The drive arm of the box section construction is made from type 205 stainless steel for high strength and welding compatibility to type 347 stainless steel bellows.

The probe made from titanium 6A1 4V for lightness was designed for the design loads taken simultaneously. If the hoop is displaced up to 1/8 inch sidewise during magnetic levitation, the hoop socket is designed to catch the ball end and deflect the probe to home with approximately a 50 pound lateral load. The probe is also electrically insulated from its mounting and a wire extending externally is provided for instrumentation purpose and fail safe electrical circuits. The ball end position is radially adjustable ± 1/4 inch by varying the shim thickness between the drive arm pivot block and the housing in addition to a 1/8 in. eccentric adjustment of the ball center by rotating the probe about its mounting axis. The lower position of the ball center is adjustable by changing the length of the connecting link as shown in Figs. 2 and 3. The vertical upper position of the ball center is adjustable ± .4 in. by rotating the threaded dummy piston rod guide. To overcome the detrimental effects of inertia on an oscillating mounted actuator the actuator body was rigidly mounted to the vacuum chamber and a light ball socketed hollow connecting link was designed. Each end of the connecting link is lubricated through a common grease fitting. Driving the piston of the actuator upwards withdraws the probe from the induced magnetic field to a position outside ψ critical.

Pneumatics was chosen over hydraulics for the actuator for reasons of simplicity and economy while retaining dependability.

Basically, the principle of operation of the actuator is very simple. A piston is manipulated between a constant intermediate pressure P-3 on one side and a high pressure P-1 or low pressure P-2 on the other. Switching from P-1 to P-2 then back to P-1 drives the piston in one direction and back. Check valves and adjustable volume chambers provide the desired characteristics.

A detailed discussion of the operation of the levator follows. It is divided into five sections, each referenced to a figure corresponding to it.

Starting Conditions

Figure 4a shows the actuator and probe in their primary function, that of supporting the hoop, which they will do 99.7% of the operating time. The solenoid is de-energized, P-1 is connected to the top of the piston. The force of P-1 (~ 200 psig) has to be greater than the combined weight of the hoop and the force of P-3 to provide the necessary reaction for countering the energy of the hoop fall. This additional force also holds the piston against the adjustable dummy piston rod guide, thus properly locating the hoop vertically.

Probe Withdrawal

In Figure 4b we show the probe being retracted. The solenoid valve has been energized connecting the top of the cylinder to P-2. The piston starts moving when the pressure above it falls below P-3 ($\sim$70 psig). The delay between the start of the electric pulse and the piston movement is 35 ms and depends on the values of pressures as well as line impedances and inertia of moving parts. The value of the intermediate pressure P-3 depends on the speed needed for probe withdrawal.

Probe Deceleration

Figure 4c shows the piston being cushioned and the probe about to clear ψ critical. The main exit port is blocked by the cushion nut and CV-2 prevents the air from leaking out of the cushion.

A soft cushion is desirable for prolonging the life of the mechanism but it also stores a lot of energy causing the piston to bounce, and the probe to penetrate ψ critical at the very instant plasma is being confined. The problem was solved by incorporating an adjustable volume chamber AV-1 in the cylinder head with a check valve CV-3, such that this volume was part of the cushion only in one direction. The stored energy in it was trapped, and was unavailable to do work on the piston to bounce it. The air in AV-1 bleeds out through a restricted line into the cylinder exit port. This line gets blocked off as soon as the cushion nut enters the cylinder port. In this way we have almost eliminated the bounce while retaining a soft cushion.

The duration the probe remains withdrawn depends on the length of the electric pulse to the solenoid valve. At present, it is adjustable between 10 - 35 ms.

Partial Reinsertion of the Probe

In order to catch the hoop as it is dropping, the probe has to be partially reinserted into the plasma chamber. Figure 4d shows the probe catching the hoop which had dropped from the level where it was released.

The solenoid valve is de-energized, returning the top of the cylinder port to the high pressure P-1. Check valve CV-2 allows the pressure to act over the whole piston moving it rapidly downward. As the piston moves down it compresses the air under it. The air cannot return to P-3 because of CV-1 but can go into the adjustable volume chamber AV-2 through CV-4. The piston slows down and stops against a very soft cushion.

Absorbing the Energy of the Hoop Fall

As the hoop contacts the probe (Figure 4e) it drives it down forcing the piston up. Check valve CV-4 is closed and the air in AV-2 is trapped. As the piston moves up, the air under it expands and its pressure drops. CV-1 remains closed until the pressure drops below P-3 after which it stays at P-3. The pressure on top of the piston rises above P-1 as the piston moves up since the air is trapped in the line due to CV-5. It is this constant pressure rise which counters the fall energy of the hoop. The system is now equivalent to a mass on springs and performs several oscillations with a period of 300 ms before it damps out. Then as the air in AV-2 bleeds back to P-3 through a needle valve the piston slowly moves down, returning the hoop to its starting location as shown in Figure 4a.

A primary concern in the design of the actuator was to insure that the hoop would not bounce off the probe at any time. If while approaching the maximum point of its first oscillation (region of possible hoop bounce as marked by asterisk on Figure 4e) the probe, on which the hoop is now supported (but not attached to), decelerates faster than one g, then the hoop can separate from the probe. The rate at which the air bleeds out of AV-2 during the first oscillation determines how far the piston returns downward and how fast it decelerates. The adjustment of the needle valve which bleeds the air out of AV-2 is critical, but once done, should not have to be readjusted. In our tests we were actually able to make the load bounce at will. A simple adjustment of the needle valve corrected this condition.

A prototype levator was constructed and tested extensively with and without load. Check valve modifications were necessary to improve performance and prolong life. Otherwise, performance was as predicted.

The load consisted of a steel bucket filled with lead bricks. It was suspended from the probe on straps which were fitted with an aluminum block and a socket of Ampco alloy similar to the hoop socket. The levator was then pulsed and the load caught under strictly gravity conditions. This is the toughest situation the levator will ever be confronted with. A total of 15,000 pulses with full load have been made on four different levators with no apparent signs of wear or failure. These tests were performed under simulated operating conditions with two levators fed from one set of pressure reservoirs, as will be the case in the actual device.

The bellows was also tested under simulated operating conditions with the probe in a vacuum chamber. Although more tests are forthcoming, the bellows has so far withstood 2000 pulses with no ill effects.

Linear variable differential transformers and conventional piezoelectric pressure transducers were used to monitor displacement and pressure respectively. The outputs were displayed on a memory scope which proved to be invaluable for studying reproducibility. Outputs of an upper and a lower levator were also simultaneously displayed on the scope. From these tests it became apparent that separate electric pulsing systems for the solenoids of the upper and lower levators would be desirable. It also became apparent that throttling valves or the P-2 lines of the upper levators would be useful for impedance matching.

Acknowledgments

The authors wish to acknowledge the helpful discussions with Dr. D. W. Kerst, Dr. F. E. Mills, Dr. H. K. Forsen, and the help from the engineering department and instrument makers of the Physical Science Laboratory and the University of Wisconsin Physics Machine Shop. The work of Al Cavallo in testing the levator is also appreciated.

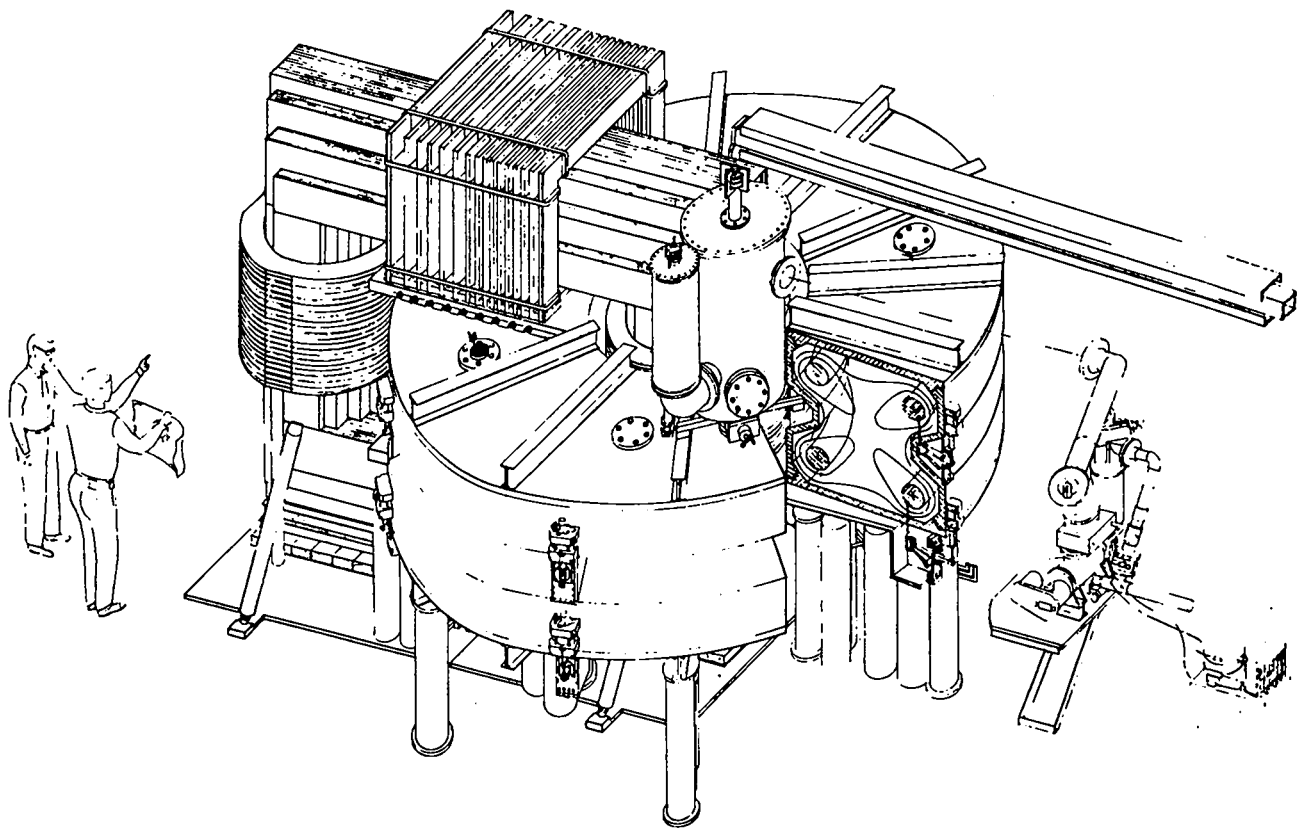

FIGURE 1 WISCONSIN LEVITATED OCTUPOLE

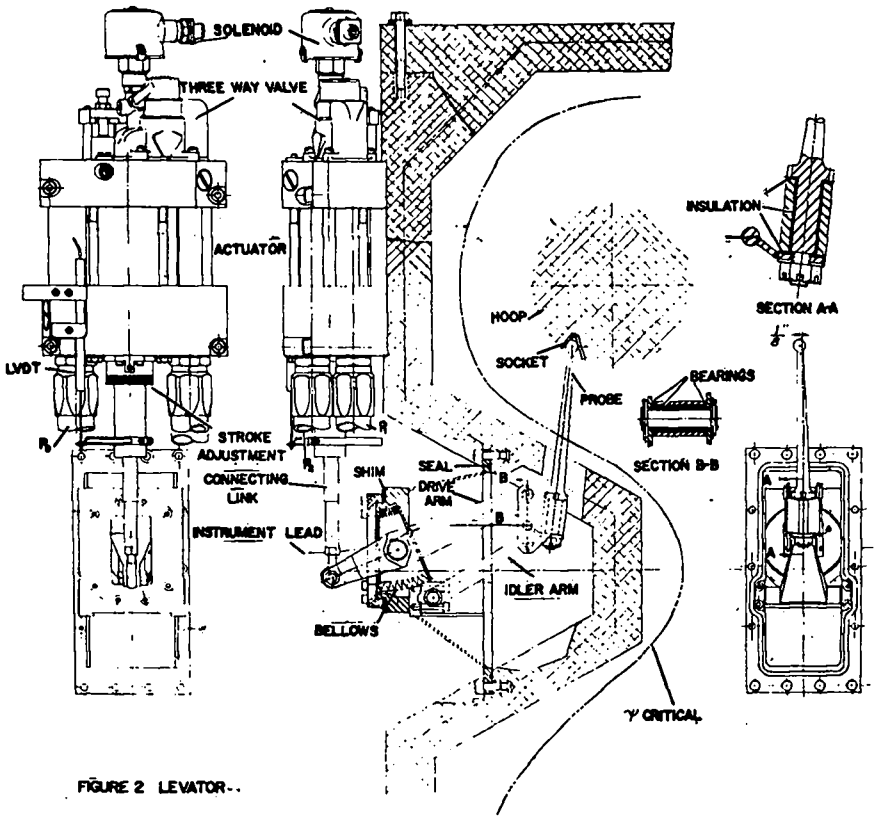

FIGURE 2 LEVATOR--

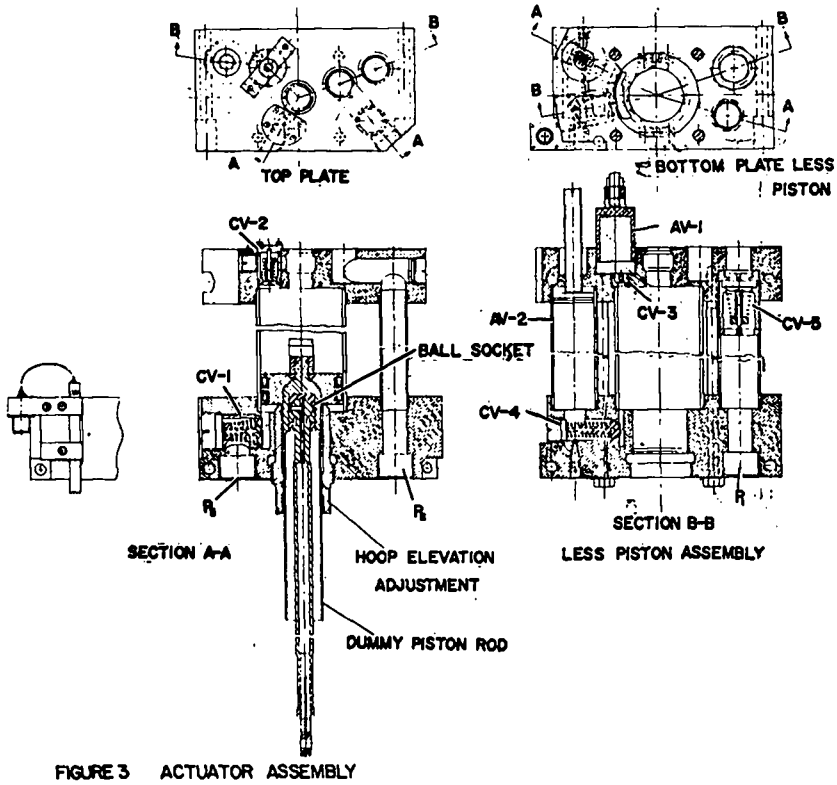

FIGURE 3 ACTUATOR ASSEMBLY

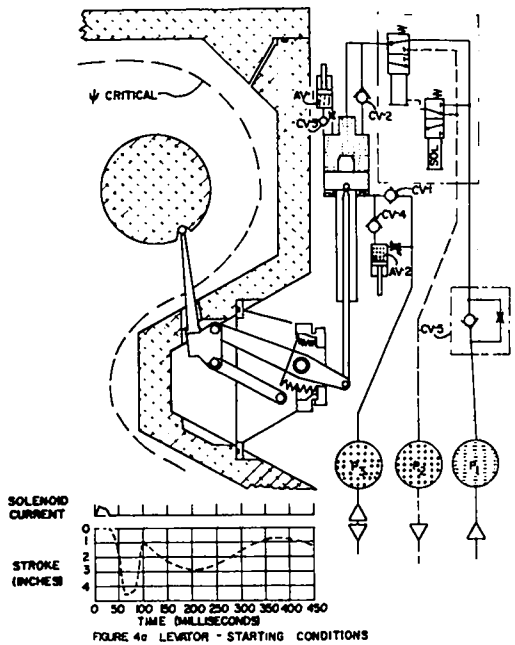

FIGURE 4a LEVATOR - STARTING CONDITIONS

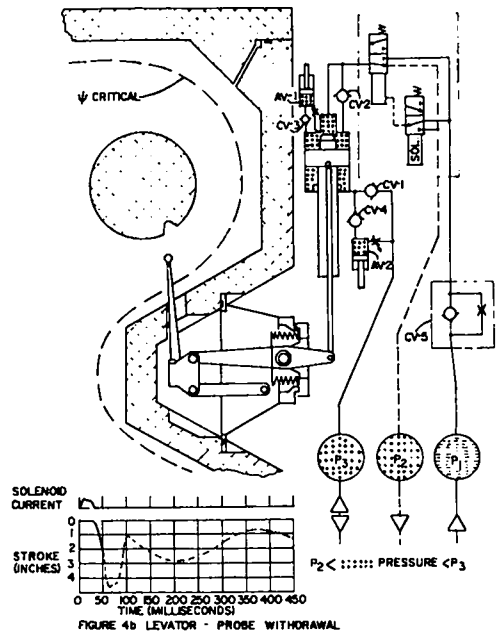

FIGURE 4b LEVATOR - PROBE WITHDRAWAL

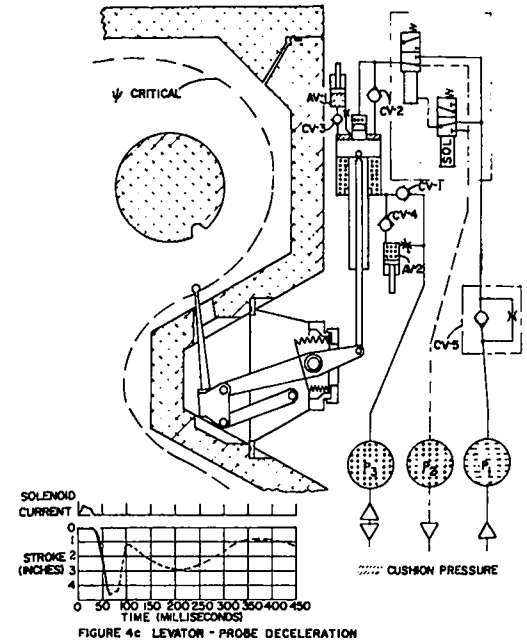

FIGURE 4c LEVATOR - PROBE DECELERATION

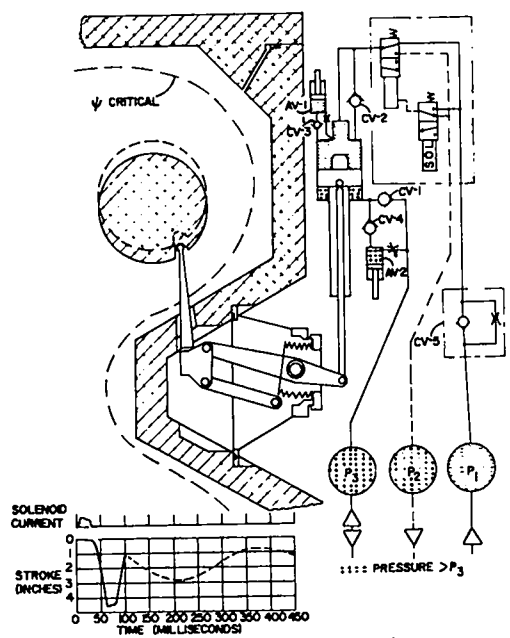

FIGURE 4d LEVATOR - PROBE PARTIAL REINSERTION

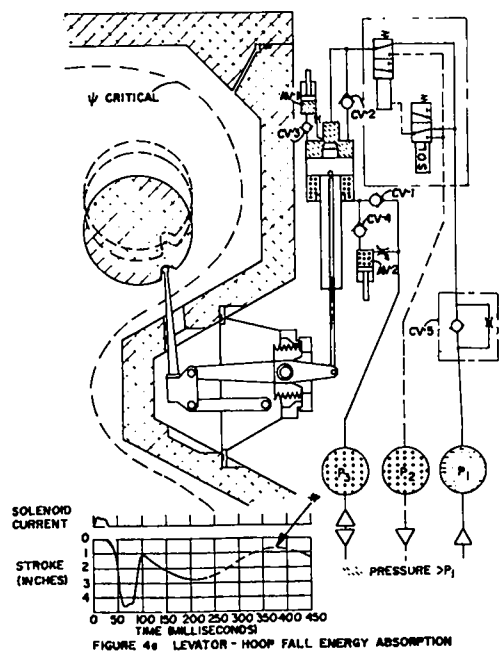

FIGURE 4e LEVATOR - HOOP FALL ENERGY ABSORPTION

MAGNETIC PROPERTIES OF THE ORNL LEVITATED TOROIDAL QUADRUPOLE*

by

M. Roberts, I. Alexeff, W. L. Stirling, and W. Halchin
Oak Ridge National Laboratory
Oak Ridge, Tennessee

ABSTRACT

Electromagnetic levitation of internal conducting hoops in a toroidal quadrupole has been achieved, producing a magnetic field for plasma confinement experiments. High magnetic field strengths are now available in this low-inductance quadrupole and a possible technique for producing time-invariant magnetic fields in the device is presented.

INTRODUCTION

The useful plasma confinement properties of the toroidal multipole field configuration[1] require the current carrying conductors to be embedded in the plasma. Optimum use of this geometry necessitates levitation of the conductors, the highest magnetic field strength and time invariant magnetic fields.

LEVITATION

Electromagnetic levitation[2] is accomplished by the induction of eddy currents in the walls surrounding the current carrying conductors (Fig. 1a). The eddy current magnitude is proportional to R^{-1} or $\sigma^{1/2}$ (since the wall thickness (r_h) is greater than the electromagnetic skin depth (δ)). With liquid nitrogen cooling (from 273°K), eddy currents are increased a factor $\sim 10^{1/2}$ and most (> 90%) of the field is confined to the vacuum space; cooling also increases the L/R magnetic field decay time. As the ratio of repulsive (hoop-wall) forces to attractive (hoop-hoop) forces (Fig. 1b) is equal to $\sigma^{1/2}\ r_{hh}/r_{hw}$ equilibrium is achieved by both cooling and separating the hoops; it is necessary that $r_{hh} \gtrsim 2r_{hw}$ to prevent collapse of the toroidal quadrupole.

A downward displacement of the hoops produces a difference in magnetic pressures equal to the force of gravity (Fig. 1c). When sinusoidally excited the hoops oscillate at a low frequency ($f \sim 16$ Hz) with a small amplitude ($\Delta x/x < .25$) apparently resulting from the non-smooth time variation of the force. In model experiments, severe hoop oscillations have resulted when the iron core was driven into saturation resulting in a nonlinear coupling.

The sketch (Fig. 2) shows that the quadrupole is basically a transformer with the plasma filling the toroidal chamber between the two hoops and the contoured wall. Figure 3 shows the lower half of the quadrupole (with the hoops levitated); the entire apparatus is enclosed inside a four foot diameter vacuum tank.

HIGH MAGNETIC FIELD

A maximum magnetic field (or current) requires a minimum of secondary inductance since the iron core has a maximum flux density. The simplest scheme of making a minimum inductance quadrupole is to form a dual coaxial toroid (Fig. 4), driving the wall currents and inducing the hoop currents; this scheme requires an extremely high supply current (.4 MA)--but has very little excess energy storage, using a strip-line connection from the generator. In practice, a transformation ratio (Fig. 4b) is usually used, which then introduces a third element, (Fig. 4c) the wall carrying induced eddy currents. This current carrying wall serves as a magnetic wall

*Research sponsored by the U. S. Atomic Energy Commission under contract with the Union Carbide Corporation.

to minimize stored energy in the coupling field. The field between the hoop current and eddy current is the confining field, and that between the primary current and eddy current, the coupling field. Energy comes from the source through the coupling field to the quadrupole field via the connecting gap. Since the confining wall has a radial cut to prevent shorting the emf there is a section of azimuth at which the magnetic wall (the eddy current distribution) does not match the vacuum field shape. Proper placement of the primary windings matching the wall current density can provide a nearly continuous azimuthal current pattern, although only an approximation (two horizontal current sheets) to that density profile exists in our present model.

At present, 1/3 of the maximum fields (Fig. 4d) are available for use (representing 140 kA out of possible 420 kA). The wall currents are carried around the iron core by a copper jumper inside which the primary coil is placed. The total quadrupole inductance (calculated and measured) is about 170 nH and the total jumper-primary inductance is about 30 nH. With the fields in the jumper strip-line presently at $\sim$ 6-1/4 kG ($\sim$ 1/3 max), the pressure separating the coil from the copper is 1.5 atm ($\sim$ 1/10 max).

Figure 5 shows the three components of the power supply. A slow (high inductance) 18 kJ capacitor bank is being used to supply the single half-cycle main field. The levitating field is supplied by a triangle shaped pulse envelope of 60 Hz sine waves; the 3 Ω resistor prevents the capacitor discharge from shorting through the a.c. supply. A battery supplies mmf biasing currents through a protective diode. All three supplies use the same 38 turn primary coil pair. Biasing the iron core allows a change of magnetic flux from $-\phi$ to $+\phi$ inducing 2I in the secondary, although only a single half cycle is possible in this mode.

TIME INVARIANT MAGNETIC FLUX

The difference

$$\frac{\dot{\phi}_{core} - k(r)\,\dot{\phi}_{quad}}{r}$$

where k(r) varies from 0 to 1 in the cross section represents an azimuthal electric field at radius r having consequences potentially dangerous[3] to plasma confinement. There is a decay of ϕ_{quad} or an increase in ϕ_{core} because the ohmic loss in the hoop must be supplied either from the quadrupole magnetic field or from the driving source. The poynting vector can be made zero (no energy input) only by providing a source of energy inside the material of the hoop or using superconductivity.

Taking advantage of the low propagation velocity of energy into a good conductor, it is possible to store energy in the copper material in the form of the magnetic field of a non-simple current distribution (Fig. 6). The amount of energy available is the difference in magnetic field between the initial current distribution and the final relaxed distribution. The material thickness (radius) must be greater than about two electromagnetic skin-depths to allow a radial current variation; the relaxation time varies inversely with the excitation frequency.

Figure 7 shows an equivalent circuit for the energy storage. The net current passes through parallel annular paths in the copper hoop represented by the parallel L-R strings. Upon active crowbarring of the primary (supplying the primary ohmic loss) the charged internal inductors can relax, supplying the internal ohmic losses as long as $dL_{int}/dt = R$, a time related to the excitation frequency. The equality $dL_{int}/dt = R$ represents a possible mode, but not a necessary one and it presumably requires deliberate programming of the current excitation for optimum benefit. As long as $dL_{int}/dt = R$, then I and ϕ_{core} are constant resulting in a steady, time invariant situation indistinguishable from the superconducting case. The wall current also must not change if there is to be no time varying flux anywhere; the same energy storage arguments do apply to the wall as well.

Figure 8 shows the type of measurements made with a typical result indicating a reduction of 250 in electric field when a solid cold hoop is used instead of a hollow cold hoop. A factor 6 in this represents the reduction in driving force resulting

from the smaller resistance in the solid hoop leaving a factor 40 of improvement attributable to energy storage. More recent accurate data show two orders of magnitude reduction in E for 10 μsec and one order of magnitude reduction for 100 μsec. These data (using the solid hoop only) come from comparing E at the same B but during the second and first quarters of the cycle, when one would and would not expect energy storage. Further experiments with programmed currents are evidently necessary to lengthen the period of time invariance for useful results.

REFERENCES

1. T. Ohkawa and D. W. Kerst, Nuovo Cimento 22, 784 (1961).
2. E. C. Okress et al., J. Appl. Phys. 23, 545 1413 (1952).
3. Report of the Study Group on Low-Beta Internal Ring Devices, Princeton Plasma Physics Laboratory, February 1969.

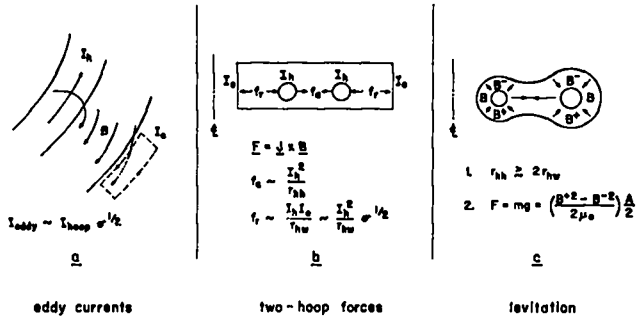

Fig. 1. Eddy Current Levitation. (a) Wall eddy current induced by the changing field of the hoop. (b) Attractive and repulsive forces between two hoops and the wall. (c) Levitation by using the difference in magnetic pressures.

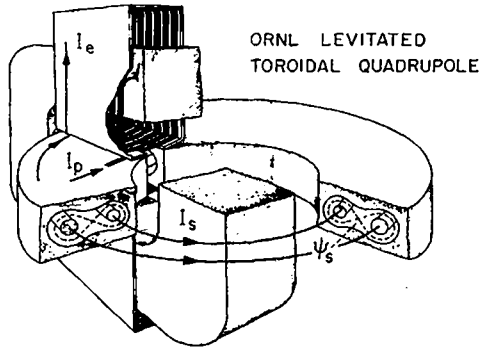

Fig. 2. A representation of the ORNL levitated toroidal quadrupole illustrating the primary (I_p), secondary (I_s), and eddy (I_e) currents and the magnetic separatrix ψ_s.

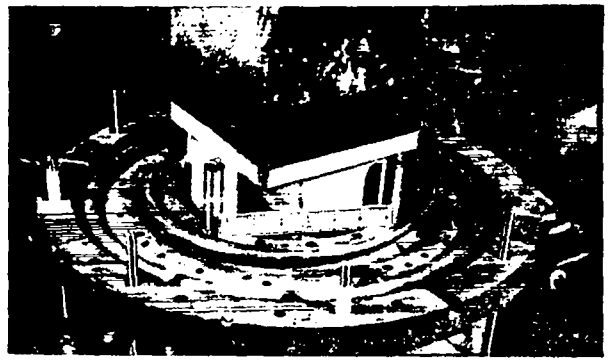

Fig. 3. The lower half of the ORNL quadrupole showing the hoops levitated and illustrating the access holes, the iron core, and the jumper beneath.

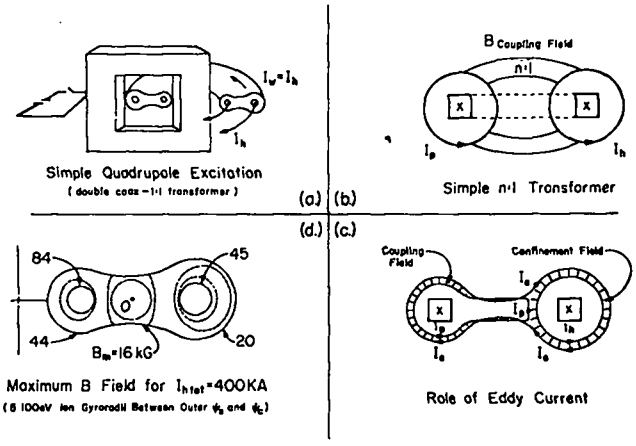

Fig. 4. Quadrupole Magnetic Field Design. (a) The simplest low-inductance quadrupole. (b) Stored coupling field of an n:1 transformer. (c) Use of a flux-conserving wall to minimize the coupling field; use of the primary mmf to smooth the azimuthal discontinuity in field. (d) Approximate maximum field strength plot expected with present design.

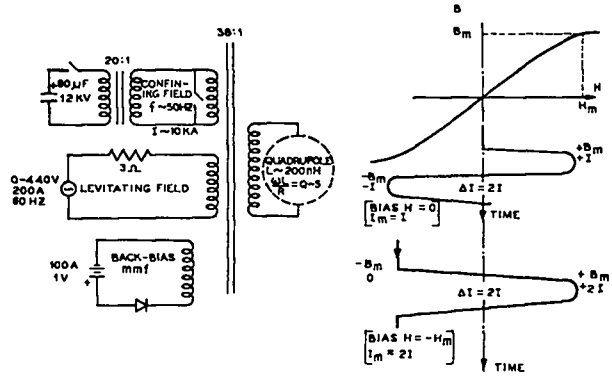

Fig. 5. The Quadrupole Power Supply with an Illustration of the Back-Bias Technique.

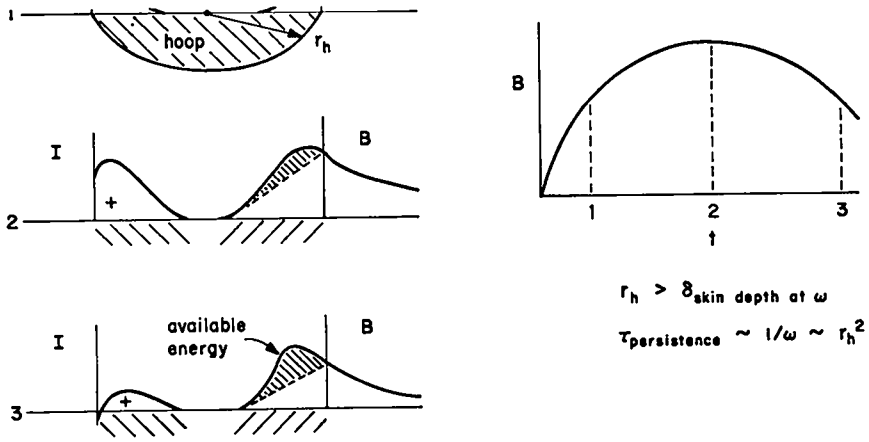

Fig. 6. The Energy Storage Concept. Showing typical current and field profiles at three times in the cycle.

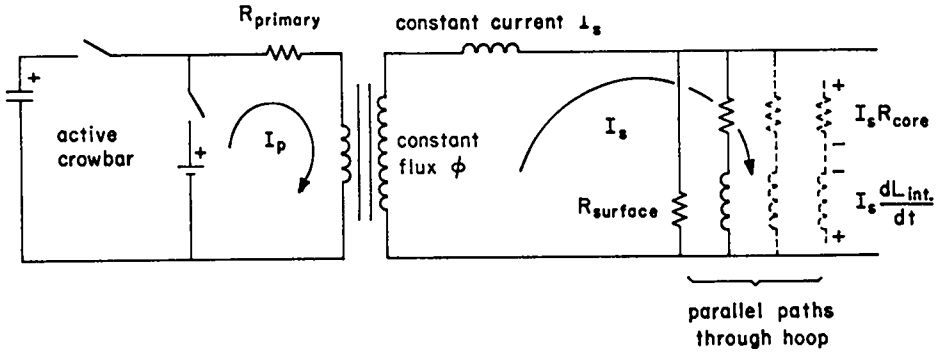

there exists a steady state as long as $\frac{dL_{int.}}{dt} = R_{core}$

Fig. 7. Equivalent Circuit for Energy Storage.

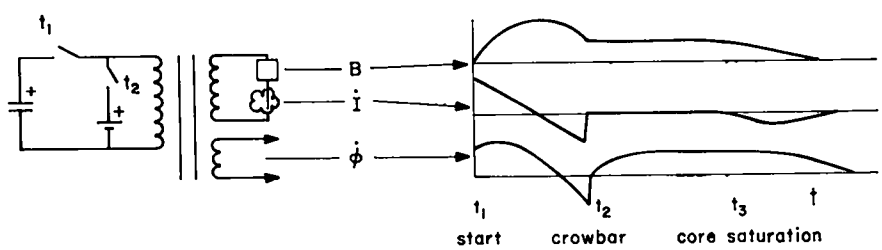

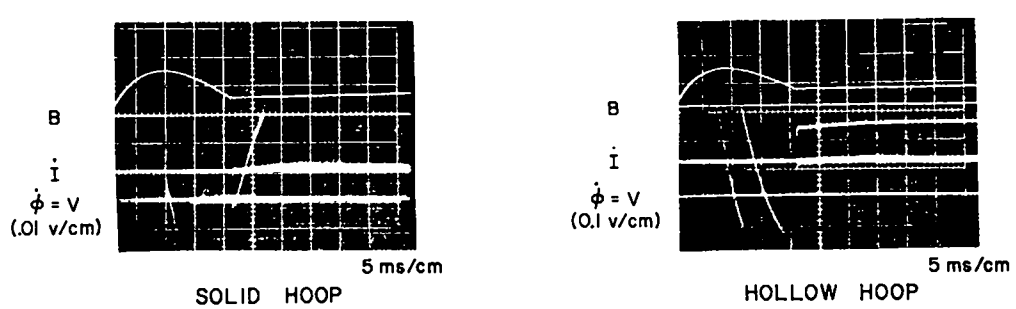

Fig. 8. Energy Storage Measurement. Illustrating that $r_h > \delta$ is a necessary requirement for energy storage. Hall probes, Rogowski belt and simple voltage coils are used.

MECHANICAL DESIGN OF A QUADRUPOLE INJECTION EXPERIMENT

by

R. W. Kewish, Jr., R. S. Dike, J. E. Hammel, and A. R. Sherwood

Los Alamos Scientific Laboratory, University of California
Los Alamos, New Mexico

ABSTRACT

A plasma gun is frequently used as a source of plasma for containment experiments in controlled fusion. In these experiments usually guns with low plasma energy output have been used. We have designed and are building an injection experiment using the much more energetic plasma from a coaxial gun. The coaxial gun plasma with its highly directed energy will be injected into a quadrupole geometry capable of stopping the 2.5-keV stream. The limitations placed on the design by the experimental requirements are: (1) an injection field of at least 6.5 kG but less than 10 kG (for self-depolarization of the plasma stream); (2) an MHD stable configuration which has at least 10 gyro radii across the stable region for 2.5-keV protons; (3) a maximum of 0.8 MJ in the magnetic field (because of availability); (4) coils suspended at one point by a dipole guarded current feed. With 2.5-keV ions it is mandatory that the support and feed be guarded because bombardment of any obstruction would hopelessly contaminate the system; (5) a maximum field of 40 kG; and (6) maximum current of 600 kA (because of current joints which lead to the necessity of designing a two-turn coil).

The quadrupole coils, liners, and flux-smoothing shrouds were designed with the aid of a computer code developed by Baker and Mann.[1] The guarded feed is a force-free configuration with its null line closed by a cross-feed at the coil surface. The design of this complicated region was guided by an examination of the analytic expression of the dipole field supplemented by probe measurements of a model of the feed region. This paper will discuss the results of the model analysis and the mechanical design of the experiment with the imposed constraints.

I. INTRODUCTION

A plasma gun is frequently used as a source of plasma for containment experiments in controlled fusion. The process by which a plasma stream enters and is trapped in the containment geometry is not well understood. A toroidal quadrupole has been designed which will be used to study the injection and trapping processes and the efficiency of these processes in producing a quiescent plasma within the quadrupole field. This quadrupole design is distinguished by an arrangement in which each interior coil is suspended from a single support which is magnetically guarded by a linear dipole current. Also in this experiment the increased plasma loss produced by such a dipole guarding field will be measured.

The experiment is designed within certain constraints which are as follows: (1) a minimum of about 10 gyro-radii of MHD stable field for 2.5-keV ions was felt to be reasonable; (2) the maximum field must be no larger than 40 kG, a restriction imposed by design considerations and materials available; (3) the total field energy must not exceed 0.81 MJ, because this is the bank energy readily available in the

*Work performed under the auspices of the U. S. Atomic Energy Commission.

[1] D. A. Baker, J.E. Hammel, and L.W. Mann, Bull. Am Phys. Soc. Ser. 2 12, No. 6, 909 (1967).

experimental area; (4) from past experiments with the coaxial gun streams, the limits of the injection field must be between 6.5 and 10 kG to assure plasma penetration and self-depolarization; (5) coil design must include a dipole guarded current lead from which the coil can be suspended or supported; and (6) maximum current should not exceed about 700 kA because of design limitations on current connections.

II. GENERAL CONFIGURATION

The quadrupole field is formed by a pair of driven coils inside a conducting liner and baffle system. The usual toroidal multipole has an outer wall which completely encloses the confinement region (Fig. 2a). With the magnetic field geometry independent of the vacuum vessel, greater freedom in the quadrupole design is possible. It is desirable to have the outer field shaping conductors as open as possible for ease of injection and diagnostic observation. A completely open design (see Fig. 2b) could not be found because the requirements on the injection field strength could not be met. A baffle arrangement was able to produce the desired injection field strength while retaining many of the advantages of a completely open design. The baffles are shown in Fig. 2c. Openings to the interior of the containment geometry are completely symmetric which allows injection and diagnostic access without field perturbing ports. Since the baffles see large magnetic forces, they are supported by aluminum channels which are in turn supported by steel rods from the liners. All these supports are well outside the containment region.

A computer code developed by Don Baker and Lawry Mann[1] was used to calculate the field configuration from many possible coil, liner, and baffle arrangements. The computation assumed the skin depth to be infinitely thin. The design chosen was that configuration which had the largest number of ion gyro-radii of MHD stable flux within the imposed constraints. Some results of the optimized computer design are shown in Fig. 1. A schematic of the final design is shown in Fig. 3. The outer conductor surfaces are not part of the vacuum vessel so the whole machine is placed within a 7-ft.-diam. stainless steel tank. More detailed views of the arrangement are shown in Fig. 4.

III. COIL DESIGN

Because of limitations in current joint design,[2] the coils each have two turns. In order to match the calculated current distribution, the ring was split along the symmetry axis for the two-turn configuration. The major problem on the design of the coil itself is the cross-over region where the first turn connects to the second turn. Figure 5 shows the design of the region in expanded view. Epoxy and fiberglass hold the two parts together; this is discussed later.

By previous experience we knew that the two-turn coil would have perturbations in the magnetic field caused by the two-turn design. A solution to this problem is the use of a copper shroud covering the coil as seen in Fig. 6. The shroud is more than two skin depths thick, which forces the field to conform to the shape of the shroud. In order that the shroud not be a shorted secondary turn for the coil, it is interrupted by two 1/2" Micalex insulators which are held in place by the epoxy. The coil assemblies are thus a three-part sandwich of an Al alloy two-turn coil covered by an epoxy-fiberglass insulator which is in turn covered by the copper flux-smoothing shroud. Great care has been taken to assure impregnation of the fiberglass with no voids. The space occupied by the fiberglass is evacuated prior to the epoxy pour with the copper shroud itself being used as the potting vessel. Figure 7 shows the apparatus for casting. Epoxy is mixed and heated in a separate container then evacuated to remove all of the air. The fiberglass-wrapped coil and the shroud are evacuated in the same tank that will house the final assembly of the experiment. The epoxy is then pressure-fed into the bottom of the coil in several places. Several stand pipes indicate when the coil is fully impregnated. Finally the apparatus is let up to air, and the coil with the epoxy is cured in water at 90°C for 24 to 36 hours. A prototype coil has been so made, and careful disassembly showed that there were no voids in the epoxy.

The highest field is 40 kG at the surface of the inner coil and this puts the inner coil at high tensional stress. A computer problem was run by D. Baker and L. Mann on the stress in a coil when energized and crowbarred.[3] On the basis of these results it was decided to use a special aluminum alloy to meet the

strength requirements. This alloy, 7039-T64, caused us many problems. Vendors bidding to make the coil have not been able to demonstrate that they can satisfactorily weld 7039; therefore, Kaiser Aluminum Metallurgical Laboratory (the original developer of the alloy) was finally called in to do the welding.

IV. DIPOLE GUARD AND CURRENT FEED

Because bombardment of a current feed with 2.5-keV protons would contaminate the system, it is mandatory to use a current feed magnetically shielded by dipole guarding. The dipole guard field added to the quadrupole field produces a field similar to that depicted in Fig. 8. This configuration can be arranged to produce no net magnetic force on the leads and thus reduces the strength requirements on the leads. Two line nulls in the field are produced by this arrangement, and plasma entering the null region will flow unimpeded along a null line. To prevent contamination, only flow toward the outside of the machine can be tolerated; therefore, a special design is made which closes these nulls as they approach the inner conductor. The closing of the nulls is accomplished by adding a steeply rising field to the dipole field as the coil is approached. This added field is produced by a cross-over current between dipole legs just before the coil surface is reached. A computer solution to the field of a simple hairpin of current in a background field showed that the null region could thus be effectively closed. A more accurate study of the effect of the dipole cross-over current in closing the null was studied by magnetic probing of a mock-up of the dipole guard region. A full-scale mock-up of the dipole and cross-over combined with a background field simulated by a Helmholtz coil was used to find the configuration needed. The model was driven at 1 kHz (to approximate the skin depth in the real case) and probed by a small coil mounted so that amplitude and direction of the field could be measured. Figure 9 shows the field in the plane of the nulls and how the field lines dip under the dipole cross-over current element. Figure 10 shows one of the field plots made in studying the dipole. The length of each arrow is proportional to the field strength. In a later design, Fig. 11, the dipole cross-over is lowered to the surface of the coil. The advantage of this design is that it minimizes the perturbation of the dipole on the quadrupole field.

Thus the design at the two dipole legs feeding the coil is as shown in Fig. 12a and it is equivalent electrically to the current shown in Fig. 12b. The legs of the dipole field elements are made of Amzurk, a high-strength, high-conductivity copper alloy.

V. LINERS

The liners are 1/4" copper cylinders backed by aluminum rings for mechanical strength. The 24 aluminum backing rings on each liner form a cylinder $2\frac{1}{2}$" thick. Each liner must have a port through which the dipole current feed for the coil can pass, but a simple port in the liner would cause a large perturbation in the field.

To reduce this perturbation, a scheme similar to that proposed by John Marshall[4] was employed in the liner design. This scheme depends on the fact that a wall can be moved outward from the containment region of the machine without disturbing the interior field, if the wall is placed on a flux surface which would be an extension of the interior field. If this is done locally at the port position, the port perturbation can be reduced to a negligible amount. In our case the extension is not straight-forward because a separatrix is crossed in moving the wall. An analog method was used to give an approximate shape and position for the wall, and a magnetic probing of a model of the port region gave the final configuration for the port region. For this reason the liner is slotted down its entire length with small tabs extended from the edge of the slot. A bridge the same width as the coil crosses the slot at a larger radius than the liner surface, Fig. 13. This bridge has a hole to accommodate the dipole current feeds. Extensive probing with the model shows no appreciable perturbation of the magnetic field in the experimental region due to the dipole port, and only a small perturbation at the baffles which are completely circular. A conducting shield is placed in the slot at the same radius as the inside surface of the liner to minimize the field distortion due to the baffles.

VI. HEADERS AND CROWBARRING

The machine includes headers which feed the coils coaxially up to the point where the configuration is changed to form the dipole. The field rises to the peak in 250 μsec. Finally, this experiment is to be crowbarred using a fast metallic solid dielectric

switch.[5,6] The entire assembly of the machine is shown in Fig. 14.

References

1. D. A. Baker, J. E. Hammel, and L. W. Mann, Bull. Am. Phys. Soc., Ser. 2 12, No. 6 (1967).
2. R. S. Dike and W. H. Borkenhagen, "High Current Joint Techniques", paper E8, this Symposium.
3. P-18 Quarterly Report, p. 11, April 1968.
4. J. Marshall, Los Alamos Scientific Laboratory Report LA-3202-MS, p. 10 (1964).
5. I. Henins and J. Marshall, Rev. Sci. Instr. 39, 1481 (1968).
6. V. A. Finlayson, "Characteristics of the Scylla IA Theta Pinch with Crowbar", Los Alamos Scientific Laboratory Report LA-4042 (1968).

FINAL QUADRUPOLE DESIGN

Field energy	0.81 MJ
Turns/Coil	2
Number of gyro-radii across stable region	5.5 (2.5 keV deuterons)
Injection field	7.3 kG
Maximum field inner coil	40.0 kG
Maximum field outer coil	24.1 kG
Field inner bridge at the separatrix	32.4 kG
Field outer bridge at the separatrix	19.6 kG
Current/turn, inner coil	0.61 MA
Current/turn, outer coil	0.41 MA

Fig. 1. This table shows some of the results of the final computer design.

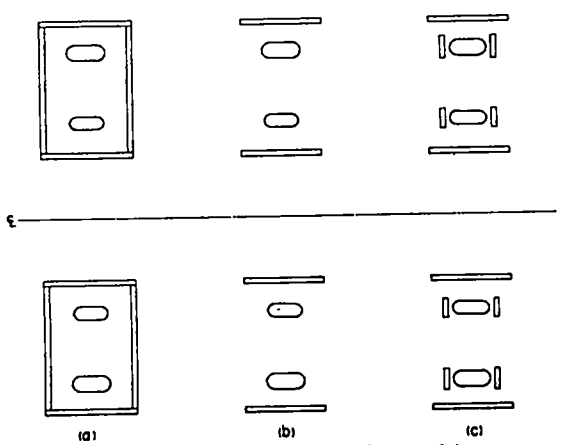

Fig. 2. Alternative designs of the machine, open and closed, and the final design baffled or semi-open machine.

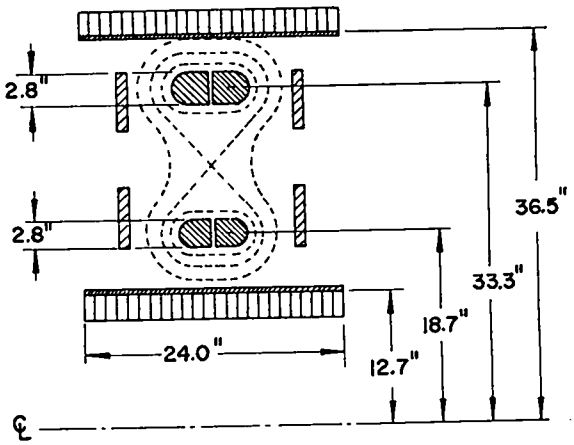

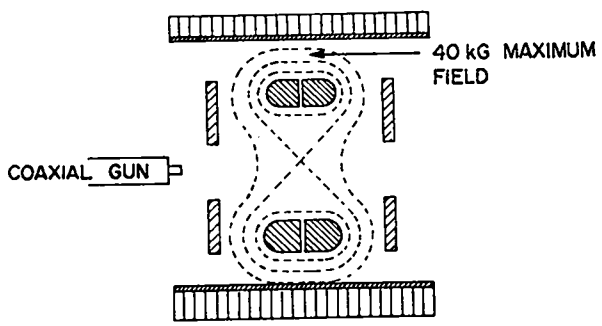

Fig. 3. The major parts of the quadrupole, dimensions, and general field configurations.

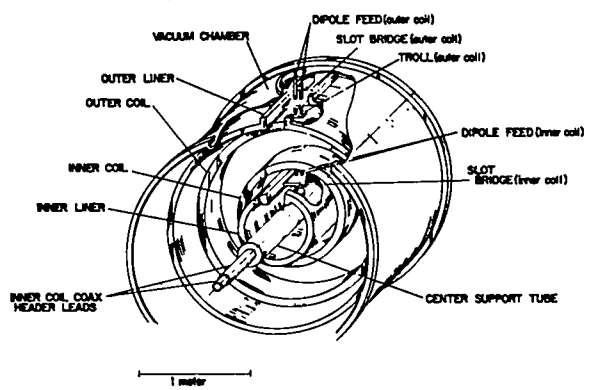

Fig. 4. Simple picture of the quadrupole without the baffles.

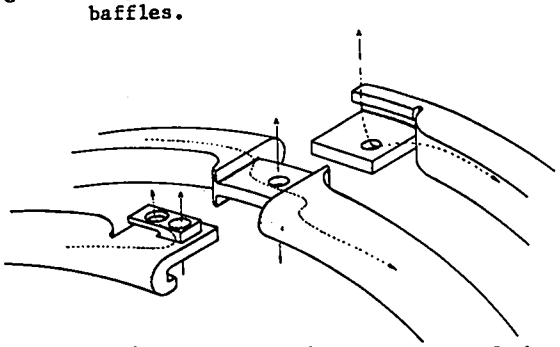

Fig. 5. Exploded view at the cross-over of the two-turn coil. Current feed path is shown.

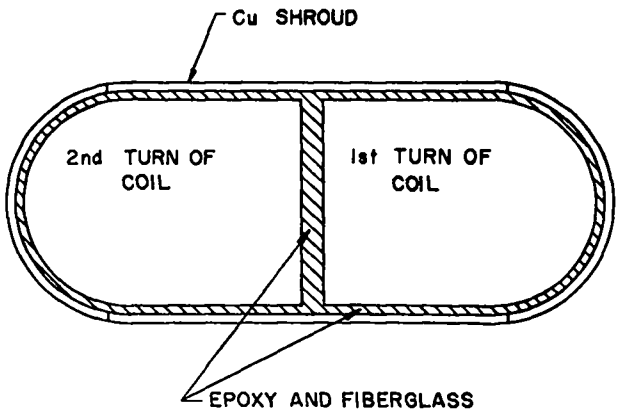

Fig. 6. Cross-sectional view of a coil.

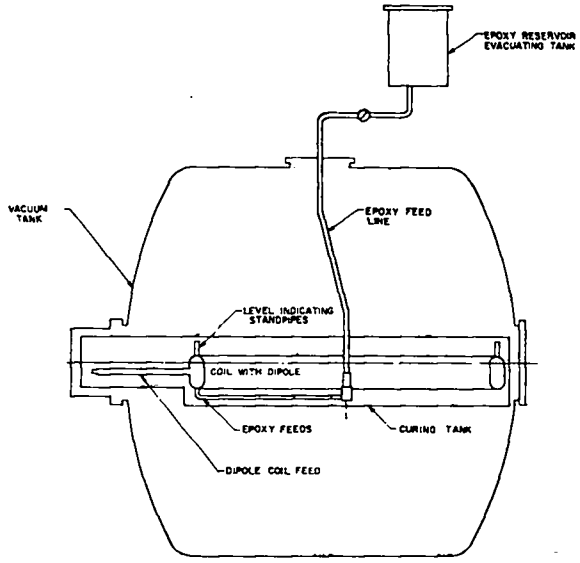

Fig. 7. Epoxy casting apparatus.

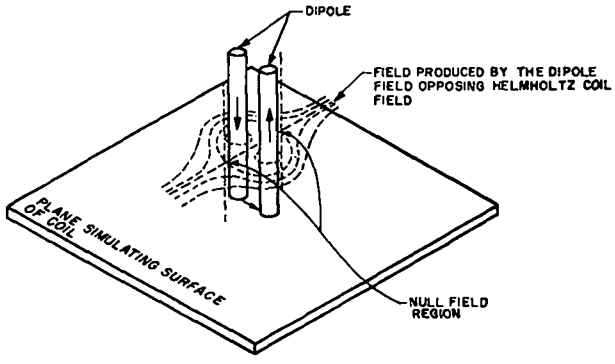

Fig. 8. Representation of the combined dipole field and the field produced by the coil. Line null is shown.

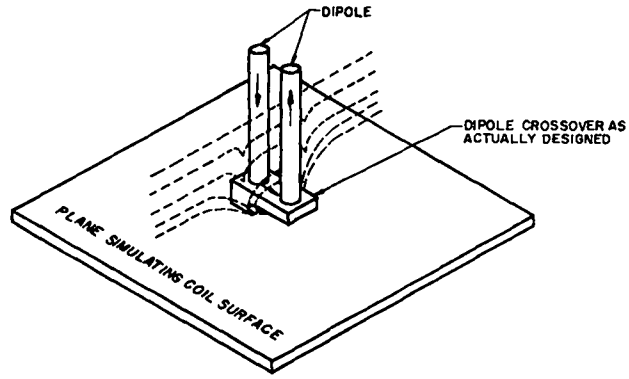

Fig. 9. Field in the mid-plane of the dipole legs. Field lines from the region of the null become large before dipping under the cross-over.

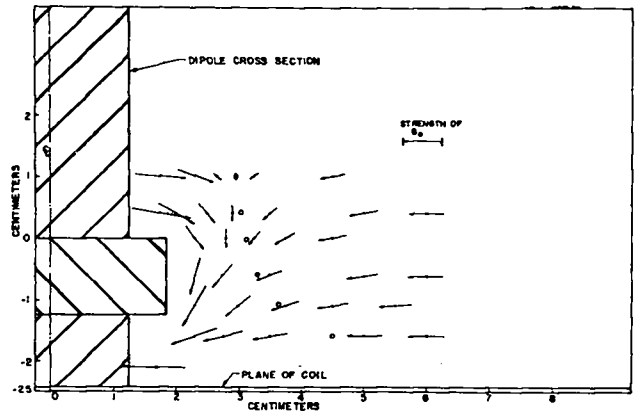

Fig. 10. Magnetic field plot of the model near the current cross-over.

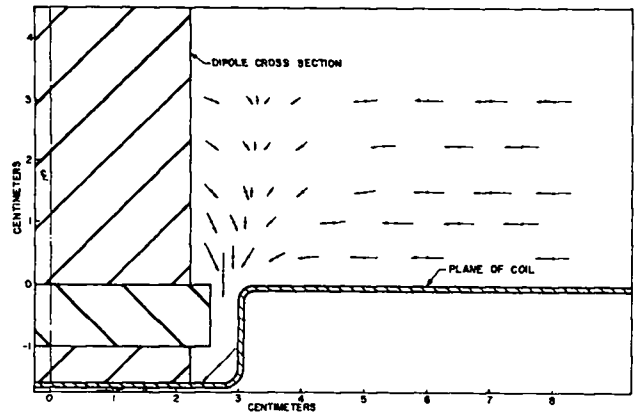

Fig. 11. Dipole and cross-current design giving a smaller perturbation in the containment region than the design shown in Fig. 10.

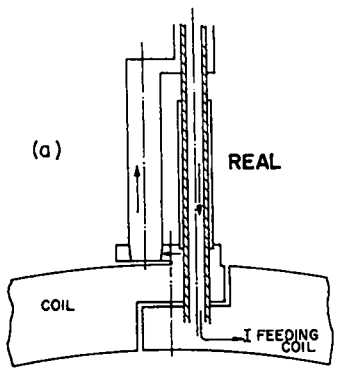

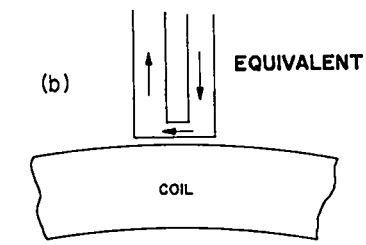

Fig. 12. Real configuration (a) of the coil feed in cross-section, (b) equivalent current.

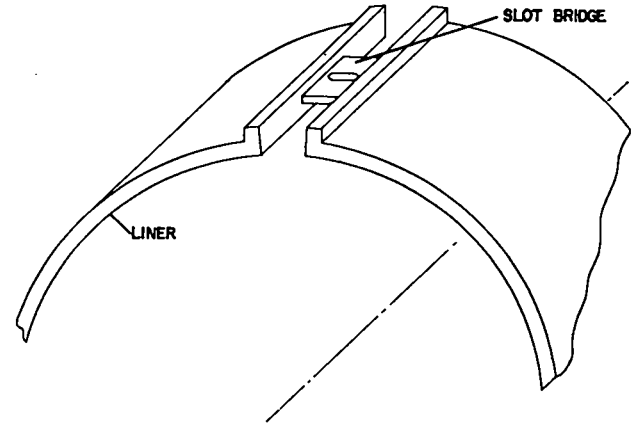

Fig. 13. Liner with slot and hole for current leads.

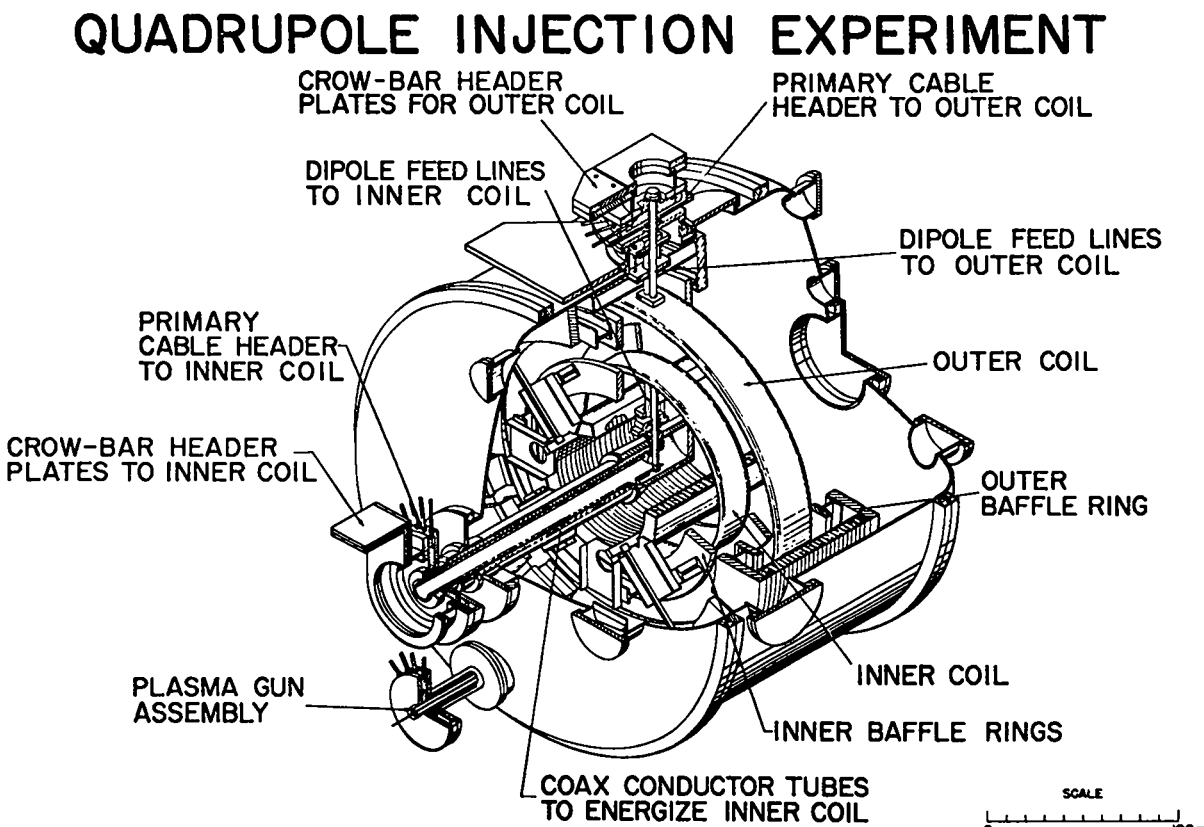

Fig. 14. A detailed illustration of the final design of the machine.

THE PRINCETON SPHERATOR*

by

P. Bonanos, U.R. Christensen, D.H. Mullaney
Plasma Physics Laboratory
Princeton University
Princeton, New Jersey

ABSTRACT

The engineering aspects of the Princeton spherator are presented. The magnetic and mechanical design of the coils, structure, and vacuum system are described. Recent modifications including the installation of a superconducting poloidal field coil suspended within the vacuum tank are also related.

A cross section of the spherator assembly is shown in Fig. 1. The main elements of the machine are:

a. A 60-inch diameter, 40-inch high vacuum tank with an internal volume of 1900 liters.

b. A ring coil of circular cross section suspended within the vacuum tank, which produces a poloidal field. (PF coil)

c. A system of four coils external to the vacuum tank arranged in symmetric pairs and producing an axial field. (EF-1 and EF-2 coils)

d. A linear conductor centered about the vertical axis of the machine which produces a toroidal field. (TF coil)

The magnetic system of the spherator is a superposition of the three field configurations. The poloidal field opposes the axial field within the bore of the PF coil giving rise to two stagnation points. The addition of a toroidal field component generates a set of nested toroidal surfaces. The surface passing through the stagnation point is a separatrix within which the surfaces are closed. It is the visible plasma boundary. Figure 2 shows how the separatrix varies with the ratio of poloidal to an ideal homogeneous axial field. If the height and radius of the separatrix surface are equal, the plasma volume appears spherical, hence the name of the device.

The magnetic geometry is altered by selecting, in advance, the number of active turns in each of the four EF coils. Each EF coil contains 24 turns, 4 layers at 6 turns per layer. Each layer is provided with an electrical tap at the inner and outer turns and one layer has a tap per turn. With suitable external jumpers, therefore, from 1 to 24 turns from each coil may be energized. The polarity of each coil is reversible. The cross section and tap arrangement of EF-1 and EF-2 coils are identical; the only difference is their diameter.

The center conductor of the toroidal field coil has a cross section as shown in Detail "A" of Fig. 1. Eighteen hollow trapezoidal copper conductors are arranged in a circle around a phenolic core. Each conductor is taped with Dupont "H" film, and the assembly is overwrapped. Around the conductor bundle are the OH coil segments - three copper sheets running the length

*Work performed under the auspices of the U.S. Atomic Energy Commission.

of the conductor. The composite is again overwrapped and enclosed by a stainless steel pipe that is also the central wall of the vacuum vessel. The return bus, also of hollow copper construction, completes the series connection of the TF coil and is visually the dominant feature of the machine. The coil is rated at 520,000 ampere-turns when pulsed.

The major engineering effort on the spherator since the original assembly has been in modifications to the poloidal field coil.

The first coil was of hollow copper construction, water cooled and with a substantial lead passing through the plasma volume to feed current and coolant to the coil. It was supported and guyed by six 1/8-inch diameter Inconel 718 rods. The coil was rated at 130,000 ampere-turns. Early experiments with the machine indicated a high plasma loss to the supports and current lead. A second coil wound with solid No. 15 AWG enameled wire with a 0.148 inch O.D. coaxial lead was installed. The coil, weighing 200 pounds, is hung on three wires, each with a diameter of 0.035 inch. The coil was rated at 34,000 ampere-turns, could be pulsed 200 times a day, and then had to cool down overnight. The third coil is a superconductor suspended from three 5/32-inch O.D. tubes, which are also used to fill the coil Dewar with liquid helium and allow the vent gas to be recovered and liquified. The coil is rated at 130,000 ampere-turns.

The spherator structure consists of two main elements, the EF support rings and ribs and the TF support cage. The major load on the EF-1 coils is mutual attraction, while the EF-2 coils experience vertical loading in either direction depending on the poloidal field geometry. The self load on the TF return bus tends to open the rectangular loops. Interaction with the axial field produces a torque on the horizontal rays. The torque is in one direction on the upper rays and in the reverse direction on the lower rays. Figure 3 is a photograph of the assembled machine. The top structural spider, vertical TF bus support columns, cross bracing to restrain the applied torque, and vacuum tank are clearly visible.

A general specification is shown in Table 1.

Table I

Spherator Characteristics

Toroidal Field Coil	
No. of turns	18
Ampere-turns	520,000
Maximum current (amperes)	28,900
Pulse duration (eq. sq. wave sec.)	0.6
Maximum current density (amps/in.^{2})	145,000
Material	Hollow OFHC Copper
Resistance cold/hot (milliohms)	11.2/15.4
Peak power (megawatts)	12.7

Axial Field Coils (EF Coils)	
No. of turns (max)	24
Ampere-turns	260,000
Maximum current (amperes)	10,830
Pulse duration (eq. sq. wave sec.)	1.5
Maximum current density (amps/in.^{2})	13,500
Material	Hollow EC Aluminum
Resistance cold/hot (milliohms)	
EF-1 coils	15.4/16.0
EF-2 coils	9.4/9.8
Peak power (megawatts)	
EF-1 coils	1.88
EF-2 coils	1.15
Poloidal Field Coils	
First Coil	
No. of turns	12
Ampere-turns	130,000
Maximum current (amperes)	10,830
Pulse duration (eq. sq. wave sec.)	1.5
Maximum current density (amp/in.^{2})	94,000
Second Coil (Installed June 1968)	
No. of turns	1,620
Ampere-turns	48,600
Maximum current (amperes)	30
Material	No. 15 AWG ETP Copper Wire
Third Coil (Installed March 1969)	
No. of turns	2,275
Ampere-turns	130,000
Material	Nb_3Sn
Maximum current (amperes)	57.1
Dewar capacity (liters)	12
Liquid helium consumption (ℓ/hr)	20-32
Superconducting life with 200 liter supply Dewar (hrs)	6
Vacuum System	
Volume (liters)	1,900
Internal Surface (sq. cm.)	10^5
Base Pressure (torr)	4×10^{-8}
Pumping Speed (ℓ/sec.)	2680

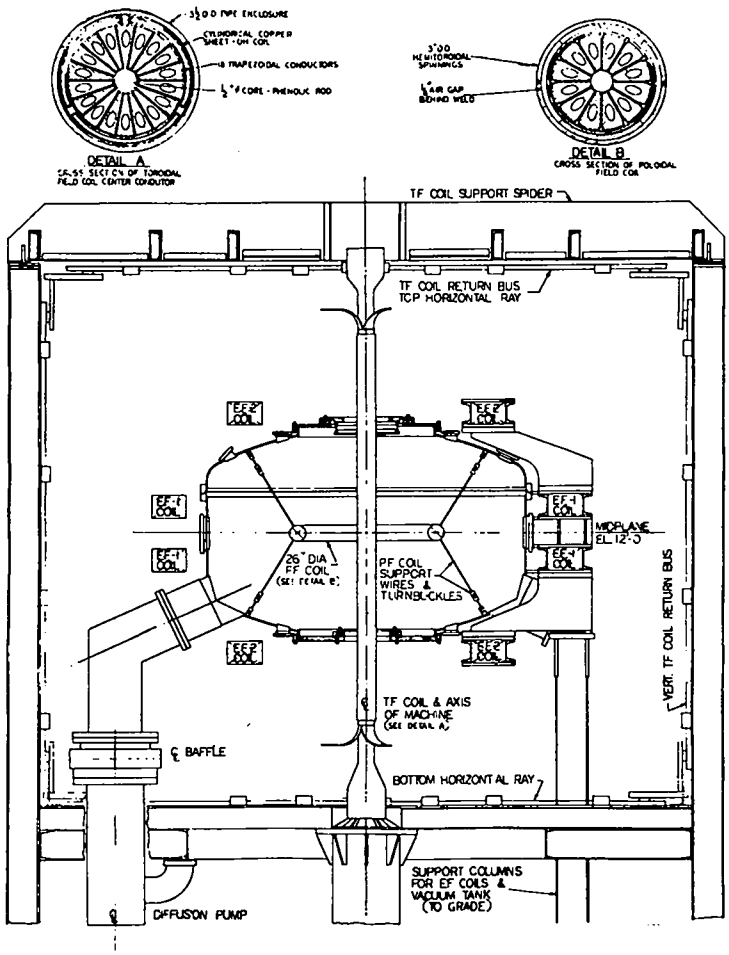

Fig. 1. Spherator cross section.

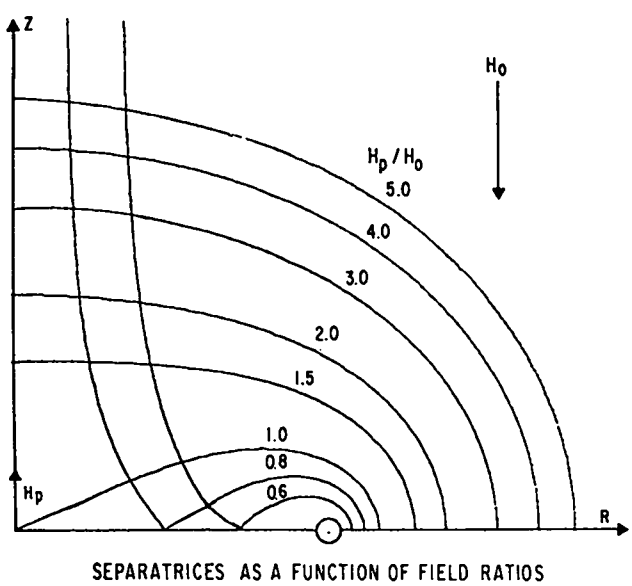

SEPARATRICES AS A FUNCTION OF FIELD RATIOS

Fig. 2. Separatrix as a function of poloidal to axial field.

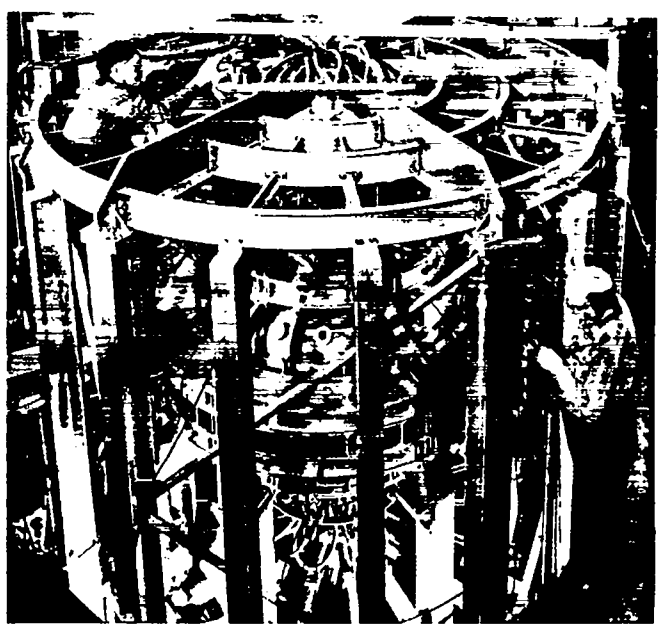

Fig. 3. View of assembled spherator.

COILS FOR THE SUPERCONDUCTING LEVITRON*

Clyde E. Taylor and Thomas J. Duffy
Lawrence Radiation Laboratory
University of California
Livermore, California 94550

ABSTRACT

The Superconducting Levitron system now under construction consists of an 80 cm diam, 600 kA, superconducting levitated ring wound with Nb_3Sn tape conductor; six stationary superconducting coils wound with Nb-Ti wire; and an array of stabilizing control coils, also superconducting, wound with multi-core Nb-Ti material designed for low ac loss. The coil system is described in detail. Tests were made on several inductively energized Nb_3Sn coils to determine critical temperatures. These tests are described.

INTRODUCTION

The Superconducting Levitron is a dc single floating-ring apparatus which represents about the minimum advance over the present Levitron in size and complexity which will achieve significant plasma parameters. It is designed to produce a variety of field configurations including a minimum $\langle B^2 \rangle$ well, and the quasi-linear field.** Although initial plasma will be produced by gun-injection, the machine is designed to accommodate neutral beam injection at a later date.

Figures 1 and 2 show a cross section of the machine. The main features of the magnet system are:

a) The floating ring.
b) Six non-floating coils which provide a variety of field shapes.
c) Twelve superconducting stabilizing coils which are elements of the servomechanism which maintains the ring in the desired position.
d) The toroidal coil which is water-cooled Al and Cu.
e) The large magnetic damping plates located on either side of the ring.

The main purpose of this paper is to describe the main parameters and design considerations involved in each of the above mentioned magnet systems. The vacuum chamber is a rather conventional, all-metal, stainless steel tank with 77 flanged aluminum foil gasketed joints. The large cover flange is 82 in. in diameter.

FLOATING RING

This coil must be superconducting because any support member or electrical lead would penetrate the plasma which completely surrounds the ring and would therefore seriously limit plasma lifetime because of collisions with the solid material.

The ring parameters are listed as follows:

a) Major diam — 80 cm.
b) Minor diam (overall) — 9 cm.
c) Design current — 160 A/turn at 12° K.
d) Maximum field at conductor — 34 kOe.
e) Heat capacity between 5° and 12° K — 500 J.
f) Number of turns — 3750.
g) Stored energy — 250 kJ (self-ind. only).
h) Inductance — 19.5 H.
i) Conductor — Nb_3Sn tape, 0.5 cm wide × 0.0065 in. total thickness, varnish insulated. Thickness includes 0.002 in. copper on each side.
j) Conductor length — 32,400 ft.
k) Mass of ring (incl. steel container) — 109 kG.

The minor diameter of the ring must be as small as possible to allow maximum plasma volume; therefore, high current density is a require-

*Work performed under the auspices of the U. S. Atomic Energy Commission.

**$|B| \approx$ constant on flux surfaces.

ment. The operating time available between ring re-cooling cycles depends on having minimum heat input and maximum heat capacity. The latter requirement favors Nb_3Sn as the superconducting material because its high critical temperature of 18° K allows a much higher operating temperature compared to Nb-Ti, and therefore a much greater heat capacity. Figure 3 shows the internal energy per unit volume vs. temperature for a number of materials. It is apparent that helium gas at a density corresponding to 100-atm pressure at 300° K has a much higher heat capacity than nearly all metals, with the notable exception of Hg. The superconducting levitron ring will be pressurized with helium gas to about 100 atm at room temperature and permanently sealed. Thus, all available void volume around the conductor will be filled with helium. At 4.2° K, the pressure will be about 1 atm, and the ring will contain very little liquid. The coil operating environment will therefore be gaseous helium rather than liquid.

The limited space available in this small ring makes it difficult to design electrical leads which pass through a highly stressed, internally pressured shell, and which are reliable for ultra-high vacuum service. Therefore, the ring will be inductively energized, thus eliminating the need for external electrical connections. The coil turn-on procedure is to energize the external coils while the ring is in the normal state; this generates a pre-determined magnetic flux linking the ring. The ring is then cooled to the superconducting state. The currents in the external coils are then set to the desired levels (in general, with opposite direction from that used to generate the ring flux) and the ring current will automatically adjust to maintain the initial flux linkage constant.

After much testing, the material selected for the ring conductor is 0.5-cm-wide by 0.0065-in.-thick tape made by General Electric Company. This tape has 0.002 in. of copper soldered to each side of the core, which is a 0.001-in.-thick Nb alloy strip with Nb_3Sn in a thin layer on both sides. The tests that were necessary to evaluate this material required operation at temperatures well above 4.2° K in order to duplicate the actual ring operating conditions. Several small coils were made using 0.5-in.-wide material of various designs. These coils were energized inductively in a gaseous helium environment and, while persistent, were allowed to slowly warm up to the temperature where resistive heating begins. It was discovered that under certain conditions a maximum temperature is often reached which is well below that temperature which might be expected from "short-sample" performance.[1] This appears to be a type of "stability" limit imposed by the existence of local diamagnetic currents which cause critical conditions to be reached locally somewhere in the conductor while the overall transport current in the conductor is well below critical. This general type of "stability" problem has been analyzed by Hart.[2] Figure 4 shows some preliminary results using several types of tapes. The main problem is that the critical temperature of high current-density coils which are "stability limited" is apparently decreased when the thickness of the Nb_3Sn supperconducting layer is increased. Therefore, there is an optimum conductor design which will allow maximum current density under any given operating conditions. Our small coil tests are continuing using an improved calorimeter and 0.5-cm-wide tape.[3] Our condition of 160 A at 34 kOe and 12°K requires enough superconductor to carry 656 A at 34 kOe and 4.2°K,[4] or 152 A at 100 kOe and 4.2°K.

The ring consists of six double "pancake" modules. Each module has one "spiral-in" and one "spiral-out" coil connected in series at the inside radius. The entire coil is connected in series. Three different grades of tape are used, depending upon the maximum field expected at various locations within the winding. There will be about 30 internal series connections in the tape. Figure 5 shows a cross section of the ring.

RING RE-COOLING

Many re-cooling methods were considered, but the simplest appears to be heat conduction to helium-cooled blocks which are mechanically pressed against the ring. Since heat conduction across mechanical contacts in high vacuum is poor, especially at low temperatures, an experiment was conducted to obtain design data.[5] Figure 6 shows typical heat flux vs. temperature of the warmer

contact surface for a particular contact pressure, using one indium-coated surface and one plain copper surface. These data agree closely with some earlier preliminary measurements made by Bradford at Culham.[6] An approximate analytical model of ring cool-down time can be easily calculated by approximating the data of Fig. 6 by the straight-line relation:

$$q/A\ (W/cm^2) = 0.03\ (T - 4.2°K).$$

Since the ring heat capacity is mainly due to the helium gas, the change in internal energy of the ring is approximately $C_v \Delta T$ where the average C_v between 6°K and 12°K is, from Fig. 3, 2.8 J/g - °K for v = 65.2 cc/g.

The cooling rate is given by

$$q = -m \frac{du}{dt}$$

where

m = mass of helium gas, g
t = time, sec
q = watts
u = internal energy, J/g.

Separating variables and integrating, we get the time τ for cooling from temperature T, to temperature T:

$$\tau = \int_0^T dt = -m \int_{Ti}^T \frac{du}{q/A \cdot A}.$$

From above, $du = C_v\, dT$ where C_v = 2.8 J/g - °K and

$$q/A = B\ (T - T_0)$$

where B = 0.03 W/cm^2 - °K. We have

$$\tau = -m \int_{Ti}^T C_v\, dT/A\ B\ (T-T_0) = \frac{m\, C_v}{A\ B} \log \frac{T_1 - T_0}{T - T_0}.$$

In this case, m = 25 g of helium, A = 10 cm^2, T_1 = 12° K, T = 6° K, T_0 = 4.2° K, τ = 5.5 minutes. Actually, we expect about 15% greater heat capacity due to the internal energy of the metal, but a more refined calculation allowing for this additional effect (i.e. $C_{v\ metal} \approx C \cdot T^3$) does not change the time very much. We will use a higher contact pressure than the data of Fig. 6, which will increase heat transfer. Therefore, recooling is expected to require less than 10 minutes.

Data on a copper-mercury contact using a copper cone in a socket was reported by a group at Garching,[7] who found a higher heat transfer coefficient than we find for flat copper-indium contacts. However, the later contact system was chosen because it is simpler for our configuration and seems to result in a reasonably short re-cooling time.

The ring coil form is also the inner half of the pressurized toroidal shell. The remainder of the shell is formed by welding two additional segments in place after the coil is wound. This shell must withstand not only the 100 atm internal helium pressure but must also withstand the bending forces that occur if the ring drifts laterally out of its magnetic equilibrium position, which can happen if the servo-system fails. High local stress can occur if the ring goes out of control at maximum current and comes to rest against the surrounding stops. For this reason, the shell material is forged ARMCO 21-6-9 steel which has high strength and toughness at cryogenic temperatures.

To keep ring heating minimum, a single reflective heat shield is placed outside the shell.

MAIN FIELD COILS

Table I gives the dimensions and maximum performance required of the non-floating coils. Dimensions are for the winding, and not the coil form.

These coils will be layer-wound, using a single-core Nb-Ti composite conductor with oxide "insulation" and with fiberglass cloth between layers. The smaller coil uses 0.015-in. core, 0.030-in. o.d. wire, and the two larger coils use 0.014-in. core, 0.032-in. o.d. wire. Total wire required is 50,000 ft of 0.015-0.030 and 133,000 ft of 0.014-0.032. The coils are now being wound using Supercon wire. Each coil is wound in a single-piece stainless steel form with 0.25-in. inner wall thickness and 0.5-in. wide flanges; the thick sections are required for stiffness. A 0.060-in. cover is welded over the coil after winding. Liquid helium is supplied to the enclosed coils by a gravity circulation system. The coil leads pass through the helium piping to the external supply dewar

where a terminal connection is made between the superconducting leads, the normal leads, and a persistent switch.

STABILIZING COILS

The ring de-stabilizing forces, which can occur at maximum current levels, are expressed as "spring constants" for small displacements from the central position. Referring to Fig. 7, the major "spring constants" are identified as

$$\frac{\Delta Fy}{\Delta y}, \frac{\Delta Fz}{\Delta z}, \frac{\Delta Mx}{\Delta \theta_x}.$$

In the presence of a toroidal field, there are, in addition to the above,

$$\frac{\Delta Fy}{\Delta \theta_x}, \frac{\Delta Mx}{\Delta y}.$$

The above forces are given for two field configurations produced by the currents given in Table II.

The ring current is -600 kA and the toroidal current is 1200 kA. Table III gives the forces on the ring. These forces are very large; for example, in Case 1:

$$\frac{\Delta Fy}{\Delta y} = 2{,}220 \text{ lb/cm} \quad \text{and} \quad \frac{\Delta Mx}{\Delta x} = 3{,}330 \text{ ft-lb/cm}.$$

Note that the axial force $\Delta Fz/\Delta z$ is negative, indicating that the ring is highly stable for axial motion. It is obvious that very high velocities can be acquired by a ring which is out of control. Therefore, two large plates are located parallel to the plane of the ring, above and below the ring outside the plasma region. The plates provide eddy current damping which will limit the velocity of the ring to safe values in case of loss of control.

The control coils are superconducting. The choice of superconductor rather than conventional copper coils is based on several factors:

a) Lower cost.
b) High current density, therefore smaller coils.
c) It is easier to cool the coils with liquid helium in our case, than to shield the low temperature environment against thermal radiation from warm coils.
d) Mechanical support is simpler if the coils can be attached directly to the eddy-current plates.

Much recent progress has been made in the development of low-loss conductors for pulsed applications. One of the control coils is now being wound with a twisted multicore material for testing. The four pairs of x-y control coils are located at $z = \pm 17$ cm, parallel to the plane of the ring (see coordinate system of Fig. 7), with the centers at x, y = 48 cm, coil diam = 56 cm. The coil cross section is shown in Fig. 8.

To balance the maximum $\Delta Fy/\Delta y$ destabilizing force for 1-cm displacement, given in Table III, these coils must carry 7342 A-turns each or 14,684 A-turns for a "gain" of two.

The two pairs of tilt-stabilizing coils are located with their centers at x, y = 60 cm, normal to the plane of the ring, with coil diam = 50 cm. The coil cross section is identical to that of the x-y coils. 9790 A-turns are required for a "gain" of two.

TOROIDAL WINDING

This coil is water-cooled and located outside the vacuum tank. It must be easily demountable to gain access to the vacuum tank for removal of the cover, etc. The return conductors are located at a radius of 200 cm to permit a man to have access to flange covers on the perimeter of the tank.

The coil must be matched to four existing 300-kW Temescal power supplies. This requires 90 turns. Direct current operation allows 600 kiloampere-turns using the four power supplies in parallel and 1200 kA-turns at four times overload for 45-sec pulses using the supplies in series-parallel. At 1200 kA-turns, the current is 13,333 A, V = 250 volts, and the overall current density in the 6.5-in.-diam core is 5600 A/cm^2. The core is subjected to very large twisting forces and the conductors must, therefore, be integrally bonded together to have enough strength.

The core will be copper, using wedge-shaped hollow conductors to fit together efficiently, and the remaining conductor will be aluminum, water-cooled. About 0.8 of the total power is dissipated in the core.

Azimuthal uniformity requirements on the toroidal field will allow grouping the 90 return conductors into 30 equal groups of 3.

It is interesting that this single piece of apparatus includes four quite unique types of coils.

REFERENCES

1. Reported at the 1968 Applied Superconductivity Conference, "The Critical Temperature of Some Persistent Nb_3Sn Coils," Thomas J. Duffy and Clyde E. Taylor.
2. H. R. Hart, Jr., "Magnetic Instabilities and Solenoid Performance: Applications of the Critical State Model," General Electric Co. Rept. 68-C-297, Sept. 1968.
3. To be published at a later date.
4. Paul R. Aron and Gary W. Ahlgren, "Critical Surfaces for Commercial Nb_3Sn Ribbon and Nb 25% Zr Wire," Advances in Cryogenic Engineering, Vol. 13, 1968.
5. Results to be published.
6. R. Bradford, personal communication.
7. L. Donati, H. Haeglsperger, R. Scherzer and K. H. Schmitter, "A New Thermal Contact for Cryogenic Applications," Fifth Symposium on Fusion Technology, Oxford, July 2-5, 1968.

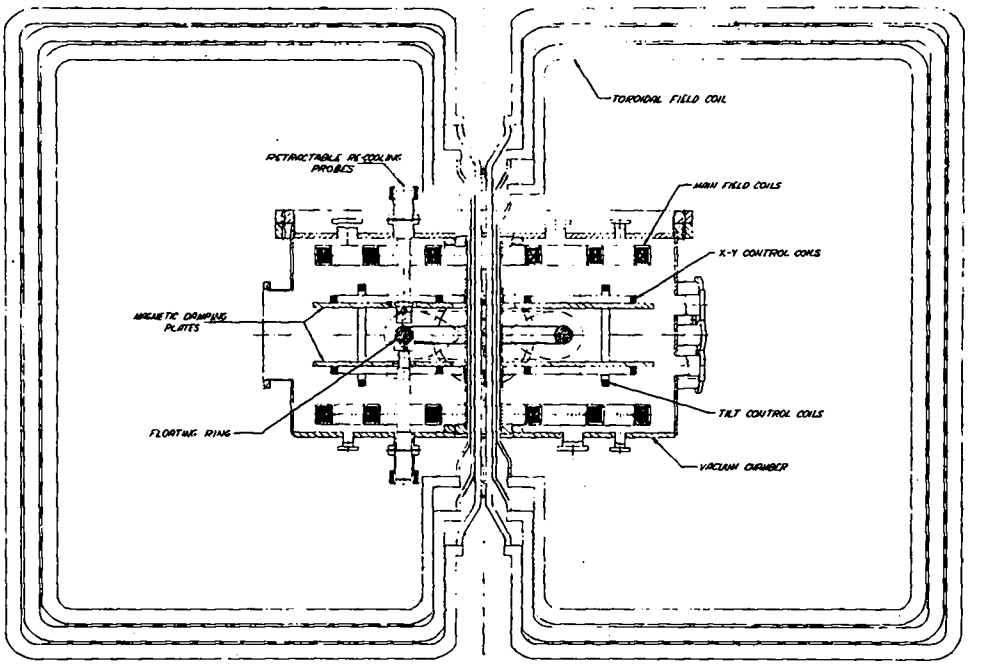

Fig. 1. Cross section of superconducting levitron, showing the coils.

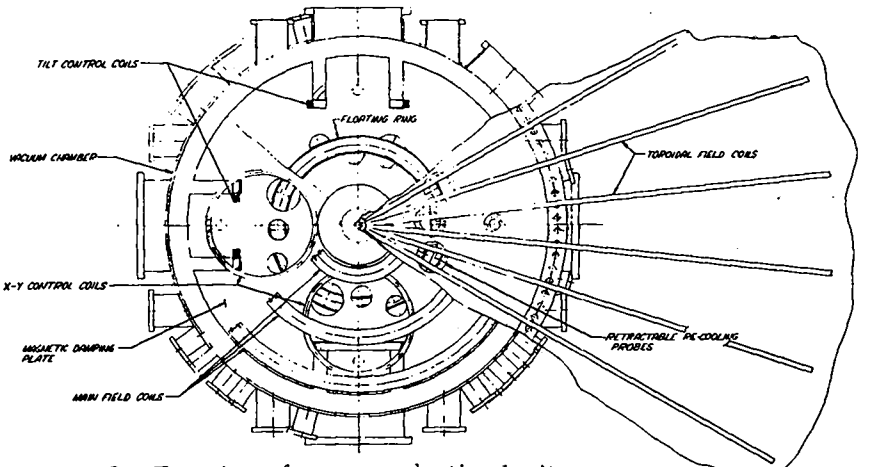

Fig. 2. Top view of superconducting levitron, showing the coils.

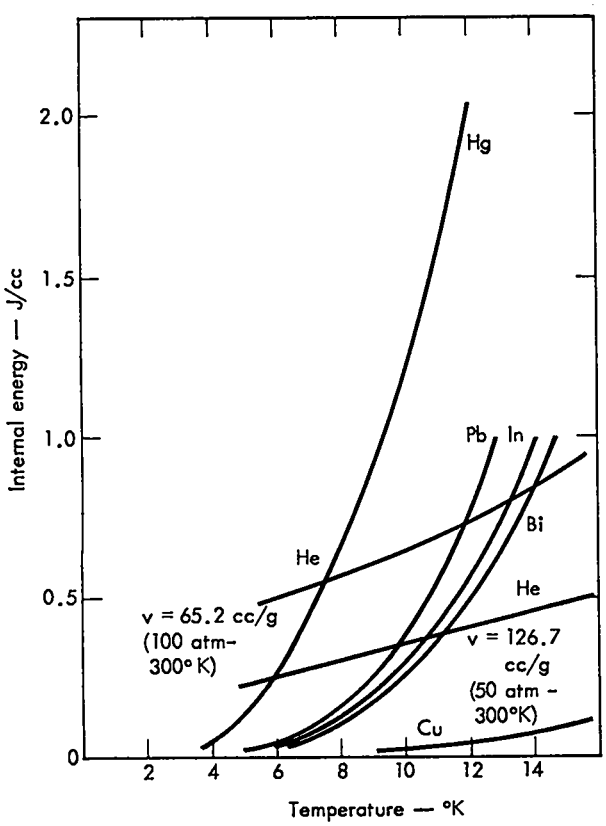

Fig. 3. Internal energy vs. temperature for several metals compared to helium gas.

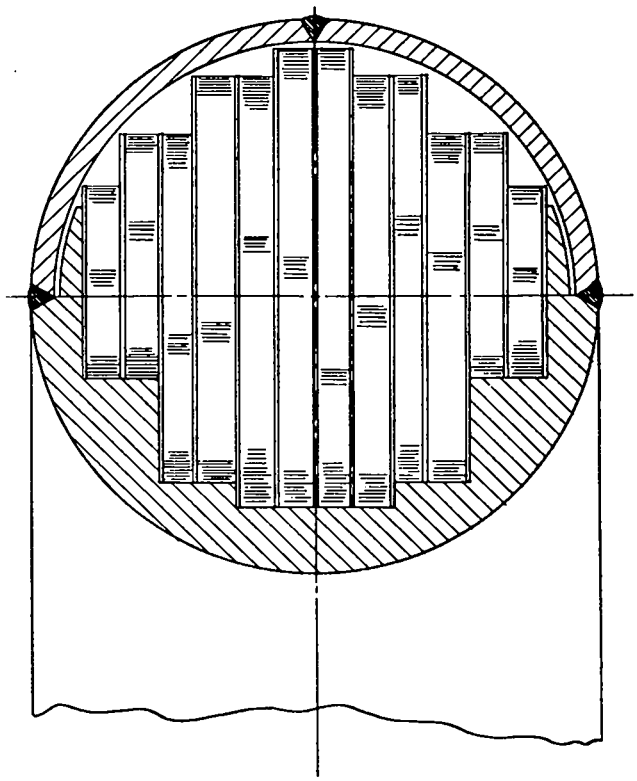

Fig. 5. Cross section, superconducting levitron floating ring.

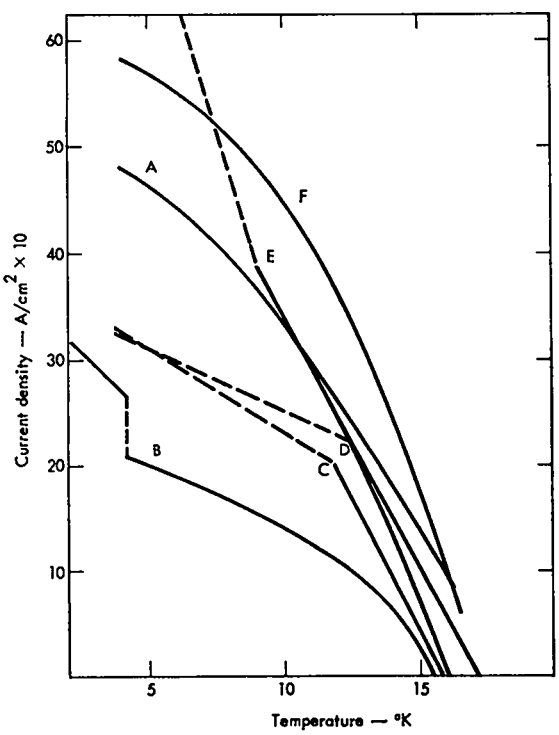

Fig. 4. Persistent coil current vs. "quench" temperature for several types of Nb_3Sn tape.

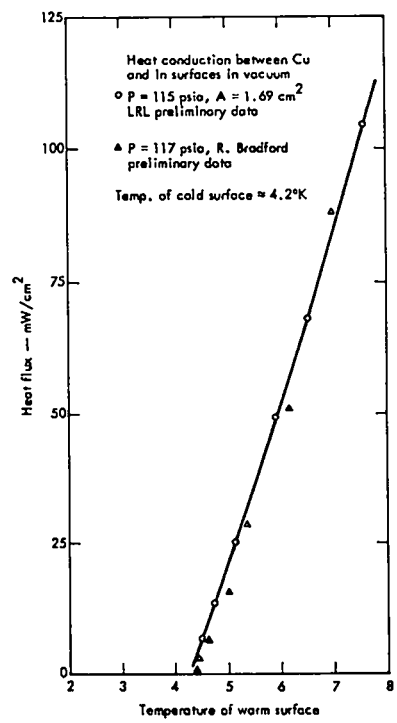

Fig. 6. Heat flux vs. temperature at warm surface for heat transfer across flat surfaces pressed together in a vacuum.

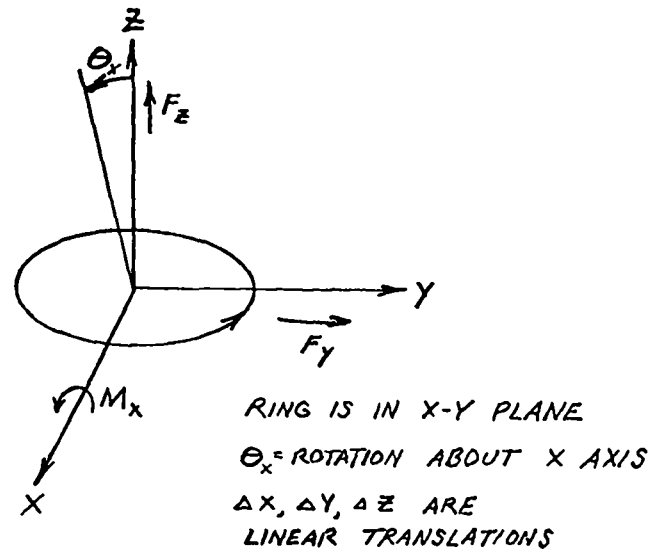

Fig. 7. Coordinates for identifying forces on the ring.

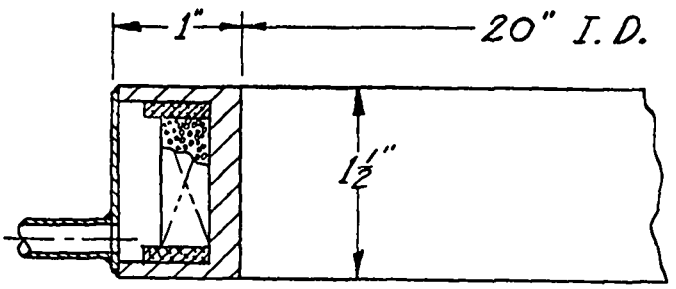

Fig. 8. Cross section of control coil.

Table I

i.d.	o.d.	Length	N turns	A turns	i	B_{max}
17.480"	21.500	2.5	4380	657,000	130a	
43.138"	44.898	2.5	1720	258,000	150a	
61.403	64.363	2.5	2827	424,000	150a	

Table II

Nominal coil diam	Case 1 B^2	Current	Case 2 "quasi-linear"
50 cm	540 kA		658 kA
112 cm	258 kA		-72 kA
160 cm	282 kA		424 kA

Table III

	$\frac{\Delta Fy}{\Delta y}\left(\frac{dyn}{cm}\right)$	$\frac{\Delta Fy}{\Delta \theta}\left(\frac{dyn}{deg}\right)$	$\frac{\Delta Fz}{\Delta z}\left(\frac{dyn}{cm}\right)$	$\frac{\Delta Mx}{\Delta \theta}\left(\frac{dyn\text{-}cm}{deg}\right)$	$\frac{\Delta Mx}{\Delta x}\left(\frac{dyn\text{-}cm}{cm}\right)$
Case 1	9.89×10^8	7.89×10^8	-1.98×10^9	4.42×10^9	4.52×10^{10}
Case 2	6.16×10^8	7.89×10^8	-1.23×10^9	8.54×10^9	4.52×10^{10}

10^5 dynes = 0.2248 lb

THE PRINCETON FLOATING MULTIPOLE MACHINE*

J. File

Plasma Physics Laboratory
Princeton University
Princeton, New Jersey

ABSTRACT

The Plasma Physics Laboratory has undertaken the fabrication of a major toroidal quadrupole machine (FM-1) that utilizes levitated superconducting rings. The device has the flexibility to be used as either a spherator or a quadrupole. The detailed design of the FM-1 represents the major effort of the Engineering and Development Division of the laboratory during the past year.

The vacuum vessel, external coils, superconducting rings, cryogenic equipment, stabilizing servo system, and associated equipment are described. The design of some of the major components is presented, and the progress to date of the effort is summarized.

INTRODUCTION

The Plasma Physics Laboratory has since December 1967 undertaken the design and fabrication of a major toroidal machine. It is designed to operate with stabilized, levitated superconducting rings of the type described by File et al.[1,2] The device is to be operated in two modes: with one sixty-inch diameter ring as a spherator, and with two rings, forty and eighty inches in diameter respectively, as a quadrupole. Figure 1 shows a partial full scale mock-up of the spherator mode. Figure 2 shows the major components of either mode and demonstrates the steps required to convert from one mode to the other. The spherator mode will be the first assembled and unless otherwise noted, all discussions pertain to this mode. Some major components of the FM-1 will be described.

DESCRIPTION

A. Vacuum Vessel

The vacuum vessel, shown in Fig. 3, is made of Type 305 stainless steel. The main tank is diffusion pumped while titanium sublimation is used in the divertor section.

B. Toroidal Field Coil

The toroidal field is generated by a linear conductor centered about the vertical axis of the machine. The current returns along rectangular loops which extend beyond the outside diameter of the vacuum vessel. The toroidal field coil is shown in Fig. 3.

The return loops are subjected to substantial magnetic forces that tend to open the rectangular loops. The coil was designed to be self-supporting, and therefore the loops are constructed of six-inch by one-inch hollow, water-cooled aluminum (Grade 6106) extruded conductor, which dually serve as beams and columns capable of carrying the loads.

C. The Ring Positioning and Emergency Ring Catching Systems

The ring positioners, shown in Fig. 3, are hydraulically operated cylinders that move into position in about two seconds. They are capable of the following:

*Work performed under the auspices of the U.S. Atomic Energy Commission.

1. Centering the ring with respect to the toroidal field column.

2. Adjusting the vertical height of the ring to a very close tolerance.

3. Rotating the ring to such a position that it can be filled and energized.

The emergency ring catchers, placed on the top and bottom of the vacuum vessel, are designed to move eight inches in 100 milliseconds. They are pneumatically operated cylinders preloaded in the catch position. The catchers are actuated by any one of several fault conditions when the stabilizing system ceases to hold the ring. A pneumatic solenoid valve opens that actuates a pneumatic cylinder, which in turn releases the piston.

D. The Support Structure

The gravitational and magnetic loads are generally moderate except for those on the toroidal cage. In the case of that cage, shown in Fig. 3, which experiences large forces tending to open the rectangular cage, and to twist the top and bottom of the cage, a unique method of support is used. The vertical members of the toroidal coil are self-supporting in compression and tension. They are kept from bowing out by glass epoxy structural channels placed flange to flange to form a box beam with the toroidal coil inside the box. These shapes have the dual role of supporting against the forces and acting as electrical insulators. Glass epoxy shapes have become commercially available in the past few years. The remainder of the structure is conventional and made of standard aluminum shapes.

E. Other External Coils

Other external coils for the spherator mode are shown in Fig. 4. They are conventional, glass epoxy insulated, and pancake-wound of water-cooled, hollow copper conductor. The pancakes are then vacuum impregnated.

F. The Superconducting Rings

The spherator mode has one ring 60 inches in major diameter and is shown in Fig. 5. Wound from RCA 90 mil Nb_3Sn ribbon, it will be capable of producing 375,000 ampere-turns. The coil form is constructed from Type 305 stainless steel drop ring forging.

The quadrupole mode will have two rings, 40 inches and 80 inches in major diameter respectively, with current ratings of 500,000 and 250,000 ampere-turns. They, too, will be wound of RCA ribbon.

In both modes the rings will be operated isochorically from 4.2 to 12°K. In conventional Dewars experimental time of two to three hours is expected.[2,3] Recently Martin[4] has described a new lead-shielded Dewar that will increase the experimental time by a factor of five or more. Figure 6 shows a cross section of such a Dewar. The lead shield is cooled to 5 - 10°K, and all heat leaks are dissipated in the lead shield. The very favorable properties of lead up to 30 - 40°K are then exploited. Figure 7 shows the expected life of a lead-shielded Dewar with varying shield thicknesses and stainless steel supports between the respective layers. Experimental results from this type of Dewar are expected shortly.

G. The Levitation and Stabilizing System

Levitation of the ring is accomplished by energizing a conventionally wound levitating coil, placed on the bottom plate of the vacuum vessel. The signal from the optical control system, shown in Fig. 8, is amplified and in turn energizes the proper stabilizing coils shown in Fig. 2, moving the ring opposite to the direction sensed.

H. Power and Controls

Steady state power for the conventionally powered coils will be provided by the existing motor-generator facility.

The FM-1 control system is unique in that it will use a stored program digital controller. This permits a much greater flexibility in the use of the controls as described during this conference in the paper by Simon et al.[5]

PROGRESS TO DATE AND SCHEDULE

The development and design of components are mostly completed. Purchasing of materials for all of the components is in an advanced stage. Manufacture of the structure, vacuum vessel, external coil, and superconducting ring has started and, in the case of the external coils, is almost completed. Initial stages of machine assembly should begin early in June 1969. The controller is on hand, and test programs are being debugged. The expected completion date is July 1970.

References

1. J. File, G. D. Martin, R. G. Mills, and J. L. Upham, J. Appl. Phys. 39, 2623 (1968).
2. J. File, G. D. Martin, R. G. Mills, and J. L. Upham, Princeton Plasma Physics MATT-657 (1968); to be published in J. Appl. Phys.
3. J. File, Princeton Plasma Physics MATT-Q-26 (1968) p. 249.
4. G. D. Martin, Princeton Plasma Physics MATT-Q-26 (1968) pp. 237-238.
5. E. D. Simon et al., Symposium on Engineering Problems of Fusion Research, Los Alamos Scientific Laboratory (April 1969); to be published.

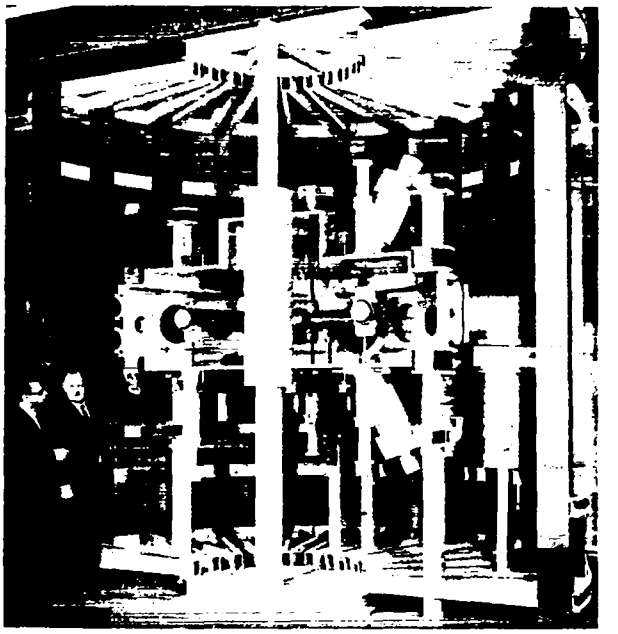

Fig. 1. Photograph of partially completed, full scale mock-up of the FM-1 spherator mode.

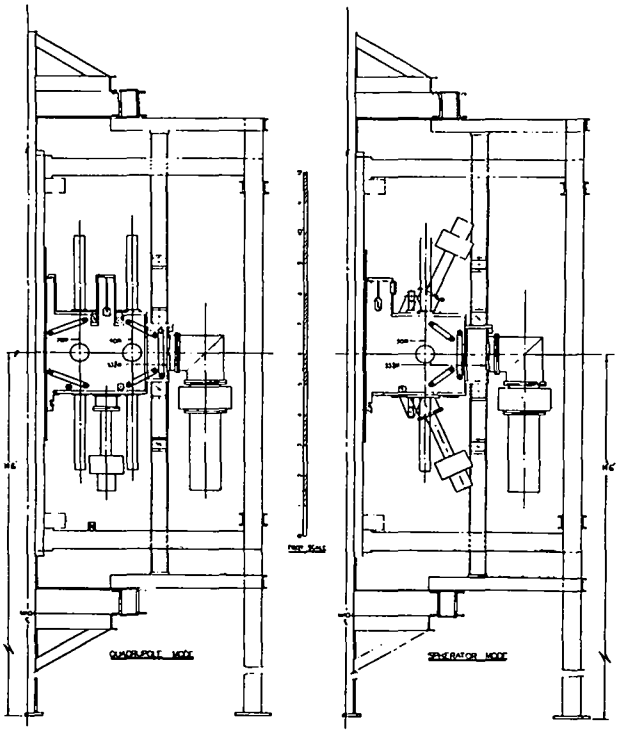

Fig. 2. Sketch of both quadrupole and spherator modes showing construction differences.

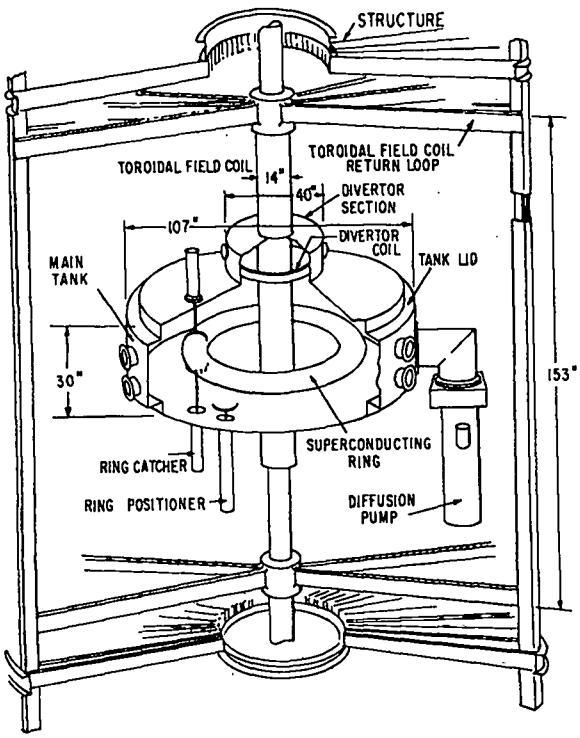

Fig. 3. Sketch of the vacuum tank and some attached components.

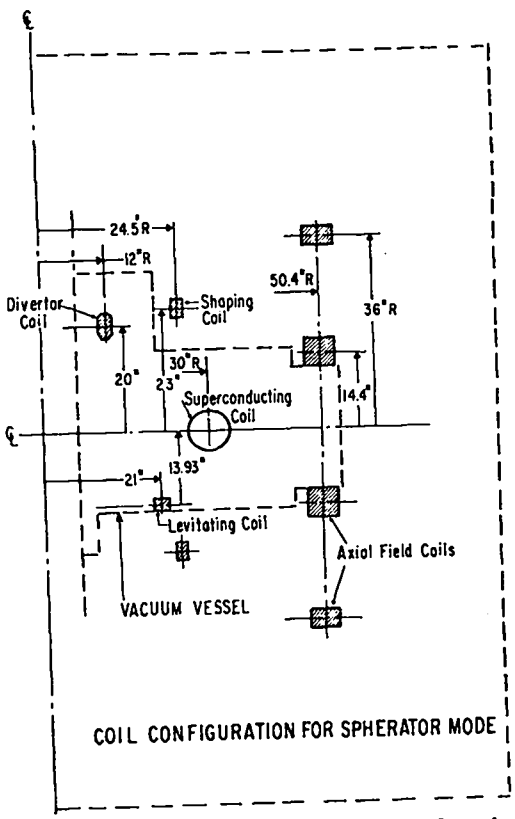

Fig. 4. External coil configuration for the spherator mode. The vacuum vessel is shown by dotted lines.

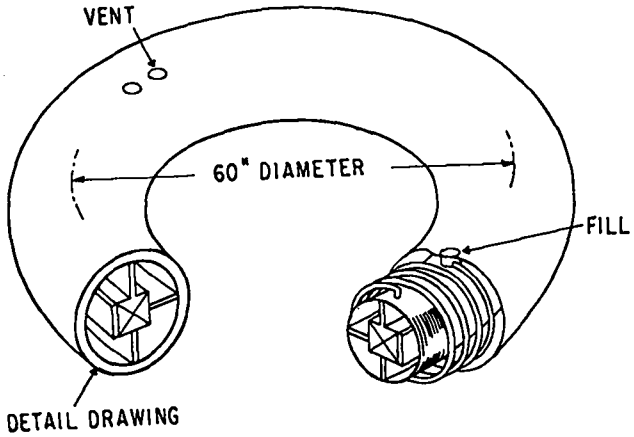

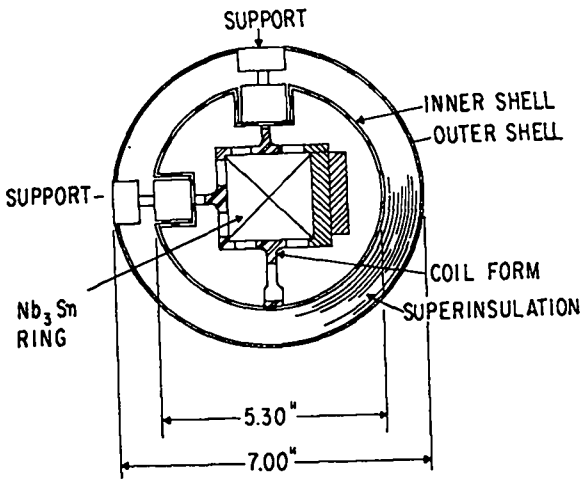

Fig. 5. Sixty-inch diameter Nb_3SN ring and Dewar showing construction details.

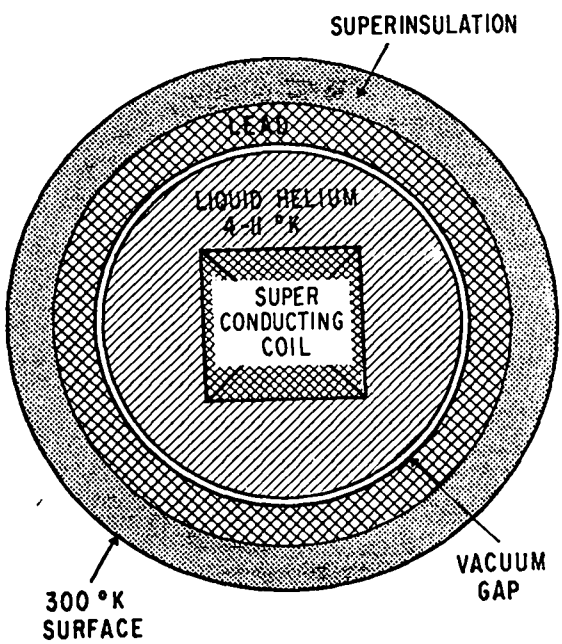

Fig. 6. Cross section of a lead-shielded superconducting ring and Dewar.

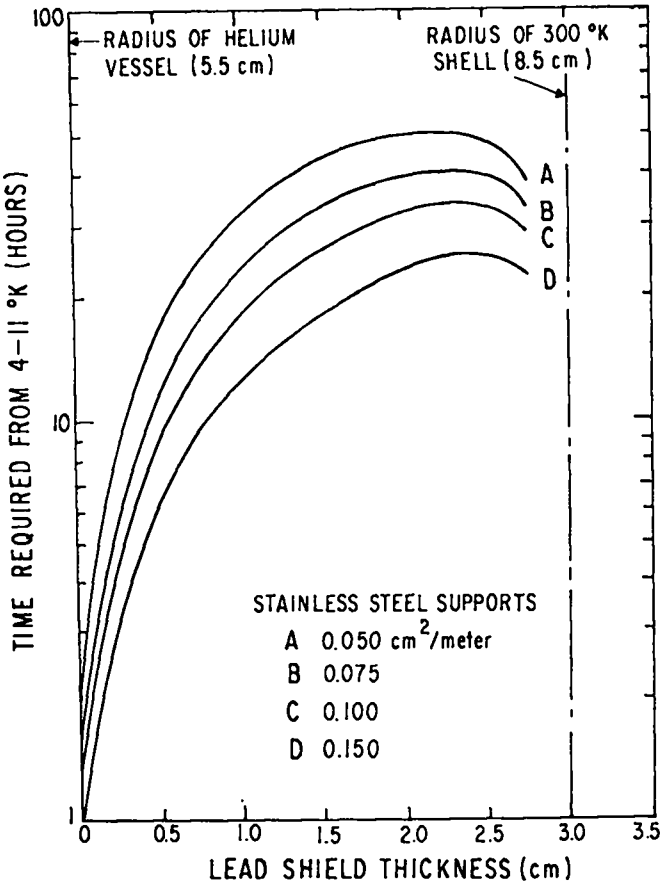

Fig. 7. Plot of lead shield thickness versus time required to raise the temperature of the lead shield from 4°K to 11°K.

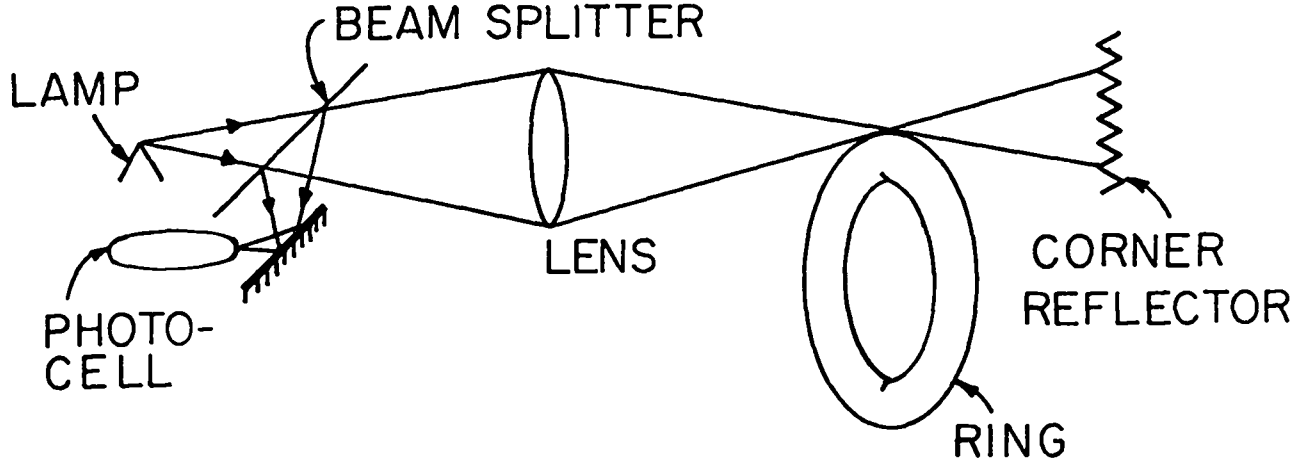

Fig. 8. Optical system arrangement.

THE PROBLEM OF CONTROL OF THERMONUCLEAR REACTORS*

R. G. Mills

Plasma Physics Laboratory
Princeton University
Princeton, New Jersey

ABSTRACT

Of the various types of hypothetical thermonuclear reactor that have been considered as candidates for the eventual generation of commercial electric power, none has yet been proven to be physically possible. If a number of them proves to be possible, the most economical type will be adopted for practical applications.

It appears at the present time that the least expensive would probably result if a machine could be fabricated in which a steady-state nuclear fire burns continuously with cold fuel injection. If such a machine is not possible, and the injection of energetic particles is necessary, the cost of such injection equipment would tend to raise the investment cost of a fusion power plant.

Assuming a cold fuel injection machine, one in which the fuel is heated to the operating temperature by the plasma itself, it can be stabilized by feedback control of the plasma confinement time as well as other operating parameters. It is interesting to note that Bohm-type diffusion (in the sense that the diffusion rate varies with the plasma temperature) results in stable operation.

It should also be noted that the operation of such a system requires a particular value of the product of the ion density and the plasma confinement time of the system. This $n_i\tau$ criterion also implies a certain fuel percentage burnup per pass through the machine.

I AN EQUILIBRIUM CONDITION OF A REACTOR

If sufficient plasma confinement time can be achieved, a steady-state reactor may be possible in which cold fuel, possibly in the form of small droplets of liquid DT, is continuously injected at a rate of m ions per cubic centimeter per second. This fuel would be heated to reactor temperature by the heat being released by fusion and retained in the plasma in the form of the 3.52 MeV alpha particles that result from D-T fusion.

In such a system the ion density, n_i, will change in time as given by

$$\frac{dn_i}{dt} = m - \frac{n_i}{\tau} \qquad (1)$$

where τ is the confinement time against all losses for the plasma ions. In a steady-state equilibrium

$$m = \frac{n_i}{\tau} \qquad (2)$$

represents particle conservation.

Energy conservation in the plasma requires that

$$n_i \frac{d}{dt}\left(\frac{3}{2}k(T_i+T_e)\right) = n_i^2 p(1-p)(\overline{\sigma v})cE^* - \frac{3}{2}mk(T_i+T_e) \qquad (3)$$

*Work performed under the auspices of the U.S. Atomic Energy Commission.

where p is the tritium fuel "richness", or n_T/n_i, $(\overline{\sigma v})$ is the reactivity of the plasma, E^* is the 3520 keV liberated to an alpha particle in a D-T fusion event, and c is the fraction retained in the plasma, the balance being radiated. T_i and T_e represent the ion and electron sea temperatures respectively.

For steady state we may replace m by (2) to give

$$n_i^2 p(1-p)(\overline{\sigma v}) c E^* = \frac{3}{2}\frac{n_i}{\tau} k(T_i + T_e) \quad ,$$

which leads to an $n_i\tau$ equilibrium condition:

$$n_i\tau = \frac{3k(T_i + T_e)}{2p(1-p)(\overline{\sigma v})cE^*} \quad . \quad (4)$$

This exact condition must be maintained, as can be seen from (3), if the plasma conditions are not to change.

Since the rate of reaction in the plasma is $n_D n_T (\overline{\sigma v})$ events per cm^3 - second, the probability per second of the loss by fusion of a triton is $n_D(\overline{\sigma v})$. The mean life for fusion loss of a triton, τ_F, is therefore given by

$$\tau_F = \frac{1}{n_D(\overline{\sigma v})} = \frac{1}{n_i(1-p)(\overline{\sigma v})}$$

and

$$n_i\tau_F = \frac{1}{(1-p)(\overline{\sigma v})} \quad . \quad (5)$$

Thus the relative burnup, b, of tritium in a single pass through the reactor can be found from the ratio of (4) to (5) or

$$b = \frac{3k(T_i + T_e)}{2pcE^*} \quad (6)$$

which for practical cases is a few percent.

Figure one shows, on the left, the percentage burnup as a function of the ion temperature. On the right is shown the $n_i\tau$ criterion vs ion temperature. Below the equilibrium condition is shown the Lawson criterion,[1] frequently referred to in the literature. The Lawson criterion represents the minimum $n_i\tau$ at which a fusion reactor is physically possible. Neglecting bremsstrahlung, which is small except near the ignition point, one can derive it by equating the energy needed to heat the fuel to the reacting temperature, T, to the entire energy content of the reacting gas multiplied by a recovery efficiency, η, or:

$$\left(3n_i k T + n_i^2 p(1-p)(\overline{\sigma v}) U \tau\right)\eta = 3n_i k T \quad (7)$$

where U is the total energy released per fusion, about 23.3 MeV. This yields an $n_i\tau$ criterion shown in Fig. 1 for efficiencies between 35% and 45%.

It is remarkable that these two criteria differ by a factor of only six, especially when one finds that an $n_i\tau$ representing classical confinement lies five orders of magnitude above the top of Fig. 1, while Bohm confinement lies below the bottom.

It is not known yet what $n_i\tau$'s will be achievable in plasma confinement apparatus. A device producing an $n_i\tau$ greater than (4) could be applied only to transient or pulsed reactors. One providing a value below the Lawson region cannot be a reactor, and one falling between the two criteria requires energetic injection of fuel, possibly an expensive proposition. One would prefer to control his reactor to keep it exactly at the equilibrium condition.

II THE TEMPERATURE DIFFERENCE BETWEEN THE ELECTRON AND ION SEAS

In order to compute $n_i\tau$, percent burnup, and other related quantities, it is necessary to find the electron temperature as a function of the

ion temperature. At temperatures of principal interest the alphas deliver most of their energy to the electrons. The electrons radiate some of this energy. The ions receive some energy directly from the ions but must receive most of it from the electrons. This requires the electron sea to have a higher temperature than the ions to permit this heat flow. An earlier misconception that the necessary heat flow was so great that electron temperature runaway could result under some conditions has been corrected by R. Carruthers.[2] Consideration of the amount of heat directly passed from the alphas to the ions[3] results in the electron sea temperature elevation shown on the upper left of Fig. 2. At higher ion temperatures a greater spread is needed for heating the incoming fuel unless the electron temperature is high enough that a significant amount of heat passes directly from the alphas to the ions. The necessary temperature difference then declines.

After T_e has been found, a number of interesting characteristics can be computed. For example, in order to find the optimum operating temperature of the reactor, the quantity $\overline{\sigma v}/T^2$ is relevant.[4] D.J. Rose has pointed out[5] that the quantity $\overline{\sigma v}/(T_i + T_e)^2$ is more precise, and this function is shown on the upper right in Fig. 2. The optimum temperature is about 12 keV. The quantity $\overline{\sigma v}/(T_i + T_e)$ is significant for stability and is also shown in Fig. 2.

III STABILITY CONSIDERATIONS

Let us examine the stability of this equilibrium. From (4) we find a quantity that must be constant

$$n_i \tau\, p(1-p)c(\overline{\sigma v})/(T_i + T_e) \quad .$$

The quantity, c, could be written in the form $(1 - \delta)$ where δ is relatively small at temperatures of principal interest and which varies with the square root of the temperature when bremsstrahlung dominates the radiation loss. The effects of synchrotron radiation have not been included in this paper. Known to be small in the neighborhood of 10 keV, it is expected to be relatively unimportant even at the higher ranges considered in this paper, but this point remains for further study. At any rate c will be treated as a constant in the current work.

The quantity $\overline{\sigma v}/(T_i + T_e)$ is a function of the ion temperature. For convenience we shall represent it as being proportional to T_i^n as illustrated in the lower half of Fig. 2. Finally by inserting $n_i = m\tau$, we derive a function, ψ, which must be constant for equilibrium.

$$\psi = m\tau^2 p(1-p)T_i^n \quad .$$

For stability of the equilibrium, the variation must vanish. Taking the logarithmic variation, we shall have stability when

$$\frac{\delta\psi}{\psi} \equiv \frac{\delta m}{m} + 2\frac{\delta\tau}{\tau} + \left(\frac{1-2p}{1-p}\right)\frac{\delta p}{p} + n\frac{\delta T_i}{T_i} = 0 \quad . \tag{8}$$

Thus the equilibrium is unstable against fluctuations in the fuel feed rate, the confinement time, the fuel mixture (unless $p = 1/2$), and the ion temperature, except when n falls to zero. From the graphs of $\overline{\sigma v}/(T_i + T_e)$ (Fig. 2), it is seen that this occurs at about 28 keV. Since c will not be strictly constant as assumed here, further study is required to find the exact location of the maximum as the inclusion of synchrotron radiation (which tends to depress T_e) will extend this point to higher temperature. Certainly one would prefer to operate at a lower temperature, near the

12 keV optimum. It is clear that at low temperatures control of the reactor will be necessary to avoid departure from the equilibrium condition. This control might be exercised through the feed rate, the mixture, or even the radiation losses (by injection of impurities), but probably the best method will be to control the confinement time, τ.

The variables in (8) may not be independent, and it is interesting to note that Bohm-type confinement, in the sense that $\tau \sim T_e^{-1}$ is a strongly stabilizing influence. Let m and p be held fixed, then (8) becomes

$$2\frac{\delta\tau}{\tau} + n\frac{\delta T_i}{T_i} = 0 \quad .$$

We may replace a variation with a differential if the physical system admits a continuum of equilibrium states reversibly accessible to one another. If the confinement time is a direct function of the temperature, a state of neutral equilibrium will result if

$$2\frac{d\tau}{\tau} + n\frac{d T_i}{T_i} = 0 \quad . \qquad (9)$$

Stable equilibrium will result if a differential temperature increase results in greater reduction in confinement time than given by this condition.

The solution of (9) is

$$\tau \sim T_i^{-n/2} \quad .$$

Therefore Bohm-type diffusion will stabilize for $n < 2$ or for all temperatures between about 7 and 28 keV.

Figure 3 shows the development in time of the density and temperatures of the ions and electrons as calculated by an approximate iterative procedure. Here it has been assumed that the confinement time is governed by Bohm-like diffusion of sufficiently reduced coefficient to allow equilibrium conditions. Future work is planned to improve the accuracy of this code.

References

1. J.D. Lawson, Proc. Phys. Soc. (London) B 70, 6 (1957).
2. R. Carruthers, private communication.
3. R.G. Mills, Princeton Plasma Physics Laboratory MATT-656 (1969).
4. L. Spitzer et al., Rep. No. NYO-6047, USAEC, Washington, D.C. (1954).
5. D.J. Rose, Oak Ridge National Laboratory Report, ORNL-TM-2204 (1968).

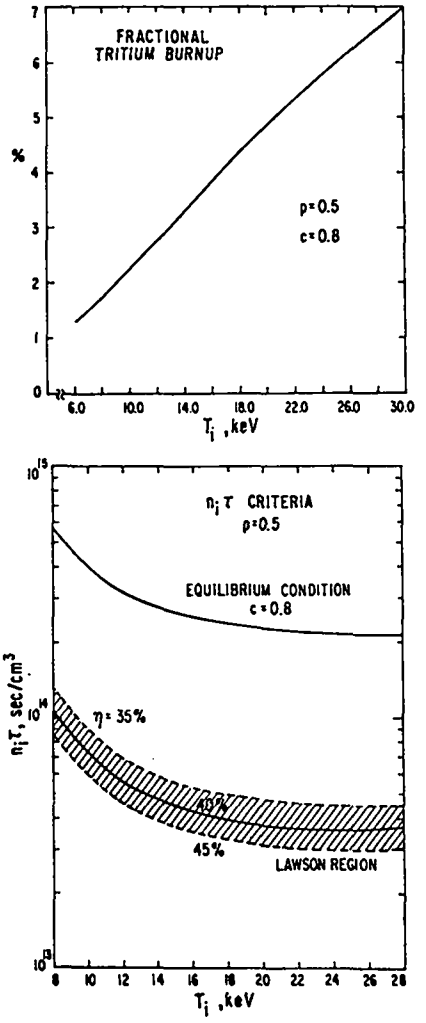

Fig. 1. Percentage burnup and $n_i\tau$ criteria.

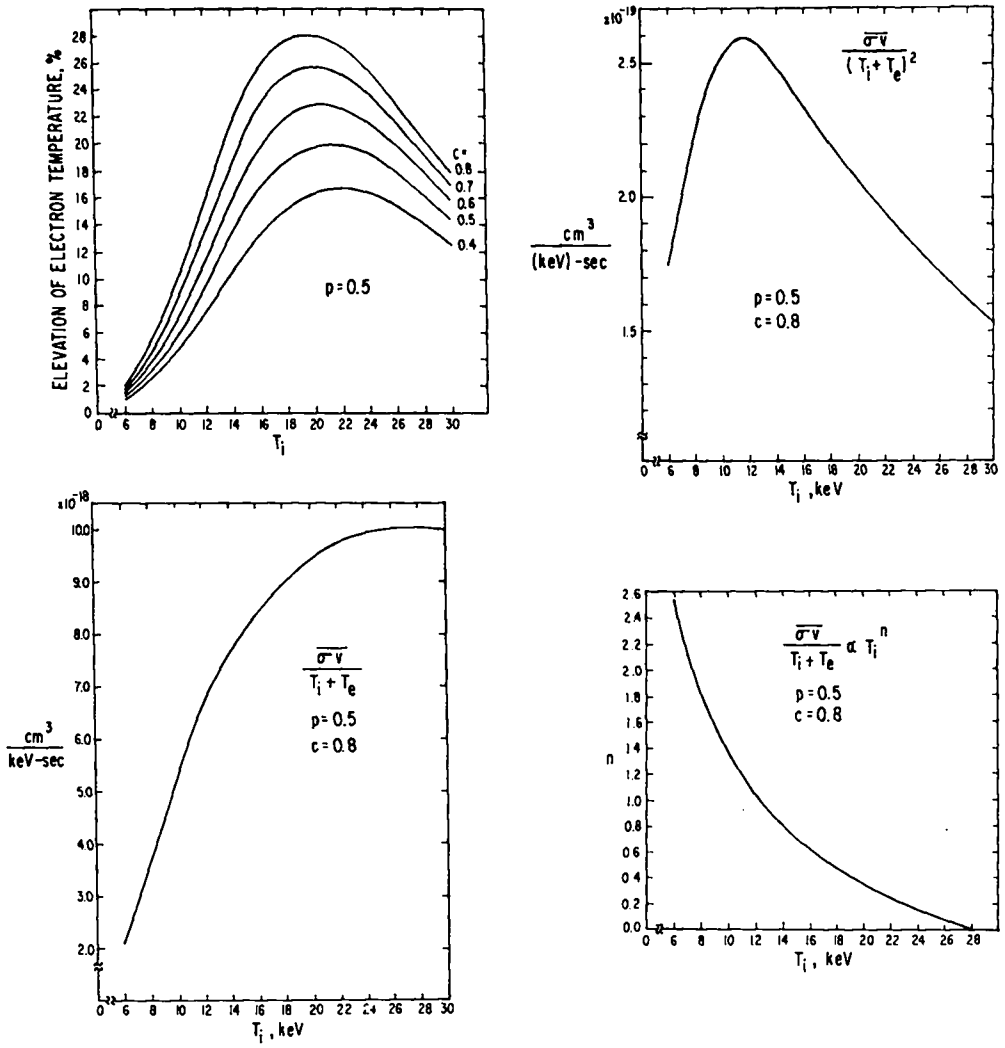

Fig. 2. Plasma parameters as a function of ion temperature.

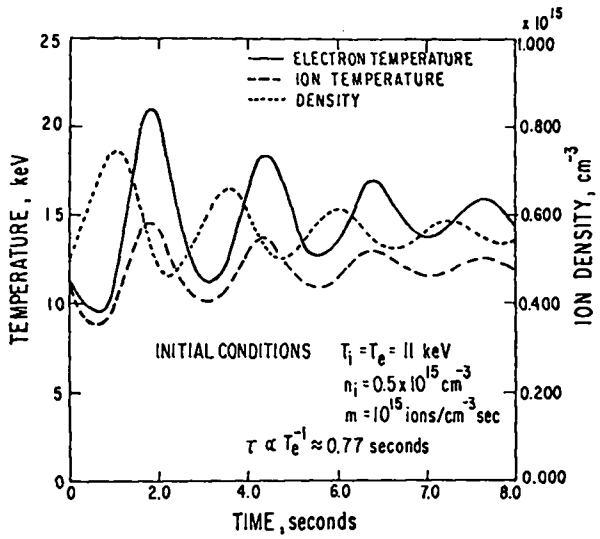

Fig. 3. Plasma conditions as a function of time.

PRESENT AND FUTURE 2X DATA SYSTEMS*

George E. Vogtlin
Lawrence Radiation Laboratory
University of California
Livermore, California 94550

ABSTRACT

The data systems on the 2X Machine are rapidly changing to meet the requirements of increased plasma life and density. In particular, the study of multiple ion species, including the effects of carbon impurities, has greatly increased the number of channels and the complexity of measuring the ion cyclotron frequencies.

The present data system on the 2X Machine uses oscilloscopes and Polaroid film cameras. A key diagnostic system is the raster oscilloscope, which permits the measurement of frequencies to 100 MHz and has recently been delayed between sweeps to permit sampling at intervals of 10 μsec. An important feature of these measurements is the use of band-pass filters. A computer program was written to speed the design of M-derived filters.

The use of computers is now limited because of the time required to digitize and process the data. In addition, the recent extension of plasma life has made the time-resolution of the present oscilloscope inadequate. A new data system is being purchased that has a 40-channel analog disc recorder and a digital computer. This unit should be able to record 30 msec of data with a 500-kHz frequency response and a high signal-to-noise ratio. The information can then be digitized by a single analog-to-digital converter and processed on a computer.

The rotational speed of the disc permits the computer to sample data recorded on a channel at 30 times per second. The data will be processed for immediate use and stored in digital form.

INTRODUCTION

The 2X Machine is a pulsed mirror machine with a quadrupole. The deuterium ion density is 5×10^{13} per cm^3 with energies from 1 to 50 keV. The plasma life is of the order of milliseconds. Some of the diagnostic measurements are (1) thermonuclear reaction rate (energetic neutrons), (2) plasma density, (3) analysis of the transverse charge-exchange flux to derive the ion-energy distribution as a function of time, (4) correlation of multiple ion probe and/or electron probe data, (5) electron temperature as a function of time (derived by means of neutral beam techniques), and (6) end-loss patterns or radial density distributions. All of this data is taken simultaneously during each firing of the machine.

To achieve the necessary analysis of the experimental results requires processing of all of this data by computer. Several alternative systems for feeding the data to the computer were considered. The one selected is described in the following section on "The Basic System," and the reasons for its selection are discussed. Particular problems in acquiring the data and specific solutions for them are presented in succeeding sections.

THE BASIC SYSTEM

Disc Recorder

The present data system for the 2X Machine uses Polaroid film and oscilloscopes. This system is marginal for the present operation. The time of plasma confinement has been extended from hundreds of microseconds to milliseconds, and many additional measurements have been added, such as

*Work performed under the auspices of the U.S. Atomic Energy Commission.

ion-energy distribution as a function of time. To achieve time resolutions of 10 μsec over 3 msec may require as many as six oscilloscopes with the present methods. Many alternatives were considered, including tape recorders. However, their cost-per-channel and signal-to-noise ratio at the required bandwidth have appeared marginal. Besides, the data would have been stored with no quick way to make the extensive calculations required for the ion-energy distribution as a function of time. Another alternative was analog-to-digital conversion and then operation on the stored data by computer. The cost of 40 channels of high speed analog-to-digital (A-D) conversion and the necessary core storage made this system prohibitively expensive.

The system now being purchased and constructed will have a disc recorder as an intermediate storage device, and a single, slow-speed A-D converter to put the information into a computer.

The characteristics of the disc recorder are a signal-to-noise level exceeding 46 dB with a bandwidth of 500 kHz. The bandwidth limitation can be extended to at least 6 MHz with signal-to-noise ratios above 40 dB. The cost of this system is significantly lower per channel than that of tape recorders, and slow-speed A-D conversion by repetitive sampling each disc rotation results in an extremely flexible and powerful data system. This system is shown in block diagram in Fig. 1.

The initial uses of the computer will include (1) thermonuclear reaction rate on both linear and log plots, (2) plasma density on linear and log plots, (3) the ion-energy distribution as a function of time (this measurement, which is derived from the charge-exchange flux by the use of the multichannel mass-energy analyzer, may use as many as 10 to 20 channels), (4) correlation of multiple ion probe and/or electron probe data, (5) electron temperature as a function of time (derived by means of neutral beam techniques), and (6) end-loss patterns or radial density distributions.

SPECIFIC DATA ACQUISITION PROBLEMS

A particular challenge has been the reduction and recording of high-frequency signals on the ion and/or electron probes. The probes used have been shielded Faraday cups, loops, or, more commonly, a Langmuir probe. These particular Langmuir probes are 50-ohm coaxial from the plasma to their termination. A miniature Teflon-insulated coaxial cable is used at the plasma end. Signals from these probes are in a frequency range of from 1 to 100 MHz and from 100 V to below the ambient noise level. The noise problem on this machine is particularly difficult because ignitrons are used to fire and crowbar the capacitor banks.

Filters

One of the most effective ways found to improve the signal-to-noise ratio on the Langmuir probes was to incorporate band-pass filters. The kind of filter generally used is designed according to the equations in Terman's "Radio Engineers Handbook." The filters, M-derived ladder types with passive components, have been found to meet all our requirements.

To speed the designing and improve the selection of components, a filter design was written by C. Harris, an LRL summer student. All that is required is four data cards specifying the following information: M, load resistance, lower frequency limit, and upper frequency limit.

Comb Filter

The measurements of radio frequencies have been greatly assisted by the design of comb filters. These are of the standard M-derived type, but are constructed without the shunt portion of the end sections. They have been used in up to six sections. A standard setup uses diode detectors and a multichannel scope to present all bands for direct comparison. Figure 2 gives an example of the data from a filter of this kind. There is a single input with six outputs. This response was generated with a sweep generator operating into the input. This comb has pass-bands of 1-4, 4-8, 8-15, 15-28, 28-50, and 50-150 MHz.

Raster Oscilloscope

The frequencies of the signals on the Langmuir probes are from 2 to 100 MHz. The particular predominant frequency on one of these probes can be distorted by in-phase higher harmonics or two or more frequencies occurring simultaneously. A filter alone cannot determine this. An extremely

useful device for direct observation of frequency is the standard LRL raster oscilloscope Model L-10, which, however, was designed for accurate measurement of time and not as a linear device. The incorporation of wideband amplifiers resulted in adequate data (Fig. 3). Each sweep is 2.5 μsec in duration with approximately 0.1 μsec retrace time. Timing marks are 0.5 μsec apart.

A problem is that these scopes cover only about 40 μsec. A useful modification was to delay each sweep for 7.5 μsec. This gives a 2.5-μsec sample every 10 μsec, and the oscilloscope then covers 150 to 200 μsec.

Predominant Frequency Device

Attempts to determine the frequencies present are made more difficult by variations in amplitude of from 100 V to the ambient noise level. A system was devised that always gives the predominant frequency. It consists of six or more amplifiers, which are diode-clipped at the input and connected in series to give sufficient gain so that the ambient-plus-system-noise is fully clipped at the output. System overload is prevented by fast diodes that limit the swing, positive or negative, to ±0.5 V. Each amplifier in turn has a gain of 10 and an overload voltage of 8 V. The result is a system that detects all zero crossings. Assuming that noise is random it is quite simple to observe coherent signals. A raster picture of the clipping is shown in Fig. 4.

Digital

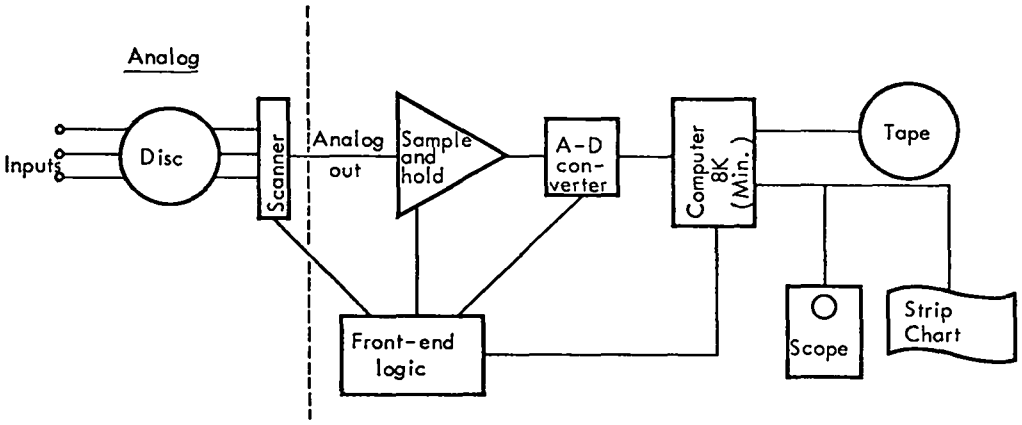

Fig. 1. Proposed 2X data system.

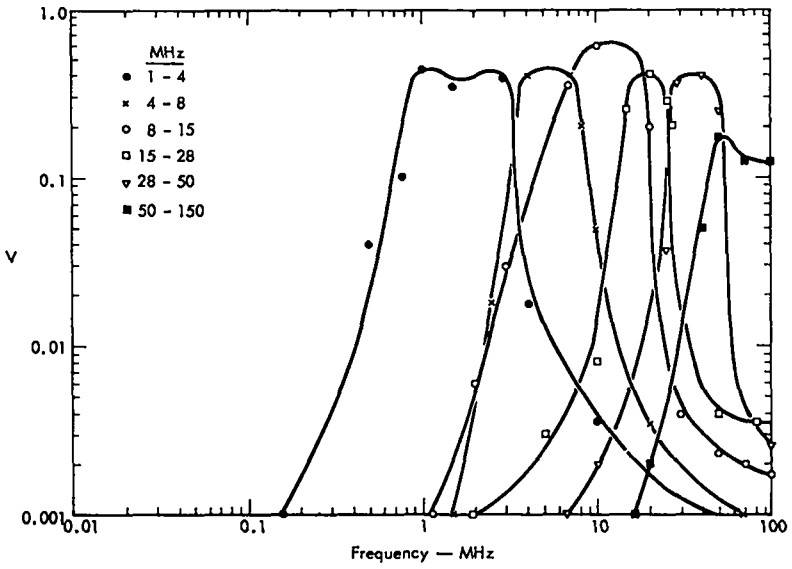

Fig. 2. Electrical response of the comb filter, 1 to 150 MHz, 50 ohms.

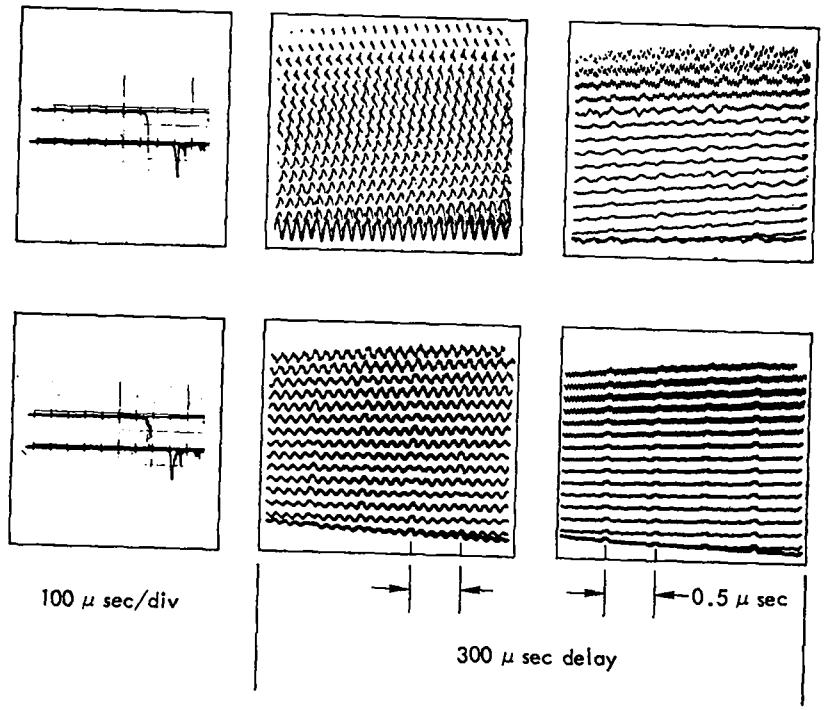

Fig. 3. Raster scope display.

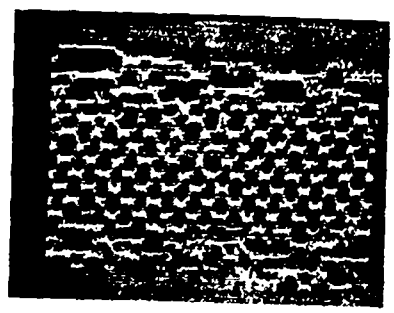

Coherent signal

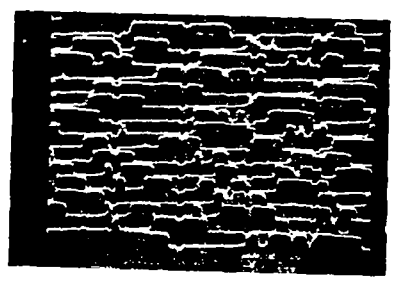

Noise

Fig. 4. Predominant frequency.

THE DATA ACQUISITION SYSTEM FOR THE SCYLLAC DEVICE

by

R. F. Gribble, D. Brown, J. W. Lillberg,
G. A. Sawyer, and D. M. Weldon

Los Alamos Scientific Laboratory, University of California
Los Alamos, New Mexico

ABSTRACT

An automatic data acquisition and processing system utilizing a small digital computer is being constructed for use with the Scyllac toroidal theta pinch. "Scan converters" (storage oscilloscopes) will be the principal means of recording data. In a scan converter tube the signal is stored on a zinc sulfide screen in the form of low mobility electron holes written on the screen with a conventional oscilloscope gun. Reading of the data is accomplished by scanning the opposite side of the screen with a 1-kV electron beam and recording the position of those points where a change in secondary electrons from the screen indicates the presence of holes. The screen is scanned in a non-interlaced raster format with the read-beam position controlled by digital to analog circuitry so that the position of the beam is available in digital form when the stored trace is found. Accuracy of 0.2% (512 steps) is expected in reading either the vertical or time axis. On the write side of the tube, the sweep speed is variable from 1-μsec to 5-msec full scale, and the vertical rise time is adjustable to a 5-nsec minimum.

Output from the scan converters is fed to an on-line digital computer for processing. Permanent storage on magnetic tape and temporary storage on a 0.37 million word (16bit) magnetic disc will be available. Data from any scan converter can be brought into core from the disc on command, processed as desired, and sent to a CRT display system for inspection. This display system is fully buffered by a second magnetic disc which stores the data in the form of a television signal. The display scopes are ordinary television monitors driven by read heads scanning different tracks of the display storage disc.

The computer will also monitor performance of Scyllac power supplies and spark-gap switches.

I. INTRODUCTION

The size and complexity of the Scyllac toroidal θ pinch now under construction at Los Alamos has made it necessary to develop methods of automatic data acquisition and processing in order to carry out the experimental program expeditiously. Details of this system have been, for the most part, dictated by the properties of the Scyllac machine itself. The Scyllac device is a toroidal θ pinch of 5-m major diameter and 10-cm minor diameter. Energy for the main B_z field and auxiliary fields comes from capacitor banks switched and crowbarred by over 6000 spark gaps, and each machine pulse is of the order of 100 μsec. Ideally a data acquisition system should be able to record automatically initial conditions for each shot (e.g., charging voltages of the capacitor banks), monitor the behavior of the spark-gap switches, and process and display signals from various diagnostic devices. Detailed considerations show that approximately 100 parameters are required to specify initial conditions, 6480 data readings are required to monitor the firing time of the spark gaps, and roughly 30,000 data points to record the signals from 100 diagnostic devices. Estimates of these numbers come from a typical selection of diagnostic devices

and their sampling times which can range from once every 1 μsec for simple magnetic pickup loops measuring B_z, to once every 50 nsec for measurements pertaining to the initial implosion. The high sampling rates preclude the possibility of recording data in real time. Accuracy of 1/2% should be adequate for all of these data readings.

Because of the high frequencies required to sample diagnostic devices, we have decided on scan converter tubes for recording fast data rather than storage on magnetic tape or disc. Each scan converter, or recording oscilloscope, records data by storing a trace on a ZnS screen in the form of electron holes written with a conventional oscilloscope gun. A second gun scans the screen and the position of the trace is marked by a change in secondary electrons from the screen. Position of the trace is digitized with a maximum accuracy of 512 steps in either the signal or time axis. External controls are similar to those of a conventional oscilloscope with a sweep speed variable from 1-μsec to 5-msec full scale and variable gain amplifiers to adjust for signal size. Rise time of the vertical amplifier is variable down to a 5-nsec minimum. Data from each scan converter is read into an on-line digital computer for further processing and display. Time required to read a single scan converter is about 0.1 sec if the maximum number of vertical and horizontal steps (512) is selected. Reading the full complement of 100 tubes should be accomplished in a few seconds.

Recording of the initial conditions of each shot is accomplished by a relay multiplexor which continuously samples voltages from power supplies during the Scyllac charge cycle and passes these voltages to an analog to digital converter (ADC) for digitizing and examination by the computer. Values sampled just prior to a machine pulse will be saved for permanent record. The computer also exercises a control function during the charge cycle in that it uses its internal clock to calculate charge rates and will terminate a cycle if it detects a malfunction.

Successful operation of the Scyllac device requires each of the spark-gap switches to fire at the correct time with less than 50-nsec jitter. By measuring the firing time of all gaps it will be possible to identify not only those gaps which are completely malfunctioning but also those whose anomalous behavior indicates the need of preventative maintenance. The gap firing time is measured by starting to charge a small low-leakage capacitor at the time the trigger is sent to the gap and terminating the charging when the gap fires. The voltage on each measuring capacitor gives the firing time of the respective gap. Reed relays isolate the measuring capacitors after each shot and a second set of relays connects each measuring capacitor in turn to an ADC to measure the firing time. Prefiring gaps can also be identified with this device by allowing a prefire of any bank to start the measuring cycle. Prefiring gaps will have zero time between the start of the measuring cycle and the gap firing time.

Once all the above information is read into the computer it is processed and the results of the calculations presented either by printing out on a teletype or displaying data in graphical form on a cathode ray tube (CRT), display system. The teletype has the advantage of producing a hard copy of data for later reference, but its speed of only 10 characters per second is a drawback. Therefore a software character generator will be made to allow display of alpha-numeric data of transitory interest on the CRT display. A line printer may be added at a later date if the need arises for a hard copy of large amounts of data.

II. DETAILS OF THE SCAN CONVERTER RECORDING SYSTEM

The scan converter tube consists of two independent sections, a write-side and a read-side; the only common part being a zinc sulfide semiconductor target that records and stores information in the form of low mobility holes. Figure 1 is a picture of a scan converter tube. A conventional 10-kV electron beam performs the "writing" by producing secondary electrons that are collected on a positive ring, leaving a positive charge where the beam strikes the target. The input connections to the tube are the same as for an oscilloscope in that a sweep voltage is applied to a set of electrostatic deflection plates to provide a time axis and the signal is connected to an orthogonal set of plates to record the signal as a function of time.

A 1-kV electron beam is utilized on the read side to retrieve the recorded information. This read operation can follow the write operation by

anywhere from zero to about 72 hr. The presence of stored information on the target is detected by observing the rate of collection of secondary electrons emitted as the read beam moves over the target; when the beam hits a region of the target where the hole concentration is high (the written trace) the number of collected secondaries changes. Covering the target in a non-interlaced raster manner, the read beam is controlled by special digital-type circuitry (the logic chassis) that outputs digital information automatically. Each set of orthogonal electrostatic deflection plates is driven by a separate digital-to-analog converter (DAC) and a synchronous binary counter serially connected to a 2.5 mHz clock. The "horizontal" counter indexes once for each complete scan of the "vertical" counter, and a frame is completed when the horizontal counter reaches full count. The terms counter and DAC are used interchangeably here because the DAC output is an accurate analog voltage proportional to the count of the counters. Figure 2 is a schematic diagram of the scan converter controller.

The "horizontal" read deflection plates are closely aligned parallel to the sweep plates of the write-side. Since the digital information obtained on each vertical scan is proportional to the recorded signal at a time related to the count of the horizontal counter, and since the horizontal counter and DAC index sequentially, the digital output represents a serial sampling of the signal where the sampling interval is the reciprocal of the product of the write sweep-speed in steps per second and the number of horizontal steps taken on the read-side. Only the vertical counter words need be recorded; the position of the word in a frame sequence indicates that time at which the sample was taken.

The procedure by which actual reading is accomplished involves the use of a current activated switch and a gate for the read beam. A preamplifier for the switch monitors the secondary electron current from the read beam. When that current is larger than a set threshold value, the switch toggles, the counter is stopped, and a command is sent to the computer to read the contents of the counter. Because of transients at the DAC output whenever it changes state, the read beam or the switch must be disabled while the DAC settles following each step. Gating or unblanking of the beam is the more economical in that target information is conserved while the bean is off. A convenient procedure is to unblank the beam during the second half of each clock pulse while the counter is running.

Because the width of the written trace varies with writing rate, focus conditions, etc., the trace may cover several read positions of the read beam, resulting in several output words per vertical scan. (Words on the same vertical scan are distinguished from those in adjacent scans by a flag bit inserted in each data word indicating even or odd scan number.) In addition, there may be "noise" spots on the target that cause spurious word output. The read logic may transmit all data words, letting the computer determine the center of each trace; or it can automatically determine and transmit the trace center (or spurious noise spot center). In any event, the computer or computer operator must decide which data is spurious.

The logic chassis can be programmed to read a tube either one or three times; the latter is to provide more reliable data when desirable. In the output flow of data words, each frame will be separated by a word of all zeros (a zero word) and successive tube will be separated by two zero words. The counter and DAC are connected such that there will be no zero or zero complement data words. In the event that a large signal produces an off target deflection of the write beam so that the written trace disappears, the logic chassis will insert words containing all ones for the vertical read scans of the lost section of the data. These events will cause an operator flag to be raised indicating the need for a change in gain.

Information available on the scan converter tube indicates that the target is capable of a resolution of about one part in 600. The maximum number of horizontal and vertical steps was therefore chosen to be 512, requiring a 9-bit counter. However, the logic chassis can be programmed to select for each tube either 64, 128, 256, or 512 steps for either the vertical or horizontal direction. The time required to read one frame is proportional to the product of vertical and horizontal steps. Therefore, total readout time can be reduced by using fewer steps for readout of those signals that do not require higher resolution.

Because the digital output of the system is a

sampling process, it is possible that signal information can be lost if there are components in the signal having frequencies greater than twice the equivalent sampling frequency. The digital data may be meaningless if the high-frequency components are large. The signal can therefore be filtered at the input to the write amplifier to limit the bandwidth to a value consistant with the selected sampling rate. As an example, a 50-mHz signal can theoretically be faithfully recorded and reproduced where the write sweep-speed is 5-μsec per target width and 500 samples are taken on the read side. Since for Scylla or pulse-type experiments the most rapidly time varying part of most signals occurs during the first few microseconds, a simple procedure to allow faithful recording over 100 μsec or so is to use an exponential writing sweep that expands the time scale during early parts of the sweep.

The design philosophy is not unusual in that every attempt is being made to build the circuitry for utmost reliability, freedom from maintenance and adjustment, and ease of any maintenance that is necessary. The use of capacitive coupling to deflection plates with multi-turn potentiometers and stable power supplies should remove all beam drift problems. This requires DAC's having zero average output. The circuits are all solid state with maximum use of integrated circuits. Nearly all of the components will be built up on plug-in printed circuit boards that can be easily replaced.

It is anticipated that eight scan converters will be plug-in mounted in pairs in one 84-in. high standard relay rack. Each scan converter will have its own read and write amplifiers and sweep generators, but the eight in one rack will share power supplies, gun filament transformers, and read logic chassis. The prototype model will be an independent unit with automatic sequencing of tube readout. As such, the prototype, as well as the "production" model, can be used independently of a computer on any experiment with the addition of a recorder such as an IBM card punch, paper tape punch, etc., and a recorder controller. The prototype uses a paper tape punch as a recorder. To convert for Scyllac use only one printed circuit card in the logic chassis must be changed. Figure 3 is a preliminary printout from the prototype.

For Scyllac operation each logic chassis will be slaved to a master controller that directly connects to the computer. The controller will direct the reading sequence for all of the tubes in a selected order, or it will be able to allow the computer to select any or all tubes in any sequence desirable. The controller will insert a few words preceeding each tube readout giving the date, the shot number, the nominal signal gain, and the sweep speed. In addition it can provide a programmed contact closing signal to a reed relay at the front end of selected signal amplifiers, connecting the amplifiers to a time and vertical axis calibrating source. The computer will then take the readout of the selected tubes and calculate calibration factors for these tubes where maximum accuracy is desired.

III. PROCESSING AND DISPLAY OF DATA

A. The Computer

The computer configuration used in the data acquisition system consists of an SDS Sigma 2 processor containing 16,384, 16-bit words of core storage, a 375,000 word disc, a 7 track magnetic tape unit, and an ASR 35 teletype. Figure 4 is a block diagram of the computer configuration. The central processor contains hardware multiply and divide, 2 real time clocks, 4 priority interrupts, and digital input/output adapters for interfacing the scan converters and display system. Cycle time of the computer is 0.9 μsec. Temporary storage of data and subroutines used for processing data is provided by the magnetic disc. Average access time to the disc is 17 msec. Permanent recording of data is provided by the magnetic tape unit; tapes written on this unit are compatible with tape units on larger computers in the Los Alamos central computer facility. Until such time as the computer is provided with a card reader, the magnetic tape unit will serve to read programs into the computer. Control of computer operations, selection of data for display or printing will be chiefly through the teletype.

Several points relating to the computer software should be pointed out. All of the programming can be done in Fortran except for the I/O handlers for the scan converters and other special peripheral equipment being built at Los Alamos. Because of the size of the data acquisition program (~ 30,000 words)

and the large volume of data read into the computer (~ 36,000 words/pulse) we make profitable use of that part of the software system which can automatically overlay subroutines from the disc, and which can perform all the bookkeeping connected with maintaining data files on the disc. The Real-time batch monitor provided with the computer is capable of writing an executing program onto the disc upon receiving a priority interrupt, reading in a second program to work on data requiring immediate processing, and then restarting the interrupted program. This feature is to be used to allow the operator to interrupt the data processing at any time to prepare a new CRT display. In this way maximum delay time in changing a display will be a few seconds.

Although the word length is just 16 bits, the Fortran compiler optionally allows multiple precision of either 2 or 3 computer words for floating point words so that accuracy of 6 or 9 decimal digits is possible in performing calculations.

B. The Display System

The display system being developed for use with the Scyllac data acquisition system is a medium resolution, (~ 480 x 250) low cost, (~ $12K) system. Figure 5 is a block diagram of the display system.

The memory used for refreshing the CRT's is a rotating magnetic disc. The CRT's used are standard T. V. monitors which are refreshed once each revolution of the disc (i.e., once every 1/30 sec).

The disc has four independent read/write heads and one sync track which is used to syncronize the T. V. monitors with the disc. These four heads supply the video signals for refreshing four monitors, each one having a different display. In addition, one of the heads can be moved radially, so that up to 50 different displays (tracks) can be recalled independently of the computer which generated them.

The control panel of the display system has a video mixer. This consists of a set of switches which allows the video signal of one or more displays to be superimposed on any of the monitors. Also it is possible to record this mixed signal on any of the four tracks independent of the computer.

The information to be displayed is outputed from the computer as the coordinates of a series of points. The display "writes" these points on the disc at the appropriate time (in relation to the sync track). Once written, a point is outputed on the T. V. monitor(s) connected to that track each time the point passes under the read head (i.e., 30 times a second).

The information for the display is outputed from the Sigma 2 Direct I/O interface in a series of 16 bit words. The time to output a single display not counting time to generate data to be displayed is 1-3 seconds, depending on the complexity of the display. Each of the T.V. monitors is rotated through 90° so that the raster lines are in a vertical direction. In plotting a point, the abscissa of the point determines the number of the raster line on which a point is written while the ordinate determines the position along line. Data is sent to the display system as 16 bit words which are sent to one of four registers. Two bits in each word are reserved for selecting the proper register. The bits in the first register (Command Register) select which of 4 write heads is to be used and whether data is to be written or erased. An erase command causes the entire track to be erased.

The bits in the second register (Line Selection) are the binary value of the T. V. line on which the data in the "Data on the Line" register will appear. Because of the vertical retrace time of the T. V. raster only about 480 lines will be visible and the first line visible will be about number 22. Due to the field interlace in the T. V. raster the next line visible would be line (262 + 22) = 284. The lines then follow in sequence 23, 285, 24, etc.

The binary value of the bits in the third register (Position of Data) determine the relative position of the data on the selected line. A value of zero corresponds to the start of a T. V. line (left end of line in a normal T. V. raster) while a value of 1023 corresponds to end of the T. V. line. Although any one point can occupy any of 1024 positions along the line the next point on the same line should be separated by at least the resolution of the disc (i.e., ~ 1024/250 ≅ 4) in order to be visible.

The third register (Data on the Line) contains the bit pattern that will be written along the selected line. The first bit (if = "1") will be written as a point on the line at a distance from

the start of the line as determined by the "Position of Data" register. The second bit (if also equal to "1") would be written one resolution element further along the line. This continues for the other eight bits. This register will be useful in writing parts of letters that appear on the same line and in writing a coordinate axis on a T. V. line. After the 10 bits of data are written on to the line the contents of this register will be reset to output a single point (i.e., the first bit = "1" and all others equal zero). Note that all other registers are unchanged by a write or erase operation. One bit of every word sent to the display is reserved for an execution command. Upon reception of this command a signal is written on the disk at the place corresponding to the contents of the various registers. After the write command is executed, this bit is reset to zero.

IV. CONCLUSION

The data acquisition computer has been received and is being installed temporarily in the Scylla IV area. The computer will be used on Scylla IV until Scyllac is ready. A prototype scan converter system, and the CRT display unit are nearly completed. We will be able to test the system on Scylla IV before Scyllac is operating.

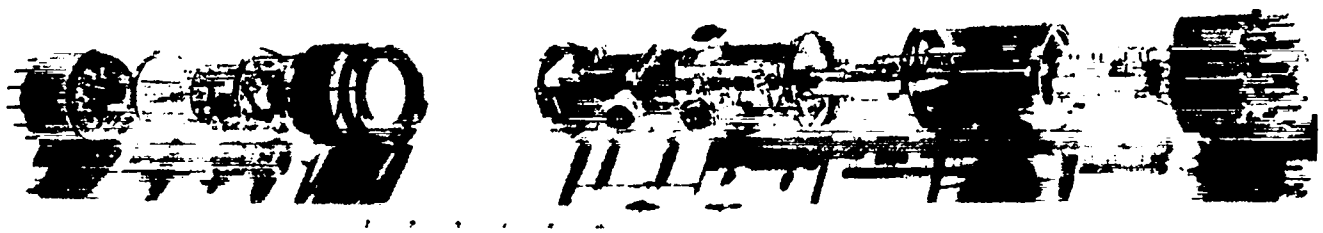

Fig. 1. A scan converter tube. Read-side is to the left.

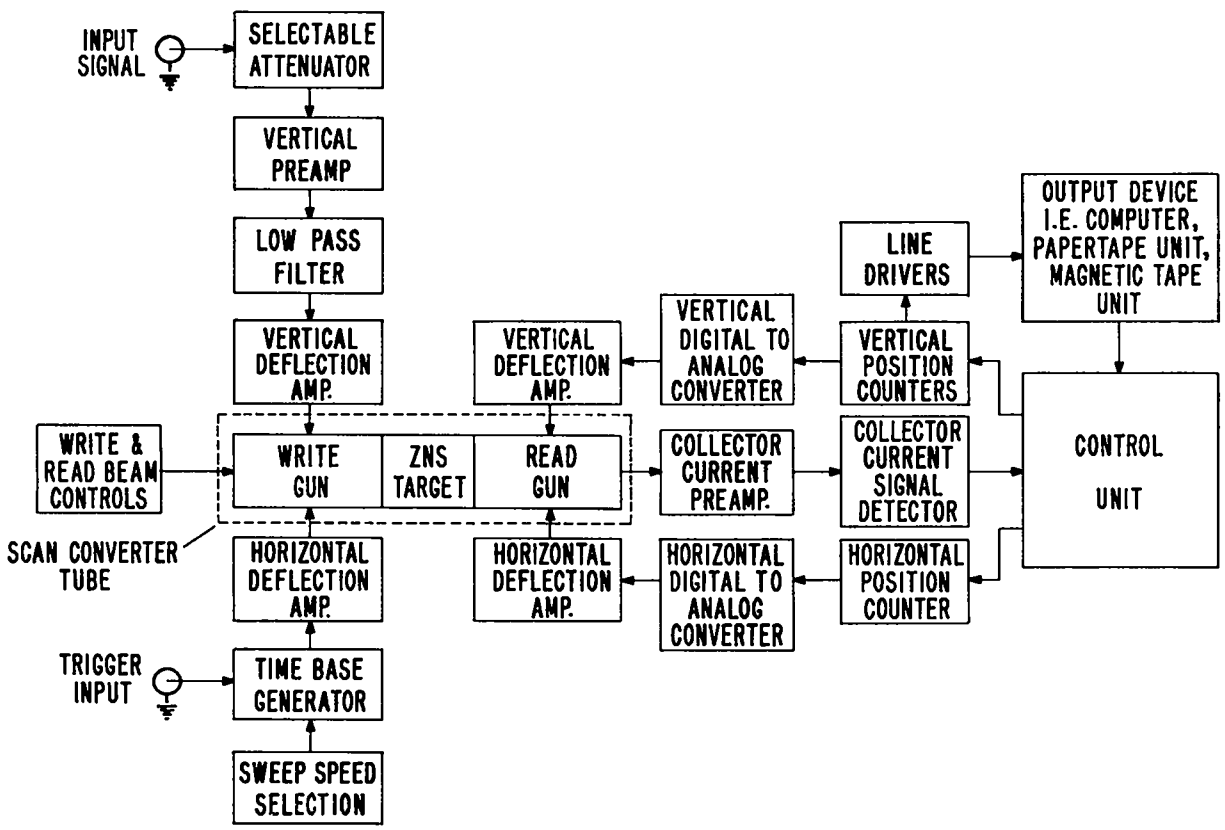

Fig. 2. Block diagram of the scan converter controller.

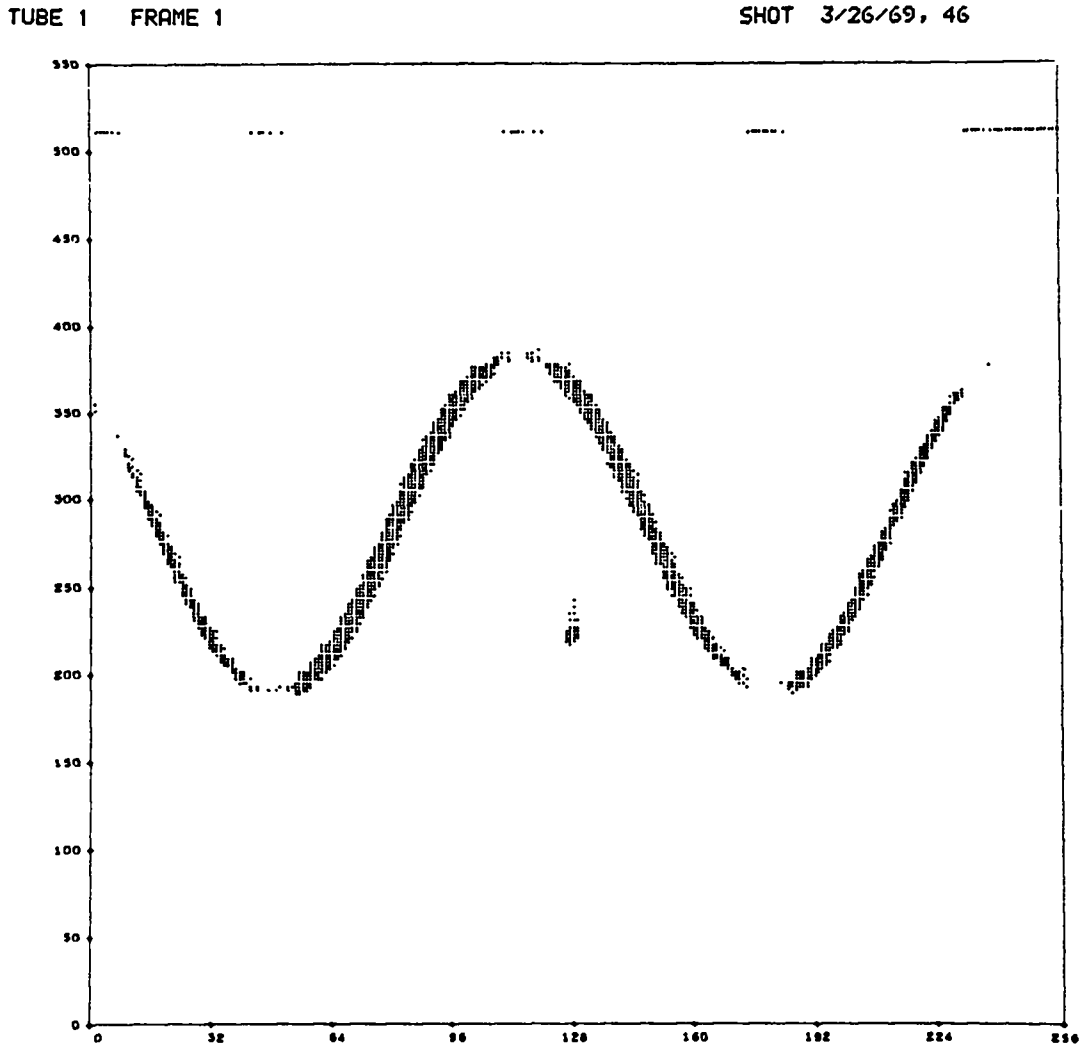

Fig. 3. Preliminary printout of a sine wave recorded on a scan converter tube.

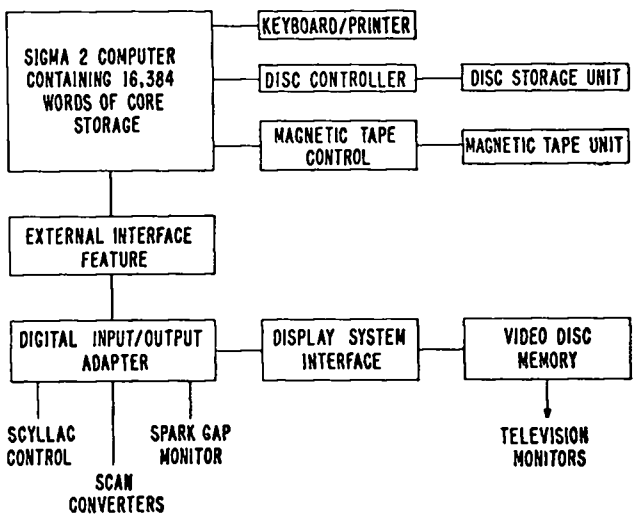

Fig. 4. The computer configuration.

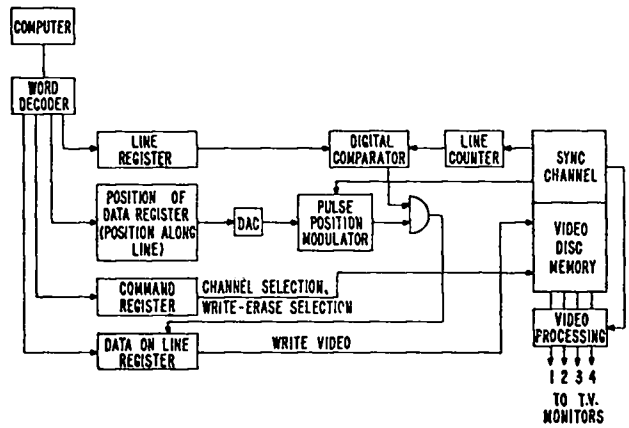

Fig. 5. Block diagram of the display system.

DATA ACQUISITION FOR THOMPSON SCATTERING EXPERIMENT ON CHALICE*

SIT-2582-30

by

Wayne E. Carr
Stevens Institute of Technology
Hoboken, New Jersey

ABSTRACT

In a fast-rise, single-shot experiment such as Chalice, there are several difficulties which must be overcome in data acquisition. The rapidly rising magnetic fields induce large emfs which must be discriminated against. In addition, the maximum possible amount of information must be obtained from each shot. Presented here is a system for collecting data from a Thompson scattering experiment. This system measures the frequency width of the scattered light from a 2 joule pulsed ruby laser by means of an 8-channel polychrometer. The detection device consists of a Spex 3/4 meter monochrometer spectrometer, 8 plastic light guides connected to photomultipliers, followed by fast self-contained preamplifiers driving coaxial cables. These outputs are passively delayed and combined in such a way that the information is displayed on one oscilloscope.

Introduction

In the course of experimental plasma research it is usually necessary to know the temperature of the plasma in question. High-β, pulsed plasmas, such as CHALICE,[1] offer some particularly challenging problems in attempting to make measurements of the plasma electron temperature.

There are several possible methods which may be tried, each having its own particular problems. Impurity line spectra give some temperature information, but the regime where present calculations apply is limited. In addition, time resolution is not possible except at low temperature.

Continuum radiation offers another possibility. Here, however, the temperature dependence is not very pronounced, radiated intensity is proportional to $T^{1/2}$. In addition small amounts of high-Z impurities render this method useless, since radiation emitted from the impurities $\sim (Z)^2$.

Probably the most reliable method is Thompson scattering[2]. The experiment is quite clean and it is possible to obtain both spatial and temporial resolution through the use of a focused, pulsed laser.

The characteristic features of the scattering depends upon the relative magnitudes of the Debye wave number k_D and the wave number of the light, k. For $k_D^2 >> k^2$ the scattering is essentially from free electrons. In the Chalice experiment we have densities, $\gtrsim 3 \times 10^{16}$ cm^{-3} and temperatures, $T \sim$ 100-200 eV. Thus $k_D^2 \gtrsim 5 \times 10^8$ cm^{-2}. For a ruby laser $k^2 \gtrsim 8 \times 10^9$, and hence the scattering is from individual electrons. For this case the scattered power is given by

$$P_s = N\left(\frac{e^2}{mc^2}\right)^2 f\left(\frac{\Delta\omega}{\Delta k}\right) \Delta\Omega\Delta\omega_s,$$

where N is the total number of electrons participating in the scattering process, $f\left(\frac{\Delta\omega}{\Delta k}\right)$ is the 1-dimensional electron distribution function evaluated at the incident minus scattered frequency divided by incident minus scattered wave vector. $\Delta\Omega$ is the solid angle which intercepts the receiver and $\Delta\omega_s$ is the frequency width of the receiving system.

With a very sensitive, selective receiver one could, in principle, determine the electron distribution function quite accurately, but our first task is to determine the temperature.

The Scattering Experiment

The experimental arrangement is shown in fig. 1. The laser light is admitted from below into the cusp region. The receiver is positioned horizontally at 90^{o} with respect to the incident beam. For the laser source we are using a pulsed ruby laser, capable of delivering several joules in approximately 40 nanoseconds. It belongs to Dr. W. H. Bostick, of the Stevens Physics Department, who has consented to our using it.

We now turn to the subject to be given major emphasis here, the receiver system. The scattered light from the plasma is transmitted through a SPEX model 1700, 3/4 meter, spectrometer, equipped with a spectrograph attachment. This is admirably suited to the scattering experiment since the spectrograph has a 500 Å spread with a dispersion of 11 Å/millimeter.

The expected frequency width of the scattered light is approximately 200 Å, thus to make the temperature determination we decided to use 8 regions of width 1 millimeter, each separated by 1 millimeter, at the focal plane of the spectrometer. The number 8 represents a somewhat arbitrary decision. The number of points necessary for a temperature determination is 3. To improve the accuracy one would like 5. The center of the region, where unshifted laser light from incidental scattering is presented, is useless. In addition, there may be one to two emission lines strong enough to mask the scattering. Thus the number 8.

The light from the 8 regions is transmitted to eight Amperex photomultipliers by means of plastic light guides. The photomultiplier output thus gives the scattered intensity vs. frequency needed to determine the temperature.

Engineering Considerations

We now turn to the problem of collecting and displaying this information. There some obvious solutions; 8 oscilloscopes equipped with polaroid cameras; 8 pulse height analyzers. Solutions of this type are very costly, and they suffer from other drawbacks.

The Chalice experiment has a very rapid capacitor bank, and the magnetic field rises to $\sim$ 50 K Gauss in 1 microsecond. With this type of rapidly varying field, every cable leading to the experiment represents another inductive loop in which an extraneous emf is induced. Thus receiver systems with many cables and connections to earth must be avoided. Additionally it is undesirable to have too many complex components because of the chance of malfunction.

Incidentally, the possibility of simply photographing the scattered light was considered. Here the scattered light spectrum could be measured after the shot with a densitometer. The intensity is too low for photography, but not by as much as one might think. The total received energy is $\sim 10^{-12}$ joules. This falls on about 1 cm^2 of film. We experimentally determined the intensity of red light needed to expose Polaroid 3000 speed film, using a 1 mw gas laser. The energy required is about 2×10^{-9} joules/$_{cm}{}^2$. Strangely, we have not noticed in the literature any quote of the energy density required to expose film.

The Data Acquisition System

The system which we finally designed and constructed is shown schematically in figure 2. The photomultiplier outputs are amplified in self-contained preamplifiers, admitted into coaxial cables of various lengths, combined into one composite signal and displayed on one oscilloscope.

The photomultiplier preamplifiers are very simple transistor circuits, diagrammed in figure 3a. The circuit is a Darlington pair emitter-follower. The 8 circuits are powered by one 6 volt battery which is inside the shielded container holding the photomultipliers. The amplifiers are forward biased just enough so that they are in the conducting region. Quiescent current is approximately 1 milliampere each, so the battery lifetime is quite long. Transistors are TIXM101, which have a cutoff frequency of 1GHz. The input capacity is less than 1 pf. It is this very fast preamp which allows us to resolve the 40 nanosecond laser scattering pulse.

To observe these outputs on one oscilloscope it is necessary to delay the various pulses

enough so that they do not overlap. To do this we used RG8/U coaxial cable because of its relatively low cost and high frequency response. We measured the propagation speed and found it to be 1.6 nanoseconds/foot. Using this information we determined the appropriate lengths. The cable lengths for the eight signals are given by the following formula:

$$L_N = 5 + (N-1)\ 32 \text{ (feet)}$$

where N is the channel number. Thus each successive channel is delayed by 51 nanoseconds with respect to the previous one. The 8 delayed signals are then combined in the circuit shown in figure 3b. This operates similarly to a logical "or" circuit in that the output voltage is equal to the largest of the eight inputs. The transistors here are 2N963, only 250 MHz since the source impedance is 50Ω and the capacity of the transistor is not as important. Again, this circuit is powered by batteries.

The delay cables, along with the combining circuit, are housed in an ordinary 30 gallon steel drum, connected to the photomultiplier housing via a flexible pipe. These are physically close together. Thus the only electrical connections to the entire receiver system are the high voltage cable to power the photomultipliers and the composite signal cable to the oscilloscope.

The actual scattering experiment has not yet been performed but the main part of the receiver system has been constructed and tested. Figure 4 shows an oscilloscope photograph of the performance of the delay unit. It was performed under the following conditions: an input pulse upper trace, was simultaneously launched in the 8 cables. The delayed, recombined pulses are shown in the lower trace. Observe that the system is indeed fast enough, since each pulse is distinct. The lack of uniformity is due to slight variations in transistor characteristics. This will be compensated by adjustment of the photomultiplier preamplifiers.

In summary, we have designed a very simple, reliable, inexpensive receiver system capable of displaying the information from a Thomspon scattering experiment on a single oscilloscope trace.

References

1. Paper by G. Yevick, given this symposium.
2. There are many articles in the literature. See e.g. Gerry & Rose, J. App. Phys. 37, 2715 (1966).

---

* Supported by the Atomic Energy Commission.

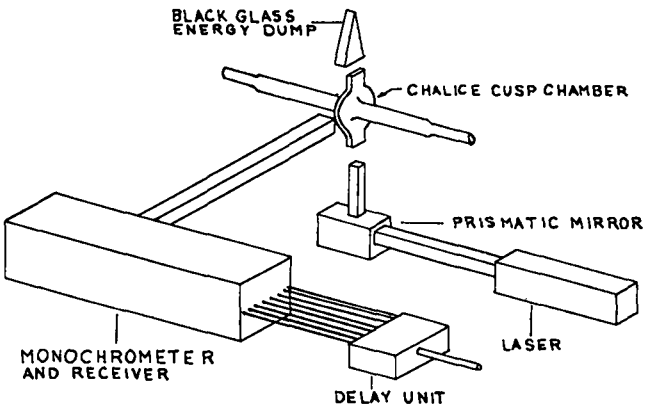

Figure 1: Schematic Diagram of Scattering Experiment.

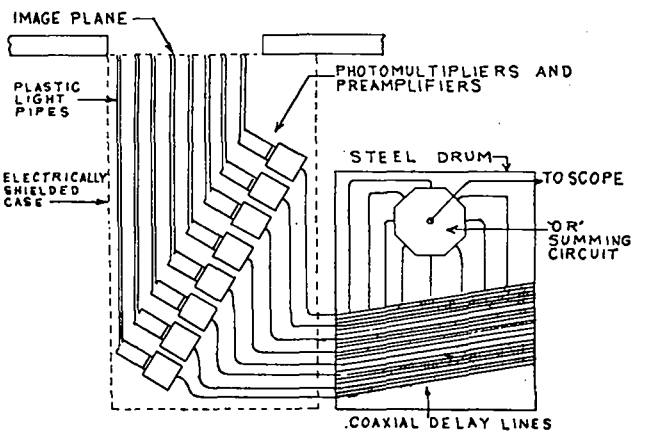

Figure 2: Schematic of Data Acquisition System.

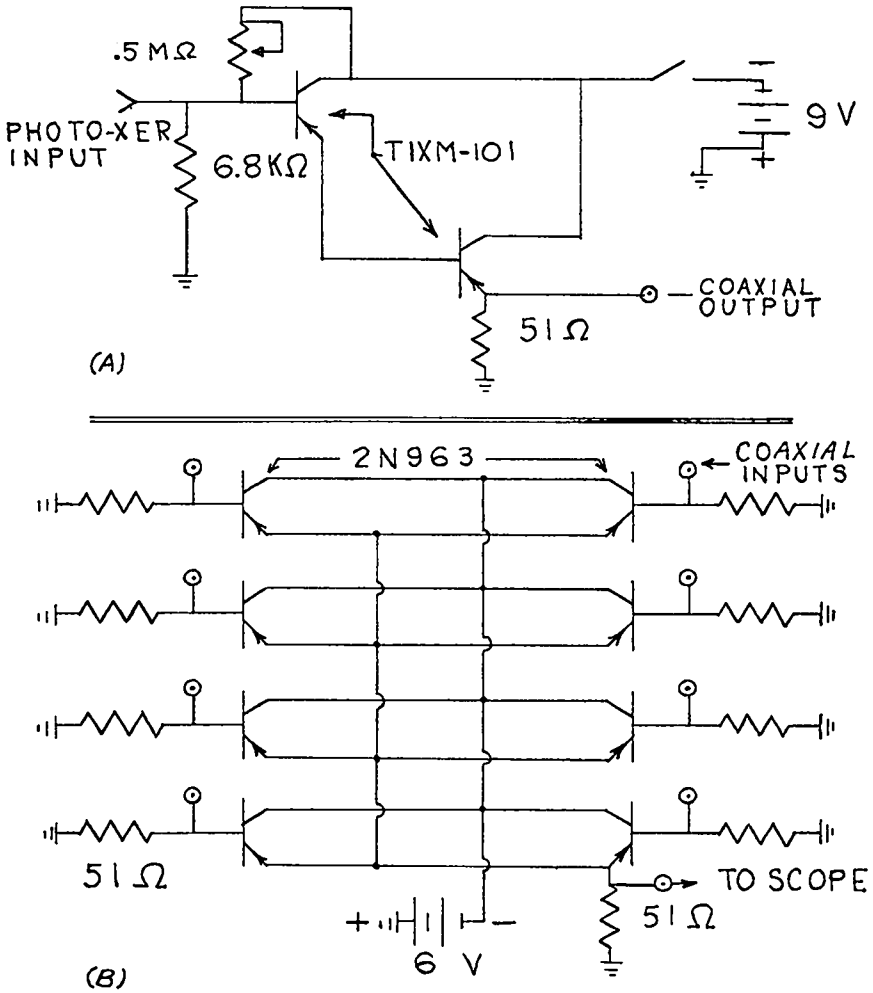

Figure 3: Electronic Circuits for Data Acquisition System - a. Photomultiplier Preamp.
b. "OR" Summing Circuit

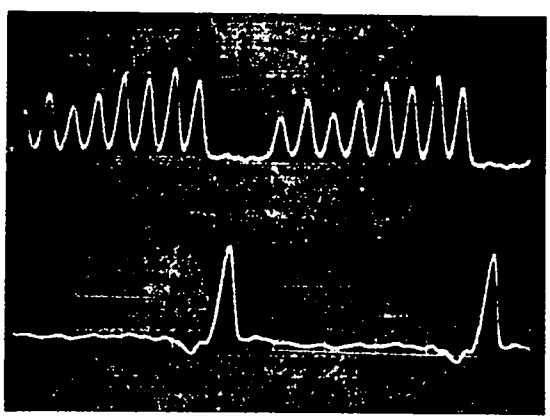

Figure 4: Oscillogram Showing Delay and Summed Output. Horizontal Scale = 0.1μs/ large div., Vertical Scale = 0.02 Volts/ large div.

THE IMP FACILITY AT OAK RIDGE NATIONAL LABORATORY*

R. J. Colchin, J. L. Dunlap, R. S. Edwards, D. P. Hammond,**
L. A. Massengill, T. F. Rayburn, R. G. Reinhardt, and E. R. Wells†
Oak Ridge National Laboratory
Oak Ridge, Tennessee

ABSTRACT

IMP (Injection into a Microwave Plasma) is a fusion device for investigation of hot ion accumulation by injection of an energetic H^o beam and trapping by resonant charge exchange on a target plasma established by high-frequency (35 GHz and/or 55 GHz) microwave heating. Principal components are a neutral injector, a superconducting coil system within a 200 cu. ft. vacuum chamber, and a beam dump. After a brief description of these principal components, we will review the design criteria and discuss more fully mechanical assembly and the vacuum pumping system. Details specifically related to the magnet system (field contours, winding layouts, winding techniques, and choice of superconductor) will be covered in other papers.

INTRODUCTION

IMP (Injection into a Microwave Plasma) is an experimental facility which is being constructed for investigation of hot ion accumulation by injection of an energetic H^o beam. Proton production will be by resonant charge exchange in a target plasma that is established by heating electrons with high-frequency microwave power (35 GHz and/or 55 GHz). The facility will operate in steady state, that is, the magnetic field is dc, the microwave power is CW, and injection is continuous.

Reference to Fig. 1 will make the scheme more clear. Microwave power at kilowatt levels is fed into a high mode cavity, and the microwave electric fields initially cause ionization of some of the ambient neutral hydrogen background. The resulting electrons are further heated by these fields, and a steady-state target plasma composed of hot electrons and relatively cold protons is created. The population of cold protons captures electrons from the incoming 20 keV H^o atoms to form a 20 keV hot proton component. Here we have made use of charge exchange as a trapping rather than a loss process. We expect target densities of about 10^{13} cm^{-3} and conversion of several per cent of the fast neutral beam to trapped protons.

The facility is initially being constructed with a mirror coil pair to provide the plasma confinement field. Later this year we will add four more coils in quadrupole configuration to make a "minimum B" geometry. Our discussions below relate to the mechanical design for operation with only the mirror coils, but the design philosophy for handling the full coil set is the same and most of the components of the facility will not be affected by the change. These coils are all superconducting at 4.2^oK, so the mechanical design has treated numerous cryogenic problems. Further discussion of the magnet system is outside the scope of this particular paper. We refer those interested in the electrical design and in winding techniques to other papers at this meeting.[1,2]

Also we are not concerned here with much detail on the microwave power sources. The initial power will be 1 kilowatt at 35 GHz; 10 kilowatts at 55 GHz

* Research sponsored by the U.S. Atomic Energy Commission under contract with the Union Carbide Corporation.

** On leave from Culham Laboratory, England.

† Denotes speaker.

will be added next year. These items will be near duplicates of those presently in use at our Division's ELMO facility, and are the result of some years of development work by M. C. Becker, R. A. Dandl, H. O. Eason, Jr., and J. C. Ezell in collaboration with several manufacturers. Some basic design features were reviewed in a paper at an earlier meeting, and the two systems are being described in another paper here.[3,4] We do note that the use of microwave power has influenced the mechanical design, principally from two considerations: first, kilowatts are dissipated on the cavity walls and therefore the problem of thermal protection of the liquid helium is severe; and secondly, all ports and leads into the cavity must be designed to permit only negligible leakage of microwave power.

In the sections that follow, we consider in detail the other principal components of the facility. These are:

1. the beam injection and burial lines;
2. the main vacuum system; and
3. the cavity, coil assemblies, and helium vessel (all suspended within the main vacuum system).

We conclude with discussion of cryogenic aspects.

BEAM INJECTION AND BURIAL LINES

The injection system (Figs. 2 and 3) consists of a modified duo-plasmatron ion source optimized for 40 keV H_2^+ production, a focusing coil, a beam neutralizing section, a coil system to remove the charged portion of beam, a flexible joint, and a valve to isolate the system from the main tank. Pumping in the injection area is accomplished with one ten-inch and two six-inch oil diffusion pumps with freon cooled baffles, two sets of titanium evaporators and several square feet of liquid nitrogen cooled copper surfaces to pump the water vapor that is used for neutralizing. Pressures in this system vary from 25 millitorr in the source region to 10^{-6} torr in the region just before the main tank.

The beam dump (Figs. 2 and 3) is for monitoring and disposal of that portion of the neutral beam (> 90%) that has passed through the plasma volume. Pumping in this section is by one six-inch oil diffusion pump with freon cooled baffle and titanium evaporated on liquid nitrogen cooled copper surfaces. The neutral beam current is monitored on a water-cooled beam stopper using a differential temperature cell.

MAIN VACUUM SYSTEM

This system is outlined in Figs. 3 and 4. The principal component is a 200 cu. ft. stainless steel tank of welded construction with full penetration welds. The removable lid is heavily ribbed since it is 7 ft. in diameter. The tank was rough polished on the inside after all welding was completed. At present most of the openings are sealed with "O"-rings, but about 1/3 use a shear type copper ring seal. All openings are designed so that they can be used with metal seals if desired.

The pumping arrangement reflects a combination of several design criteria: fairly low base pressure (10^{-9} torr range), very high pumping speeds for hydrogen gas, and an environment essentially uncontaminated by pump oil. These criteria arise because of considerations involving the electron cyclotron plasma. First, this plasma requires a clean hydrogen background in the cavity region at pressures which will probably not be less than 1×10^{-7} torr and for certain experiments may be as high as 1×10^{-5} torr. So pumping speed for hydrogen gas is emphasized rather than very low base pressure. Secondly, most of the microwave power is transferred to the cavity walls by energetic particle bombardment. This fact coupled with the requirement of a clean hydrogen background leads to the need for low hydrocarbon contamination.

The pumping arrangement that has evolved in response to these criteria involves several elements. From atmospheric pressure, the tank is initially evacuated by aspirators using compressed dry nitrogen. A vacuum of about 23 in. (Hg) is obtained in 20 minutes by this method. At this time, the aspirators are valved off and a valve to a pre-cooled Linde SN-150 cryosorption pump is opened. This pump reduces the pressure to 1×10^{-5} torr in a few minutes. Then a 15 m^2 copper liner spaced close to the tank walls is brought to liquid nitrogen temperature, and titanium evaporators are energized. Finally the cryosorption pump is valved off and the pumping load transfers to the titanium-coated liquid nitrogen surfaces. We use a total of 32 resistance-

heated titanium filaments to insure full coverage and long filament life. A 1000 ℓ/sec electro-ion pump is also installed for pumping inert gases and for holding operation in standby conditions after base vacuum is reached. A premanently mounted mass spectrometer defines the gas composition and aids in diagnosing leaks.

The tank system includes two freon baffled ten-inch oil diffusion pumps. Without the coil system in place and without baking, these pumps base out at ~ 1 x 10^{-7} torr. They have been useful in vacuum tests of the main tank and in tests of the injection and burial systems, but are not intended for use when the facility goes operational.

CAVITY, COIL ASSEMBLIES, AND HELIUM VESSEL

These elements, Figs. 3 through 5, are suspended as a package from the lid of the vacuum tank. Each of the two mirror coils fits into a liquid helium vessel. The two vessels are rigidly spaced against coil forces and are connected so as to share common fill and vent lines. The helium assemblies rest on angle supports which hang from the tank lid by thin stainless tubing. The cavity section nestles between and extends through the helium vessels. The cavity is held in position by pre-loaded spoke arrangements of stainless tubing which terminate on the walls of the helium vessels. The whole package is shrouded by a liquid nitrogen cooled radiation shield. This shield is required because of the use of titanium evaporators in the space between this assembly and the tank shield, and also because of interruptions in the outer shield at numerous port openings in the tank. In conjunction with the evaporators, it provides an additional 6 m^2 of pumping surface.

The cavity is fabricated from 3/16 in. thick copper and is liquid nitrogen cooled to remove the power that originates from the microwave sources. Ports for diagnostic probes are sealed against loss of microwave power by locking a copper-plated stainless steel knife edge into a copper ring that is part of the probe itself. Beam entrance and exit ports are sealed against these losses by using 1/4 in. thick tungsten plates with 85% transparent pattern of honeycomb grids cut by electrical discharge machining. The grid openings are beyond microwave cut-off, (1/8 in. x 1/8 in. mesh size is used for 35 GHz operation). Some pumping out of the cavity directly to liquid helium surfaces is provided by a number of small holes through the cavity wall. These too are beyond microwave cut-off.

The coils are series connected internally, and the two external conductors are brought through the top of the helium can and then out of the lid of the tank through helium gas-cooled leads.[5] A vacuum tight electrically insulated joint was required here. One using brass and Stycast 2850 GT epoxy was devised to provide matched coefficients of expansion so that the integrity of the joint can be maintained from room temperature to 4.2°K.[6]

The helium vessels are of 1/2 in. thick 304 stainless steel. All closures are welded, so future access to the interiors will require grinding away weld seams. Since ultra-high vacuum is not essential, the radiation shield about these vessels has deliberately been arranged for limited pumping conductance to the helium surfaces. We estimate this conductance to be a few hundred ℓ/sec and believe that this amount, along with the electro-ion pump, will provide sufficient handling capacity for inert gases.

CRYOGENIC ASPECTS

We have already mentioned several features of the designs which are intended to minimize helium consumption. Others include the use of thin wall (0.010 in.) stainless tubing for helium fill and vent lines, cool-down lines, instrumentation leads, etc. that pass through the tank lid.

With mirror geometry, cool-down will be accomplished by gradual cooling with cold nitrogen gas flow through the radiation shields and through lines built into the coils and into the helium vessels for this purpose. Once the system is cooled to 77°K, helium will then be transferred from a storage dewar through the fill lines, which open at the coils themselves. It is estimated that approximately 300 ℓ of liquid helium will be required to reach 4.2°K. Thereafter, standby losses are expected to be about 100 ℓ/day, with an additional 2 ℓ/hour during field operation. No attempt to recover the helium gas will be made since at the present time recovery, purification, and reliquefication is prohibitively expensive.

The change to quadrupole geometry will include

installation of a helium refrigerator. Then the nitrogen cool-down will be eliminated and all cooling will be done with the refrigerator, which operates with a closed cycle and so does provide for gas recovery except in the event of catastrophic loss of liquid helium.

Thermal contraction during cool-down made it necessary to use bellows seals on the tubes through the tank lid. Upward displacement of the coil system axis has been calculated as 1/8 in., so adjustments are provided for precise alignment of the coil system with the axis of the neutral beam.

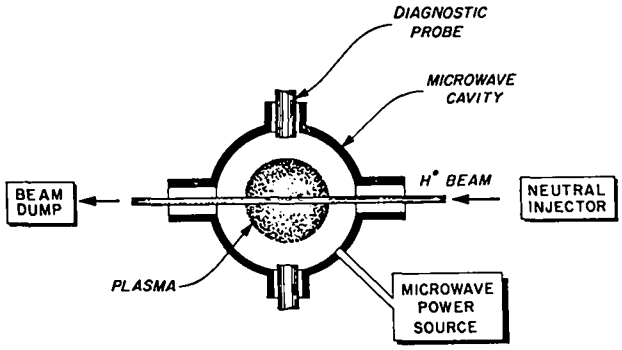

Fig. 1 (ORNL Dwg. 69-3596) Conceptual schematic of the IMP facility.

REFERENCES

1. D. L. Coffey and W. F. Gauster, "Superconductor Evaluation Tests for IMP".
2. R. L. Brown, "Winding Techniques for Superconducting Magnets".
3. H. O. Eason, Jr., "CW Microwave Systems for Electron-Cyclotron Heating Experiments", Proc. Engineering Problems of Controlled Thermonuclear Research Symposium, pp. 168-175 (Gatlinburg, Tennessee, October 1966), CONF-661016.
4. H. O. Eason, Jr., "Electron-Cyclotron Heating at Millimeter Wavelengths".
5. K. R. Efferson, Rev. Sci. Inst. 38, 1776 (1967).
6. This development is also due to K. R. Efferson.

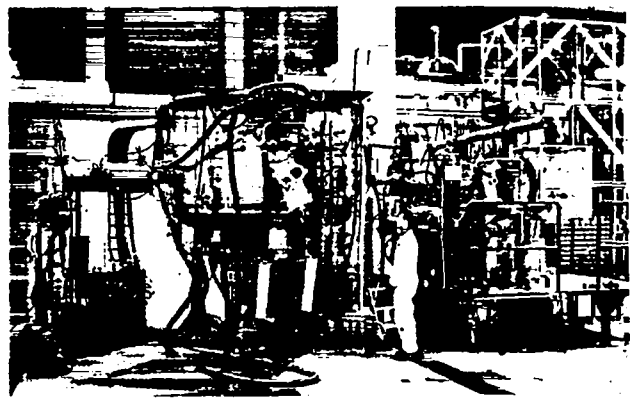

Fig. 2 (ORNL Photo 76636) Photograph of the IMP facility. The beam injector is on the right and the dump is on the left.

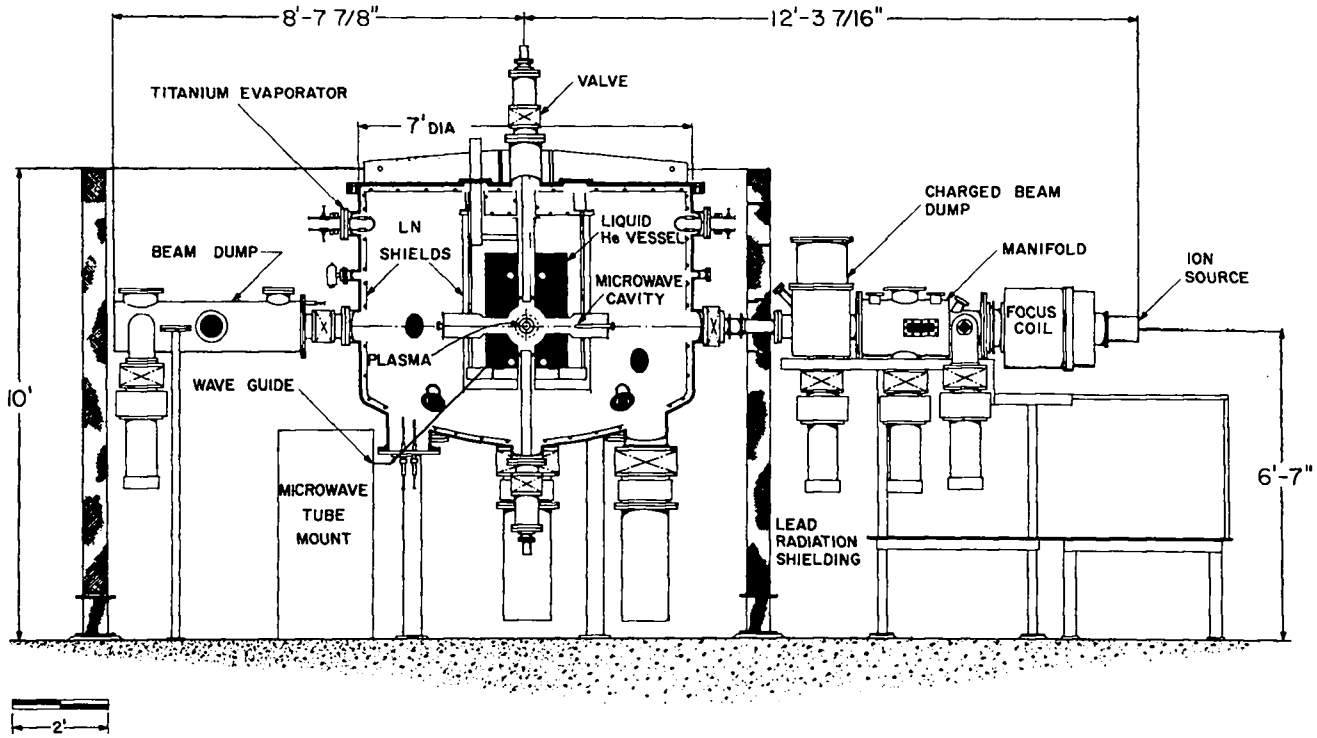

Fig. 3 (ORNL Dwg. 69-3253) Schematic diagram of the IMP facility.

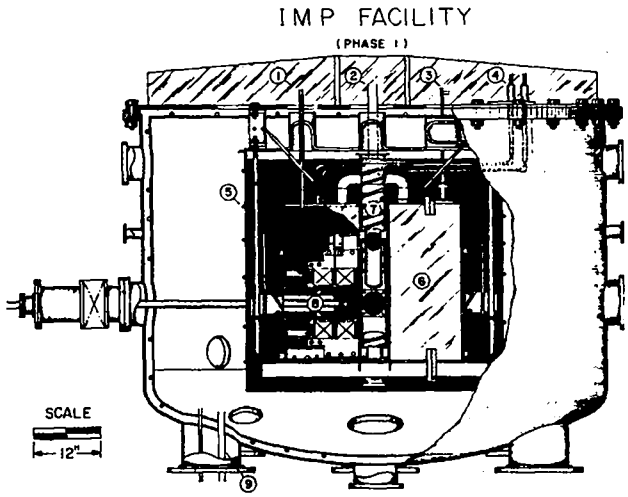

Fig. 4 (ORNL Dwg. 69-3332) Sectional view of the IMP vacuum tank showing the suspended assembly for mirror coil operation.

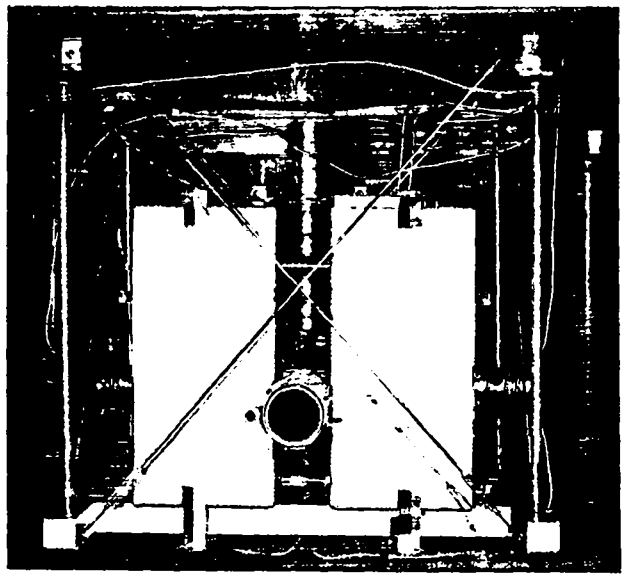

Fig. 5 (ORNL Photo 76637) Photograph of the suspended assembly minus radiation shielded.

NEW ASTRON ACCELERATOR AND MAIN CHAMBER*

Charles A. Hurley
Lawrence Radiation Laboratory
University of California
Livermore, California

ABSTRACT

Astron has gone through a remodeling period in which the main trapping chamber and the linear induction electron accelerator were completely redesigned.

Greater operating reliability combined with mechanical flexibility and accuracy were the desirable qualities included in the design criteria of the main trapping chamber. This chamber consists of an aluminum vacuum chamber approximately 90 ft long, 63 in. o.d., with 4-in.-thick water-cooled walls, supports an "infinite" solenoid coil system of 1100 gauss at the center, and accommodates 250 diagnostic port penetrations. The inside diameter of the chamber is lined with 10-ohms-per-square resistors made of 0.0015-in. tungsten wire. The chamber can be aligned to within 0.040-in. in length and can be moved by floating on a thin film of air. This chamber became operational in early February 1968.

The primary electronic requirements for the new accelerator were to increase the current output from 400 to 1000 amp, to include additional space for the diagnostics and monitoring, and to increase the energy above 4 MeV. The new accelerator is housed in a wing added to the original building and is oriented to allow injection into the main trapping chamber from the south at an angle of 94°.

The accelerator was completed early in December 1968 and the building in April 1968.

The physical design features of the accelerator consist of an increasing gradient gun followed by four constant-gradient 8-in.-bore injector sections. Fifteen identical, 20-core units, each with a 4-in. aperture, make up the remainder of the accelerator. Between these units is space for beam diagnostics, focussing, and steering.

Design changes in the gun were made to eliminate sparking. The diameter of the ceramic seals have been increased from 13 to 15-1/4 in. and the insulator length was approximately doubled. This change required the construction of a larger vacuum furnace to braze the accelerating column.

INTRODUCTION

The Astron program has been through a long modification period in which the main trapping chamber and the induction electron linear accelerator were completely redesigned. The main chamber construction was completed in early February 1968 during a 2-month shutdown. The accelerator, housed by adding a wing on the south side of the existing building, was installed while the existing accelerator continued to operate and inject into the new main chamber. During a 1-month shutdown in November 1968, the switch-over to the new accelerator took place. As can be seen in Fig. 1, injection into the main chamber is at a radius of 35 cm and an angle of 94° and is now at the bottom and on the opposite side of the chamber. In the late fall of 1969, the old accelerator will be cannibalized to extend the new accelerator from 4 to 6 MeV.

This report describes this modification

*Work performed under the auspices of the U. S. Atomic Energy Commission.

program from a mechanical engineering viewpoint.

MAIN CHAMBER

Mechanical accuracy and reliability were found to be very critical in the operation of the main chamber. These inadequacies prompted the new construction which included a new coil system, vacuum vessel, resistor hardware, and inflector.

The coil system (Fig. 2) consists of 116 individual 18-turn coils spaced on 9.6-in. centers, with a $4\frac{1}{4}$ in. gap between, for penetrating through the vacuum chamber, an important feature which did not exist in the original machine. Details of these coils will be covered by another Symposium paper.[1] The coil cross section is $4\frac{1}{4}$ in. by $1\frac{1}{2}$ in. with a 65 in. i.d. The assembly of coils develops a 1000-gauss infinite solenoid field in the region of the experiment.

The vacuum tank consists of eight 96-in.-long units and one 48-in.-long unit (the injection section). Each tank is 63 in. in o.d. with a 4-in.-thick double wall with mild bakeout and water cooling capabilities. There are approximately 250 ports penetrating the walls. These ports are designed to flex throughout the thermal cycle to minimize the stress on the weld which forms the vacuum seal.

Plates of 1100 aluminum, 2-2/3 in. thick, 8 ft wide by 20 ft long, were rolled so that only one longitudinal weld was necessary. These cylinders were machined, slipped together, end-welded, then finish-machined.

The 4-in.-thick high-conductivity wall is required to cancel or to reduce the slow time-varying field (or "ripple") created by the main magnetic dc power supplies. This field can have a disturbing effect on the E-layer buildup, if it penetrates the vacuum chamber wall.

Accurate alignment of the vacuum tanks was achieved, first, by fabricating to close tolerances and secondly, by installing a fixed optical system. The tanks are moved by floating on a thin film of air (Fig. 3). At assembly they move on air to the O-ring contact range, are lowered to rest on rollers, are then aligned using outboard targets at each end of the tanks and a system of adjustments to control horizontal, vertical, and rotational positions. The tanks are then bolted together and the alignment is rechecked. This system will allow an accuracy of 0.040 in. in approximately 100 ft.

Resistors are mounted in the i.d. of the tanks in axial rails, which have leaf springs for electrical contact. The resistors are 10 ohms per square, made of 0.0015-in. tungsten wire mounted on U-shaped stainless steel cans, 18-in. long, which have built-in springs to keep the resistor wires taut (Fig. 4).

This new main chamber design is quite successful in that it yields improved experimental results and saves operating and maintenance time.

1000-A 4-MeV INDUCTION ACCELERATOR

A high current beam of electrons is one basic requirement in the Astron program. The old accelerator had some serious limitations in this regard. Among its limitations, the inability to increase the beam current output to desired levels and the lack of diagnostics space between units and at the end of the accelerator were the most critical.

To increase the beam current, it was decided that an increase in beam focussing per unit length was the most economical approach. As a result, the accelerator sections were shortened to approximately 20 in., with 20 cores per unit. These units are constant gradient, have a 4-in. aperture, with a ceramic-to-metal vacuum seal (Fig. 5). There are 15 of these sections and each section adds about 0.19 MeV to the beam energy.

The space between these units is used for beam optics, diagnostics, and pumping. Focussing the beam is accomplished by iron-shrouded solenoid magnets, capable of fields up to 1000 gauss. Combined with these are boxes which house diagnostics gear that indicates the position and current of the beam. Cosine-type air-core coils to steer the beam and correct for the ambient earth magnetic field are spaced at approximately 12-ft intervals. Included in some of these spaces are the six vacuum pumping stations which consists of 6-in. mercury diffusion pumps, valves, and liquid nitrogen baffles, with an operating

pressure of $1\text{-}3 \times 10^{-6}$ torr (Fig. 6).

All components are mounted for easy alignment and interchangeability by using jack screws at three support points and gimbal-type mechanisms.

The injection section of the acclerator consists of a variable gradient gun with an output energy of 0.55 MeV, and four 8-in.-bore units, three of which have 22 cores and one 20 cores. These units are identical to the accelerator units except in size, and increase the beam energy 0.22 and 0.19 MeV, respectively.

The gun is installed in a pressure tank with freon at 30 psig to provide cooling and to control sparking and corona. This tank is mounted on air pads for easy handling, by a method similar to that used for the main chamber.

In an attempt to eliminate sparking, the gun has been redesigned. This redesign involved increasing the ceramic seal diameter from 13 to $15\frac{1}{4}$-in. and increasing the insulator length between electrodes, thus reducing the gradient on the ceramic from 24 to approximately 10 kV/cm. This, in effect, puts all the reentrant hardware inside the vacuum, with the advantage of easier maintenance and assembly as well as better voltage-holding characteristics (Fig. 7). There are 44 instead of 45 cores to accommodate more insulation.

To reduce the probability of freon contamination of the cathode, double O-ring seals with pump-outs are included and the sliding seal will be replaced with a bellows.

The new ceramic accelerating column is too large for the old vacuum furnace, so one has been built with the capability of heating parts 20 in. in dia by 20 in. long to 1200°C at a pressure of 2×10^{-6} torr.

Diagnostics at the end of the acclerator consists of an on-line energy analyzer (still in design), a spectrum energy analyzer, a beam chopper, and a beam emittance measuring device.

An extension of the accelerator to 6 MeV is planned in the late fall of 1969. An additional 80 ft is to be added to the building. The injection section will be moved back and additional accelerating units will be inserted ahead of the present system to give the 2-MeV increment.

REFERENCE

1. Arthur E. Harvey, "Fabrication Techniques for Recent Complex Magnet System," Lawrence Radiation Laboratory, University of California, Livermore, Report UCRL-71540, to be published in Proceedings of the Symposium of Engineering Problems of Fusion Research, 1969.

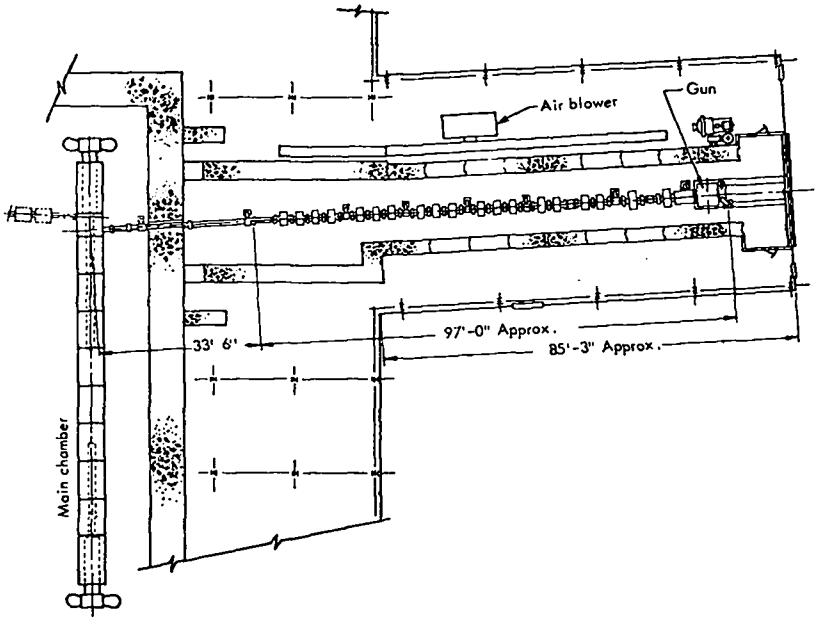

Fig. 1. Plan view of Astron Accelerator.

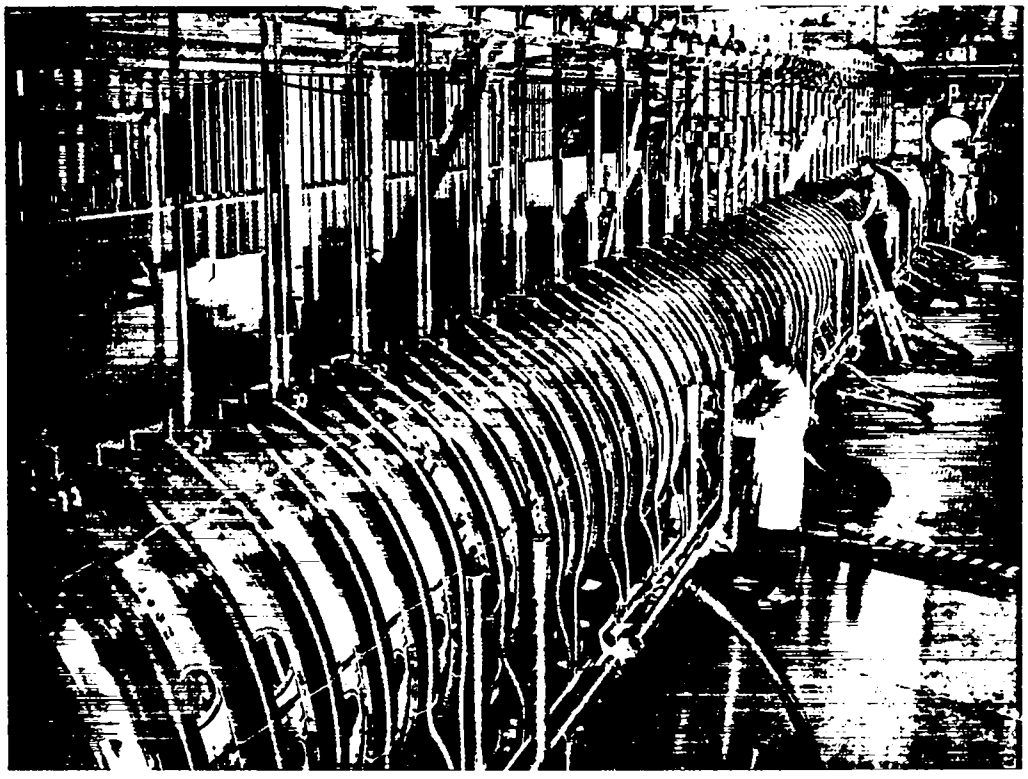

Fig. 2. Overall view of Astron main chamber.

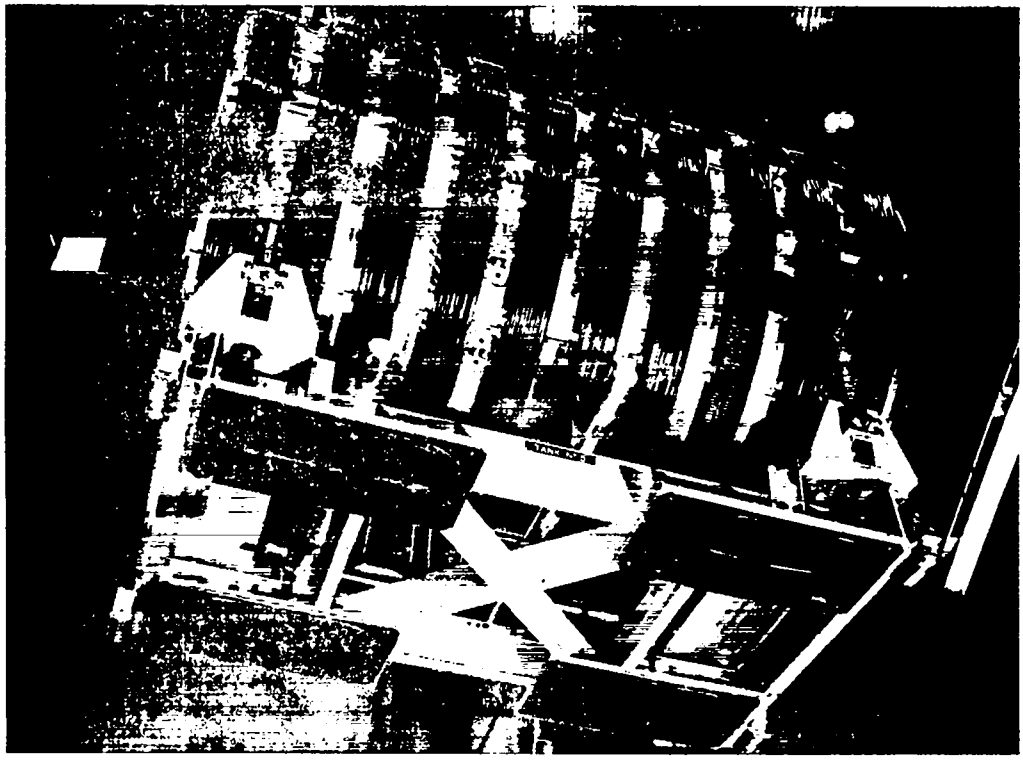

Fig. 3. Air pads for moving Astron main chamber.

Fig. 4. Resistors in Astron main chamber tank.

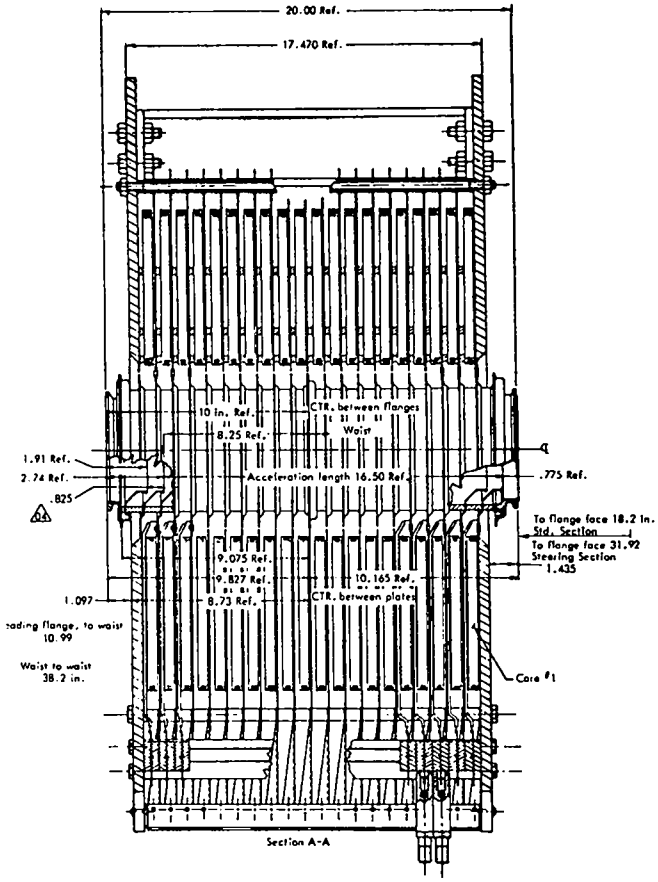

Fig. 5. Cross section of accelerating 20-core unit.

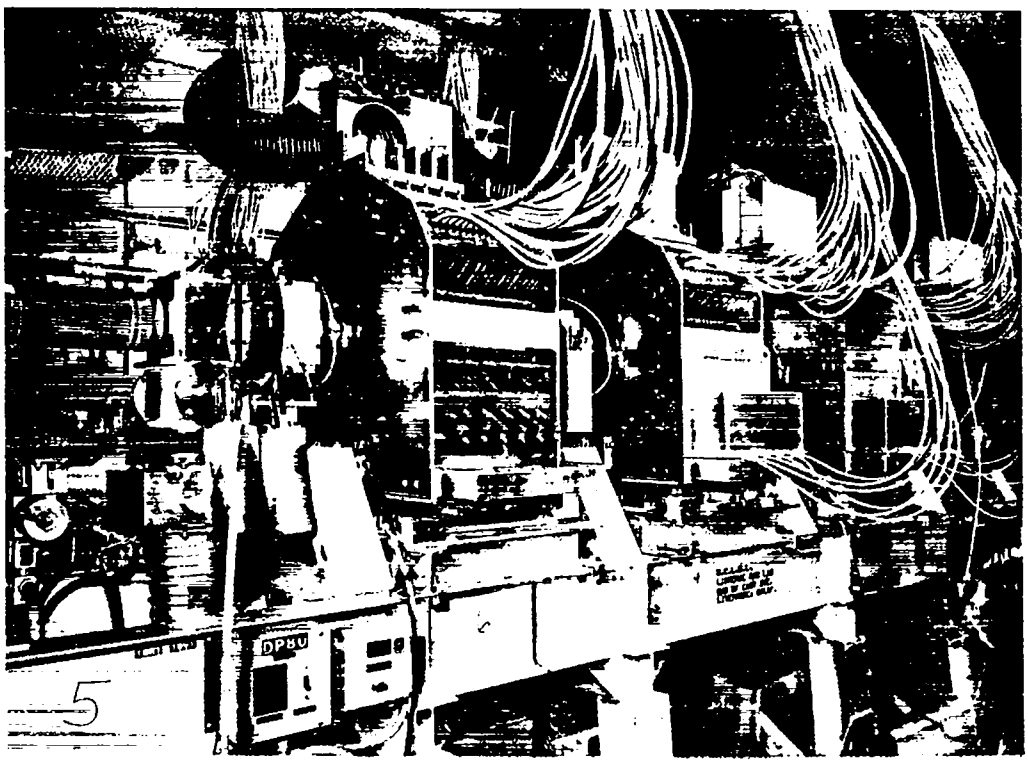

Fig. 6. Accelerator pump and diagnostic station.

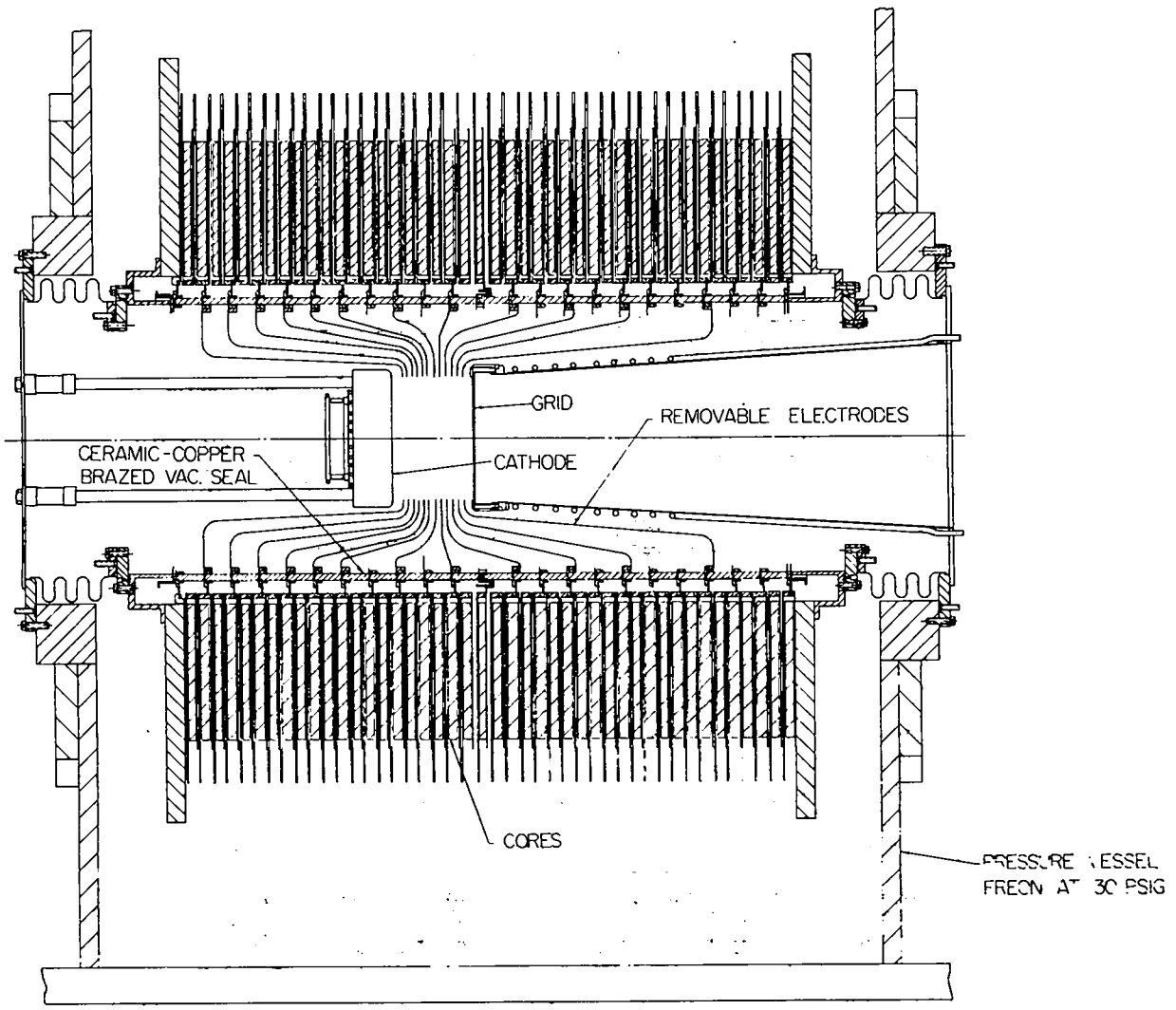
GRID
REMOVABLE ELECTRODES
CERAMIC-COPPER
BRAZED VAC. SEAL
CATHODE
CORES
PRESSURE VESSEL
FREON AT 30 PSIG

Fig. 7. New gun.

TECHNOLOGICAL PROBLEMS ASSOCIATED WITH THE ADDITION OF A HARD CORE TO THE PHAROS 2 MJ θ-PINCH

by

Marvin P. Young
Plasma Physics Division
Naval Research Laboratory
Washington, D.C. 20390

ABSTRACT

An axial current conductor (hard core) has been added to the Pharos θ-pinch facility for a series of stability experiments. The axial conductor is made from thick-walled aluminum tubing (1.27-cm outside diameter and 0.16-cm wall thickness). It is wrapped with Mylar and polyethylene and further insulated from the plasma by a quartz tube (2.1-cm outside diameter and 0.3-cm wall thickness) which forms the inner wall of the plasma-containment vessel. An adjustable-tension wire structure inside the 335-cm-long conductor eliminates its sag, and an overall axial alignment of less than ±1 mm is maintained.

A 700-kJ, 100-kV capacitor bank supplies the energy for the hard-core circuit. The bank, assembled from 20-kV capacitors and switches, operates as a five-stage Marx-type circuit to generate the required 100-kV energy source.

An oil-filled coaxial 100-kV current collector terminates the 28 coaxial cables from the parallel capacitor bank sections and mechanically supports the axial conductor.

A molded polyurethane housing with an inflatable chamber to affect a constricting O-ring surface provides a vacuum seal for the ends of the plasma-containment tubes. This technique allows quick assembly and eliminates the heretofore required close tolerances of eccentricity and outside diameter of the large quartz tubes.

INTRODUCTION

Magnetic-compression experiments, relating to controlled thermonuclear research, have been performed continuously in the Pharos[1] 2-MJ facility since 1961. A number of additions and changes of major features have been made to investigate various facets of plasma confinement[2,3,4,5]. An axial current conductor (hard core) has now been added, and a new series of experiments is presently being conducted[6,7,8] to explore the possibility of shear stabilization in high-β plasmas.

Concurrent with the hard-core addition, the Z-field load coil inside diameter was increased to 18.4 cm, the plasma-containment tube inside diameter was increased to 17 cm, and mounting techniques were included that allowed proper coil segment alignment and eliminated the causes of the previous collector-plate failures. Two rooms were added in close proximity to the experimental area to house the 700-kJ hard-core capacitor bank.

HARD-CORE CIRCUIT DESIGN CRITERIA

A hard-core current pulse is required which will produce a θ-magnetic field at the inner surface of the plasma that is equal in rise time and amplitude to the Z magnetic field at the outer surface of the plasma. The Z field is generated by the 2-MJ energy-storage bank and load coils. A full energy discharge current pulse of 11 MA, with a 25-μsec rise time and subsequently clamped to give a 200-μsec decay time constant, generates a peak Z field of about 70 kG.

Due to the mechanical configuration, the hard core and return current conductor will have a self-inductance of approximately 1.5 μH. Assuming a 2.5-μH total circuit inductance and a current of 1 MA, the corresponding L(di/dt) = 100 kV. Therefore, a 1-MJ energy source operating at 100 kV to produce a 1-MA current pulse is required to produce the θ-field.

ENERGY STORAGE BANK DESIGN

The economic and time advantage gained by use of an existing 1 MJ of 20-kV capacitors and high-voltage power supply, proven designs and experience with 20-kV starting switches, clamp switches, and trigger system influenced the design of the energy-storage bank. We therefore built a bank consisting of 28 parallel sections of Marx-type circuits (Fig. 1). Each section has five 20-kV series stages to give a 100-kV output pulse.

Erection of the Marx-type circuit is initiated by triggering the starting switches[9] of the first two stages.

The extreme insulation requirements for a trigger system for the advanced stages of a Marx-type circuit led us to develop self-contained trigger circuits[10] for the clamp switches[11]. These units, mounted piggy back on each clamp switch and using energy from the charged bank, initiates a trigger automatically at the first current maximum of the bank discharge.

THE PLASMA CONTAINMENT ARRANGEMENT

The plasma-containment tube, θ-coils, and hard-core load conductors are shown in Fig. 2.

The vacuum seal and hard-core support on the high-voltage input end is a flexible polyurethane housing with constricting O-ring surfaces. After the housing is easily placed on the tube, it is inflated to constringe the O-ring surfaces. This housing permits greater diameter and roundness tolerances for the quartz tubes, provides the necessary electrical insulation, and provides shock absorption of the pulsed forces transmitted between the ends of the inner and outer quartz tubes.

The hard core consists of a 335-cm-long aluminum tubing (1.27-cm outside diameter and 0.16-cm-thick wall). The type 606IT-6 aluminum has a resistivity of 4.31 microhms-centimeter, which gives a resistance for the hard core of 4 milliohms. Numerous high-current contact arrangements were used. The most satisfactory for both mechanical assembly and current-carrying capability was the compressed split-ring type of the Imperial fittings. The line-current density at this connection point is 250 kA/cm.

Axial alignment of the 335-cm-long aluminum tube to better than ±1 mm at each coil slot is achieved by an adjustable-tension-wire structure inside the 1.27-cm-diameter hard-core tube. The alignment is verified by a cathetometer and mirror arrangement. Field penetration of the aluminum tubing for the 25-μsec, 1/2-cycle pulse is insignificant; thus no current flows on the wire bridge supports, and no arcing is observed there. The self-swaging forces for a 350-kA pulse were enough to collapse the thin wall (0.09-cm) aluminum tubing initially used.

DIFFICULTIES IN BANK OPERATION

Isolating the 100-kV high-energy pulse from ac power lines, control cables,

etc., in the small capacitor bank rooms was a very difficult task. We therefore eliminated all cables to the capacitor bank room except the three basic ones: (a) charge, (b) trigger, (c) discharge. The bank is charged through a single RG 17/AU coax cable from the externally located 20-kV charging power supply. An air-actuated relay in the bank room switches from charge position to grounded position. A single RG 8 cable brings a trigger pulse from the control room to a self-contained trigger-distribution system inside the capacitor bank room. Energy for the trigger system is taken from the hard-core main bank capacitors and comes on automatically with the bank. A single RG 218/U cable connects the output of each section of Marx-type circuit to the load.

The trigatron starting switch on each stage of the Marx-type circuit was designed as a triggered switch. Used in this way on the first two stages, it operates satisfactorily. Used as an overvoltaged switch in the last three stages, it deteriorates very fast. The failure point is the insulating plate behind the electrodes. This plate must be replaced about every 50 shots to give a satisfactorily low prefire rate.

The ground returns under the capacitors cover the entire floor of the capacitor bank room. To cover this large area, it was necessary to use parallel sheets. Small electrical sparks between parallel ground sheets closely spaced eventually burned through the insulation and allowed a direct breakdown, with catastrophic results. The parallel sheets are now either solidly connected or well insulated with spark-resistant insulation included at the joints.

The vacuum switch clamp system has operated satisfactorily on six sections; however, they are considered too poor in prefire reliability to use for the complete system (140 switches). Vacuum clamp switches used directly on the capacitors will inherently prefire during the bank charge; however, this action cleans the vacuum switch, and performance improves after a few initial prefires. In their use on the Marx-type circuit, a clamp-switch prefire will cause the complete Marx section to pre-erect, and the resulting high-energy discharge through a single vacuum switch will tend to reduce its life drastically rather than clean it up. The vacuum clamp system has been removed, and a single solid-dielectric type switch is being considered.[12]

DIFFICULTIES IN THE TRANSMISSION LINE AND COAXIAL COLLECTOR

Figure 3 shows the initial capacitor bank, transmission line, and load arrangement. This arrangement eliminated a rotation of the 100-kV flat-plate transmission line that would be required for the upstairs capacitor bank if its ground return did not pass under the capacitors.

The current return conductors are symmetrical, which results in symmetrical magnetic forces on the hard core. However, if either the upstairs or the downstairs bank fires independently, the force from the asymmetrical current would break the plasma-containment tube. A coaxial current collector is now being used so that the return currents are always symmetrical (Fig. 2). In this arrangement, RG 218/U coaxial cable replaces the flat-plate transmission line, which suffered numerous failures. Most failures were caused by surface flashover due to various debris on the insulation from the experimental area, and dielectric breakthrough at sharp edges and junction points of the conductors. We have experienced no failures in the RG 218/U coaxial cables.

After experiencing two catastropic failures of the coaxial collector assembly, it became evident that the static 150-percent voltage tests (both in air and

5-psi freon) with a high-impedance power supply were inappropriate. Subsequent breakdowns with the high-energy bank completely ionized the freon and disintegrated the chamber. The chamber is presently filled with oil, and no failures have occurred.

PRESENT SITUATION

Plasma-instability studies are presently being made at reduced energies (150 kJ) to optimize the early time and amplitude relationships between reverse field, θ-pinch field, and hard-core field. Approximately 1500 discharges have been made at this energy. The parallel operation of Marx-type circuits with the corresponding stages of each section directly strapped together has been achieved. Out-of-phase erections, reverse erections resulting from prefires in other sections, and erections both ways from center stages will occur but without catastrophic results.

Changes in the design and adjustment of the circuit parameters continue to be made as required to assure a reliable operating system and to meet the changing demands of the physics program.

REFERENCES

[1] Kolb, A.C., and Lupton, W.H., "A Pulsed-Field Plasma Experiment - PHAROS in High Magnetic Fields", Proc. of the International Conf. on High Magnetic Fields, Mass. Inst. of Tech., Cambridge, Mass., Nov. 1961, Cambridge MIT Press, pp 693-700, 1962.

[2] Hintz, E., Kolb, A.C., Lupton, W.H., Griem, H.R., "Drift of a θ-Pinch in a Ioffe Multipole Field", Physics of Fluids, Vol. 7:153-154 (Jan. 1964).

[3] Hintz, E., Kolb, A.C. and Lupton, W.H., "Some Technological Problems in the NRL θ-Pinch Program," Third Symposium on Engineering Problems of Thermonuclear Res., Munich, Germany, June 1964.

[4] Young, M.P., Lupton, W.H., and Kolb, A.C., "Clamp System for the Pharos 2-MJ Capacitor Bank" NRL Report 6422, Jan. 25, 1967.

[5] Young, M.P., "Operating Experience with the PHAROS 2-MJ Magnetic Compression Experiment" 4th Symposium on Engr. Prob. in Thermonuclear Res., Rome, Italy, May 1966.

[6] Kolb, A.C., McLean, E.A., Elton, R.C., Griem, H.R. and Young, M.P., "Recent Studies in a Large Theta-Pinch with Reverse Trapped Magnetic Fields", Ninth Annual APS-DPP Meeting, Austin, Tex. November 1967.

[7] Kolb, A.C., Young, M.P., McLean, E.A., "Hard Core Theta-Pinch with Reversed Trapped Magnetic Fields", APS Topical Conf. on Pulsed High Density Plasma, Los Alamos, N. Mex., Sept. 1967.

[8] Kolb, A.C., Dixon, R.H., Dűchs, D. Elton, R.C., Young, M.P. "Confinement of High-β Plasma in Pulsed Toroidal System with High Shear", Third Conf. on Plasma Physics and Controlled Nuclear Fusion Res., Novosibirsk, USSR, 1-7 Aug. 1968.

[9] Lupton, W.H. "Fast Triggered Spark Switches for a Two Megajoule Capacitor Bank", Proc. Fifth International Conf. on Ionization Phenomena in Gases, Munich, Germany, 1961; Amsterdam North Holland Publishing Co., Vol. II, pp 2059-2068, 1962.

[10] Young, M.P., "The Pharos Hard Core Experiment and its 700 kJ Marx Circuit Capacitor Bank" Fifth Symposium on Fusion Tech., Oxford, England, 2-5 July 1968.

[11] Young, M.P., "A 5-kJ Vacuum Clamp Switch for the PHAROS 2 MJ Capacitor Bank", NRL Report 6418, Aug. 31, 1966.

[12] Kopoplus, P., "A Fast Metal-to-Metal Switch with 0.1 μsec Jitter Time", Fifth Symposium on Fusion Tech., Oxford, Eng., 2-5 July 1968.

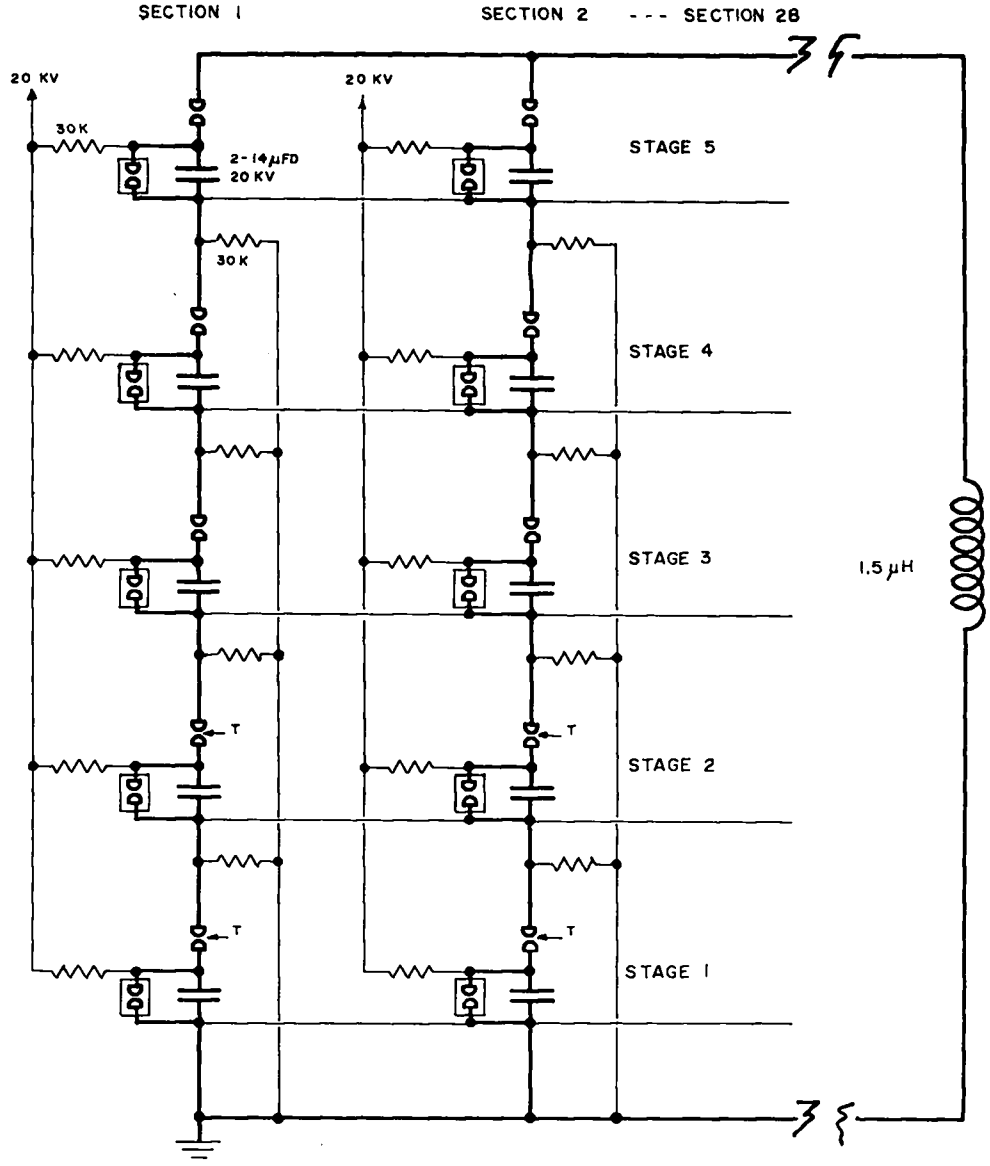

FIGURE 1. 100-kilovolt Marx-type bank circuit schematic

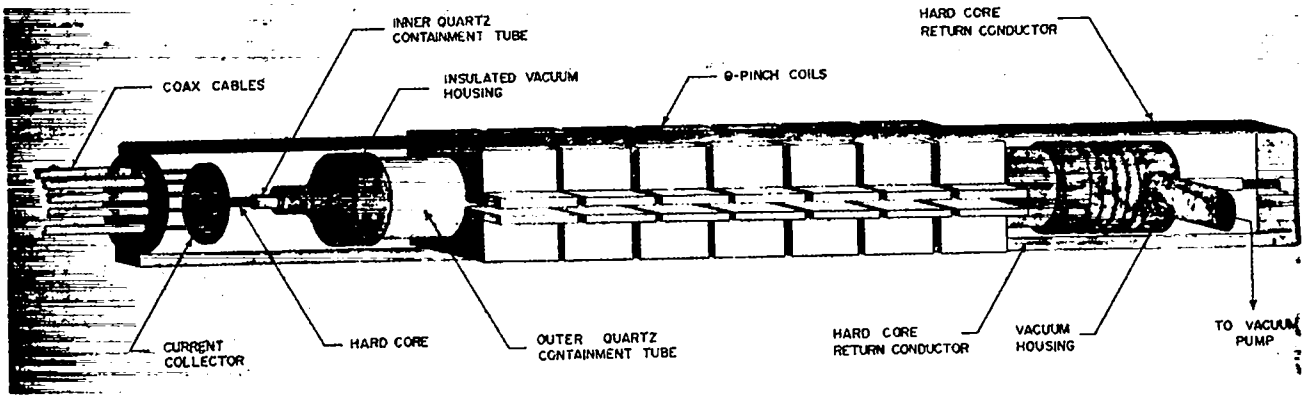

FIGURE 2. Arrangement of containment tube, θ-coils and hard-core conductor

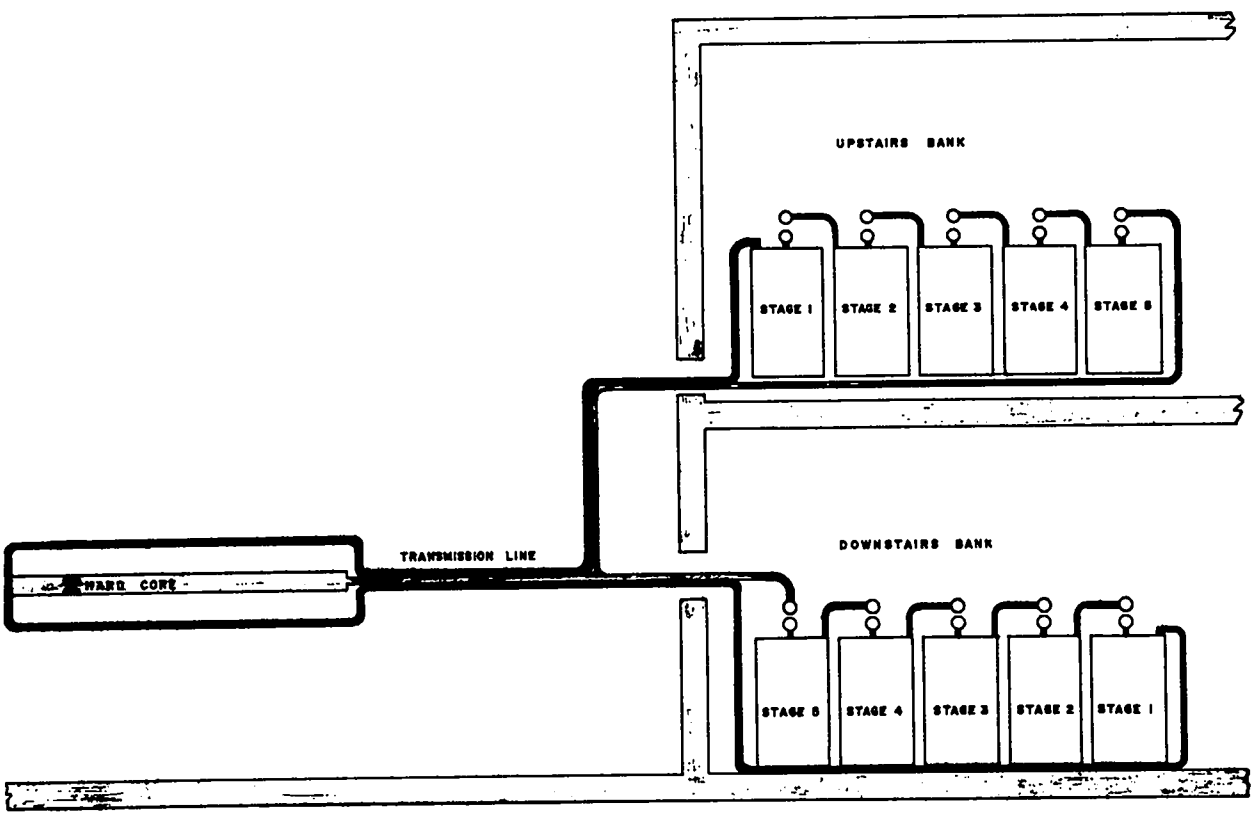

FIGURE 3. Undesirable hard core circuit arrangement (asymmetric load current following prefire)

SOME REMARKS ON THE ENGINEERING PROBLEMS ENCOUNTERED IN THE CHALICE EXPERIMENT*

by

G. J. Yevick, R. Harvey, W. Carr, and J. Karol
Stevens Institute of Technology
Hoboken, New Jersey

ABSTRACT

The Chalice experiment[1] involves the production of hot dense plasma by means of two θ-pinches. The plasma is then injected into a cusp field for long time confinement. A description of the new electrical tie-up is presented along with a novel self-crowbarring, metallic contact, solid dielectric series switch. A modular coil-switch system, now operating at 20 kV and 1.5 megamps, has been designed and tested. Diagnostic measurements have included density measurements, with a Mach-Zehnder and temperature measurements making use of the C_V line. In order to increase the sensitivity of the density measurement a Michelson interferometer has been built and tested. For temperature measurements, Thompson scattering will be performed. Serious thought has gone into finding an inexpensive, powerful, easy-to-handle method for measuring the space-velocity distribution function $f_n(\vec{x},\vec{v},t)$ for both ions and electrons. At the present time, the density $\rho(\vec{x},t) = \int f(\vec{x},v,t)\, d\,v$ is measured somewhat crudely with a Mach-Zehnder. Thompson scattering does provide information on the velocity distribution and in principle could yield $f(\vec{x},\vec{v},t)$. The possibility of using two different frequencies and picking up the beat is now being investigated and preliminary theoretical analysis indicates considerable promise in this direction.

Introduction

The Chalice experiment[1] is a high density, high temperature experiment which in essence attempts to confine the hot plasma produced by two fast θ-pinches in a cusp field for as long a time as possible.

The engineering problems encountered in building the system have been described elsewhere [2,3]. Genuine improvements in switching[4] over the past year have resulted in improved performance of the system. Along with this, a new effective means for high voltage isolation by means of an air core transformer have been developed and the data on this is presented in a separate paper in these Proceedings[4].

Our major effort, however, no longer lies in engineering and building components but rather in concerning ourselves with inexpensive, powerful easy-to-handle diagnostic tools. Needless to say, the going has been rough.

The basic physical data that we would like to measure, subject to the three engineering criteria of low cost, powerful in scope, and easy to handle, is the position-velocity distribution function for both electrons (n = 1) and ions (n = 2) as a function of time, i.e. $f_n(\vec{x},\vec{v},t)$. If we know these two distribution functions for a plasma, we indeed know a great deal and can begin to understand the complex behavior characterizing a plasma. It is important to stress, however, that history may prove that this may not be enough and that a deeper probing of the plasma will be required; e.g. it may become necessary to measure the two-body time-dependent correlation function.

Present Chalice System

Fig. (1) shows a schematic diagram of Project Chalice as it now is electrically tied together. The fundamental changes made in the old system[3] are (a) the two-coils of the θ-pinch are now energized by the same switch so that there is

absolutely no question as to whether one θ-pinch fires before the other, (b) the single switch on the fast θ-pinch bank acts also as both series and crowbar switch (see below).

Fig. (2) is a close-up view of the experimental area of Chalice. Because of the mini size of Chalice, the volume available for diagnostics is small, and great ingenuity must be exercised in order to fit the diagnostic equipment around the plasma chamber.

Self-Crowbarring Solid-Dielectric Switch with Metallic Crowbar[4]

Because the coils are connected in anti-parallel, only a single series switch is required to activate them (See Fig. (1)). Since the inductance of the θ-pinch bank is around 3 nh, an extremely low inductance switch is necessary, and this is why considerable work has gone into dielectric switching. Following the pioneering work done at Los Alamos[5], we now crowbar our system using metallic contact. Fortunately, Chalice is so constituted that the gases generated by the series switch can be used to drive the aluminum electrode.

Fig. (3) is a schematic diagram of the self-crowbarring solid dielectric switch system in the arc mode without the use of metallic contact. Fig. (4) shows more clearly the folding arrangement for the metal-metal mode of self crowbarring; and Fig. (5) illustrates the typical decay time involved. Peak currents of 1.5 megamps have been handled and the switch has been operated between 5 and 20 kV. The closing time of the crowbar is very short, around 1 μsecond, and can be regulated by varying the thickness of the dielectric. The e-folding time of the current is 27 μsec. Single channel resistance is measured to be 0.26 milliohms and the inductance of the single channel crowbar 0.4 nanohenries.

New Coil Configuration

The present coil configuration is 10 inches long and 1.5 inches in diameter. It is constructed in modular form so that it can easily be taken out and put back in. A precision-built fiber glass box serves as a mold into which accurately epoxied interchangeable coils can be placed. Fig. (6) shows the fiberglass strong-box with cusp coils for a 2.5" assembly. Fig. (7) is a photograph of a large diameter assembly. Fig. (8) shows the 1.5 inch assembly now in operation along with a top view of the switch.

Magnetic Fields

At the present time, the θ-pinch bank is operating at 20 kV and the cusp bank at 10 kV. The preheater is fired at around 7 kV. The various magnetic fields for different voltages and positions is shown in Table 1.

TABLE 1

MAGNETIC FIELDS FOR 1.5" COILS

Cusp Bank	B (Line Escape)	B (Point Escape)	B Center of θ-Coils
10 kV	52	46	24 kg
θ-Pinch Bank			
20 kV	10	20	40 kg

DIAGNOSTICS

Density Measurements

The density of the plasma has been measured with a vertical Mach-Zehnder suspended with rubber bands for mechanical isolation. Direct viewing through the cusp allows density measurements in the cusp alone. Unfortunately, because the length of the plasma in the cusp is very short, only a fraction of a fringe is measured even for high densities ($n \approx 5 \times 10^{16}$ particles/cm^3). In order to increase the sensitivity, a Michelson interferometer (See Fig. (9)) has been built which allows a double transit of the light.

Temperature Measurements

Temperature measurements using the decay time of C_V line have given us some indication of the temperature. In order to improve on this data, we have commenced to build the apparatus for a Thompson scattering experiment. A separate paper[6] on this subject is presented in this Symposium. Unfortunately a high powered laser and a number of expensive photomultipliers apparently cannot be avoided in this experiment.

Some Remarks on Diagnostics

In Thompson scattering, using a finely focussed beam, and measuring in different directions at different positions, we can theoretically evaluate the one body space-velocity distribution (certainly for electrons). This would be very difficult in practice. The ion distribution function is even more difficult to measure. Using two different wavelengths and measuring the beat frequency, the full fourier transform of the spatial one body distribution function plus the velocity distribution with only one integration in the direction of the cross product of the two vectors involved can be obtained.

References

1. For a more detailed description on the nature of the Chalice experiments see Proc. of APS Topical Conference on Pulsed High Density Plasmas Sept. 19-22, 1567. Los Alamos Report LA 3770, paper A6.
2. Proc. of 1965 Symposium on Eng. Problems of CTR, Lawrence Radiation Lab., Livermore, Conf. 650512 p. 35.
3. Proc. of 1966 Symposium in Eng. Problems of CTR, Oak Ridge Nat. Lab., CONF 661016 p. 206.
4. Air Core Transformer for Chalice, R. Harvey, this symposium.
5. Finlayson, V. A., Bull. of APS 13, 557, 1968.
6. Data Acquisition for Thompson Scattering Experiment on Chalice, W. Carr, this symposium.

---

* Supported by the Atomic Energy Commission.

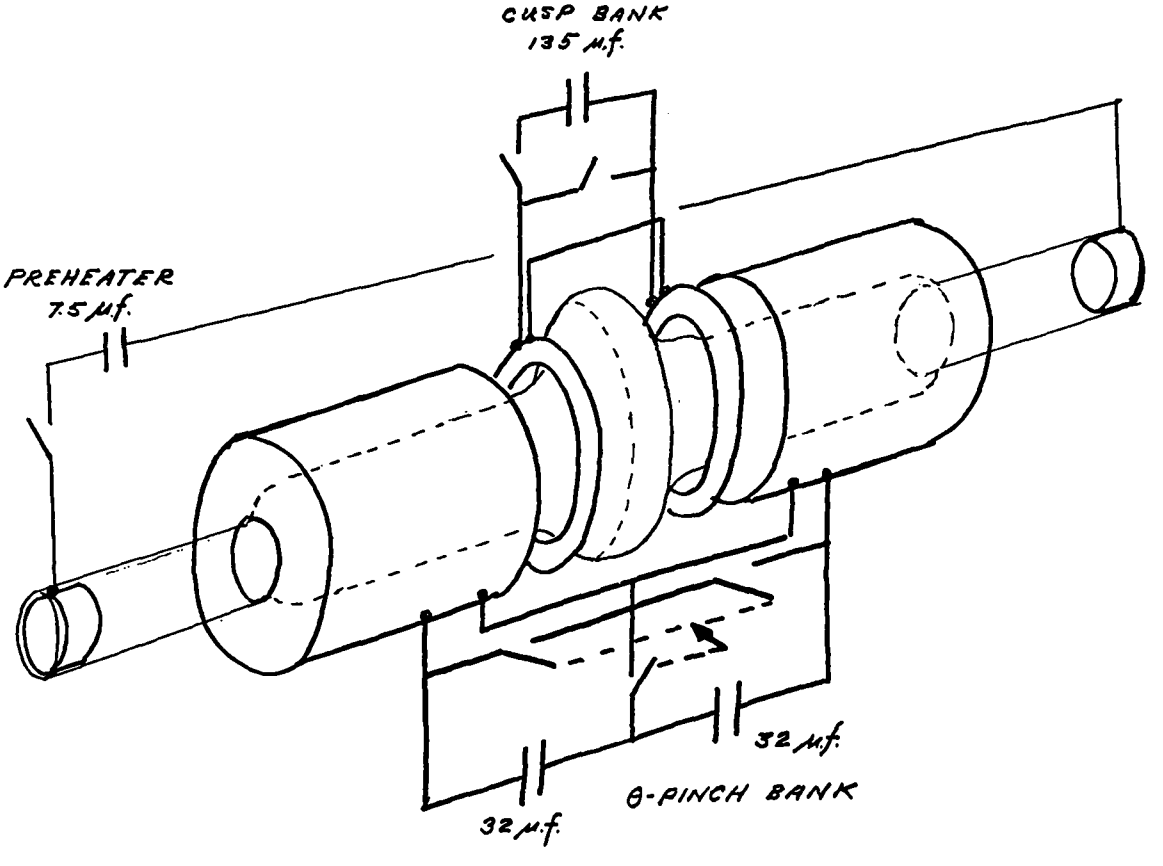

Fig. (1) Schematic Diagram of Project Chalice.

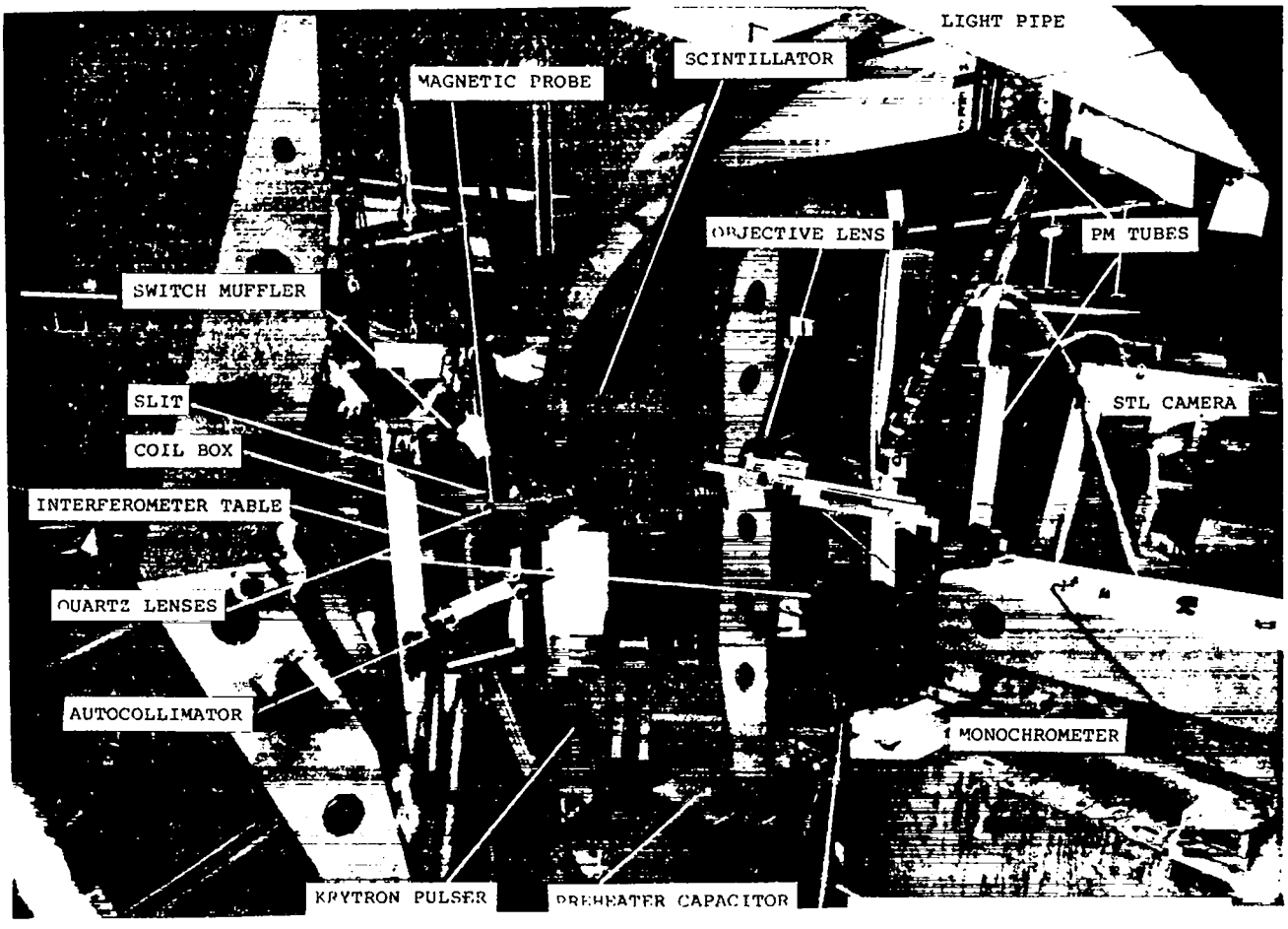

Fig. (2) General View of Experimental Set-Up in Chalice.

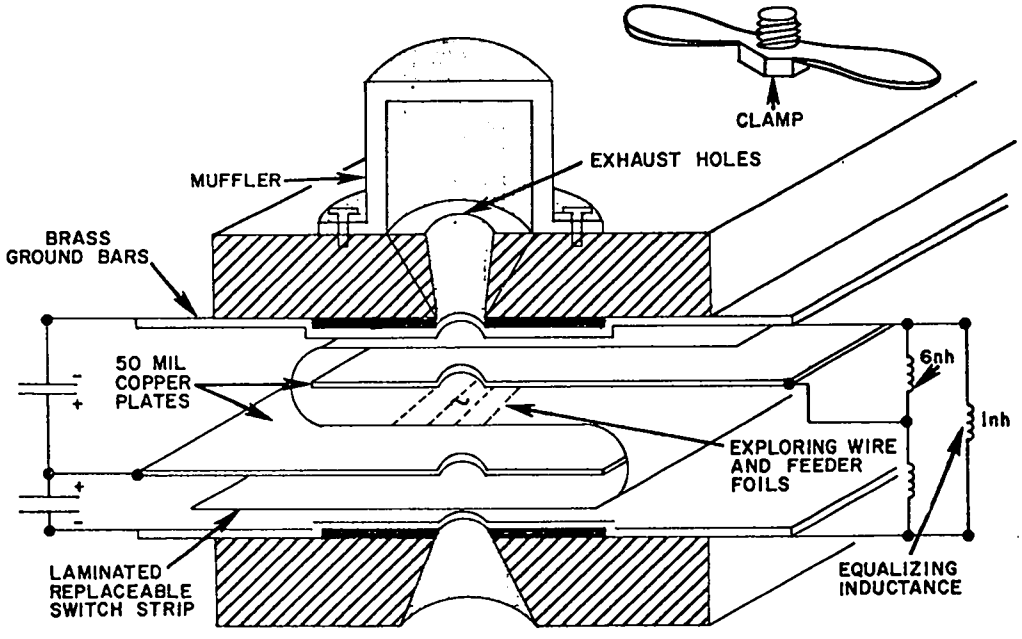

Fig. (3) Schematic Diagram Showing Cross Section of Arc Mode for Self-Crowbarring Solid Dielectric Switch System.

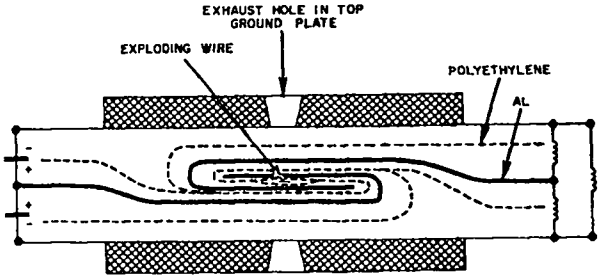

Fig. (4) Schematic Diagram Showing Metal-Metal Mode of Self Crowbarring Solid Dielectric Switch System and Replaceable Folded Insert.

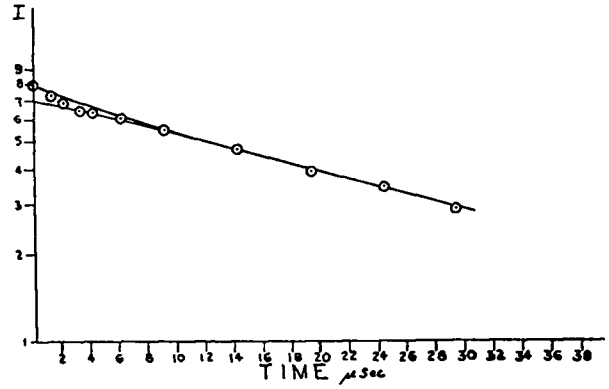

Fig. (5) Current vs. Time for Self-Crowbarring Solid Dielectric Switch.

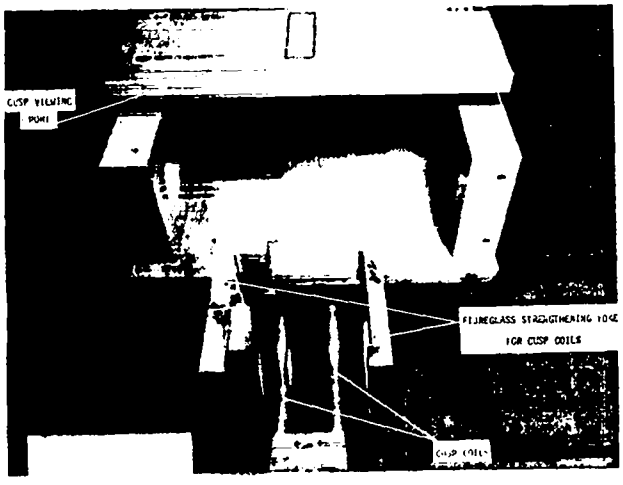

Fig. (6) Fiberglass Strongbox Larger Diameter Tube Assembly.

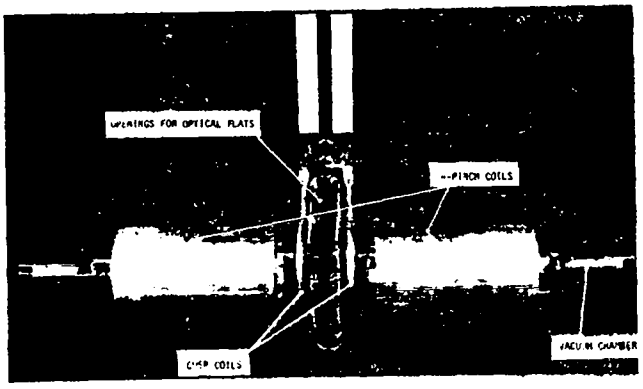

Fig. (7) Large Diameter Coil Assembly with 2.5 Inch Diameter Chamber.

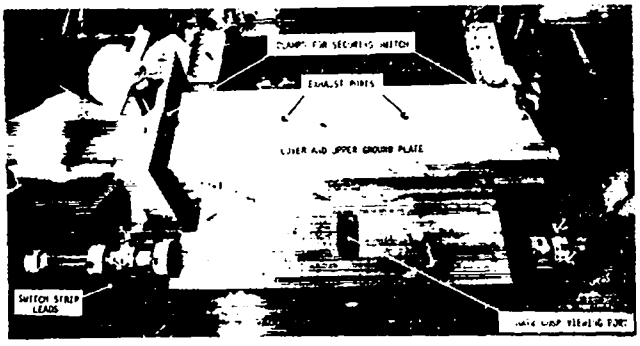

Fig. (8) Top View of Modular Series-Crowbar Solid Dielectric Switch in the Chalice Bank System Along with Coil Assembly.

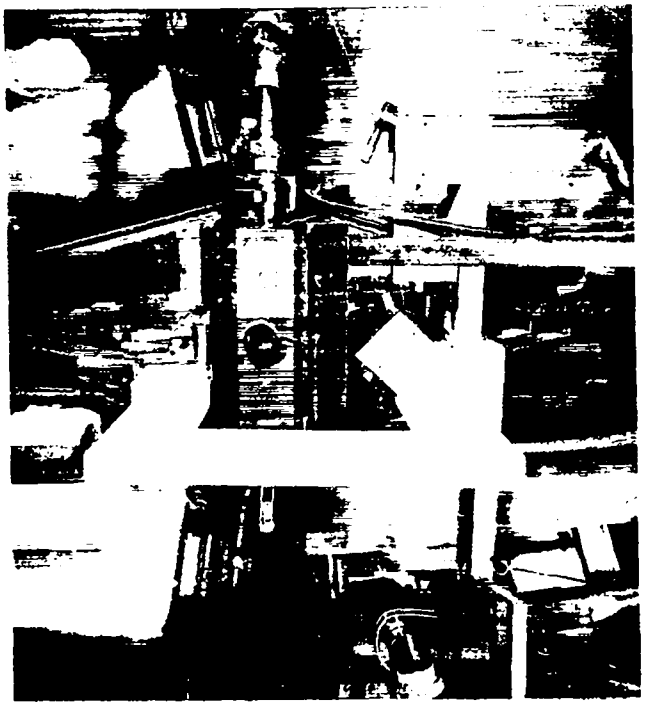

Fig. (9) Michelson Interferometer.

CAPACITOR DEVELOPMENT FOR SCYLLAC*

by

Grenfell P. Boicourt

Los Alamos Scientific Laboratory, University of California
Los Alamos, New Mexico

ABSTRACT

The capacitor requirements for Scyllac are described. The history of the development of the 1.85-μF, 60-kV primary bank capacitor is covered in detail. During the development of this unit, it was found that many areas were not being properly controlled during manufacture. As a result it is felt that the successful development of the 1.85-μF capacitor has resulted in a significant upgrading of general manufacturing practices. The life characteristics and electrical products of the 1.85-μF, 60-kV unit are given. Some attention is given to the developmental problem of high density B_o capacitors, the preionization capacitor, and high-Q stabilization capacitor.

I. INTRODUCTION

Scyllac is the latest in a series of theta-pinch machines built at Los Alamos Scientific Laboratory. The Scyllac proposal[1] describes the aims of the machine. In a very general way Scyllac is intended to duplicate the plasma characteristics of Scylla IV[2] while at the same time reducing the end losses from the plasma. The overall engineering aspects of Scyllac have been described by E. L. Kemp in References 3 and 4. What I propose to discuss here are the capacitor requirements for Scyllac. The four main types of capacitors required are the primary bank capacitor which supplies the energy for the main discharge; the B_o capacitor, so-called because it supplies the energy for the bias magnetic field; the preionization capacitor which is discharged before the main bank to preionize the gas in the discharge tube; and the high-Q stabilization capacitor which is intended as the energy source for a rapidly oscillating stabilization system.

II. DEVELOPMENT PROCEDURE

In May 1966 a meeting was held in Los Alamos to discuss the Scyllac capacitor requirements with the capacitor manufacturers. Eight manufacturers sent representatives to this meeting. The ground rules for qualification to bid on future capacitor orders for Scyllac were laid down at this meeting. The procedure was as follows: Upon receipt of word from a manufacturer that he wished to qualify to supply a given capacitor, we would buy two to four tender-loving-care prototype units. These units would be given a standard qualification test. If these units performed satisfactorily, an order for 25 production units would be made. Qualification to bid on Scyllac orders was to be contingent on the satisfactory performance of this 25-unit sample. Units which failed during testing were to be given postmortem examinations to determine the cause of

* Work performed under the auspices of the U. S. Atomic Energy Commission.

failure, if possible. Information obtained from these examinations would be channeled back to the manufacturer to be used in the design and manufacture of subsequent units. Both steps of the procedure, the small group of T.L.C. units followed by a production lot, were found to be justified by later events.

III. PRIMARY BANK CAPACITOR DEVELOPMENT

We now turn to a detailed look at the development of the primary bank capacitor. The primary bank capacitor originally assumed in Ref. 1 was to be a 60-kV, 2-μF, low-inductance unit similar to the existing 50-kV, 2-μF unit supplied by several manufacturers. The Scyllac primary bank voltage was increased to 60 kV from the 50 kV used in Scylla IV to offset the loss in transfer efficiency which was expected to result from the use of longer transmission lines to the load. The longer lines themselves were due to the 15-fold increase in total bank size. It was hoped that the case size, the low-inductance, and the 85% voltage reversal capabilities of the 50-kV capacitor could be retained. For reasons which will be given in the sequel, the specification was subsequently changed to 1.85 μF at 60 kV.

When we first started on this development we expected only a few individual production problems since the proposed 60-kV unit design was in essence a copy of the 2-μF, 50-kV unit used in the Scylla IV primary bank. The original 50-kV unit, Fig. 1, was developed jointly by several capacitor manufacturers and Los Alamos specifically for Scylla IV. The original unit installed in Scylla IV had a diphenyl impregnant and exhibited a life of the order of 3,000 to 4,000 shots in our standard test. After units had been delivered for Scylla IV, the impregnant was changed to castor oil with a dramatic increase in pulse life. Figure 2 shows a schematic of this unit.

Life test data is taken in our standard capacitor-cable test system. The capacitor is constant-current charged to its rated voltage then discharged through six series cables which connect to a small doubling capacitor with load cables connected to it. (See Fig. 3). The test repetition rate is 6 pulses per minute. The main discharge oscillation, so far as the capacitor is concerned, involves the capacitor and the load cables which are shorted fifty-foot lengths of RG 218/U. This oscillation has a period of approximately 13 μsec. The capacitor voltage reversal in the test is 85%. We feel that it is desirable to maintain this voltage reversal requirement even though it is expected that Scyllac will be crowbarred since it seems inevitable that there will be system malfunctions which result in the capacitors being subjected to equal or worse transients. It is known that a suitable decrease in the allowed reversal would result in a ten-fold, perhaps even a hundred-fold, increase in life of these units. The test system is described in more detail in Ref. 6.

Figure 4 shows a Weibull plot of life data on a set of 2-μF, 50-kV castor oil-impregnated capacitors along with the 90% confidence band. The median life of this sample is 76,000 shots and the distribution displays an 18,000-shot positive location parameter. It was the existence of this relatively large location parameter which made the step up to 60 kV appear easy, for it indicates that failures earlier than 18,000 shots are not to be expected from the 50-kV unit. A theta-pinch experimental apparatus is rarely used more than 3000 shots per year and thus the life of the apparatus is quite likely to be shorter than the capacitors. It thus seemed reasonable to try to get a unit for Scyllac with a location parameter of approximately 10,000 shots. This was to be accomplished by adding one section to the 8-section, 50-kV winding and allowing the pad stress to increase to keep the capacity unchanged. Our data indicates that the pad life is inversely proportional to the 8th power of the charge voltage in our test so we expected that the Weibull median life would decrease mainly at the expense of the location parameter. One other seemingly minor change was made, the interior margins were reduced from 1" to 3/4" in order to help keep the capacity up.

The first two units delivered to this specification operated well but as other manufacturers delivered, it became quite apparent that something was badly wrong either with the design of the units or the manufacturing procedure. Painstaking postmortem examinations were made on virtually all units after failure. It was soon obvious that at least part of the problem was due to poor manufacturing quality control. Among the problems of this sort which were found to have caused failure in the dissected units

were low impregnant level, missing sheets of dielectric, missing foils, excessive wrinkling, shorted foils, poor solder connections, dirt in the winding, damaged major insulation, and icicles. Icicles are stalactites of solder which drop down between packs during scrub solder operations. Perhaps one of the more interesting items found during the postmortem examinations were insects, in certain cases, large numbers of them. In most cases these insects are built into the paper. Figure 5 shows one such animal. To my knowledge nobody has investigated the dielectric properties of insects but when one drops from the paper leaving a hole, there is little doubt that the effect will be bad. These problems are considered in greater detail in Ref. 7.

Dimensional checks made in the windings showed that in many cases the machine set-ups were responsible for producing the wrong margin and active widths. Cross-checks were made on the older 2-μF, 50-kV unit and it was found that roughly the same absolute margin and active width variations were present but these were not as large percentage-wise due to the smaller number of sections. A number of the 50-kV capacitors were then run at 60 kV. This group had a Weibull median life of 17,500 shots which is in close agreement with an inverse 8th power law voltage dependence. An analysis of the dependence of the voltage distribution in the pack on the margin and active width variations was made for both the 8-section and 9-section packs.[7] The results indicated that the 9-section pack with 3/4" margins was marginal when the voltage enhancement due to the variations was considered.

It was decided to return to an 8-section pack with 1" margins. The insulating pad was increased to increase the pad life and as a result a capacity of 1.85 μF was achieved. The various manufacturers were informed of the areas where better control was needed. This new design gave the desired results at least when properly built. Figure 6 shows the raw data from part of one production lot. The pronounced angle in the plot is due to a dual failure mechanism. In this case the reason for the steeper sloped portion, which is also the portion with shorter median life, is known. Gas formed by hydrogenation of the castor oil collects in the top of the case, the case swells and the oil level drops exposing the header connections which then arc over to the case. Had these units been run at a slower repetition rate, some of the gas would have been absorbed and then these failures might have been avoided; however, more complete filling of the case would also have increased the life. A second production group from the same manufacturer appears to have a median life of approximately 70,000 shots.

The situation is not quite so good when manufacturing defects are allowed to creep in. Figure 7 shows the raw data on a lot of twenty units submitted by a second manufacturer. The plot shows two steps indicating that there are three separate distributions in the sample. Figure 8 shows the separated data with 90% confidence bands. For the capacitors in the very short-lived portion the cause of failure though different from unit to unit was a glaringly obvious problem, the median-lived portion showed indication of lack of proper care during manufacture, but it was usually difficult to pinpoint the cause of failure. The long-lived portion failed due to old age, the median life being close to that expected from these units.

The knowledge gained from the development of this unit has resulted in a significant upgrading of the general quality of energy storage capacitors.

IV. OTHER CAPACITORS UNDER DEVELOPMENT

We now turn to the other three types of capacitors under development. The B_o capacitor is to be a 170-μF, 10-kV, high-energy density unit. Test samples of this unit have been under evaluation at LASL for some time and it was felt that the savings in cost and space obtained by the use of this unit will be substantial. The relative isolation of the B_o bank from the rest of the system makes possible the use of an ignitron crowbar which can hold the voltage reversal on the B_o capacitors down to below 25%. Four companies have supplied the 170-μF, 10-kV, high-energy density, B_o capacitor for testing. These units were given three types of tests, a high-current test to determine if the unit could withstand the high currents caused when another unit failed close by, an electrification test to insure that the life of the unit would not be determined by the relatively long times these capacitors would be required to be on charge, and a bank test which simulated the actual bank discharge conditions.

The tests show that this design is feasible

provided good quality control is maintained during manufacture. The test data indicate that a median life of 50,000 shots is to be expected if the crowbar can hold the voltage reversal on the capacitors to below 25%. However, the Weibull slopes are low, usually about one-half, so early failures are to be expected. Since only about 240 units will be in service and these will have fairly easy accessibility, this is considered a minor price to pay for the great savings in cost and space effected by using the high-density unit.

The philosophy on the preionization capacitor has changed considerably from that proposed in Ref. 1. The Scyllac proposal called for the use of the Tobe ESC Model 250 which is a 0.8-μF, 120-kV capacitor. This unit is very bulky, expensive, and requires a very expensive spark gap header. The extremely high-voltage rating is required because the preionization bank, unlike the B_o bank, is not electrically isolated from the system and as a result gets pulse-charged by the primary bank to approximately twice the primary bank charge voltage. The dc charge voltage for this application need not exceed 75 kV and NET-1[5] calculations indicate that the voltage on the capacitor does not reverse during the main bank pulse charge. These facts lead to the concept of a capacitor nominally rated at 75 kV with 85% reversal but with margins and major insulation designed to withstand dc pulses up to 120 kV. The present aim is a 75-kV unit with a capacity of about 1 μF in a case having the same base area but perhaps taller than that used for the 60-kV primary capacitor.

Several types of 75-kV capacitors have been made. These include 1/4-μF, 1/2-μF, and 1-μF models. All these models were in the same case used for the 1.85-μF, 60-kV unit. The 1/4-μF and 1-μF models were made before we began to understand the voltage problems accompanying large percentage variations in active widths. Consequently these units were made with 10-section packs and wide margins. The result was that the 1-μF units did not operate well while the 1/4-μF units operated adequately, mainly because the pad was so thick that the pack would not fail even with one section shorted. The 1/2-μF and 2/3-μF units are made by series connecting packs with fewer sections. The 1/2-μF design has been tested and operates well. The 2/3-μF unit has not been tested yet.

The bushing used on these capacitors is the same as used on the 60-kV capacitor. Some bushing failures have occurred on capacitors from one manufacturer. This particular bushing has less radial spacing between electrodes than is used by other manufacturers. Over-the-top failures have also occurred when developmental spark gaps which projected above the bushing barrier were used. Since the spark gap problem has been solved no change in the bushing for the 75-kV unit is projected at present.

The high-Q stabilization capacitor specifications call for a 0.1-μF unit at 75 kV. The Q must be as high as possible and at worst should be of the order of 300 at 2 MHz. The physical dimensions of this unit are still open.

The high-Q development has barely gotten under way. This is a relatively new field for energy storage units. Some of the first work in this field was done by Mather[8,9], Tenney[10], and Wurmser[11] at Princeton. The work at Princeton was concerned with an application at 100 kHz. Axel and Sangamo ultimately produced production units with Q's of approximately 400 and 500 respectively at this frequency. Preliminary checks made on these units show that the Axel unit has a Q of about 40 at 1 MHz while the Q of the Sangamo unit seems to be about 75 at 600 kHz. Other measurements indicate that the Q of both units may now be below the values reported by Mather.[8] The units which we checked were from the same group measured by Mather hence our lower measurement tends to strengthen some previous evidence that the Q of these units may decrease with aging.[12] At the present time only one new unit has been received at Los Alamos. The packs of this unit show a Q of approximately 160 at 1 MHz but the Q of the assembled unit is only about 60 at the same frequency. This still represents an advance over the previous units but indicates that a long path still lies ahead.

V. SUMMARY

Summing up the Scyllac capacitor situation, we have developed a reliable, 1.85-μF, 60-kV, low-inductance capacitor for the primary bank. During the development of this unit we have shown that rigid quality control is required during manufacture if these units are to perform properly. The proposed 170-μF, 10-kV, high-density, B_o unit has been shown feasible and is close to realization. Seventy-five kilovolt preionization units and 0.1-μF, 75-kV,

high-Q capacitors are now under active development and some successes have been achieved.

ACKNOWLEDGEMENTS

Capacitor development is always a team effort involving many people. Special mention should be made of the contribution to the above work by E. L. Kemp, M. J. Hollen, and J. A. Meyer.

REFERENCES

1. Project Sherwood Personnel, Los Alamos Scientific Laboratory Report, LA-3487-MS (1966).
2. E. L. Kemp, T. M. Putnam, W. E. Quinn, and F. L. Ribe, Los Alamos Scientific Laboratory Report, LAMS-2609 (1961).
3. E. L. Kemp, "The Engineering Aspects of the Scyllac Proposal", Proc. 1966 Symposium on Engineering Problems of CTR, Conf. 661016, p. 179.
4. E. L. Kemp, "The Design of Scyllac, a 15-Meter Theta Pinch Machine", Proceedings of Fifth Symposium on Engineering Problems of Fusion Technology, Culham Laboratory, England (1968), to be published.
5. G. P. Boicourt, "Application of the NET-1 Network Analysis Program to Distributed Circuits", paper E7, this Symposium.
6. G. P. Boicourt, "Evaluation of Coaxial Cable Performances at High Voltages: an Interim Report", Proceedings 1966 Symposium on Engineering Problems of CTR, Conf. 661016, p. 13.
7. G. P. Boicourt, "Some Practical Problems Concerning the Design and Manufacture of Energy Storage Capacitors", Los Alamos Scientific Laboratory Report LA-4142-MS (1969).
8. N. W. Mather, "High-Q Capacitor Development", Proceedings 1965 Symposium on Engineering Problems of CTR, Conf. 650512, p. 201.
9. N. W. Mather, "Analysis of a Ringing Circuit Containing a Spark Gap", Plasma Physics Laboratory, Princeton University Tech. Memo. No. 190, Feb. 18, 1964.
10. F. H. Tenney, "Investigation of Bushing Stress on Sangamo Electric Company High-Q Capacitors", Plasma Physics Laboratory, Princeton University Tech. Memo. No. 195, May 1964.
11. J. F. Wurmser, "Prediction of Q in Low Loss Energy Storage Capacitors", Plasma Physics Laboratory, Princeton University Tech. Memo. No. 166, Nov. 1962.
12. P. Hoffman, Maxwell Laboratories, private communication.

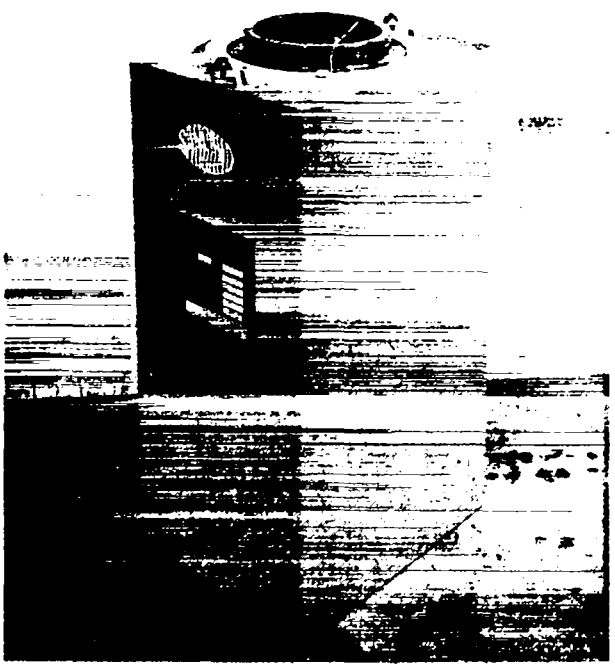

Fig. 1. 2-μF, 50-kV energy storage capacitor.

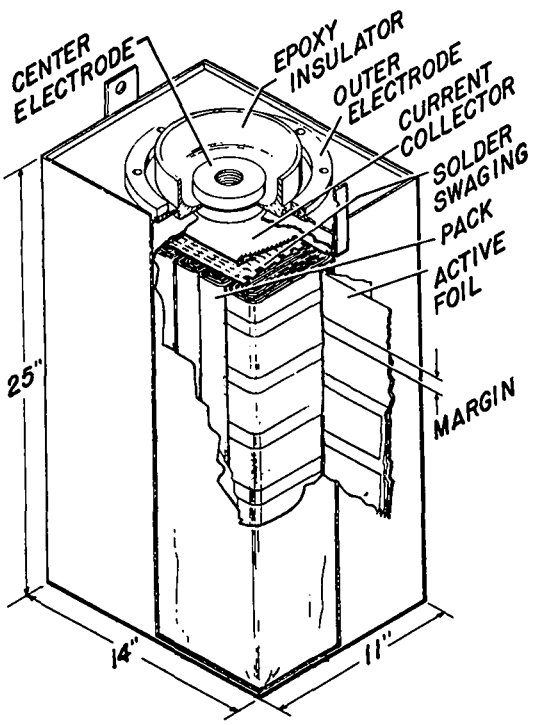

Fig. 2. Schematic of 2-μF, 50-kV energy storage capacitor.

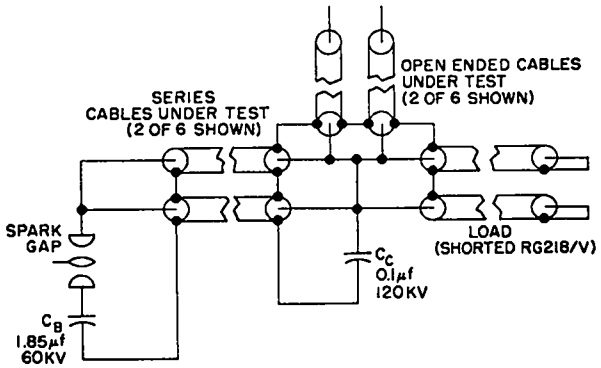

Fig. 3. Capacitor test circuit.

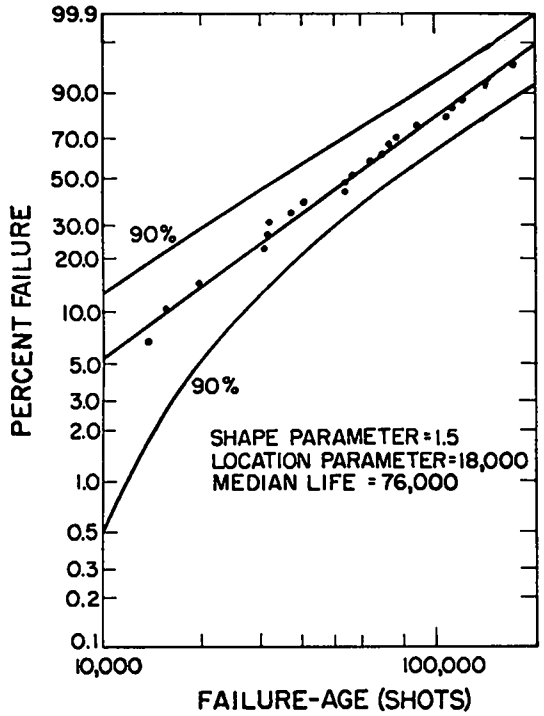

Fig. 4. Life data on a set of 2-μF, 50-kV capacitors plotted according to Weibull statistics.

Fig. 5. Insect found embedded in capacitor dielectric.

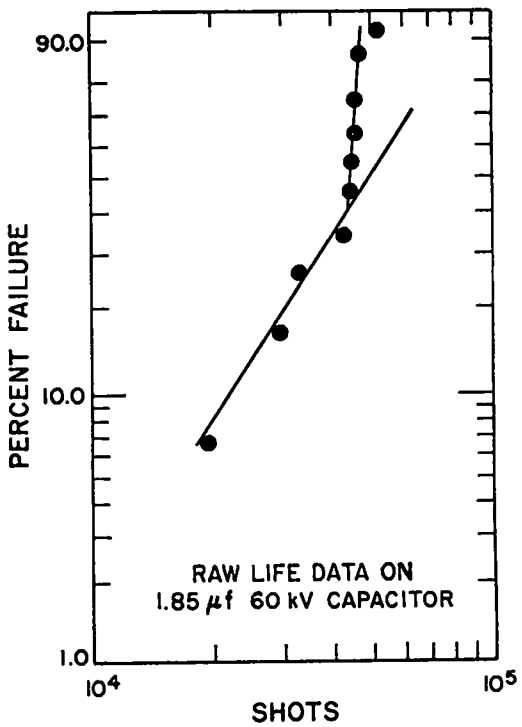

Fig. 6. Raw life data on 1.85-μF, 60-kV capacitor plotted on Weibull paper.

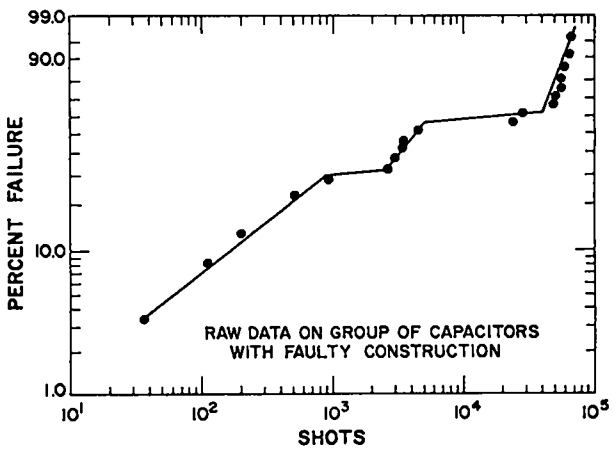

Fig. 7. Weibull plot of raw data on group of capacitors with faulty construction.

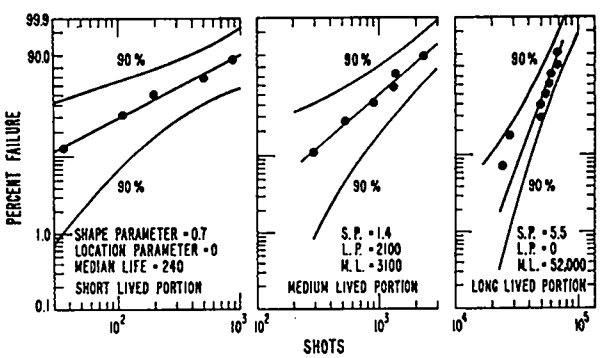

Fig. 8. Data on the capacitors in Fig. 7 separated according to Weibull statistics.

THE DEVELOPMENT OF RELIABLE, HIGH-VOLTAGE, LOW-INDUCTANCE CABLE FOR SCYLLAC*

by

G. P. Boicourt and E. L. Kemp

Los Alamos Scientific Laboratory, University of California
Los Alamos, New Mexico

ABSTRACT

Scyllac requires over 750,000 feet of low-inductance coax cable. There will be over 25,000 individual cables operating simultaneously and any cable failure will stop operation of the entire system. A cable development program involving several companies in the cable industry was begun in 1966 to develop a reliable cable to operate as load cable in a capacitor bank charged to 60 kV and switched with pressurized gaps. The cable has a foamed polyethylene core and uses the braid of RG 14/U cable as the center conductor. The main insulation is extruded over the inner braid and the outer conductor is braided over the insulation. A final jacket is applied to make a cable that approximates the size of RG 17/U. The inductance of cable made in this manner is less than 40 nH per foot but this cable will not operate reliably at 60 kV. It was found during the development program that the voltage reliability could be improved by extruding conducting dielectric screens adjacent to each side of the main insulation. Reliable cable with an inductance of about 45 nH per foot is now commercially available. This paper describes the tests used for evaluation and details some of the problems encountered in this development.

I. INTRODUCTION

Coaxial cable has many advantages as a transmission system for energy storage capacitor banks. Cable is compact and mechanically flexible so many lengths can be easily paralleled to transmit large currents from numerous capacitors to a single load. The cylindrical construction of cable presents an optimum geometry for containing the magnetic forces generated by large currents. When used in parallel, coaxial cables provide a low-inductance transmission system that competes favorably with strip lines. It is also a commercial product and is inexpensive for this type of application.

The inductance of coaxial cable is directly proportional to the logarithm of the ratio of radii of the inner conductor to the outer conductor and for RG 17/U the inductance is 86 nH/ft at 40 kHz. This inductance is primarily due to the relatively small diameter of the inner conductor. About 1956 the Los Alamos Scientific Laboratory required lower inductance coaxial cable for use in the Controlled Thermonuclear Research program. The first approach was to use a center core of polyethylene, a braid for the center conductor, then more polyethylene braid, and a jacket. As capacitor voltage increased it became necessary to increase the cable size in order to maintain sufficient insulation. A standard

*Work performed under the auspices of the U. S. Atomic Energy Commission.

cable when developed was type 17/14 which used a foamed polyethylene core, the outer braid of RG 14/U for an inner conductor, and the braid of RG 17/U as the outer conductor. The inductance of this cable was 36 nH/ft at 50 kHz. For high voltage this design had the advantage of lowering the circumferential stress at the inner conductor boundary but it increased the average radial stress when compared to RG 17/U, since the total insulation thickness was reduced. Another disadvantage was discovered with use. The small wires composing the inner conductor would break and be restarted during manufacture. Often these ends would penetrate a small distance into the polyethylene dielectric and form a high-voltage stress point. Type 17/14 cable would often fail at these points.

In 1962 Scylla IV was built using 50-kV capacitors and over 1300 individual type 17/14 cables. In operation at 50 kV it was normal to lose one cable for every 10 shots. Naturally this failure rate could not be tolerated so a new cable design (see Fig. 1) was developed.[1] The basic design change was to add a thin conducting screen on the outside of the inner braid and on the inside of the outer braid. The function of these conducting screens was to terminate the wire ends in the screen and thus equalize the stress. When properly manufactured, this design greatly improves the high-voltage reliability of low-inductance cable.

II. SCYLLAC CABLE REQUIREMENT

Scyllac will contain over 3000 energy storage capacitors operating at 60 kV. Each capacitor will have a spark gap and use 6 low-inductance coaxial cables to carry the current from the capacitor to the collector plate and load. The load is a single-turn solenoid coil that appears electrically as an almost pure inductance. There are several connections between the capacitors and the load and each connection presents an unmatched termination point which creates high-voltage transients throughout the system during discharge. The cables must sustain these high voltages without failures.

The energy density requirement of Scyllac dictated close packing of the cables. Figure 2 shows a one-quarter scale model of one collector plate of Scyllac with 1/4" polyflow tubing used to simulate cables. The model was used to determine the actual cable lengths and configurations in the machine. It is obviously very difficult to isolate and change a failed cable and it is also not possible to operate with a failed cable in the system. Reliable cable is absolutely essential for Scyllac.

III. DEVELOPMENT PROCEDURE

The need for reliable cable was recognized when Scyllac was proposed. Some preliminary development work had shown that voltage gradient screens improved the life of cable but the use of screens was not common among cable manufacturers. An optimized cable was designed and a target specification written using MIL specifications as a guide. Three well-known cable manufacturers, Amphenol, Belden, and Plastoid were invited to comment on the target specification. Each company was visited to discuss the specification and also to become acquainted with cable manufacturing methods. Each company suggested changes in the specification which they felt might improve the reliability of the cable. In some cases these changes involved special manufacturing techniques developed by the company. After all suggestions had been evaluated, it was decided to write eight different specifications specifically designed to test the new features and methods. Each company would make the two or three cable types which used their own special expertise. One thousand feet of cable was ordered to each specification. When the eight different cables had been evaluated a composite specification was written using the features found to be essential from all eight specifications. The composite specification was used to order 1000 feet of cable from each of the three manufacturers. When the production problems were worked out for the 1000-feet prototype samples, 5000-feet production lot samples were ordered and tested. When these production samples operated satisfactorily and met all dimensional requirements, the manufacturer was approved for supplying this cable for Scyllac. After the composite specification was written, several other companies became involved in this development.

IV. TEST PROCEDURES AND DISCOVERIES

The first eight cables were made to eight different specifications. The primary features evaluated were: the effectiveness of conducting screens; the best method of applying conducting screens,

wrapping or extruding; multiple extrusion of the insulating polyethylene vs single extrusion; the best type of braid wire to use, round or flat, bare copper or plated copper; and finally, the best material for the main insulation, normal polyethylene or other more exotic insulating materials. A testing program was established to evaluate these parameters.

Three tests were used to evaluate each prototype sample cable; a dimensional check, an ac test, and a pulse test. The dimensional check was to determine the actual diameter and radial thickness of each layer of the composite system. The method of measurement was carefully described in the specification so each manufacturer could perform the same test for quality control.

The second test was a 60-Hz ac test; 55-kV rms was applied to an 18-ft sample of cable, the ends of which were terminated in logarithmic spiral stress cones. The time to failure was recorded for each sample. Usually 6 or more samples were tested from each new reel of cable. It was hoped that the ac test could be correlated with the pulse test so the ac test could be used as a final test before installing the cables into the Scyllac system. Unfortunately, this test did not correlate with the pulse test. The ac test did show up cable with thin insulation and cable with contaminated polyethylene. However, it would not find certain other bad features that the pulse test would disclose immediately.

The pulse test schematic is shown in Fig. 3. A 1.85-μF, 60-kV capacitor and 4-element spark gap were used to pulse charge a 0.1-μF, 120-kV capacitor. Two lengths of shorted RG 218-U cable were used as a load. The length of these two cables and the 1.85-μF capacitor determined the fundamental frequency which was 73 kHz, essentially the Scyllac ringing frequency. The six test cables, each 16 feet long, were connected to the 0.1-μF capacitor and were open-ended in a pot of oil. The initial current pulse-charged the 0.1-μF capacitor to about 88 kV. The voltage on the test cables was a combination of the pulse-charged capacitor voltage and the reflected voltage from the open ends. The peak voltage on these cables was computed to be 123 kV. This test was run at a rate of 6 shots per minute on a 24-hour-a-day basis for 100,000 shots on each sample of six cables. A microphone detector automatically stopped the test when a cable failed.

The ac test does not show up two types of cable faults which have proven to be disastrous for pulse cable. The first problem is any short range periodic variation in the cable insulation thickness. These variations arise from a manufacturing extrusion problem called galloping and from wrapped conducting screens. Galloping occurs when the cable is not pulled through the extruder at a uniform speed. The resulting cable varies in insulation thickness at a periodic rate. The wrapped conducting screens have spiral ridges which are uniformly spaced down the cable. The periodic discontinuities which result from galloping or the presence of ridges produce voltage reflections when a pulse is applied and the resultant increased voltage will usually puncture the insulation after a few thousand shots even though the cable may run indefinitely on ac. The second type of fault is a cut in the insulation. This fault is usually the result of careless dressing but may sometimes occur during manufacture.

Some cable gave poor performance on both ac and pulse test although no specific manufacturing problem was apparent. A fourth test was used to identify the cause of the poor performance. The polyethylene insulation was carefully examined under a microscope and an inventory of all particulate matter was made for a typical one-inch sample. All cable, good or bad, has some particles which are apparently anti-oxident that is in the bulk polyethylene material supplied to the cable manufacturer. When this material is very small it seems to cause no degradation in high-voltage performance. But in some cable this material is easily visible under a two-power glass and this cable displays a somewhat poorer performance on both electrical tests. Other types of particulate matter can make the cable unsuitable for use. One large sample of cable was received and found to have a considerable amount of metal particles imbedded in the polyethylene. The metal was later found to have come from a worn part in the extruding machine. This cable was also very poor on both tests. The ac test quickly identified all cable with the contaminated polyethylene insulation.

The following conclusions were made from the test results of the first eight different cables. The conducting screens improved the high-voltage performance of this type cable. The inner screen is

essential. The outer screen seemed to have some effect although it may be argued that an equivalent amount of active polyethylene would be equally effective. The final design uses both screens. Due to the voltage reflection phenomena, wrapped screens are worse than no screen at all for pulse cable. There is no obvious difference between multiply-extruded and singly-extruded polyethylene provided no dirt is allowed to collect on the interior interfaces. No improvement was detected for cable with ribbon braid or with silver-plated round copper wire. The final design uses bare, round copper wire. One cable was made with high-density, cross-linked, polyethylene insulation. This cable performed well, especially on ac, but it was not markedly better than well-made standard polyethylene cable in the pulse test. It was more expensive and considerably stiffer. The final design uses standard polyethylene. From the dimensional analysis it was discovered that eccentricity between the conductors is not a serious problem provided that a minimum insulation thickness is maintained.

The final specification requires an inner foam core of 0.370" nominal diameter. Two layers of bare copper are braided over this core. Then a thin layer, 0.027" of conducting polyethylene or conducting polyvinyl chloride is extruded over the braid. The main polyethylene is then extruded with a nominal wall thickness of 0.140". The outer screen is conducting polyvinyl chloride with a nominal wall thickness of 0.030". The outer braid of bare copper wire and a PVC jacket is then applied to complete the cable. The tolerance and absolute variation given for each nominal dimension is specified. The method of measurement and the method to be used for calculating each dimension is given in an appendix to the specification. The philosophy of the specification is to produce the best pulse cable possible while taking into account the limitations of the industry. All dimensions and tolerances in this specification are within the manufacturing state-of-the-art of the cable industry.

Cable made to this specification has a life in the pulse test of over 100,000 shots with no failures. The median life on the ac test at 55-kV rms should be approximately 70,000 cycles. Its inductance should be 45 nH/ft and its resistance should be about 1.25 mohms/ft.

V. MANUFACTURING PROBLEMS

The test on the original eight types provided most of the basic information for making reliable cable for this application. The largest problem was getting cables to the tolerances required in the final specification. The first serious problem for the manufacturer was the extrusion of the thin conducting screens. Few manufacturers had any experience in extruding thin layers of this material, in fact, conducting polyethylene has been commercially available only since about 1967. Conducting polyvinyl chloride is also a relatively new material and certain of the companies experienced problems at first in extruding it. A different problem was discovered during the dimensional check of another manufacturer's cable. In this case the main polyethylene was applied in two passes through the extruder. After the first pass, the warm insulation was sized through a heated sizing die. Instead of merely removing the outer irregularities, the sizing die also compressed the warm cable assembly and reduced the diameter of the inner braid. The final cable had extra insulation and gave excellent high-voltage performance but the inductance was high by about 15%. The dimensional check identified this problem and the manufacturer deduced the reasons and corrected the processing.

In one case untrained personnel inadvertently provided us with cable from which we gained the information required to design a preinstallation test. Figure 4 shows a piece of this cable. When the outer screen was being extruded, bubbles and bare spots formed along portions of the cable. A workman removed these portions of screen by cutting around the cable, points A in the figure, and then along the cable, B, in the figure. The whole area was then wrapped with conducting polyvinyl chloride tape. The result in the pulse test, a blowout on one portion of the cut, is shown just below the right-hand point A. It was possible to detect such areas by merely examining the jacket of the cable. A group of sections having such faults was assembled and tested in the pulse test. The data, plotted according to Weibull statistics, are shown in Fig. 5 along with the 90% confidence band. This plot shows that we need approximately 6000 shots to eliminate 50% of the cables with cuts made during manufacture or dressing.

Even though the most serious manufacturing problems have been identified and corrected, it is still possible that new problems will occur. For this reason the production cable will undergo a series of tests prior to installation. When the cable is received for Scyllac, some typical samples will be dimensionally checked. Then the cable will be cut into appropriate lengths and terminated on each end. Then all cables will be pulse tested in a system similar to the development pulse system. NET-1 computations[2] indicate that the proposed test will be equivalent to the standard development test and we hope to eliminate all bad cable before installation in the Scyllac system.

VI. SUMMARY

After testing and examination of a group of different cable designs, we have been able to formulate a specification, which, when adhered to, will result in a highly reliable, low-inductance, high-voltage pulse cable. The single most important factor in maintaining high reliability in such cable is the strict adherence to good quality control procedures during manufacture. We have been able to give suitable criteria for a preinstallation test which should preclude very early cable failures in Scyllac.

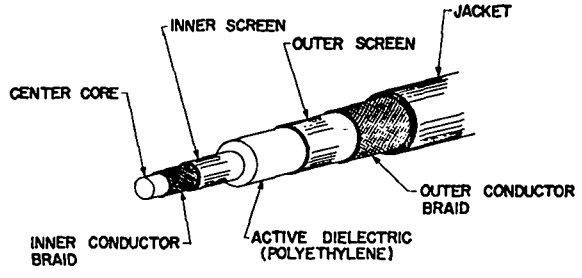

Fig. 1. Low-inductance coaxial cable with screens.

Fig. 2. Quarter-scale Scyllac model showing cable congestion.

ACKNOWLEDGEMENTS

The authors would like to express their deepest appreciation for the help of M. J. Hollen and J. A. Meyer during the cable development project.

REFERENCES

1. G. P. Boicourt, "Evaluation of Coaxial Cable Performance at High Voltages: An Interim Report", Proc. 1966 Symposium on Engineering Problems of Controlled Thermonuclear Research, Conf. 661016, p. 13.
2. G. P. Boicourt, "Application of the NET-1 Network Analysis Program to Distributed Circuits", paper E7, this Symposium.

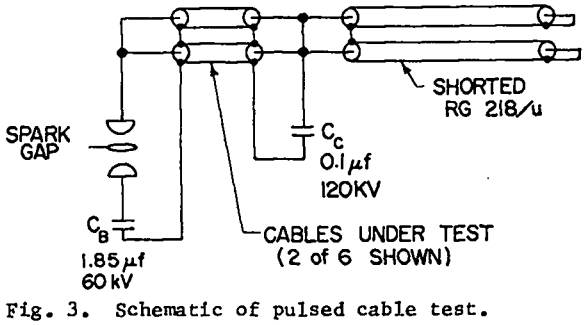

Fig. 3. Schematic of pulsed cable test.

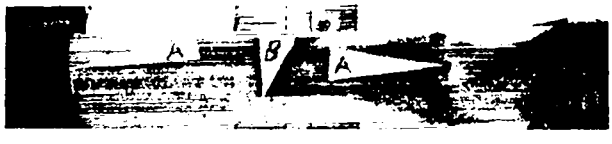

Fig. 4. Section of cable showing cuts made during manufacture.

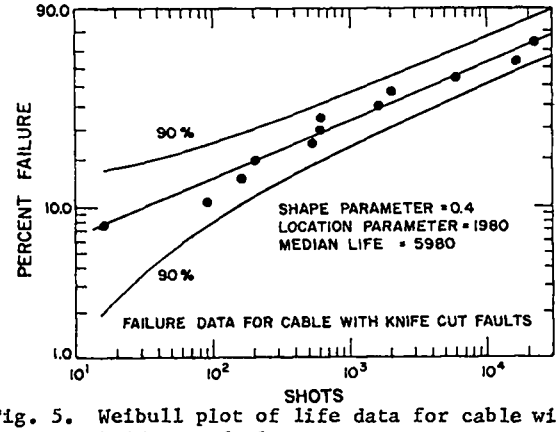

Fig. 5. Weibull plot of life data for cable with knife cut faults.

THE DESIGN AND DEVELOPMENT OF CABLE CARTRIDGES FOR SCYLLAC*

by

K. W. Hanks and G. P. Boicourt

Los Alamos Scientific Laboratory, University of California

Los Alamos, New Mexico

ABSTRACT

One of the critical components in the Scyllac system is the cable cartridge. The primary function of the cable cartridge is to terminate coaxial cables into a parallel plate transmission line. Each cartridge has been designed for minimum inductance and must hold off the 60-kV primary voltage plus any superimposed transient voltages which may occur in the system. These short duration peak voltages may reach as high as 143 kV. In addition, the cartridge geometry must efficiently transfer 120,000 amps. The magnetic forces which are generated between the collector plates are retained by a through-bolt which is incorporated into the design of each cartridge. Both mechanical and electrical problems have developed with respect to materials used for the basic components of the cartridge. These problems and solutions will be discussed. The final design of the linear Scyllac system requires four different types of cartridges. One hundred-twenty-three total cartridges are required for each meter of machine of which there are 59 top-fed and 64 bottom-fed cartridges. Each meter of machine uses only two types of cartridges. Each adjacent meter uses a set of reversed polarity cartridges. Each type of cartridge has been initially certified in a 75-kV test system for a minimum of 5000 shots with voltages being applied that are characteristic of the Scyllac system. Each set of top- and bottom-fed cartridges will have their final certification when they are installed in the Scyllac prototype machine. The history of the development of these cable cartridges and methods of testing and evaluation will be presented.

The mechanical and electrical design of the Scyllac system has been in process for the past two and one-half years. One of the critical components in the system is the cable cartridge. Figure 1 shows the physical location of the cable cartridge as a part of a typical Scylla system. The primary function of the cable cartridge is to terminate coaxial cables into a parallel plate transmission line. In other words, it is a transition device for transferring electrical energy from a coaxial cable system to a parallel plate system.

The evolution of the cable cartridge started with a device which terminated a single cable. Prior to this cables were installed in Scylla systems in the manner shown in Fig. 2. This method was adequate, but cables had to be installed on the edges of the collector plates and left little freedom in designing collector plate systems. In addition, the strip-back length on the cable had to be quite long to hold off the system voltages.

A section of the single cable adapter is shown in Fig. 3. The main reason for this device was to have a hermetically-sealed unit which would allow cables to be installed or removed in collector plates without disturbing the SF_6 system. A cable would be installed into each unit with adequate strip-back in air for the system voltages. This device has the advantage that it can be installed at any location desired in a collector plate geometry. A proposed workable geometry where this adapter is utilized is shown

in Fig. 4. Twelve cables are grouped around a bolt and a complicated molded polyethylene insulator is required to meet the voltage hold-off requirements of the system. The disadvantages are the added inductance due to the space required for the molded insulators and the large number of penetrations in the plates. Also it was found that the pipe thread on the cable adapters were not parallel with the longitudinal axis of the adapters and this made reliable installation very difficult. In addition, this type of geometry was very costly.

The first cable cartridge system was installed in the 50-kV Scylla IV machine three years ago. Prior to this the method for terminating the cables had been similar to the method as shown in Fig. 2 where cables were installed along the side edges of the collector plates except that the cables were installed under oil with a short strip-back. Many electrical failures had occurred using this method and the decision was made to investigate other possibilities. Employing the basic concepts of the single cable adapter, a cable cartridge was developed. This device is shown in Fig. 5. Twelve cables are grouped around a bolt and the polarity of the cartridge is such that the bottom collector plate is at high voltage with respect to ground. The current is carried down the center braid of the cable through a brass connector to an aluminum block and down through the cartridge through an aluminum sleeve around a bolt. A close-fit slit-finger device transfers the current to the bottom aluminum collector plate through a copper washer current joint. After the current has been transferred around the coil of the machine, its ground return is back through a copper washer current joint to the horizontal aluminum flange of the can and up the inner surface of the can to the top aluminum plate. From here the current is transferred to the outer braid of the coaxial cable that is clamped to the top plate. Polyethylene insulators in a SF_6 environment at 60 psig are used between the collector plates to provide sufficient voltage creepage path between adjacent plates. Oil is used as the dielectric media in the region of the strip-back on the cables. The main insulator was molded from diallyl phthalate and it was discovered that due to preloading the $1\frac{1}{2}$"-dia. bolt the insulator was developing cracks in the area of the radii. These areas were overstressed locally mainly due to the stress concentration at the radii. The insulators were finally molded from glass-filled epoxy and the cracking problem was eliminated. To date these cartridges have proven functional in the 50-kV Scylla IV system.

With the knowledge and experience gained from the Scylla IV cartridge and the previous single cable adapter the design criteria was established for designing the 60-kV Scyllac cable cartridge. The basic geometry was to be similar to the Scylla IV cartridge with the voltage hold-off requirements being 60 kV plus any superimposed transient voltages on the system. The current joints would have the capacity to carry a minimum of 120,000 amperes or the current from two 1.85-μF, 60-kV capacitors through twelve cables. Sulfurhexofloride and oil would be used as the dielectric media. A plug-in feature would be incorporated for each cable. In addition, the geometry was to be designed for minimum inductance, ease of assembly, and low cost. It was imperative that the cartridge geometry be established to enable the collector plate design to proceed since the collector plate design was dependent on the geometry of the cartridge.

With the basic design criteria established the first Scyllac cartridge was designed and is shown in Fig. 6. The polarity is shown as reversed from that of the Scylla IV cartridge with the top collector plate being at high voltage with respect to ground. This allows the current to be transferred directly to the top collector plate and eliminates using a dielectric member of complex geometry which is required when transferring current to the bottom collector plate. In addition, the basic geometries of the components are of a less complex nature and therefore are relatively inexpensive to manufacture. The outer housing is fabricated from transparent acrylic resin tubing. This allows for the oil level to be monitored visually. A one-inch AISI C1144 steel bolt retains the complete assembly as well as restrains the magnetic forces which are generated between the collector plates. A brass sleeve around the bolt acts as the ground return to the braid of the cable through a slit-finger current joint geometry. A cloth-base phenolic dielectric compression member with laminations parallel to the axis of the bolt is utilized.

This cartridge functioned successfully for 2000 shots in a 60-kV test system where the cartridge was

subjected to 53.5 kV which was calculated by inductive voltage division. The gas pressure on the cartridge was 60 psig. Following this initial certification, 36 of these cartridges were installed in the Scyllac prototype machine which is shown in Fig. 7. The function of the prototype is to evaluate all components and circuits of the Scyllac system. It was believed that it was possible for the transients in a multi-capacitor system such as the prototype to produce voltages that were not obtainable in the single capacitor test system. The machine is essentially a one-third scale model of one meter of Scyllac. Since the 1.85-μF, 60-kV capacitors were not fully developed at this time, seventy-two 2-μF, 50-kV capacitors were installed in the bank (180,000 joules). Sixty kilovolt capacitors were to be installed as soon as they become available. The geometry of the machine is scaled to acquire Scyllac electrical parameters at the coil. The horizontal collector plates are 23 in. wide by 97 in. long and have skirts which extend 40 in. vertically along each side of the machine. The skirts increase the width of the machine and effectively lower the inductance. The coil bore diameter was determined for a current density of 100,000 amperes per centimeter across the width of the coil.

Two load coils were designed for this machine, a low-inductance coil to test for current problems and a high-inductance coil to test for voltage problems of the system. As initially assembled, the low-inductance load coil was used. After assembly it was found that the SF_6 could not be maintained at 60 psig. This was due to inadequate surface finishes and flatness of the surface of the collector plates as received from the manufacturer. Nevertheless, it was felt that 40 psig would be sufficient due to the lowered bank voltage and the use of the low-inductance load. It was also noted that the dc breakdown voltage in SF_6 was higher at 40 psig than at 60 psig even though the corona inception voltage was lower.

After 50 successful shots at full bank voltage the decision was made to remove the skirts in order to put more peak voltage across the cartridges. On the first shot a major failure occurred on five cartridges at the rear of the machine. Figure 8 shows the result of this failure. The mode of failure appeared to be voltage creepage from the corner of the bottom aluminum plate up the surface of the polyethylene wrap located around the brass sleeve to the ground return plate. This geometry was in a SF_6 environment. Since all the energy of the bank was dissipated in these cartridges, it was very difficult to determine the cause of failure. It was discovered that there was not a leak-tight solder joint at the base of the brass tube which could have resulted in gas leakage; thus it was possible that there may not have been 40 psig pressure on the SF_6. It was noted at this time that the slit-fingered current joints were arcing.

The decision was made to reassemble the machine. Each brass tube was resoldered and checked for leakage and supplemental precautions were incorporated to verify that there was in fact 40 psig pressure on the SF_6.

On the first shot at full bank voltage, the second major failure occurred on a single cartridge at the rear of the machine. The type of failure looked identical to the first. It was also noted that the creepage may have occurred on the surface of the phenolic compression member rather than the surface of the polyethylene wrap. There was also the possibility that the creep may have been along the laminations in the phenolic where air possibly could have been trapped.

To alleviate these problem areas the cartridge was redesigned as shown in Fig. 9. The phenolic insulator was lengthened and was fabricated with its laminations perpendicular to the center line of the cartridge. In order to alleviate the arcing problems, the slit-fingered current joint was replaced by $\frac{1}{4}$"-diam. copper tubing which was loaded in a confined geometry between the phenolic compression member and the top aluminum plate. The brass sleeve and 1" through-bolt were replaced with a $1\frac{1}{2}$"-diam. steel bolt which performed the functions of the brass sleeve and the 1"-diam. bolt. In earlier tests this type current joint successfully carried 400,000 amps ringing with a period of 200 μsec with 50% reversal.[1] Two thousand successful shots were put on this cartridge geometry in a 75-kV test system which subjected the cartridge to peak voltages of 140 kV[2] calculated using the NET-1 computer program. The SF_6 in the cartridge was pressurized to 60 psig.

Thirty-six of these redesigned cartridges were again assembled in the prototype machine and on the first shot at 50-kV charge voltage, six cartridges at the rear of the collector plates failed. To say the

least, this was very discouraging, but for the first time the cartridges had not been completely destroyed and the area of failure could be readily identified unlike in the previous two failures. Voltage crept along $\frac{1}{4}$" of polyethylene insulator from the corner of the high-voltage termination plate and punctured 0.100 inch of polyethylene wrap to the steel bolt. From here the arc cascaded to the top ground return plate. The problem was tentatively identified as a corona phenomena which essentially broke down the dielectric stability of the pressurized SF_6. With the main cause for failure identified a series of tests were set up to try and determine the dielectric characteristics of SF_6 as it is used in the cartridge environment. It was determined that a minimum pressure of 60 psig was required on the gas to minimize the effect of the corona.

The cartridges were again assembled in the prototype system and the gas pressure was raised from 40 psig to 60 psig. The counterbores on the bottom collector plates were opened up to accept O-rings to minimize gas leakage. The system operated successfully for 100 shots at 50-kV charge voltage and a significant amount of engineering data obtained. As might be anticipated on the 101st shot, a single cartridge at the rear of the machine failed. Again, after postmortem, it was established that the cause of failure was the breakdown of the SF_6 due to corona generated on the edge of the bottom high-voltage termination plate. It was also clear that the voltage at the rear of the collector plates was considerably higher than near the coil. Figure 10 clearly shows the voltage gradient along the length of the collector plate. This voltage gradient was also predicted by the NET-1 calculations.

What is hopefully the final version of the top surface cartridge is shown in Fig. 11. The main compression member has been redesigned to extend through the cartridge and into the top collector plate. This insulator will be molded glass-filled diallyl phthalate. This geometry essentially hides the corner of the bottom high-voltage plate from ground. These cartridges have been installed in the prototype machine that is now equipped with 60-kV capacitors and the high-inductance load coil to increase the voltage on the collector plates. To date the system has functioned without failure.

A one-meter section of the linear Scyllac machine is shown in Fig. 12. The original concept called for all cartridges to be of a single design. The physical layout of the cable cartridges in the collector plates is such as to optimize the inductance of the geometry. There are a total of 123 cartridges in each meter of the machine. The linear layout of the machine alternates adjacent one-meter sections of the machine 180° resulting in a continuous coil. The current flow from each adjacent meter of machine to its neighbor must be in the same direction around the coil. This was to be accomplished by charging one-half of the capacitor bank positive and the remaining half negative. After evaluating triggering characteristics of the spark gaps, it was determined that there was considerable jitter in the two polarity systems. The conclusion was reached that the entire capacitor bank would have to be charged to the same polarity. This indicated that there had to be an opposite polarity cable cartridge for each adjacent meter of machine.

Concurrently with the cartridge development, a study was made to determine the feasibility and complexity of actually installing the required 1476 coaxial cables in such a cartridge distribution. It was concluded that possibly the first installation could be made, but replacement of blown cables would be very difficult. A design study was undertaken to develop cartridges which would terminate cables into the bottom of the collector plates. It was determined that with a cartridge distribution of 59 top-fed and 64 bottom-fed cartridges that the average cable length could be reduced from 30 feet to 22 feet. This also would essentially split the mass of cables into two groups and installation and replacement of blown cables now looked feasible.

With this new concept of cable distribution, there is a requirement for four different types of cable cartridges for the linear Scyllac system. The four types are shown in Fig. 13. The top surface cartridge (T.S.) as described previously is shown in the top right-hand corner. Its matching bottom-fed cartridge (B.R.T.) is shown in the bottom right-hand corner. In both geometries the top collector plate is at high voltage with respect to ground. A set of opposite polarity cartridges is shown on the left-hand side of the figure. Their geometries are such that the bottom collector plate is at high voltage with respect to ground.

In both bottom cartridges the stripped-back portion of the load cable is located in a reservoir of oil. The problem here has been to find a reliable seal to prevent oil leakage around the cable insulation. The oil seal is made on the polyethylene insulator where the diameter can vary by 0.040" from cable to cable. A compression gland device has been designed for this purpose. Soft O-rings are seated by loading a nylon pusher geometry after each cable is terminated into the cartridge. The outer braid of the cable is clamped to a brass sleeve which is shrunk into the aluminum plate. Although this method for sealing each cable is functional, it is difficult to assemble. Several new methods are currently being evaluated.

The bottom reach-through cartridge has been by far the most difficult to design. In the cartridge shown the oil level terminates at the bottom of the brass connectors on the center high-voltage terminal of each cable and consequently there is an oil-air interface at this point. The oil could not be allowed to cover these terminations since the center braid of the cable forms a leakage path down the center of the cable. The cartridge was tested in the 75-kV test system and after 2000 shots a failure was generated. A voltage-boring phenomena took place at the surface of the oil and penetrated the nylon insulator to the outer ground return cylinder. The insulator is shown in Fig. 14. The cartridge was redesigned to allow the oil to completely cover the cable terminations and to extend upward into the cartridge. The problem here was to find a reliable method for sealing each cable end so that the oil would not run down the center braid. The cables were successfully sealed by forcing a silica rubber compound down the center braid of each cable. This redesigned geometry was successfully tested for 5000 shots in the 75-kV test system.

The top reach-through cartridge has the same polarity as the original Scylla IV cartridge but has been designed to eliminate the problem areas of the original cartridge. Two dielectric insulators replace the single complicated molded insulator in which mechanical strength problems developed when preloading the cartridge. A glass-filled diallyl phthalate insulator again is used as the main compression member. Initial testing of this cartridge yielded a puncture failure through the outer nylon insulator from the bottom corner of the high-voltage termination plate to the outer ground return cylinder. The nylon insulator was replaced with a heavier walled polyethylene insulator, additional space was obtained for oil, and generous radii were machined on the high-voltage termination plate. With these changes, 5000 successful shots in the 75-kV test system were obtained.

The bottom surface cartridge employs the basic geometry of the top surface cartridge with minor deviations. The cast acrylic outer housing has been convoluted for additional voltage creepage path. This cartridge has also been certified in the 75-kV test system for 5000 shots.

The inductance of each of the four types of cartridges has been experimentally determined. These measured inductances are as follows:

Type of Cartridge	Measured L
1) Top surface	27.7 nH
2) Bottom reach-through	29.8 nH
3) Top reach-through	31.9 nH
4) Bottom surface	30.7 nH

Each value of inductance includes the inductance from twelve one-foot lengths of cable as well as a representative area of collector plate.

The final layout of the cartridge distribution in the Scyllac collector plate system is shown in Fig. 15. The linear system uses the four types of cartridges. When the machine is converted to a toroidal geometry a single polarity cartridge system will be required. The top reach-through and bottom surface cartridges will be installed since their respective inductances are very close in value compared to the set of opposite polarity cartridge inductance values.

At the present time we feel that these cartridges will be functional in the final Scyllac design. Final evaluation of the four types of cartridges will be accomplished in the 60-kV Scyllac prototype machine and will be complete in the near future.

Acknowledgements

The authors would like to recognize the contributions of the following people: E. L. Kemp, R. S. Dike, C. F. Hammer, T. S. Jervis, J. A. Meyer, and W. L. Willis.

References

*Work performed under the auspices of the U. S. Atomic Energy Commission.

1. E. L. Kemp, "The Design of Scyllac, a 15-Meter Theta-Pinch Machine", 1967 Symp. on Eng. Problems of Fusion Research, Culham, England (to be published).

2. G. P. Boicourt, "Application of the NET-1 Network Analysis Program to Distributed Circuits", paper E7, this Symposium.

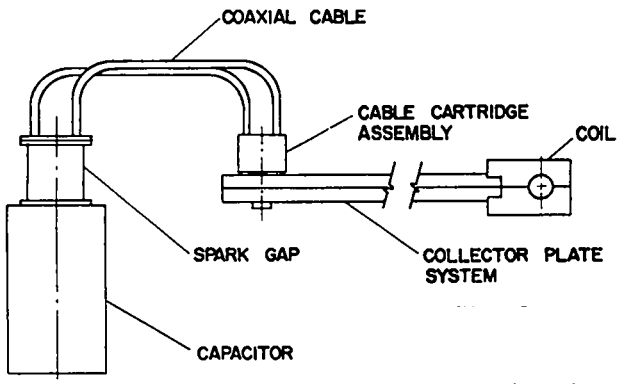

Fig. 1. Typical Scylla machine component locations.

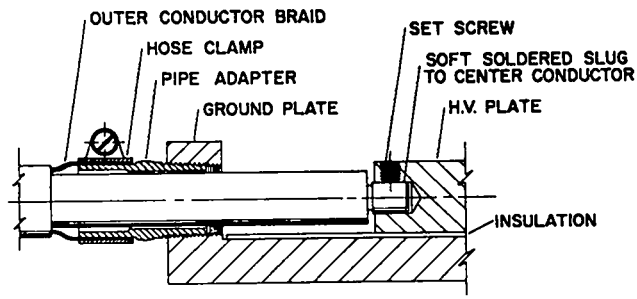

Fig. 2. Cable side plate header.

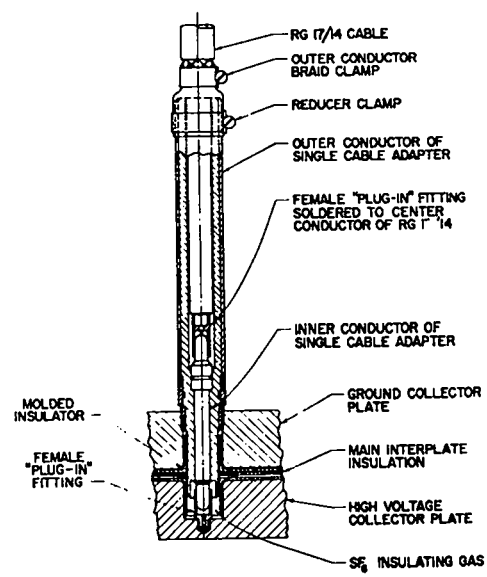

Fig. 3. Single cable adapter.

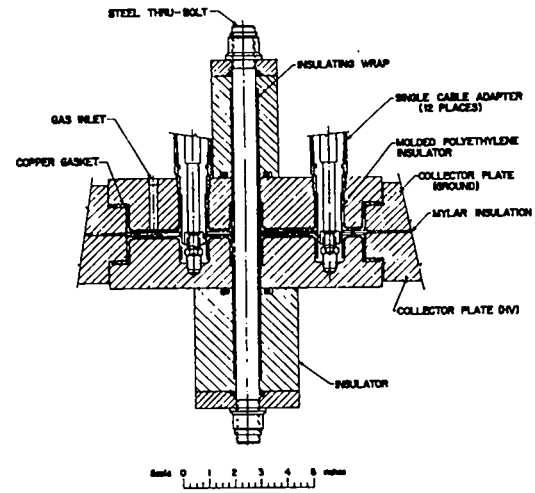

Fig. 4. Single cable adapter assembly.

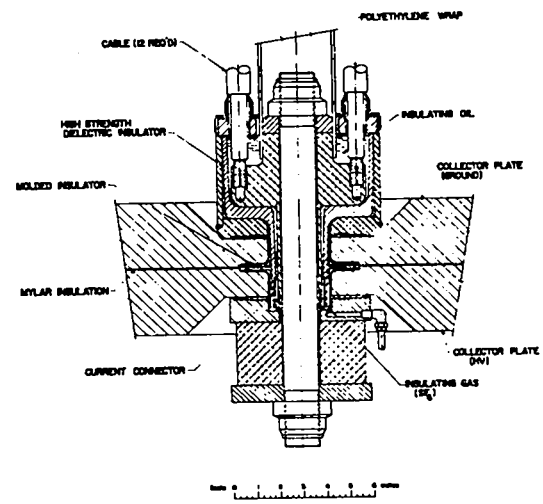

Fig. 5. Scylla IV cable cartridge.

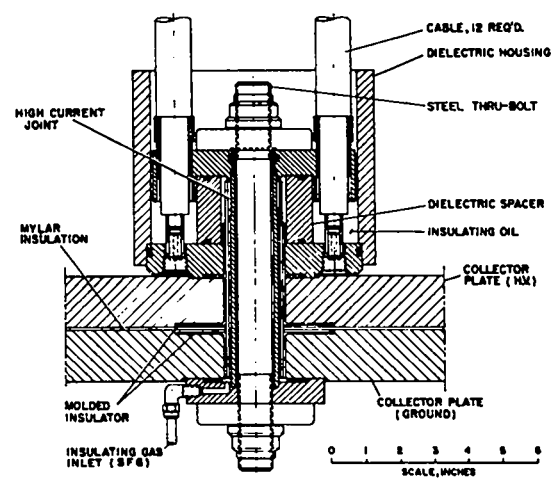

Fig. 6. Scyllac cable cartridge - design No. 1.

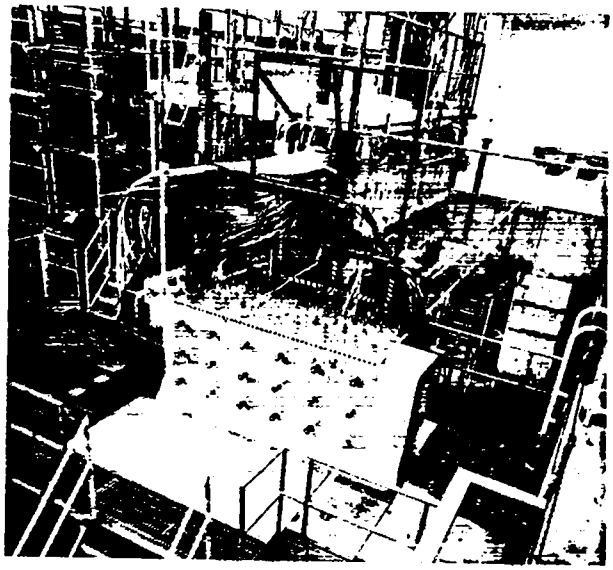

Fig. 7. Scyllac prototype machine.

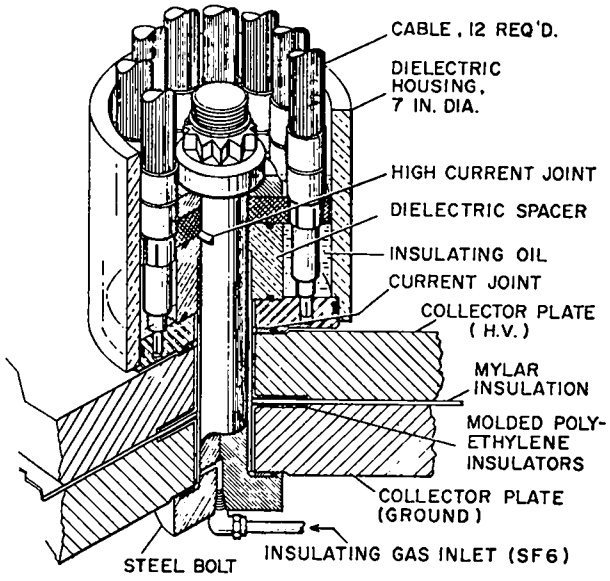

Fig. 9. Scyllac cable cartridge - design No. 2.

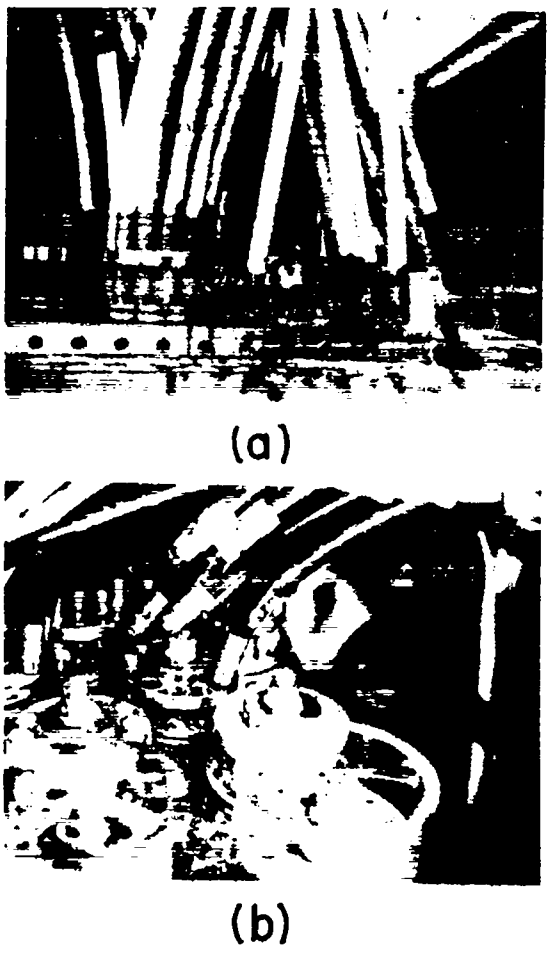

Fig. 8. (a) and (b). Cable cartridge failure.

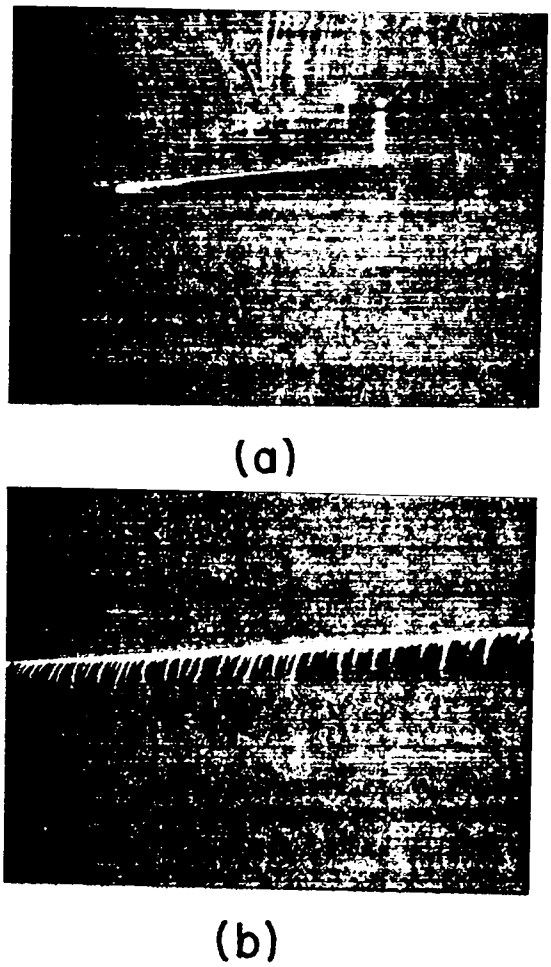

Fig. 10. (a) Photograph of arc tracking indicating voltage gradient along edge of prototype collector plates.
(b) Close-up of arc tracking phenomena.

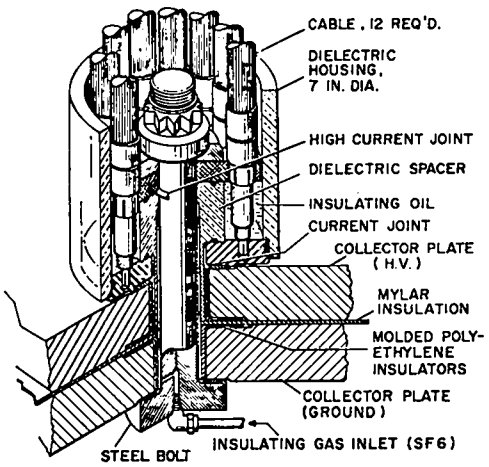

Fig. 11. Scyllac cable cartridge - design No. 3.

Fig. 14. Failure of nylon insulator from bottom reach-through cable cartridge.

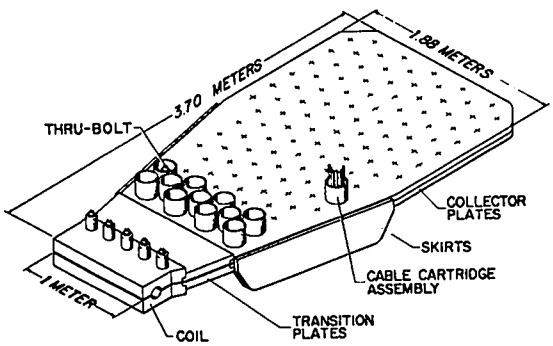

Fig. 12. One-meter section of linear Scyllac collector plate system - original proposal.

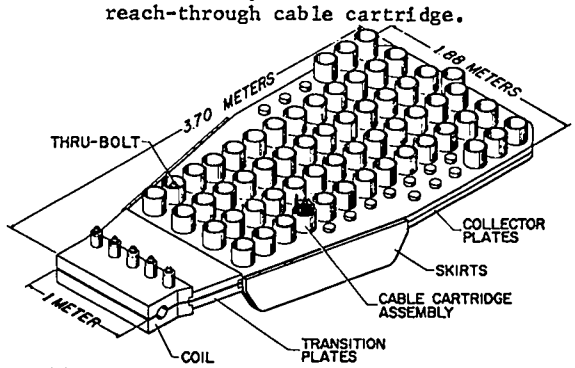

Fig. 15. One-meter section of linear Scyllac collector plate system - final configuration.

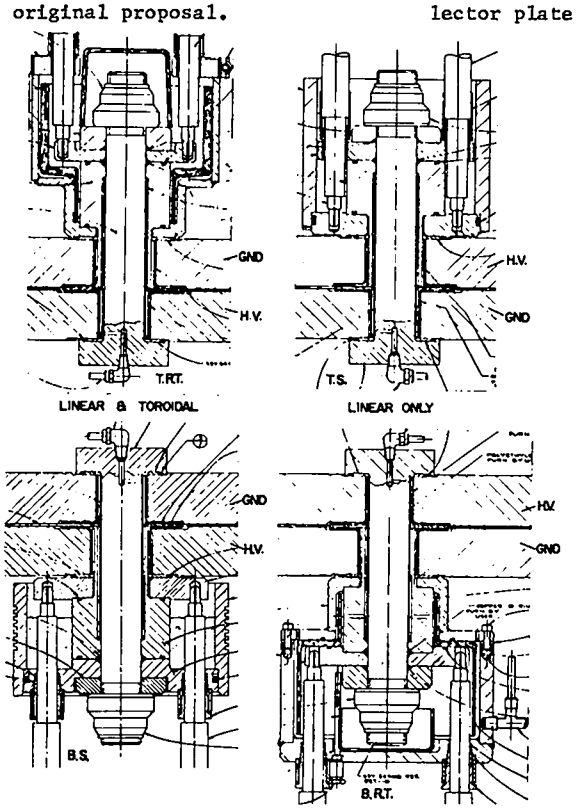

Fig. 13. Four types of cable cartridges required for the linear Scyllac system.

AN INERT-FLUID COOLED AND MAGNETICALLY SHIELDED LOW-POWER KLYSTRON MILLIMETER SOURCE*

W. P. Ernst

Plasma Physics Laboratory
Princeton University
Princeton, New Jersey

ABSTRACT

The cooling effectiveness of completely immersing a low power, millimeter reflex klystron in an inert fluorochemical liquid bath is reported. A closed cooling system, not requiring liquid circulation, is provided by the boiling -- vaporization -- condensation cycle of the cooling process. The operating temperature of the klystron tube is controlled by the boiling temperature of the fluorochemical. Klystron warm-up time and long time frequency stability, using the inert fluid cooling are compared to that provided by forced air. Since the inert fluid cooling is a closed system, more effective magshielding may be used. With the klystron millimeter source applied to a microwave spectrum analyzer, operating performance is compared using two types of cooling; (a) forced air with klystron tube inside a long cylindrical magnetic shield and (b) inert fluid cooling with magnetic tape completely lining the fluid reservoir.

INTRODUCTION

In the field of controlled fusion research, microwave diagnostic techniques play an important role in the various measurements associated with the study of hot plasmas. The typical plasma experimental machine always has a magnetic field associated with it, either steady state or pulsed, and the stray magnetic fields frequently are appreciable in magnitude. Diagnostic system microwave signal sources, e.g. klystrons, magnetrons, and backward wave oscillators, are extremely frequency sensitive to magnetic fields, and also dissipate tens of watts of power. We have then dual requirements for cooling the microwave source and providing an effective magnetic shield.

The usual method of cooling the microwave signal source is with forced air convection cooling. Since the cooling process requires free air flow, any magnetic shield will have openings for intake and outgoing air passage. These openings considerably reduce the effectiveness of the magnetic shielding. Secondly, the fan itself can introduce mechanical vibration to the microwave tube elements and thus cause unwanted frequency modulation, as can the stray 60 cycle magnetic field from the fan motor.

In this paper we will demonstrate the advantages of an alternate cooling process--evaporation cooling with inert fluorochemical liquids. The system allows more effective magnetic shielding and eliminates the disadvantages of the forced air method.

Evaporation Cooling Using Inert Fluorochemical Liquids

*Work performed under the auspices of the U.S. Atomic Energy Commission.

h_v = vapor side condensing film coefficient, watts/in^2/^oC

h_a = air side film coefficient, watts/in^2/^oC

x = condenser thickness, in

k = thermal conductivity of condenser material, watts/in^2/^oC/in

A = condenser area normal to heat flow in^2

Q_a = heat flow rate, watts

U_{cond} = overall heat transfer coefficient, watts/in^2/^oC

Test Results

Using the test set-up shown in Fig 3, the following data were taken.

(1) Klystron body temperature vs time for two conditions.

(a) forced air cooling 3" fan 60 ft^3/min.

(b) vaporization cooling.

Figure 4 shows in chart form the warm up time and maximum operating temperature for each cooling method. Significant points are:

1. Maximum body temperature is reached in a considerably shorter time with air cooling (15 min vs 1.5 hrs). The relatively slow warm up time with the evaporation cooling could be reduced by providing a heater element to maintain the liquid near operating temperature when the klystron tube is off.

2. The maximum temperature attained is approximately the same for each method.

3. At turn off there is a 10^o rise in temperature with the forced air cooled method indicating for those applications using air cooling it would be advisable to continue the cooling for a short time after power turn off.

(2) Stability of body temperature with ambient temperature change.

When the ambient temperature was raised at a rate of $10^0/h_r$ to 54°C the klystron body temperature increased at a rate of 4°/ hr to a temperature of 99°C. The same change of ambient temperature for the forced air cooled method would have caused the body temperature to increase to the maximum recommended of 120°C.

(3) Klystron output power spectrum .

A phase locked 35 GHz klystron (stability 1 in 10^8) was used with a harmonic mixer to heterodyne the output of the 70 GHz klystron under test. The difference frequency was applied to a low frequency spectrum analyzer. Figure 5 shows the spectrum with forced air cooling and evaporation cooling. A signal from a low frequency oscillator was also applied to the spectrum analyzer as a reference. It is plainly evident that there is significant frequency modulation with the air cooled method, mainly due to mechanical coupling of the fan vibration through the magnetic shield. The evaporation cooling method produces a more stable output frequency. The fine structure on the spectrum is primarily due to noise on the klystron power supply voltages.

(4) Magnetic shield effectiveness .

For the forced air cooled tube a cylindrical magnetic shield 3 1/2 inches in diameter and 8 inches long was used. (Manufactured by Perfection Mica Co., Magnetic Shield Division under the brand name Netic Co-netic). The tube was placed at the center of the shield with the fan mounted at one end.

The direct evaporation cooled klystron was shielded with a adhesive magnetic foil, 004"

A liquid that has a lower boiling point than the surface temperature of the heat source will provide the highest rate of heat transfer. The technique of cooling with an evaporating liquid is known by various names; ebullient, vaporization, ev-grav, and direct evaporation cooling. The development of dielectric coolants [1,2], has provided the ideal coolant for the direct evaporation method. They are chemically inert, have very high dielectric strengths, and a wide range of boiling points. Below in table 1 we compare the properties of "3M" brand, FC-75 fluorochemical to that of water.

Table I

Properties of Inert Fluorochemical vs Water

Property	F.C. -75	Water
Nominal Boiling Point, ^{o}F	216	212
Vapor Pressure at 77° F, mmHg	30	23.7
Density @ 77°F, lbs/ft^3	110	62.4
Viscosity @ 77°F, CP	0.8	0.89
Pour Point, °F	-135	32
Heat of Vaporization at Boiling Point BTU/lb	38	969
Dielectric Strength @ 77°F, Kv/0.1 inch	55	---
Dissipation Factor @ 77°F, 3 GHz	0.0065	0.15
Dielectric Constant @ 77°F, 1 GHz	1.87	78

Heat Transfer Process

Figure I is a simplified diagram of the heat transfer process of the evaporation-condensation cooling cycle. At steady state conditions the process is as follows:

Initially the heat flow is from the klystron tube body to the liquid and the rate of heat flow is controlled by a liquid film coefficient, h_L. In steady state conditions this rate of heat flow is given by

$$Q_c = h_L A_c (T_1 - T_2) \qquad (1)$$

where

Q_c = rate of heat flow, watts

A_c = surface area of klystron, in^2

h_L = boiling liquid film coefficient, watts/in^2/°C

R_1 = component surface temp, °C

T_2 = bulk fluid temp, °C

The heat is given off in the form of vapor bubbles which rise to the surface of the liquid pool. As previously indicated the heat is transferred from the vapors, through the condenser and to the air. The rate of heat transfer from the vapors to the condensing liquid-condenser surface interface is given by.

$$Q_v = h_v A (T_3 - T_4) \qquad (2)$$

The rate of heat transfer across the condenser is given by

$$Q_{cond} = \frac{k}{x} A (T_4 - T_5) \qquad (3)$$

And finally, the rate of heat transfer from the air-condenser interface to the bulk air is given by

$$Q_a = h_a A (T_5 - T_6) \qquad (4)$$

In steady state operation

$$Q_v = Q_{cond} = Q_a$$

We may show that the final rate of heat transfer is controlled by the individual thermal resistance. So that

$$Q_a = U_{cond} A (T_3 - T_6) \qquad (5)$$

where $$U_{cond} = \frac{1}{\frac{1}{h_v} + \frac{x}{k} + \frac{1}{h_a}}$$

T_3 = vapor temp, °C

T_4 = vapor side condenser surface temp, °C

T_5 = air side condenser surface temp, °C

T_6 = bulk air temp, °C

thick, 80% nickle-iron alloy (Manufactured by Magnetic Metals Co. under the tradename Shieldmu 30). Two layers were wrapped around tube and one layer lined the container walls.

The data obtained by observing the harmonic mixer output frequency on the spectrum analyzer. A permanent magnet was placed a fixed distance away from the tube and oriented to produce the maximum charge in the observed intermediate frequency. The hall probe placed along the axis of the tube measured the peak magnetic field. Following are the results of this test procedure:

Condition	Δf MHz
1. Forced air cooled, no magnetic shield	30
2. Forced air cooled, with magnetic shield	1
3. Evaporation cooled, without magnetic shield	30
4. Evaporation cooled, with magnetic shield	3

Peak magnetic field was 50 Gauss when magnet was 2 1/2 inches away from tube axis. No increase of maximum operating temperature was observed in the case of the magnetically shielded, evaporation cooled tube.

Conclusions

Comparison has been made of two types of cooling (a) forced air convection and (b) evaporation condensation with inert fluorochemical liquid. The latter type cooling had the following advantages.

(a) More stable operating temperature with ambient temperature changes.

(b) No spurious frequency modulation due to the cooling method.

(c) Potentially can be made insensitive to magnetic fields with a more effective shielding enclosure.

Disadvantages:

(a) Extra protection must be provided to monitor liquid level or provide some interlocking if tube temperature exceeds maximum.

(b) Relatively slow warm-up time which could be improved by a pre-heating arrangement.

REFERENCES

1. R. J. Armstron, (Technical Bulletin EL-11 E. I. duPont deNemours & Co. Engineering Dept., Wilmington, Delaware, 1966).
2. E. T. White, (Technical Bulletin Y-IHTC Minn. Mining & Mfg. Co., Chemical Division, St Paul, Minn., 1965).

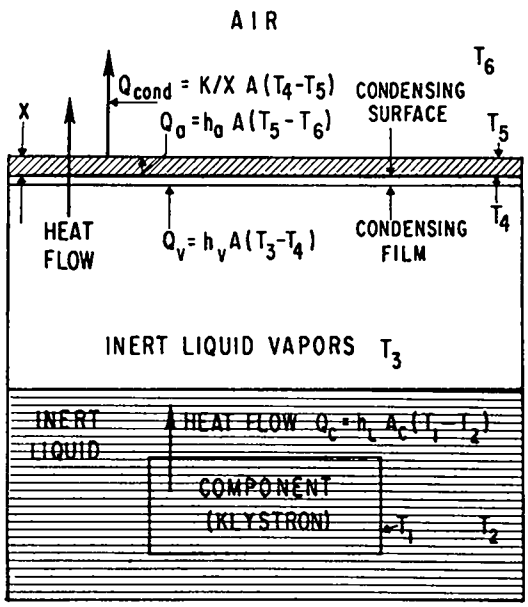

Fig. 1. Klystron heat transfer process.

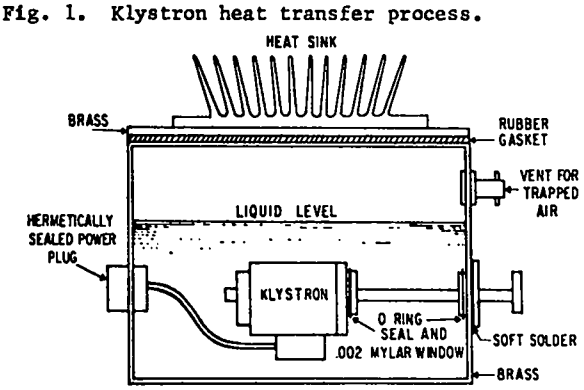

Fig. 2. Drawing of Klystron cooling enclosure.

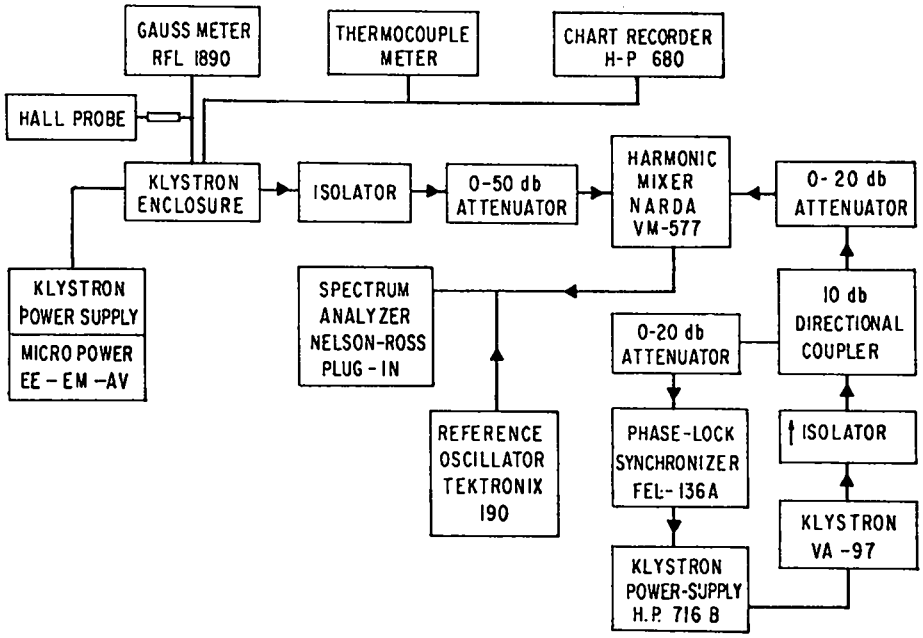

Fig. 3. Block diagram of measuring set-up.

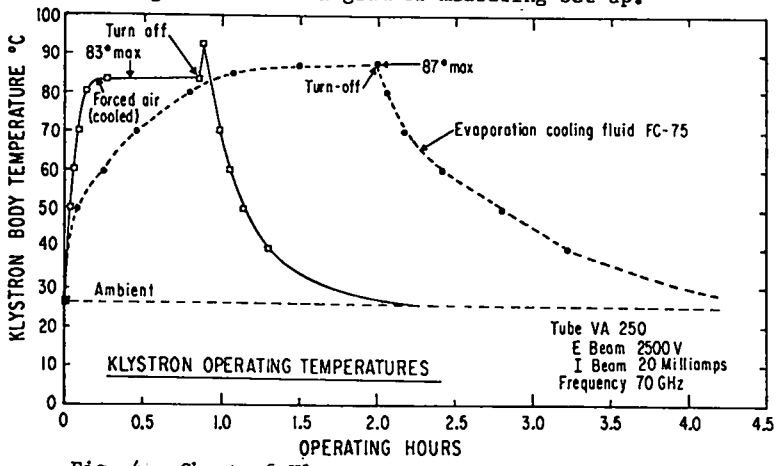

Fig. 4. Chart of Klystron warm-up time and operating temperatures.

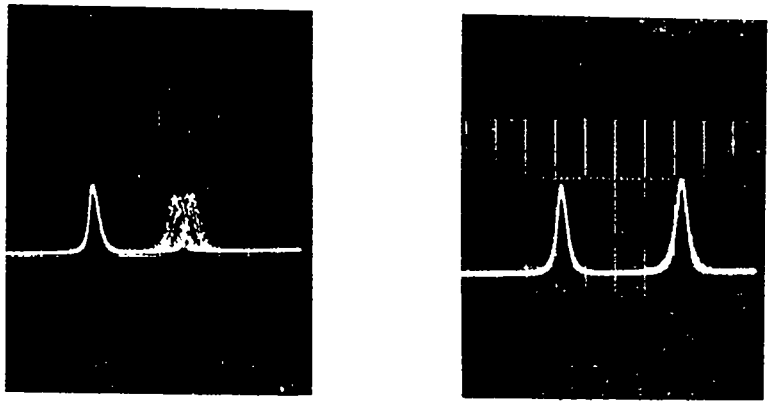

(a) (b)

FORCED AIR COOLED EVAPORATION COOLED

Fig. 5. Oscillograms of Klystron output power spectrum. Scope calibration.

considered for its ability to produce high power pulses with control of the waveshape. This system turned out to be more complex than the existing thyratron-modulated system. Also, the vacuum tube system would require considerable development to produce a working, reliable accelerator.

Another method of increasing the output energy from the accelerator is to improve the performance of the existing system. A simplified block diagram of this system (Fig. 4) shows that this is basically a thyratron-switched, line-type modulator. The output of the modulator is then shaped with a resonant pulse shaper to produce a flat topped accelerating voltage to the beam. The energy is coupled to the beam of electrons through a pulse transformer whose primary winding is excited by the modulator, with the beam completing the secondary. The pulse-forming networks are first charged to approximately 32 kV, then discharged which produces a 10 to 12 kV pulse at the accelerating core. The cores are made of square-loop magnetic material. A negative current pulse to drive the cores to negative saturation between accelerating pulses is supplied by the core reset pulser.

Improving the Existing System

There are several ways to increase the accelerating voltage from this type of system. The PFN voltage can be increased, the source impedance decreased, or the load impedance increased. In this case, however, the PFN voltage and the source impedance are limited by the ratings of the thyratron.

The load presented to the modulator consists of the beam current plus the core excitation current. Since the beam current is fixed in the range of 500 to 1,000 amperes, the core excitation current is the only variable that can be used to increase the accelerating voltage. The magnetic cores used in the accelerator are toroids with an $8\frac{1}{2}$-in. ID, 24-in. OD, and are $\frac{1}{2}$-in. thick. They are wound with 1-mil tape of 50-50 NiFe. It has been determined that the core excitation current is a direct function of the tape thickness, and is an inverse function of the thickness of the core and the inter-lamination resistance.[1,2]

The inter-lamination resistance cannot be significantly increased without seriously affecting the stacking factor or volume of magnetic material within the core. This leaves the tape thickness and the width of the core as the primary variables for increasing the output voltage from the modulators.

To permit using as much of the existing hardware as possible, the overall dimensions of the cores are to remain unchanged. With the dimensions of the cores fixed, each modulator is required to drive more than one core. Decreasing the excitation current for a 1-mil lamination core requires increasing the width of the core. Since the primary winding for the cores is a single-turn, two cores driven in series has the same effect as having a core twice as wide as the original. If the tape thickness of the cores is to be reduced, the cores must be driven in parallel to keep from saturating the cores before the end of the pulse. Figure 5 shows the modulator output voltage as a function of beam current for the two cases considered. Also, a single 1-mil core (as presently used in the accelerator), is included for reference. This shows that the greatest gain can be made by decreasing the tape thickness. However, the cost of cores produced with $\frac{1}{2}$-mil material is approximately three times the price of a 1-mil thick material. Economics then determined that the accelerator would be improved by using two 1-mil cores driven in series by each of the modulators.

System Details

The system designed on this basis is shown in Fig. 6. The accelerator consists of an electron gun section, 7 large bore accelerator sections, and 35 accelerator sections.

The electron gun section consists of 44 magnetic cores (18-in. ID by 33-in. OD by $\frac{1}{2}$-in. thick) wound from 1-mil tape. Alternate cores will be powered by either two or three switch chassis and pulse shapers. Two reset channels of the modular reset system are supplied to each core.

Each large-bore accelerator section consists of 20 magnetic cores wound from 1-mil tape. These cores are 13-in. ID by 33-in. OD by $\frac{1}{2}$-in. thick. Each core is powered by one switch chassis followed

by one pulse shaper. Two reset channels of the modular reset system are required for each core.

The remaining accelerator sections consist of 700 magnetic cores, also wound from 1-mil material. These cores are $8\frac{1}{2}$-in. ID by 24-in OD by $\frac{1}{2}$-in. thick. These are grouped in 35 sections of 20 cores each. Each group of two cores, in series, will be powered by one switch chassis followed by one pulse shaper. One reset channel is required for each pair of cores.

Figure 7 shows the expected beam energy as a function of beam current for the accelerator described above. This shows the design energy of 8 MeV at approximately 750 A of beam current.

CONCLUSIONS

The Astron electron accelerator, which is rated at 4 MeV at 1,000 A, presently consists of 428 accelerating cores, driven by 504 modulators. This accelerator can be extended to 8 MeV at 750 A. It will consist of 884 accelerating cores, driven by 600 modulators. Doubling the energy will then be accomplished by sacrificing 25% of the beam current and by increasing the active electronics by approximately 20%. The remaining additions to obtain the energy are magnetic cores, or passive components.

An intermediate step will be taken where no additional electronics are added. This will give an output energy between 6 and 7 MeV. The remaining electronics and cores can then be added as required for the Astron experiments.

REFERENCES

1. Berg, Gary G., "Experimental Study of 50-50 NiFe Tape-Wound Magnetic Cores for The Astron Accelerator," Lawrence Radiation Laboratory, University of California, Livermore, Report UCRL-71553 submitted to Symposium on Engineering Problems of Fusion Research, April 8-11, 1968.
2. Winter, S. D. and Kuenning, R. W., "Analysis of Flux Reversal in Tape Cores," Lawrence Radiation Laboratory, University of California, Livermore, Report UCRL-71552 submitted to Symposium on Engineering Problems of Fusion Research, April 8-11, 1968.

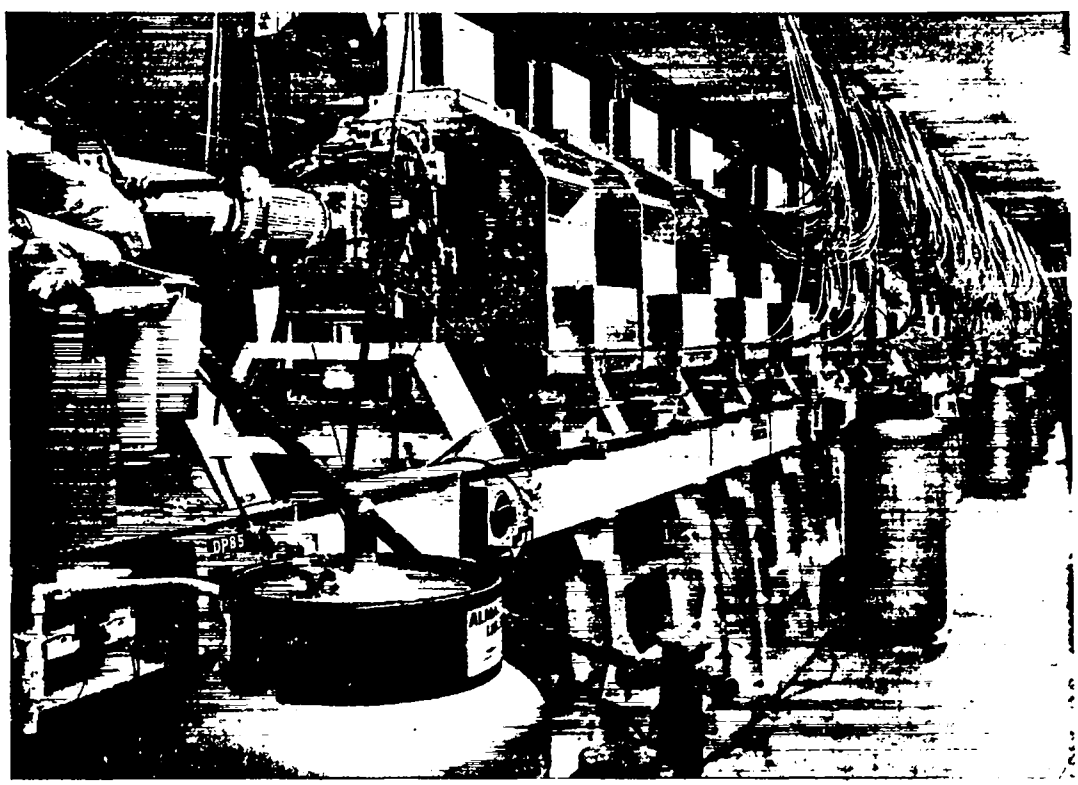

Fig. 1. Astron linear induction accelerator.

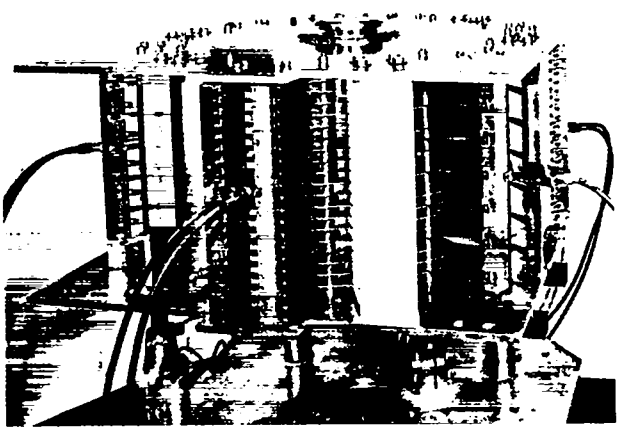

Fig. 2. Twenty-core accelerator stack.

Fig. 3. Approximately $\frac{1}{2}$ of the modulators for the Astron 4-MeV Accelerator.

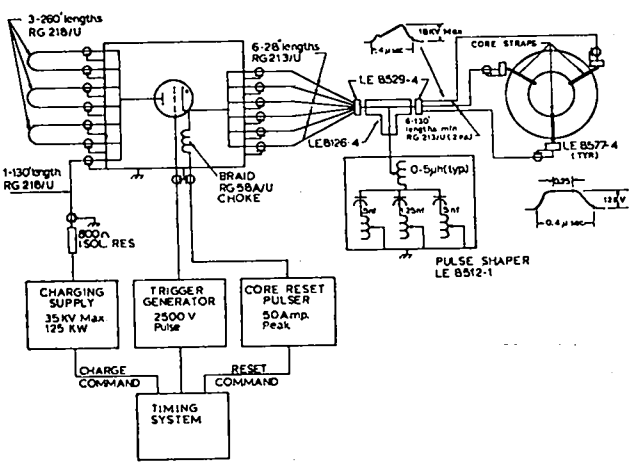

Fig. 4. Block diagram of accelerator modulators.

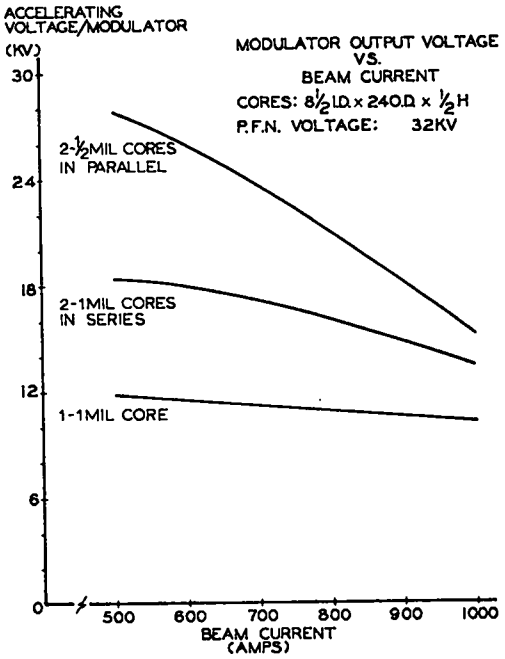

Fig. 5. Modulator output voltage vs beam current for different core types.

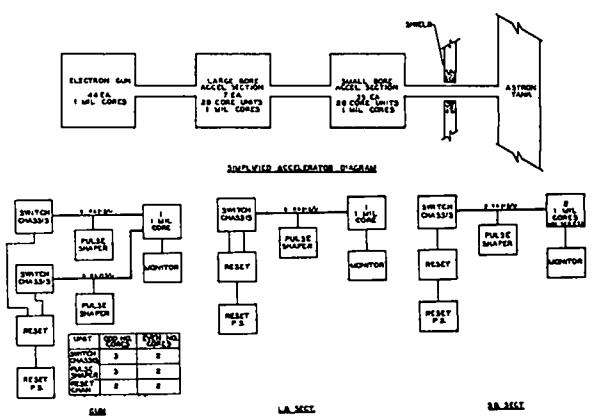

Fig. 6. 8-MeV Astron Accelerator, simplified block diagram.

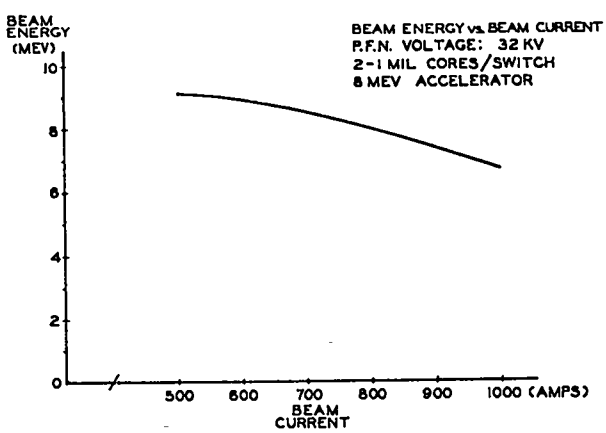

Fig. 7. 8-MeV accelerator beam energy vs beam current.

ANALYSIS OF FLUX REVERSAL IN TAPE CORES*

S. D. Winter and R. W. Kuenning
Lawrence Radiation Laboratory
University of California
Livermore, California

ABSTRACT

Part of a study on magnetic cores which are used to couple energy to the beam in the Astron accelerator was the development of a theory explaining the drive requirements of the cores. The cores consist of 1-mil 50-50 NiFe tape, 1/2 inch wide, wound spirally to form a toroid having a rectangular cross-section with typical i.d. and o.d. dimensions of 8-1/2 and 24 inches, respectively.

These cores have sufficient flux to support a 10-kV pulse for 400 nsec; however, during the pulse, there is an increase of current losses within the tape and more and more drive current is required to maintain constant voltage output. An existing theory on flux reversal, "the saturation-wave theory," predicts just such an increase throughout the pulse for cores with an aspect ratio (o.d./i.d.) of 1. To obtain quantitative results for the Astron cores, first it was necessary to extend the theory to include an aspect ratio greater than 1. Excellent agreement was then achieved between predicted and measured values of "good" cores during the latter part of the pulse. Next, a threshold level of the magnetic field to cause a change of induction in the tape was introduced which led to close agreement between the predicted and measured currents throughout the entire pulse. Comparison of predicted and measured currents are given for both "good" and "bad" cores with a qualitative discussion on the causes of "bad" cores.

INTRODUCTION

Of prime importance to the operation of the Astron accelerator is the performance of the 400 transformer cores which couple energy from the pulse forming networks to the beam. The purpose of this paper is to describe how flux reversal proceeds in the cores during the pulse in order to predict accurately the drive power required to support a given level of acceleration per core.

The first set of cores for the Astron accelerator were bought on a "best-effort" basis. Fortunately, the manufacturer's "best-effort" was compatible with the existing electronics and a workable accelerator was achieved. However, the amount of excitation current required among the cores varied. The prospect of having to obtain future cores without specifications on the performance limits was not encouraging. In order to write a set of specifications, a study program was initiated to educate ourselves and core manufacturers as to what could be expected from cores. This study proceeded along two paths concurrently: (1) an empirical investigation of the contributing factors to variations in the drive currents among cores and (2) a theoretical determination of what should be the minimum current required in a perfect core.

ANALYSIS OF FLUX REVERSAL

A review of the literature[1-4] showed one theory, the saturation-wave theory, which appeared to take into account adequately the eddy currents which are present in each wrap of the core during flux reversal. Figure 1 is a picture of a typical core and some tape material. Figure 2 shows a cross-section of a single wrap of tape and the dimensions relevant to the analysis.

When a voltage pulse is applied, flux reversal begins and three regions then exist within the tape: (1) an interior region in which no flux reversal has

*Work performed under the auspices of the U. S. Atomic Energy Commission.

occurred, (2) an exterior region in which all of the flux has been reversed, and (3) an intermediate region in which flux reversal is taking place. Typically the thickness of the tape, d, is 0.001 inch and the width, w, is 0.5 inch, so end effects can be neglected. In our case, the intermediate region has essentially zero thickness leaving only an interior and exterior region separated by a "wall."[5] The wall between these regions moves from the edge to the center during the pulse. The velocity of this wall depends on the position of the wrap in the core, so "a," the distance of the moving wall from the surface, will be a function both of time and radius.

For a single wrap, the total change of flux $\delta\phi$ up to time t in MKS units is

$$\delta\phi = 2\Delta B_s a w \tag{1}$$

where ΔB_s is the flux density change from the starting value to positive saturation. The voltage at time t for one wrap is

$$\delta V = -\frac{d}{dt}\delta\phi = -2\Delta B_s w \frac{\partial a}{\partial t}. \tag{2}$$

A path for eddy-current, i_e, exists within the saturated exterior region since this region surrounds the changing flux. The resistance associated with this eddy current, Re, is

$$Re = \frac{\rho w}{\pi r a} \tag{3}$$

where ρ is the resistivity of the magnetic tape material.

Combining Eqs. (2) and (3) we achieve an expression for "a,"

$$a\frac{\partial a}{\partial t} = \frac{i_e \rho}{2\pi r \Delta B_s}. \tag{4}$$

In order to solve this equation, infinite permeability of the magnetic material is assumed. Thus, negligible magnetic field intensity, H, is required to reverse the flux density; and since the flux density has not reversed in the interior of the wrap, H must be zero there. Hence, H must go to zero at the wall. For this to be so, the eddy current in each wrap must be equal and opposite to the primary excitation current, i_p. Since i_e for all wraps is equal, i_e is not a function of radius but depends only on time. Therefore, it is possible to obtain a solution for "a" in Eq. (4) by assuming a product solution for "a" in terms of radius and time. The details of this analysis for the general case of non-constant applied voltage is covered in three papers by Kuenning.[6-8] From such an analysis, it is found that the inner wrap will be the first part of the core to saturate. The time at which it saturates, τ_i, can be found from the expression,

$$\int_0^{\tau_i} V_a\, dt = \Delta B_s w S(\text{i.d.}) \left[\left(\frac{\text{o.d.}}{\text{i.d.}}\right)^{1/2} - 1\right]. \tag{5}$$

Prior to saturation of the inner wrap, the eddy current, and hence the primary current, i_p, is given by

$$i_e(t) = i_p(t) = \frac{\pi V_a d^2 \int_0^t V_a(\tau)\, d\tau}{4\rho \Delta B_s w^2 S^2 (\text{i.d.})\left[\left(\frac{\text{o.d.}}{\text{i.d.}}\right)^{1/2} - 1\right]^2}. \tag{6a}$$

From the onset of saturation at the inner wrap until the core is completely saturated, the eddy current can be found from

$$i_e(t) = \frac{\pi V_a d^2}{4\rho w S} \times \left[\frac{1}{1 - \left(1 - \frac{\text{i.d.}}{\text{o.d.}}\right)^{1/2}\left(1 - \frac{\int_0^{\tau_m} V_a\, dt}{\Delta\phi\ \max}\right)^{1/2}} - 1\right]^{-1} \tag{6b}$$

where $\Delta\phi$ maximum is the total flux change available in the core and τ_m is the time at which total saturation occurs. If the voltage across the core remains constant throughout most of the pulse, Eq. (5) predicts that the drive current begins at zero and rises linearly until the inner wrap saturates. Figure 3 shows the comparison between the predicted and measured currents for a typical 1-mil core used in the accelerator. The values are in good agreement after 150 nsec but lack agreement prior to that. The measured current begins with a step current of 500 A. Figure 4 shows a similar comparison for a 1/2-mil core. Here the lack of agreement is even more pronounced. The

main reason for this discrepancy lies in the assumption that H is zero at the wall. A more accurate assumption would be that the velocity of the wall, v_w, depends on H at the wall, H_w, by the relation

$$v_w = \alpha\left[H_w - H_0\left(1 - e^{-H_w/H_0}\right)\right] \qquad (7a)$$

which qualitatively fits most data that has been published. In the above equation, α and H_0 are constants. Unfortunately, we were unable to obtain analytical expressions for τ_i or i_e except where $H_0 = 0$, which is equivalent to the analysis just discussed. However, the problem can be approached numerically.

The core was broken into six concentric sections, each section having six concentric subsections. The voltages of the wraps within a subsection were assumed to be equal. Also to simplify the program, Eq. (7a) was replaced by a three-part linear approximation of the form

$$v_w \simeq \alpha(H_w - H_{0i}) \qquad (7b)$$

where H_{0i} takes on one of three values depending on the value of H_w. At the end of short time intervals, the voltage of each subsection, which depends on the primary current, is calculated and added together. If the sum of the voltages is close enough to the applied voltage, another time step is made; otherwise, the current is changed and the calculations are made over. This continues until τ_m is exceeded.

While the program was being written and debugged, cores consisting of six concentric sections were obtained, and the relation of current and section voltages to the applied voltages were measured. These measured values were then compared to the calculated values to determine appropriate values for H_0 and α which were 1.3 and 1500, respectively.

These calculations have made manufacturers more willing to accept our specifications for pulse performance. Figure 5 shows the comparison between the measured and computed values for recently obtained 1/2-mil and 1-mil cores. The agreement is quite good throughout the pulse.

REFERENCES

1. A. G. Ganz, Trans. AIEE 65, 177 (1946).
2. MIT Radiation Laboratory Series (McGraw-Hill, New York, 1948), Vol. 5, p. 633.
3. F. Voelker, Analysis of Iron Cores Driven With Fast Pulses and High Voltages Per Turn, Lawrence Radiation Laboratory, Livermore, Rept. UCID-827 (1958).
4. H. W. Van Ness, W. S. Mitchell, and R. M. Searing, Preliminary Investigation of Astron Magnetic Cores, Lawrence Radiation Laboratory, Livermore, Rept. UCID-5097 (1965).
5. S. D. Winter, Magnetization of Tape Assuming Uniform Distribution of Nucleating Centers Throughout the Tape, Lawrence Radiation Laboratory, Livermore, Rept. UCID-5042 (1966).
6. R. W. Kuenning, Saturation Wave Analysis For Eddy Currents Entirely Within the Magnetic Strip, Lawrence Radiation Laboratory, Livermore, Rept. UCID-15029 (1966).
7. R. W. Kuenning, Eddy Current Analysis Extended for Non-Constant Applied Voltage, Lawrence Radiation Laboratory, Livermore, Rept. UCID-15030 (1966).
8. R. W. Kuenning, Eddy Current Analysis Extended for Times After the Inner Wrap Completely Saturates With Non-Constant Applied Voltage, Lawrence Radiation Laboratory, Livermore, Rept. UCID-15031 (1966).

Fig. 1. A typical accelerator core. Dimensions of this core were: i.d. = 8.5 inches; o.d. = 24 inches; width = 0.5 inches.

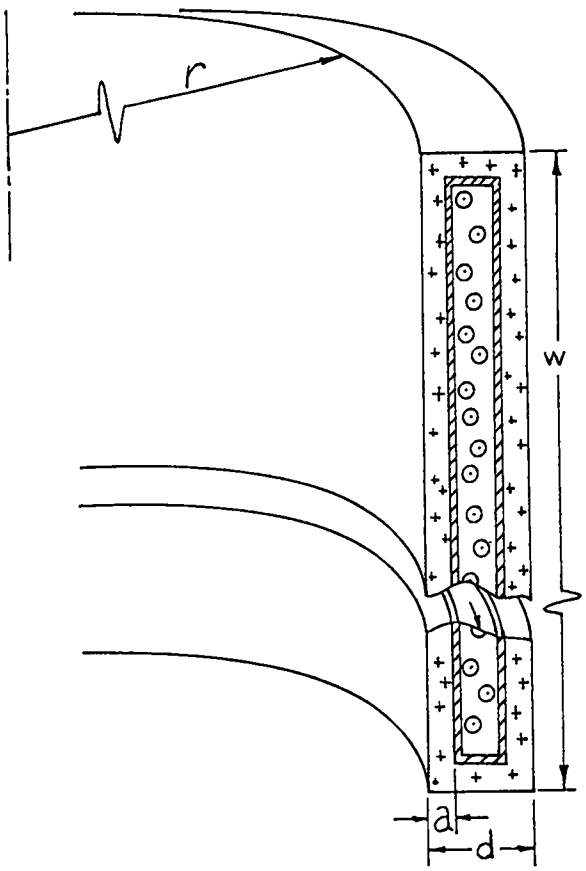

Fig. 2. Cross section of a single wrap of tape.

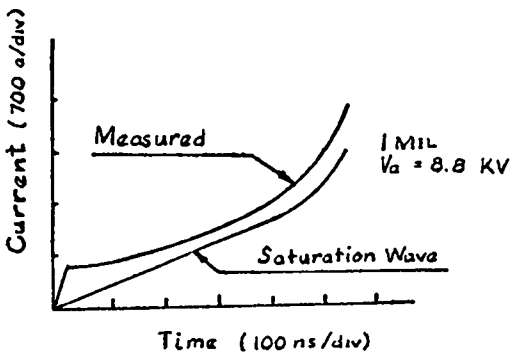

Fig. 3. Comparison of measured and predicted (saturation wave) current for 1-mil core.

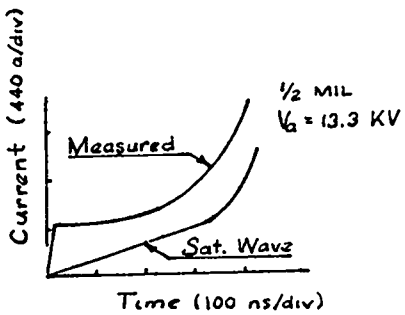

Fig. 4. Comparison of measured and predicted (saturation wave) current for 1/2-mil core.

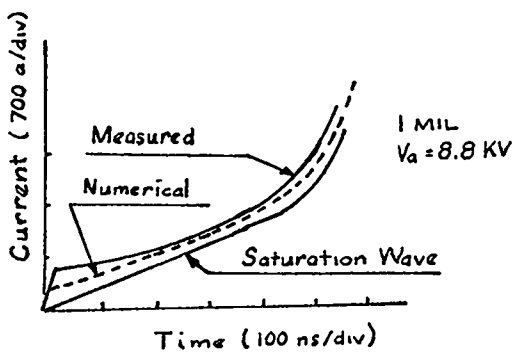

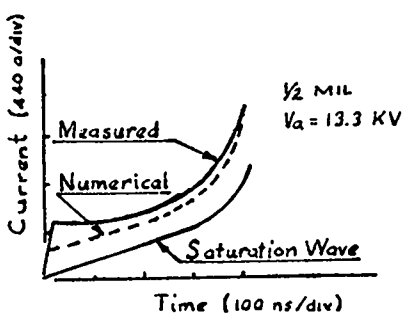

Fig. 5. Comparison of measured and computed currents [$v_w = v(H,\alpha,H_0)$] for 1-mil and 1/2-mil cores.

EXPERIMENTAL STUDY OF 50-50 Ni-Fe TAPE-WOUND MAGNETIC CORES FOR THE ASTRON ACCELERATOR*

Gary G. Berg
Lawrence Radiation Laboratory
University of California
Livermore, California 94550

ABSTRACT

Two of the fundamental limitations on the Astron accelerator have been the poor quality and uniformity of pulse properties in the accelerator cores. An experimental and theoretical study to improve these properties was undertaken. The primary goal of the study was to determine which parameters affect the excitation current of a 1-mil tape-wound core when it is energized by kilovolt pulses. The most significant conclusion from our research is that eddy currents form the dominant component of excitation current. Furthermore, eddy currents in several adjacent, poorly insulated turns of tape seem to be the prime cause of the lack of quality and uniformity of cores. Following this core study, an order for 266 cores was placed, and for the first time, manufacturers had the knowledge to respond to performance specifications. The contractor was provided with special pulse test equipment so that cores could be tested and reprocessed, if necessary, until they did meet these specifications. Consequently, cores of higher quality were purchasable.

INTRODUCTION

In the Astron accelerator, several hundred large magnetic cores are, in effect, used as pulse transformers in which the common secondary load is the beam. The primary driving networks consist of charged, coaxial transmission lines which are switched to the cores when this beam is present. The driving networks must supply the excitation current of the cores as well as that of the beam. From Fig. 1, we can see that the accelerating voltage applied to the core (V_{accel}) decreases as the total primary current ($i_{core} + i_{beam}$) increases, due to the source impedance, Z_0. Therefore, to obtain maximum energy from the beam, we must have cores with minimum excitation current. Finding the parameters affecting this excitation current was the goal of the core study described here.

Typical core size is 8-1/2-in i.d. by 24-in. o.d. by 1/2-in wide, wound of 1-mil, square-loop, 50-50 Ni-Fe tape. These cores are excited by voltage pulses of 10 to 12 kV, lasting for 0.3 μsec.

PROBLEM

Since the cores purchased for Astron in 1960 had no specification for performance, they were found to be higher in excitation current than anticipated, and varied excessively from core to core. This performance variation resulted not only in lower total beam energy, but made core compensation difficult as well. The compensating circuit forces the voltage across the core to be flat, making the beam energy constant throughout the pulse. The lack of uniformity in excitation current resulted in varying accelerating voltages from core to core, or non-constant beam accelerating field gradients. This complicated the beam-focusing problems.

Since there were plans to buy additional cores for the extension of the accelerator, we began an experimental and analytical[1] study to determine the parameters important to the excitation current of thin-gauge cores at high-drive levels.

CORE TESTER

The first need of the experimentation was a core-testing device that would duplicate the drive system of the Astron accelerator, but which would still exclude all phenomena not resulting directly from the core. We needed a flat-top voltage pulse, but without the complicated compensating network

*Work performed under the auspices of the U.S. Atomic Energy Commission.

used on the accelerator. To keep current and voltage independant, the source impedance should be minimum. The circuit had to have a rise time of tens of nsec and be capable of providing kV pulses at thousands of amperes. Pulse length could be as long as long as several μsec.

Our solution was to fabricate a capacitor discharge circuit with a low inductance switch coaxially arranged to limit distributed inductance. The capacitance of this system is large enough to provide the core with its excitation current until it saturates with a negligible voltage drop. The switch used is an air-pressurized spark gap. The gap is adjusted so that at 100 psi it is just below the breakdown threshold. When the pressure is relieved, the voltage-holding ability of the gap is reduced to breakdown. The gap then ionizes and initiates conduction.

The signals to be monitored from the energized core are excitation current and core voltage as a function of time. Since there is no secondary load, all the primary current is core excitation current. This is monitored by recording the voltage across a small resistor in series with the primary turn around the core. The voltage is measured from a high-impedance secondary turn around the core. These signals are applied directly to the plates of a modified Tektronix 551 oscilloscope.

Since a number of experimental cores were to be purchased with no application other than for this study, we performed most of our experiments on small cores, typically 2- to 3-in. o.d. (as compared with 24-in. to 33-in. o.d. on the cores used in Astron). Nearly all the results were applicable to the large cores making the study less expensive.

Experiments

The experiments performed were concerned with the effects of "interwrap eddy currents", or eddy currents circulating in more than a single turn. This is a result of shorting between adjacent turns due to various possible causes, such as: Inadequate insulation between turns, which allows metal-to-metal contact; the formation of a burr on the tape which bites through the insulation into the next turn; or the scratching or marring of the surface of a completed core, which tends to pull one turn into the next.

The first experiment was an attempt to relate dc "o.d.-i.d. resistance" of a core to its pulse properties. In a perfect core, the o.d.-i.d. resistance would exactly equal the total strip resistance, since the only current path for the ohmmeter is through every turn. In the presence of interwrap shorts, however, some turns are bypassed resulting in a lower o.d.-i.d. resistance. This appeared to be a quick and easy check on the interwrap shorting and therefore, on the interwrap eddy currents. We selected a core, which was pulsed, had a strip resistance calculated to be 60 ohms, and a normal o.d.-i.d. resistance measured at 26 ohms. The core was then squeezed radially until the o.d.-i.d. resistance dropped to 12 ohms, when it was again pulsed. Finally, it was compressed to a point where the o.d.-i.d. resistance was 2 ohms, then once again tested. A comparison of the results showed that there was detectable but slight degradation of pulse properties as the o.d.-i.d. resistance changed by a factor greater than 10. One point of touching between adjacent wraps of tape will significantly affect the dc o.d.-i.d. resistance, but two points of touching are necessary to form a closed path for interwrap eddy current flow. Therefore, we can say that a core having a high o.d.-i.d. resistance measurement should be relatively free of interwrap eddy currents, but we can draw no conclusion about a core having a low reading.

The second experiment was an attempt to simulate interwrap shorting by connecting a one-turn loop with a series resistor around part of the core. The current generated in this loop has the same shielding effect on core pulse performance as the effect of interwrap eddy currents in the section enclosed by the loop. The magnetic field in the enclosed section is proportional to the primary excitation current minus the current in the loop. This causes the rate of change of flux in this area to be reduced, but since the total rate of flux change of the core must remain constant $\left(V = \frac{d\phi}{dt}\right)$, the flux rate outside the enclosed section is increased. As a result, the non-shielded section will saturate first, then the required total flux change must occur within the shielded section. This results in an increase in the slope of the excitation current at the time of saturation of the non-shielded section. In the simulation where the shielding is discreet, the

changes are abrupt. In real cores, where the shorts are uniformly distributed, the current tends to rise non-uniformly, concave-upward, making compensation in the accelerator at the end of the pulse very difficult.

In the third experiment, a core was deliberately scratched across the windings and was checked for changes in pulse characteristics at several stages. The results show that the current increase due to the scratching is not significant until the scratches become extensive and are on both sides of the core. This tends to confirm the results of the first experiment.

In the fourth experiment, a core was selected whose pulse waveforms had the concave-upward current typical of cores having interwrap shorting. This core was carefully rewound with 1/4-mil mylar tape between the wraps. In this way we forced the core to be absolutely free of interwrap shorting. In the process of rewinding, however, some of the dc magnetic quality was sacrificed. The formerly "square" hysteresis loop was skewed until the residual flux density differed markedly from the maximum. As is shown in Fig. 2, the removal of interwrap shorts greatly improved the pulse properties of the core. It also appears that the damage done to the dc properties had little effect on the pulse properties.

CONCLUSIONS

After the work on small cores was done, it was necessary to buy several large cores to verify that the conclusions drawn from the small cores applied to the larger ones, and to check the manufacturers' ability to apply these conclusions in making better cores. It turned out that the large cores were indeed improved, but there was a greater difference between the theoretical minimum excitation current and the measured current in the large cores as compared to those of the small ones. This seems reasonable due to the increased bulk of material and greater circumference per turn. For example, if there is an average of 3 feet per short in the magnetic tape, a small core would have about five turns per short, while a large core would have about two shorts on each turn.

After giving the manufacturers some parameters to follow to make consistently good cores, we were able to buy cores under a specification that had pulse performance limits.

The bid winning company was provided with a core tester to be located within their plant and operated by their personnel. This enabled them to test the cores, and to improve or salvage those having excessive currents before the application of the edge-strengthening material prohibited these operations. The tester's location in the manufacturer's plant also allowed and encouraged experimentation on improving our cores. Since the core tester was to be operated by non-LRL personnel who might not have high voltage pulse experience, it had to be made as safe, simple, portable and self-contained as possible. The basic circuit was identical to that used in the original study but was scaled up to accommodate the large size cores (see Fig. 3).

The cores that were received from this order were considerably higher in quality and more uniform than those from earlier orders. Table I summarizes a comparison of magnetic core currents of this last core shipment with previous orders, and with the theoretical optimum values of current when driven with a 9-kV pulse.

REFERENCE

1. S. D. Winter and R. W. Kuenning, "Analysis of Flux Reversal in Tape Cores," Lawrence Radiation Laboratory, University of California, Livermore, Rept. UCRL-71552, submitted to the Proceedings of the Symposium in Engineering Problems of Fusion Research, April 8-11, 1969.

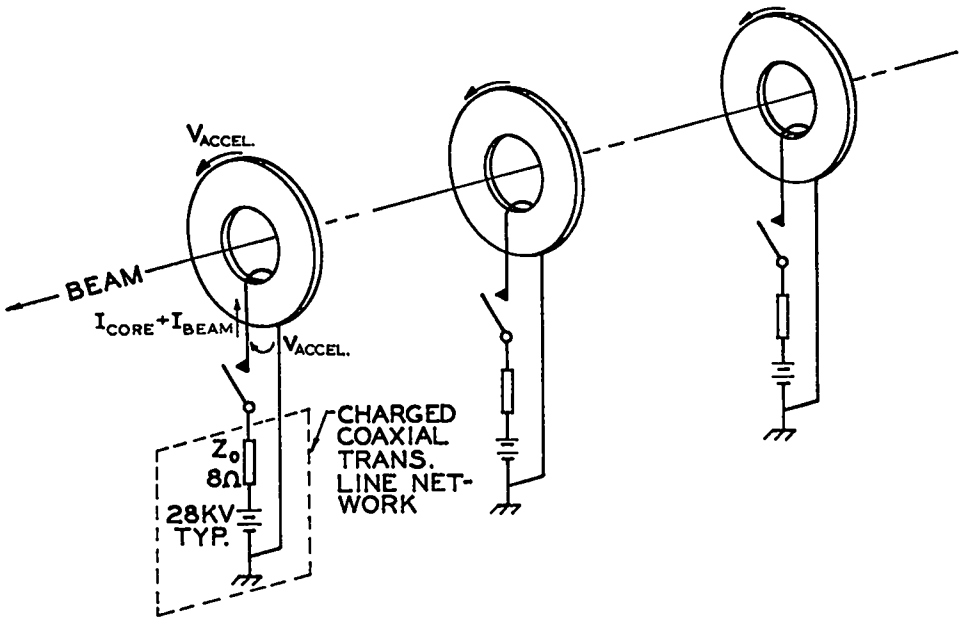

Fig. 1. Conceptual schematic of the Astron Accelerator.

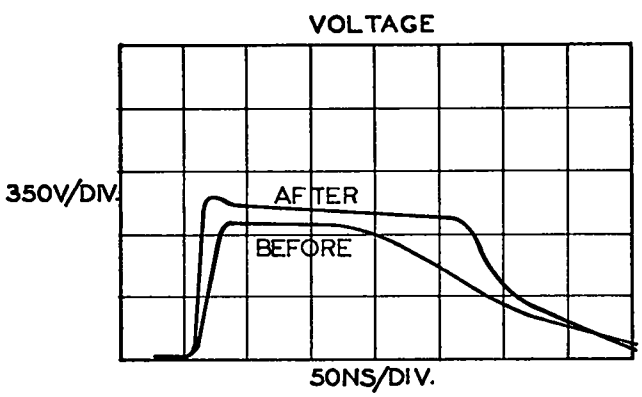

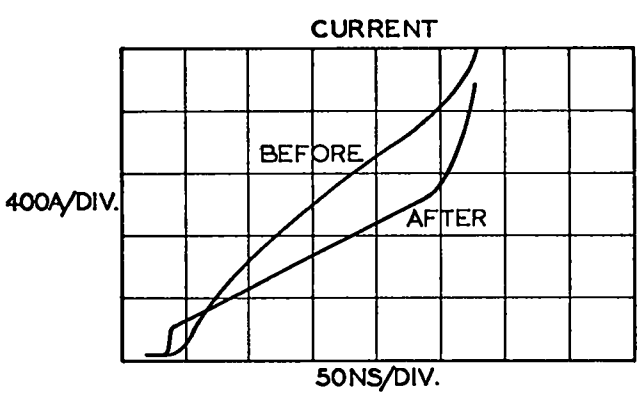

Fig. 2. Comparison of core pulse properties before and after insulating adjacent turns with mylar.

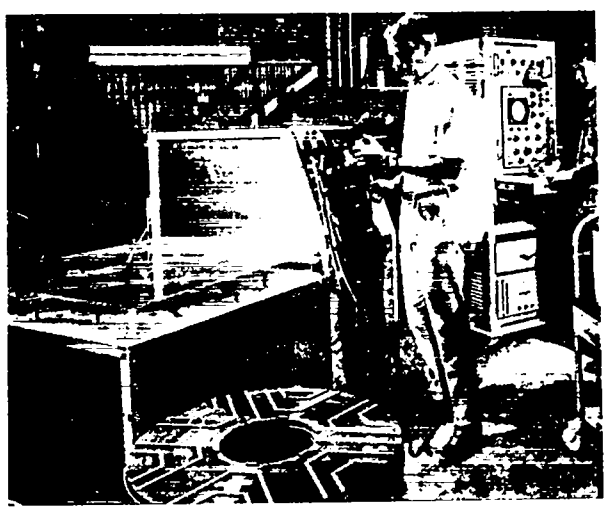

Fig. 3. Portable core tester.

Table I. Comparison table of the mean excitation current and spread of the latest core order, earlier orders, and theoretical optimum.

	Latest Core Order (Amp)	Earlier Core Order (Amp)	Theoretical Optimum (Amp)
Mean Initial Current (At t - 50 nsec)	510	720	372
Current Spread to Include 90% of the Cores	120	250	0
Mean Final Current (At t - 400 nsec)	1270	1620	1130
Current Spread to Include 90% of the Cores	320	535	0

DIGITAL CONTROL OF A RESEARCH DEVICE *

E. D. Simon S. P. Duritt M. Pelovitz

Plasma Physics Laboratory
Princeton University
Princeton, N. J.

ABSTRACT

Operation of the FM-1 research device at the Plasma Physics Laboratory will require an entirely new control complex. This system will provide the functions of start-up, shutdown, enable-disable, arm-disarm and start-stop.

In providing these functions the control system must be designed in such a way that failure will not cause a hazard to personnel or equipment.

Experience with the existing control systems at PPL indicated the following shortcomings in relay systems. First, they are very inflexible. They do not provide detailed status information. Relay systems are also very costly. By comparison digital process control is very flexible and can give extensive status information but the initial cost is high.

The FM-1 operator will use lighted push buttons in the console. Conditions which prevent the normal sequence of operation will be displayed on a storage scope. Field levels and timer settings can be set by a 10-button "touch tone" input. The normal operations log will be printed on the typewriter. Parameter settings will be punched on cards.

THE NEED FOR CONTROLS

The FM-1 research device will require the simultaneous operation of some twenty separate subsystems. Part of these systems is shown in Fig. 1. Each subsystem interacts with the FM-1 device and in most cases a subsystem must interact with a number of other subsystems. An obvious example of this is the need for removal of coil current in the event of loss of water flow, followed by removal of other fields due to the loss of the first, and the cutoff of rf heating due to field loss.

This subsystem interdependence creates the necessity of having an overall system which can accomplish the following objectives.

1. Supervise all interactions between subsystems.
2. Cause subsystems to operate in a manner that will not permit undesirable interactions.
3. Protect operators and equipment from injury.
4. Survey itself and revert to a safe condition in the event it is unable to continue the above tasks.
5. Convey to the experimenter information about the subsystems.

It is important at this point to emphasize that if the experiment is to be an organized, efficient, coordinated operation, the control system must be

* Work performed under auspices of the U. S. Atomic Energy Commission.

treated as an integrated system separate and distinct from the subsystems. Bringing together a dozen remote control boxes does not of itself create a central control system.

LEVELS OF OPERATION

The FM-1 subsystems contain energy sources which can be dangerous to equipment and personnel. For this reason control action is taken according to the following priority schedule.

1. Personnel safety.
2. Equipment safety.
3. Experiment parameter requirements.
4. Sequence timing.

The following levels of operation are standard on large research devices at the Plasma Physics Laboratory.

1. Shutdown In this level, all ac power sources are disconnected from a subsystem, access may be had to all areas, and no connection exists to the loads.

2. Startup but Disabled AC power is connected, auxiliaries are energized and operating access is not permitted to a subsystem. However, no connection exists from subsystem to load and access may be had to the FM-1 device. All high voltage equipment is deenergized. This is the normal access state when an experimental run is made.

3. Enabled but not Armed The subsystem is now connected to the load. Access to the FM-1 device is NOT permitted.

4. Armed but not Started All high voltage sources are energized, energy storage banks are ready, and generator fields are energized. System only requires timer pulse to deliver energy.

5. Start All steady state fields come on, sequence timer begins its operation.

The system may be placed in each successive level of operation if and only if all requirements for that level have been met. It is also required that increasing levels of operation be taken one at a time. The ascending levels of operation are shown in Fig. 2.

DIGITAL VS RELAY

Two approaches may be taken to plasma device control systems. One can utilize hardware such as relays, gates, etc., and produce the required logic of wire connections between elements, or one can utilize a computer and produce the logic via programming. The relay system is inflexible, requiring hardware changes to effect a change in logic. The digital approach is very flexible since all logic is incorporated in the programming. Since the logic is programmed, the changes take less manpower and less overall time to complete. A digital system also permits one output device to convey detailed information on all aspects of the control system.

Unfortunately, the initial cost of a digital system is high and at first glance may indicate that the digital system is not feasible. However, a plasma device is a research device and research demands change, change in controls as well as experiments. A large relay system may demand the full time services of a draftsman and a technician to make these alterations. Over a period of years these changes will cost more than the initial digital system cost. Further, the time required to get a needed change operational on a relay system seldomis less than a month, whereas a digital system can be changed in days, including debugging.

For these reasons, the FM-1 control system will be based on a programable digital computer.

SYSTEM DESCRIPTION

The controller is an IBM 1800 data acquisition and control system. The control processor has a 16,000 word random access memory. Instruction execution takes 2 microseconds. The core memory is augmented with a 512,000 word disk storage unit. Programming input and output

is done via a card reader-punch which reads at 300 cards per minute and punches at 80 cards per minute. Since our system requires only occasional printout, the output printer is a typewriter unit which operates at 900 characters per minute.

Process inputs include 416 binary points in 16 point groups and 128 binary interrupts in 16 point groups. Analog inputs include 45 analog points multiplexed through one analog to digital converter which has a conversion rate of 20,000 conversions per second.

Process outputs consist of 480 binary points in 16 point groups and 12 digital to analog converters.

Supporting software on the system includes an executive system which permits programs to be transferred into core from the disk and executed without external intervention. Time sharing with non-process programs is also implemented.

Since this processor is responsible for preventing injury to people or equipment the following steps have been taken. The cpu and the disk unit are equipped with two extra bits on every stored word, one is a parity bit and the second is a storage protect bit. Each is checked by the hardware. There is an operations monitor which must be reset every 5 seconds or an alarm is tripped. All outputs are pulse type with a duration of 80 milliseconds. The processor must up-date at the end of 80 milliseconds or the output reverts to a fail safe condition. All inputs are scanned at the same rate. Thus, any failure of cpu, disk, or program causes a system shutdown.

CONTROL SYSTEM OPERATION

The FM-1 control system and data acquisition station will share a room with another system which is used on another research machine. The room layout is as shown in Fig. 3.

In order to avoid problems with training operators to be proficient typists, and in order to make the FM-1 controls similar to existing systems, the processor-operator interface is a console with lighted push buttons. Each button lights when it can be pressed and contains a micro instruction such as "Push to Enable." When pressed, the button goes dark and another button lights saying "Push to Disable." Thus, in a darkened control room, all useful buttons are lighted. Further, someone not intimately familiar with the system can be lead through the operation by the push buttons themselves.

The push buttons will be augmented by storage oscilloscopes on which system status information will be written. A typical assortment of messages is shown in Fig. 4. These messages may be followed up with supplementary information as shown in Fig. 5.

Parameter settings such as field levels, timer settings and voltage settings may be entered via a ten button data entry panel. The operator enters a 2 digital number, followed by a 5 digital variable. Confirmation of the input appears at the bottom of the scope face. When the operator is satisfied that the data is correct, he presses "ENTER" and the system updates that parameter. A portable version of this terminal may be plugged in right at the FM-1 device for on the spot debugging of the interlocks. One of these units is

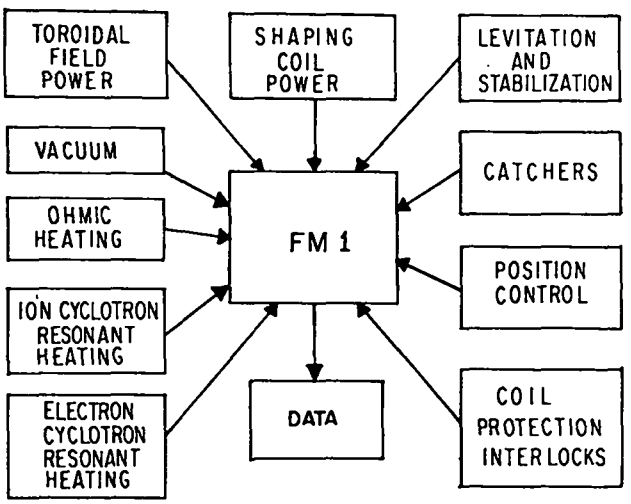

Fig. 1. Major systems on FM-1.

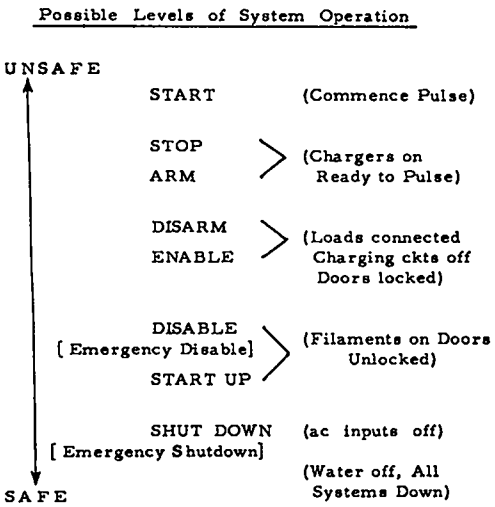

Fig. 2. Possible levels of system operation

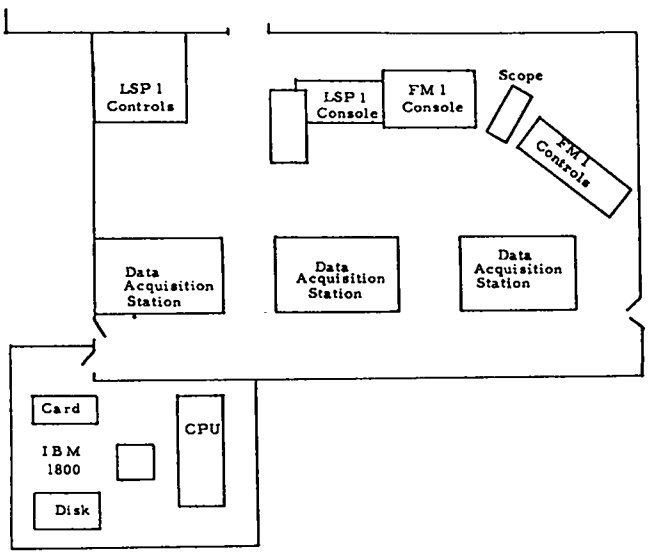

Fig. 3. FM-1 control room layout.

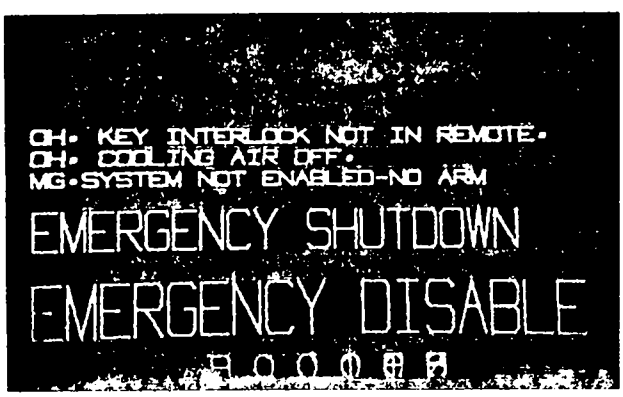

Fig. 4. Typical storage scope messages.

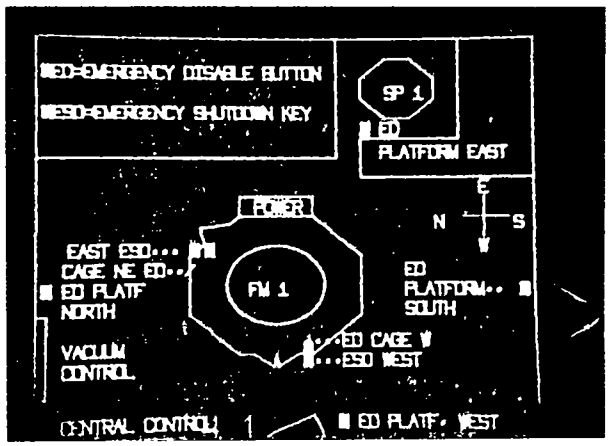

Fig. 5. Storage scope supplementary information.

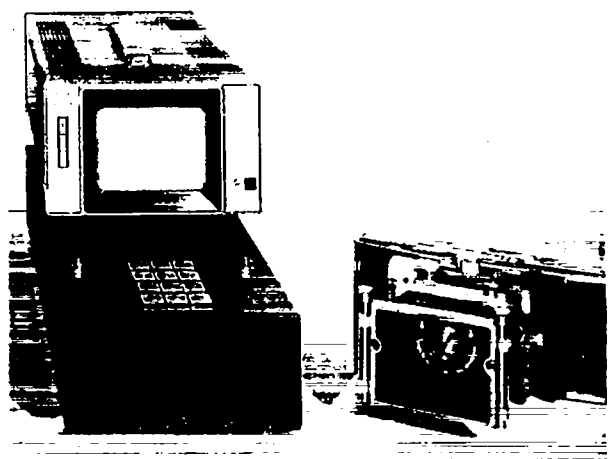

Fig. 6. Portable scope keyboard terminal.

PROGRAMMING LOGIC USING AN IBM 1800 PROCESSOR CONTROLLER*

M. Pelovitz S. P. Duritt E. D. Simon

Plasma Physics Laboratory
Princeton University
Princeton, N. J.

ABSTRACT

The IBM 1800 Processor Controller responds to input signals from push buttons or monitoring devices through several logic systems. These include a priority interrupt level scheme, a continuous scan of all digital input strips, and calls from a queuing table where programs are stored with a given priority to await execution. Outputs are handled by programming the controller to update all output terminal strips every 80 milliseconds. During this time interval any desired output changes are made by programming these changes into the contents of the machine addresses where the output information is stored.

Differences in design concept for an existing relay system and this programmed system are described. Some of the problems which might be encountered in the programming are pointed out, as well as the steps necessary for establishing a program using the controller's full capabilities.

Inputs and Outputs

Several different types of inputs are available on the controller, and the machine recognizes and processes the signals received in different ways. One hundred twenty-eight input terminals are recognized by the machine on different priority levels Sixteen terminals may be connected on each one of these levels. Figure 1 shows a layout of this priority system. Each terminal strip represents one of the PISW (program interrupt status word) blocks on the drawing. Other machine functions such as typewriter, disks, etc., also have assigned levels in the controller as shown.

When a switch or monitoring device connected to a terminal point operates, the controller interrupts its present operation and immediately proceeds to execute the subroutine servicing the activated terminal point. The only exception to this rule is if an interrupt at a higher priority interrupt level requires service. Servicing of the lower priority interrupt would then be delayed until completion of the higher.

Many input devices should have action taken both when they are energized (contact closure) and when they become deenergized (contact opening). Examples of such devices are water flow switches and door interlocks. These must be closed for a system to be operable and deactivate the system if they open during system operation. Eight digital input terminal strips of sixteen contacts, or bits each are employed for this. Any contact connected to these points will not immediately be noticed by the controller, since the strips are sensed only by a program command.

At present each of these eight strips is scanned every 80 milliseconds. Using an IBM-supplied fortran subroutine, each one of the 16 bits or

---

* Work performed under auspices of the U. S. Atomic Energy Commission.

contacts is compared against a corresponding 16 bit word located in core. If, for example, a contact has closed since the last scan, the particular terminal strip being compared will have a one in the bit position associated with that contact. A non-comparison will result when the subroutine compares this word against the word in core and the scanning program will branch to another subroutine. As part of the subroutine to which the program branches, the comparison word in core is changed and a one bit is now placed in the bit position which did not compare. As long as the contact which had closed remains closed the terminal strip containing that contact will again compare with the revised comparison word in core. However, when the contact reopens another non-comparison results and upon branching, the appropriate control action can again be taken.

Thought has been given to the problem of a process controller failure and its resultant effect upon machine operation. For example, if a controller failure were to occur while the controller was on line, it could enter a wait state and be unresponsive to any inputs. In order to prevent a potentially dangerous situation, a fail safe system for signal outputs is employed. All output signals from the controller are on for a maximum of only 80 milliseconds. If they are not updated at the end of that time, they will immediately revert to their off positions. Consequently, our programming procedure is to update all outputs every 80 milliseconds. The actual updating is performed by calling an IBM subroutine which sets the sixteen transistor switches of the particular output terminal strip either off or on depending upon whether it finds a zero or 1 in each of 16 bits of some designated address in core.

The 80 millisecond time interval is chosen as a compromise. If this updating time is made much shorter, the program begins to occupy an appreciable percentage of the process controller time. If the time were much longer there would be too much delay in recognizing any depressed buttons on the scanned input strips and in performing stop functions.

Steps in Programming a System

Figure 2 shows a portion of a relay-oriented control system for a motor generator set at Plasma Physics Laboratory. The M-G sets can be controlled from several locations in the building through a control transfer system. Figure 3 shows the corresponding fortran programming to perform the same functions. The section shown controls the operation of the disconnect switches linking the M-G sets to the load. This is known as the "enable-disable" function. Figures 4 and 5 show portions of the controls for the performed function after the system is enabled.

The "arm-disarm" circuit allows the fields of each 2.5 MW generator to be excited and start the current flow into the load.

The most important priorities are assigned high priority level input positions. Any "emergency stop" procedure is on the uppermost level. Normal stop functions generally occupy higher priority positions than start functions. If the length of time to perform a function is relatively unimportant, the subroutine associated with it may be stored on the disk instead of in core memory. It can be called into core for execution in a maximum time of two seconds. This results in more efficient utilization of the 16K word core and 500K disk. However, the controller logic for handling interrupts can cause a hazardous situation and must be guarded against by the programmer. If, for example, the operator pushed a start action button associated with a disk routine and a machine fault occurred within the two second period of execution, an attempt to abort this start function by pushing stop, which is on a higher priority, could produce undesired results. The controller would leave the start routine, which is not yet completed,

service the stop and then revert back to the start. The result being that the start action would continue.

Logic Differences

Some differences between control relay logic and fortran logic are shown in Figs. 4 and 5 as examples. Note that while there is only one relay control ladder for this portion of the circuit, there are two separate subroutines. SK063 turns on or arms, the system and SK065 disarms it.

Comparing SK063 with the first relay chain, shows that the logic consists of simply checking different core addresses to see if either a certain bit in the sixteen bit word at that address is on or if some other criterion has been met before an output can be given. Many relay logic necessities, such as hold-in contacts around start buttons and contact noise suppressors are eliminated. Statement 20 of the program is an example describing in greater detail the exact technique used. This statement checks to determine if the system has been enabled, a necessity before arming, and corresponds to contact CS-2 in the relay chain. If the MG system has been enabled, a 1 will be placed in bit position one of a word called KOUT1(2). This is accomplished by statement number 60 of SK062 (Fig. 3). In that statement a 1 is placed in bit positions 3 and 15 which will perform other related output enabling functions.

If the decimal number 20481 in statement 60 is converted to a 16 bit binary number, stored in the controller, it will appear as 0101 0000 0000 0001. Note that bits 1, 3 and 15 of this word are 1's (16 bit words are labelled starting from bit 0 to bit 15). When a fortran IOR sub-program is performed using the contents of KOUT1(2) and 20481, the corresponding bits of each word will be compared and if either bit is on, a 1 will be placed in that position of the resultant word. If not, a 0 will be placed in that bit position. Hence bits 1, 3 and 15 will be turned on, but all other bits of the resultant word will remain as they were.

In order for statement 20 of SK063 to check if bit number 1 of KOUT1(2) is on we perform an IAND sub-program with KOUT1(2) and binary 0100 0000 0000 0000 corresponding to decimal 16384. With this sub-program the corresponding bits of each word must both be on in order for a 1 to be placed in that particular bit position of the resultant word, otherwise a 0 will be placed there. The entire resultant word will be either positive if the bit had been on or zero if it had not. The "IF" statement then determines what action to take by either printing a message on the oscilloscope or continuing to test the other contacts.

This type of logic is used throughout the programming. The versatility of being able to change a fortran statement instead of rewiring field components is a decided advantage in increasing flexibility of the control systems.

Level ↓	0	1	2	3	4	
0	PISW #1	Timers A, B, C				
1	PISW #2	Disk (2310)				
2	PISW #3	Tape (2401)				
3	PISW #4	Printer/ Keyboard (1816)				
4	PISW #5					
5	PISW #6	Analog Input	Digital Input	Digital Analog Output		
6	PISW #7					
7	PISW #8	Card (1442)				
8	Console Interrupt					
9						
10						
11						

Fig. 1. Priority interrupt level table.

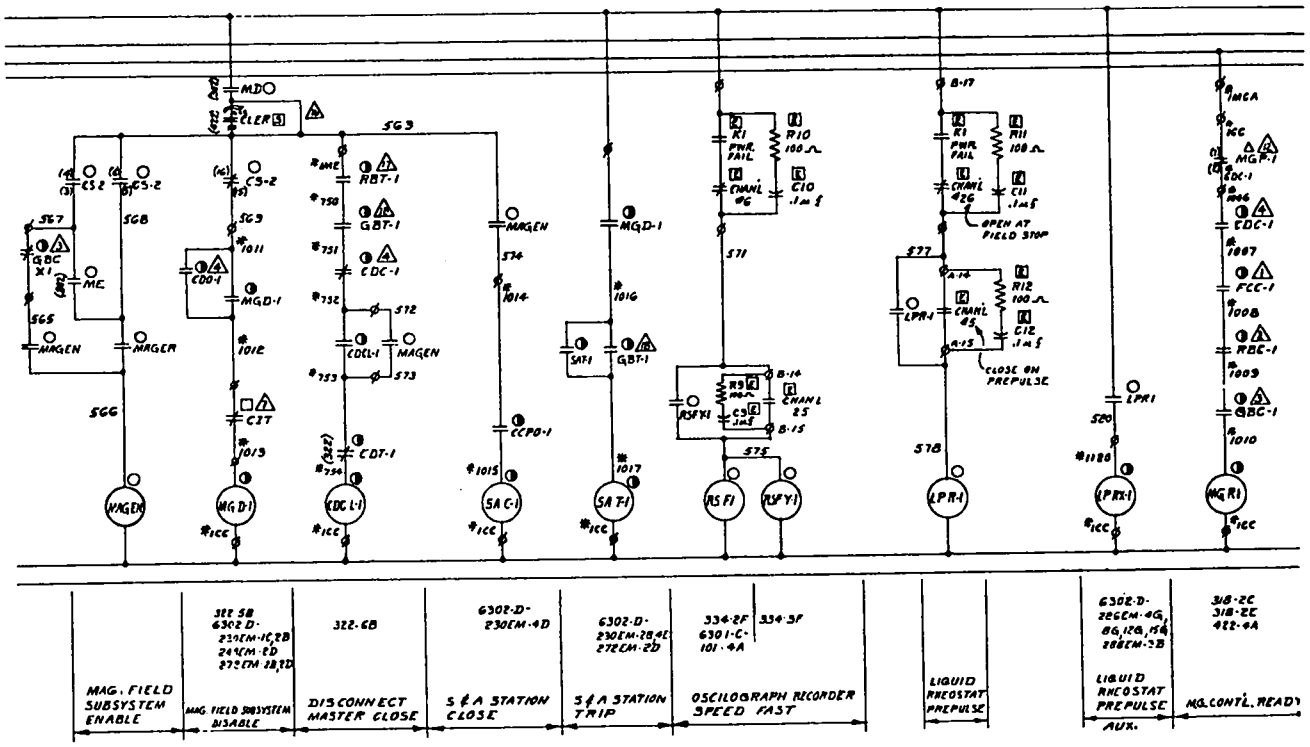

Fig. 2. MG system, enable-disable function.

```
      SUBROUTINE SK062
C     AN SYSTEM CONTROLS ENABLE FUNCTION (LEVEL 6, BIT 00)
      COMMON/INSREL/IR(3),IO(3),INP,IND,NTIME,ITABL(9),KOUT1(5),KOUT2(10
     1),KCO,KCSC,IHSTO(10),INTAB(3),HSTO(7),HRT(15),IX,KEBAS,KY,JX,KOO1B
     2,KOO1A,KOO1B,IHD01,BIND,HESS(10),II,KOO2B,KOO2A,KOO3B,IHD03,IHD02,
     3PUL1,INBT,HASIB,ITIME,TICK,HGS1(3),HGS2(3),HGS3(3),LPRE,RANGE,
     4HGSO1,HGSO2,HGSO3,HGP01,HGP02,HGP03,PUL2,PUL3,DUH1,DUH2,DUH3,
     5L1,L2,L3
C     IS CONTROL SYSTEM ON?
      IF(KOUT1(2))5,100,100
C     IS MG OPERABLE?
    5 IF(MIHD-10)10,10,20
   10 CALL SCOPE (23)
      GO TO 100
C     IS GBC CLOSED
   20 IF(IAND(ITABL(5),16))30,30,40
   30 CALL SCOPE (24)
      GO TO 100
C     IS CBR RELAY CLOSED
   40 IF(IAND(ITABL(5),32))50,50,60
   50 CALL SCOPE (22)
      GO TO 100
C     CLOSE ENABLE CONTACTS AND LIGHTS (BITS 1,3 &15)
   60 KOUT1(2)=IOR(KOUT1(2),20481)
      KOUT1(2)=IAND(KOUT1(2),-8193)
  100 IF(BASIB)102,102,104
  102 CALL INTEX
  104 RETURN
      END
```

```
      SUBROUTINE SK065
C     SYSTEM DISABLE (LEVEL 3, BIT 00)
      COMMON/INSREL/IR(3),IO(3),INP,IND,NTIME,ITABL(9),KOUT1(5),KOUT2(10
     1),KCO,KCSC,IHSTO(10),INTAB(3),HSTO(7),HRT(15),IY,KEBAS,KX,JX,KOO1B
     2,KOO1A,KOO1B,IHD01,BIND,HESS(10),II,KOO2B,KOO2A,KOO3B,IHD03,IHD02,
     3PUL1,INBT,HASIB,ITABL,TICK,HGS1(3),HGS2(3),HGS3(3),LPRE,RANGE,
     4HGSO1,HGSO2,HGSO3,HGP01,HGP02,HGP03,PUL2,PUL3,DUH1,DUH2,DUH3,
     5L1,L2,L3
C     TURN OFF CONTACT & LIGHTS (106-15,01)
      KOUT1(2)=IAND(KOUT1(2),-2)
      KOUT1(2)=IAND(KOUT1(2),-16385)
C     TURN ON PUSH TO ENABLE LIGHT IF CONTROL POWER ON
      IF(KOUT1(2))10,20,20
   10 KOUT1(2)=IOR(KOUT1(2),16384)
   20 CALL SK065
      IF(BASIB)40,40,50
   40 CALL INTEX
   50 RETURN
      END
```

Fig. 3. MG system programmed enable-disable function.

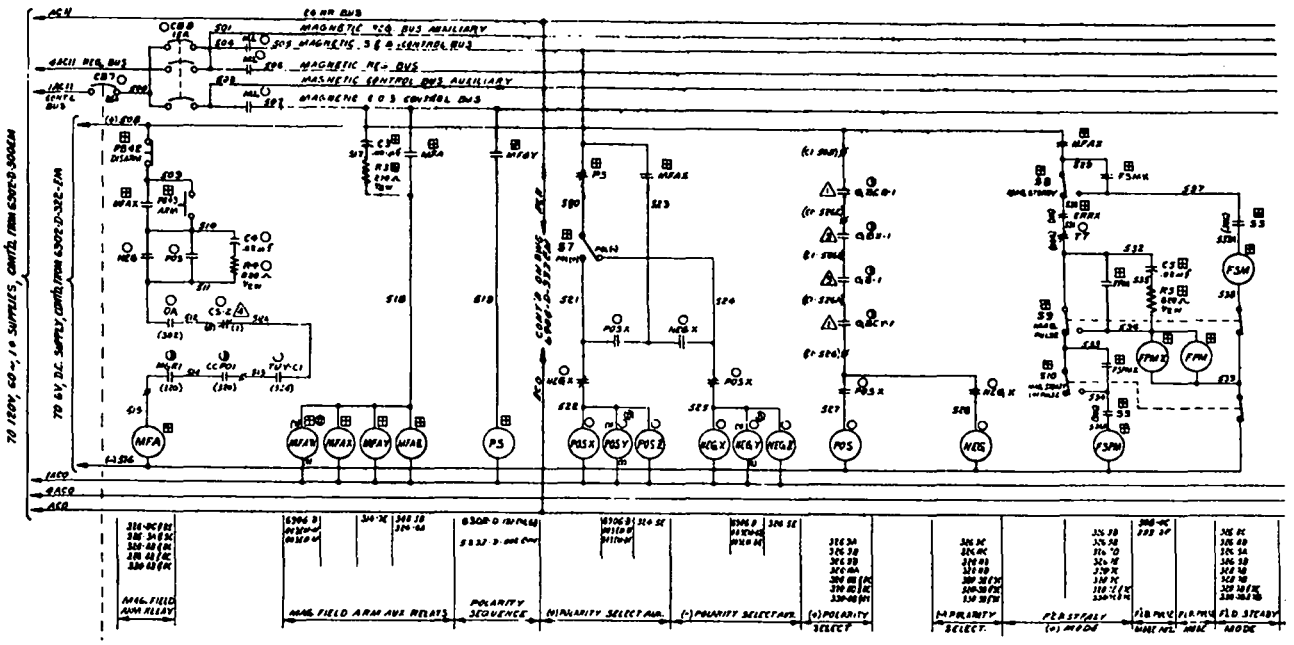

Fig. 4. MG system, arm-disarm function.

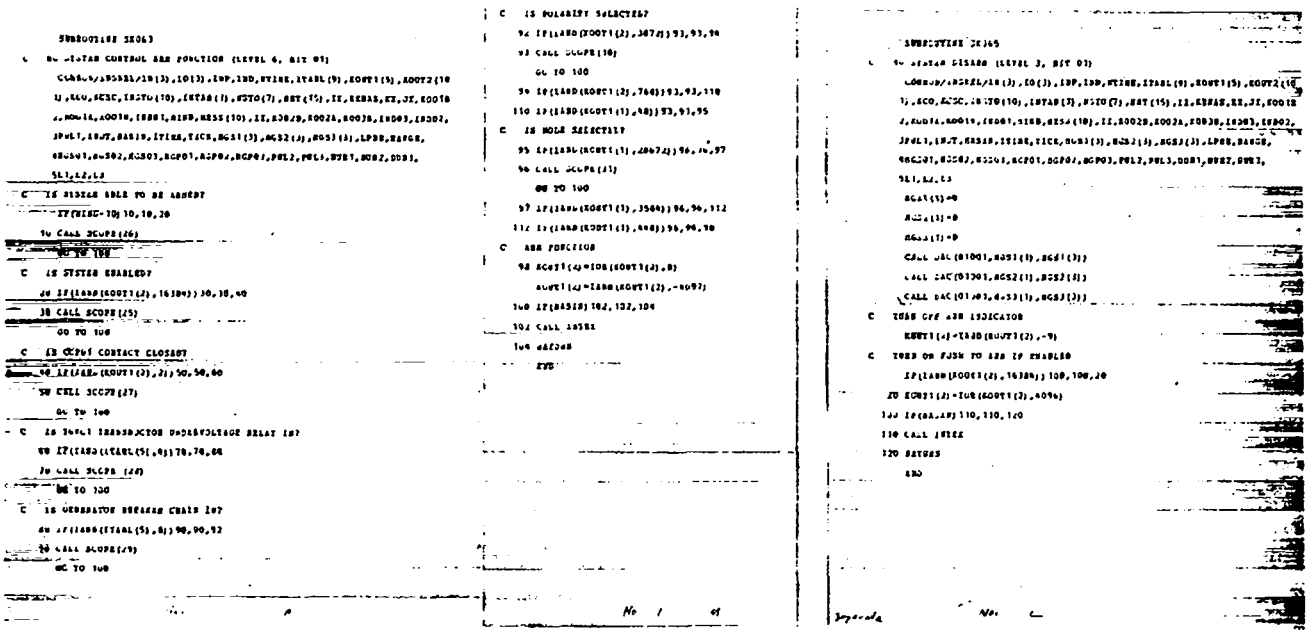

Fig. 5. MG system, programmed arm-disarm function.

DESIGN AND TESTING OF SERVO STABILIZING SYSTEMS* FOR LEVITATED SUPERCONDUCTING RINGS

P.A. Thompson, G.V. Sheffield, and F.H. Tenney

Plasma Physics Laboratory
Princeton University
Princeton, New Jersey

ABSTRACT

The general problem of providing stability for one or two levitated, current-carrying rings is presented, and the desirability of using an active system of correcting coils, servoed to ring displacements, is discussed. Computer codes for calculating systems parameters for a linearized analysis and for simulating complete ring dynamics for an actual system design are described. A comparison of the computer studies to results obtained with the magnetic model test stand for the FM-1 machine is given, along with technological developments associated with these results which have special implications to the computer work.

INTRODUCTION

As was described earlier in the Conference,[1] the levitated superconducting rings in the Princeton floating multipole machine will be stabilized by means of a servo control system of correcting coils. The either one or two rings are in the mid-plane of the axisymmetric arrangement of external coils required for producing the combined antiparallel poloidal and toroidal magnetic fields necessary for meaningful plasma experiments with these isolated ring currents. The very nature of these requisite external or "shaping" fields renders the ring unstable for at least two of the three possible types of motion: slide, tilt, or vertical.[2]

The general problem of stably levitating an object with electromagnetic fields has been considered by many workers,[3-7] all of whom have concluded that it is possible only for diamagnetic or superconducting bodies. As applied to non-servo stabilization of superconducting rings of the sort of interest here, the most significant studies are those by Rehban and Salat[6] and Neil and Cooper.[7] It can be shown that Earnshaw's theorem as applied to the lack of a stable region in the magnetic field configuration produced by any system of fixed current coils does not exclude the possibility of finding such a region when flux conserving, superconducting coils are involved. In fact, there are at least two cases of field configurations produced entirely by constant-current, fixed windings that provide positive stability for a single superconducting ring.[8] These are shown in Fig. 1.

Despite the great academic interest in these passive stabilizing schemes for levitated rings, the demands of the experimental physicist for flexibility in the external fields in which the rings of a practical plasma device would be immersed are such that it is deemed appropriate to consider only a high gain, servo stabilizing system.

*Work performed under the auspices of the U.S. Atomic Energy Commission.

COMPUTER PROGRAMS

We shall return to stability analyses for levitated rings presently. First historically, however, came a straightforward computer program for following the dynamics of one or two floating superconducting rings in a system of arbitrarily shaped and positioned windings with both fixed currents and variable currents servoed to the displacement in any of the five significant degrees of freedom and to the associated velocities of the rings. For each step of the time interval the mutual inductances between each ring and all other elements of the system are calculated, the flux conserving changes in ring currents are evaluated, and the forces and accelerations determined. The equation for the conservation of total flux through a superconducting ring,

$$L_R I = L_R I_O - M_{R1} I_1 - M_{R2} I_2 - \ldots M_{Rn} I_n \quad ,$$

determines the current in the ring at any time in terms of its original current and changes in all the other windings in the system. These changes may take the form either of changed currents or different mutual inductances resulting from changes in spatial relationship to the superconducting ring. For the case in which there are two superconducting rings, a pair of simulta neous equations of this form must be considered.

Although neither especially elegant nor extremely efficient, this Ring Dynamics Code is perfectly general* and has proved quite useful for calculating the positions and velocities of rings under a variety of conditions. However, it simply simulates proposed designs, thus can be used only for a rather expensive type of "cut and try" design engineering.

*Provision is made for superconducting correction coils.

Much more insight and guidance in magnetic design can be gained with a minimal expenditure of computer time by a Stability Criterion Code based on the small amplitude analysis[8] of the motion of a thin superconducting ring about its equilibrium position in an axisymmetric magnetic field. The geometry is that of the lower diagram in Fig. 1; the equations of motion are shown in Fig. 2, in which ϕ is the tilt angle about a horizontal axis through the center of mass. It should be noted that the lateral displacement and tilting motions are coupled, but that the vertical motion is completely decoupled from the rest of the motion. The "spring constant" variables, k_1 and k_3, are introduced to simulate the effect of stabilizing, non-axisymmetric, time dependent, magnetic fields. None is provided in the equation for vertical motion, since in the configurations of interest there is always stability for this motion.

The formal stability criterion (the right side of Fig. 2) is derived from the equations of motion for x, y, ϕ_x, and ϕ_y. Assuming a time dependence of the form $\exp(i\omega t)$, these four equations have a non-trivial simultaneous solution only if the appropriate determinant of the coefficients of the unknowns vanishes. This leads to a biquadratic equation in ω^2, both values of which may be made positive, thus assuring real ω and stable motion. The factor $(k_1 - n)$ is identified with lateral motion and the factor $(1 + n + k_3)$ with tilting motion. The regions above and below the curves are stable, and the second criterion relates the proper region for the ring being either in tension or compression under the influence of the external fields.

The computer coding of these stability criteria calculates the fields and their spatial

derivatives at the ring produced by all the other coils in the system, and this together with the size, mass, and current of the ring determines whether it is an environment which is stable in the slide and in the tilt modes. The code also calculates the "spring constants" necessary for producing minimal stability (points A and B). By translating these constants into engineering terms of forces and torques necessary to be produced electromagnetically by external stabilizing windings, it is possible then to determine the minimum "gains" (in terms of amps/inch or amps/degree) required of a servo feedback system to given stabilizing winding geometries. In fact, the differential force or torque azimuthally about the ring (which is printed out by the code) indicates the relative efficiencies of the shape and location of correction windings. And although the analysis used in the Stability Criterion Code is applicable only to single ring configurations, this feature of describing the details of the effectiveness of a given stabilizing winding for producing forces and torques on one ring with minimum effect on the other ring has been extensively used in the design of the stabilizing system for two-ring or quadrupole-mode machines.

Another feature of this code is that it calculates from the equations of motion the growth rates of instabilities or the frequencies of normal mode oscillations. Thus, not only can proposed machine designs be evaluated, but also the parameters of a test setup can be prescribed for a ring environment with any combination of slide and tilt stabilities.

EXPERIMENTAL STAND FOR LEVITATED RINGS

In the first experiments at the Laboratory with a single 20-inch-diameter levitated superconducting ring, stabilization was provided by existing circular coils.[9] After extensive analyses with the Ring Dynamic Code of the problems to be encountered in stabilizing a pair of such rings, a system of winding was designed for a general purpose test facility for experiments using one or two prototype rings. These rings, both wound with RCA SR-2100 superconductor, are a 20-inch-diameter ring with a capability of 100 kiloampere-turns and weighing 65 pounds in its Dewar filled with liquid helium, and a 36-inch-diameter ring with 160 kiloampere-turns weighing 192 pounds.

The test stand was designed to leviate and stabilize each ring separately or both rings simultaneously in either the slide-unstable mode alone or the combined slide-unstable, tilt-unstable mode. The levitation coils, which are shown schematically in Fig. 3, produce the slide instability, while the shaping pair induce the flip instability when desired. The circular tilt-stabilizing coils shown in the single, 20-inch-diameter ring case in Fig. 3 are simply moved out radially for both the single, 36-inch-diameter ring and the two-ring cases.

The shape and placement of the stabilizing windings is dictated by the combined requirements that they be magnetically efficient in producing the desired forces on the rings, yet physically remote from what would be the plasma region surrounding the rings. Stabilizing windings of the shape indicated in the conceptual drawing in Fig. 4 fulfill these requirements for slide stabilizing of the general two-ring configuration. For tilt correction a rectangular coil on a cylindrical surface is the most efficient. However, for ease of construction and so that the same coils could be used with both the small and the large rings, a less efficient circular coil shape was used for the test stand.

From comparisons of experimental results on the test stand with calculated predictions it has been possible to establish interpretation criteria in terms of engineering parameters. Computer calculations have been thus used to design a levitating and stabilizing system for a support-free 36-inch-diameter ring for the present Princeton spherator and to design a set of interchangeable correction coils for both the one and two ring modes of operation for the floating multipole machine.

A detailed study on the current-accuracy requirements for the non-servoed, axisymmetric coils used for field shaping in these machines indicates that special shunt-correction power supplies will have to be used along with the M-G set power to provide the necessary long-term stability for ring positioning.

TECHNOLOGICAL DEVELOPMENTS

The feedback loop from the ring displacements to the servoed power supplies for the correction coils is provided by five autocollimated combined light source-photocell heads, the light beams from which graze the ring Dewar and are returned by corner-reflector mirrors. A recent improvement to the system has been automatic head tilting motors connected to circuits which seek a null in correction coil currents, so that any non-axisymmetric fields from the stabilizing system can be eliminated when the ring is properly positioned. It can be shown that a knowledge of stability for each mode of ring motion is necessary in order to adjust the circuit for proper null seeking; the Stability Criterion Code provides this information.

Recalculations and extensive redesigns of the levitating and stabilizing windings for both the spherator and the floating multipole machines were necessary as a result of another technological advancement: The high heat capacity Dewar, in which a thermal mass of lead and/or mercury is substituted for part of the liquid helium in order to obtain longer lifetimes for isochoric (non-vented) operation in the same overall size Dewar. The weights and inertias of the rings increase by as much as a factor of three in order to provide these longer experimental times.

ACKNOWLEDGMENTS

The test stand work and the technological development cited above were done by G. D. Martin and J. L. Upham.

References

1. J. File, Symposium on Engineering Problems of Fusion Research, Los Alamos Scientific Laboratory (April 1969); to be published.
2. P. A. Thompson, Princeton Plasma Physics Laboratory MATT Q-26 (1968) pp. 220-223.
3. W. Braumbek, Zeitschrift fur Physik 112, 753 (1939).
4. A. H. Boerdijk, Philips Research Report 11, 45 (1956).
5. E. R. Laithwaite, Proc. of IEE 112, 2361 (1965).
6. E. Rebhan and A. Salat, Z. Naturforsch 22A, 1920 (1967).
7. V. K. Neil and R. K. Cooper, Rev. Sci. Instr. 40, 295 (1969).
8. F. H. Tenney, Princeton Plasma Physics Laboratory MATT-693 (1969).
9. J. File, G. D. Martin, R. G. Mills, and J. L. Upham, J. Appl. Phys. 39, 2623 (1968).

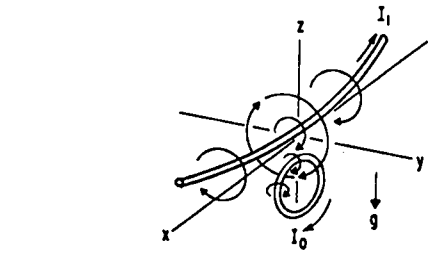

STABLE FOR $I_1^2 > \dfrac{mg\, L_0 \left(\frac{\delta^2 M_{10}}{\delta z^2}\right)}{\left(\frac{\delta M_{10}}{\delta z}\right)^3}$

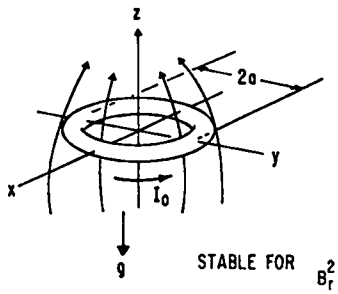

STABLE FOR $B_r^2 > \frac{L}{(2\pi a)^2} \cdot mg\left(\frac{1}{B_r}\frac{\delta B_r}{\delta z}\right)$

and $\frac{a}{B_z}\frac{\delta B_z}{\delta r}\left(1+\frac{a}{B_z}\frac{\delta B_z}{\delta r}\right) < -\left(\frac{a}{B_z}\frac{\delta B_r}{\delta r}\right)^2$

Fig. 1. Two static external magnetic field configurations for providing stability for a single superconducting ring.

EQUATIONS OF MOTION IN AXISYMMETRIC FIELDS

$$\ddot{Z} = -2\left(\omega_1^2\, n + \omega_3^2\right) Z$$

$$\ddot{X} = \omega_1^2\left[(n-k_1)x - qa\phi_x + pa\phi_y\right]$$

$$\ddot{y} = \omega_1^2\left[(n-k_1)\,y - pa\phi_x - qa\phi_y\right]$$

$$a\ddot{\phi}_x = \omega_2^2\left[-(1+n+k_3)a\phi_x - qx - py\right]$$

$$a\ddot{\phi}_y = \omega_2^2\left[-(1+n+k_3)\,a\phi_y + px - qy\right]$$

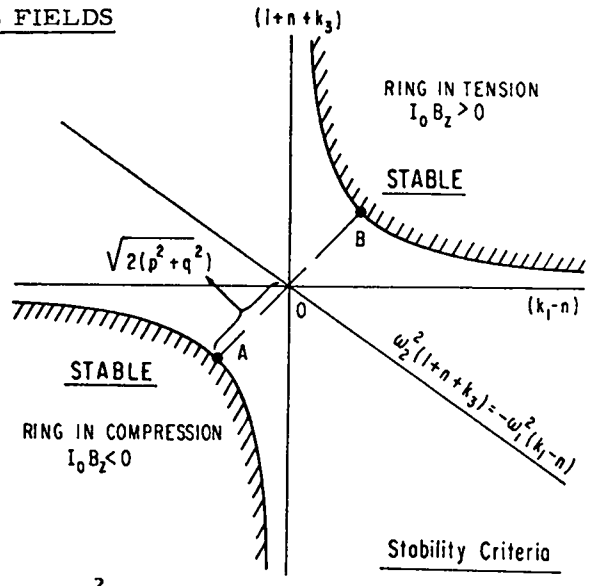

where:

$$\omega_1^2 \equiv \frac{I_0 \pi B_z}{m} \qquad \omega_2^2 \equiv \frac{ma^2}{I_{xx}}\,\omega_1^2 \qquad \omega_3^2 \equiv \frac{2(\pi a B_r)^2}{Lm}$$

$$n \equiv \frac{a}{B_z}\frac{\partial B_z}{\partial r} \qquad p \equiv \frac{a}{B_z}\frac{\partial B_r}{\partial r} \qquad q \equiv B_\theta / B_z$$

Stability Criteria

$$(k_1-n)(1+n+k_3) > p^2+q^2 > 0$$

$$\omega_2^2(1+n+k_3) > -\omega_1^2(k_1-n)$$

Fig. 2. Stability analysis for single superconducting ring in an axisymmetric field.

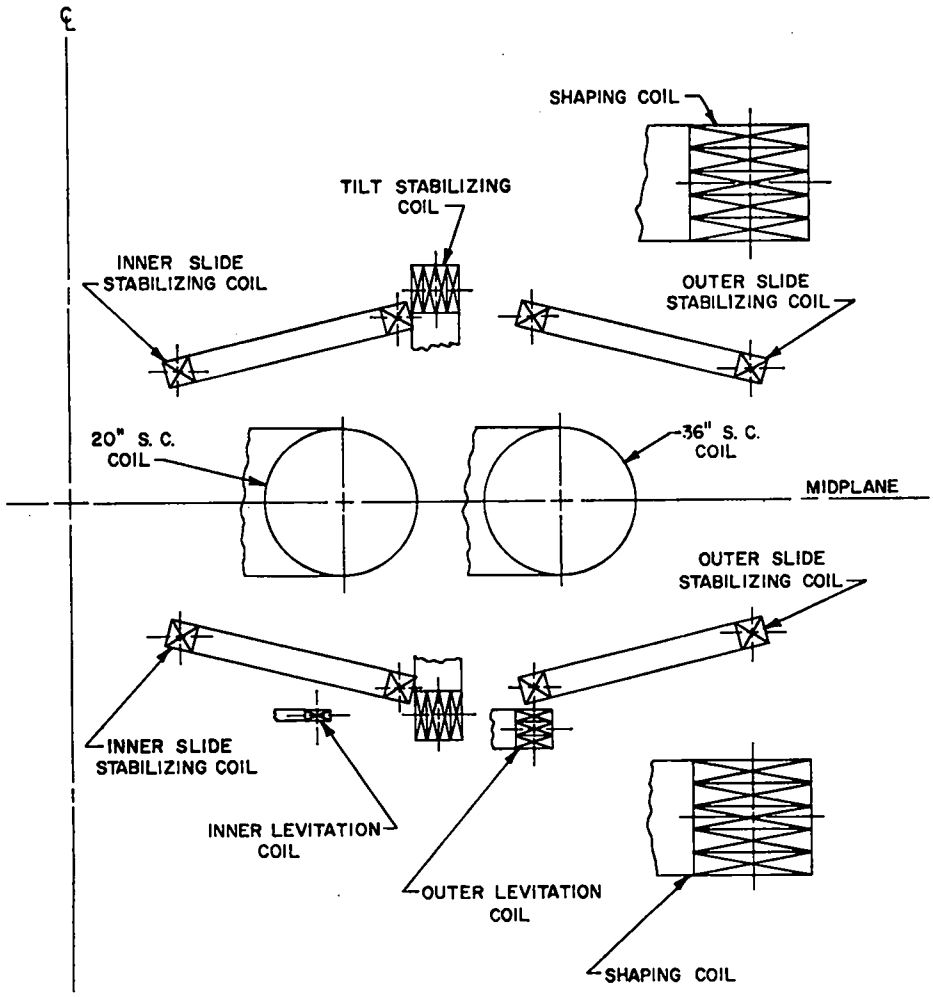

Fig. 3. Experimental test stand for ring stabilization.

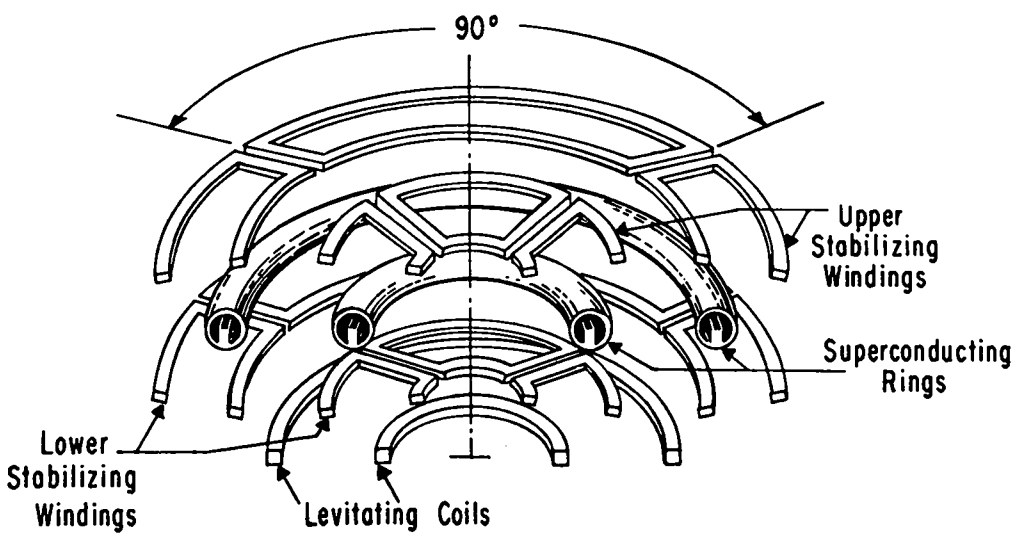

Fig. 4. Coil system for levitating and slide stabilizing two concentric rings.

REDESIGNED CONTROLS FOR THE ASTRON MAGNETIC FIELD USING OPERATIONAL AMPLIFIERS*

Jerry W. Robinson
Lawrence Radiation Laboratory
University of California
Livermore, California

ABSTRACT

The Astron machine has undergone several stages of modifications. Each of these changes has required either increased flexibility or increased output from some subsystem. One of the more adaptable subsystems has been the voltage reference scheme used to control the shaping of the main solenoidal field.

However, a recent 70 percent increase in the required number of outputs, from 65 to 110, dictated a major expansion of the reference subsystem. Complete redesign and rebuilding proved to be more advantageous than expansion both in cost and system flexibility. Several factors leading to this conclusion and a description of the resulting system are presented.

REFERENCE SYSTEM

A system to control the magnetic field of the Astron Machine has been in service for five years. During this period the number of power supplies has increased from 65 to 80, and operating methods have changed several times. As originally built,[1] the system was flexible enough to handle these changes with but minor modifications. As with nearly all systems adapted to revised uses, there were inconvenient and inadequate features.

The change from 65 to 80 outputs was not really a problem since we had built in seven spare channels, and several power supplies needed identical reference voltages and could be paralleled. Real problems were encountered though, as soon as more than two regions of control were needed.

At this point a brief description of the system requirements is in order. The Astron chamber is a long, evacuated tank in which relativistic electrons are trapped in a shaped solenoidal field as a cylindrical current sheet. When the current level is high enough, closed field lines will encircle the electron layer forming a magnetic bottle.

A view of the Astron experimental area, Fig. 1, shows one end of the tank with its encircling dc magnet coils. Each coil is fed from a separate power supply to allow fine control of the dc solenoidal field shape.

Two separate areas of control are required. One gives the basic mirror field shape and the other reinforces the central field as it is opposed by a field from trapped electrons. The transition from one region to another must be gradual and differences between adjacent coils should be small. All of the current-regulated power supplies are controlled with voltage from the reference system.

A block diagram of the original system is shown in Fig. 2. The three reference supplies "M," "A," and "B" are voltage regulated. The main or master reference M is used to match the field strength in Astron to the energy of electrons injected so that the proper radius of gyration can be obtained.

Mirror field shapes are set in with both the series dropping resistors and percentage taps chosen on the two voltage dividers across A and B. In practice, a shape is chosen and expressed in percentages of maximum. These percentages determine divider tap settings and then with "A" or "B" turned up, the variable resistors are set

*Work performed under the auspices of the U. S. Atomic Energy Commission.

to cancel the effect of the divider. Then, by taking A or B from minimum to maximum, the mirror depth will go smoothly from maximum to minimum. M sets the general field level, while "A" and "B" control mirror depth.

Reference voltage applied to each supply is a function of six variables. In equation form, $V_R = M + KA + K'B - (M + KA + K'B/R_S + R_{IN})^{R_S}$ where M, A, and B are the voltages of those three reference power supplies respectively, K and K' are voltage divider tap percentages, R_S the series dropping resistance, and R_{IN} the input resistance of the power supply it is controlling. Choosing the radio R_S/R_{IN} equal to the ratio $(KA + K'B)/M$ for each supply fills the requirement that the field be flat or $V_R = M$ when mirror depth is a minimum. This restriction that $R_S = R_{IN}/M - (KA + K'B)$ makes it impossible to have two superimposed shapes, since the two shape functions K and K' are not independent.

As the system is constructed, the shape functions are set on a patch board and R_S is one of 72 in an array of potentiometers. If, during the course of an experiment, it is desired to optimize the field shape, the only readily available control is R_S. This could be adjusted for optimum conditions but any change of A or B would then change the mirror shape as well as depth, instead of just the depth as intended.

Water-cooled voltage dividers are used across A and B to handle the 200-A divider current. These are shown in Fig. 3. Although up to 6.5 A are taken from divider taps, loading of the divider is tolerable with 65 supplies but becomes marginal with 80 supplies to control. Water leaks have been very infrequent, but, being in the control room, they attract attention. Also unfortunate from the human engineering standpoint is noise from the reference supply cooling blowers which are also in the control room.

This background of reasonable operation, adaptation to evolving methods, and minor inconveniences preceded a request to expand the system to accommodate 110 outputs. What formerly has been a minor annoyance or slight inconvenience promises to become an active problem as the system doubles in size.

Reestablishing Criteria

Establishing criteria for the expanded system has proven to be more difficult than would be the case for an entirely new system. Most difficult has been finding common ground in understanding the operation of the old system. Each member of the operation staff has developed his own effective methods of operating based on his mental picture of the system. Ideally, the new system either would allow each person to maintain his unique approach or it would be entirely different so he could learn without interference from the past.

Several system features are not in question and have been used as a very basic common ground. First of all there are 110 coils each with its own power supply. These dc power supplies are all current-regulated and voltage-controlled. They are used at the same basic level but are of four different maximum ratings. Front panel controls can be used to obtain identical transfer functions of 60 A per volt on all supplies.

Injection of electrons into the Astron machine requires a field strength in the region of the inflector which is proportional to accelerator beam energy. One master reference voltage (M reference) can still be used to set the inflector region field level for optimum injection. Any field shaping is done as needed by adjusting the field in the rest of the machine with respect to this basic level.

Individual coil currents along the machine axis are changed in two ways, either as individuals or in groups. Group changes using a single control require that an intra-group relationship be set in some part of the control circuitry in advance of the desired group action. These settings should not impose restrictions on the amount of field shaping that can be done on an individual basis while smooth proportional group control is maintained.

Since fine adjustment of individual coil currents has sometimes proven effective in the past, this capability should be included. For most effective use of hand tuning, a proportionate change should be made in the group settings at the same time. This change in the proportion of group movement

reflected in an individual channel should be such that, for some one particular setting, the region current profile would be flat. In this way the shape function for a group ($\cos^2$, etc.) could be varied in amplitude smoothly without the function itself being changed.

Since in the past, there have been more than two regions of group control desired, the new system should include provision for several regions of group control with possible additional expansion. Transitions between regions should be relatively smooth but the option should be retained for a small offset if desired.

Each person on the operating staff has at one time or another wanted to superimpose two shapes in one region. Knowing this to be impossible with the old system, however, no one listed this as a requirement for the new system until asked directly. Functions to be controlled by the operator include:

1. Field at electron beam injection point.
2. Base field level for each region.
3. Transition between regions.
4. Magnitude of region shape.
5. Region shape.
6. Individual coil currents.

Design of The Reference System[2]

System functions and criteria point to each reference channel as being a basic level with some superimposed amount of regional and individual change.

First we need a basic level proportional to accelerator beam energy and this forms a basis for all shaping modifications. This master level M modified by some function F_2 provides a base level for region B adjacent to the inflector. The n^{th} channel in the B region needs the base level F_2M modified by some proportion $\pm f_n$ of the region amplitude control B. Reference voltage to the n^{th} channel of the first region should then be $V_R = F_2M \pm f_nB$.

For a smooth transition between regions, the second region C needs to follow the base and shape functions of the first. Base level for the C region would be $F_2M \pm F_3B$. An individual n^{th} channel receives $V_R = F_2M \pm F_3B \pm f_nC$.

This form requires an algebraic sum of terms for each channel. Operational amplifiers used as gain of one summing amplifiers are a natural in this service. Recent cost reductions and expanded operating ranges of operational amplifiers have allowed us to choose one that fits both our system and budget. We need at least +14 V and +150 mA per channel while the under $50.00 amplifiers purchased will provide ±20 V and ±200 mA.

Refer back to a typical channel in the C region where $V_R = F_2M \pm F_3B \pm f_nC$. Shape within the region is determined by all of the f_n terms. This f_n is also the individual coil control term so that hand tuning the region shape automatically follows hand tuning the individual controls and vice versa. Figure 4 shows two typical channels of the total 110 channels and two regions of the seven which will be used.

In addition, each channel will have provision for an f_n and an additional summing resistor so that superimposed shapes will be possible.

RESULTS

The largest problem in designing the reference system has been sorting memories out of the list of requirements. Once the requirements have been clearly stated, most other problems with the new system become minor when compared with the former system.

No longer will there be noise from large power supplies in the control room or water leaks from voltage dividers. Small 5-A supplies with grounded center taps will be our new high current reference supplies. These can be purchased off-the-shelf as can the entire amplifier array with its bias supply for less than regulated high current supplies would have cost.

There will be no problems of divider loading and all adjustments and controls are noninteracting. All controls will be available for use during operation and no separate program boards will be needed. Any future expansion of the system either in number of channels or in regions of control will involve only the addition of small modules.

Central to the ease of design are low cost, high gain operational amplifiers. They have made it possible to satisfy all electrical requirements

quickly and spend the time saved trying to satisfy the human engineering problems.

REFERENCES

1. D. O. Kippenhan, Magnetic Mirror Field Control in The Astron Experiment, Lawrence Radiation Laboratory, Livermore, Rept. UCRL-70035 (1966).
2. N. C. Christofilos, Lawrence Radiation Laboratory, Livermore, private communication (1968).

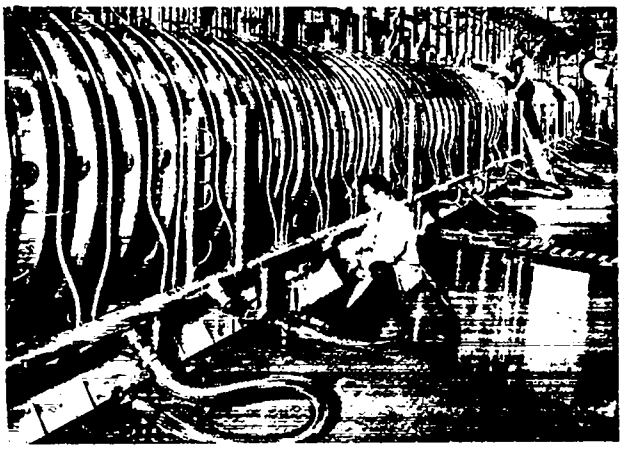

Fig. 1. View along the Astron tank.

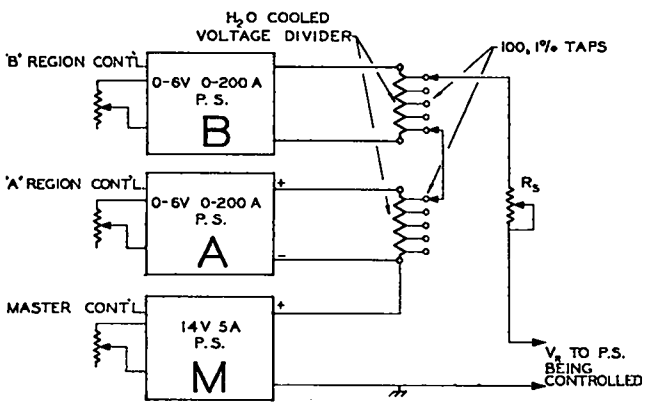

Fig. 2. Block diagram of original reference system.

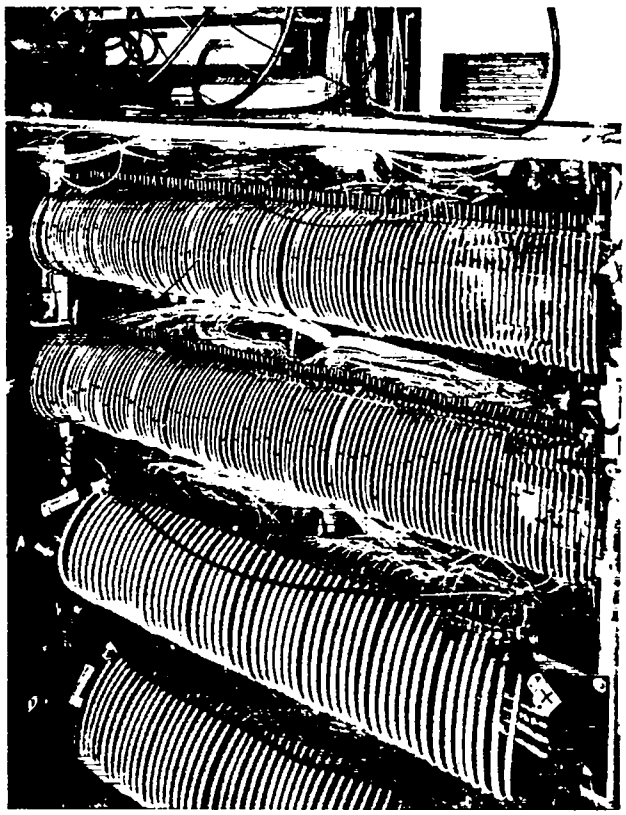

Fig. 3. Water-cooled divider coils.

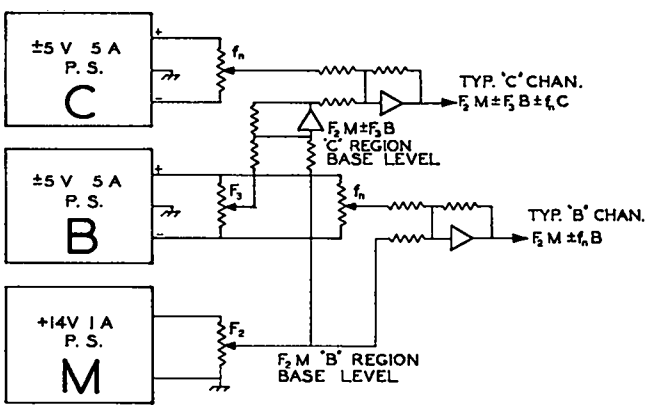

Fig. 4. Block diagram of new reference system.

A COMPUTER-CONTROLLED ELECTRONIC SEQUENCE TIMER*

S. Schweitzer

Plasma Physics Laboratory
Princeton University
Princeton, New Jersey

ABSTRACT

An Electronic Sequence Timer which may be controlled either by a set of thumbwheel switches or by an IBM Model 1800 Process Controller is described. Unusual features of the logic employed, and of the output circuitry, are described in detail.

INTRODUCTION

One of the requirements of the Princeton floating multipole machine is a source of pulses which are displaced in time from a start signal in precisely controlled, adjustable increments. These pulses may be used to trigger oscilloscopes and other diagnostic instruments, or to trigger associated equipment such as the breakdown oscillator. The floating multipole machine will be controlled by an IBM Model 1800 process controller. Although it is possible for this computer to supply the required timing pulses, there are several reasons for building a separate timer which may be controlled by the computer. The timing pulses must be 175 volts in amplitude when driving a 75 ohm load. Also, each pulse must be electrically isolated from every other pulse. If the computer supplied the timing pulses, a multichannel pulse amplifier would be required. Also, during machine maintenance times, or when the computer is down, it is very useful to have timing pulses available. This is readily accomplished by having a separate timer which can be controlled either manually (by means of a set of thumbwheel switches) or by the process controller.

*Work performed under the auspices of the U.S. Atomic Energy Commission.

Specifications. The basic requirements for the timer were the following:

Number of Channels: 20

Timing Range for Each Channel: 10μs to 999.99 ms in 10 μs steps.

Channel Start: Each channel may be started by any other channel, or by the start input.

Channel Setting: The channel timing may be set by either of two sources. In local control, all channels are set by means of twenty 5-digit thumbwheel switches — one for each channel. In external control, all channels are set by the process controller.

Timer Output: The timer output is a pulse of 175 volts amplitude into 75 ohms, with a rise time of 1 microsecond maximum. The maximum repetition rate is 10 pulses per second.

60 Hz Tie: There is a 60-Hz tie associated with the timer input such that the timer start output will occur at the next positive slope zero crossing of the timer 60-Hz power input after a start signal has been received.

Recycling Timer: There is a recycling timer output which may be connected to the timer start input when a recycle mode is desired. The recycling time is adjustable from 0.1 second to 99.9 seconds in 0.1 second steps.

Basic Approach. The basic approach selected for the timer was to use five BCD down counters connected in tandem for each channel. Each channel is preset to whatever time is required, and after a start signal is received, a gate is turned on which allows a very accurate 100 kHz signal to be counted. When the counter reaches zero, an output pulse is generated. When the timer is being controlled locally, each output pulse presents its counter to the number selected by the thumbwheel switch associated with that counter and also gates off the 100kHz clock signal. The channel is then ready to accept another start signal. When the timer is being controlled by the process controller, the output pulse gates off the 100kHz clock only. At a later time (before the next start signal) the process controller must supply the channel setting information. It does this by utilizing twenty-six lines of the process controller register outputs. Twenty lines contain the channel setting in BCD form. Five lines contain the channel identification number in binary form. The twenty-sixth line is used to insure that the information is correctly interpreted by the timer. It goes to 1 after all the other lines have settled to their proper value, and then it goes to 0 before any of the other lines have changed. After the channel is set, it is ready to accept another start signal.

DETAILED APPROACH

There are several refinements to the basic approach discussed above. These will be described in the following sections:

End of Count Determination. To determine when the counters reach zero requires a twenty-input AND gate or its equivalent. Since standard, commercially available integrated circuits were to be used for the timer, this would require several packages including the necessary inverters (since most logic families use inverting gates). Also, because of propagation delays in the counters, cross-over signals would be generated, requiring additional gating, or delayed strobing, or some equivalent logic to insure that only the correct all-zero condition of the counters was recognized. Also, the printed circuit pattern would become quite complex because the gate inputs would come from many other packages. As an alternative, it was decided to add an additional flip-flop to the counter chain. This flip-flop would be triggered when the counter chain changed from 00000 to 99999. This provides a simple, unambiguous signal to show when the counters have reached the all-zero state. However, this signal occurs one clock pulse after the all-zero state. Also, this signal is delayed by the full propagation delay of the counter chain. Therefore, this signal is used to gate the next clock pulse. The next clock pulse provides a signal which is free of propagation delay errors, but is two clock pulses late. To make this signal occur at the proper time, there is a circuit at the input of the counter chain which adds two counts whenever a start signal is received. This circuit, which consists of less than two IC packages is simpler and more reliable than using a gate to detect the all-zero condition. The two added counts must occur before the first clock pulse (in case the channel is set for one clock pulse, or 10 microseconds). Therefore, a 1 MHz signal is distributed to all the channels, and the two added counts are added at a 1 MHz rate. The system clock is actually a crystal-controlled 1 MHz oscillator. This is divided by ten, to 100kHz, to provide the 100kHz required by the counters.

Counter Presetting. To preset the counters to any number requires some special techniques, because ripple counters are employed. Synchronous counters would ease the presetting problem, but the large amount of

additional logic required meant that it was more economical to use the presetting system described below. Each flip-flop set input is connected to a dual two-input AND-OR gate. One of the AND-gates is connected to the thumbwheel switches, and the other is connected to the process controller register buffers. The second inputs of these AND-gates is controlled by a front-panel switch such that one set of AND-gates is always off, so that timing control is performed from one source only. Whenever a counter set signal is received from one of the three possible sources (a channel identification number from the process controller in external control, or a channel output pulse or a front-panel reset switch operation in local control), a one microsecond pulse is generated and applied to all the flip-flop reset inputs. This sets all the decades to a count of 15 (which normally cannot occur in a BCD counter), which means that all the flip-flop outputs which are used to trigger another flip-flop are set to the 0 state. After the one microsecond pulse has returned to its normal state, whichever set gates are active set their associated flip-flops. All the flip-flop carry output transitions at this time are from the 0 to the 1 state, which cannot trigger another flip-flop. Thus all the flip-flops are correctly set, independent of the flip-flop states before the set command is received.

Multiplexer. For some machine experiments, and for some maintenance procedures, it is more convenient to have the timing set by the thumbwheel switches, although the process controller is controlling other machine operations. When this is done, it is useful to have the channel setting available to the computer, so that they may be displayed at remote computer readouts, or possibly to be used in internal computations. This is done by having a multiplexer built into the timer. In local control, when a channel identification number is received, the settings of the thumbwheel switch associated with that channel are transmitted over twenty lines to the computer. The computer can request this information at any time without upsetting the operation of the timer.

Output Pulse Amplifier. The output pulses are generated in SCR pulse amplifiers. The high voltage supply which is connected to the SCR's is isolated from the low voltage supplies used for the rest of the timer. The trigger signals from each channel are transformer coupled to the SCR gates. Each SCR output is transformer coupled to an electrically isolated BNC connector, so that there is no common ground connection between the outputs and any other circuitry. A series diode protects the SCR circuit from back-feeds from the load of up to 1000 volts. Outputs may be short-circuited indefinitely, because SCR current is limited by an internal resistor. The output pulse is 350 volts with 75 ohm source impedance. When terminated in 75 ohms, the pulse is 175 volts with a width at half amplitude of approximately seven microseconds.

Construction. With the exception of the output pulse amplifiers and the power supply, over 95% of the timer circuitry is comprised of integrated circuits. Each channel is contained on two plug-in printed circuit boards. Two boards are used because of pin limitations of the connector used. In addition to the forty channel boards, there is a common board which contains the recycling timer (which operates by counting down from the 60-Hz line), the system clocks, the 60-Hz tie circuitry, and the timer start cicuitry. There are three computer interface boards. One interface board decodes the channel identification (which is in binary form) and operates the appropriate channel board. The second interface board acts as a buffer for the channel

setting information. It is necessary because twenty channels are connected to each line. The third interface board amplifies the multiplexer outputs to the high voltages necessary for the computer voltage sense inputs. The output amplifiers are contained on three plug-in boards. The timer is packaged in a 14 x 17 x 18 inch package. The height is dictated by the control switches on the front panel, since the circuitry occupies only a portion of the total volume available. The timer power supply is in a separate 5 1/4 x 17 x 18 chassis.

DIAGNOSTIC DRIVES AND CONTROLS*

by

V. S. Foote, Jr.
Plasma Physics Laboratory
Princeton University
Princeton, New Jersey

ABSTRACT

Present day plasma research devices, with their multiplicity of diagnostics in combination with limited operator access, can pose many problems in the acquisition of the required data. The evolution over a number of years of the drive and remote control systems for diagnostic positioning devices now in use at PPL is described with examples. Drives used with positioning devices for both "in-plasma" and "external" diagnostics are discussed, as well as questions of reliability, safety, convenience, cost, and standardization. Present trends in design such as automatic logging and programmed control of probe positioning mechanisms are discussed, and a new type of incremental drive motor (utilizing stray magnetic fields between solenoid coils) presently under test is introduced.

INTRODUCTION

The experimental devices and machines utilized in present day physical research often have inherent characteristics which necessitate the remote operation of the diagnostic devices with which they are equipped. High voltage, radiation, temperature extremes, and often economics preclude access to these diagnostics for repositioning between readings.

Experience over the last nine years at PPL in meeting these requirements has resulted in a philosophy or design approach utilizing standardized (almost modular) components and techniques to meet a broad variety of requirements.

DEVELOPMENT OF DIAGNOSTIC DRIVES

Initial Work

In 1960, studies[1] of runaway electrons in the B-3 stellarator, utilizing a lead x-ray collimator which had to be re-aimed for each data point (with attendant shutdown and restart of the machine) suggested the desirability of a remotely operable positioning device. A two-axis positioner (Fig. 1) utilizing reversible, capacitor-run instrument motors and potentiometers in a simple Micropositioner^{TM} servo system permitted the experimentalist to set in the desired coordinates from the control room. Concurrently, several half meter Jarrell-Ash Ebert Monochromators had been more or less successfully modified for remote operation. The significant improvement in data-gathering speed and economy was apparent.

At this time the Model C stellarator was nearing first-stage completion and instrumentation was being designed. A Smith-type Mass Spectrometer was being constructed for use in the vacuum vessel and a request was made for a remotely-operable drive for the instrument. The drive would position the device within 0.1 mm radially with readout to 0.01 mm and, most importantly, provide two 11 kilovolt breaks in series between the vacuum vessel and the control room in

*Work performed under auspices of the U.S. Atomic Energy Commission.

accordance with C stellarator safety specifications. These breaks were placed in the flexible shaft between the positioning mechanism and the drive unit. Never installed, the probe positioning mechanism and drive were duplicated several times for an early Langmuir probe mechanism now referred to as a Type IP (Fig. 2). Results[2] with these probes, positioning mechanisms, and drives have formed the basis for most subsequent work.

Other Approaches

During this period, the L-2 reflex arc device was utilizing four Langmuir probes spaced axially. On request, these were modified for remote control. Space limitations on the control console, together with operating procedures, suggested a single switched readout of probe position with ultimate expansion to 12 probes. To avoid synchronization difficulties, an analog readout from a position potentiometer (with buffer amplifier) to a D'Arsonval meter was utilized. The 1/2% meter was calibrated from 0 to 64 mm into the plasma and could be read to 1/2 mm or 1 part in 128. Proven adequate in service, the system was later expanded and provided with variable speed radial scanning. It was subsequently duplicated on the Q-1 cesium plasma device.

Meanwhile, the C stellarator was being readied for installation of the SF-2 stabilizing field coil.[3] Locating the position of the plasma in the U bend dictated installation of four probes 90° apart at the center of the U bend. Miniaturization fitted the mechanisms through the SF-2 torus. Faced with the requirement for four nearly identical drives and with more in the offing, a modular design was evolved. Featuring cast-aluminum gear boxes, adjustable limit switches, metric conversion gearing, reduced size and cost, and greater reliability, these became the prototype for most future work. Relaxation of the requirements for position readout to 0.1 mm - permitting the use of smaller synchros for transmission - allowed the controls for all four probes to be mounted on one 5-1/4 inch high relay rack panel (a design which holds to this day).

Standardization

As requests from C machine experimenters for more and varied probes, mechanisms and drives proliferated, an intensive development program was begun. As outlined by Christie,[4] this work culminated in the Type IIIP mechanism shown with its drive and control panel in Fig. 2.

Adoption of a metric lead screw in the probe positioning mechanism eliminated the cumbersome metric conversion gearing in the drive. One revolution of the drive and flexible shaft moves the probe tip one mm. The local and remote counters (coupled by synchros) read out to 0.1 mm. By use of readily interchanged floating gears, the limit stop mechanism is easily modified to provide travels of from 50 to 400 mm $\pm$ 0.1 mm. Depending on speed and torque requirements of the positioning mechanism, gear head motors of from 18 to 186 rpm (both synchronous and induction) are installed. Approximately 50 of these drives have been built in this standard form. By suitable selection of gearing, and if necessary changing the shaft locations, almost any reasonable requirements may be met.

Fabrication and assembly of a drive and control panel represents approximately 70 man-hours of shop time and $350.00 for components.

Special Drives

Development of the longitudinal "shuttle probe" mechanisms[4] for the Q-3 linear cesium plasma device posed an interesting problem. The Z-axis position of the probe tip is a cosine function of the input shaft rotation. By using a surplus mechanical resolver (from a fire-control system) to drive the synchro transmitter, this function was generated to an overall accuracy of 0.5 mm in 197 mm.

Also, experience on other linear machines with use of the analog probe position voltage to drive one axis of an X-Y recorder suggested the inclusion of a potentiometer in parallel with the synchro transmitter (Fig. 3). This output was used with both recorders and oscilloscopes and the convenience in data acquisition soon suggested the addition of readout potentiometers to other Q-3 drives of the standard IIID type.

Figure 4 shows the most recent refinement of this analog equipment. Experiment showed that paralleling a second synchro receiver affected the standard control panel readout by less than 0.05 mm. This second receiver drives a ten-turn potentiometer through a 20:1 reducer. The assembly can be quickly coupled to the readout for any probe positioner. Application of the potentiometer signal to the horizontal axis of an oscilloscope permits the recording of probe voltage as a function of both probe position and time.[5]

External Diagnostics

A number of monochromators are in use at PPL. Two Jarrell-Ash 1-Meter Ebert Vacuum Monochromators have been modified for remote operation, with a novel counter assembly which reads out wavelength directly in the first through fourth orders and a calibrated vernier for correction of minute tracking errors. A tilting quartz plate before the exit slit permits fine readout to 0.01 Ångstrom. Also, a number of half meter monochromators have been modified in an unsophisticated manner by addition of Size 5 Synchro Receivers and chain drives to permit remote manual scanning. Several control panels for these have had a synchronous motor with six-speed transmission added. By applying the detector output to a strip-chart recorder, plots of intensity versus wavelength are readily obtained.[6]

An investigation of the decay of persistent current in a superconducting solenoid[7] required a special drive for a mechanism positioning an NMR probe. The drive (Fig. 4) permits scanning (at preselected speeds) between preset limits of travel, automatic reversal or stop on reaching either limit, and digital printout of the probe position.

Recent Work

A set of four "tiltable" probe mechanisms (providing linear and angular positioning in a normal plane) have recently been installed at one port cross of the C stellarator. Equipped with a 1 mm square "flag", each probe can sweep out one quadrant of the 15 cm diameter aperture in connection with electron gun plotting of line closures. The desired one mm resolution requires some 2000 data points per quadrant, with radial and angular repositioning of the probe between each shot. Since operation at one pulse per second will require about three hours to map out the aperture, rapid and accurate positioning is essential. Until now, monel flexible shafts have been used to permit placing the drive motors and position transmitters outside the machine's magnetic field.[2] However, the spectre of eight flexible shafts at one port cross (with perhaps four additional probes and shafts and, probably, waveguides) coupled with the fact that the mechanism ends would be tilting through a 40° arc led to a different approach. By utilizing the stray field ($\approx$ 600 gauss) between the confining field coils, two nonferrous stepper motors consisting of orthogonal Faraday coils with slip rings could be mounted directly on each probe positioning mechanism (Fig. 5). Each motor requires about 40 pulses (10 revolutions) to move the probe one mm. A remote-readout counter (11 wires/digit) direct-coupled to each motor transmits the probe position via a local decimal-binary converter to the control console and the data-acquisition system. Future plans envisage the use of the process controller system[8] to perform the coordinate transformations required to permit the probe to follow any desired path in machine coordinates.

References

[1] E. B. Meservey and L. P. Goldberg, Phys. Fluids 4, 1307 (1961).

[2] J. M. Chapuk, V. L. Corso, V. S. Foote, R. M. Sinclair, W. L. Harries, J. L. Upham and S. Yoshikawa, Rev. Sci. Instr. 34, 1377 (1963).

[3] J. B. Joyce, Proceedings of the 1966 Symposium on Engineering Problems of Controlled Thermonuclear Research. Gatlinburg: Oak Ridge National Laboratory (October 1966) pp. 370-378.

[4] R. S. Christie, "Probe Positioning Mechanisms", Symposium on Engineering Problems of Fusion Research. Los Alamos Scientific Laboratory (April 1969) to be published.

[5] W. L. Harries, Rev. Sci. Instr. 39, 1294 (1968).

[6] A. S. Bishop, A. Gibson, E. Hinnov and F. Hoffman, Phys. Fluids 8, 1541 (1965).

[7] J. File, Proceedings of the 1966 Symposium on Engineering Problems of Controlled Thermonuclear Research. Gatlinburg, Oak Ridge National Laboratory (October 1966) pp. 116-119.

[8] E. D. Simon, S. P. Duritt and M. Pelovitz, "Digital Control of a Research Device", Symposium on Engineering Problems of Fusion Research. Los Alamos Scientific Laboratory (April 1969) to be published.

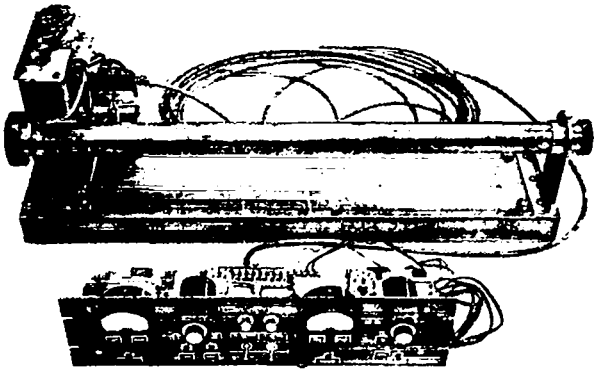

Fig. 1. X-ray collimator, two-axis positioning and remote control panel.

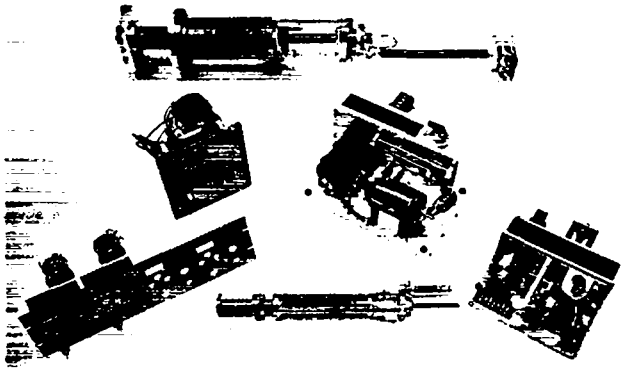

Fig. 2. (Top) PPL Type IP probe positioning mechanism with 90:1 reducer, Type ID drive and control cabinet.
(Bottom) PPL Type IIIP PPM (4 inch stroke), Type IIID (4) Drive and Quadruple Control Panel.

PROBE POSITIONING MECHANISMS*

by

R. S. Christie
Plasma Physics Laboratory
Princeton University
Princeton, New Jersey

ABSTRACT

For many years instrumentation of plasmas has made use of movable probes usually provided with a linear motion only. From these single degree of motion positioning mechanisms a PPL "standard design" has evolved after three major developmental modifications. Minor alterations in the design of this probe mechanism and variations in the method of mounting it, have increased its flexibility and usefulness to the extent that it is able to position a probe anywhere in a specified volume. The standard device, special mechanisms designed to solve particular positioning and measurement problems and probes of an unusual and miniature nature are described and illustrated. The probe tip motions obtained by the mechanisms are shown through use of multiple exposure photography.

STANDARD MECHANISM

As plasma research machines become larger and more complex so do the experiments performed with them. The advent of operating machines on a shift basis, the desire for more data, and a reluctance to break vacuum for probe changes led to instrumenting machines with two or more sets of probes. Because the number of diagnostic ports on a machine is fixed, two or more probe positioning mechanisms had to be located where one had been previously. More than just in and out motion also became a requirement. At PPL there have been three major design modifications made in the last several years which led to a "standard design" probe positioning mechanism used to meet these changing conditions and requirements.

Early single degree of motion mechanisms used formed bellows to obtain linear motion in ultra high vacuum systems. As length of stroke and degrees of motion increased, formed bellows were no longer adequate. Welded metal bellows were introduced. The first major change in design came with the use of welded bellows. Manufacturers of these bellows were few, and they were reluctant to guarantee the bellows' ability to perform. Outside diameters were relatively large, but stroke per inch of free length far exceeded that of formed bellows.

As experience was gained, the diameters improved favorably. Bellow diameters were reduced from 2.75 inches to 1.125 inches. The second major modification came as a result of this reduction and the use of an on axis lead screw instead of an off axis ball screw as the means of stroking the mechanism. The diameter of the positioning mechanism was substantially reduced.

Removal of the bakable in place requirement for the devices plus ingenuity resulted in the third design change. Some parts which were stainless steel only because of bake requirements were

*Work performed under auspices of the U. S. Atomic Energy Commission.

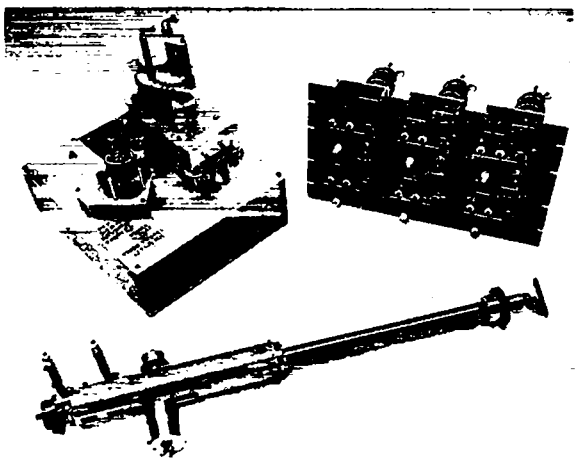

Fig. 3. Q-3 shuttle probe, Z-axis resolver drive, and control panel (R and Z Axes-three probes).

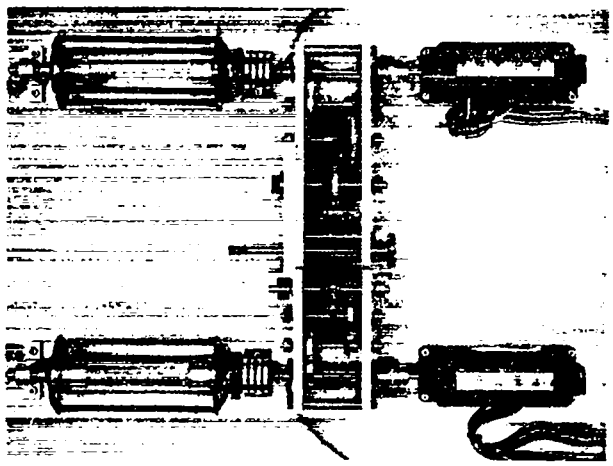

Fig. 5. Dual-axis drive and readout for "Tiltable" probe positioning mechanism.

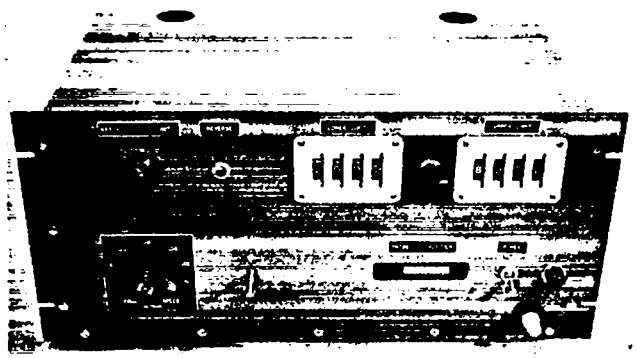

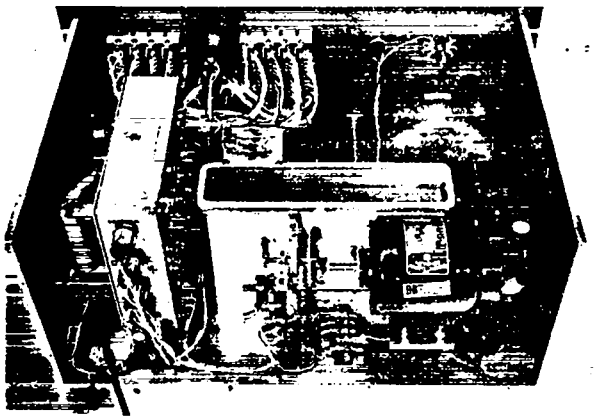

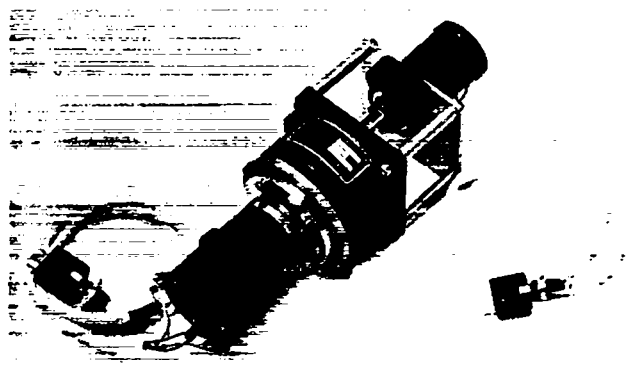

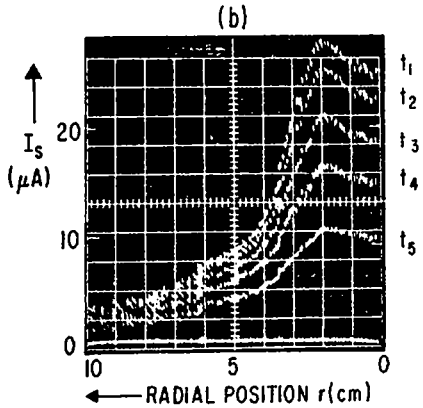

Fig. 4. (Top) NMR probe scanning drive (front and rear views).
(Bottom) Probe position sensor with typical oscillogram (I_s vs at $t_1 \ldots . t_5$, Reference 5).

diameter ceramic container. In the center is a "double-double" probe which is a modification of a probe made by D. Dimock.[3] There are two grids and two collectors plates all in a shield. The overall diameter is .096". The tip shown at the top of the figure is a miniature Langmuir probe made of drawn quartz tubing over .001" diameter tungsten wire. Miniaturization to this extent, (tip diameter of .004") reduces the disturbing effect of the size of the probe on the plasma.

Many changes have been made in probe positioning mechanisms. Standard components, new materials, relaxation of restrictions on materials used in vacuum systems and ingenuity in design have resulted in mechanisms which provide a means of placing a probe anywhere within a specified volume. Present designs, together with remote drive, control and readout[4] enable the measurement and collection of data to be accomplished with a minimum of difficulty.

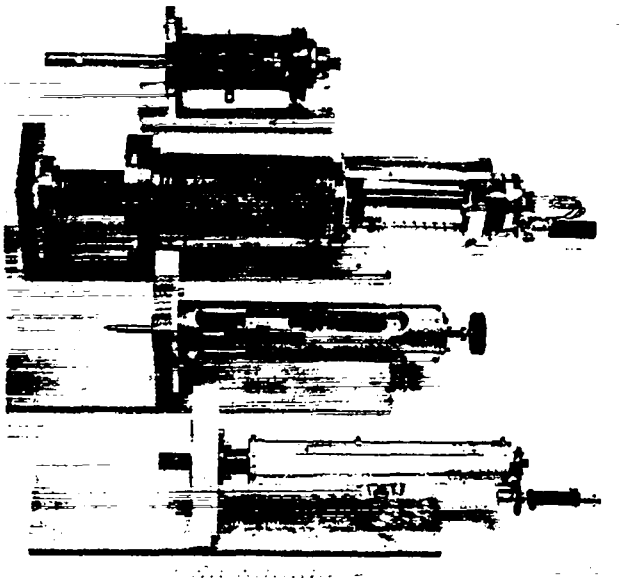

Fig. 1. Comparison of early type probe positioning mechanism and IP, IIP, and IIIP models.

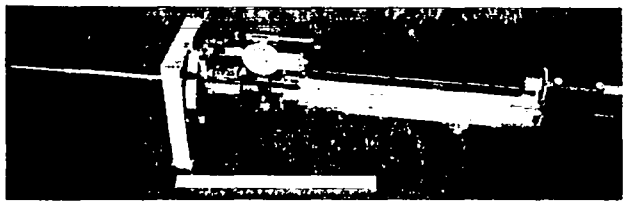

Fig. 2. IIIP probe positioning mechanism modified to have three degrees of motion.

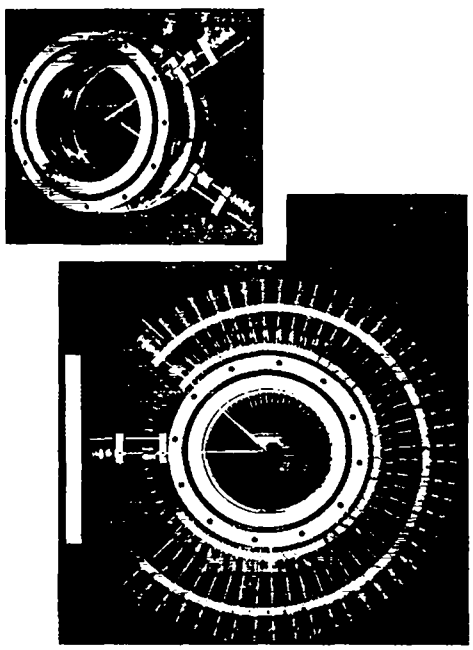

Fig. 3. Rotating twin probe assembly and multiple exposure photograph of probe motion.

References

[1] T.H. Batzer, Lawrence Radiation Laboratory, UCRL-7830 (1964).

[2] R. S. Christie, Proceedings of Aerospace Symposium, Lubricating Techniques and Design Studies of Bearings and Gears for an Orbital Manned Space Laboratory, Detroit, Mich. (1965) p. 30.

[3] N. D'Angelo, D. Dimock, J. Fujita, G. Grieger, M. Hashmi and W. Stodiek, Particle Losses of a Cesium Plasma in a Stellarator, Proc. 6th Inter. Conf. on Ionization Phenomena in Gases, Paris, July 1963., Vol. I, 399-403.

[4] V. S. Foote, Jr., "Diagnostic Drives and Controls", Symposium on Engineering Problems of Fusion Research. Los Alamos Scientific Laboratory (April 1969) to be published.

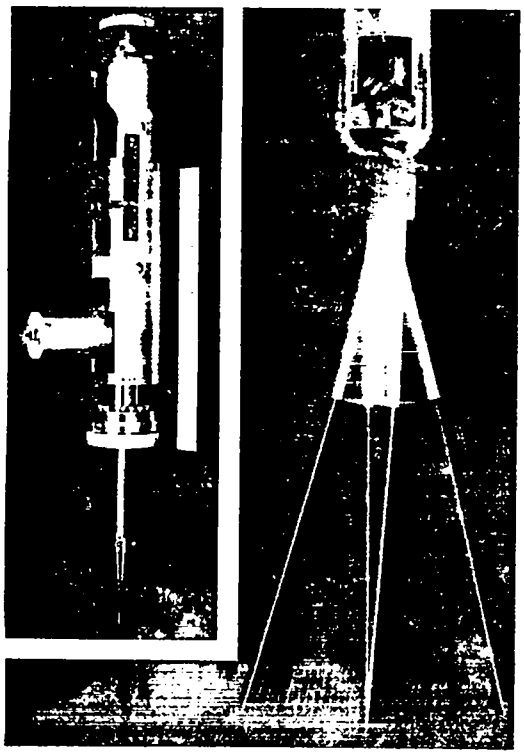

Fig. 4. Double probe and multiple exposure photograph of tip motion.

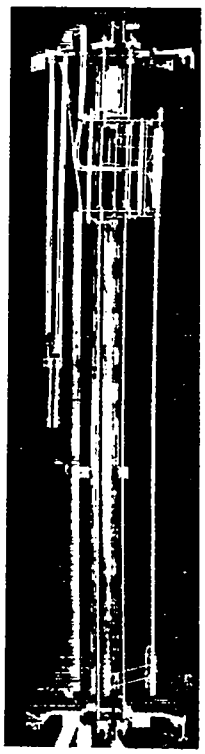

Fig. 6. Travelling probe mechanism.

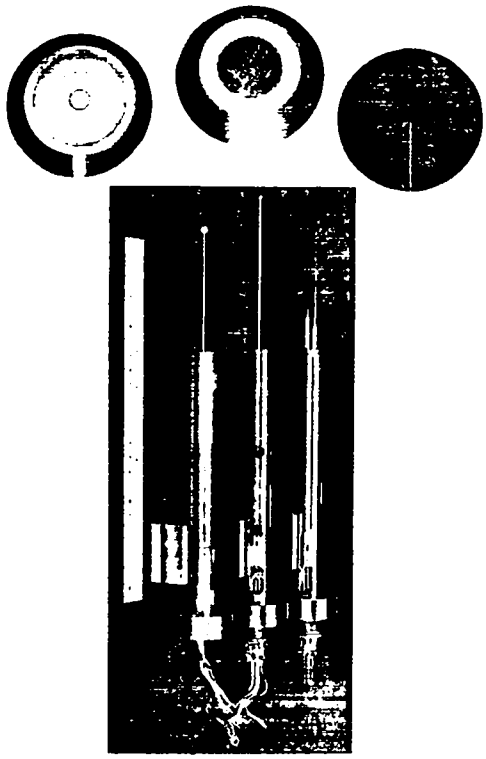

Fig. 7. Probe tips.

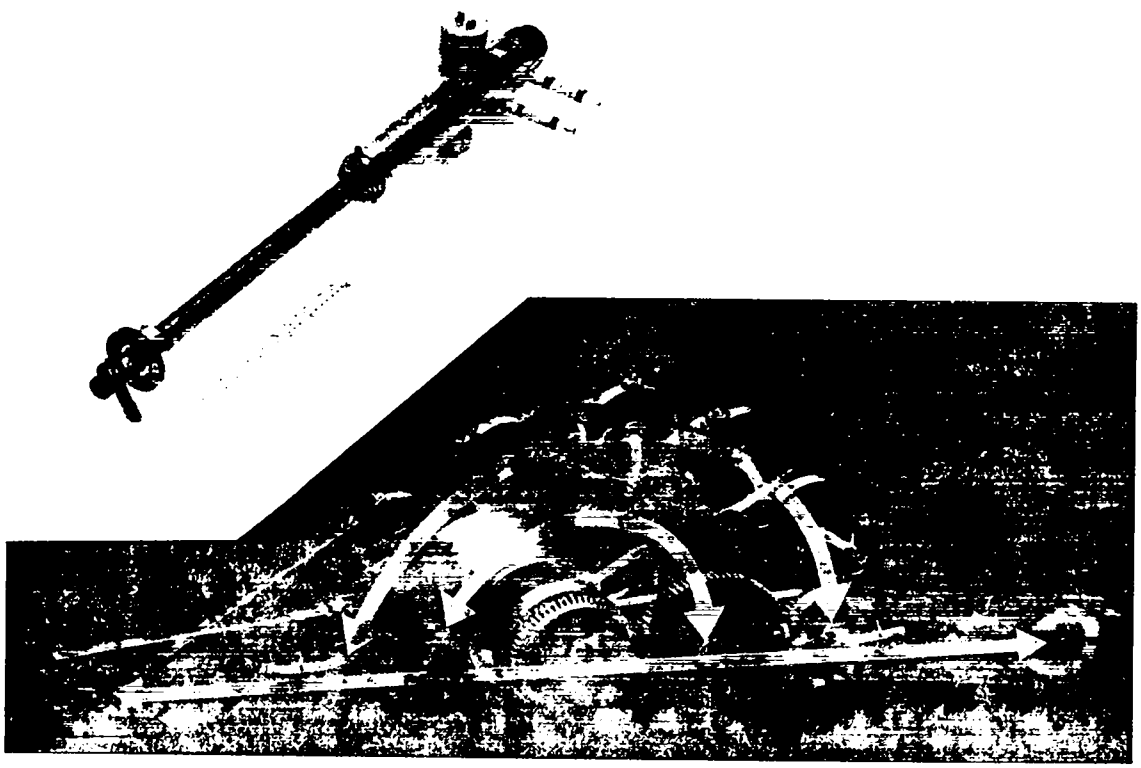

Fig. 5. Shuttle probe positioning mechanism and multiple exposure photograph of mechanism motion.

INDUCTIVE CIRCUIT SWITCHING *

J. G. Murray G. Bronner

Plasma Physics Laboratory
Princeton University
Princeton, N. J.

ABSTRACT

Two experiments of inductive energy switching are described. 1. A direct current interrupter utilizes a relatively small external power supply to drive the breaker current to zero. 2. Inverters in inductive storage systems can be used to limit the voltage on interruption and to facilitate efficient energy transfer.

1. DIRECT CURRENT INTERRUPTER[1]

The difficulty in interrupting a direct current inductive circuit lies in the fact that there is no point of current zero where the arc channel can deionize and build up dielectric strength to a value where it can hold off the recovery voltage of the circuit. Tests have been made to show that the switching could be accomplished by providing a current zero with a small pulsed power supply. As a result of these tests, engineering of a dc interrupter is possible for arbitrary circuits. The accuracy in the prediction of breaker performance has been found satisfactory.

Description of the Circuit

The basic circuit in the tests is shown in Fig. 1. A dc source of 2000 amperes, was used to charge a $\frac{1}{2}$ henry inductor with a 3 second time constant. When interruption of the circuit was required, the circuit breaker was tripped and an arc was drawn. After a few milliseconds, the discharge circuit, which consisted of a capacitor C_d, an inductor L_d, and an ignitron IG1 was fired to force a current zero. The bank of load resistors (Z_2) limited the peak voltage when the current was interrupted. To protect the breaker in the event of malfunction a crowbar ignitron was placed across the breaker.

The circuit breaker used was a Westinghouse type DB50, rated at 1600 amperes, 600 volts, 60 Hz or 250 volts dc.

Experimental Results

The time required for the breaker from energization to contact separation was about 25 milliseconds. The arc voltage climbed from 20 volts to about 400 volts in 5 to 10 milliseconds. This increase was interpreted as the result of the arc traveling up into the arc chute.

The discharge circuit was fired when the arc voltage reached 350 volts. This circuit then would drive the current to zero in about 0.5 millisecond. Typical currents and voltage waveforms are shown in Fig. 2.

The highest current, within the limits imposed by the load inductor, 2000 amperes, was interrupted with peak voltages up to 16 kV generated across the circuit breaker contacts. The maximum $\frac{dv}{dt}$ was 10 kV/μsec. The energy required to force a current zero was 2 kJ or 0.2% of the stored energy in the inductor. The current interrupted was 125% of the breaker's rating, the

* Work performed under auspices of the U. S. Atomic Energy Commission.

voltage on interruption was 2500% of its ac rating.

These findings were utilized in engineering dc breaker applications in inductive circuits. Performance of the breakers confirmed the usefulness of this method of using standard low voltage interrupters in circuits where high induced voltages are present.

2. INVERTER CIRCUIT IN AN INDUCTIVE STORAGE DEVICE

An inductive energy storage system using ignitron switching was developed and tested at PPL. Preliminary results have been reported by E. D. Simon.[2]

On transferring energy from an inductive storage device the voltage across the inductor can reach undesirable levels. Most attempts to regulate this voltage are inherently wasteful. The application of an inverter, however, can limit the voltage without appreciable loss. A pertinent circuit is shown in Fig. 3.

An inverter was built to test the use of standard (5555) ignitrons in such a circuit. Provision has been made to series and parallel inverter bridges (Fig. 4), such that a bridge can be used as a building block to assemble arbitrary systems. The storage inductor was a 2000 ampere, 0.5 henry coil (Fig. 5), of 3 second time constant. The plan view of the installation is shown in Fig. 6.

Description of the Circuit

Assume an initial energy stored in the inductor (Ls) and an initial negative voltage on the commutating capacitor C_c. If we simultaneously fire IG1 and IG2 the storage current (i_s) will gradually change the originally negative voltage of C_c. When this voltage reaches a preset value, a sensing circuit will fire IG3 and IG4, thus an inverter action begins. Meanwhile IG7 acts as a rectifier, C_T as a filter, and L_L load can be supplied with dc current through IG9 (Fig. 3). The object of the testing was to determine: a) How much current can be inverted with one set of 5555 ignitrons. b) What inverter voltage can be used. c) What $\frac{dv}{dt}$ and $\frac{di}{dt}$ can be tolerated. d) Finally to determine if series and parallel combination of inverters is feasible.

Experiments

The charging circuit is separated from the storage inductor by a string of 5 ignitrons (IG5 of Fig. 4). At the end of the storage current buildup the inverter is started. The first step of the inverter reduces the current in IG5 to zero thus separates the current supply from the inductor. The rate of rise of voltage and the rate of current change is determined by the size of C_c (of Fig. 4). Changing C_c and finding the limits (in current and voltage) of reliable commutation yields the permissible values of $\frac{dv}{dt}$ and $\frac{di}{dt}$. The inverter action continues until the stored energy is exhausted. Failure of inversion results in short circuiting the storage inductor, thus damage to any component is unlikely. Ignitron life is quite long since the tubes are not excessively stressed.

Conclusion

The experimental results show that about 1000 amperes can be inverted by s single set of 5555 ignitrons. The peak inverter voltage has to be kept below 4.5 kV. A rate of voltage rise of 1 volt/μsec, and a rate of current change of 1 A/μsec are permissible. Series and/or parallel combinations of inverters are quite feasible without any reduction in the performance quoted above.

References

1. G. D. Edmonds, J. G. Murray, and R. R. Robertson, Princeton Plasma Physics Laboratory MATT-559 (1967).

2. E. Simon and G. Bronner, IEEE Transactions on Nuclear Science, Vol. NS-14, 33 (1967).

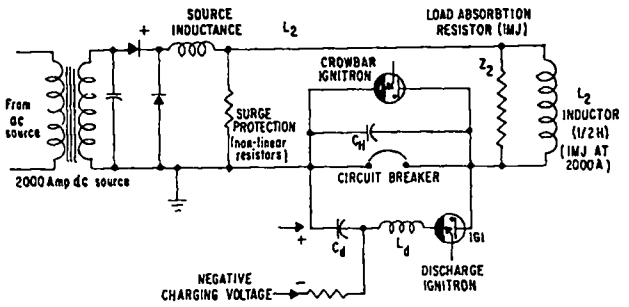

Fig. 1. Test circuit for dc interrupter.

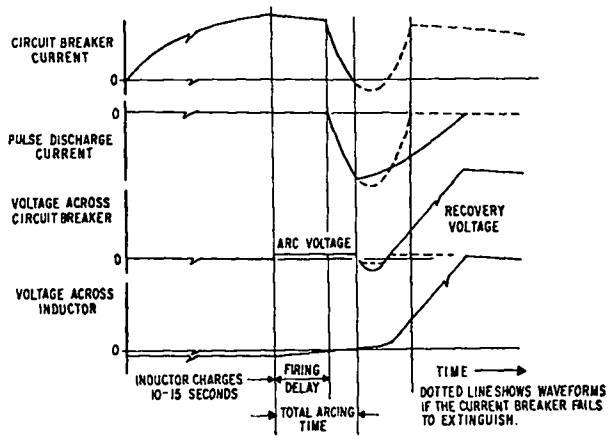

Fig. 2. Current and voltage waveforms for the dc interrupter.

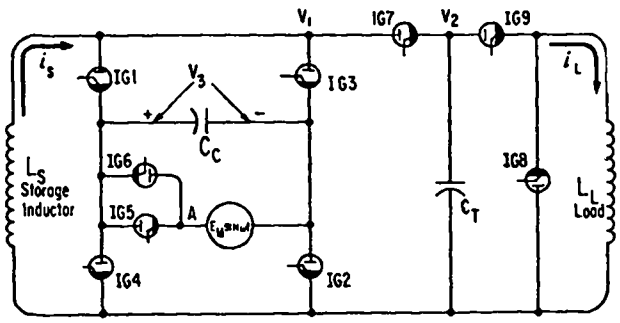

Fig. 3. Inductive energy storage circuit using an inverter.

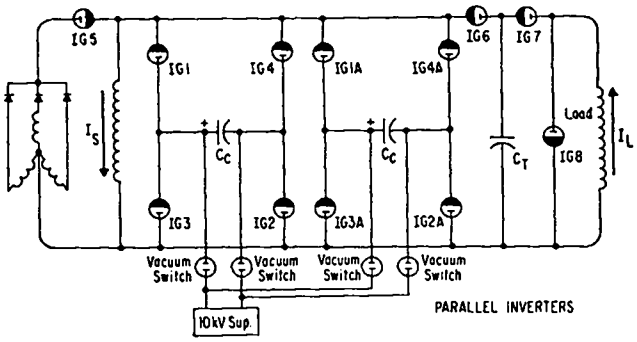

Fig. 4. Parallel inverters for an inductive energy storage system.

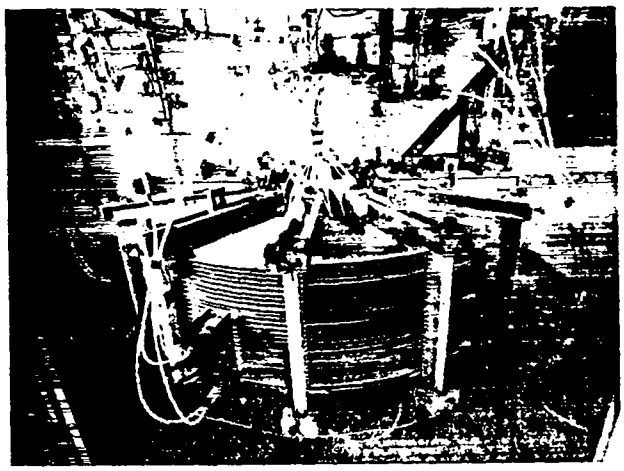

Fig. 5. One megajoule storage inductor.

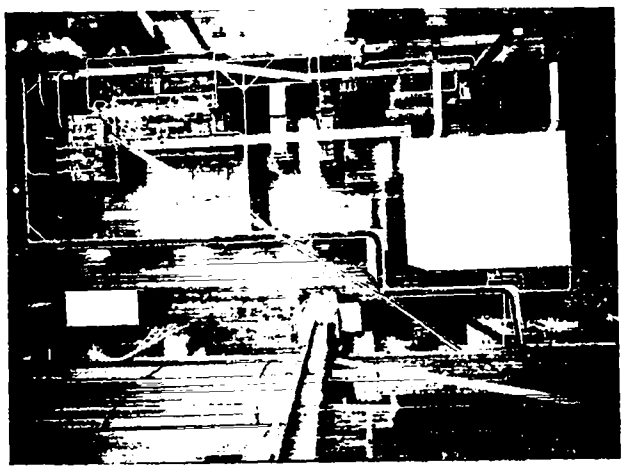

Fig. 6. Plan view of the inductive energy storage system.

STANDARD COMMERCIAL IGNITRONS AS HIGH VOLTAGE SWITCHES *

Nicholas M. Turitzin

Plasma Physics Laboratory
Princeton University
Princeton, N. J.

ABSTRACT

Test results performed on ignitrons types 5550 and NL-1053 used as high voltage switches are given. Static voltage breakdown, dynamic voltage breakdown, internal dark and bright tube resistance, tube voltage drop, arc transfer, ignitor resistance and factors influencing the tube life have been investigated. A high voltage ignitron switch using series connected ignitrons is described.

INTRODUCTION

At the beginning of the fusion research little was known about the characteristics of ignitrons used for switching and crowbarring high voltage, high energy capacitor banks. In 1959 the Plasma Physics Laboratory conducted a testing program of available ignitron tubes mass produced for resistance spot welding to determine their pulse characteristics.[1] Since that time and after many applications two tubes emerged which fulfilled approximately 90% of all the switching and crowbarring requirement: the two inch ignitron size A, type 5550, and the seven inch ignitron size D, type NL-1053. To bring the data on these tubes up to date and gain additional information, new tests were initiated. The intention of these tests was not to obtain exhaustive results but to secure sufficient data for design purposes, and to find factors which could forecast the approach of tube failure.

I. DESCRIPTION OF TESTS

The ignitrons were tested for the following characteristics:

1. Static voltage breakdown.
2. Dynamic voltage breakdown.
3. Tube resistance.
4. Voltage drop.
5. Arc transfer.

Eight tubes type 5550, and nine tubes type 1053 were tested.[2, 3] The tubes were heated initially for 16 hours with 250 watt heat lamps, which remained on during all tests. The jacket of the type 1053 ignitron was filled with standing water. Measurements were made before the beginning of tests, and at the end of life after the tubes failed repeatedly to fire. Table I shows the results obtained experimentally.

1. Static Voltage Breakdown Test

The static voltage breakdown test indicates the ability to withstand indefinitely a maximum static or slowly rising voltage for positive and negative polarities. All breakdowns for the 1053 ignitrons occurred internally. For the 5550 ignitrons all breakdowns in the initial tests took place across the outside of the glass neck, in the final tests they all occurred internally. Thus the insulation of anode limits the voltage standoff of the 5550 ignitron.

* Work performed under auspices of the U. S. Atomic Energy Commission.

To test for the internal breakdown, the glass neck was first coated with a layer of silicone rubber sealant adhesive to provide an elastic bond between glass and epoxy, and then potted to the size of the external diameter of the tube with an epoxy compound. Four tubes were thus treated, they all broke down internally at an average value of 31 kV.

2. Dynamic Voltage Breakdown

The dynamic breakdown voltage indicates the ability of the tube to withstand a fast rising voltage. The ignitrons were subjected to a voltage rising at a rate of 7.5 to 60 kV per microsecond. When the value of the static breakdown voltage was applied dynamically all the tubes withstood it. For the 50% breakdowns the voltages are shown in Table 1. Seventy-five percent of the times 1053 ignitrons broke down externally. All the 5550 tubes flashed over on the outside. For a 100% breakdown the voltages were found 20% higher.

The dynamic breakdown voltages were identical for rise times from 7.5 kV to 60 kV per microsecond. A tube selected on the basis of static breakdown will be able to withstand a larger voltage applied dynamically. The test showed that standoff voltage is not a reliable indicator of the tube life.

3. Tube Resistance

The leakage current of unfired ignitrons with 15 kV rms, 60 Hz across, was measured to determine their dark resistance.

When 15 kV was applied to the failed 5550 tubes they broke down several times internally before they were able to support this voltage. The leakage current was then measured. The similarities of before and after resistance indicate again that this is not a sure indicator of the impending failure.

4. Internal Voltage Drop

The knowledge of the internal voltage drop is necessary for the calculation of the tube impedance and heating. This voltage drop is made up of two parts: the cathode and anode fall of potential, which is independent of the current and equal to about 12 volts, and the bright resistance of the conducting medium which varies with current.

Figure 1 shows the results for the type 5550 ignitron. Two straight lines are drawn through the experimentally obtained points; the first line corresponds to the voltage drop before arc transfer to the wall, and the second line after the arc transfer. A similar condition has been obtained for the type 1053 ignitron except that the break point occurs at about 7 kA at a voltage drop of 28 volts. The slopes of these curves give the internal resistance of a few milliohm shown in Table 1.

5. Arc Transfer

Arc transfer is said to occur when an appreciable amount of current gets suddenly diverted to the ignitron metal jacket. To illustrate this phenomenon a type 5550 ignitron was cut horizontally. A teflon ring was installed between the two sections, the tube was reassembled, pumped down and electrical connections with current transformers inserted were made from the two sections to the return conductor as is shown in Fig. 2. The ignitron was triggered to pass a large pulse of current. As the current begins to rise it flows mostly through the mercury pool, then as it reaches a certain value a sudden current jump is registered in the upper portion of the tube showing the effect of the arc transfer.

In the actual tests the current at which the arc transferred to the wall was determined from the ignitron current and voltage drop. A downward jump of voltage indicates the arc transfer, as shown in Fig. 3. The total coulombs Q_T transferred by the tube is equal to the sum of Q_M transferred through the mercury pool and Q_J transferred through the tube jacket. Figure 4 shows this for two waveforms of current carried by a 5550 ignitron. Similar curves were obtained for

type 1053 ignitrons, except the initiation of wall current started at 7000 amperes.

6. Arc Transfer and Tube Failure

The arc transfer with its erosion of the steel jacket appears to be the major cause of the ignitron failure. This assertion is based on a number of observations such as pitting of the tube walls, the measurement of ignitor resistance, the relationship of tube failure to fire to the maximum current, operating experience and the study of gamma ray photographs. Figure 5 shows two such pictures of the same tube. The picture on the left represents the condition of the mercury level in the good 5550 tube before the beginning of the tests. The surface of mercury is sharply delineated and the meniscus at the walls is convex upward. The picture on the right shows the same tube at the end of its life after repeated passage of high current. The mercury surface is now fuzzy and the convex meniscus has disappeared. This is due to the metal particles knocked off the metal walls floating on top of mercury. It is well known that certain impurities added to a liquid alter the contact angle considerably.[4]

When a hole was drilled in the metal jacket the air oxidized the metal particles, restored sharpness to the mercury surface and brought back the convex meniscus.

The wetting action occurring at the walls also takes place at the ignitor changing the mercury-ignitor interface and reducing its resistance. In both ignitron types the average resistance dropped from the average original value of 32 ohms to 1 ohm or less at the end of life. This was found to be the most reliable indicator of the impending failure of the tube.

A certain amount of arc transfer can be tolerated by the tube without serious reduction of life. As a case in point, one 1053 ignitron has been pulsed for 1000 times at a repetition rate of 1 pulse per minute, with a total charge transfer of 100 coulombs, of which 50 coulombs were flowing through the jacket. During this time the ignitor resistance decreased from 42 to 36 ohms. The charge was increased to 150 coulombs, with 100 coulombs transferred through the wall. The tube failed after 73 pulses with ignitor resistance decreasing from 36 to zero ohm. Similar results were obtained for the 5550 ignitrons.

II. SERIES CONNECTION OF IGNITRONS

Both types of tubes just described have been used extensively to switch high voltage circuits either singly or in series arrangement. In these applications the standoff voltage of the 5550 ignitron without potting has been limited to 15 kV per tube, while the 1053 ignitron was used to hold off reliably 20 kV.

Figure 6 shows a switch with 5 ignitrons type 1053 connected in series. It has been used in a 100 kV circuit as a crowbar to discharge 2 megajoules of energy, as a series switch supplying energy to rf oscillators, as a crowbar in the rf tank circuit, as an oscillation suppressor in the pulse forming network.[5] In this switch the anode current begins to flow one microsecond after the input signal has been applied to the firing circuit.

III. CONCLUSION

The experience shows that while the change in any of the parameters tested can indicate a deterioration of the tube only the ignitor resistance seems to be a reliable measure of the impending tube failure. It is suggested that all of the parameters tested be periodically checked in an actual installation, and a trend if any be considered as significant.

The standard commercial ignitron represents a satisfactory building block for high voltage switches. It is a standard industrial product, easily obtainable, relatively cheap and rugged in construction. It lends itself to series connections for high voltage use. Up to ten ignitrons have been operated in series and fired in a microsecond time.

These factors contribute to the continued use of ignitrons by the Plasma Physics Laboratory for switching high voltage, high energy circuits.

The author wants to acknowledge the contributions made to this paper by Messrs. George Bronner and John Murray.

References

1. C. Nittrouer, Princeton Plasma Physics Laboratory MATT-30 (1960).

2. J. G. Murray and G. Bronner, Princeton Plasma Physics Laboratory TM-243 (1968).

3. G. Bronner and J. G. Murray, Princeton Plasma Physics Laboratory TM-249 (1969).

4. F. W. Sears and M. W. Zemansky, University Physics, (Addison Wesley Publishing Co., 1963), 3rd ed., p. 306.

5. N. M. Turitzin, Proceedings of 1965 Symposium on Engineering Problems of Controlled Thermonuclear Research, Lawrence Radiation Laboratory Conf. 650512, pp. 213-220.

TABLE I

IGNITRON TYPE	NL-1053				5550			
TEST	INITIAL		FINAL		INITIAL		FINAL	
POLARITY	POS.	NEG.	POS.	NEG.	POS.	NEG.	POS.	NEG.
STATIC BREAKDOWN kV	27.4	30.0	25.3	27.6	20.0	19.2	9.0	9.5
STAT. BKDN. STD. DEVIATION kV	6.3	6.1	6.7	7.2	0.9	1.3	4.3	4.3
50% DYNAMIC BREAKDOWN kV	46.0	47.0	46.6	47.5	25.9	27.5	14.0	16.9
" " STD. DEVIATION kV	3.1	2.9	2.9	2.5	0.7	0.7	4.0	4.0
IGNITOR RESISTANCE OHMS	31.8		0.6		32.2		1.05	
" " STD. DEVIATION "	8.8		0.88		6.1		0.77	
DARK TUBE RESISTANCE MEG.	16.0		15.9		24.5		23.3	
" " STD. DEVIATION "	7.0		5.5		2.4		2.2	
BRIGHT TUBE RESISTANCE BEFORE ARC TRANSFER OHMS	2×10^{-3}				8.2×10^{-3}			
AFTER ARC TRANSFER OHMS	0.87×10^{-3}				2.3×10^{-3}			
START OF ARC TRANSF. AMPS	7000				1500			

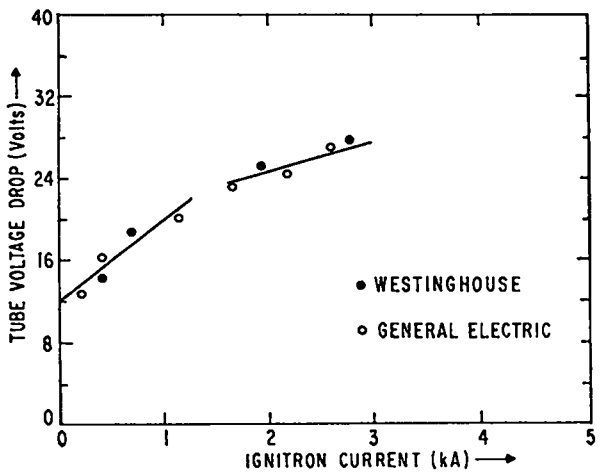

Fig. 1. Internal voltage drop vs current - ignitron 5550.

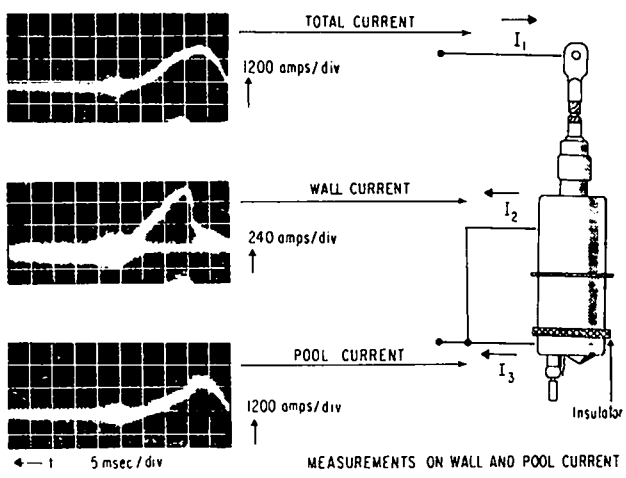

Fig. 2. Measurements of wall and pool current - ignitron 5550.

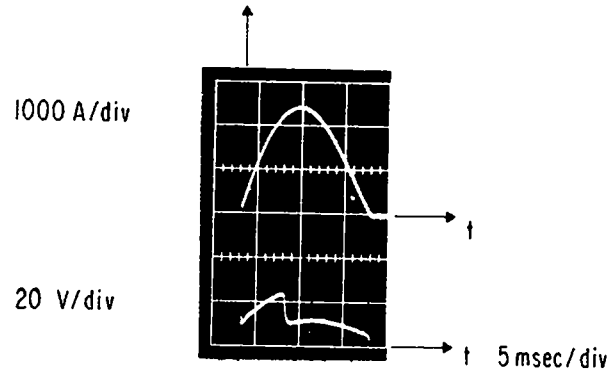

Fig. 3. Occurrence of arc transfer - ignitron 5550.

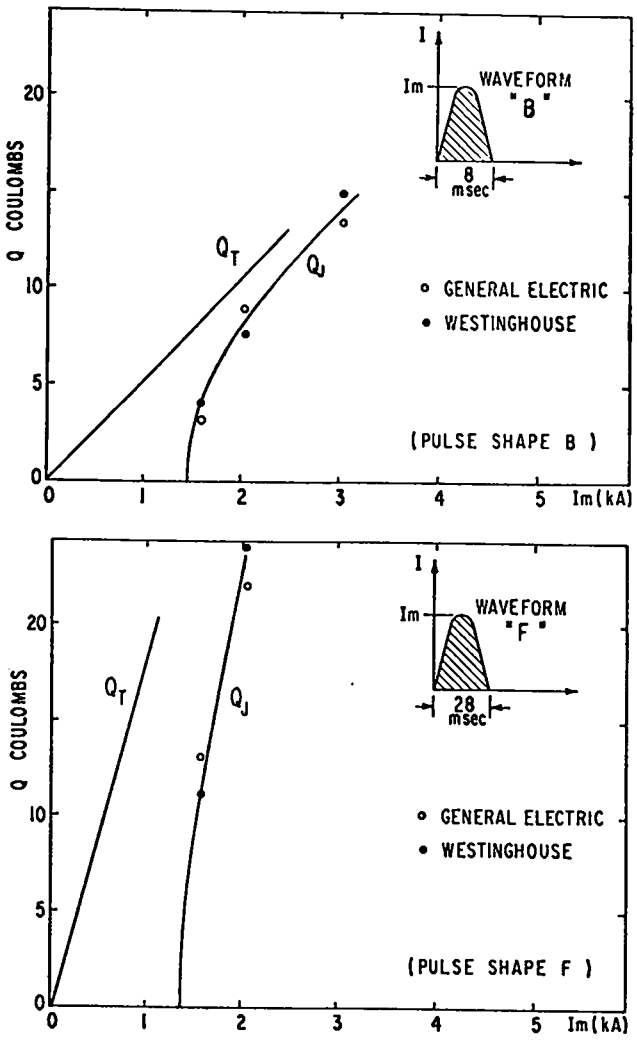

Fig. 4. Arc transfer vs peak current - ignitron 5550.

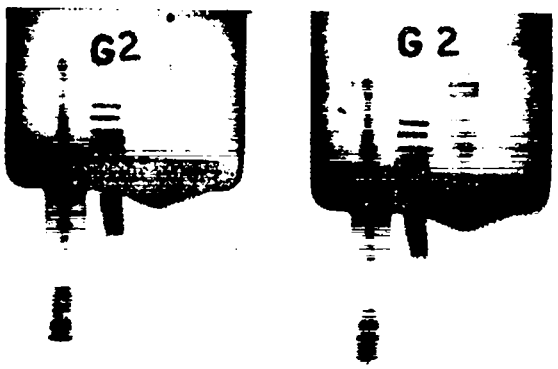

Fig. 5. Mercury pool surface for the same 5550 ignitron, new (left) and defective (right).

Fig. 6. 100 kV ignitron switch 5 units high.

100 KV PRESSURIZED TRIGATRON SWITCH

by

J.K. Burton
W.R. Glock
W.H. Lupton

Plasma Physics Division
Naval Research Laboratory
Washington, D. C.

ABSTRACT

A pair of low-cost trigatron switches have been developed for use at 100 kV. The switches exhibit a delay of less than 10 nsec and a jitter less than 5 nsec. One of the switches was initially designed for low-current use with medium inductance for a 10^6 volt LC generator. The second switch was designed for a system requiring a low-inductance switch with high current capability (140 kA). No degradation appears in the operating characteristics of the high-current switch after 200 operations.

INTRODUCTION

In many areas of plasma physics research there is a frequent need for high-voltage switches capable of controlled operation over a voltage range of 20 to 100 kV. The requirement for switches in the 100 kV range was undertaken as part of the high voltage generator development program. These generators were of two types - the multistage impulse type and the pulse transformer type. The multistage generator is a variant of the Marx-type circuit and is known variously as an LC generator or "swinging Marx." This machine operates at 100 kV per stage and requires triggering of all switches. The second generator is a storage capacitor pulse transformer type high-voltage device that produces 500 to 600 kV. This machine requires only one switch with command triggering and a high current (100 kA) capability.

LOW CURRENT SWITCH

Our previous experience has been with low voltage (20 kV), unpressurized trigatron switches[1]. The electrodes for this type switch, which was designed and developed for the Pharos program, were available at NRL, so these were incorporated into a pressurized housing with no major redesign of the electrode. The switch that evolved from this development is shown in Fig. 1. A coaxial trigger pin made from 2.5-mm-diameter copper with the ends rounded to a hemisphere, with an alumina insulator, is brought through the trigger electrode. The trigger electrode is mounted flush with the main electrode, resulting in a trigger discharge gap of 3.0 mm. The body of the switch is stock nylon tubing. A pressure fitting in each of the electrodes is provided so that, in a surge generator, the switches may be pressurized in series, and only the voltage from one stage appears across the connecting pressurized line. Both the electrodes can easily be replaced in case of damage, and the nontriggered electrode has the additional feature that washers may be inserted under it to reduce the gap. Five switches of this design

were manufactured on contract at a total cost of $985.00.

SWITCHING TIME AND JITTER MEASUREMENT

The circuit arrangement shown in Fig. 2 was used in all the switch delay time and jitter measurements. In this test circuit, the load consists of a single-turn two-microhenry inductor and 19-ohm copper sulphate solution resistor. The trigger generator consists of a spark gap discharging a 0.01 μF capacitor into a 50-ohm line. The capacitor is charged by a 20-kV supply, and the amplitude for the trigger voltage is determined by the output gap spacing. In addition to firing the switch, the trigger gap couples through a suitable resistive divider to provide a trigger voltage for the oscilloscope. The coaxial (RG/8) cable coupling the trigger to the switch is wound on a coil to provide the isolating inductance between the switched high voltage and the trigger generator. The trigger cable is broken 12 in. before it connects to the switch, and a circuit is installed for monitoring the trigger signal as it is impressed on the switch electrode. The two-microhenry inductor in series with the load resistor can be monitored to provide a voltage proportional to the time rate of change of the current in the load circuit.

Figure 3 shows typical waveforms obtained from the test arrangement. The upper positive-going waveform is a monitor of the trigger signal and shows that the trigger rises at the rate of about one kilovolt per nanosecond. A number of trigger pulses superimposed on one film show the jitter in the trigger to be less than one nanosecond. This stability permits monitoring the switch closing without simultaneously monitoring the trigger pulse. Switching time in this test is defined as the time between the peak point of the trigger pulse and the peak current in this discharge circuit. Operating conditions with a negative charge (V_s) and a positive trigger (V_t) are shown in Fig. 4, curve A. The self-breakdown voltage (V_{sb}) of the switch in this case is 98 kV, which is about 10 kV lower than the V_{sb} when the polarity of the charge voltage is plus. This lower value of V_{sb} is undoubtedly due to the slight asymmetry introduced into the switch by the trigger electrode assembly. This switch configuration is interesting and useful, and while it does not have the fast switching characteristics available with a positive charge and negative trigger, it does have the advantage of broad operating range with only a modest increase in delay at the lower voltage. The jitter at 70 percent of V_{sb} and above is in no case greater than 10 nanoseconds, and the delay ranges from a high of about 40 down to about 15 nsec.

The second useful switch configuration, when the trigger V_t is negative and the charge is positive, is shown in Fig. 4, curve B. This configuration has the fastest switching time and the lowest jitter of any of the four possible combinations; however, below about 70 percent of V_{sb} the jitter and the delay become very large. For example, reducing the applied voltage to 60 kV results in nearly twice the delay as in the previous configuration. In this figure one can pick out rather clearly the fast and the slow regions in the trigatron operations. In the fast region the trigger spark travels in the air between the two electrodes and not along the ceramic to the neighboring electrode[1]. This region of low jitter and low delay extends to somewhere in the neighborhood of 70 to 75 percent of V_{sb}. In the voltage below 70 percent of V_{sb} the delay in the jitter becomes strongly dependent upon its applied voltage. A plot of jitter versus applied voltage for positive charge and negative trigger is

shown in curve C. Here the jitter is below 10 nsec throughout the fast region. In the fast region the delay and the jitter are generally less than 5 nsec. It is quite apparent that below a V_{sb} of 75 percent the jitter climbs very rapidly to a generally intolerable figure.

HIGH-CURRENT SWITCH

The high-current switch intended to operate at 100 kV and capable of switching at least 100 kA is shown in Fig. 1. This switch was constructed to be a low-inductance version of the first switch, and the electrode inductance is about 2 nH, while that of the small electrode switch is about 4.8 nH. However, in the 1 to 10 nsec region most of the inductance is still in the spark gap. The inductance of one discharge channel can be approximated by the following expression[2]:

$$L = 0.002\ell(\log_e 2\ell/\rho) - 0.75\ \mu H/cm$$

where ℓ is gap length and ρ is channel radius. It is assumed that the channel radius at 1 nsec after closure[3] is 10^{-3} cm and that this will expand at an initial velocity of 10^6 cm/sec and slow to an expansion velocity of 10^5 cm/sec at 1 μsec[4]. The channel inductance per centimeter decreases from 13.8 nH at 1 nsec to 9.7 nH at 10 nsec, so even though the electrode inductance can be reduced to a reasonable minimum, it is still the gap that causes problems in gas switches. For very fast risetime pulses, the use of oil, water, or polyethylene rather than gas is much preferred.

TEST PROCEDURE

This switch was intended primarily to handle high-current switching problems, and its ability to perform under these conditions was determined by measuring V_{sb} of the switch versus pressure as the switch was initially received and then remeasuring this value after a series of runs at a definite load current. The plot of V_{sb} versus pressure for this switch is shown in Fig. 5. First a new switch having a 1-cm gap was checked and showed a standard deviation of 13 percent for an average V_{sb} of 83 kV. This switch was then operated 100 kA for 100 shots. At the end of this series the average V_{sb} was reduced from 83 kV to 77.5 kV, and the standard deviation was 5.5 percent. The switch was then operated an additional 100 times, and at the end of this series the V_{sb} had increased to 79.3 kV, but the standard deviation went from 5.5 to 10.4 percent. The switch was disassembled and cleaned by wiping the electrodes and housing with alcohol. There was no visible damage, so the switch was retested and the standard deviation was back to 5.5 percent.

Recently the performance of a high current trigatron with a gap of 1.5 cm was tested at 140 kA. The initial characteristics of the switch after a conditioning run at 100 kA were a standard deviation of 4 percent and a V_{sb} of 94.4 kV. After a series of 25 shots the characteristics were remeasured and the V_{sb} had dropped to 83.4 kV and the standard deviation had risen to 10 percent. Upon disassembly, the electrodes were found to be heavily coated with what is presumed to be carbonized nylon. The switch components were cleaned with alcohol and reassembled with a close fitted 0.250-in.-thick lucite sleeve inside the nylon housing. The initial characteristics were rechecked and the switch was then run for 200 shots. The V_{sb} was measured and had dropped from 94.4 to 89.9 kV while the standard deviation had improved from 4 to 2.5 percent. The switch was disassembled and showed only some discoloration of the lucite liner and of the switch electrodes.

CONCLUSION

Two versions of the trigatron switch have been developed for use in the 100-kV

SCYLLAC SPARK GAP AND TRIGGER SYSTEM DEVELOPMENT*

by

C. F. Hammer and R. F. Gribble

Los Alamos Scientific Laboratory, University of California
Los Alamos, New Mexico

ABSTRACT

The Scyllac primary energy system consists of three-thousand two-hundred forty 1.85-μF, 60-kV capacitors with a 4-element spark gap mounted on each capacitor. When triggered the spark gap transfers the stored energy from the capacitor to the load coil. The Scyllac trigger system must trigger all 3240 spark gaps and with a jitter (or simultaneity) of 10 nsec rms.

Each 4-element spark gap is required to hold off the 60-kV bank voltage until triggered, then carry a peak current of about 60 kA. The spark gap consists of 3 main electrodes and an illuminating spark plug. The gap spacings are 1/4" and 1/2". It is pressurized to 20 psig which raises the voltage hold-off capability to 120 kV. The gap is operated with the capacitor charged negative, and the center electrode biased to 1/3 the capacitor voltage. A 1-3/4" wide brass ring is attached to the center electrode to provide additional capacitance to the fast-rising trigger pulse. A major consideration in the design of this gap was to be able to operate the gap in a fast swinging cascade mode.

The Scyllac trigger system uses charged coaxial cable as the energy source for the fast trigger pulse. The system has been designed so that each trigger gap will trigger fifty-four 4-element spark gaps. Therefore, the Scyllac trigger system consists of 60 sub-master trigger gaps and one master trigger to trigger all the sub-master gaps. The coaxial source cables are charged to 100 kV with a pulse which has a risetime of 12 μsec. The trigger system delivers an 80-kV pulse with a risetime of 100 nsec, when measured with a coaxial 50-Ω resistive load. The trigger gap is also a 4-element spark gap with electrode spacings of 1/16" and 1/8" and is pressurized to 45 psig. Low inductance was an important design criterion for this gap. A detailed description of the 4-element spark gap, trigger gap, and trigger system will be included in this paper.

I. INTRODUCTION

In the Scyllac proposal, the Scyllac trigger system and spark gaps were thought to be identical with those being used in Scylla IV only larger in number. At that time a program was initiated to develop an electronic device which would measure the variation in firing delay or jitter of each of of the Scyllac spark gaps. While trying to arrive at a method to measure the gap jitter it was discovered that the Scylla IV gaps were not "cascading" properly, allowing the delay to vary considerably. Gap jitter had not previously been thoroughly investigated simply because the Scylla IV system had been tremendously successful from the standpoint of producing plasma and there were no indications to suspect that the gaps were not firing properly. It was felt that for a system as large as Scyllac it would be desirable to control jitter and minimize it as

*Work performed under the auspices of the U. S. Atomic Energy Commission.

much as possible. Another development program was then started which produced an improved spark gap, which operated "fast swinging cascade"[1], and a trigger system which generated a very fast high-voltage trigger pulse. These improvements have been installed in Scylla IA, the Scyllac prototype, and are now being installed in Scylla IV-3.

II. SCYLLAC SPARK GAP

Upon determining that the Scylla IV gap was not cascading correctly, an investigation was started to determine how the situation could best be remedied. It was decided that the spark gap configuration should be optimized and that a fast trigger system would be designed.

A prototype trigger circuit was built which was capable of delivering to an open circuit, RG/17, 50-Ω coaxial cable, a fast pulse of 60-nsec duration that rises to 300 kV in about 4 nsec. Shown in schematic form in Fig. 1 is the prototype trigger circuit which was used throughout the spark gap development.

Considerable effort went into setting up the instrumentation for the spark gap test system. Two types of measurements were made on the spark gaps; voltage and emitted light. To measure voltage, capacitive voltage dividers were connected to the top and center electrodes of the gap. A photomultiplier was coupled to a rigid light pipe which was inserted into a shallow hole in the gap insulators to observe the emitted light at each gap. By comparing the voltage data with data obtained from the light emission measurements, a method was established to determine when the individual gaps would fire. This is illustrated by the waveforms shown in Fig. 2.

Approximately a year was spent developing the spark gap, about half of this time was devoted to taking hundreds of Polaroid oscilloscope pictures. The spark gap configuration decided on as being the best we had examined is shown in Fig. 3 and will be used in the Scyllac system. The main spark gap is shown in the lower portion of the illustration, the upper portion shows the piggyback crowbar which is being reported on by Robert Gribble.

The Scyllac spark gaps hold off the bank charge voltage of 60 kV, and carry peak current which may be in excess of 60 kA. Low inductance is an important design criterion for all of the Scyllac components, this is particularly true of the spark gaps, since the gap inductance has a direct effect on the voltage transfer efficiency. The inductance of the gap and capacitor assembly has been measured to be 61 nH.

The new features included in the improved spark gap are: the center electrode has a 3/4" diameter hole in the center with a radius of curvature of 1/4" on the edge of the hole. A metal ring has been attached to the center electrode which increases the center electrode capacitance to ground by 100 p.f.

Major changes from the previous design are the reduction of gap spacing to a ratio of 2:1 and pressurizing the gap. When using this center electrode geometry with a lower gap spacing of 1/2", the upper 1/4" gap pressurized to 14 psig, and the capacitor charged to -59 kV, the average delay was 34 nsec and the rms jitter was 2 nsec in 50 samples taken from 1100 shots. The center electrode swing was + 80 kV in 22 nsec to lower gap breakdown. Six nanoseconds later the overswing reached a peak of -80 kV relative to the upper electrode. The top gap breakdown occurred 4-6 nsec after the overswing peak. The gap did not operate satisfactorily for a positive charge less than 55 kV, whereas the useful range extends down to 40 kV for a negative capacitor charge. At 59 kV the delay was reduced by a factor of 5 by charging the capacitor negatively.

Use of grooved insulators was found to produce a very good static hold-off. At 14 psig the gap would hold 90 kV all day and at 20 psig it would hold 95 kV indefinitely.

The final gap configuration has been installed in Scylla IA (36 gaps) and has operated successfully for several months. Seventy-two gaps have been installed in the Scyllac prototype which is in the debugging stage. Three-hundred-fifty gaps are being installed in Scylla IV-3 and will be operating soon.

III. SCYLLAC TRIGGER GAP

The prototype trigger circuit used in the spark gap development consisted of five, 50-Ω, RG/17 source cables, one RG/17 output trigger cable, and a simple overvolted spark gap that connects the two sets of cables. A Marx circuit produces a rapidly rising charge voltage on the source cables, variable from 60 to 150 kV. The gap was pressurized to 35

psig with compressed air. The output pulse was quite stable, with a value of 75 to 85 kV and a risetime of less than 4 nsec. When operated into a load gap spark plug the pulse doubles and is slowed by the R. C. of the cable impedance and the electrode capacitance (R.C. $\approx$ 5 nsec).

Modification I trigger gap is essentially the prototype trigger gap except that it is designed to trigger 36 spark gaps, using 36 source cables. This gap has been installed as the master trigger in both Scylla IA and Scylla IV-3.

Modification II trigger gap is quite different from Modification I in that it is a 4-element spark gap and is capable of triggering 72 spark gaps. Mechanically it is considerably larger, the electrodes are 30 in. diameter and the assembled gap weighs about 800 lbs. This gap was installed in the Scyllac prototype and was used in developing the Scyllac trigger gap. Data taken during this development indicated the gap spacings should be 1/8" and 1/4" for an overall spacing of 3/8". This configuration would break down at 100 kV with a pressure of 40 psig, and is operated at 45 psig min.

Low gap inductance is of particular importance in the trigger circuit since the trigger pulse risetime, $\frac{\text{Gap Inductance}}{\text{Out Trigger Cable Z}}$, must be very fast in order that the load gap will operate fast cascade. The inductance of Modification II gap was measured to be about 45 nH, which gives a 28-nsec delay to the $\approx$ 130-kV breakdown potential of the lower gap of the load gap. If additional time were available for further development of the trigger gap it would be spent trying to reduce the gap inductance even further.

Modification III trigger gap is shown in Fig. 4 and is the design which is to be used in the Scyllac trigger system. This design incorporates all of the findings from the previous developments. The gap is much smaller and much easier to assemble than Modification II. It is designed to trigger 54 spark gaps, using 60 source cables (RG 17/14) each 20 feet long, pulse charged to a maximum of 120 kV. This gap configuration is being installed in Scylla IV-3 and the Scyllac prototype.

IV. THE SCYLLAC TRIGGER SYSTEM

Figure 5 shows the trigger system being proposed for Scyllac. The system consists of a master trigger which triggers 60 sub-masters. Each sub-master will in turn trigger 54 load gaps. The complete system consists of 61 trigger gaps and 3240 load gaps, all to be triggered with a jitter (or simultaneity) time in the order of 10 nsec rms. The master and sub-master trigger gaps are mechanically identical but operated at different pressures because of voltage hold-off requirements.

During the load gap development it was found that the 4-element spark gap would trigger with less delay and jitter, with the capacitor charged negatively than with it charged positively. Since a positive trigger is needed for the load gaps, it would seem logical that the trigger source cables be charged positive and the sub-master triggered with a negative pulse. This now means that a jitter problem may have been shifted from the load gap to the sub-master. To try to overcome this problem the gap spacings have been reversed, so that the small gap is connected to the source cables and the larger gap connected to the output trigger cable. By applying a fast positive high-voltage pulse, the larger gap will be overvolted first and the shorter gap will follow a short time later. To show this the electric field intensity of both gaps has been plotted as a function of time in Fig. 6. The top electrode is biased to -20 kV dc. The center electrode is at + 66 kV and the lower electrode is at + 100 kV when the trigger pulse is applied to the center electrode. The trigger pulse is a positive pulse which rises to 200 kV in 50 nsec. This means the electric field of the top gap goes from $\approx$ + 344 kV/in. to $\approx$ + 1140 kV/in. in 50 nsec and the lower gap goes from $\approx$ - 272 kV/in. to $\approx$ + 1330 kV/in. in the same time. The polarities are taken with respect to the applied trigger. Assuming the gaps break down at $\approx$ 800 kV/in. as shown in the graph, the larger (upper) gap would be overvolted first and some 6 nsec later the shorter (lower) gap will be overvolted. Using 200 kV as the trigger pulse is being somewhat conservative since in the system the trigger pulse may easily exceed 300 kV. This means that slope of the two curves would be increased, and that delay time to breakdown would be decreased. The voltage at which the gaps breakdown is controlled by gap spacing, pressure, and electrode configuration, the point at which the two curves intersect represents simultaneous gap breakdown. This type of operation is desirable but is very difficult to maintain. The

foregoing explanation may also be used in analyzing the load gap operation.

V. SUMMARY

During the past 18 months the Scyllac spark gaps have been improved, while the Scyllac trigger system has been completely redesigned. The entire triggering system should meet the design requirements and be a more reliable system than the previous one.

This is supported by data obtained from Scylla IA after the new trigger system and improved spark gaps had been installed. The neutron output had increased by a factor of 2. Streak pictures show a much better defined ingoing plasma sheath and a less diffuse plasma column. This was presumably a result of the faster voltage rise brought about by the new system.

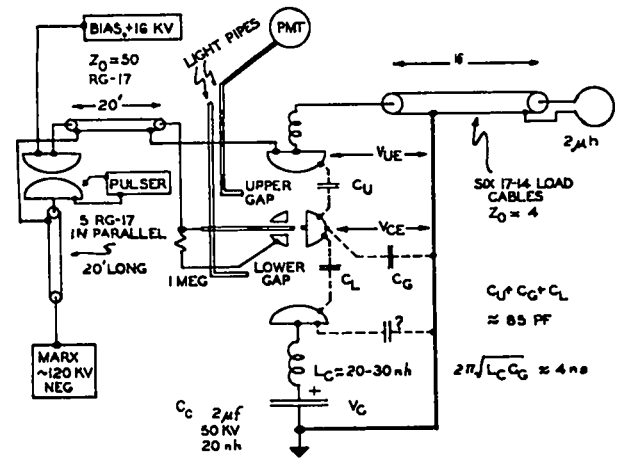

Fig. 1. Circuit diagram of spark gap test setup.

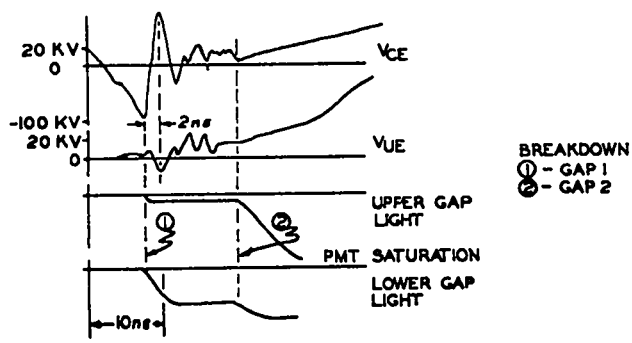

Fig. 2. Typical waveforms obtained from Fig. 1.

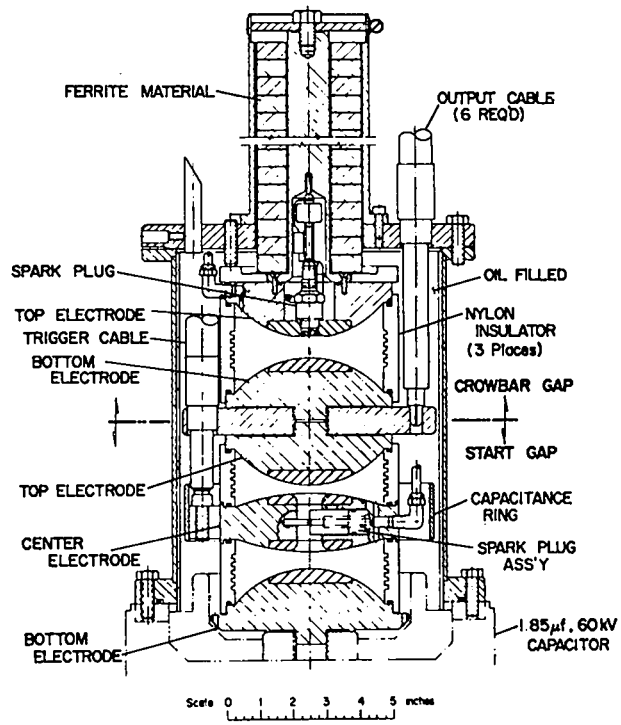

Fig. 3. Scyllac 4-element spark gap with piggyback crowbar.

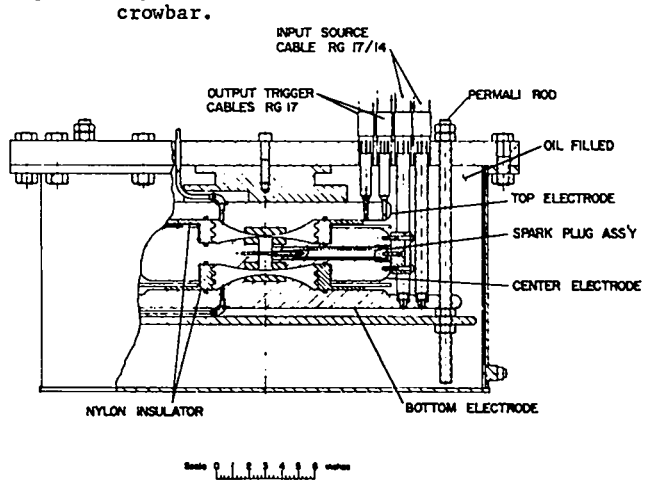

Fig. 4. Scyllac trigger gap.

REFERENCES

1. R. A. Fitch and N. R. McCormick, Proceedings of 4th International Conference on Ionization Phenomena in Gases, Uppsala, 1, p. 463 (1959).

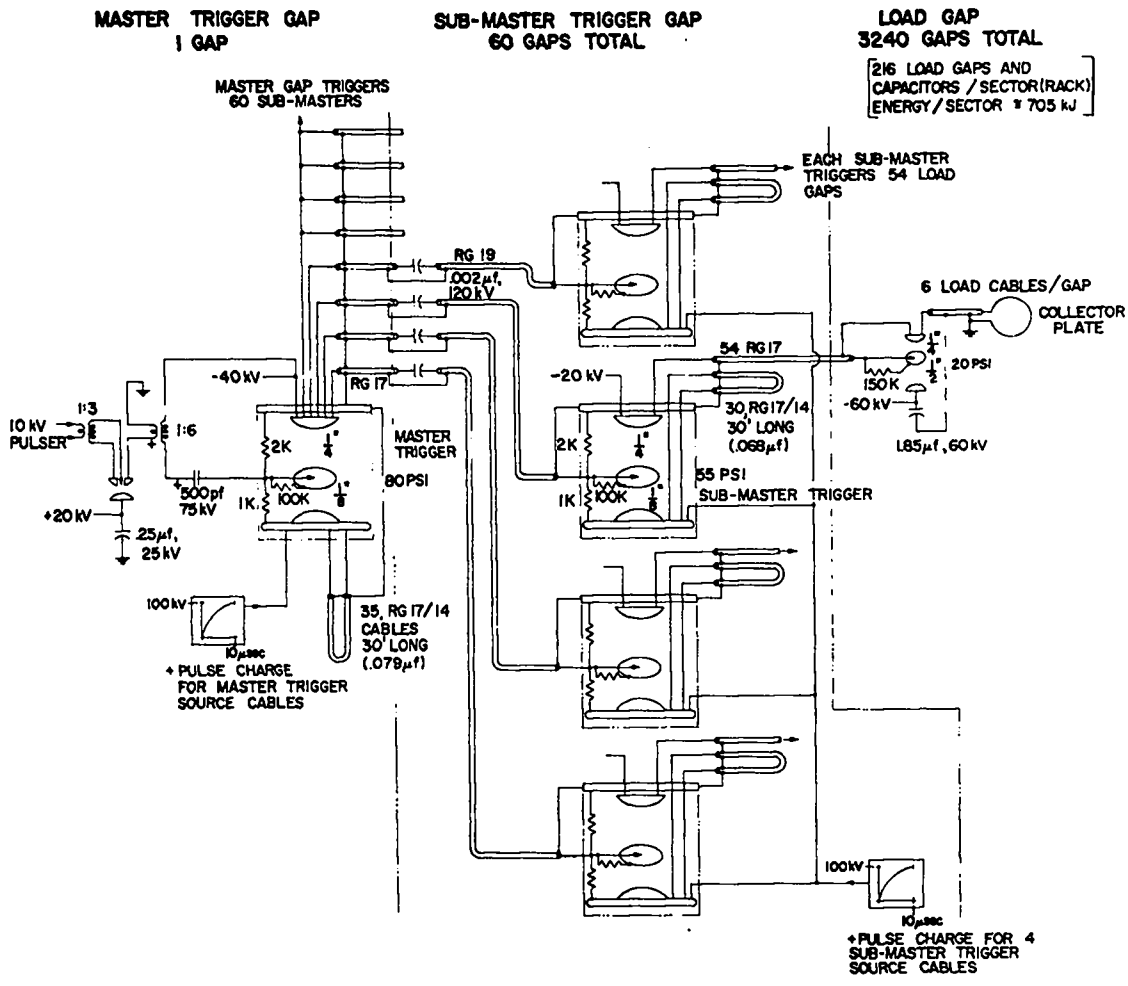

Fig. 5. Schematic diagram of the Scyllac trigger system.

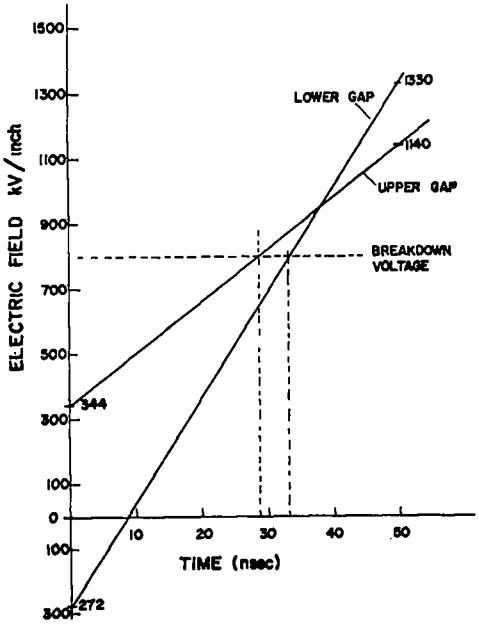

Fig. 6. Spark gap electric field intensity vs time.

A FERRITE LOADED PIGGY-BACK CROWBAR GAP

by

R. F. Gribble

Los Alamos Scientific Laboratory, University of California,
Los Alamos, New Mexico

ABSTRACT

To provide a reliable, low-maintenance, passive crowbar for Scyllac a pressurized, ferrite loaded spark gap was developed to connect directly to the load start gap on each primary bank capacitor. Use of ferrite for trigger decoupling is similar to that of Isar I at the Institute for Plasma Physics, Garching, West Germany.[1] The ferrite introduces a saturating inductance between the trigger electrode and ground or load return. Trigger current from a 75-kV capacitor passes through the coaxial housing containing ferrite toroids and across a spark plug in the trigger electrode. Polarity is such that the crowbar switch does not break down when the crowbar trigger is switched one-half trigger current period before load current peak. During the first half cycle the trigger current at the spark plug drives an ionizing fountain into the inter-electrode region. At the end of the first half cycle of the trigger and at the load current peak the crowbar gap is closed by the pulse on the trigger electrode as the trigger current passes through zero, switching saturation states of the ferrite. For an experimental arrangement consisting of two parallel 2-μF, 50-kV capacitors and gaps having a quarter cycle load current risetime of 4 μsec and a crowbar trigger current of 10-kA peak at 500 kHz, the crowbarred load current modulation was 6%, and the e-folding decay time was 310 μsec.

A crowbar system different from those in present use has been developed for the Scyllac experiment. Employing pressurized air gaps containing ferrite material for trigger decoupling, it differs from the ferrite loaded gaps developed at the Institute for Plasma Physics, Garching, West Germany[1] in the method of triggering. Current provided from a trigger capacitor drives a plasma from the spark plug in the gap for one-half of a trigger current period. Passing through the ferrite circuit the trigger current produces a trigger voltage pulse across the gap when the ferrite switches saturation at the first trigger current zero crossing. A two-load capacitor circuit with parameters similar to that of Scyllac has a crowbar current modulation of 6% and e-folding decay time of 310 μsec.

The crowbar gaps are located on top of the start gaps and within the same return housing; hence the term, piggy-back. A crowbar-gap-start-gap combination is mounted on top of each load capacitor of which Scyllac will employ 3,240. The drawing of Fig. 1 shows this combination. The crowbar gap electrodes, containing heavy metal inserts, are very similar to those of the start gaps. The lower electrode of the crowbar is fastened directly to the upper or output electrode of the start gap.

Containing 50 cm^2 of toroidal ferrite cores,

the top coaxial housing provides the return path for the crowbar current. The crowbar trigger electrode is fastened to the inside cylinder of the ferrite housing. Mounted within the trigger electrode is a champion L-19 spark plug modified by hard soldering a heavy metal washer to the face of its outer electrode. The crowbar trigger lead is placed in a groove in the trigger electrode and connected to the spark pin so that trigger current passes across the face of the plug and through the ferrite housing.

The ferrite material used presently is type 0-5 manufactured by the Indiana General Corporation. Specifications on the material include a saturation flux of 4700-G at 25 Oe, initial permeability of 3000, maximum permeability of 4800 and a core loss at 100 kHz, 1000-G peak of 0.3-W per cm^3. The core is 7.4-cm o.d., 3.9-cm i.d., and 1.3-cm thick. There are indications that a higher frequency core with lower loss and somewhat lower permeability might perform more satisfactorily.

Three set screws clamp the double gap assembly together. The grooved nylon insulator contains O-ring seals. The crowbar gap length is 1.6 cm. Operating gap air pressure is 8 psig at 50-kV capacitor charge and 12 psig at 60 kV.

A 75-kV - 1-μF capacitor triggers 18 crowbar gaps. Gaps on these trigger capacitors are identical to the load start gaps and are triggered by similar sub-master switches. Twenty-foot lengths of 25-ohm cable connect the trigger capacitor to the crowbar gaps.

Crowbar triggering occurs in two steps. During the first half cycle of the trigger current the crowbar gap is effectively shortened as plasma is driven away from the spark plug by the trigger current. The gap is then closed by the pulse of voltage produced as the ferrite switches saturation states during the first trigger current zero crossing. The measured value of this pulse is about 60 kV. Trigger current initiation ideally occurs one-half trigger current period before the main current peak. In practice, the timing is arranged so that the zero crossing occurs a short while before load current peak to utilize a portion of the load capacitor voltage to help close the crowbar.

The polarity of the initial pulse when the crowbar trigger capacitor is started is the same as the load capacitor voltage so that the possibility of a prefire is reduced. In addition a 1000-pf capacitor and a 200-ohm resistor are connected in parallel across the spark plug to prevent a premature spark when the load gap fires. The tendency to prefire is due to the voltage capacitively coupled to the crowbar trigger electrode by the start gap output electrode. Since the trigger electrode is isolated from ground by the ferrite, it tends to swing with the lower crowbar electrode until the ferrite saturates. But the spark plug pin is connected to ground through the trigger cable impedance and hence, without the RC circuit the pulse would appear across the plug.

Most of the crowbar gap performance was obtained from a two capacitor developmental arrangement. However, the crowbar gap has recently been installed in the Scylla IA experiment. Performance of the gap in Scylla IA with 36 capacitors is satisfactory. The developmental arrangement consists of two 2-μF, 50-kV capacitors and gaps connected in parallel to a 1.5-μH load to simulate the Scyllac quarter-cycle rise time of 4 μsec.

For the estimated saturated crowbar inductance of 100 nH and the load inductance per gap of 2.9 μH, 6.6% modulation is calculated where the percent modulation here is defined as the difference between the first current maximum and the first minimum divided by the first maximum. The measured modulation was 6%.

Operating pressure range for a particular load capacitor voltage is defined as that range of gap air pressures where with high reliability the gap will not prefire when the start gap connects and the gap fires reliability near the load current maximum. For Scylla experiments the peak voltage applied to the crowbar gap by the load capacitor when the start gap fires is about 1.6 times the capacitor charge voltage. The developmental arrangement using 50-cm^2 of ferrite has at 50-kV bank voltage a range from 6 psig to 14 psig. Ferrite area here refers to that normal to the field. No crowbar prefires were observed for pressures of 6 psig and above.

Figure 2 shows data for the two parallel gaps where each exposure is an overlay of 10 shots. The upper trace of each is the load current and the

lower is the crowbar current in each gap. A discontinuity at the end of the trigger current half cycle shows the start of the crowbar. The Rogowski loop was placed around the center conductor of the coaxial ferrite housing so that it detects the sum of the trigger and crowbar currents. The crowbar current waveform shown for the slower sweep speed droops due to the fact that the integrators employed had insufficient time constants.

The piggy-back crowbar operates reliably in the developmental arrangement and preliminary data for Scylla IA indicates proper performance in a 36-gap system. Because of uncertainties in the magnitude of line transients in larger systems, especially at 60 kV, work on the crowbar gap is continuing in an attempt to improve the holdoff capability and triggering reliability.

REFERENCE

1. E. van Mark and H. Wedler, IIP 4/59, (June 1968).

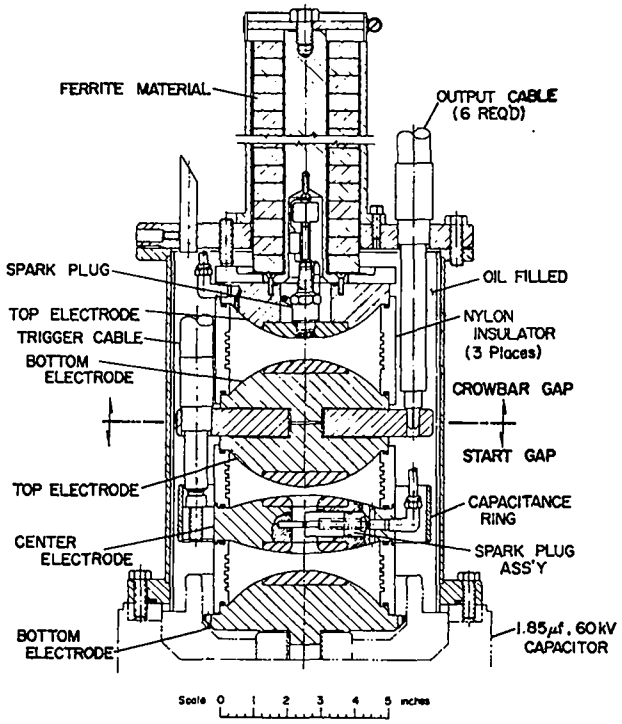

Fig. 1. Drawing of the start-gap and piggy-back crowbar gap.

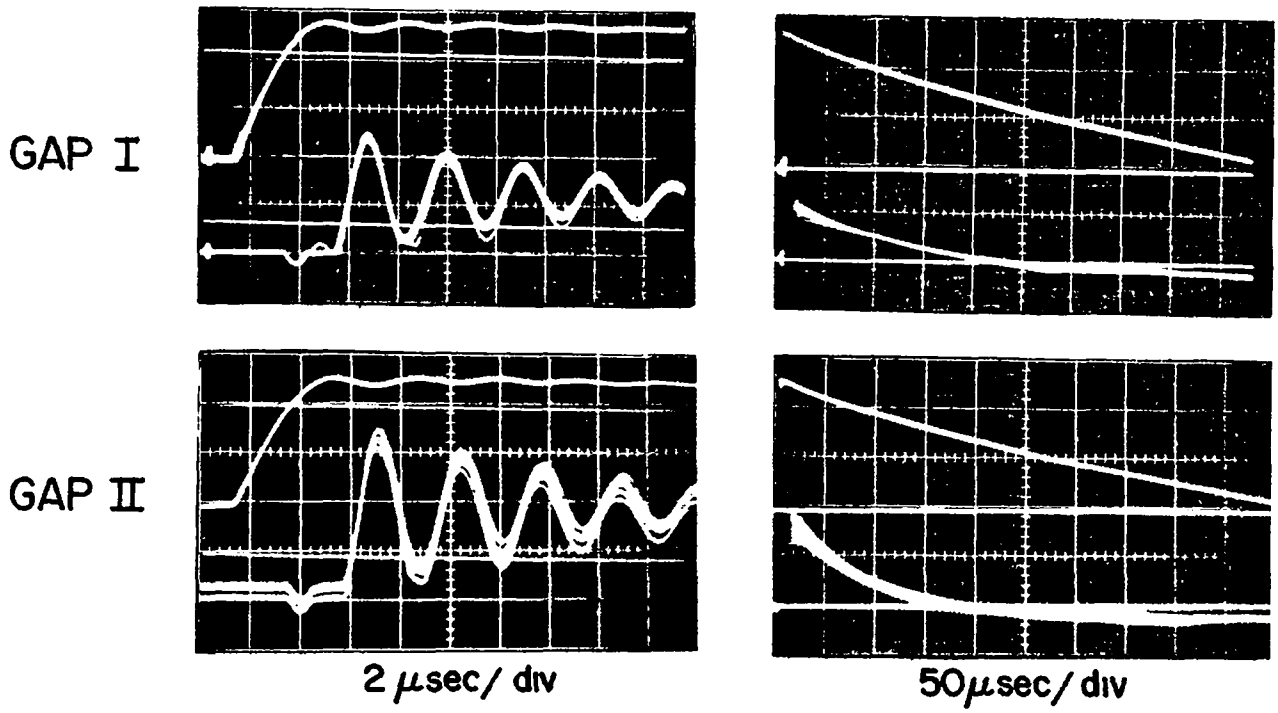

Fig. 2. Crowbar data. Top traces show the load current; lower traces are the sum of trigger and crowbar gap currents.

SOLID DIELECTRIC CROWBAR SWITCH*

by

Darrell L. Call

Los Alamos Scientific Laboratory, University of California
Los Alamos, New Mexico

ABSTRACT

Development work on the Marshall-type solid dielectric switch for Scyllac and other machines is reported. Scyllac will have a peak current of 10 MA per meter section which requires a minimum total switch length of about 12 inches per section to carry the current with a reasonable margin of excess capability. The switch was originally developed as a 2.5-inch switch so that four or five switches per section of Scyllac would be required, which is a formidable operating problem. Assemblies which would close 6 inches of switch were tested in a machine where the switch operated as a start switch. Foil shape, foil exploding capacitor bank, compressive pressure on the switch assembly, foil encapsulation laminating process, and switch insulation thickness were parameters varied during testing. The extruding portion of the switch (switch plate) was changed to a slotted, flattened tube for convenience and to direct the current in a path which uses magnetic pressure to keep the switch closed after closure. Maximum current-carrying capability of this type switch was determined with a one-inch-long exploding foil and found to be just above 1 MA per inch of switch length. This one-inch switch is suitable for many modest crowbarring problems where up to 60 kV must be held off and up to 1 MA is to be crowbarred. Switch closure time jitter with the 2.5-inch switch is 0.01 μsec. As switch length was increased to 4, 5, and 6 inches, the jitter increased to the order of 1 μsec. Jitter and closure time are affected by almost all physical parameters of the switch. Closure time is strongly dependent on impedance matching between the exploding foil energy source and the exploding foil itself. Optimization of this matching was studied. The possibility of driving the exploding foil with an inductive energy source is suggested. Some initial studies and tests using high explosives instead of an exploding foil are reported. Study of the crowbar problem on the NET-1 circuit analysis program is reported where the solid dielectric switch acts to relieve a piggy-back spark gap or ignitron crowbar switch and where it is the only crowbar switch in the system.

I. INTRODUCTION

A low-resistance and low-inductance switch to crowbar the 10 MA of current in each of the 15 sections of Scyllac is necessary. This is a total of 150 MA of current in Scyllac which must be switched, but fortunately it is to be done in 10-MA portions. The switches to be discussed here are modifications of the Marshall-type solid dielectric switch. The original work by Marshall, Henins, and Finlayson[1,2] was with a switch 2.5 inches long. The 2.5-inch switch clearly could not mechanically handle the 10 MA of current and would have too much resistance and inductance for Scyllac even if the switch would stay together.

Operations on Scylla IA with the 2.5-inch switch indicated that the 2 MA carried by that switch was

* Work performed under the auspices of the U. S. Atomic Energy Commission.

near the maximum capability of the switch. Based on this experience, development was started on a switch which was 6 inches long. Two 6-inch switches would be adequate for each section of Scyllac.

II. EXPERIMENTAL HARDWARE AND INSTRUMENTATION

The switch tested is shown in Fig. 1. The switch plate electrode is made of 1100-H14 aluminum 0.091-in. thick which has been formed into a flattened tube with a slot down the length of it. The purpose of the slot is to cause the current to flow in a path which creates forces that help to hold the switch closed. Without the slot, current would flow in the shorter current path where the magnetic pressure tends to reopen the switch. The "flattened tube" switch plate is easier to install in the machine and confines the debris of the explosion to the tube. The previous design was U-shaped and open to the main insulation of the collector plates and sometimes flying debris damaged the collector plate insulation. The second electrode is the slotted die plate made of 2024-T3 aluminum. The main insulation of two or three sheets of 6-mil polyethylene separates the two electrodes. The exploding foil was molded into polyethylene insulation to isolate the exploding foil current from the machine. The whole switch assembly was held together by a big C-clamp.

For ease of operation, this switch was operated as a start switch in the circuit shown in Fig. 2. The capacitor banks were charged up to a preset voltage, the foil capacitor bank was fired to explode the foil and close the solid dielectric switch, and finally current flowed in the main capacitor bank loop. Current in the closed solid dielectric switch was about 200 kA per kilovolt initial charge on the main capacitor bank. Closure time of the switch was defined as the time from when current started flowing in the exploding foil to when current started flowing in the solid dielectric switch. The foil exploding capacitor bank C_2 was varied to give different amounts of energy and different circuit parameters in the foil exploding circuit. The inductance varied with each C_2 as listed in Fig. 2. Two nominal 15-μF, 20-kV capacitor combinations were used. The first combination was a low-inductance capacitor header with an oil-filled folded return, low-inductance triggatron spark gap.[3] The second was a high-inductance capacitor header with a high-inductance, air-insulated triggatron spark gap. The 170-μF, 10-kV capacitor had the high-inductance triggatron for a spark gap and the 5.3-μF, 25-kV had the low-inductance, oil-filled gap. Triggering of the two spark gaps (when C_2 was two capacitors) was by use of a charged cable, triggered spark gap trigger system.

Data recorded included the current in each foil bank capacitor to determine that they fired simultaneously, total current in the exploding foil circuit, current through the switch after switch closure, and the voltage across the exploding foil. Current measurements were made by electronically integrating the output of Rogowski loops. Voltage was measured with a string of resistors and a Tektronix P6041/CT2 current probe. The resistor string was about 1000 ohms and connected in parallel with the exploding foil. Current through the resistor string was measured with the current probe. The back emf due to the inductance of the exploding foil was subtracted out using the voltage from a di/dt loop placed near the exploding foil. Presumably this resulted in the True Resistive Voltage (TRV) of the exploding foil.[4]

III. TESTS AND RESULTS WITH SIX-INCH SWITCH

Different methods of laminating or molding the copper foil between two sheets of polyethylene were tried. The usual procedure is to take two sheets of 1/32-inch-thick polyethylene laid on top of one another with the copper foil between them. These pieces are then put into a hydraulic press equipped with hot platens. After the polyethylene sheets have melted and run together, the part is cooled in a cold press. This results in a part which has the copper foil imbedded or molded inside a sheet of polyethylene insulation. When the foil is exploded the copper vapors can expand only into a volume created by moving the switch plate. Attempts to try to glue the two sheets of polyethylene together weren't successful. With the best adhesive available there was considerable loss of vapors between the two layers of polyethylene. Increasing the clamping pressure on the switch decreased the venting some but never enough to be satisfactory. The maximum pressure used on the switch parts was limited by mechanical capacity of the C-clamp to about 2500 psi.

The thickness of polyethylene around the copper foil laminates was marginal for the voltage hold-off. In the original laminating process the polyethylene was heated long enough to make it flow quite a lot which resulted in the overall thickness of the laminated assembly to be about 50 mils. By lowering the platen temperature, hydraulic press pressure, and the length of processing time, it was possible to still make the two pieces of polyethylene flow together but resulted in an end product with 55 to 60 mils thickness. This extra thickness did help the voltage hold-off problem.

Uneven closure of the switch along the length of the exploding foil was a major problem. Sometimes the full six inches would close completely and simultaneously. Usually only part of six inches would close. The amount that didn't close varied from 1 to 4 inches. A large number of shots were fired to determine the cause of this problem. A definite answer was never determined, but a lot of evidence indicates that the laminating process was the problem. Our own LASL plastics group laminated most of the foils for us. Some batches would be better than other batches and suddenly one batch was perfect. Every switch fired in that one batch closed perfectly. We never were able to reproduce the batch that worked perfectly every shot. Varying the platen temperature, press pressure, and processing time all varied the end results. Copper foil batch, milling to shape, and handling were eliminated as causes, as was the possibility of differences in polyethylene used for laminating. The impedance matching problem (to be discussed in Section V) was found to affect the closure quality but a complete solution to the uneven closure problem was never found.

A number of shapes for the exploding foil were tried. Those shapes tested are shown in Fig. 3. Shape A is the standard 6-inch foil. Shapes B and C are attempts to make use of a tapered foil. Tapered foils were tried to see if a "blowout" problem could be solved. When the switch with a shape A foil was fired quite often the short tab of exploding foil would blow out the end of the flattened tube and cut through the main insulation. Current would flow in an arc through the hole in the insulation and bypass the switch. The shape B tapered foil did reduce the problem a little but not sufficiently. It was observed that for shape B the maximum length of switch closed was never any longer than the straight 5/16-inch wide portion of the exploding foil. The transition to the tapered part of the foil ended the length of switch closure. Eighteen different combinations of the length Z and dimensions X and Y of the shape B foil were tested. For foil shape C, the length Z was varied from 3/8 to 3/4 inch. In this short exploding foil case the length of switch closed was usually more than the length Z. The length closed in this case was determined by the amount of energy in the foil exploding capacitor bank.

The blowout problem was solved by lowering the clamp pressure. When pressure on the switch was in the 650 - 1000 psi range, there was no blowout. When the pressure exceeded 1250 psi the blowout problem was severe. At higher pressures blowout could be relieved a little by sliding the exploding foil inside the tube away from the end where blowout occurred. This never did cause blowout at the other end but also didn't solve the blowout problem.

Figure 3 also indicates total foil lengths were varied between 12.5 and 14 inches. This was done primarily on shape A where dimension W, which is the current feed tab length, was varied from 4.5 to 6 inches. The polyethylene insulation molded around the foil was adequate to hold off the voltage kick of the shorter foil but would quite often break down on the longer foil in the place marked area 1. The higher voltage was caused by the higher inductance on the long tab on the foil. This small change in the foil length indicated that the foil insulation was marginal for voltage hold-off. The longer foil would be necessary on a plasma machine to reach a point for connecting to the rest of the circuit. Increasing the laminated thickness from 50 to about 58 mils helped to relieve the problem but it still was marginal for machine operation.

Closure time data for 84 shots with pressure on the switch ranging from 1200 to 2500 psi is shown in Fig. 4. Blowout described above was a big problem for this series of shots. In this series 150 shots were fired to get 84 shots which didn't suffer from blowout. Blowout causes an apparent switch closure time of about 5 μsec when observing the current starting to flow in the main capacitor bank. Closure time jitter is about 1 μsec.

Data for a group of 46 shots in which the clamp

pressure was varied between 600 and 900 psi is shown in Fig. 5. These shots were all good ones. There was little or no arcing of the switch parts, the entire length closed to the same depth and there was no blowout. When Fig. 5 is compared to Fig. 4, we see that the average closure time with the lower clamp pressure is about 0.9 μsec higher than with the higher clamp pressure. Longer closure time with lower clamp pressure is a general pattern that has always held true for good or poor switches.

The main switch insulation thickness was varied to determine the effect on closure time. It is a linear function which changes at the rate of 0.31 μsec/mil of polyethylene. This performance can be compared to two other similar switches. The 2.5-inch switch developed by Finlayson varied at a linear rate of 0.27 μsec/mil.[2] In another similar but smaller switch, Dokopoulos in Julich, Germany, reported a linear factor of about 0.11 μsec/mil.[5] Since this relationship always turns out to be about linear, it can be assumed that the switch plate is moving at a constant velocity which is the reciprocal of the numbers noted above. These velocities are shown in Fig. 6. It is also possible to calculate the rate at which voltage is falling in a machine during the first quarter-cycle before closing the crowbar switch. Assuming about 70% of the bank voltage transfers to the crowbar switch location, the 60-kV Scyllac machine will put about 40 kV across the crowbar switch. Also, assuming a 4-μsec quarter-cycle drop to zero, the voltage will be changing at a rate of 16 kV/μsec when it crosses zero at 4 μsec. Polyethylene can be used at a stress level of 3 kV/mil in this application. We want to have the switch plate move fast enough to always leave at least enough insulation to keep the stress level at or below 3 kV/mil. This requires a minimum velocity of 5.3 mils/μsec for the switch plate and is about 2 mils/μsec faster than the velocity measured. The low velocity results in arcing of the switch parts when the switch closes.

IV. TESTS AND RESULTS WITH ONE-INCH SWITCH

In the experimental machine for testing six-inch switches the capacitor bank switched on by closing the exploding foil switch would produce a maximum of about 2 MA, which is not enough to test the maximum current capability of the six-inch switch. To find the maximum current capability of this type switch, switches with an exploding foil length of one inch were fired. The one-inch switch was the same as the standard six-inch switch except the narrow exploding part of the copper foil was one inch long instead of six inches and the overall foil length was also shortened a little as was the slotted tube length.

The maximum current per inch of switch was found to be 1 MA. At 1.14 MA the mechanical damage to the switch was so severe that the switch was not useful. Switching current to 1.0 MA presented no problems. The exact transition from good to poor closure was not determined because of the extreme damage to the experimental machine when 1.14 MA was switched.

Closure time as a function of foil capacitor bank energy for the one-inch switch is shown in Fig. 7. Switch insulation thickness was 12 mils of polyethylene. The two curves are for the same high- and low-inductance capacitor headers which were described for the 6-inch switch system.

This one-inch switch would be useful for some modest switching problems where up to 1 MA was to be switched. Voltage capability is determined by switch insulation thickness and the geometry of the application.

V. IMPEDANCE MATCHING

The need for proper impedance matching between a capacitor bank and an exploding wire for maximum power transfer is well documented.[6-9] Theories worked out by the various authors for a properly matched source and load do not agree, but the general requirements they suggest are all consistent. If the resistance of the load for a given capacitor bank is too low, the current simply is a damped oscillation. Power dissipation in the load is low and the wire hardly explodes. As the resistance of the wire is increased more power is put into the wire. The current has less reversal until finally at maximum power dissipation in the wire, there is essentially no current reversal and the current trace looks like a critically damped discharge. If the resistance is increased further there appears to be a current "restrike" before the current has completed the first half cycle. Bennett[6] has presented a range of circuit resistance as a function of $\sqrt{(L/C)}$ for

maximum power dissipation in the circuit resistance. L and C are the total inductance and capacitance of the discharge circuit. For maximum power at the first current peak $R_{opt} = 1.1\sqrt{(L/C)}$. For maximum integral power (energy) deposited in the circuit resistance at some time in the second quarter of the current cycle $R_{opt} \approx 1.3\sqrt{(L/C)}$. Leopold[8] confirms these results in a study of optimizing circuit parameters for bridge wires when the load resistance is determined by calculating

$$\bar{R} = \frac{\int_o^t R\, I^2\, dt}{\int_o^{t_1} I^2\, dt}$$

with t_1 taken at the upper energy plateau.

Exploding foils seem to function the same as exploding wires in determining the proper impedance match. When one 5.3-μF capacitor was used to try to explode a one-inch foil, the resistance of the foil didn't reach $\sqrt{(L/C)}$ anytime during the discharge and no metal was moved in the switch. By increasing the capacitance to 10.6 μF, the optimum resistance was lowered and the switch closed very well. Similar performance was noted for the longer switches and different capacitor banks. Total energy in the capacitor bank was found to be not as important as the impedance match. Unfortunately, it has been after much testing that the current waveform shape was discovered to be a key in determining the quality of the impedance matching. Many shots have been fired with a current waveform that indicates that the foil resistance is too high and a thicker foil should be used.

A series of tests were run with foils which had exploding foil lengths of 2.5", 4", 5", and 6" to determine the effect of changing the circuit inductance. Inductance was varied by changing the length of the feed tab on the copper foil. These tests indicated that for any given exploding length, there is an optimum total foil length or circuit inductance. The exploding foil cross-section was the same for all tests and only the length was varied. Complete optimization of the impedance match requires varying cross-section parameters as well as the length.

Data for a six-inch switch that fired and closed properly and was typical for switches that always closed properly was used to determine the energy distribution in the exploding foil circuit as a function of time. From the voltage and current traces, instantaneous power during the discharge was calculated and plotted. Peak power was 2750 MW. The power curve was integrated to get the energy deposited into the foil. On Fig. 8, E_R is the energy vs time curve for the I^2R heating of the exploding foil in which the foil bank was one 14.6-μF capacitor and one 5.3-μF capacitor. Peak current was 170 kA which is 4.2×10^7 amps/cm^2 through the exploding foil. A total of 6.9 kJ/gm was deposited in the exploding portion of the foil. Spark gap energy loss was estimated to be 450 joules.

Figure 8 also shows the energy stored in the inductance of the circuit. That energy is labeled E_L and was determined by calculating $1/2\ LI^2$ where L = 151 nH and I was the total foil current. E_R and E_L are added and compared to what $1/2\ LI^2$ would be if the circuit was lossless and oscillating. The energy balance is within the accuracies of the experiment. Vaporization of the foil started at 2 μsec and the voltage peak occurred at 2.7 μsec. During this time foil energy increased 1820 J. Curve E_L indicates that 1490 joules were supplied by the inductance of the circuit. Integration of the current trace indicates that about 360 joules came from the capacitors during this time so that again, with experimental error, energy balance was preserved. This performance suggests there may be a quicker way to get the energy into the foil and lower the closure time of the switch. If all of the energy of the capacitors was first transferred to the inductive energy storage and then delivered to the foil, a much faster rate of energy transfer into the foil would be possible. A method for inductive energy storage is briefly outlined by Janes and Patrick[10] and recently has been improved to the state of a workable system by DiMarco and Burkhardt[11] of LASL.

VI. HIGH EXPLOSIVE-DRIVEN SWITCH

Since there has been considerable difficulty in developing a workable switch six inches long using an exploding foil to drive the switch plate, some other designs are being considered. A review of high velocity metal-forming techniques indicates that if the exploding wire could be put under water, higher efficiency in terms of moving metal would be possible.[12] Water (or any other liquid) inside the collector plates of a Scylla-type machine is an untenable

proposition. Magnetic field pressure large enough to do the job seems difficult.

High explosive technology is now being considered. An initial test was run with H.E. in which a regular six-inch foil was exploded with a piece of Detasheet H.E. lying in contact with the copper foil. The Detasheet was 0.312" wide, 6" long, and 0.18" thick. The whole assembly was clamped tightly together. The test conclusively proved that the exploding foil would not detonate the Detasheet even though the copper foil explosion moved metal in the switch. Other high-explosive techniques are being considered.

VII. CIRCUIT ANALYSIS

The simple lumped parameter circuit description of the crowbar problem shown in Fig. 9 has been studied. The circuit includes a leg (R_5 and L_5) which is the piggyback spark gap crowbar. All circuit component values except R_6 and L_6 were determined either by experiment or computer calculations. R_6 and L_6 are educated guesses based on experience. R_2, R_3, L_2, and L_3 are time-varying components on a Scylla machine but were held constant for all results reported here.

In Fig. 9, R_6 and L_6 are labeled as the in-plate crowbar. An in-plate crowbar is a solid dielectric crowbar switch which is built into the machine collector plates as close to the load coil as possible.

Three computer codes have been used to study the behavior of the circuit. NET-1 was used to get initial conditions for the crowbar problems.[11] The outside loop of Fig. 9 was run from time zero without the two crowbar legs in the circuit. Currents and voltages in the single loop circuit at the first current peak in the load were used as initial conditions for crowbar calculations. These initial conditions were used in two different crowbar solutions. The first calculation was done with a code called TAF which was developed by the Rover Reactor Controls group of LASL.[12] This code was used because it can be used to calculate the time-varying parameter case. NET-1 cannot handle time-varying parameter problems. The second crowbar calculation was with NET-1. The third code was a Fortran program to calculate the eigenvalues of the circuit's A matrix. The A matrix is that of the state variable network analysis equation $\frac{d}{dt}[X] = [A][X]$.

The case of both the piggyback and in-plate crowbar switched on simultaneously at the first load current peak was run with the TAF code using the initial conditions determined by NET-1. The results are shown in Fig. 10. Time zero on Fig. 10 corresponds to 4.2 μsec circuit time. Current in the in-plate crowbar rises relatively slowly.

The eigenvalues of the A matrix are the natural frequencies of the circuit. This circuit has four degrees of freedom so there are four eigenvalues. One of these eigenvalues is the time for the load current to decay to 1/e (e-folding time) of its maximum value. For the circuit element values of this circuit, that time is 146 μsec and is essentially determined by the load and in-plate crowbar loop (R_3, R_6, L_3, and L_6).

An exact solution for currents and voltages in the circuit is very complex and completely masks the dominating circuit parameter combinations which effectively determine circuit behavior. By using the results of the eigenvalue and the TAF code calculations, it was possible to deduce good approximate solutions for the currents in the circuit. Those results are listed here.

$$I_1 = I_{10} e^{-\alpha_1 t} \cos 2\pi(t/\tau)$$

$$I_2 = I_{20} e^{-\alpha_2 t}$$

$$I_3 = I_{30} e^{-\alpha_3 t}$$

$$I_5 = I_{10}[e^{-\alpha_2 t} - e^{-\alpha_1 t} \cos 2\pi(t/\tau)]$$

$$I_6 = I_{30}[e^{-\alpha_3 t} - e^{-\alpha_2 t}]$$

where

$$\alpha_1 = \tfrac{1}{2} \frac{R_1 + R_5}{L_1 + L_5}$$

$$\tau = 2\pi\sqrt{[(L_1 + L_5)C_1]}$$

$$\alpha_2 = \frac{R_2 + R_5 + R_6}{L_2 + L_5 + L_6}$$

$$\alpha_3 = \frac{R_3}{L_3}$$

It should be stressed that these solutions are approximate and valid only for the assumptions given and the component values of the order of magnitude used in the calculation.

The e-folding time of the load current in the circuit when only the piggyback crowbar is used is about 70 μsec. The in-plate crowbar is seen to increase the e-folding time by a factor of about two.

Again it is important to note that constant parameter circuit values have been used in this study. The parameters really vary so that the e-folding time on a machine will be much longer than predicted with these unrealistic worst case calculations.

The results for the case of using only the in-plate crowbar run with NET-1 are shown in Fig. 11 where only the load current was plotted. Time zero is also zero circuit time. The only significant difference between the load current in Fig. 11 and the load current shown in Fig. 10 is that with only the in-plate crowbar there is 16% modulation of the load current. With both crowbars in the circuit the load current sees no modulation at all. The decay time is about the same in both cases.

VIII. FUTURE PROGRAM

A switch suitable for use on Scyllac has not yet been developed but notable progress has been made in determining how to (more notably, how not to) make the switch. More methods of laminating the exploding foils and impedance matching of the exploding foil to the energy source are to be studied.

A usable switch is expected to be developed using high explosive technology. Circuit analysis using existing codes and the new NET-2 program which can handle non-linear and time-varying circuits will be used to study the behavior of capacitor discharge circuits. By the time Scyllac is operational, a low resistance and inductance crowbar switch is expected to be a reality.

ACKNOWLEDGEMENTS

The author is grateful to E. L. Kemp for encouragement and many fruitful discussions, to R. Jarvis and R. Benavidez for technical assistance, to C. M. Fowler and D. B. Thomson for high explosives tests, and H. Sass for typing and editing the manuscript.

REFERENCES

1. I. Henins and J. Marshall, "Fast Metallic Contact Solid Dielectric Switch for High Voltage and Current", Rev. Sci. Instr. 39, 1481 (1968).
2. V. A. Finlayson, "Characteristics of the Scylla IA Theta Pinch with Crowbar", LASL Report LA-4042 (1968).
3. E. L. Kemp, E. M. Dolnick, R. S. Dike, G. A. Sawyer, and J. L. Tuck, "Scyllacita -- Compact High Voltage Theta Pinch Machine", Rev. Sci. Instr. 37, 1065 (1966).
4. R. J. Thomas and J. R. Hearst, "An Electronic Scheme for Measuring Exploding Wire Energy", IEEE Transactions on Instrumentation and Measurement IM-16, 51 (1967).
5. P. Dokopoulos, "Fast Metal-to-Metal Switch with 0.1 μsec Jitter Time", Rev. Sci. Instr. 39, 697 (1968).
6. F. D. Bennett, "Energy Partition in the Exploding Wire Phenomenon", Ballistic Research Laboratories Report No. 1056, Appendix 1 (1958).
7. A. Caggiano et al, "Capacitor Discharge Metal Forming", Republic Aviation Corporation Report No. ASD-TR-7-844 (V), (1962).
8. H. S. Leopold, "Capacitance-Voltage Relationships for the Initiation of PETN by Exploding Wires", Exploding Wires (Plenum Press, Inc., New York, 1968), Vol. IV, p. 319.
9. Ch. Maissonier, J. G. Linhart, G. Gourlan, "Rapid Transfer of Magnetic Energy by Means of Exploding Foils", Rev. Sci. Instr. 37, 1380 (1966).
10. G. S. Janes and R. M. Patrick, "The Production of High Temperature Gas by Magnetic Acceleration", Conference on Extremely High Temperatures, H. Fischer and L. C. Mansur (Eds.) (Wiley, 1958), p. 3
11. J. N. DiMarco and L. C. Burkhardt, "Fast Z-Pinch", LASL Report LA-4975-MS, p. 3 (1968).
12. D. L. Bagnoli and D. J. Molella, "Application of High Velocity Hydro-Electrical Discharge as a Non-Destructive Testing and Metal Forming Tool", Picatinny Arsental Tech Report No. 3228, p. 29 (1965).
13. G. P. Boicourt, "Application of the NET-1 Network Analysis Program to Distributed Circuits", Paper E7, this Symposium.
14. T. E. Springer and O. A. Farmer, "TAF - A Steady State, Frequency Response and Time Response Simulation Program", Fall Joint Computer Conference, p. 359 (1968).

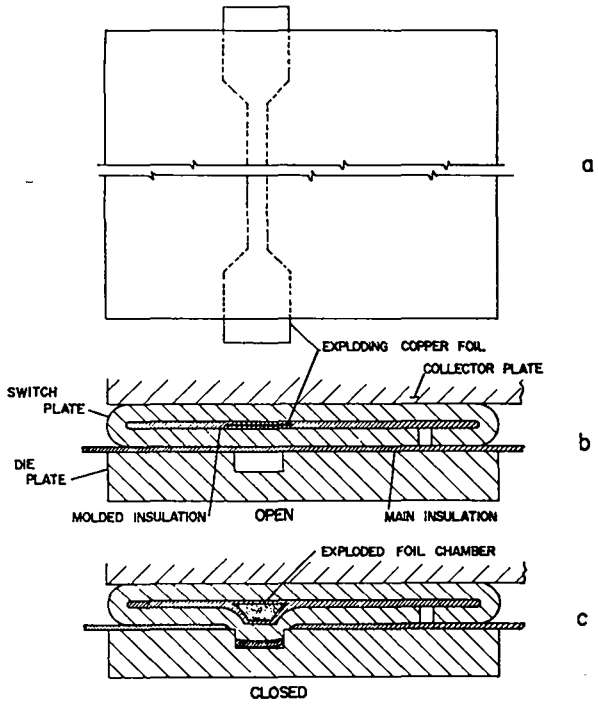

Fig. 1. Metal-to-metal solid dielectric switch. (a) The exploding foil is shown in place inside the switch plate. (b) The switch is made of the slotted switch plate which contains the exploding foil, main switch insulation of polyethylene film, and the slotted die plate. (c) When the foil is exploded a low-resistance switch contact is formed.

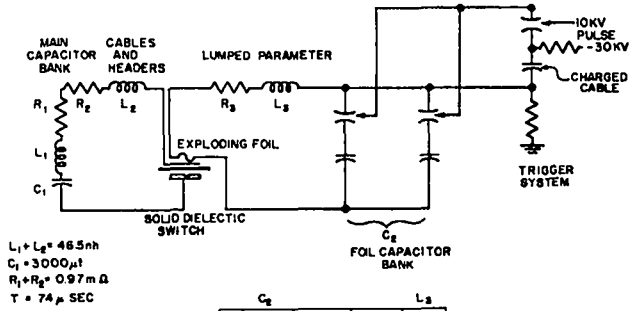

C_2 NO.	EACH Cμf	TOTAL Cμf	MAX KV	L_3 nh
1	14.6	14.6	20	177
2	14.6	29.2	20	99
1 and 1	14.6 5.3	19.9	20	151
1	5.3	5.3	25	118
1	170	170	10	
2	150	300	20	182

Fig. 2. Experimental machine circuit schematic. On the left is the solid dielectric switch used as a start switch. The right side is the exploding foil circuit and trigger system. The table lists values of C_2 and the corresponding inductance L_3 used during the experiment.

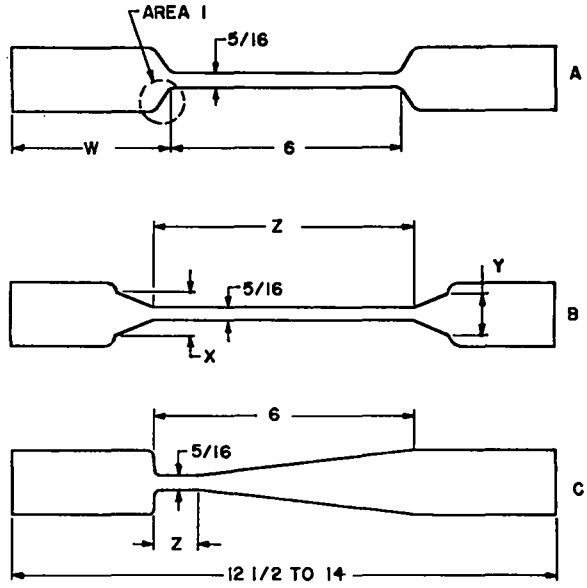

NOTE- ALL FOILS ARE 2 MILS COPPER

Fig. 3. Exploding foil shapes tested. (A) The feed tab length was varied for the standard six-inch exploding foil. (B) Tapered foils were tested to see if a blowout problem could be solved. (C) A very short exploding foil closed a switch length which depended on energy input.

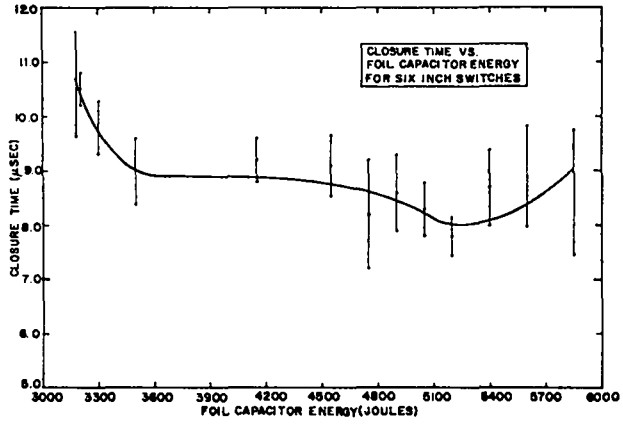

Fig. 4. Closure time vs foil capacitor energy for six-inch switches. This curve shows a closure time of about 9 μsec and relatively large jitter when switch compressive pressure was high.

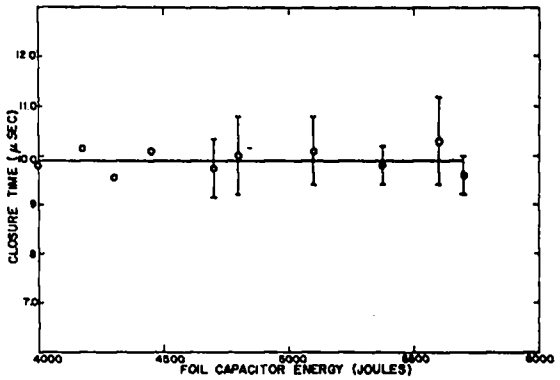

Fig. 5. Closure time vs foil capacitor energy for six-inch switches. Closure time was 9.9 μsec when the switch compressive pressure was low.

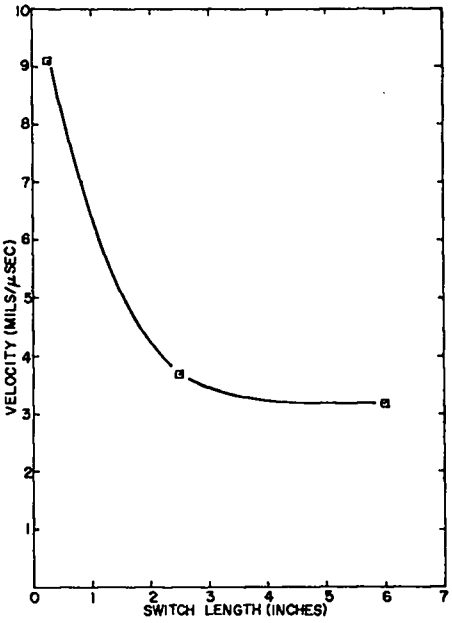

Fig. 6. Velocity of switch plate metal. Velocity of the switch plate is seen to decrease as the switch length increases for three different lengths of switches.

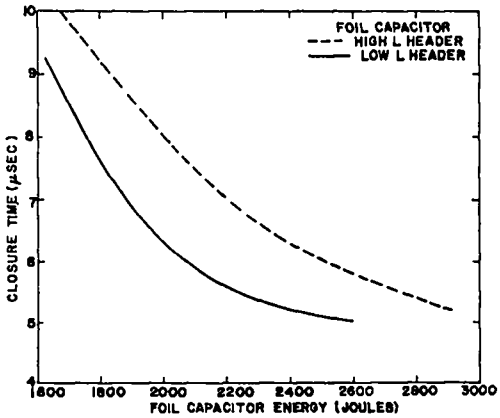

Fig. 7. Closure time vs foil capacitor energy for one-inch switches. The two curves show the effect of different amounts of inductance in the foil capacitor bank.

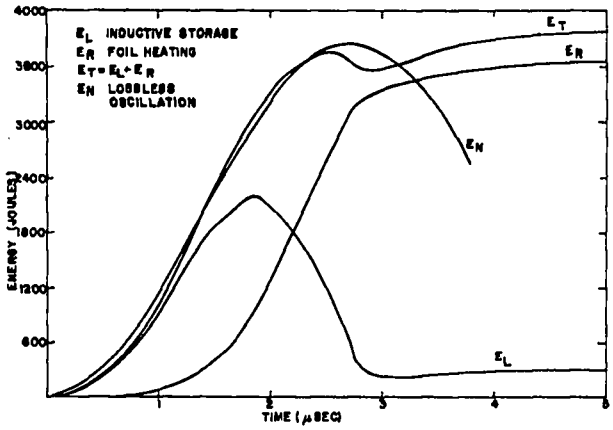

Fig. 8. Energy distribution during exploding foil discharge. E_R is I^2R heating of the exploding foil. E_L is the energy stored in the foil-exploding circuit inductance. E_N is a check to see if energy balances during the discharge.

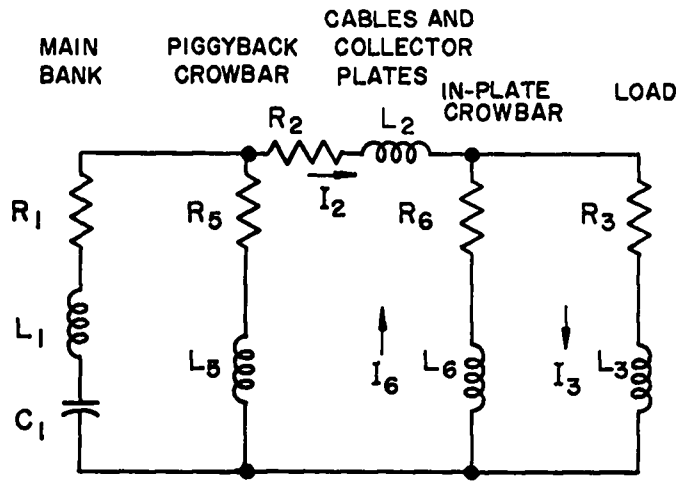

$R_1 = 69\,\mu\Omega$ $L_1 = 0.28\,nh$

$R_2 = 151\,\mu\Omega$ $L_2 = 4.46\,nh$

$R_3 = 83\,\mu\Omega$ $L_3 = 12.95\,nh$

$R_5 = 16\,\mu\Omega$ $L_5 = 0.31\,nh$

$R_6 = 1\,\mu\Omega$ $L_6 = 1\,nh$

$C_1 = 399.6\,\mu f$

Fig. 9. Simple circuit for analysis of the crowbar problem. "Piggyback crowbar" is a spark gap mounted on top the start gap. "In-plate crowbar" is a solid dielectric switch located near the load coil in the collector plate system.

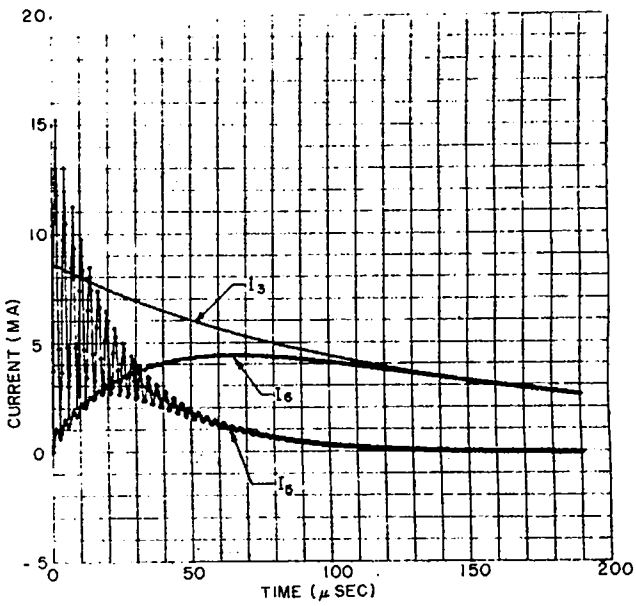

Fig. 10. Computer solution to crowbar problem with both crowbars switched on at maximum load current. I_3 is the load current, I_5 is the piggyback crowbar current, and I_6 is the in-plate crowbar current.

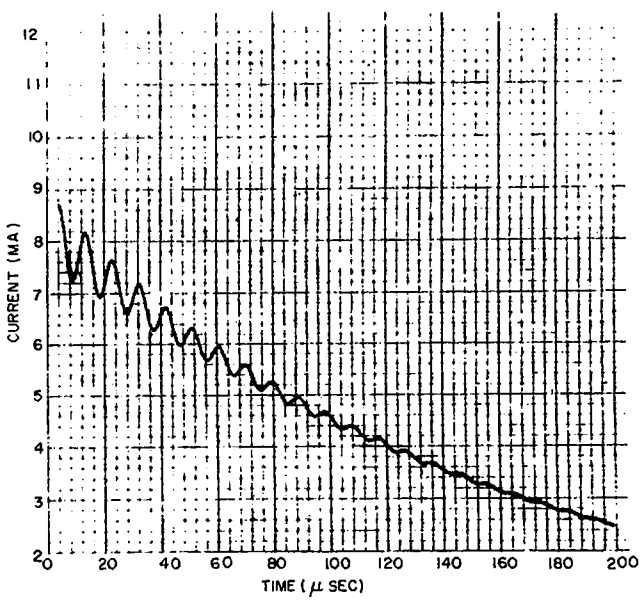

Fig. 11. Computer solution to crowbar problems with in-plate crowbar only. Only the load current is plotted.

PULSED POWER FROM EXPLOSIVE GENERATORS*

by

M. Cowan and E. C. Cnare

Sandia Laboratories
Albuquerque, New Mexico

April 1969

ABSTRACT

For the past few years, explosive generators have undergone engineering development in connection with experimental programs being carried out at Sandia Laboratories. As a result, this technology has taken on a versatility not previously extant. Explosive generators may now be considered competitive with capacitor banks as a source of pulse power for a larger range of applications. Recent developments in characterizing performance capabilities of explosive generators along with techniques which extend the capabilities of a given generator design will be presented. A new explosive generator facility which allows isolation of the high explosive effects will be described.

INTRODUCTION

During the past few years at Sandia Laboratories, explosive generators have been utilized in experimental programs for producing pulse power. As a result, an explosive generator technology has evolved which may have useful applications in fusion research. If pulses of very high energy are required, the explosive generator may be a more practical source than the capacitor bank.

The purpose of this paper will be to describe very briefly the capabilities and limitations of some of our explosive generators along with some recently developed operational techniques and facilities which make them more generally useful.

PRINCIPLES OF OPERATION

The principles of operation for explosive generators are well documented.[1,2,3,4,5] The essence of their simplest operational mode may be understood by analysis of a circuit which consists of a series arrangement of an inductive load L_f, the generator inductance L_g, and the circuit resistance R. The analytic solution for the current I(t) is

$$I(t) = \frac{I_o L_o}{L} \exp\left(-\int_o^t \frac{R}{L}\, dt\right)$$

where $L = L_g + L_f$, and $\exp\left(-\int_o^t \frac{R}{L}\, dt\right) = \epsilon$, the flux efficiency. The original current I_o is usually established with a capacitor

*This work was supported by the U. S. Atomic Energy Commission.

bank. Thus, as the generator inductance is explosively reduced, current and electromagnetic energy in the circuit increase, provided R is not too large. Since a negligible amount of energy is stored in electric field, the capacitance of the circuit is ignored.

GENERATOR DESIGN

The generator may have any geometry which allows explosive fuel to forcibly reduce its inductance; however, this discussion will deal with the one shown schematically in Figure 1. Two identical copper helical windings are coaxially aligned with an explosive-filled aluminum tube as shown. At their adjacent ends, the windings are electrically connected in series with the load. Prior to detonation, the winding and tube are electrically connected at one end of the generator and the starting current is injected at the opposite end. Soon after detonation the expanding tube isolates the generator circuit by crowbarring the original current source. As it continues to expand, the tube makes contact with the windings at two points which move smoothly along the helical path of the windings from the ends to the middle of the generator and thus forcibly reduce generator inductance to zero.

Three specific devices of this kind have been used often enough to have empirically established performance characteristics. While they do not necessarily represent the best that can be done in generator design, their capabilities and limitations will serve well to illustrate the general possibilities. Table 1 gives a summary of some of the important characteristics of these three generators.

FUNDAMENTAL LIMITATIONS

The performance limitations of a given generator design depend on both the load into which it works and the capacitor bank that provides the starting flux. However, there are some limitations which are largely independent of these. One is the maximum current limitation or saturation current which is listed for each of the three generators in Table 1. This limitation has its practical basis in a physical effect which occurs when conductors are required to support high magnetic fields ~1 MG and the associated high current densities.[1] Ohmic heating which results will start to make important increases in resistivity which will lead to a greater rate of ohmic heating and result in nonlinear diffusion losses. Generally, the nonlinear diffusion effect is sufficient to end the generating process. Thus, each generator design has a built-in saturation current which is nearly independent of other operating conditions. In fact, it is really the temperature increase in the conducting metal which determines the onset of terminating diffusion losses. For this reason, "saturation current" varies slightly with load inductance, being smaller for larger load inductances.

There is, of course, an energy limitation associated with a given design having to do with the amount of explosive employed. The energy in the generated pulse must be less than the kinetic energy of the expanding tube which in turn must be less than the chemical energy released by detonation. The generators of Table 1 use a plastic bonded explosive, designated PBX 9404, which has a heat of detonation of 2.7×10^6 joules/lb. Their expanding tubes convert 30-40% of this detonation energy to kinetic energy, and a maximum of 15-20% of the kinetic energy appears as electromagnetic energy in the load. Thus, the overall chemical-to-electrical conversion efficiency ranges from 5-8%.

PERFORMANCE CHARACTERISTICS FOR NORMAL OPERATION

For a wide range of inductive loads, including the ones which optimize current and energy gain, the generators of Table 1

produce a current pulse which, for most of its duration, rises exponentially or approximately so. The e-folding time for current rise is listed for each generator.

Unlike the capacitor bank discharge, voltage at the load is low at the beginning of the explosive generator pulse and high at the end when current is high.

An empirical technique is used for determining generator performance with different capacitor banks and load inductances. First, a few well chosen shots are conducted using a given bank to determine the flux efficiency curve, L_o/L vs. ϵ. Then, with a knowledge of generator inductance history, which may be calculated reasonably well, and saturation current, performance curves may be constructed for a load inductance range and a given capacitor bank injector.

Examples of operating curves which may be obtained from flux efficiency curves, are given in Figure 2. Final energy E_f is shown for the three generators as a function of load inductance when the 140 kJ capacitor bank at one of our firing sites is used to establish the original flux. Peak energy for each generator indicates the load inductance which optimizes energy output. All load inductances less than optimum fail to receive as much energy because of the saturation current of each generation design. Load inductances greater than optimum do not reach saturation current.

If a higher energy bank is used to provide a larger starting flux, the tendency will be for both the optimum inductance and the final energy to become larger. However, in making such extrapolations, one must keep in mind the fundamental limitations on pulse energy for each design. Also saturation current is not really constant for a given design but becomes somewhat smaller as load inductance increases.

The peak pulse energies shown in Figure 2 for the 106 and 169 generators are close to their fundamental design limits. That is, an injector bank larger than 140 kJ will not lead to significantly greater pulse energies from these two generators. However, the 612 generator is far from achieving its design limitation. For example, when it is operated with the 600 kJ bank at our new test facility it will produce a pulse energy of 6 MJ.

A point which seems to disagree with most intuitive appraisals of explosive generators is the fact that their output can be highly reproducible and reliable. This was shown by a series of 51 identical tests of a design similar to those of Table 1.[6] A histogram of current gain for these tests is shown in Figure 3. The data exhibit a spread which is nearly small enough to assign completely to experimental error in current measurement. Data for peak dI/dt are equally good.

OPERATIONAL OPTIONS

Many applications for pulse power are incompatible with normal generator operation as exemplified by Eq. (1). For example, a short duration fast rising pulse like that produced with a fast, high-voltage capacitor bank may be required. Also, an experiment may require higher voltages or currents than the single generator capability. In these cases there are operational options that may still allow successful and practical application of explosive generators.

Some of the experimental techniques which may be used to alter the output pulse have been described.[5,7,8,9] High voltage is produced by first inductively storing the generated energy and then switching it to the load.

Recent tests at Sandia Laboratories have shown feasibility of simultaneous operation of several generators in parallel-series arrays. This technique allows matching the impedance of a wide range of experimental loads without going through a costly creation and evaluation of new generator designs. It also provides other advantages.

Operation of generators in parallel is straightforward. This increases the saturation current to n times the single generator value, where n is the number of generators used. It also increases generated pulse energy by a factor n, provided the starting flux per generator is maintained.

However, operating generators in series is not trivial, because to avoid diminishing return the generators must be charged with their original flux while connected in parallel. The parallel charging and series operation ("Marxing") of generators has been accomplished with only the closure switching (crowbarring) which is part of their normal operating sequence. Marxing generators of a given design injected from a given capacitor bank allows one to produce at least the pulse energy produced by a single generator, but in a load inductance which is n times that of the single generator. Thus the flux linkage finally established in the load increases as $\sqrt{n}$. Even though the series array produces relatively high voltage at the load, electric fields inside a single generator in the array are no higher than normal. In principle, using parallel-series arrays, any combination of current and energy can be established in an inductive load using a given capacitor bank and a single generator design.

ISOLATING THE HIGH EXPLOSIVE EFFECTS

For many applications it is necessary to protect the load from the generator explosion. A facility soon to be operational at Sandia Laboratories will provide this capability as shown in Figure 4. The starting capacitor bank is located in a large underground vault beneath the firing pad. Generator output may be fed through a slot in the front wall into a laboratory which is designed to withstand the effects of magnetically exploded conductors, or for low current density experiments, it may be fed through a ten-foot wide slot in the ceiling of the vault. The building is designed for a 200-lb. detonation at 35 feet from the front wall. Its cost with the 20 kV, 600 kJ starting bank was approximately 0.8 million dollars.

SUMMARY

Explosive generators may be a more practical source than a capacitor bank for very high energy electromagnetic pulses. They can be constructed to have very reliable and reproducible performance which can be predicted for varied applications. The load can be isolated from the generator explosion. Several operational options can be utilized to provide a wide variety of output capabilities for a given facility with a few established generator designs.

REFERENCES

1. "Proceedings of the Conference on Megagauss Magnetic Field Generation by Explosives and Related Experiments," EUR 2750.e, (1965).
2. F. Herlach and H. Knoepfel, "Megagauss Fields Generated in Explosive Driven Flux Compression Devices," Rev. Sci. Instr. 36, No. 8, (August 1965).
3. A. D. Sakharov, "Explosive-Driven Magnetic Generators," Uspekhi Fizicheskikh 88, No. 3, p. 725 (April 1966).
4. J. W. Shearer, et al., "Explosive-Driven Magnetic Field Compression Generators," J. Appl. Phys. 39,

p. 2102 (1968).

5. J. C. Crawford and R. A. Damerow, "Explosively Driven High-Energy Generators," J. Appl. Phys. 39, p. 5224 (1968).
6. A. E. Binder and J. G. Kohl, private communication.
7. R. A. Damerow, et al., "Use of Explosive Generators to Power the Theta-Pinch," These Proceedings.
8. C. M. Fowler, et al., "High Altitude Pulsed Plasma Power Supply," These Proceedings.
9. H. Knoepfel, H. Kroegler, R. Luppi, and J. Van Montfoort, "Generation and Switching of Magnetic Energies in the Megajoule Range by Explosive Systems," Rev. Sci. Instr. 40, 60 (January 1969).

Table 1

Summary of Generator Characteristics

Generator Model	106	169	612
Length (in.)	17	25	31
Diameter (in.)	7	10	13
Weight (lbs.)	23	62	108
Explosive Weight (lbs.)	5	17	37
Inductance (μh)	4.6	18.1	3.5
Operating Time (μsec)	28	45	55
e-folding Time (μsec)	5.0	7.5	10.0
Saturation Current (Ma)	3	7	12
Typical Energy (MJ)	0.6	1.5	6.0

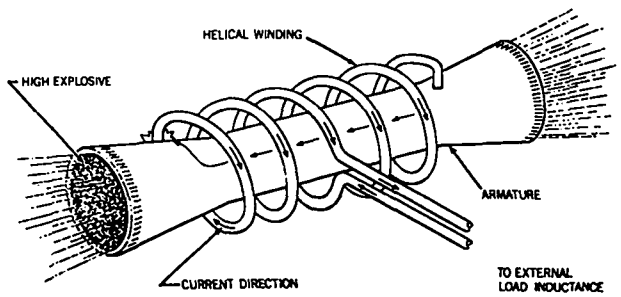

Fig. 1. Schematic of generator design.

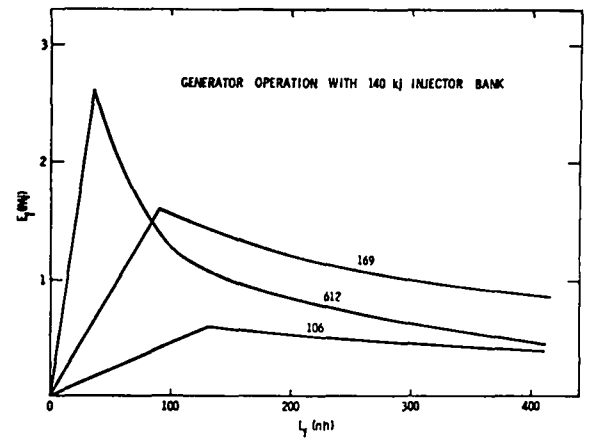

Fig. 2. Operating curves for the three generators of Table 1 with a 140 kJ capacitor bank.

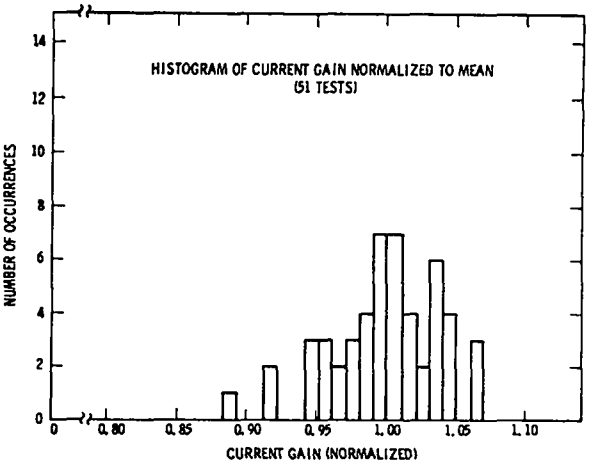

Fig. 3. Current gain histogram for 51 identical tests.

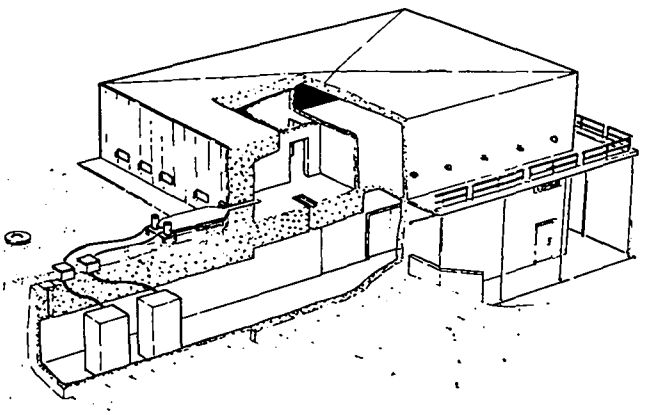

Fig. 4. Electro-explosive research facility.

USE OF EXPLOSIVE GENERATORS TO POWER THE θ-PINCH*

by

R. A. Damerow and J. C. Crawford
Sandia Corporation, Albuquerque, New Mexico

and

D. B. Thomson, R. S. Caird, K. J. Ewing, W. B. Garn, and C. M. Fowler
Los Alamos Scientific Laboratory, Los Alamos, New Mexico

ABSTRACT

Explosive-driven generators have been used to create neutron producing plasma in conventional θ-pinch coils. The generators were spiral wound flux compression devices which were loaded with 5 lbs, or 17 lbs, of high explosive depending on the model. When used with an exploding wire switch, the generators have produced θ-currents of approximately 2.5 MA, or 5 MA, respectively. The smaller generator has provided switched currents into 25 cm long θ-coils with rise times of 1.6 to 2.7 μsec, corresponding to peak fields of 106 to 128 kG. The highest neutron yield from this system was about 7×10^5. For the larger generator, peak currents ranging from 4.2 to 5.1 MA were switched into θ-coils of lengths 25 and 35 cm. Peak magnetic fields obtained varied from 141 to 220 kG with rise times ranging from 2.1 to 4.0 μsec. Coil voltages around the θ-coils at time of switching ranged from 37 to 70 kV. Neutron yields as high as 1.4×10^8 were produced. These results indicate that the larger generator, on a one shot basis, compares favorably with present high energy fast condenser banks for θ-pinch production. Engineering problems which relate to matching the generator to the θ-pinch, such as the importance of the operation of the high voltage switch, and the features unique to the single shot nature of the experiments, are discussed. Comments are made on some plasma conditions that might be reached if substantially larger generators are used.

INTRODUCTION

The creation of a neutron emitting θ-pinch has generally required a strong radial-shock heating stage followed closely by magnetic compression and containment. The development of reliable high current explosively driven helical generators that could be switched[1] at voltages high enough to produce the radial shock heating made possible a series of experiments[2,3] in which explosively produced magnetic energy was used to create neutron emitting θ-pinches in conventional (nonimploding) θ-coils.

This report includes a brief summary of the operation of the explosive generators and related switching, a review of plasma initial conditions used, and a discussion of the experimental results and their significance.

THE GENERATORS

The explosive generators used here (Sandia models 106 and 169) have been discussed in detail previously[1]. Figure 1 illustrates the operating principle for either generator. An external capacitor bank establishes initial current in the helical winding and armature of Fig. 1.

Following this, the inductance of the generator is forcibly reduced by explosively expanding the armature with a consequent increase in current. As shown in Fig. 1, the explosive is detonated simultaneously at both ends, and the output terminals are located at the center of the helix.

The model 106 generator uses 5 lbs of PBX 9404 explosive and produces a current output of 3 MA in loads of 65 nH, or less. Peak current is limited by joule heating in the helix.

The model 169 generator uses 17 lbs of PBX 9404 explosive detonated similarly. It consists of a 16 turn coil, 24 inches long, with an inside diameter of 9 inches, and has an aluminum armature of 4.5 inch outside diameter and 0.400 in. wall thickness. When injected with 90-100 kA, it produces currents up to 6-7 MA into inductive loads up to 70 nH with a normal operating time of 48 μsec.

HIGH VOLTAGE SWITCHING

A switching circuit was devised that shapes the output current pulse from the generator to produce the high values of dI/dt necessary for θ-pinch production. The switching technique has been previously described in detail[1,2,3] and therefore is only shown briefly on the schematic in Fig. 1. L_g is the generator and load. The exploding wire fuse (R_w, L_w) is designed to burst (open) near peak generator current. As burst is approached, R_w increases drastically in a time of about 1 μsec.

The dielectric switch is designed so that the exploding wire voltage spike punctures the dielectric (switch closure). Most of the total generator current then flowing is deflected into the θ-coil load (L_ℓ) in a very short time (1.6 - 4 μsec). With the model 169, this switch produced voltages (V_θ) as large as 65-70 kV around the θ-coils used. The switched generator outputs are self crowbarred and decay very slowly compared to the rise time.

THE θ-PINCH INITIAL CONDITIONS

Application of the switched generator outputs to produce a keV θ-pinch requires the same parameters and initial conditions that are used for first half cycle neutron production in the laboratory[4,5]. These conditions are a clean fully ionized deuterium plasma, a suitable reverse field, and a discharge tube whose walls have been adequately preconditioned[5] by electrical discharges prior to application of the principal fast-rising magnetic field pulse.

In these experiments, the initial plasma was created in a 2 mm-wall Pyrex or quartz discharge tube by means of a 40 kA linear discharge between two electrodes 60 cm apart. The linear discharge was obtained from a 7.5 μF capacitor (at 15 kV) crowbarred after one-half cycle (6 μsec) to minimize axial current prior to plasma compression started 15-20 μsec later. A separate coil pair (driven by 440 μF at 6-12 kV) provided reverse field prior to preionization. The initial deuterium pressure was 80-90 microns.

Since the explosive generators are one-shot devices, tube warm-up was achieved by first coupling an auxiliary low inductance 290 μF condenser bank, ($\leq$ 17 kV) to the θ-coil.

The procedure for each shot was to install a new, well-cleaned, discharge tube at the firing point, pump on the system overnight ($\sim 10^{-4}$ mm Hg, Model 106 series; $\sim 10^{-5}$ mm Hg, Model 169 series); warm-up the discharge tube with six to ten θ-pinch shots from the auxiliary fast bank; disconnect this bank; attach the explosive generator and fire it, together with the preionization and reverse field banks (within 30-60 minutes of the last warm-up shot).

θ-PINCH SHOT SERIES

With Model 106

Results of the five θ-pinch shots fired with the Model 106 generator, described in detail previously[2,3], are presented in Table I. Neutron

yields were obtained on shots 1, 2, and 5. Lack of yield on shot 3 is ascribed to zero bias field, and on shot 4 to poor switching.

With Model 169

Results of the four θ-pinch shots fired with the Model 169 generator are summarized in Figs. 2, 3, 4 and Table I.

A longer coil (35 centimeters) was used for the first two shots; neutron yields of 10^5 and 4×10^5 were produced.

The last two shots used 25 cm coils, giving higher values of coil voltage (V_θ = 70, 65 kV) and peak magnetic field (B_{max} = 220, 180 kG). For these last two shots, use of shorter coils together with linear discharge preionization (instead of R. F.) resulted in stronger warm-up shots, each producing small neutron yields ($\sim 10^3$). On one shot, there was no preionization, but a large yield, 8×10^6 neutrons, was observed, apparently due to high (70 kV) θ-coil voltage and good warm-up.

On the last shot, warm-up, reverse field, linear discharge, and switching all performed well, and the highest yield, 1.4×10^8 neutrons, was obtained.

Figure 2 shows that the switching used with the Model 169 resulted in fast rising θ-coil voltages on all four shots. Current rise times varied from 2-4 μsec for these shots, due partly to small adjustment of the resistance of the exploding wire fuses made from shot-to-shot in an effort to optimize the output.

DISCUSSION

Neutron Yield Rate

Highest yield rates were achieved for the shots (8 and 9) with highest coil voltage (70, 65 kV), for which the warm-up was substantially better, and for which peak magnetic field was highest.

Figures 3 and 4 show that the yield rate always drops drastically after 2 μsec regardless of continued buildup of field. This indicates that plasma containment decreases significantly after two μsec, typical of the short coils used (25 and 35 cm). For short coils ($\leq$ 35 cm) the magnetic field rise time should not exceed 2 μsec if yield rate is to be optimized for a given current.

In shot 9, the peak yield rate was 9×10^7 neutrons per μsec at B = 100 kG. These values, together with the known initial pressure and volume, allowed an estimate[3] of the ion temperature of T ~ 1.4 kV at an ion density of $\sim 5 \times 10^{16}$ ions/cc.

Comparison With Other θ-Pinches

Comparison of the results of this shot series with those of a series of five explosive generator shots recently reported[6] by the Frascati group appears to bear out the importance of high V_θ and fast rise time. In the latter case, higher magnetic fields (320 - 380 kG) with longer rise times and lower coil voltages gave smaller, or unobserved, yields and yield rates.

The results of shot 9 are given in Table II for comparison with those of large laboratory θ-pinches. The yield rate per unit coil length on shot 9 is comparable to those obtained with the highest yielding laboratory θ-pinches. This is encouraging in view of the one-shot nature of the generator experiments. Parameter studies and improved warm-up should enable substantial improvement in yield rate for the generator system.

Higher Intensity θ-Pinches

Helical explosive generators with long rise time (> 10 μsec) capable of delivering currents greater than 10 MA have been developed at the Lawrence Radiation Laboratory[7], Sandia Laboratory[8], Los Alamos[9], and in Russia[10]. Coaxial generators, using the helical generators as input stages, can deliver currents in excess of 100 megamperes[7, 10]. Development of fast rise time (< 2 μsec) switching for these generators is still needed. The successful use of generators to drive the θ-pinch, particularly shots 8 and 9,

leads to speculation as to use of the higher current generators with suitable switching.

Preliminary calculations[9] have been made using a very simplified model in which the θ-pinch is assumed to be heated in two separate stages; first a shock heating stage of constant $\dot{R}$ for which $\dot{R}^2 = KV_\theta$, and $T \sim \dot{R}^2$, where K is a scaling factor; and then a purely adiabatic magnetic compression stage. The calculations are cut off 2 μsec after start of the B field (based on Figs. 3 and 4) to minimize containment loss effects. These calculations use experimental results to determine the scaling factor K. Fully warmed-up laboratory θ-pinches require a 60% larger value of K to fit the observed neutron yields than that required for the firing point experiments.

The calculations[9], using values of initial $V_\theta \sim 83$ kV, and $B \sim 250$-290 kG at $t = 2$ μsec, predict neutron yields of 5×10^9 to 5×10^{10} in coils similar to the present ones. Ion temperatures of ~2 keV, at densities of $\sim 4 \times 10^{17}$ ions/cc are predicted. The calculations indicate that the present filling pressure (~ 85 μD_2) is about optimum. Improved warm-up increases the predicted yield.

The calculations also show that with the use of much higher filling pressures (1-100 mm Hg D_2) seeded with a high Z gas, temperature may be sacrificed to achieve large amounts of Bremsstrahlung radiation with less stringent requirements for V_θ and warm-up. For example, with $V_\theta = 50$ kV, and $B = 285$ kG (rise time ≤ 2 μsec), radiation rates of ~ 20 kJ/μsec (or greater) at electron temperatures of 50-100 eV and densities of 10^{18} - 10^{19} electrons/cc are predicted.

The possibility of achieving these interesting and unique plasma conditions makes the development of rapidly switched higher current generators very desirable.

REFERENCES

1. Crawford and Damerow, J. Appl. Phys. 39, 5224 (1968).
2. Thomson, Caird, Ewing, Fowler, Garn, Crawford, and Damerow, "An Explosive Generator Powered θ-Pinch," Proc. of Conf. on Pulsed High Density Plasma, Los Alamos Report LA-3770 (1967), Paper H3.
3. Damerow, Crawford, Fowler, Caird, Ewing, Garn, Thomson, Sandia Corp. Research Report - 69 - 51 (1969).
4. Little and Quinn, Phys. Fluids 6, 875 (1963).
5. Los Alamos Report LA-3863-MS (1968).
6. Hamm, Knoepfel, Krogler, Linhart, and Verbeek, "Very High Density θ-Pinch," I. A. E. A. Conference, Novosibirsk, U. S. S. R., Aug. 1-7, 1968, Paper K-8.
7. Shearer, Abraham, Aplin, Benham, Faulkner, Ford, Hill, McDonald, Stephens, Steinberg and Wilson, J. Appl. Phys. 39, 2102 (1968).
8. Cnare and Cowan, "Pulsed Power from Explosive Generators," Symposium on Engineering Problems of Fusion Research, Los Alamos Report , Paper DI8 (1969).
9. Los Alamos Report, LA-4150-MS (1969).
10. Sakharov, et al., Soviet Phys. Doklady, English Transl., 10 (11):1045, (1966).

*Work performed under the auspices of the U. S. Atomic Energy Commission.

TABLE I

Plasma Shot Results

Plasma Shot No.	Date	Generator	I_{MA}	V_θ (kV)	$-B_0$ (kG)	B_{max} (kG)	$t_{90\%}$ (μsec)	L (cm)	Neutron Yield (at source)	Neutron Half Width (μsec)	Containment Time[d] (μsec)
1	2/10/67	Mod 106[e]	2.9	25	1.7	128[h]	2.1	25	2×10^3	-	-
2	3/8/67	"	2.6	25-34	1.7	114	1.6	25	7×10^5	0.9	1.7
3	3/21/67	"	2.4	34	0	106	1.8	25	0	-	-
4	4/11/67	"	2.8	g	1.7	121	2.7	25	0	-	-
5	4/21/67	"	2.4	34	1.7	106	1.6	25	3×10^4	1.0	2.0
6	9/6/67	Mod 169[f]	4.4	37	3.0	141	3.2	35	10^5	1.4	1.75
7	9/13/67	"	4.9	55	3.0	157	2.1	35[b]	4×10^5	0.9	1.85
8	10/17/67	"	5.1	70	3.5[a]	221	4.0	25[b]	8×10^{6c}	1.25	2.0
9	10/26/67	"	4.2	65	3.5	181	2.6	25[b]	1.4×10^{8c}	1.6	2.25

a. Pre Ionizer Failed

b. Quartz Tube

c. Made Neutrons on Warm Up

d. Measured from B = 0 to end of neutron half width

e. θ-coil i.d. = 66 mm; tube i.d. = 60 mm

f. θ-coil i.d. = 72 mm; tube i.d. = 66 mm

g. Poor rise

h. All B values have had bias field subtracted

TABLE II

Nominal Characteristics of Present High Energy θ-Pinches

Parameter	Los Alamos Scylla III	Los Alamos Scylla IV	NRL Pharos	General Electric	Culham England	Garching Germany	Model 169 Explosive Generator
Voltage (kV)	80	50	20	60	40	40	100
Capacitance (μF)	52	454	10,920	278	1344	3330	-
Energy (MJ)	.166	0.6	2.0	0.5	1.1	2.65	.225
Coil Length (cm)	18.7	100	180	36	200	150	25
Coil Diameter (cm)	9.2	10	10.5	19	10	10.6	7.2
Peak Current (MA)	2.5	9.4	17	3.5	12.1	21.3	4.2
E_θ (at tube i.d.)(kV/cm)	~ 1.6	1.1	0.33	0.9	0.55	0.66	2.6
Peak Field (kG)	120	93	120	54	76	178	184
Quarter Period (μS)	2.5	3.7	16	7.4	5.95	9.5	2.6[a]
Neutron Yield	10^8	1.5×10^9	4×10^7	10^7	8×10^7	4×10^9	1.4×10^8
Yield Rate Half Width (μsec)	2.0	2.4	~8	~ 3.5	3	6	1.6
Peak Yield Rate (Neutrons/ μsec)	5×10^7	6×10^8	5×10^6	3×10^6	2.3×10^7	7×10^8	9×10^7
Peak Yield Rate/cm length	2.8×10^6	6×10^6	2.9×10^4	8.3×10^4	1.4×10^5	4.8×10^6	3.6×10^6
t_c (μsec)[b]	3.0	5[c]	>14	7	5	10	2.25

a. Rise time as measured from zero to 90% of the peak magnetic field

b. Containment time as measured from B = 0 to end of neutron half width

c. With crowbar

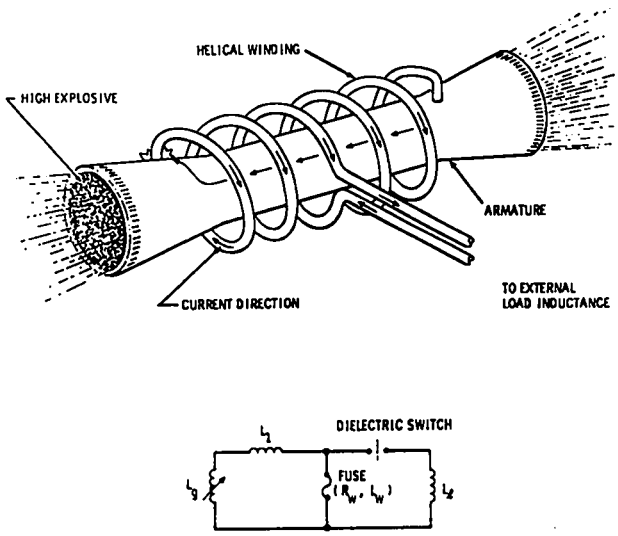

Fig. 1. Sketch representing the operating principle of the Model 106 and 169 generators. Also shown is the equivalent circuit, including the exploding wire switching.

SHOT NUMBER	V_θ COIL VOLTAGE (KV) VS TIME	REVERSE FIELD (KG)	PEAK FIELD (KG)	RISE TIME (μsec)	NEUTRON YIELD
6		-3.0	141	3.2	10^5
7		-3.0	157	2.1	4×10^5
8		-3.5	221	4.0	8×10^6
9		-3.5	181	2.6	1.4×10^6

Fig. 2. Coil voltage vs. time and summary of results of the four θ-pinch shots using the Model 169 generator.

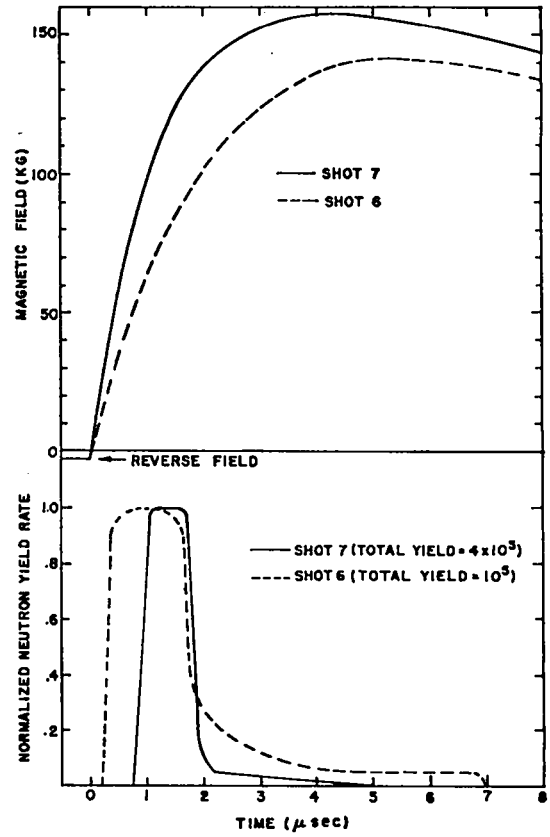

Fig. 3. Plots of field and yield rate vs. time for two shots using a 35 cm long θ-coil with the Model 169.

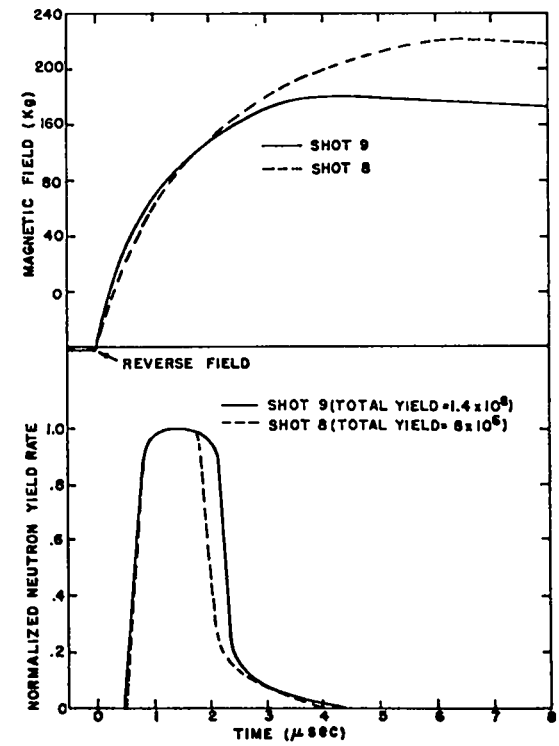

Fig. 4. Plots of field and yield rate vs. time for two shots using a 25 cm long θ-coil with the Model 169.

HIGH ALTITUDE PULSED PLASMA POWER SUPPLY*

by

C. M. Fowler, D. B. Thomson, K. J. Ewing, R. S. Caird, and W. B. Garn
Los Alamos Scientific Laboratory, University of California
Los Alamos, New Mexico

ABSTRACT

A pulsed power supply under construction is described which can be used in space physics experiments. The supply considered here is designed to drive a coaxial plasma gun. Rocket and plasma gun requirements which the supply should meet include the following. The payload vehicle is approximately 11 ft long, has a maximum diameter of about 2 1/2 ft and allows about 500 lbs for the power supply. In the early flight stages, accelerations of 10-15 g's are encountered. A stabilizing spin of 3.5 rps is required, which subjects peripheral components to accelerations greater than 20 g's. The plasma gun will require pulsed energy of 2-400,000 joules, switched in at a voltage of between 5-10 kV across the gun breech, and a subsequent operation time of several tens of microseconds. The basic power plant consists of two explosive-magnetic generators operating in sequence. The first generator amplifies the energy obtained from a small capacitor bank (18,000 joules, 250 lbs weight) sufficiently to supply the output generator. It, in turn, after further amplification delivers energy to the plasma gun. A dielectric switch is designed to switch the plasma gun into the circuit at a time when 5-10 kV will be placed across the gun breech. The present status of the power package will be reviewed including current results and environmental testing procedures carried out on various components. Explosive generators may make accessible space physics experiments which would normally be prohibitive from the standpoint of payload weight limitations.

INTRODUCTION

The explosive power supply is, of course, only a part of the particular space physics experiment for which it is designed. In its final configuration, it will have to conform to the specifications imposed by a number of people.

The particular application discussed here was proposed by H. Hoerlin of Los Alamos. A number of people in other Los Alamos groups, as well as at Sandia Laboratories, are involved in the project. Hoerlin and D. Kerr, also of Los Alamos, guide the project and work closely with the various people involved. Of the many technical requirements we are concerned here, however, only with those that most directly affect the power plant design. These include electrical requirements of the plasma gun and limitations set by the rocket.

The electrical requirements were set forth by J. Marshall and I. Henins of Los Alamos. The power supply should deliver a minimum energy of about a quarter of a megajoule to the gun, should place a few kilovolts across the gun breech at switch time, should rise to peak current in a few tens of microseconds, and remain crowbarred for several tens of microseconds.

From the rocket group at Sandia Laboratories (W. F. Adams is presently coordinating the extensive Sandia participation), a weight limit of around 500 lbs was set for the supply. Components

were required to function properly under a prescribed acceleration regime, including a stabilizing rocket spin of 3.5 to 4 revolutions per second. Finally, some space requirements, set not only by the geometry of the rocket payload vehicle, but also by explosive blast protection, imposed additional demands upon the design.

The essential feature of the power supply is the use of explosive generators to amplify the energy contained in a small capacitor bank. The supplies are, of necessity, one-shot devices, but there appears to be no other way at present to achieve the high current - high energy pulse required in the prescribed weight limit.

As will be seen in the next section, the power supply requirements have been essentially met or surpassed. Since explosive generator outputs may be varied over wide ranges of current, voltage, energy, and time, it appears that their use may make other types of high altitude experiments accessible.

THE POWER SUPPLY TO DATE

The operating principles of explosive generators have been described in some detail[1,2]. Basically, explosive energy is converted into magnetic energy by compression of magnetic flux as the explosive forcibly reduces the inductance of flux enclosing circuits[3]. The initial flux is normally supplied from condenser bank energy. The enormous energy content of explosives (2 MJ/lb) compared to that of high energy density capacitors (100 J/lb), makes its use particularly appealing where weight and volume impose limitations on a pulsed power supply. For example, the power supply described below will eventually be completely self contained and weigh about 500 lbs. In its final test (before coupling to a plasma gun), it delivered 500 kilojoules into a load roughly simulating the plasma gun. Owing mainly to development time limitations and rather generous allowances for weight and volume, the present power supply is not particularly efficient from the standpoint of weight. Components already available were selected when possible. Our previous experience with the Sandia model 169 generator[4] led us to select it as the output stage, almost immediately. A number of schemes to supply the 169 generator would, no doubt, appear more efficient on paper than the one adapted here (use of more input generators, perhaps inductively coupled, but with a smaller primary capacitor bank). Again time limitations, particularly involving the question of one-shot reliability, led us to the present design. It is our feeling that should the need arise comparable sized supplies could be built which would deliver similar energy pulses in the megajoule range.

Figure 1 gives a schematic drawing of an explosive generator typical of those used here. The generator consists of a cylindrically wound spiral concentric with an explosively loaded metal armature. As shown, an external load, L_1, is in series with the generator and the primary capacitor bank, which supplies initial current (flux) to the circuit. The explosive is detonated at such a time that the subsequent expansion of the armature will short out the generator at about maximum current. As explosive detonation proceeds, the expanding armature wipes the spiral turns, pushing flux into the load, L_1. If there were no losses, both current and energy gain in L_1 would be given by the ratio L_0/L_1, L_0 being the initial generator inductance.

Figure 2 shows in schematic form the setup for the last power plant development shot, while Fig. 3 is a photograph of the assembly on the firing table. In order, the various components are as follows:

A. Leads from a permanent capacitor bank, 1430 μF energized to 18 kJ. A special bank of Maxwell Laboratory capacitors, 1360 μF, 18 kJ, weight 250 lbs, will be used on the rocket shots.

B. LASL Mark V feed generator, inductance

of 390 μF, 11 lbs cyclotol explosive, designed to supply the output generator with 75,000 amperes.

C. Sandia model 169 output generator, inductance of 18 μH, 17 lbs 9404 explosive, designed to supply plasma gun.

D. Dummy load, 0.56 μH, heavy copper ring. It carries the output current until the plasma gun is switched into the circuit, sets the voltage across the gun breech at switching time and partly determines the current branching after switching.

E. Detonator switch: isolates plasma gun until proper switch time. It is closed by jets formed from two detonators.

F. Plasma gun mockup, fixed coaxial load, 0.11 μH inductance. This inductance value was selected for a first trial since its value lies between the variations expected for the actual plasma gun.

The shot results were about as we had hoped for. Of the 18 kJ stored in the capacitor bank, approximately 12 kJ were delivered to the generators at an injection current of about 7600 amperes. The feed generator amplified the current to approximately 80 kA and the energy to about 60 kJ. The detonators switched the simulated plasma gun into the circuit at a time when approximately 7 kV were across the gun breech. Signals from magnetic probes placed in the coaxial load showed that the load current rose to about 3 megamperes, (energy ~500 kJ) in 25 μsec, at which time the output generator was finished. A characteristic of these generators is that they are self-crowbarring at burnout. In the present case the coaxial load current still exceeded 2 megamperes 50 μsec after crowbar.

Most of the components have been subjected to a vigorous regime of acceleration on a shake table, and have been spun at rates such that centrifugal forces far exceeded those expected on the rocket. The capacitors to be used on the rocket have also been tested electrically and mechanically to conditions far exceeding those required for the rocket flight.

Space is not available to describe a number of additional studies made in connection with the supply, nor to detail other shots in the series leading up to the present design. The next stage involves coupling to the actual plasma gun itself. How the system will behave then, partly in view of the varying gun inductance, is not known with certainty. Considerable variation in gun input can be achieved, however, by varying the dummy load inductance and detonator switch time. In any event these tests will carry us to a regime new to both plasma and power supply people, and therefore they should be interesting and, hopefully, productive.

ACKNOWLEDGEMENTS

The authors are greatly indebted to a number of people who have contributed in many ways to this project. Firing point operations were ably carried out by P. Sisneros and J. King. Many technical problems in design and fabrication were solved by R. Livingston of Los Alamos and V. Willerton of the Bendix Corporation. D. Gill and P. Mace, of Los Alamos, and more recently R. Syler of Sandia Laboratories, have contributed some supplemental shot diagnostic measurements. Helpful discussions were held with M. Cowan and members of his magneto-explosives division at Sandia Laboratories, particularly on their model 169 generator. We are grateful to E. Kemp and G. Boicourt of Los Alamos for helpful discussions on the high energy density capacitor bank to be used in flight and for electrical testing of the capacitors. Finally, we are indebted to the Los Alamos explosive group, GMX-3, for use of their acceleration test equipment, and particularly, to H. Ballance for his care in supplying our explosive needs.

REFERENCES

1. Shearer, et al., J. Appl. Phys. 39, 2102 (1968).

2. Crawford and Damerow, J. Appl. Phys. 39, 5224 (1968).
3. Fowler, Garn, Caird, J. Appl. Phys. 31, 588 (1960).
4. Damerow, Thomson, et al., "Use of Explosive Generators to Power the θ-Pinch," this conference.

*Work performed under the auspices of the U. S. Atomic Energy Comission.

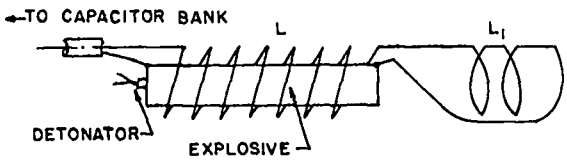

Fig. 1. Schematic of explosive generator, with load coil, L_1. The explosive loaded aluminum armature pushes magnetic flux into the load coil as detonation proceeds down the armature core, expanding it against the outer helix.

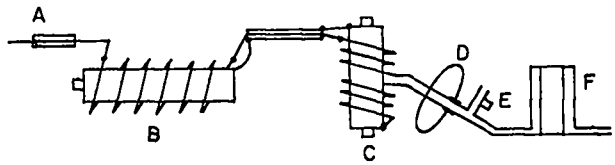

Fig. 2. Schematic of the explosive pulsed power supply as tested. The components indicated by letters are described in the text.

Fig. 3. Photograph of power supply components on the firing table. The feed generator may be seen at the left. The output generator is mounted vertically and the transmission plates take off about the generator midplane. The dummy load (heavy circular ring) may be seen just before the detonator switch. The coaxial plasma gun mockup load, far right, is switched into the circuit after the detonator switch is activated.

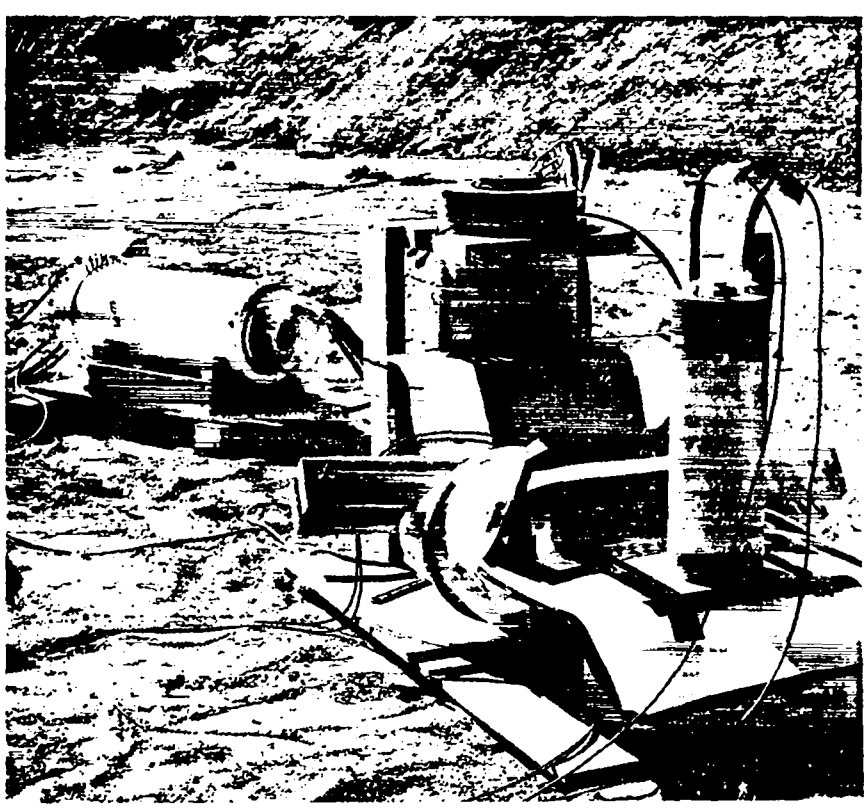

MOLECULAR FLOW AND SURFACE ABSORPTION IN GENERAL AXIALLY SYMMETRIC GEOMETRIES BY THE MONTE CARLO METHOD OF CALCULATION*

K. E. Wakefield

Plasma Physics Laboratory
Princeton University
Princeton, New Jersey

ABSTRACT

The vacuum chamber of the Princeton Floating Multipole contains a divertor situated such that the ionized particles approaching the walls of the main reaction chamber are guided by the magnetic field lines to a baffle deep within the divertor structure; neutral particles, which originate at the point of impact, are prevented from easily returning to the main plasma by a labyrinth of vanes and other structural members. The backflow of neutral particles can be substantially reduced by coating the vanes with a gettering material, especially if the design is such that the average particle makes many collisions with walls so coated before finding its way back to the main reaction chamber. Since the gettering material saturates when a monolayer of gas has been absorbed, this improvement is practical only when the plasma is formed on an intermittent basis, with reapplication of the getter after each pulse.

This paper describes a Monte Carlo computer program for evaluating such a system, taking into account the intricacies of the geometry and the absorption properties of those elements containing the getter, including possible local saturation effects. The program can simulate any axially symmetric configuration containing combinations of absorbing surfaces having a specified sticking probability and saturation density, non-absorbing surfaces, and escape or entrance ports. Results are valid only for gas densities such that the frequency of intermolecular collisions is small compared to the frequency of collisions with the wall.

Applications of the program to the divertor described above is illustrated. The program has also been used to determine the emission of neutral particles from a Marshall type gun as a function of time, and to optimize the conductance of an optically opaque section of vacuum line.

I. INTRODUCTION

The study of molecular flow rates or conductance in practical vacuum systems is severely limited by the lack of appropriate analytical tools. Before 1960 one depended on past experience, measurements on models, or subdivision of the system into elements amenable to analysis and combining the results to obtain an estimate of the system's performance.

With the advent of the digital computer, workers in the field began making use of the Monte Carlo method in evaluating molecular flow rates in systems whose geometries, though still rather simple, are beyond the present state of the art of analysis. Typically, a computer program based on this method traces the histories of a large number of molecules, following each molecule through successive wall collisions until it escapes through an exit or entrance port. The path each molecule follows

*Work performed under the auspices of the U.S. Atomic Energy Commission.

after each wall collision is determined using a random number generator in such a way as to cause the distribution of these reflected paths to follow the cosine law. Sometimes the random number generator is also used to determine whether or not a particle is absorbed on the wall during each collision. The assumption is made that the frequency of intermolecular collisions is small compared to the frequency of collisions with the wall. For a given geometry, the accuracy varies as the square root of the number of molecules traced, and is typically near the 1% level, usually quite adequate for the purpose.

The first use of the new method by Davis[1] treated the straight cylinder, cylinder with disk-shaped baffle, cylinder with restricted openings, cylindrical annulus, and cylindrical elbow. Levenson, Milleron, and Davis[2,3,4] applied the method to straight rectangular channels, cubic elbows, and extended the work with cylinders by providing for other than smooth surfaces. Ballance[5] undertook a more basic study of arrays of infinitely wide plates.

More recently Chubb[6] treated a coaxial system made up of cones or cylinders placed end to end. His program contains a novel feature whereby the history of a particle may be terminated by ionization if it enters a cylindrical region near the axis.

The present paper describes a program capable of simulating any axially symmetric configuration whose cross section can be represented by a number of straight lines, not necessarily connected. Each surface element may be non-absorbant, absorbant with a specified sticking probability and saturation density, wholly absorbant, or may represent an escape or entrance port. The program output gives the fraction which have escaped, have been absorbed, or are still active as a function of time (path length); the mean path length per collision; the mean number of collisions before escape or absorption; the fraction absorbed or escaping at each surface element; and the distribution of these as a function of position on each element, expressed in terms of the saturation limit of that element.

This program was written to assist in the design of the vacuum structure for the FM-1 divertors, an example of one being shown in Fig. 1. Ionized particles approaching the walls of the main reaction chamber are guided by the field lines to a point deep within the divertor structure where they are intercepted by a baffle. Now neutralized, the motion of the particles is no longer affected by the magnetic field, and their rate of return back to the main reaction chamber is governed only by the molecular flow characteristic of the system. The back flow can be substantially reduced by coating the vanes with a gettering material, such as titanium. Since the probability of capture by the getter is, for hydrogen, typically only about 0.1 per collision, an effective system requires the addition of vanes and other structural members to increase the number of wall collisions the average particle experiences before escaping. When a monolayer of gas has been absorbed, the getter saturates; therefore, this improvement is practical only when the plasma is formed on an intermittent basis and the getter is reapplied after each pulse.

II. DESCRIPTION OF THE PROGRAM

A. The geometry of a particular system is described by a series of data cards containing the variables, K, N, R, and Z, each

card defining a point (R, Z). The points are ordered in sequences one obtains by simulating the cross section of the geometry by a number of straight lines, the end points of which are the points in question, and progressing along the line segments until either the starting point or the axis has been reached. Several independent sequences may be required to describe the geometry. For the initial point in each sequence, K = 1; otherwise K = 0, except as noted below. For all the remaining points in the sequence, N specifies the type of the surface element whose definition is completed by that point. If N = 0, the element is one that absorbs molecules with a sticking probability specified on a later data card. If N = 1, the element is a port through which molecules can escape. If N = 2, the element is a non-absorbing surface. If N = 3, the element absorbs all molecules impinging on it. In the completed set of data cards there will be as many cards containing K = 1 as there are independently defined line sequences. The card defining the last point of the last sequence contains K = 9.

If the geometry is charted on a graph with + Z at the top and + R to the right, the direction of travel along the line sequences must be such that the region containing the molecules to be studies is on the right. In making up the sequences of points, entry and escape ports are treated like part of the structure, and thin plates or vanes extending into the molecular region must be traversed twice, each time with the molecular region to the right.

B. Following these are one or more cards, each specifying a set of parameters for a case history in the given geometry. Each case is computed independently and the results printed. These parameters include the starting point or origin of the molecules to be studied, the direction about which the first segment of the path is to be randomized, the probability of a molecule being captured during a collision with any N = 0 surface, the total number of molecules represented by the case history, the number of molecular paths to be traced, and a length of time. The latter is more convenient for presenting tabulated results than using units of path length. The conversion from path length to units of the specified length of time assumes the molecular velocity to be 1.7×10^5 centimeters per second, the velocity at about room temperature. The total number of molecules is needed to determine the degree of saturation of the absorbing surfaces. The saturating density is assumed to be 6.0×10^{14} molecules per square centimeter.

If a blank card is encountered, or the specified number of molecular paths to be traced is zero, the program will start again until there are no more cards to be read.

C. In computing each case history, the specified number of molecular paths are traced, each of which is begun at the specified starting point along a path which deviates randomly from the direction specified. A weighting parameter QUANT having an initial value of 1.0 is associated with this path. In a manner which is described below, the path is followed until it strikes one of the surface elements, at which time one of three things may happen.

1. If the surface is non-absorbing, the direction normal to the surface at the point of impact is computed, and a new path which deviates randomly from this direction is chosen. The method used to select a new path

insures that the distribution of these paths with respect to the normal direction obeys the cosine law.

2. If the surface is absorbing with a probability of STICKF that the molecule will be captured, the quantity absorbed is QAB = QUANT * STICKF unless this causes the surface to saturate. In that event, QAB is reduced to the minimum amount required to achieve saturation. QUANT is then reduced by QAB and the path continued as for a non-absorbing surface.

3. If the molecular path strikes an escape port or a wholly absorbing surface, the current value of QUANT is considered to have escaped or been absorbed, and that path is terminated.

If not terminated by escape or complete absorption, the path is terminated if QUANT takes on a value less than 0.005 or if the total path length exceeds that defined by 100 units of the specified length of time.

The program records the quantities escaping and being absorbed in 100 value tables, the location in the table being determined by the number of time units corresponding to the total path length when the event occurs. In addition, the interactions of the molecules with each surface element, subdivided into five parts, are recorded.

After all the molecular paths are traced, the program prints all the input parameters; a time history of escape rate, cumulative amounts escaped, absorbed and still active; the amount absorbed on or escaping through each element; and a five part distribution of the interactions at each element relative to the saturation limit. Also printed are the quantity whose paths were terminated other than on a surface, and the quantity for which no intersecting surface was found. The latter can occur only if an error has been made in defining the geometry.

D. The process of randomizing the path in a manner satisfying the cosine law is based on the following: In a right handed coordinate system, let the unit vector normal to the surface correspond to the Z axis. The path direction is defined by rotation through the angle TH from the Z axis toward the X axis, and by rotation through the angle PH about the Z axis. Applying the cosine law, it can be shown that the probability of the path lying between TH and TH + DTH is

$P = 2*COS(TH)*SIN(TH)*DTH = SIN(2*TH)*DTH.$

Geometric considerations show that if COS (2*TH) is assigned values uniformly distributed between - 1 and + 1, the probability of obtaining a particular value between 2*TH and 2*TH+DTH is also SIN(2TH)*DTH. Using a random number generator yielding R_1 uniformly distributed between 0 and + 1, the required range is formed by $1 - 2*R_1$. Therefore,

$$1 - 2*R_1 = COS(2*TH) = 1 - 2*SIN^2(TH) ,$$

from which $SIN(TH) = SQRT(R_1)$ and $COS(TH) = SQRT(1 - R_1)$. Values of PH being equally probable,

$$PH = 6.28318*R_2$$

where R_2 is independently obtained from the random number generator. The direction of

the path can now be computed in the normal manner.

E. In order to discover which of the surface elements is struck by a particular path, it is necessary to survey all of them, determine those which the path intersects, and select that surface for which the path length is minimum.

There is no loss in generality and the computations are eased by orienting the coordinate system so that the impact point or the point of origin of the path lies in the X-Z plane. After randomization, the path is completely defined by (XP, ZP, DXP, DYP, DZP) where XP, ZP is the impact point and DXP, DYP, DZP are the direction cosines. The surface to be tested for a possible intersection is completely defined by (RS, ZS, RF, ZF) where RS, ZS is the point at the start end of the line segment and RF, ZF is the point at the finish end as described in A, above.

1. The first test eliminates those surfaces for which both values of Z are either less than or greater than ZP and for which DZP is such that the path points away from the surface. This test eliminates about half of the candidates.

2. If ZS=ZF, the surface lies in a plane, in which case PL, the distance between the impact point and the point of intersection, is readily calculated, and the tests described in 4, below, made.

3. If ZS≠ZF, the surface is a cone or cylinder. If (X, Y, Z) is a point of intersection of the surface and path (in general there are two), a plane parallel to the X-Y plane passing through this point intersects the surface in a circle, the equation for which can be written,

$$X^2 + Y^2 = \left(RS + \frac{(Z-ZS)(RF-RS)}{(ZF-ZS)}\right)^2$$

Also, if PL is the distance from the impact point to the point of intersection, one can write,

$$X = XP + PL*DXP$$
$$Y = PL*DYP$$
$$Z = ZP + PL*DZP \quad .$$

Substituting these into the equation for the circle, one obtains an equation in which the only unknown is PL,

$$A * PL^2 + B * PL + C = 0 \quad ,$$

where A, B, and C are functions of the known parameters. The smallest positive value of PL is tested (see 4, below) and if this value fails to meet all conditions, the other positive value of PL, if it exists, is tested.

4. All the following conditions must be met; failure on any one score eliminates that value of PL.

a. Either no surface has been encountered meeting all the conditions, or if a surface has been previously tentatively accepted, the value of PL must be smaller than that recorded previously.

b. If the surface is a cone (RS≠RF and ZS≠ZF), the point of intersection must lie on the same side of the apex as do ZF and ZS.

c. R = SQRT($X^2 + Y^2$) must lie between RS and RF, or Z must lie between ZS and ZF. The first applies to flat plates and squat cones, while the second applies to cylinders and sharp cones.

d. The dot product of the unit vector (DXP, DYP, DZP) and the vector normal to the surface at the point of intersection (Pointing toward the molecular region) must be

negative. This test is performed to detect errors in defining the geometry.

5. If a trial surface meets all the conditions, it is tentatively recorded as the chosen surface and its value of PL is recorded as the shortest path length.

When all the surfaces have been tested, the one for which the path is minimum will have been identified, and the program will then take the appropriate action.

III. APPLICATIONS AND DISCUSSION

The program has been helpful in the design of the FM-1 divertors, providing a good tool in determining just how complex the interior structure must be to reduce the back flow to acceptable values, and in selecting the surfaces on which the getter is most effective.

A similar study was made of a Marshall type gun in which the rate with which neutrals escaped along the axis was determined as a function of time. Accurate evaluation of proposed geometries was easy and rapid.

The program was used to maximize the conductance of an optically opaque pumping section subject to a number of constraints making it difficult to determine intuitively the best design.

If a significant number of problems similar to the last mentioned were to be handled, the program might well be modified to allow the start position to vary randomly and uniformly over the cross section of the entrance port. However, in the study conducted, it was found convenient to run several case histories identical except for the starting point and combining the results using appropriate weighting.

Extension of the Monte Carlo technique to more complex geometries will undoubtedly take place as more powerful computers evolve. The obvious one of treating two or more intersecting axially symmetric systems probably is feasible, but there are some geometric problems pertaining to the intersecting surfaces which may prove difficult. Extension to a three dimensional system whose surface elements are generally oriented planes, perhaps in the shape of triangles, is also feasible, although computation time is bound to be a problem in a system of any complexity.

IV. ACKNOWLEDGMENTS

The author is indebted to D. H. Mullaney and F. H. Tenney of the Princeton Plasma Physics Laboratory for their assistance and advice in this work.

References

1. D. H. Davis, J. Appl. Phys. 31, 1169 (1960).
2. L. L. Levenson, N. Milleron, and D. H. Davis, Lawrence Radiation Laboratory Report UCRL-6253 (1961).
3. L. L. Levenson, N. Milleron, and D. H. Davis, Transactions of the Seventh National Symposium on Vacuum Technology, Cleveland, Ohio (1960).
4. J. O. Ballance, NASA Technical Memorandum NASA TM X-53112 (1964).
5. D. H. Davis, L. L. Levenson, and N. Milleron, Lawrence Radiation Laboratory Report UCRL-6787 (1963).
6. J. N. Chubb, Culham Laboratory Report CLM-R54 (1966).

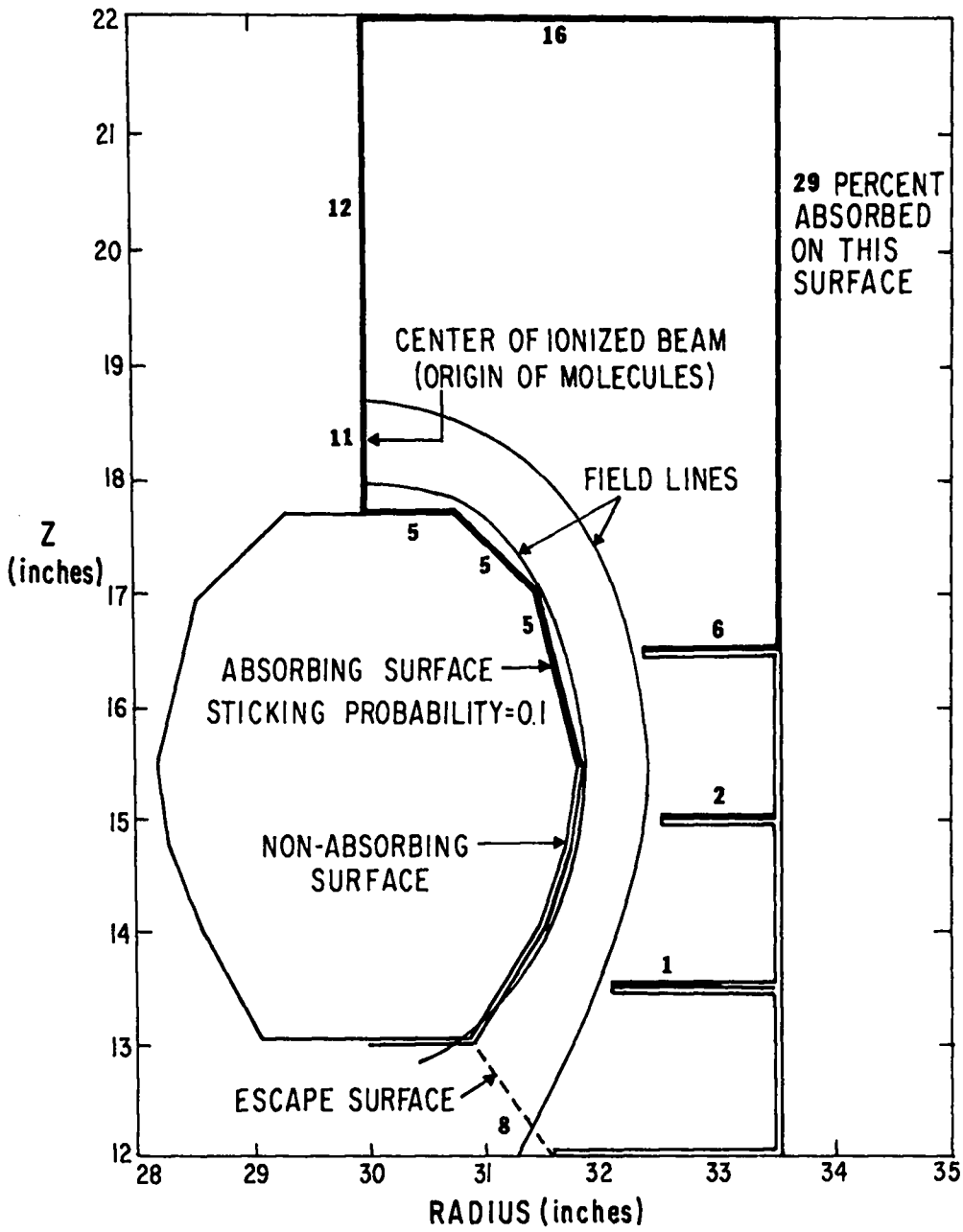

Fig. 1. Illustrative sketch showing vacuum structure of FM-1 quadrupole divertor, location of field lines, and fraction of molecules absorbed on each surface element.

THE 2X VACUUM SYSTEM*

Carl J. Anderson
Lawrence Radiation Laboratory
University of California
Livermore, California

ABSTRACT

This paper briefly describes the 2X vacuum system equipment and method of operation. Operating pressures of the order of $2\text{-}3 \times 10^{-9}$ torr and base pressures of the order of $5\text{-}8 \times 10^{-10}$ torr are obtained in a mildly baked aluminum and glass vessel of 11,000 liters. Seals are aluminum foil, TFE, Hycar, and epoxy. Titanium sublimation onto LN_2 cooled liners is used with mercury diffusion pumping. The nature of the resulting vacuum is discussed with particular regard to the predominant residual gas methane.

INTRODUCTION

Progress in the CTR program has been dependent upon the development of suitable vacuum techniques. This has been especially true for the 2X experiment.

Plasma confinement in mirror geometries was first investigated in 1952 at Lawrence Radiation Laboratory.[1] Subsequently, both neutral injection and plasma injection were attempted. Fred Coensgen performed the early experiments on pulsed magnetic compression with plasma injection in 1954 in the Toy Top machine.[1,2] The first evidence of neutrons in the Toy Top experiment was obtained in 1955.[3] Their thermonuclear origin was fully documented in 1960-62 in a subsequent experiment, Toy Top III.[4,5] A twice-scale model, the 2X machine, with quadrupole stabilization of the hydromagnetic instabilities was first operated in 1964. Two views of the 2X are given in Figs. 1 and 2.

When operations first began, 2X had eight mercury diffusion pumps with liquid-nitrogen-cooled chevron traps, titanium sublimation pumping, and Hycar seals throughout. On rare occasion the system achieved 1×10^{-8} torr with a 100°C bake. In 1967 the machine was converted to a ultrahigh vacuum system consisting of four mercury diffusion pumps with bakeable all metal traps[6] and valves,[7] titanium sublimation pumping,[8] and many seals converted to the Batzer type[7] using aluminum foil or TFE tape. A 100°C bake resulted in base pressures of the order of $1\text{-}5 \times 10^{-9}$ torr and operating pressure of $2\text{-}5 \times 10^{-8}$ torr.

The present configuration was attained in 1968 with the addition of two liquid-nitrogen-cooled liners which receive about 25% of the titanium evaporated. This configuration, which still contains some rubber and epoxy seals and undergoes only a 100°C bake, achieves base pressures of the order of $5\text{-}8 \times 10^{-10}$ torr and operating pressures of the order of $2\text{-}3 \times 10^{-9}$ torr.

Operation is currently on a 2-min cycle. Each cycle consists of a 1-min delay for cooldown followed by 1 minute of gettering during which time the 4.16 mJ capacitor banks are charged. The experiment begins with the discharge of the banks and plasma injection from deuterated titanium washer guns. The field has a rise time of 150-200 μs at which time the banks are crowbarred. The trapped and heated plasma parameters are given in Table I.[2]

PRESENT VACUUM SYSTEM DETAIL

Figure 3 is a schematic cross-section of the present 2X machine. The two end tanks are connected by a glass center section. The total volume of the vacuum chamber is 11,000 liters. Each aluminum tank is 5-ft diam × 10-ft long, has three 5-ft-diameter Batzer seals, and a welded channel for steam bakeout and water-cooling. Four mercury

*Work performed under the auspices of the U.S. Atomic Energy Commission.

diffusion pumps with barrel refrigerators and all metal valves and traps are backed by oil-sealed mechanical pumps. Liquid nitrogen refrigerated copper wool traps are used on both the foreline and roughing line. Each tank has a liquid nitrogen refrigerated liner 40-in. diam × 48-in. long made of two $\frac{1}{2}$-in. aluminum plates with a $\frac{1}{2}$-in. annular reservoir. Titanium evaporation is by means of approximately 50 ft of Ti15Mo alloy getter wire arranged so that most of the surface area is gettered.

The center section, or reaction chamber, is a 12-ft-long glass fabrication 18-in. in diameter. It is made from glass pipe and joined with epoxy glue in four places. A nonmetallic vessel is required due to skin depth considerations arising from the pulsed nature of the trapping and compression. Diagnostics and other penetrations are by means of seventeen $1\frac{1}{2}$-in.-dia Hycar seals. The glass is sealed to the end vessel by a flat Hycar gasket and isolated by two 18-in.-dia bellows.

The center section has seven retractable getters mounted so they can be inserted to the center line for deposition of the titanium and withdrawn from the plasma volume prior to the experiment. The metal is deposited on a 16-in. dia glass liner within the reaction chamber.

MODE OF OPERATION

Over several years the following general sequence has evolved. Vacuum conditions are monitored with thermocouple gauges, nude ion gauges, a helium mass spectrometer, and a residual gas analyzer, none of which is specially calibrated.

The run of January 29, 1969, was documented as follows. All getters were renewed and changes required for the physics experiment were completed. The machine was roughed-down and put on the diffusion pumps for preliminary leak-hunting. Pressures in the 10^{-6} torr range were readily obtained.

A bake by means of 15-psi steam and heater tapes was given over the weekend to the aluminum liners, valves, and the periphery of the end tanks. Figure 4 shows the first of a series of RGA mass/charge (m/e) scans of the pumpdown. It was taken while the tanks were hot. Near the completion of the bake, the getter wires were degassed giving the glass section a mild bake also. Figure 5 is an m/e scan of the system at the end of the bake.

At completion of the bake, the heaters were cut off and the water-cooling put on. The resulting m/e scan is shown in Fig. 6. Some further leak-hunting was required to get the low 10^{-7} torr range. The m/e scan shown in Fig. 7 is the one used to make the decision to proceed with the sequence. It was suspected that a small leak was present, but as the pressure was in the low 10^{-7} torr range, we began to getter down.

After an hour of gettering, a minute on and a minute off, the pressure was 1×10^{-8} torr. The methane dominance shown in Fig. 8 is typical—more will be said about that later.

The final step was to cool the liners. Figure 9 shows the resulting m/e scan at a pressure of 1×10^{-9} torr. The supposition of a leak may have been accurate, as argon dominated the system at this pressure when methane would normally dominate. However, there were only three diffusion pumps on the system for this run due to a refrigerator failure; hence, there was somewhat less argon pump speed than normal.

A quick scan of high m/e numbers might reveal a few peaks of low magnitude but there was nothing of significance.

We were now ready to begin the experiment. The seven retractable getters were inserted and run for 1 minute as the banks charged. The pressure remained at $1\text{-}2 \times 10^{-9}$ torr. The getters were turned off and retracted just prior to firing the banks and execution of the experiment. This sequence of events was repeated on a 2-min repetition rate, with a fresh layer of titanium deposited on the walls of the reaction chamber liner immediately prior to each shot.

During this run the vacuum continued to improve so that in several hours the machine was going to $5\text{-}8 \times 10^{-10}$ torr between shots. After many hours of operation, the argon peak rose due to continuous inleakage, limited pump speed, and saturated liners. Cycling the liners to a higher temperature released the argon and restored the base pressure. The same saturation effect has not been observed with methane, which was seen to come off of the

liner with the argon during the temperature excursion.

DISCUSSION

In evaluating the vacuum conditions, several parameters are important. In 2X the scattering time is 4.5 ms, the charge exchange time is greater than 8 ms, the field decay time is 4 ms, and the plasma decay time is 400 μs. Clearly, the operating pressures obtained are not a limitation.

A condition more important to the success of the experiment is the nature of the surface that the plasma "sees". The titanium layer deposited prior to every shot is put down at a pressure in the low 10^{-9} torr range where the monolayer time is very long compared to the time required to retract the getters and initiate the experiment. This results in a clean surface for every experiment thereby minimizing the contamination of the plasma due to desorbed gas. The success of the 2X program has been to a large extent dependent upon achieving these surfaces. The best results are obtained with glass liners that have been given a "tooth" by tumbling them with glass beads. Several sets of getter wires are required to condition a freshly prepared glass liner. Operation continues to improve until the layer of titanium gets so thick that it couples too strongly with the pulsed fields and begins to come loose.

In addition, current operation is being improved with the use of 1/8-in.-dia getter wire. This wire is operated in essentially the same manner as the previous 0.083-in.-dia wire and results in longer life, higher rate of deposition, and greater reliability.[9]

A more difficult question involves the effect of the constituent partial pressures on the experiment. It is not clear that there is a correlation directly between the predominant background gas, typically methane, and the plasma, but certainly there is an effect by way of the walls. In the present experiment a measurable carbon impurity contamination of the plasma is found.[10] For this reason, the origin of the methane and methods of pumping it are of interest.

Methane commonly results in vacuum systems from a number of mechanisms, several of which are as follows:

a) Holland has shown that methane production is dependent upon carbon impurities in the titanium getter.[11] Unfortunately, carbon is very difficult to eliminate from titanium. Carbon impurities of the order of 100-300 ppm are common commercially, difficult to reduce, and produce copious methane. The mechanism is not clear, as the amount of methane varies both during each getter cycle and during the life of the wire. The wire cannot be outgassed enough to noticeably reduce the methane production.

b) Chemical reactions involving hydrogen occur on the surfaces of the system, particularly on the titanium at room temperature, since hydrogen exists in the extemely reactive atomic state on clean titanium surfaces at room temperature. An example is $TiC + 4H \rightarrow Ti + CH_4 + 14$ kcal/mole. Chemical reactions are frozen out at liquid nitrogen temperatures due to the temperature-dependence of the reaction kinetics. In addition, hydrogen exists in molecular form on titanium at liquid nitrogen temperatures, preventing reactions that arise due to the presence of atomic hydrogen.[12] Della Porta[13] discusses the problem of hydrocarbon production on clean metal films and concludes that the chemistry is extremely complex.

c) Hydrocarbons undergo catalytic cracking in vacuum chambers and particularly on clean titanium at room temperature. Roberts[14] found that ethane cracks to methane in the presence of a clean surface and excess hydrogen. The production of methane was shown to vary with the temperature and cleanliness of the surface. It is reasonable to conclude that in the 2X, where most of the surface is clean titanium at room temperature, any hydrocarbons present are quickly reduced to methane.

d) Simonov et al.,[12] indicated that a titanium surface at room temperature under a flux of ions will produce methane. He showed that methane production decreased markedly

at temperatures close to those of liquid nitrogen. It was not clear whether another mechanism was present or not.

It is rather discouraging to note that all of the above mechanisms may obtain in the 2X experiment.

Various methods are being considered to reduce the methane partial pressure:

a) The pump speed for methane could be increased by adding more diffusion pumps or cryopumps. This would add to the complexity of an already complex system but might someday be necessary.

b) The fraction of titanium surfaces at liquid nitrogen temperatures could be increased. Regardless of mechanism, the effect of cooling the liners is to reduce the base pressure of a methane dominated system, hence it provides a methane "pump".

c) Cleaner wire might be obtained. The wire presently in use has approximately 260-ppm carbon. This might be improved by a factor of two or three and still be within the realm of commercial production qualities and prices.

d) Use of Ti15Ta getter alloy might help. There are claims that getters of the overwrapped type made from these metals produce less methane.[15,16]

e) A getter wire with almost no carbon, such as aluminum, could be used. In the 2X, where loss of pump speed in the center section might not be disastrous, this could be interesting.

SUMMARY AND CONCLUSIONS

The mode of operation described was used seven times during January 1969 and resulted in seven excursions, from air to ultrahigh vacuum. An understanding of the many complex competing processes occurring in the 2X may come very slowly, if at all, but the "horsepower method" of producing ultrahigh vacuum works, and in the 2X machine produces one of the cleanest plasma experiments existent today.

ACKNOWLEDGMENTS

I am indebted to the 2X group for much of this report. In particular, I must thank F. H. Coensgen, W. E. Nexsen, Jr., V. A. Finalyson, G. E. Vogtlin, R. E. Bathgate, H. C. Saulter, and J. N. Doggett (who is now associated with another project).

REFERENCES

1. A. S. Bishop, "Project Sherwood," Addison Wesley (1958).
2. F. H. Coensgen, private communication, 1969.
3. F. H. Coensgen, "Experimental Evidence for Plasma Heating by Magnetic Compression," Report WASH-289, Feb. 1955 (declassified Feb. 20, 1959).
4. F H. Coensgen, W. F. Cummins, W. E. Nexsen, Jr., and A. E. Sherman, "Evidence of Containment of a 3-keV Deuterium Plasma," Phys. Rev. Letters, Vol. 5, p. 459 (1960).
5. F. H. Coensgen, W. F. Cummins, W. E. Nexsen, Jr., and A. E. Sherman, "Production and Containment of Hot Deuterium Plasmas in Multistage Magnetic Compression Experiments," Nuclear Fusion, p. 125 (1962 Supplement, Part 1).
6. T. H. Batzer and R. F. Bunshah, "A Decade of Advances in Vacuum Equipment and Technology," Proc. of 1967 Vac. Metal. Conf., New York City, June 12-16 (1967).
7. T. H. Batzer, "Vacuum Component Developments," Proc. 1965 Symp. on Engr. Problems of CTR, Lawrence Radiation Laboratory, Livermore, California, May 3-4 (1965).
8. J. N. Doggett and G. E. Vogtlin, "Selection of a Getter Material and Mode of Operation," Proc. 1966 Symp. on Engr. Problems of CTR, ORNL, Oct. 3-6 (1966).
9. V. A. Finlayson and R. E. Bathgate, private communication 1969.
10. F. H. Coensgen, W. F. Cummins, R. E. Ellis, and W. E. Nexsen, Jr., "Decay Modes of a Dense Plasma in a Magnetic Well," Proc. Third Conf. on Plasma Physics and Controlled Nuclear Fusion Research, Novosibirsk, USSR, Aug. 1-7 (1968).
11. L. Holland, L. Laurenson, and P. G. W. Allen, "The Formation of Hydrocarbon Gas by Titanium Getters Containing Carbon and Hydrogen Impurities," Trans. 8th Nat. Vac. Symp. (1961).

12. V. A. Simonov, G. F. Kleimenov, A. G. Milsehin, and V. A. Kochnev, "Maintaining Ultra-Low Pressures of Neutral Gas in Process of Accumulation of High Temperature Plasma in Magnetic Traps with Injection," Inter. Atomic Energy Conf. on Plasma Physics and Controlled Nuclear Fusion Research, Salzburg, Austria, Sept. 4-8 (1961).

TABLE I

2X PLASMA PARAMETERS

D^+ energy range	1 to 50 keV
Maximum density	5×10^{13} cm^{-3}
Mean D^+ energy	6 to 8 keV
Electron temperature	150 to 250 eV
Central magnetic field	13.2 kG
Mirror ratio	1.33
Maximum β	5.7%
Plasma diameter (FWHM)	6 cm
Plasma length	160 cm
Plasma volume	4.5 liters
Average τ, for $dn/dt = \tau n$	300 to 400 μs
Average τ from neutron histogram	300 to 350 μs
Average τ for flat sections of stepwise decay at densities $\leq 2 \times 10^{12}$ cm^{-3}	8.5 ms
Scattering loss time	4.5 ms
Charge exchange time	> 8 ms

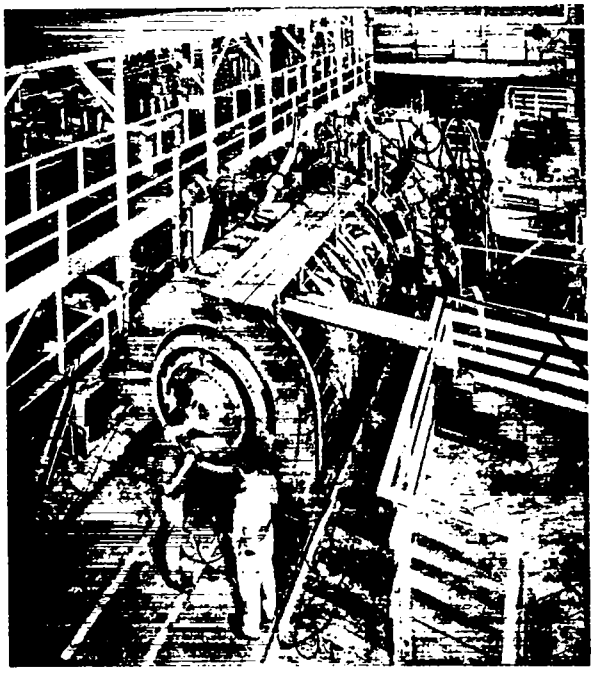

Fig. 1. Photograph of the 2X experiment taken from the west end. The west end tank is visible in place within the 6-ft. i.d. dc magnets. A portion of the capacitor banks is in the background.

13. P. della Porta and T. A. Giorgi, "Production of Hydrocarbons on Barium Films," Proc. 10th Nat. Vac. Symp. (1963).
14. R. W. Roberts, "Adsorbtion and Decomposition of Hydrocarbons on Clean Metal Films," British Jour. Appl. Phys., Vol. 14, p. 485 (1963).
15. R. A. Strehlow, private communication 1968.
16. G. D. Jarvis, private communication 1968.

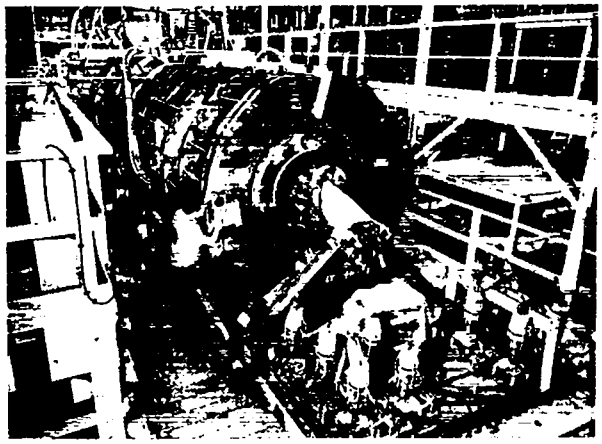

Fig. 2. Photograph of the injection, or east end, of 2X. The external portion of the deuterated titanium washer plasma sources is seen on the flange of the end tank.

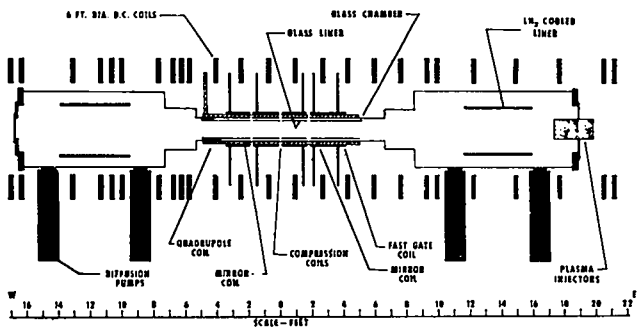

Fig. 3. Schematic cross-section of the 2X experiment. Representations of all major elements of the system are shown in approximate relative location.

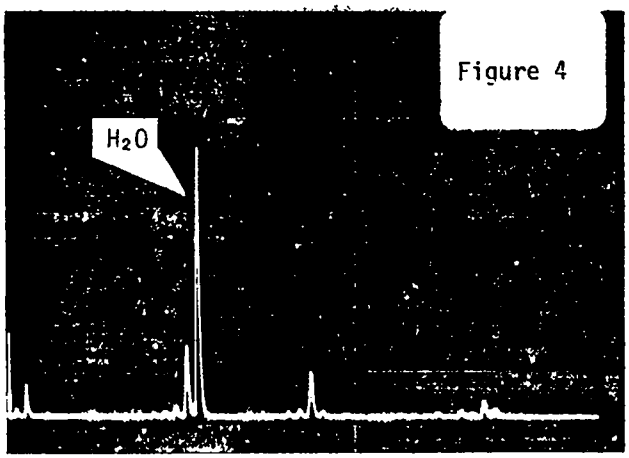

Fig. 4. Tanks, liners, and valves hot for 56 hours, 2.5×10^{-6} torr, 0.2 V/cm. 0830 hr. 1/28/69.

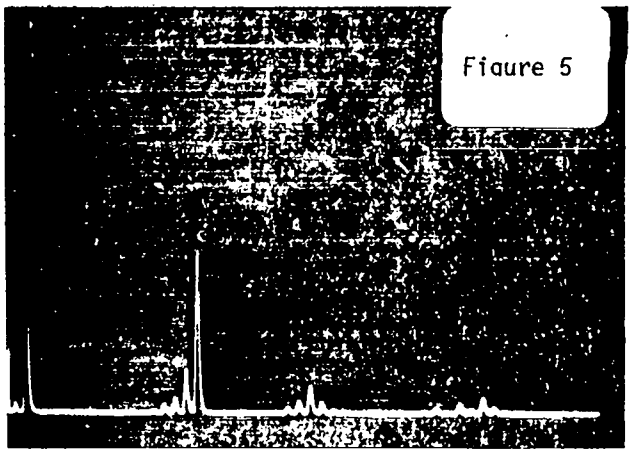

Fig. 5. Getters hot also, 7×10^{-6} torr, 0.2 V/cm, 1130 hr.

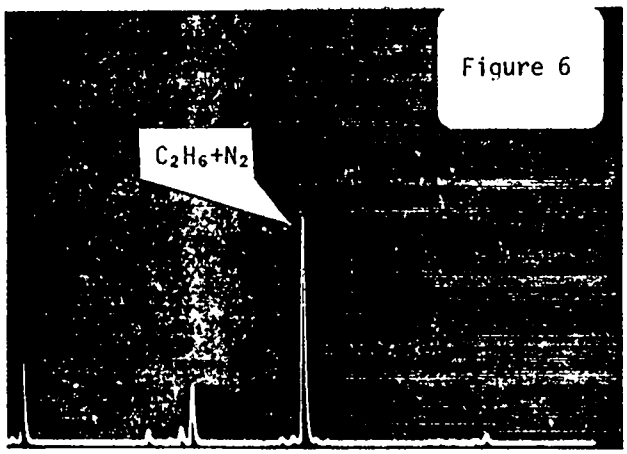

Fig. 6. Water-cooling on, 1.4×10^{-6} torr, 50 mV/cm, 1610 hr.

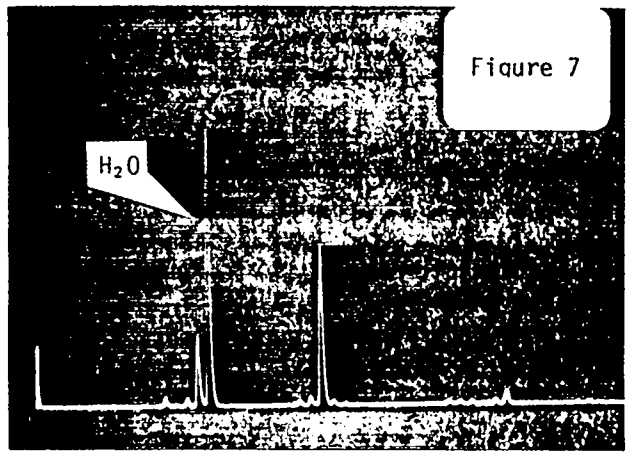

Fig. 7. Completed leak hunting, 2×10^{-7} torr, 20 mV/cm, 0900 hr, 1/29/68.

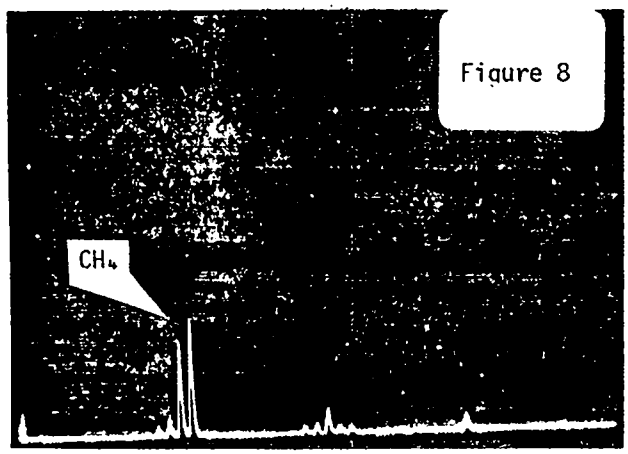

Fig. 8. Gettering down, getters off, 1×10^{-8} torr, 5 mV/cm, 1000 hr.

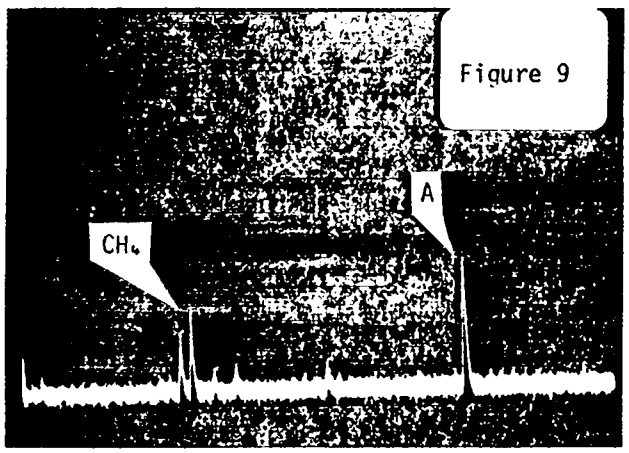

Fig. 9. LN_2 liners filled, 1×10^{-9} torr, 0.5 mV/cm, 1045 hr.

A SIMPLE, INEXPENSIVE TITANIUM SUBLIMATOR*

by

J. S. Culver
Oak Ridge National Laboratory
Oak Ridge, Tennessee

ABSTRACT

The titanium sublimator developed to pump the large gas loads in the DCX-2 machine provides a simple, rugged, inexpensive device which gives high evaporation rates and is made of commercially available materials. These filament type sublimators are run both parallel to and normal to the 12 kilogauss field in the machine.

The filaments consist of a ten inch length of tantalum or molybdenum wire surrounded by an 8 inch length of 1/4 in. x 0.065 in. wall tubing of grade II titanium. When operated at a current of 250-300 amperes, evaporation rates of 0.1 to 1.0 grams per hour are obtained. The total amount of titanium evaporated is about 10 grams per filament.

INTRODUCTION

The device to be described here is the outgrowth of an attempt to improve the reliability and reproducibility of the titanium sublimators in the DCX-2 machine at Oak Ridge.

The original, filament type, sublimator was made by winding several layers of 0.020 in. titanium wire on a core of 0.170 in. tantalum wire. As evaporation progressed, bits of wire were released and dropped into the vacuum vessel, often jamming the valve operating mechanisms. In addition to this inconvenience, these bits of wire were no longer available as material to be sublimed, thereby reducing the total material evaporated per filament charged into the machine. Hot spots frequently developed and caused high local evaporation and early failure of the filament by burnout.

By reducing the diameter of the tantalum wire to 0.118 in. and substituting 1/4 in. x 0.065 wall titanium tubing for the wire winding, the current required to evaporate 0.2 grams of titanium per hour was reduced from 320 to 240 amperes. Since a large voltage drop is encountered in the long installed cables on the machine, the reduction in current allowed 50% more titanium to be charged into the system per loading. In effect, the filaments were tailored to match the existing 20 volt, 400 ampere, dc power supplied. Six filaments can be satisfactorily operated on each of the installed supplies.

The most significant improvement was the greatly increased life before burnout and a much higher percent evaporation of available titanium.

TEST APPARATUS AND PROCEDURES

Since filament testing could not be practically pursued in the machine, a small vacuum system was constructed which allowed a filament to be installed on a holder and inserted into the water cooled vacuum chamber through an airlock. The usual operating pressure of this system was 1×10^{-7} torr.

Voltage was measured by leads brought out from the water cooled filament clamps and current was measured with a high quality shunt and precision millivoltmeter. The 30 volt, 300 ampere power supply was hand adjusted at one hour intervals if necessary. Evaporation rate was measured by removing the filament from the vacuum chamber and weighing it daily.

*Research sponsored by the U. S. Atomic Energy Commission under contract with the Union Carbide Corporation.

All tests were run by selecting an operating voltage and then adjusting the power supply to maintain this voltage throughout the run, letting the current go where it would. Since we have adopted the constant voltage mode of operation, filament burnout is a rare occurance. It can be shown algebraically that if one has a homogeneous cylindrical system that is evaporating uniformily throughout its length that maintaining a constant voltage across it will provide constant unit power at the surface and hence constant temperature in vacuum, providing uniform evaporation at the surface.

Our system is, of course, not homogeneous and does not evaporate uniformly throughout its length; however, this mode of operation has produced the most nearly constant evaporation rate of any tried to date. The curves shown later suggest that the rate increases initially and then drops off as the filament diameter decreases.

During the tests a run was arbitrarily terminated when approximately one inch of the tantalum wire became exposed, usually at the center of the filament. At this point, control becomes less precise; however, one can continue to operate the filament until virtually all the titanium is gone.

TEST RESULTS

A typical filament history is presented in Fig. 1. Run at a constant 2.5 volts, the starting current was 242 amperes. Since the voltage was held constant the current curve also represents the variation in power input to the filament. Although power is constantly decreasing, the evaporation rate increased until about one-third of the titanium was gone. Our early experience showed that constant current or constant power leads to frequest early burnout on this type of filament.

The curves in Fig. 2 illustrate performance at several voltages. The abrupt break in the lower curve at 2.5 volts is the result of poor clamping on one end resulting in overheating at that end. This filament could have been run for many more hours safely.

The two filaments run at low evaporation rates were shut down because time did not allow them to be run to exhaustion.

The group of filaments in Fig. 3 are representative of the type that run parallel to the DCX-2 magnetic field as follows:

a. A typical unused filament.
b. A filament with 6 in. of titanium tubing between clamps 8-1/2 inches apart. Note the heavy remaining titanium tube at the ends.
c. This filament had only 7-1/2 in. of titanium tubing between clamps, 8-1/2 in. apart as in b. Note the improved utilization of the ends.
d. This is a filament that ran 68 hours at an evaporation rate of about 0.02 grams/hr and still has many hours of operation left.

When it is necessary or desirable to operate a filament perpendicular to the magnetic field, it is bent in the shape of a loop as seen in Fig. 4. DC polarity must be such that the magnetic forces tend to expand the loop. If the polarity is reversed, the filament will attempt to turn over and usually shorts out.

Two liner end sections were built as shown in Fig. 5, each equipped with 16 filaments which can be run 4, 8, 12, or 16 at a time. Designed to help pump the gas load of 1-2 atmospheric cc/sec encountered in the machine when the hydrogen or deuterium arc is operated, each of the assemblies has a measured pumping speed of 60,000 liters/sec of hydrogen at 10^{-6} torr. The condensing surfaces are water cooled copper.

The magnetic field (12,000 gauss) in the DCX-2 machine necessitated a dc power supply; however, filaments have been operated satisfactorily on ac where there was no magnetic field to contend with. Molybdenum wire has been used successfully in place of the more expensive tantalum; however, the spent filaments were brittle when removed. The resistivity of molybdenum is much lower than that of tantalum requiring an adjustment in power supply capability.

The following table presents some general information on materials used in the test program.

	Tantalum	Molybdenum
Electrical resistivity 70°F	12.5	5.2
Tensil strength 2400°F	13,000 psi	16,000 psi
Yield strength 1600°F	15,000 psi	30,000 psi
2400°F	--	10,000 psi
Cost of 0.118 rod	$3.77/ft	$0.51/ft

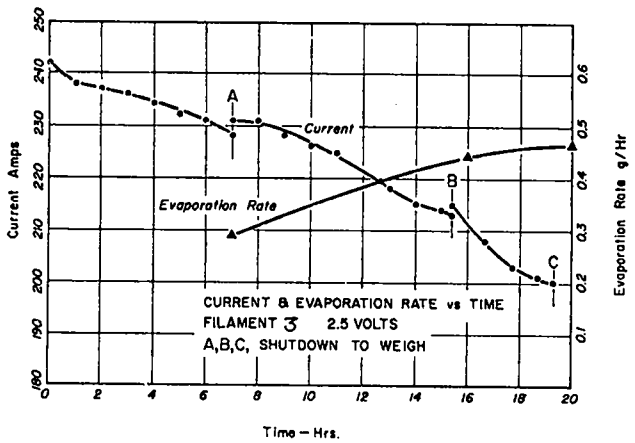

Fig. 1. Current and Evaporation Rate vs. Time.

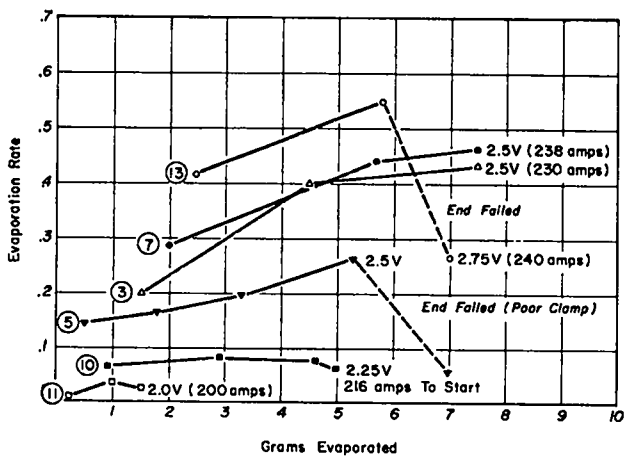

Fig. 2. Evaporation Rate vs. Grams Evaporated at Constant Voltage.

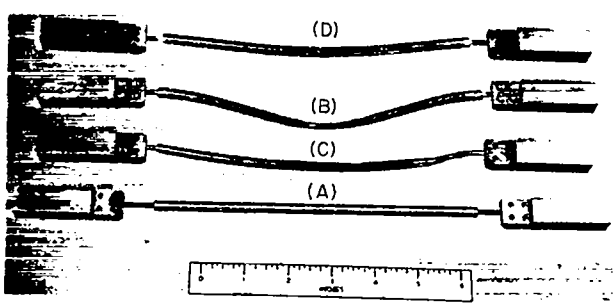

Fig. 3. New and Used Filaments.

Typical Analysis of Grade II Titanium

Carbon	0.06%
Hydrogen	0.0031%
Iron	0.14%
Nitrogen	0.006%
Oxygen	0.11%

Physical Properties

Elongation % is 2 in.	30.5
Tensile strength	72 x 10^3 psi
Yield strength	49.3 x 10^3 psi
Cost of 1/4 x 0.065 wall titanium tubing only	$1.80/ft
Material cost of one filament with Ta wire	$4.40
Material cost of one filament with Mo wire	$1.68

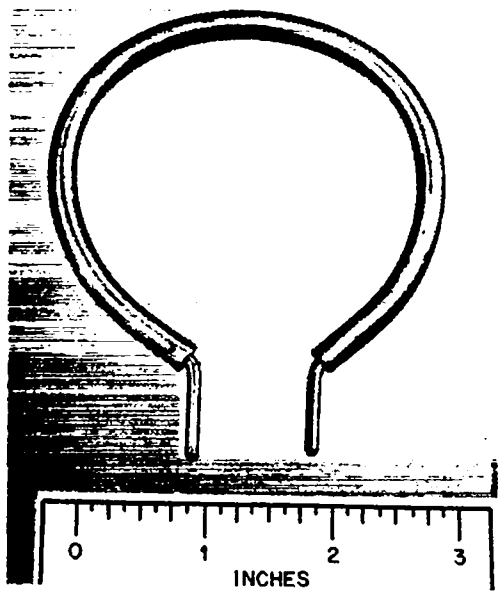

Fig. 4. Curved Filament Operated Perpendicular to the Magnetic Field.

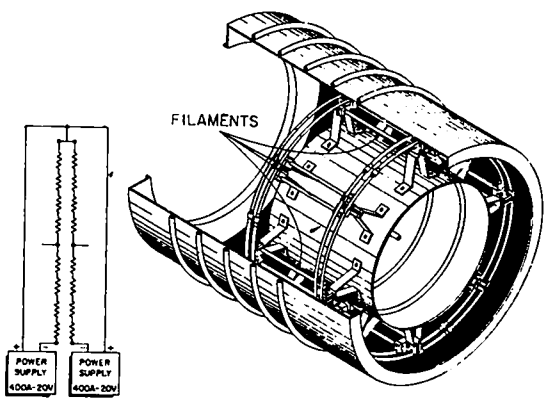

Fig. 5. DCX-2 Titanium Pump.

ACTIVE METAL BRAZING TECHNIQUE FOR METAL-TO-NONMETAL SEALS*

by

Richard H. Bulmer
Lawrence Radiation Laboratory
University of California
Livermore, California

ABSTRACT

The new Astron accelerator requires a large ceramic-metal stack assembly for the electron gun accelerating column. Vacuumtight joining of the metal and nonmetal elements of the stack will be done by the active metal brazing technique. This technique has proved to be successful previously on smaller assemblies. In the assembly, machined copper rings are sandwiched between $15\frac{1}{2}$-in.-o.d. alumina rings, resulting in an $18\frac{1}{4}$-in.-high stack with 24 brazed joints. The assembly must be aligned within 0.015 in. and must be vacuumtight against an external pressure of 3 atm. A vacuum furnace capable of 900°C with high pumping speed in the 10^{-5} torr range is required for the brazing operation. The high pumping speed is necessary to reduce the pressure resulting from evolution of hydrogen from the titanium hydride flux used for brazing. A cold-wall furnace employing refractory metal heat shields, which was designed and built specifically for this brazing operation, is described.

INTRODUCTION

An accelerating column composed of copper electrodes separated by ceramic ring insulators forms a subassembly for the Astron accelerator electron gun. The column supplies the initial 720 keV to the electrons. It also acts as a vacuumtight barrier against 30 psig. Early experience in the fabrication of these stacks has demonstrated that an active metal brazing process is the most reliable means for assembly.

Originally the stacks were produced by the sintered metal or moly-manganese technique. However, the results were unsatisfactory. Delivery was extremely long and the stacks were badly out of tolerance. Due to the failure of the first group of stacks, a different joining process was sought. The active metal process seemed a reasonable approach and adaptation of the method to large assemblies began at LRL, originally to serve as a backup. After a period of development, technicians were able to successfully braze test assemblies, and the technique was chosen for future production. The new accelerating column, being 16 in. in diameter by 18.25 in. high, was too large for existing LRL vacuum furnaces. Thus, a new furnace with a larger working hot zone was required. The active metal process required that higher pumping speed be provided in the new furnace also.

DESCRIPTION OF THE PROCESS

The active metal process using titanium hydride was originally described by Bondley.[1] Kohl[2] gives a brief but descriptive summary of the process. Krichner[3] describes application of the technique to large assemblies. Briefly, the method requires applying titanium hydride to the ceramic sealing surfaces, then heating in vacuum with a conventional brazing alloy. The titanium serves to wet the ceramic and thus creates a seal.

Figure 1 shows the ceramic rings, copper electrodes and braze alloy ready for preparation of the joint components. The mating surfaces must be free from contaminants. The surface of

*Work done under the auspices of the U. S. Atomic Energy Commission.

the ceramic to be brazed is coated with a paint made of titanium hydride powder in an easily volatized carrier. The paint is made from 200-mesh titanium hydride and nitrocellulose lacquer, using two parts by volume TiH_2 and three parts lacquer. Care should be taken so that the coating is uniform. A coating thickness of 1.5 mils is sufficient, which is equivalent to 5.7 mg/cm^2 of TiH_2; too much titanium will cause overwetting of the ceramic. A ring of Ag/Cu/Ni eutectic brazing alloy is then sandwiched between the coated ceramic and the mating copper ring. For a series of joints, such as the stack assembly, the parts are put under a nominal compressive force during brazing to insure joint uniformity and desired alignment tolerance. The assembled stack, prior to brazing, is shown in Fig. 2.

The assembled stack is placed in a vacuum furnace where heating begins after the pressure stabilizes. During the early stages of heating, the titanium hydride dissociates and a film of titanium remains on the ceramic surface. This begins at approximately 360°C, and from this point on, hydrogen is given off continuously. Just above the temperature at which the bulk of the hydrogen is evolved, the brazing alloy melts and alloys with the titanium. The highly active titanium diffuses into the ceramic, aided by the presence of the hydrogen. An excessive amount of hydrogen, however, will cause pores to develop in the braze area upon cooling.

It is important that no contaminating gases are present. Oil vapors are definitely intolerable. Water vapor, CO, and CO_2 are also harmful due to the sensitivity of titanium to oxidation. It is recommended that the pressure be kept at 10^{-5} torr or below at all times.

The alloying process between the titanium and the Ag/Cu/Ni eutectic alloy initiates at 810 °C. By the time the temperature reaches 850°C, 6% by weight of the titanium has been alloyed. This proportion yields a good braze. If the temperature is increased much above 860°C, excessive wetting occurs, as the alloy is too rich in titanium.

The total quantity of titanium hydride required for the 24-joint stack is 16 g. The hydrogen liberated is thus 0.314 mole, or 5450 torr-liters. High pumping speed is necessary to remove the hydrogen from the system and also to handle the outgassing load from the radiation shields. The stack is held at 850°C for a few minutes to insure a completed braze, then allowed to cool in vacuum or an inert atmosphere.

FURNACE

The primary design requirements were determined on the basis of a working hot zone 18 in. in diameter × 21 in. high, an operating temperature of 1000°C, and operational convenience. Tungsten stranded filaments were chosen as the heaters, due to their availability and ease of replacement. A cold-wall design was selected, primarily to reduce outgassing and to minimize cooldown time. The total amount of power required was determined by the heat-up time and heat capacities of the charge and immediate furnace components. Filaments were chosen with appropriate cross section and surface area to radiate this power at the design temperature. Much of the necessary equipment for the new vacuum furnace was on hand, including a 1000-liter chamber, mercury diffusion pumps, valves, baffles, etc.

A total power input of 10 kW was calculated as sufficient to heat up the charge within a reasonable amount of time. In order to avoid a high operating voltage, the filaments were arranged in parallel, each filament being 44 in. in length. A total of 28 filaments were used, forming a heater curtain 20 in. in diameter and 22 in. high. On this basis, the tungsten wire was chosen as 3/7/.015 which implies operation at 1200 A and 8 V, with an estimated 1600 A after the filaments age. A power supply of 30 kW, 0-10 V was available.

Choosing a method of bussing the high current into the heating region presented a problem since large-cross-section bus bars will carry heat from the filaments out of the hot zone. The best approach to the problem is to keep the high-current bus bar out of the hot zone and bring in the power through individual feed-throughs, two for each filament. These feed-throughs are insulated with alumina sleeves. An electrical conductor operating between fixed end temperatures has a critical cross section at which minimum heat loss occurs. For an insulated feed-through the optimum cross-

sectional area can be approximated by

$$A = 0.92\ IL\sqrt{\frac{\alpha\rho_0}{k}}\ \frac{1}{\lambda},$$

$$\lambda = \arctan\sqrt{\frac{T_1 - T_2}{T_1 + T_2 + 2/\alpha}},$$

where

A = cross-sectional area (in.^{2}),
I = current (A),
L = length of conductor (in.),
k = mean value of thermal conductivity (Btu/hr · in. · °F),
$\rho = \rho_0(1 + \alpha T)$ = resistivity of material (ohm · in.),
ρ_0 = resistivity at 0°F (ohm · in.),
α = temperature coefficient of resistivity referenced to 0°F (1/°F),
T = temperature (°F),
T_1 = temperature of the heated end (°F),
T_2 = temperature of the cooled end (°F).

The power feed-throughs are clamped to a hollow water-cooled bus outside the heat shield area. The bus bars circle the shields and terminate in a power/coolant manifold on the lid of the chamber.

The hot zone is insulated with radiative heat shields. The side shields are concentric cylinders, the innermost one of Ti/Zr/Mo alloy and the outer three of nickel. They are hung from the power feed-throughs and are separated with alumina spacers. The top and bottom shields are in two stages. The first stage is a stack of four 19-in.-diam sheets, the inner one of Ti/Zr/Mo alloy and the other three of Ni. In back of this set is a similar stack of 23-in.-diam sheets with a 9-in. hole in the center for pumpout. Sufficient clearance is allowed for expansion of all the shields. The shields are fabricated from 0.020-in.-thick stock with splices made by tying with 0.030-in.-diam moly wire. All sets of shields are backed with water-cooled, $\frac{1}{4}$-in.-thick stainless steel plates. The shields are sufficient to hold a heat rate of 70,000 Btu/hr at an operating temperature of 1000°C.

The vacuum chamber has a removable lid from which the shields and heaters are hung. During loading and unloading of the furnace, the lid is hoisted up far enough to allow the hearth and charge to be rolled in under it through a large door on the side of the chamber. Welded onto the side of the chamber is a manifold to which two pumping systems are attached. The parallel combination of 9-in. and 12-in. mercury diffusion pumps supply an approximate speed of 1400 liters/sec at the high vacuum valve. The diffusion pumps are backed with a 100-cfm Roots-type blower and a 15-cfm roughing pump. This arrangement yields high pumping speed in the 10^{-3} to 10^{-5} torr range where the pressure during brazing is critical. Figure 3 is a photograph of the vacuum furnace with the shields and heating elements elevated for loading and unloading. Figure 4 shows the internal parts of the furnace and associated pumping system.

Thus far only trial runs have been made in which a short ceramic-metal stack has been successfully brazed. In the future, larger cross section filaments may be installed to utilize more of the available power. The experience to date indicates that the active metal brazing process requires close supervision by capable operators.

ACKNOWLEDGMENT

Recognition is due Fred P. Brechtel whose valuable experience in active metal brazing and furnace operation provided solutions to many problems that arose during assembly and operation of the furnace.

REFERENCES

1. R. J. Bondley, "Metal-Ceramic Brazed Seals," Electronics, July 1947, pp. 97-99.
2. W. H. Kohl, Handbook of Materials and Techniques for Vacuum Devices (Reinhold Publishing Corp., N. Y., 1967), pp. 451-454.
3. K. F. Kirchner, AEC Research and Development Report MATT-228, October 1963.

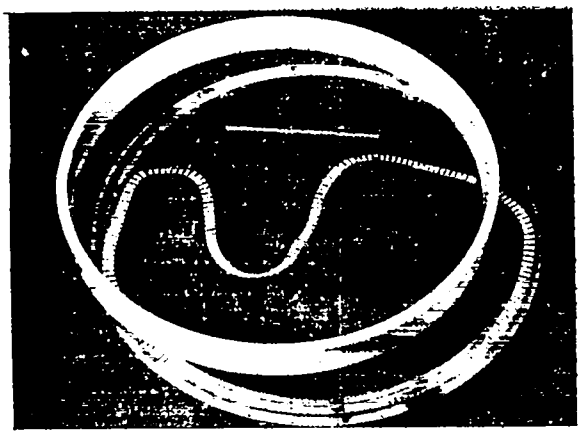

Fig. 1. Components of stack.

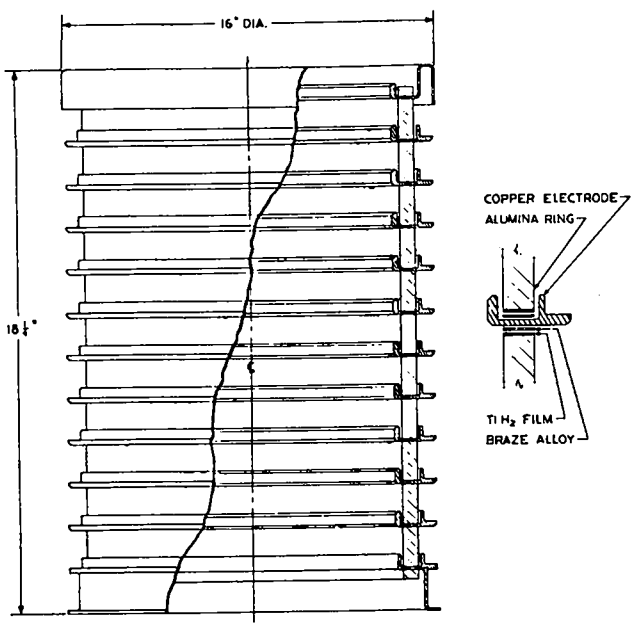

Fig. 2. Assembly prior to brazing.

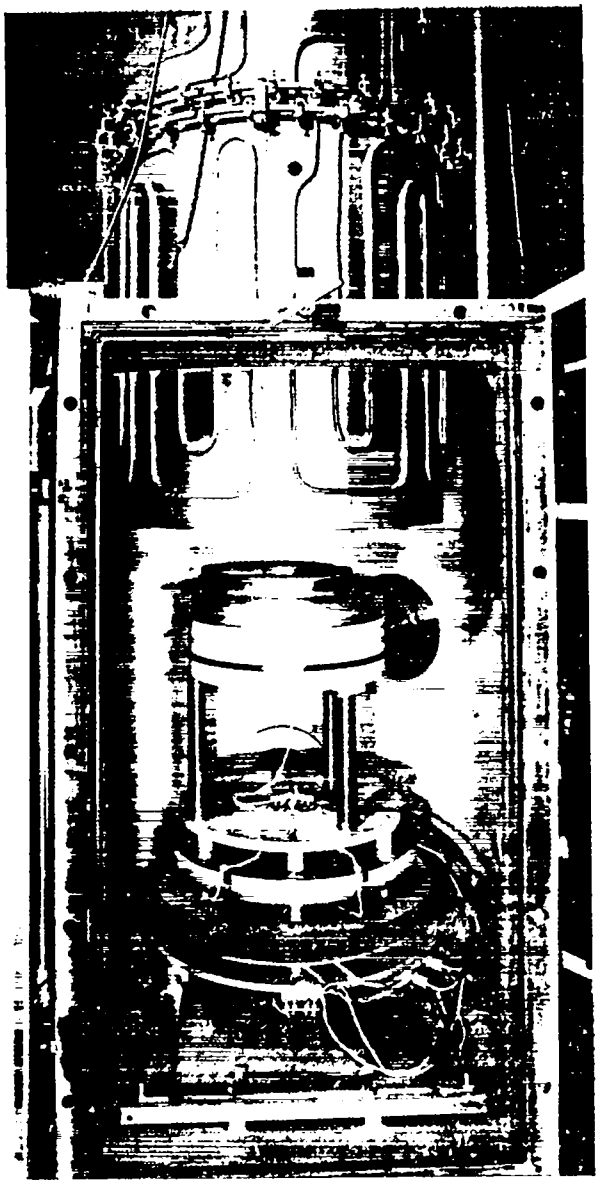

Fig. 3. Furnace ready for loading.

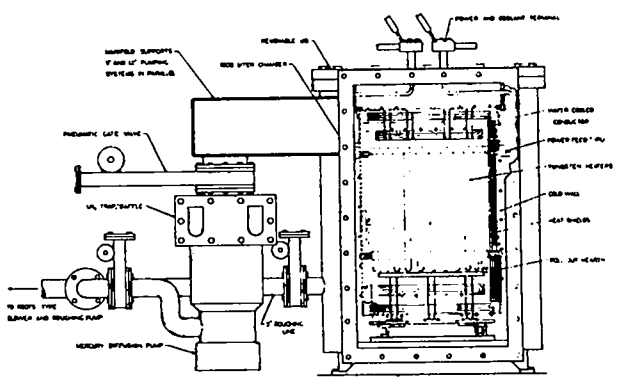

Fig. 4. Vacuum furnace.

AN ON-OFF LIQUID HELIUM CRYOPUMP*

Balwant S. Denhoy and Thomas H. Batzer
Lawrence Radiation Laboratory
University of California
Livermore, California

ABSTRACT

An on-off thermal switch for thermally isolating the LHe storage from the pumping surface is incorporated into a cryopump, which results in an increased pumping rate and efficiency as well as less-hazardous operating procedures. The switch is a hermetic volume between the LHe storage and the pumping surface. Gas is introduced into the insulating space to establish thermal contact between the LHe and the pumping surface; then the gas is evacuated to thermally isolate the pumping surface.

INTRODUCTION

The new ion source for the Alice experiment requires a hydrogen pumping capacity of 6000 liters/sec at 10^{-4} Torr. The pump must not produce any contamination and must operate continuously at the required capacity for a run of at least 8 hr. Further, the regeneration time, if required, must be very short compared with the running time. The ready availability of liquid helium and the unusual pumping requirements led to the design of a unique thermocycling cryopump.**

Pumping large quantities of hydrogen by condensing and freezing it on a cryosurface can create a potential explosion hazard. To preclude an explosion in an up-to-air accident, the amount of hydrogen (at standard conditions) pumped in this manner must not exceed 4 vol % of the pump vacuum space. This limitation requires the pump vacuum volume to be large enough to provide the specified running time. Further, a method of thermocycling the cryosurface between 4.2 and 8° K must be provided to allow the hydrogen to be periodically desorbed and removed from the pump while it is isolated from the gas source.

The two conventional methods of thermocycling the cryosurface are, first, to simply remove and replace the liquid helium and, second, to vary the pressure of the boiling liquid helium. The first method is too expensive and time consuming; the second is not practical for 8° K. A third method, using a thermal diode,[1] allows the cryopumping surface to be quickly and economically cycled through the desired temperatures without disturbing the liquid helium refrigerant.

MECHANICAL DESIGN

Figure 1 shows the cross section of a prototype thermocycling cryopump. To minimize thermal gradients, the pumping surface is copper. It is silver soldered to the bottom of the thermal switch or diode cavity, which is thin-walled stainless steel. When this cavity is evacuated to less than 10^{-3} Torr, the copper pumping surface is thermally insulated from the helium reservoir and its temperature rises to approach that of the liquid nitrogen shields. When the cavity is charged to several torr with helium gas, the condensation-evaporation process in the cavity transfers heat at a great rate (at least ten times greater than for an equivalent area of copper) from the copper to the liquid helium in the reservoir. Thus, by simply controlling the helium pressure in the cavity, the temperature of the copper cryopumping surface can be readily cycled between 4.2 and 8° K.

Further, to make such a pump work on a cycling basis, no surface can be colder than 8° K except the copper. To accomplish this the liquid

*Work performed under the auspices of the U. S. Atomic Energy Commission.

**U. S. Patent applied for.

helium reservoir is completely surrounded by a sealed-off vacuum space formed by a stainless steel jacket. Due to the radiation heat load from the liquid nitrogen shield, this vacuum jacket has an equilibrium temperature well above 8° K.

The mass of the copper should be as small as possible, consistent with allowable thermal gradients. It takes about 5 liters of liquid helium to cool a pound of copper from 100 to 4.2° K. Also, the cavity volume should be as small as possible, since it takes 373 cal/g to cool helium gas from room temperature to 4.2° K. Some liquid nitrogen precooling is desirable.

Figure 2 shows the full scale cryopump. It was designed for 6000 liters/sec at 10^{-4} Torr and a liquid helium consumption rate of 0.4 liter/hr. The Dewar capacity is 26 liters, providing ample time between fillings. Figure 3 shows a section through the center of the pump, and Fig. 4 shows the liquid nitrogen shield and liquid helium Dewar subassembly. The free volume of the pump is 200 liters, and the cryopumping surface area is 250 $in.^2$.

TEST RESULTS

The test results shown in Table I were taken on the prototype shown in Fig. 1. The temperatures were measured with calibrated carbon resistors.

The low specific heat of copper (less than 0.002 cal/g-° K below 20° K) and the small volume of the thermal diode cavity permit a complete cycle from 4.2 to 8° K and back to 4.2° K in about 60 min.

ACKNOWLEDGMENTS

The authors wish to thank Cleve A. Gunderson, Don B. Sabine, and Roger J. Chauvet for their technical advice and helpful suggestions on the development of this cryopump.

REFERENCES

1. W. E. Gifford, "The Thermal Check Valve - A Cryogenic Tool," Advances in Cryogenic Engineering (Plenum Press, New York, 1962), Vol. 7, pp. 551-555.

Table 1. Test results.

Time	Cavity pressure (μ)	System pressure (Torr)	Pumping surface temp. (° K)
11:50	1000	1×10^{-8}	4.13
11:55	< 1	1×10^{-8}	4.16
12:01	< 1	5×10^{-8}	4.2
12:02	< 1	1×10^{-7}	4.3
12:03	< 1	6×10^{-7}	4.8
12:04	< 1	5×10^{-6}	5.3
12:05	< 1	2×10^{-5}	6.0
12:07	< 1	6×10^{-5}	7.3
12:08	< 1	1×10^{-4}	8.1
12:30	< 1	5.4×10^{-4}	7.3
12:33	< 1	5.4×10^{-4}	7.3
12:34	200	4×10^{-5}	5.3
12:36	1000	4×10^{-5}	5.2
12:40	1000	1×10^{-5}	5.0
12:43	1000	1×10^{-5}	4.7
12:51	1000	2×10^{-8}	4.2
12:53	1000	1.6×10^{-8}	4.17
12:57	1000	1.5×10^{-8}	4.13

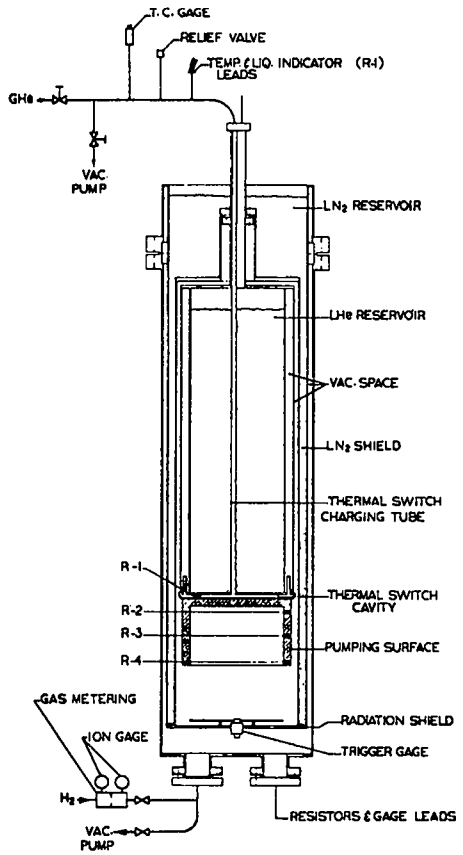

Fig. 1. Thermal switch cryopump.

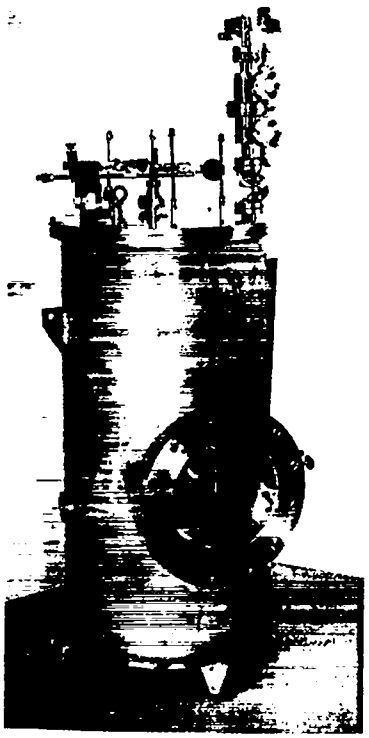

Fig. 2. On-off LHe cryopump.

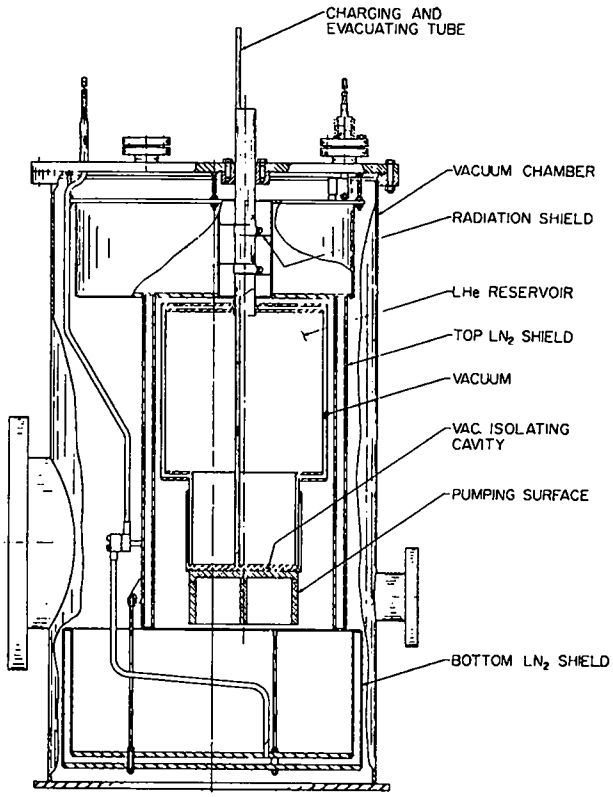

Fig. 3. On-off LHe cryopump, cross-sectional view.

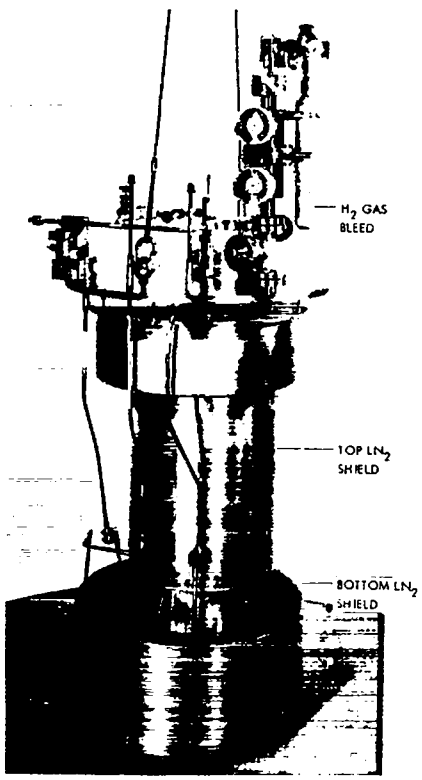

Fig. 4. On-off LHe cryopump subassembly.

Q-MACHINE HOT PLATE DEVELOPMENT*

by

F. E. Wittman, Dale B. Henderson, and Harry Dreicer

Los Alamos Scientific Laboratory, University of California

Los Alamos, New Mexico

ABSTRACT

A hot plate was designed to contact ionize an atomic beam of cesium. After testing materials and various configurations, a multiple disk construction, held in compression with draw bolts and insulated with ceramic, was used.

The hot plate consists of three stages: a conical filament, to minimize JxB forces due to the presence of an externally applied magnetic field; a cathode, heated by electron bombardment from the filament; and an anode or hot plate, three inches in diameter and 1/4 inch thick.

The grid is a ring spaced around the outside of the cathode. When the potential on the grid is made more positive than the space charge limited cathode; an increase in electron current, in the form of a coaxial ring, strikes the anode. This ring of electrons compensates for the heat losses due to the anode support. By adjusting the coaxial ring and cathode to anode current, the radial temperature profiles can be made to have positive, negative or nearly zero temperature gradients.

Tungsten is used for the hot plate, cathode, filament and cathode support rod. Tantalum is used for the filament supporting disks, grid, hot plate cap and heat shields. Molybdenum is used for the draw rods. Copper is used for the support chamber, baffles and water cooling. Al_2O_3 ceramic and boron nitride are used for voltage and thermal insulation.

Filament lifetimes average 100 hours for a tungsten foil one mil thick and a current of 0.12 ampere per mil width.

The filament requires 3700 watts at 6.7 volts, the cathode uses 4000 watts @ 2,300 volts, and the combined power required varies between 10,000 and 12,000 watts depending on the grid potential.

Temperature measurements, made on the hot plate in the isothermal case using an optical pyrometer indicate a temperature of 2200°K with a total variation of 5°K across the surface.

Conventional Q-machines depend upon a 2200 to 2500° K hot plate to contact ionize an atomic beam of cesium or potassium. The properties of the plasma produced in this manner are directly related to the surface temperature distribution on this hot plate. Moreover the efficiency with which experiments can be carried out is largely limited by the lifetime of the hot plate system. For these reasons we have been engaged in an extensive hot plate development program, some aspects of which we will describe here.

Electron bombardment is the method used for heating the hot plate (or anode) which, in our system, is electron beam welded into a thin tantalum support to prevent energetic secondary electrons from the electron bombardment source from interacting with the contact ionized plasma beam. At first wire filaments were used to provide electrons for the bombardment of the hot plate. In this construction six 97% tungsten - 3% rhenium wires arranged in a cone to reduce the JxB forces due to the strong magnetic field. These wires gave rise to localized heating of the hot plate, and since this resulted in undesirable surface temperature variations this system was discontinued.

A flat tungsten mesh was tried next. It had a long life, but it would elongate and distort with changes in the magnetic field.

A cone of 1-mil tungsten foil was also tried. Its major diameter was 1.7 inches, the minor diameter was 0.95 inches and its length was 2 inches. A cone-shaped accelerator structure placed in the

center of the filament cone increased the perveance of the system, resulting in 10^{-5} amp-volt$^{-3/2}$ with a magnetic field of 5000 gauss. The difficulty with this system was that the temperature gradient across the 2.75 inch hot plate was 260° C.

An intermediate hot plate (or cathode) was therefore incorporated into the design in order to reduce the thermal gradient on the anode. By heating this cathode until its whole surface is in the space-charge limited-regime, it acts as a uniform source of electrons. This means that the cathode can have a large thermal gradient as long as the minimum temperature is not in the temperature-limited regime.

A uniformly heated hot plate will not be isothermal, because of the heat losses to the support cap. To make up for this loss, another filament, coaxial with the cathode, is required (Fig. 1). However this complicates the design and assembly becomes too difficult. This problem was solved by increasing the diameter of the cathode until it was almost equal to the diameter of the anode and by beveling its edge. An annular tantalum acceleration structure is then located (Fig. 2) next to this beveled surface, with about 3/8 inch spacing between these two components. By varying the potential on this acceleration structure the current of electrons reaching the anode can be controlled. Moreover this voltage adjustment when combined with control of the cathode to anode current permits us to control the radial temperature profiles so that the temperature gradient has positive, negative or nearly zero values (Fig. 3). The perveance of this last design is 1.5×10^{-5} amp-volt$^{-3/2}$ for the filament to cathode and 6×10^{-6} for the cathode to anode.

The tantalum accelerator and the 2-7/8 inch diameter tungsten cathode are mounted on the same 3/8 inch diameter tungsten rod. In order to prevent sagging due to the proximity of the hot filament and the 1-1/8 pound cathode, the tungsten is purchased with a mixture of 1 to 2% thorium. A small amount of thorium in the tungsten will stop the growth of large crystals which usually form quite rapidly between 2600 and 2800° C. Water cooling is provided so that there is a temperature gradient of 2200° C in the 4 inch length. The best method for attaching the cathode to the rod is to thread both parts and screw them together. Electron beam welding was tried, but the joint was too fragile. Al_2O_3 ceramics were required in place of boron nitride filament ring supports because of the increase in electrical conductivity of the boron nitride at elevated temperatures. Boron nitride spacers required much less outgassing time when prebaked in a vacuum furnace for 1-hour at 1200° C.

To prevent excessive heating of the vacuum vessel, a water cooled jacket is placed around the support cylinder (Fig. 4). Water cooling is also provided for grid support and the cathode support structures to prolong the life of the Al_2O_3 ceramic and boron nitride insulators.

The floating high voltage power supply used to heat the cathode has a voltage stability of one part in 10^4 from 500 to 5000 volts and a current capability of 5 A. The cathode to filament voltage normally runs about 2300 V and 1.7 A. The cathode to anode power supply has the same characteristics. The anode has been operated at 1500 to 3000 V and 1 to 2.5 A depending on the grid potential. The grid supply draws no current but needs to be well regulated so that fluctuations in anode current will not occur. The filament supply is unregulated and consists of two 500 A, 15 V rectifiers connected in parallel. This supply is floated at the combined cathode and anode potential while providing 600 A at 6.7 V.

Average filament lifetime of 100 hours, controllable radial temperature gradients, and reproducible temperatures should make this hot plate module a useful tool for Q-machine studies.

*Work performed under the auspices of the U.S. Atomic Energy Commission.

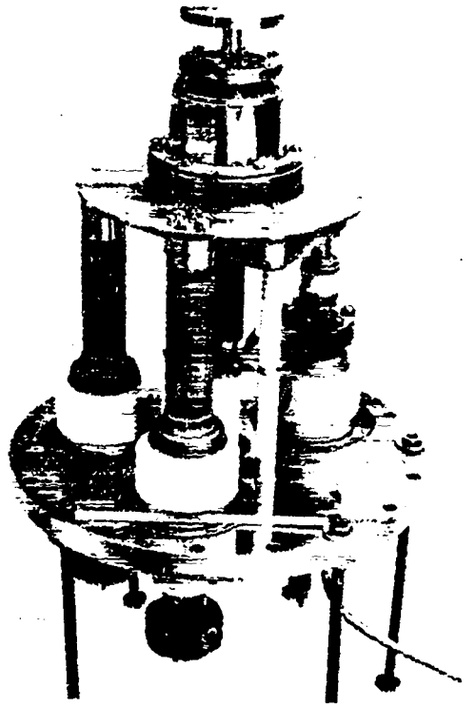

Fig. 1 Two filament and two stage hot plate structure showing only the intermediate hot plate and the two coaxial filaments.

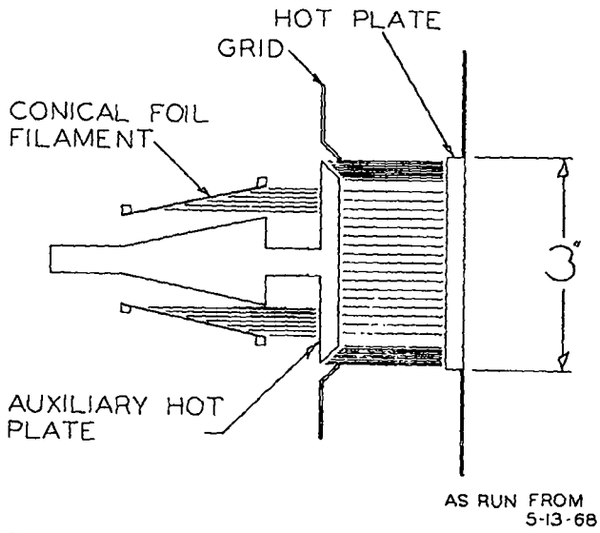

Fig. 2 Diagram of the two stage hot plate with single filament and coaxial accelerator ring.

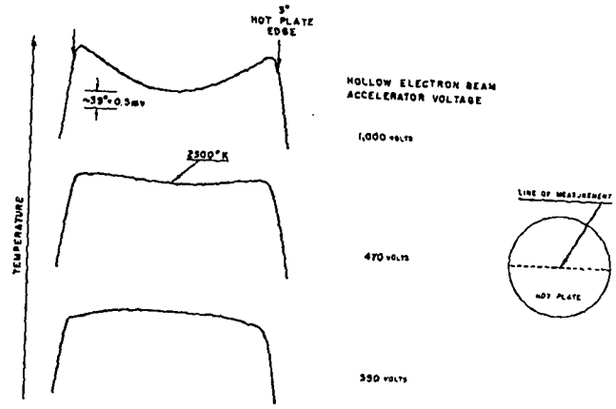

Fig. 3 Hot plate profiles. A model TD-6BTC15 Thermodot Radiometer with a bandpass filter of 1.6 to 2.7 μ was mounted on an optical bench with a drive mechanism to scan the image of the hot plate. A potentiometer was used to provide position readout to the X-Y recorder.

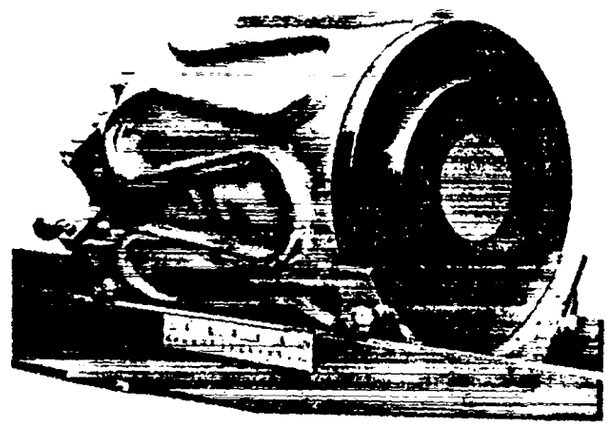

Fig. 4 Water cooling jacket on two stage system showing 3 inch hot plate.

A TWO-TERMINAL MARGINAL OSCILLATOR EASES NMR PROBE-CABLE RESTRICTION

by

A. W. Weissenburger
Plasma Physics Laboratory, Princeton University, Princeton, New Jersey

ABSTRACT

A marginal oscillator is described which satisfies a need for use in simple economical NMR systems that measure magnetic field intensity. Advantages of the basic oscillator circuit, which uses dual feedback in conjunction with a series-tuned probe, are discussed. The choice of frequency modulating the oscillator rather than employing conventional B field modulation permits the use of a simpler probe structure. A circuit diagram is given.

Marginal oscillators offer a simple means of determining magnetic field strength provided the field has sufficient homogeneity. Because of this requirement a useful by-product is a qualitative measurement of homogeneity.

A typical measuring device consists of a probe, marginal oscillator (with its associated electronics), CRO indicator, and frequency counter. A frequency counter that meets requirements is expensive. The cost problem is resolved in many cases by utilizing the marginal oscillator as a component of a modular rather than an integrated system. The modular system would be composed of a laboratory counter and oscilloscope, a probe and marginal oscillator.

The use of presently available equipment is sometimes limited because of restrictions on probe cable length. The two-terminal oscillator permits operation over a range of cable length without seriously affecting its oscillating frequency or sensitivity. The basic circuit of a two-terminal LC oscillator is shown by Fig. 1. Note that it is a series-tuned circuit in which the driving current I_o is common to all elements.

A necessary condition for oscillation is that generator resistance R_G be negative. The criterion for oscillation then becomes

$$\frac{|R_G|}{R_s} \geq 1,$$

and threshold occurs when $|R_G| = R_s$, at which point the terminal impedance falls to zero. Thus, near threshold substantial resistive and/or reactive loading of these terminals is tolerated without serious effect upon operation.

The circuit of Fig. 2 shows the probe network connected to the oscillator proper by a length of coaxial cable L. This circuit is equivalent to that of Fig. 1, provided $L \ll \frac{\lambda}{4}$ at the operating frequency. The design of the two-terminal marginal oscillator is based on this concept. Greater lengths of L unduly influence operation because the distributed elements of the cable, as shown by the equivalent circuit of Fig. 3, have become effective. Satisfactory operation has been attained with an 18 inch length of RG 174/U cable at 45 MHz.

When mechanical limits are imposed it can become difficult to achieve the desired Q within the specified volume. The condition may be alleviated somewhat by frequency modulating the oscillator thereby obviating the need for the Helmholtz coils. This approach has been employed

to provide greater space for the sample coil. The basic circuit of such a device is shown by Fig. 4. Transistor Q-1 is an emitter follower with its collector load (R-1) and its base resistor (R_F) returned to rf ground. Therefore, its output impedance (external terminals) is low. Transistor Q-2 is connected to provide negative feedback which reduces the output impedance further still and into the milliohm region. This is low enough that the Q(~ 100) of the probe circuit is not appreciably degraded.

Under these conditions emitter impedance is lowest and the voltage gain from base to collector of Q-1 is maximum at the series resonant frequency of the probe. Transistor Q-3 is now added to provide feedback from collector to base of Q-1 and the threshold of oscillation is reached when this closed loop gain is unity. Since this gain peaks at series resonance for the probe, the frequency of oscillation near threshold will essentially be determined by the probe constants L_s and C_v.

The threshold equation is given by

$$g_m^1 g_m^2 R_c R_F \left(1 - \frac{R_s}{R_o + R_s}\right) = 1.$$

It can be shown that the Q of the $C_v L_s$ network must increase with frequency in order for threshold to remain constant.

The Q of L_s tends to remain constant with frequency, because the limited volume of the probe compromises design. However,

$$Q_v \propto 1/C,$$

where Q_v is the Q of varactor C_v, and since

$$f_o \propto \frac{1}{\sqrt{C}},$$

there results a net increase in Q with respect to frequency. Such increase tends to maintain threshold constant, a characteristic that has been corroborated by tests on the model. The factor

$$1 - \frac{R_s}{R_o + R_s}$$

in the threshold equation shows that for high sensitivity both R_o and R_s should be small, i.e., Q high and output impedance low.

The internal terminals of this negative resistance oscillator are available for adjusting the oscillator to the threshold (marginal) operating point. The transconductances are set to the desired values by varying the collector currents of the transistors. Oscillating level is held at threshold by negative dc feedback via an amplified automatic gain control system.

A circuit of the test model is shown by Fig. 5. Broad-band circuits are formed by C-2, R-2, L-2, C-3, R-3, and L-3 that serve to neutralize Q-2, Q-1, and Q-3 respectively. All of these circuits are tuned to the geometric mean frequency of the desired band.

The transistors were selected for highest $h_{fe} \times f_t$ product as well as terminal arrangement.

The printed layout of the oscillator is shown by Figs. 6a and 6b. It was produced by engraving 2 oz. copper clad melamine board. Transistor Q-3 (Fig. 6b) is mounted on the circuit side of the board in order to maintain short leads, symmetry, and simplicity of layout.

The test probe is shown by Figs. 7a and 7b. Only a single cable will be used in the final version, two having been used here to facilitate testing. The oscillator and probe together with basic methods of adjusting operating point are shown by Fig. 8.

Time has not permitted adequate testing in many respects, but enough has been accomplished to indicate that frequency stability is good (at constant probe temperature) and that threshold does in fact remain quite constant over a 2:1 frequency range. Proton resonances have been

obtained in the 30 MHz region. Further work will include determination of signal to noise ratio and sensitivity relative to other marginal oscillator systems.

ACKNOWLEDGMENTS

Much credit should go to Stanley Schweitzer for his earlier investigations; and to Ulmshidi Albataew and Frank Bernath for their work in constructing the test models.

This work was performed under the auspices of the U.S. Atomic Energy Commission, Contract No. AT(30-1)-1238.

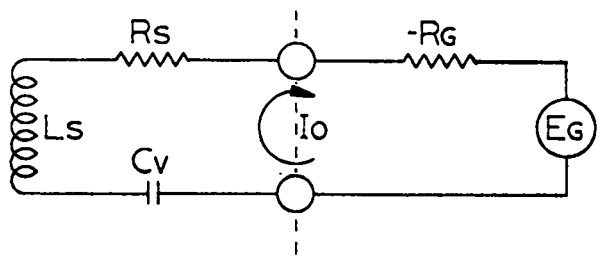

Fig. 1. Basic circuit of a two-terminal LC oscillator.

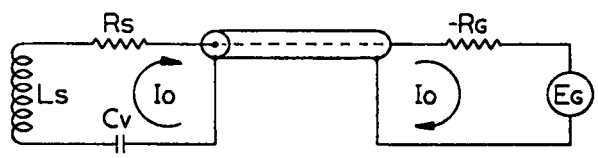

Fig. 2. Two-terminal oscillator with probe network.

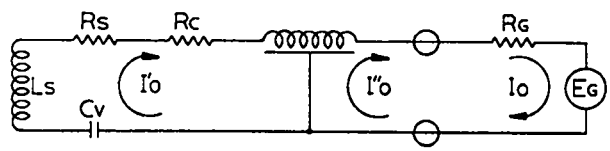

Fig. 3. Equivalent circuit of two-terminal marginal oscillator.

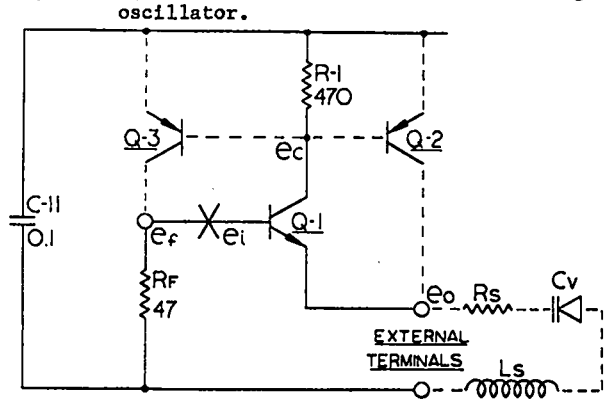

Fig. 4. Physical circuit of two-terminal LC oscillator.

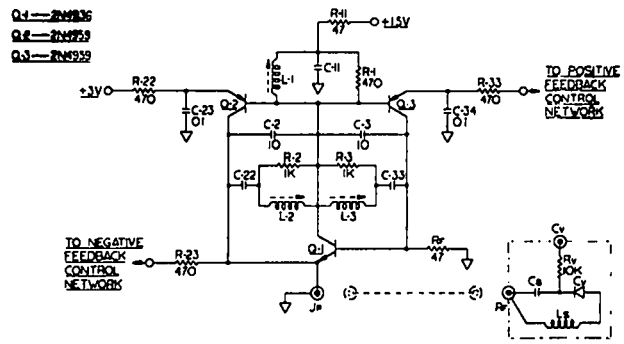

Fig. 5. Schematic of oscillator proper two-terminal marginal OSC.

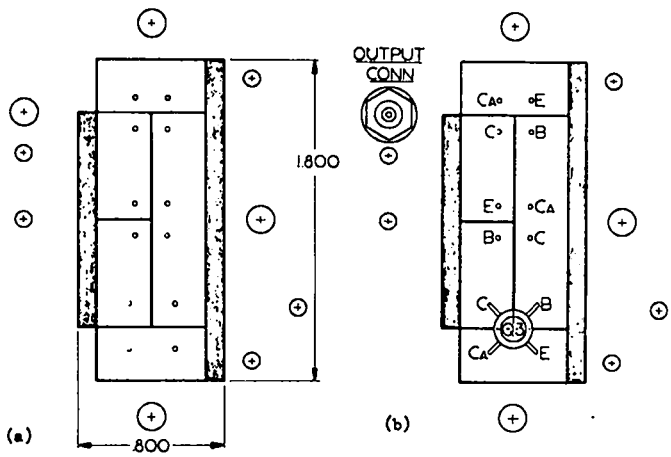

Fig. 6. (a) Bare printed circuit two-terminal marginal OSC.

(b) Output conn. and Q-3 in place two-terminal marginal OSC.

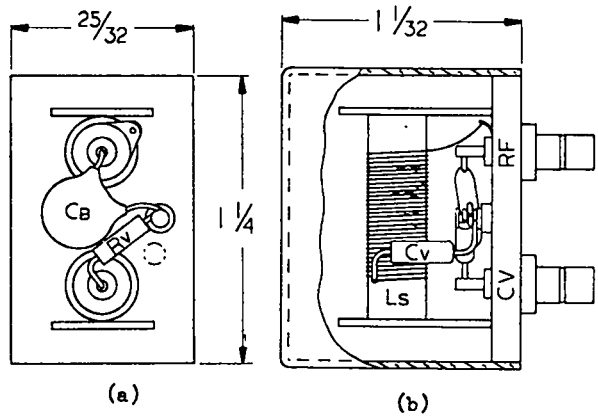

Fig. 7. (a) Probe layout less LC elements. Two-terminal marginal OSC.

(b) With LC elements in place. Two-terminal marginal OSC.

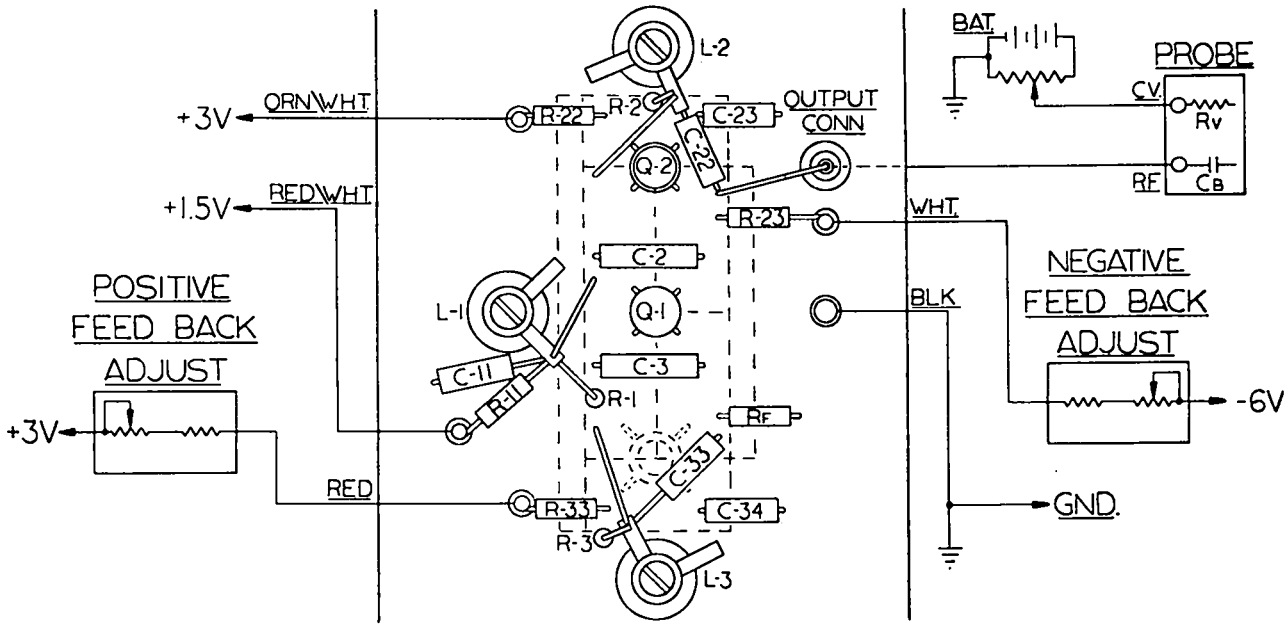

Fig. 8. Marginal oscillator showing power sources and adjustments. Two-terminal marginal OSC.

CONSTANT VOLTAGE PULSE OUTPUT SOURCE STUDY*

Francis B. Headley
Lawrence Radiation Laboratory
University of California
Livermore, California 94550

ABSTRACT

Possible methods of maintaining a constant, or nearly constant, magnitude of the pulsed magnetic field within a pulsed coil were studied. The two most promising are examined in more detail in this paper. The 2X Multi-Stage Plasma Compression Facility was used for the study comparison. The characteristics studied include resistance (R), 1 m Ω; inductance (L), 10 μH, and the corresponding time constant (TC), 10,000 μsec. This value is theoretical and would be attainable only if the crowbar circuit were to have negligible resistance and inductance. A pulse forming network (PFN) appears to be the least expensive means of maintaining a constant magnitude pulsed magnetic field. Furthermore, an impulse-operated mechanical crowbar switch connected across the coil may readily be included to prolong the pulse by forcing the field to decay slowly at the time the PFN voltage is at the point of decaying.

INTRODUCTION

Capacitor banks have been the usual source of transient energy for pulsed electromagnets. They are simple to construct, and because they are strictly a static energy storage device, require relatively little maintenance.

When an electromagnet is pulsed by a charged capacitor bank, the current rapidly builds up, essentially as a sine wave, to its peak value within a one-quarter cycle, reaching its peak in a nominal time of

$$T_r = \frac{\pi}{2}\sqrt{(L_c + L_g)(C_c + C_s)} \simeq \frac{\pi}{2}\sqrt{L_c C_c}, \quad (1)$$

where

T_r = Rise time, μsec
L_c = Pulse coil inductance, μH
L_g = Energizing source and line inductance, μH
C_c = Pulse capacitor bank capacitance, μF
C_s = Stray capacitance, μF

The circuit is oscillatory and, if left undisturbed, will oscillate with a frequency

$$f = 1/\left(2\pi\sqrt{(L_c + L_s)(C_c + C_s)}\right) \approx 1/\left(2\pi\sqrt{L_c C_c}\right) \text{ hertz.}$$

However, if the coil is crowbarred at its peak current, the latter will decay slowly, following the circuit time constant relationship

$$T_c = \frac{(L_c + L_s)}{(R_c + R_s)} \simeq \frac{L_c}{(R_c + R_s)} \ \mu\text{sec} \quad (2)$$

where

T_c = Current decay time constant in coil and crowbar circuit, μsec.
L_s = Effective shorting circuit inductance, μH
R_c = Pulse coil resistance, ohms
R_s = Shorting circuit resistance, ohms

In one time-constant period the current will decay to $1/\epsilon$ of its initial value. In five periods, it will be down to well under 1% of its value at the start of the transient. By close control of the crowbar timing, an essentially smooth transition results between the charging mode of operation and the decay mode.

From the relationship $T_c = L_c/(R_c + R_s)$ it is apparent that to prolong the current, either L_c must be increased or $(R_c + R_s)$ decreased. Increasing L_c has the inherent disadvantage that the capacitance of C_c must be increased proportionately to maintain the crest pulse current desired. This is governed by the relation

$$I = \frac{E}{Z} = E\sqrt{\frac{C_c}{L_c}} \text{ kA}, \quad (3)$$

*Work performed under the auspices of the U. S. Atomic Energy Commission.

where

E = kV across C_c

and

Z = Impedance of the pulse capacitor bank and pulse coil circuit.

Therefore, the power requirement for the rectifier power supply that charges the bank must be increased proportionately. In addition, formula (1) shows that the rise time will be increased. This is usually undesirable. The better remedy is to try decreasing the resistance of the coil and crowbar circuit. The rise time and power supply requirements are then unaffected.

Actually, for a given pulse operation requirement there is an optimum ratio of circuit component values. For a specified magnetic-field decay-time constant, the ratio of circuit inductance and resistance is established. Physical layout and economic considerations then determine the actual inductance and resistance values to be used if the coil is to be crowbarred at crest current. For the majority of pulse current applications this is the best method to date, economically and physically. However, for those instances requiring the maintenance of a relatively constant magnetic field, the application of a pulse forming network (PFN) that will maintain the current at the peak of the initial pulse current may be the best solution.

A comparison of these two methods is presented below on the basis that a 10% droop in pulse current (and voltage) over the stipulated pulse length would be permissible.

Pulse Forming Networks

PFN's have the distinct advantage over other electrical energy storage devices of being able to deliver to the load an extra high current and a high-voltage constant-current pulse over the period for which they were designed. At the end of this period all the PFN energy will have been delivered to the load, and the current will quickly collapse. Thus, an essentially rectangular pulse is delivered to the load without requiring a cutoff switch. Their limitation is that the above is true only if the effective load behaves as an essentially pure resistance.

Since an electromagnetic pulse coil is highly inductive, it would appear at first to be an unsuitable type of load for a PFN. However, if a much higher voltage, low-impedance-pulse power source were to initially establish the pulse-current level in the coil, and then a low voltage PFN (designed to supply the existing load current at the resistance voltage drop that exists across the pulse coil circuit) were switched across the circuit, it would maintain that current. The circuit and coil inductance will not now be effective, and a flat topped pulse would result.

At the end of the pulse, a rapid decay of current could cause undesirable ringing in the circuit if no preventive means were taken. The next step would logically be to crowbar the pulse coil just before the current collapses. The magnetic field would now be prolonged by the decay time constant characteristic. This dictates that from the time the current decay commences, it will continue to decrease about 63% during each time constant period. At the end of each period, about 87% of the energy existing at the start of that period would have been dissipated.

It is important to understand that the PFN is switched into the circuit only when the coil voltage is lowest (and coil current highest). Furthermore, because of the nature of PFN discharge action, practically all of the stored energy is delivered to the load. This is in sharp contrast to the use of a straight capacitor bank, in which case, even allowing a 10% voltage decay, more than 80% of initial bank energy is lost.

A typical schematic for PFN application is shown in Fig. 1. The PFN is simply a ladder network of capacitors and linear inductors, with the inductors mutually coupled to each other. When values of self-inductance and capacitance between adjacent sections are optimally adjusted, the PFN will not only be of the desired impedance, but it will deliver a practical rectangular pulse of the desired length and amplitude.

The total PFN capacitance is given by the expression

$$C_n = \frac{T_n}{2 Z_n} \ \mu F , \qquad (4)$$

and the total PFN inductance by the expression

$$L_n = \frac{T_n Z_n}{2} \ \mu F , \qquad (5)$$

where

T_n = Pulse length of PFN, μsec, and

Z_n = PFN impedance, ohms

Similarly, the PFN pulse length is

$$T_n = 2\sqrt{L_n C_n}, \quad (6)$$

where

n = Number of sections in the PFN.

The relation between network impedance, Z_n, and the components is

$$Z_n = \sqrt{\frac{L}{C}} = \sqrt{\frac{L_n}{C_n}}, \quad (7)$$

where

L = Inductance per section, μH.

C = Capacitance per section, μF.

The rise time is determined by the number of sections in the network, assuming that all capacitors are identical. For economical reasons this is usually the case. Ideally the relation is

$$t_r = \frac{1}{2}\frac{T_n}{n} \quad (8)$$

where

t_r = Rise time of wavefront, μsec,

T_n = Pulse length, μsec,

and

n = Number of sections in PFN.

However, if a larger number of sections than can reasonably be accommodated results, that number may be reduced by one-third to one-half if the increased ripple amplitude on the top of the pulse is acceptable. This is done by making one or two front sections of capacitors and inductors equal to the value calculated in equation (8), but the remaining ones may perhaps double this value, for instance. The total capacitance and inductance given by equations (4) and (5) need to be closely adhered to, however; otherwise, the pulse length will be altered. Because of the rather drastic change in section component values at the discontinuity, the components on both sides including mutual inductance must be adjusted, and perhaps even a small amount of resistance be added in the front capacitor leg.

Capacitance Comparisons

For one potential application to an existing pulse coil,

I = 500,000 amp

Δt = 3,000 μsec

Δe = 10% of coil voltage at peak current (maximum pulse voltage change allowed)

where

Δe = Drop in capacitor voltage after time interval Δt, in volts

Δt = Elapsed time of the incremental transient, in seconds

The coil was already designed and installed and could not be altered when this study was started. The resistance of the coil, plus that of the line furnishing the power from the capacitor bank, (assuming that it was installed in the most convenient location) was calculated to be 3 milliohms. Therefore,

$V_{load} = 500{,}000 \times 0.003 = 1500$ volts.

For a 10% droop, a voltage drop Δe = 150 volts.

The capacitance of a straight capacitor bank required to limit current decay to the 10% droop in 3,000 μsec, becomes very large indeed. It may be calculated by the approximate relationship that for modest fractions of the total energy loss and total transient time,

$$I \simeq C\frac{\Delta e}{\Delta t} \text{ or } C \simeq I\frac{\Delta t}{\Delta e}, \quad (9)$$

where

I = Pulse, amperes

C = Pulse power source, farads

Substituting in equation (9) above,

$$C = 500{,}000 \times \frac{3000 \times 10^{-6}}{150} = 10 \text{ farads}$$

Therefore, energy in the capacitor bank = $1/2\ CE^2$ = $1/2 \times 10 \times 1500^2$ = 11.2 MJ.

These results show that this "constant" power capacitor bank application is rather prohibitive, although the decay time constant is attractive. The time constant would be

$T_c = (R_c + R_s)C_n = 0.003 \times 10 = 0.03$ second = 30 msec.

As an alternative to a power current capacitor bank, consider a pulse forming network. Properly designed, such a network would furnish a constant average amplitude current into the pulse coil.

The amount of capacitance required is large compared to the usual applications but is appreciably smaller than for the straight capacitor bank. In the preceding application, the crowbarred coil and circuit resistance was 3.0 microhm. A constant current of 500 kiloamp was desired for 3 msec. By equation (4) the total PFN capacitance is

$$C = \frac{T}{2Z_n} = \frac{0.003}{2 \times 0.003} = 0.5 \text{ farads}.$$

For maximum power transfer and minimum ringing, source impedance should equal load impedance. Source voltage must be 3,000 V (2 × 1500), the working voltage required of the capacitors. Therefore, PFN energy, $E = \frac{1}{2} \times 0.5 \times 3000^2 = 2.25$ MJ. This value is only one-fifth the energy required to limit the voltage droop to 10% if only capacitors are used. A check of available capacitors quickly reveals that electrolytic capacitors are the only type offering high capacitance per unit volume at a reasonably high voltage. One available model having 1900 μF and a 450 working-volt rating, is about 3-in. in diameter, 6-in. long and weighs 3 lbs.

Assuming that eight capacitors were to be operated in series as a separate circuit, their effective series capacitance would be about 240 μF. For 0.5 farad, slightly over 2,000 such circuits in parallel would be required, or a total of over 16,000 capacitors.

Circuit impedance will now be considered. The resistance of the pulse coil must of necessity be very low. But for good operating efficiency, the source impedance should equal the load impedance. Now the pulse coil resistance may be anywhere between the orders of 1 microhm and 1,000 microhms. There is a practical limit to how low the impedance of a PFN may be, because the inductance coil for the network must be fairly evenly divided among all of its sections of comparable capacitance. It is necessary for the mutual inductance between sections to be about one-third to one-quarter the inductance of each section. Therefore, when the inductance becomes so low that this ratio cannot be satisfactorily maintained, a different approach is required. One remedy is to parallel the networks. The advantages are several. (a) The individual PFN impedance increases directly with the number paralleled; (b) The electromagnetic stresses within the coils decrease inversely with the square of the number of paralleled units; and (c) Available space may be utilized more efficiently by judicious proportioning of dimensions and positioning of a number of PFN's, compared with having just one unit. For the above example, the headroom was limited to 6 feet. Since it was planned to use 24 PFN's, a space 28 ft wide, 9 ft long, and 5.5 ft high was calculated to be required. This plan allows aisles between racks for ease of access to each unit.

The Crowbar Switch

The switches for crowbarring and for interconnecting the constant power pulse source into the circuit should exhibit the following qualities.

(a) Capability of reliably withstanding the high energizing pulse voltage which may range from a few kV to the 100 kV level for different applications.

(b) Capability of conducting the very high pulse currents (usually ranging between the low hundreds of kiloamperes to the middle megamperes).

(c) Low resistance, usually in the order of a few microhms maximum.

(d) Capability of an electrical closure across the low circuit voltage existing at maximum current conditions.

(e) Infrequent maintenance.

(f) Fast electrode and/or initiating fuse replacement, as required.

Three types of crowbarring switches used by industry and laboratories are spark gaps, ignitrons and mechanical switches.

Spark gaps readily qualify for condition (a), and if a sufficient number are used in parallel to bring their effective resistance low enough, they should satisfy the qualities in (b), (d), and (e) above. If (e) is acceptable, (f) is not of primary importance. However, it is doubtful that spark gaps can qualify for (a) and (d) simultaneously, except in a vacuum environment. Whether or not they can qualify for (c) will depend upon how much resistance can be tolerated.

Ignitrons qualify for condition (a) if a sufficient number are connected in series and their respective control circuits are reliably coordinated. They also qualify for conditions (b) and (c) if a sufficient number are paralleled and the crowbar circuits are arranged so that the currents within them will divide reasonably. They readily qualify for (d) and (e) only if their voltage and current short time ratings are discounted adequately for the specific

circuit conditions. Ignitrons do not fulfill the (f) consideration when replacement is necessary; however, they can be operated for innumerable times with no maintenance. Ignitrons have been used for many years for switching purposes and must be considered as being moderately successful.

Mechanical switches readily qualify for conditions (a), (b), (c), and (d). Their switch electrodes with the integral initiating fuse require replacement after each operation and they therefore do not qualify completely for (d). Other than this one drawback, maintenance of the switch assembly is minimal. Manual replacement of the contacts and fuse assembly require 1 to 2 minutes with a well-planned layout and operating procedure. A few laboratories have automatized this procedure[1] to eliminate the above shortcomings but have indicated the need for further improvements.

The mechanical switch appears to be the best switch available for crowbar operations involving high energy discharges. One mechanical switch can replace dozens of ignitron switches and their control circuitry.

One type designed in this laboratory, and now being further developed, is sketched in Fig. 2. It is a variation of the design developed at Los Alamos Scientific Laboratory.[2] Two aluminum plate electrodes are separated by a thin layer of high-dielectric-strength plastic sheeting such as polyethylene. One of the electrodes is about 0.62 cm thick and has a pair of sharp-edged parallel grooves, each about 0.62 cm wide formed lengthwise. The other electrode is of soft aluminum about 0.15 cm thick folded on itself. Inserted within the folds and insulated from them is a 3.75-cm wide, 0.005-cm thick copper foil. A rectangular hole has been cut out of the center to form two strips along the two edges about 7.5 cm long and 0.75 cm wide. Their spacing is the same as for the grooves of the other electrode. When installed into the switch, the two electrodes are positioned facing each other so that the grooves in one electrode and fuse strips within the other are aligned.

To initiate the switch closure, the fuse strips are vaporized by discharging roughly 1 kJ of energy per 2.5 cm length of fuse strip. The resulting explosion displaces the thin aluminum into the mating grooves, shearing the insulation between electrodes along the groove edges. The insulation strips are forced to the bottom by the deforming aluminum, which proceeds to make intimate contact with the sides of the grooves. The depth of the grooves should be such that the aluminum is not sheared or drawn down in thickness by more than half its thickness. The width of intimate contact along the sides of the groove varies considerably but appears to average about 0.075 cm. The resistance through two aluminum segments 0.075 square cm each side of the mating surfaces for the full 7.5 cm length of electrodes in calculated to be slightly less than 1 microhm, assuming the aluminum is completely intact. It appears reasonable that, because of the intimate contact of the contact surfaces, this value will not increase more than two or three times calculation. After each crowbar action the two switch electrodes, the insulated fuse unit, and the major insulation between electrodes must be replaced.

Other Methods Considered

Other possible methods of obtaining constant, or relatively constant, high pulse currents were studied, but they did not appear to hold any promise for our applications. These methods included homopolar generators with a heavy flywheel for storing the excessive momentary energy required, alternators backed up by a flywheel and rectified with silicon diode banks, batteries, pulse transformers, and inductive energy storage schemes, singly or, in some instances, in combination. Each appeared to be either impractical or not sufficiently developed for present consideration. The 1-MJ inductive energy storage method reported by Princeton University[3] was considered promising. It operated on the principle that as energy drains out of the large inductor, an oscillatory frequency controller speeds up to maintain a relatively constant L(di/dt) voltage output.

If economics can be ignored the most ideal method would be to develop a cryogenic pulse coil system. The system could then be pumped up to the high current desired and operated steadily at that amplitude.

Conclusions

Pulse-forming networks, rather than the

usual decaying current resulting from capacitor banks, are worthy of serious consideration for those applications for which constant pulse current is desirable.

Mechanical switches are favored over triggered spark gaps and ignitron tubes for high-current crowbar applications.

References

1. D. L. Smart, "A Survey of the Development of Solid Dielectric Switches at Culham Laboratory," fourth Symposium on Engineering Problems in Thermonuclear Research, Frascati, Rome, Italy (1966).
2. V. A. Finlayson, Doctoral Thesis, "An Exploding Foil Driven Switch for Short-Circuiting a Theta Pinch Coil," submitted to the Univ. of Utah (1968).
3. E. D. Simon and G. Bronner, "An Inductive Energy Storage System using Ignitron Switching," Symposium on Engineering Problems of Controlled Thermonuclear Research, Livermore, California (1965).

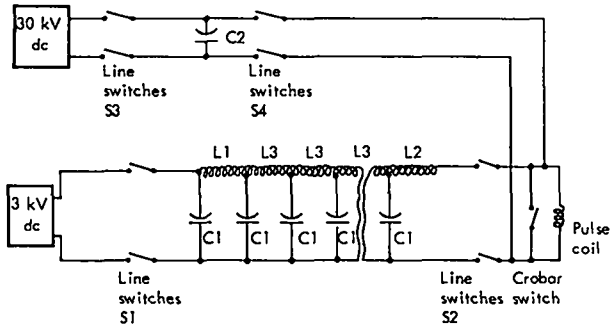

Fig. 1. Pulse-forming network schematic.

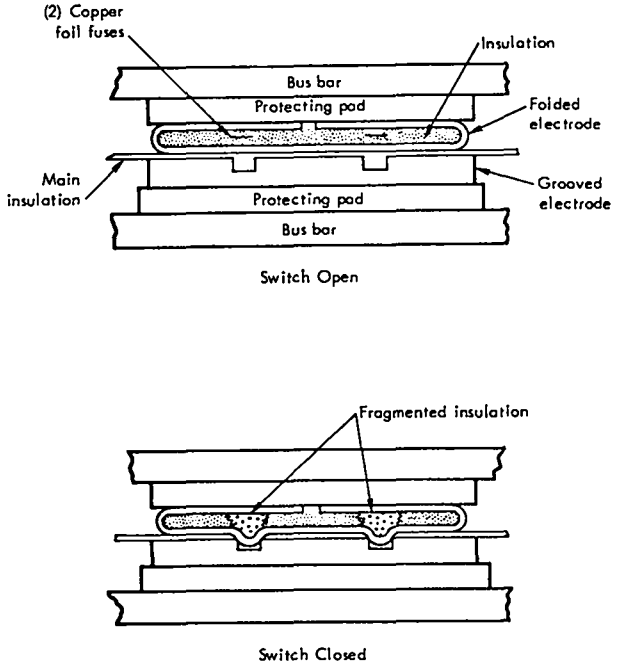

Fig. 2. Cross section of mechanical switch electrodes.

LIQUID RESISTOR DEVELOPMENT *

by

Roy A. Haarman
Los Alamos Scientific Laboratory
University of California
Los Alamos, New Mexico

ABSTRACT

Recent efforts at Los Alamos to develop a liquid resistor are described. In certain circuits containing parallelled groups of high voltage energy storage capacitors, a danger exists if a charged capacitor shorts or prefires. The energy from the adjacent groups, if large enough, will tend to discharge into the faulty capacitor and cause a violent rupture. This danger can be eliminated by either: 1. Installation of a high voltage D. C. fuse to isolate the faulty capacitor 2. Installation of a resistor that will dissipate the energy from the adjacent capacitors. In the Scyllac Project, circuit parameters require that the resistor be a 60 KV, 2000 ohm unit capable of dissipating 680 x 10^3 joules, with a discharge time constant of 0.8 seconds. Calculations and experiments indicate that a liquid resistor can meet the requirement and be undamaged by repeated discharges, eliminating replacement problems.

Basically the liquid resistor consists of two metal electrodes separated by an aqueous salt solution. Brass electrodes with a $CuSO_4$ electrolyte and stainless steel electrodes with a K_2SO_4 electrolyte were tested. The liquid resistor dissipates the energy in the form of heat according to the relationship $Q=MC\Delta T$, where ΔT is the temperature rise of the electrolyte.

Various tests were performed to verify the energy absorbtion characteristics, temperature coefficient effects, polarization tendencies and electrolysis measurement for electrode-electrolyte compatability. The procedures, results and conclusions of these tests are presented in this paper.

Introduction

The need for a resistor capable of absorbing large amounts of energy was recognized in the design of the energy storage charge system of Project Scyllac. Conditions during the operation and charge cycle of Scyllac required a resistor that could function as a 2000 ohm charge resistor carrying a 24 ma cycled current and also could periodically absorb 680 x 10^3 joules. It was apparent from observations on similar electrical systems in operation at Los Alamos that the conventional vitreous enamel wire wound resistor was not satisfactory in the particular application mentioned above; however, a study of the characteristics of liquid resistors appeared to indicate that liquid resistors could be utilized for such an application.

It should be emphasized that our approach to develop a liquid resistor for Scyllac was strongly influenced by the fact that a total of 800 liquid resistors was required; therefore, economics was introduced as one of the primary considerations in the design of the resistor. Free machining brass (61.5% Cu, 3.0% Pb and 35.5% Zn) and free machining type 303 stainless steel were the two electrode materials chosen for developement.

Application

The energy storage charge system of Scyllac consists of a constant current network and D. C. Power Supply providing constant D. C. current to charge the energy storage capacitor bank. A typical

* Work performed under the auspices of the U. S. Atomic Energy Commission.

capacitor bank consists of 36 parallelled modules of 6 capacitors each (see Figure 1). In the event that a capacitor in any module should short or prefire during the charge cycle, the other modules will dump their energy into the shorted capacitor. In the worst case, i. e. when the capacitor bank is at full voltage, the dumped energy would be 680 x 10^3 joules.

In the past, fast-acting D. C. fuses were installed in similar systems (Scylla I-A and Scylla IV) to isolate the modules in the event of such an occurrence. This was not entirely satisfactory because after a normal charge and fire sequence, a certain residual voltage is left on the modules. This potential difference exists between the parallelled modules until the modules stabilize their voltages. In the absence of any isolating resistances between modules this voltage stabilizing causes a large instantaneous circulating current that actually opens the fuses. Wire wound power resistors were added in series with the fuses in an attempt to limit the circulating current, however the result was that the resistor would often open before the fuse. In any event, replacement time and costs were incurred for each malfunction.

It is apparent therefore, that a unit installed as an isolating device between modules that has characteristics of a resistor capable of absorbing 680 x 10^3 joules at 60 KV would have direct applicability in Scyllac. The liquid resistor appears to have the characteristics suitable for use as such a device.

Test Results

Various tests were performed to evaluate those parameters of the resistor which appeared to be most important to the ultimate goal - the design of a liquid resistor for Scyllac. Consequently, certain aspects were investigated more thoroughly than others. It should be stressed that there were other factors that would have been considered had the developement of a general-type liquid resistor been desired. Basically the tests consisted of investigation in the following areas:

1. Heat dissipation qualities
2. Resistance - concentration characteristics
3. Resistance - electrolysis and polarization effects.

In conjunction with the above observations it was possible to ascertain certain mechanical features important to the final design, such as electrode configuration, tubing material and resistor orientation.

1. Heat Dissipation Qualities

The heat dissipating characteristics of the resistor can best be described by:

$Q = MKC(t_2-t_1)$

Where Q is the quantity of heat added in joules
M is mass of substance in grams
K is constant = 4.18
C is specific heat ≈ 1
(t_2-t_1) is temperature increase

In Scyllac the worst case single dump will be 680 x 10^3 joules. Rather than design the resistor to take just the one dump it was considered that 3 dumps in succession was a more practical design limit. The amount of liquid required to absorb 2040 x 10^3 joules, with a total temperature increase not exceeding 60 degrees C is 8.134 liters.

Simply stated, the testing for heat dissipation qualities consisted of passing a constant D. C. current through the electrolyte for a certain period of time and observing the temperature rise of the electrolyte. The power source used for the tests consisted of a saturable reactor controlled 10 KV 7 amp D. C. power supply. The constant current source was used to simulate as nearly as possible the total energy condition, because no stored energy was available to dump the required energy into the resistor with a practical time constant. Tests on various liquid resistors yielded comparable results showing that the observed temperature rise very nearly equals the calculated temperature rise. Typical results of one such test are shown on Table 1. It should be noted that the total duration of the test was approximately 10 minutes; therefore, no significant cooling was encountered between the 30 second energy applications. The resistance of the resistor decreased from an initial value of 650 ohms to a final value of 420 ohms in the total 58 degree C temperature increase (demonstrating the negative temperature coefficient). In many electrical circuits such a change in resistance would be unacceptable, however for the Scyllac application this decrease in resistance would be within the limits of

acceptability.

2. Resistance - Concentration Characteristics

Since the amount of salt added to the water of the electrolyte directly determines the ion-concentration of the resistor it is important to optimize the mixture. In the brass - $CuSO_4$ system the amount of Cu^{++} ions in solution is very important because the conductivity of an electrolyte is greatly dependant upon the ion-concentration. The Cu^{++} ions from the salt are attracted towards the cathode where they form Cu^{o} (metallic copper). At the anode Cu^{++} are withdrawn from the brass. Any depletion of the ions would naturally cause a change in the conductance of the electrolyte. It is advantageous to be able to construct the resistor such that the salt concentration be kept fairly high. Figure 2 represents the resistance-concentration characteristics of three types of resistors tested. The primary difference between the Scyllac and Scylla IV resistors is the electrode separation. (Scyllac - 28-3/16", Scylla IV - 15-1/16").

It is obvious from the curves that generally it is advantageous to have a higher salt concentration since any possible loss by chemical reaction of the ion-concentration would have a smaller effect on the total resistance. The expression for the resistance of a sample of material is:

$$R = \frac{\rho\, l}{A}$$

Where R = observed resistance

ρ = resistivity

l = length of sample

A = cross-section area of sample

By increasing the length or decreasing the cross-sectional area of the resistor it may be possible to design a higher concentration resistor. This was done for some liquid resistors which had a much smaller energy requirement. It was practical to construct a resistor of 2 inch I. D. with the resulting concentration of 0.5% for 2000 ohms.

It should be noted that the statement of a particular resistance value for a liquid resistor should also include the current value at which the resistance is measured. The conductivity of an electrolyte is a function of many factors including temperature, applied voltage ion concentration and frequency.[1] It is obvious that a different value of resistance will be observed at various voltages. This could be a source of concern if one were to attempt to measure the resistance of the resistor with an ohm-meter because another method of resistance measurement might give an entirely different result. This can easily be demonstrated by placing a D. C. power supply across the resistor and recording the values of current at various voltage settings. Due to the increase of ion speed as the applied voltage increases, the resistance value will decrease quite noticeably (Wien Effect).[2]

3. Resistance - Electrolysis and Polarization Effects

The phenomena of electrolysis and polarization were perhaps the most challenging because they offered the greatest possibility of extreme resistance variations within the electrolyte. In Scyllac it is felt that the resistor can function properly in the circuit as an energy absorber as long as the resistance is maintained within fairly liberal limits (a 100% or 200% change would be no great problem). Since the Scyllac resistor contains a fairly low amount of salt it is assumed that any resulting loss in ions due to chemical reactions could result in an extreme resistance variation.

Basically, two types of life tests were run. The anticipated cycle of charging current for Scyllac will be 30 seconds on and 5 minutes off. The first type of life test to be run was an accelerated test in which a constant current of 24 ma was passed continuously through the resistor for a period of approximately 7 days (equivalent to 20,000 charging cycles without the 5 minutes off per cycle). Voltage readings were noted periodically and the resulting curves drawn (see Figure 3). It was apparent from the data that the $CuSO_4$ was more affected by the current, but still within acceptable limits. Subsequent tests run on the Scylla IV liquid resistors indicated that the ion-depletion that might occur during the life of the resistor was a genuine concern. After only an equivalent 350 charging cycles the resistance did change quite drastically (see Figure 4). It was decided to attempt to observe the phenomenon more closely; therefore, samples of the electrolyte were withdrawn periodically and analyzed for Cu^{++} content by a spectrophometric method. The samples were also analyzed for pH content. It was

anticipated that these observations would verify that the Cu^{++} concentration was decreasing. Results indicated that such was the case and that as the resistance increased, the amount of Cu^{++} ions within the electrolyte decreased and the pH factor increased. It was concluded that the Cu^{++} ions were being removed from solution and forming $Cu(OH)_2$. An interesting observation of the pH variation occurs at the knee of the curve in figure 4. At this point the pH went beyond 7.0 (neutral) and $Cu(OH)_2$ indeed started to precipitate. It was felt that perhaps the addition of H_2SO_4 would keep the solution acidic and prevent the formation of $Cu(OH)_2$. It was apparent that the H_2SO_4 helped somewhat but not significantly. It appears that the addition of H_2SO_4 increases the electrolysis of water. Since the cathode reaction where H_2 gas is liberated is more efficient than the anode liberation of O_2, the pH is rapidly increased; therefore the solution becomes basic in either case. In an effort to determine whether the over-all ion concentration of the electrolyte had decreased, the electrolyte was stirred after having experienced its greatest resistance variation. The result of the stirring was that the $Cu(OH)_2$ redissolved and the resistance returned to its original value. This fact is an indication that the real cause for the extreme resistor variation is concentration polarization.

Fundamentally, concentration polarization can best be described as being caused by the existence of an area of ion depletion around the cathode and an area of ion abundance around the anode.[3] Polarization occurs to varying degrees in all electrolytes which are conducting current. Certain compensating processes occur in the electrolytes (diffusion, ion migration, etc.) which tend to overcome the concentration polarization and the rate of the compensating processes is the important factor in determining the degree to which the electrolyte will polarize (assuming a constant current density). Obviously the compensating processes in $CuSO_4$ were not sufficient to prevent polarization; therefore, the accelerated life tests were not a true indication of the 30 sec-5 minute cycle of Scyllac.

Taking the above observations into account a second type of life test was run which consisted of actually cycling the resistor for 30 seconds on and 5 minutes off. The results of this test (see Figure 4) were somewhat encouraging but not the final answer because polarization still occurred although not as rapidly. A modified method of increasing the diffusion rate was to gently agitate the electrolyte by passing a small quantity of compressed air through the resistor constantly. This effect increased the life of the resistor by a large factor and confirmed the fact that concentration polarization was responsible for the formation of the $Cu(OH)_2$, thereby causing the variation in resistance.

It should be emphasized that this polarization was only a problem in the Scylla IV resistor, primarily because the initial ion-concentration was so low. This indicates the importance of attempting to raise the level of ion concentration in a liquid resistor as high as possible to prevent the tendency of the electrolyte to polarize.

Long term corrosion of the electrodes may also have a significant effect on the lifetime of the resistor. Because the solutions used are somewhat dilute, this is not thought to be a serious problem. It was not possible to design meaningful tests to verify this. If corrosion does produce adverse effects it may be possible to bubble nitrogen gas through the electrolyte in order to retard corrosion. A secondary effect of the gas would be to agitate the solution and prevent concentration polarization.

Conclusion

It is possible to make the following statements regarding liquid resistors based on the limited testing that was performed.

1. Liquid resistors can dissipate rather large amounts of energy with a predicted temperature rise.

2. The amount of salt required to obtain a required value of resistance should be maximized by careful design considerations regarding electrode size and separation.

3. The choice of electrode and electrolyte materials depends upon the application required of the resistor. Brass - $CuSO_4$ appears satisfactory as an economic resistor for the Scyllac application. (Cobra brass electrodes are approximately 2-1/2 times cheaper than stainless steel 303).

4. In order to maintain a fixed value of resistance, careful consideration must be given to

electrode-electrolyte materials (i. e. platinum electrodes would present no contamination problem), electrolyte temperature and polarization tendencies. One possible method of maintaining fairly constant resistance would be to circulate the electrolyte by some method. This could keep the temperature constant and eliminate any polarization.

5. Distilled water should be used because tap water may contain too many impurities to be able to predict their characteristics.

Probably the most important general conclusion that can be made, based upon the tests described in this paper, is that the liquid resistor is a specialized device that is quite sensitive to many factors. The results obtained from one configuration are not necessarily applicable to another configuration and it is advisable to test prototype of the particular resistor contemplated.

A sketch of the final design of the Scyllac resistor is shown on Figure 5. It is vertically oriented so that the Cu^{O} metal formed (mostly as nodules or trees) will collect at the bottom. The metal formed has virtually no effect on the overall resistance. The upper electrode is curved to eliminate the capture of bubbles on its under surface. The top support has air-escape holes to prevent a buildup of pressure and the container is an extruded material that is not prone to checks or splits. A fully charged 0.9 mf 75 KV capacitor has been repeatedly dumped into the resistor with no sign of arcing.

Acknowledgments

Many helpful suggestions and the major design consideration were provided by James J. Banta and I gratefully acknowledge his assistance. Harry Hecht and S. W. Rabideau were also very helpful in providing additional insight into the chemical processes involved by suggestions and analysis of results.

References

1. W. Mosch, "Physical Bases of Practical Liquid Resistors for Impulse Voltages", Dtsch. Elektrotech, Vol. 9, No. 6, 214-18 (June 1955).

2. S. Glasstone, Introduction to Electro-Chemistry (D Van Nostrand Co., 1942), pp 79-105.

3. A. J. Allmand, H. J. T. Ellingham, The Principles of Applied Electrochemistry (Edward Arnold & Co., London, 1931), pp 82-85.

TABLE I

LIQUID RESISTOR - STAINLESS STEEL W/ K_2SO_4
2380 GMS., LENGTH = 21", I.D. = 2 3/4"

TIME DURATION (SEC.)	AVERAGE VOLTAGE (VOLTS)	AVERAGE CURRENT (AMPS)	OBSERVED ΔT (°C)	CALCULATED ΔT (°C)
30	1950	3.0	23.0	17.6
30	1661	3.0	15.0	15.0
31	1440	3.0	12.0	13.1
30	1260	3.0	8.0	11.4
		TOTAL	58.0	57.1

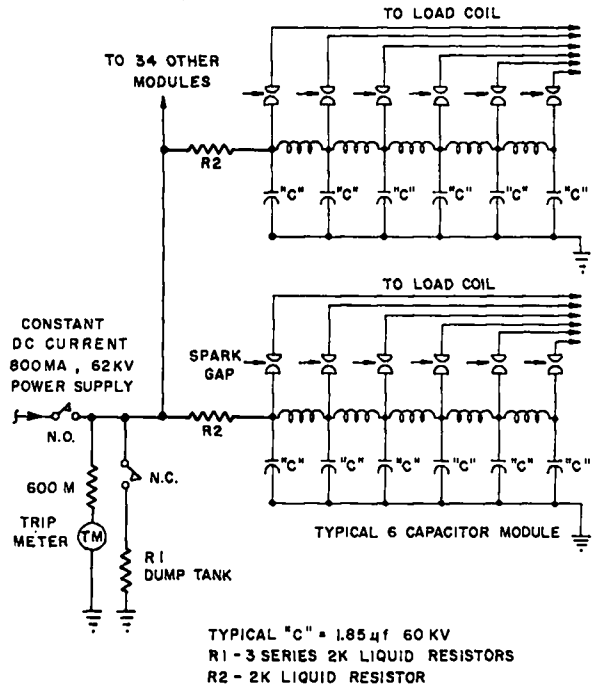

TYPICAL "C" = 1.85 μf 60 KV
R1 - 3 SERIES 2K LIQUID RESISTORS
R2 - 2K LIQUID RESISTOR

FIGURE I
PORTION OF SCYLLAC CHARGE SYSTEM

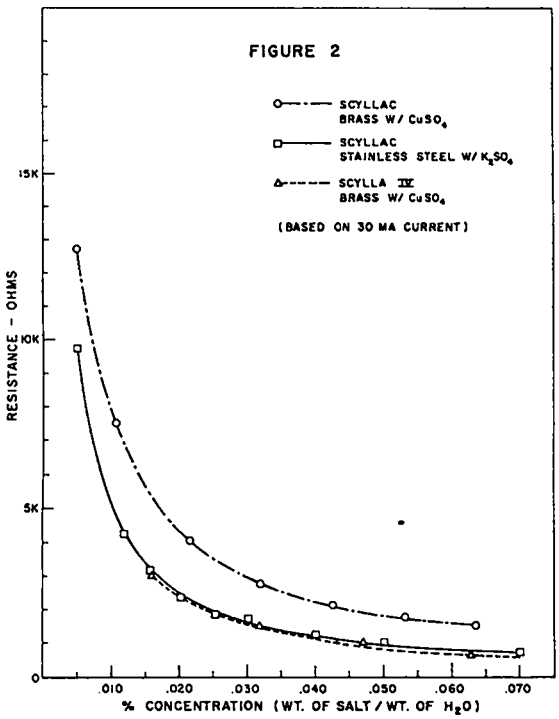

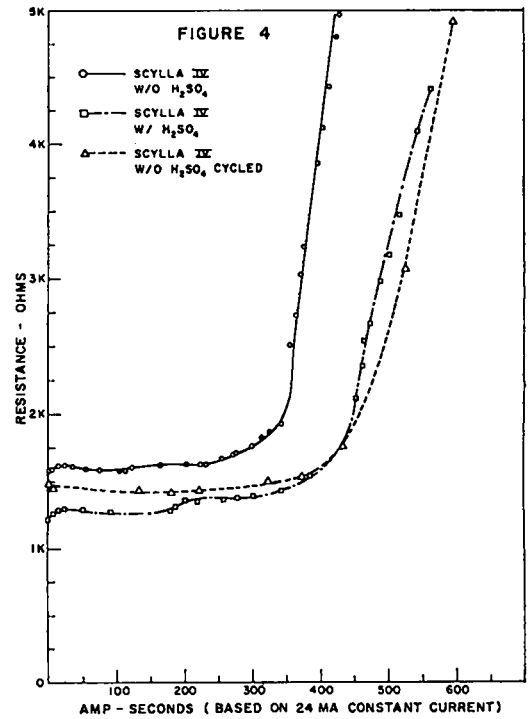

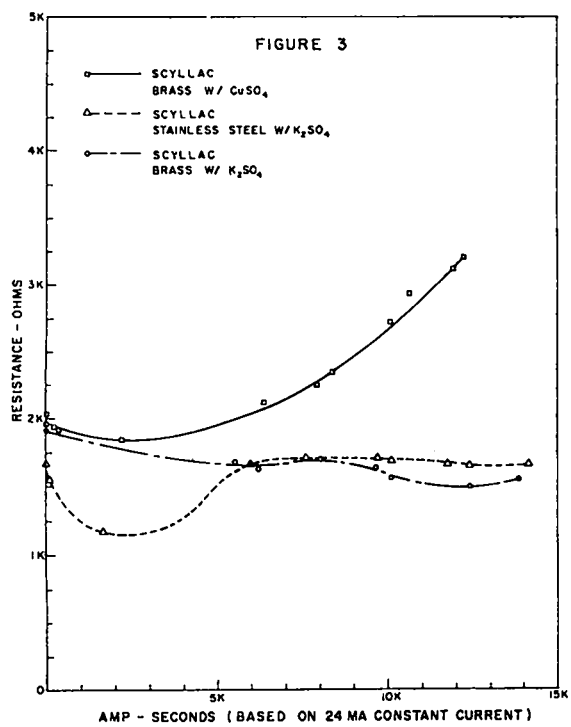

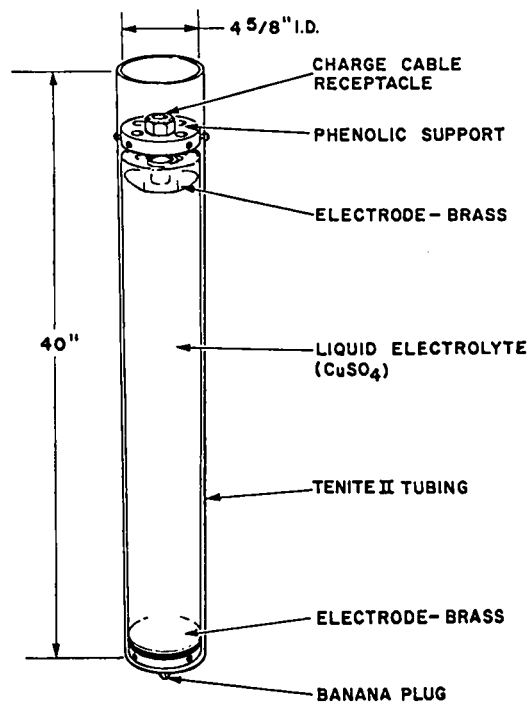

SCYLLAC LIQUID RESISTOR
FIGURE 5

SKIN-EFFECT PULSE TRANSFORMERS*

by

Robin J. Harvey
Stevens Institute of Technology
Hoboken, New Jersey

ABSTRACT

Efficient coupling of magnetic flux between two coils may be accomplished without the need for an iron core if the coils are wound in the proper way from a strip of low-inductance transmission line. The band pass of such a transformer extends from the lower limit imposed by the finite skin depth of the conductors to the cutoff due to capacitive coupling (or the speed of light to coil circumference ratio). In the case of the power-pulser-high-voltage-isolation transformers which we have built for use on the Chalice experiment the band pass is roughly 50 kc - 50 Mc. The design and construction of such "skin-effect" transformers is discussed with particular emphasis upon applications involving medium to high energy transfer (1 to 10^6 joules).

Introduction

The efficiency of the "iron-core" transformer stems from the high permeability of the core and the subsequent concentration of magnetic flux necessary for good coupling. Since a given mass of core is capable of storing a maximum amount of magnetic energy without saturating, transformers handling large amounts of energy are necessarily massive. At frequencies where the skin-depth of the metal is shorter than the core dimensions one of several variations involving laminated or powder construction must be employed.

It is the purpose of the paper to note that the skin-effect may be used to concentrate flux and thereby eliminate the need for a high-μ core. Such an air-core transformer may be readily wound from a flexible strip of parallel-plate transmission line (Fig. 1). If the frequency is high enough then the magnetic field will be excluded from the metal and forced to link the flat coils. The leakage inductance will be essentially the same as the transmission line inductance. If the ends of the strips are folded over, or right-angle tabs are included on the strips, then the in-put and out-put connections may be made to be of the parallel-plate type and their characteristic impedances matched to the rest of the circuit.

The exploding-wire-solid dielectric switches of the CHALICE experiment have required high-voltage isolation transformers to couple them to their respective low impedance pulsing units. Two one-turn transformers, 1 3/4" D, 1" L transformers with two out-puts (Fig. 2a) have been used in conjunction with a 5kv, 6μf, exploding-wire switched pulser to drive four separate solid-dielectric switches simultaneously. With the introduction of the self-crowbarring switch in the CHALICE system the need for four series and four crowbar switches was removed. The single switch insert is now triggered through a five-turn transformer (Fig. 2b) by a 3kv, 2μf, krytron switched pulser.

Table I

Symbol		Description	Formula
L_o	=	Load inductance	
N	=	Primary turns	
L_p	=	Primary transformer inductance	$= N^2\mu_o\pi r^2/\ell$
L_ℓ	=	Transformer leakage inductance	$= N\mu_o 2\pi r d/\ell$
r	=	Mean winding radius	
d	=	Insulation thickness	$\ll r$
ℓ	=	Winding width	$\gtrsim \frac{2}{3} r$
C_ℓ	=	Leakage capacitance	$= \varepsilon_o 2\pi r\ell/Nd$
C'	=	Interstage capacitance	$= \varepsilon_o 2\pi r\ell/d$

Table I Continued

Symbol		Description	Formula
Z	=	Source impedance	
δ	=	Skin depth	= $(2/\mu_o\sigma\omega)^{1/2}$
ω	=	Operating angular frequencies (must accomodate desired rise-time and pulse duration)	

Conditions for efficient operation include:

$$\omega L_p^N >> \omega L_o, Z$$

$$1/\omega C_\ell >> Z >> L_\ell \omega$$

Design Criteria

The first consideration in the design of any transformer is the specification of the source and load parameters. We have been concerned with coupling a pulse from a low impedance (capacitive) source to a D.C. high-voltage isolated, low impedance load. In the case of a linear-response, 1:1, transformer the constraints on the design are principally that the primary inductance be an order of magnitude higher and the leakage impedances be an order of magnitude lower than those of the source and load. These and other constraints are listed in Table I.

In practice, the primary inductance is proportional to the total area of a winding, the number of windings squared and inversely proportional to the width of the windings:

$$L_p^N = \mu_o N^2 \pi r^2 / \ell$$

The width of the windings ℓ must be larger than $2/3r$ if the magnetic field within the solenoid is to be uniform to within a few percent.[1] Taking $\ell \cong 2/3r$ yields

$$L_p^N \cong \tfrac{3}{2} \pi \mu_o N^2 r .$$

The leakage inductances may be calculated in two equivalent ways: by considering pairs of windings as transmission lines, or by assuming that L_ℓ is given by the ratio of the exposed edge area between windings to the total area of the windings times the single turn primary inductance

$$L_\ell = \frac{N 2\pi r d}{\pi r^2} L_p' = \frac{2d}{Nr} L_p^N \cong 3\pi\mu_o N d.$$

If $L_p^N >> Z/\omega >> L_\ell$ then Nr must be two orders of magnitude larger than 2d (the insulation thickness).

The interstage capacitance may be minimized by winding the primary and secondary turns separately. This also requires only one layer of high voltage insulation between the primary and secondary to suffice for isolation. The leakage capacitances of the individual windings are in series and lead to a net leakage capacitance of

$$C_\ell = \frac{\varepsilon_o 2\pi r \ell}{Nd} .$$

The natural frequency of such a transformer is then

$$\omega_\ell = \left(L_p^N C_\ell\right)^{-1/2} \cong \frac{c}{2\pi R}\left(\frac{2d}{Nr}\right)^{1/2}$$

$$\cong c/20\pi r .$$

This is the cut-off frequency or the upper limit of response of a skin-effect transformer due to capacitative leakage. The load and source impedances will impose conditions upon the response characteristics independently to the self-imposed cut-offs. In terms of wave length

$$\lambda_\ell \cong 20\pi r .$$

There is yet another cut-off due to the length of the windings. In this case the pulse will be transmitted through the transformer but will be distorted by the time lag as it circumnavigates

the windings. Here

$$\lambda = 8\pi N r$$

When $N \geq 3$ this will yield the upper frequency limit.

The ultimate lower frequency limit is fixed by the skin depth and the conductor thickness, t,

$$t \geq 2\delta$$
$$\omega \geq 8/\sigma\mu_0 t^2 .$$

Test Results

In an effort to establish the energy transferral efficiency of the five-turn air-core transformer, a set of wires of fixed diameter and of varying lengths were exploded with and without transformers (Fig. 3). The 9 joule 3kv, krytron pulser was used as a source and a 6 lb laminated Hypersil core with ten windings was used for comparison. It was found that both transformers would explode only 3/4 of the length of wire normally exploded by the pulser alone, yielding efficiencies of 75%.

It should be noted that the load impedance was that of a 0.003"D copper wire 2" long. With a shorter wire, the efficiencies would change. In fact, the time required to explode a wire of resistance R, and heat of vaporization E, with a sinusoidal current pulse from an L-C source ($R<\omega L$), is given by:

$$T = \left(3E/RI_0^2\omega^2\right)^{1/3} = \left(3E/R\right)^{1/3}\left(L/V_0\right)^{2/3}$$

where $I_0 = CV_0\omega$, $\omega = (LC)^{-\frac{1}{2}}$, and V_0 = the initial charging voltage.

The iron core was found to lengthen and decrease the pulse waveform. Moreover, the detonation time of a solid-dielectric switch with a 1/8" long wire was either erratic or did not take place at all. The air-core transformer showed a 25% reduction in current but no loss in rise time with detonation occurring reproduceably.

Conclusions

Once a transformer has been constructed with the proper response characteristics, the upper limit on the energy, voltage, and current will be determined by the dielectric and mechanical strengths of its constituent parts. The maximum energy that we have attempted to transfer has been 75 joules, but there is no reason to doubt that the same transformer would handle several orders of magnitude more energy.

References

1. R. Harvey, G. Yevick, and G. von Voros, Proc. of 1966 Symposium on Eng. Probs. of CTR, Oak Ridge National Lab. Conf. 661016, p. 221.

* Supported by the Atomic Energy Commission.

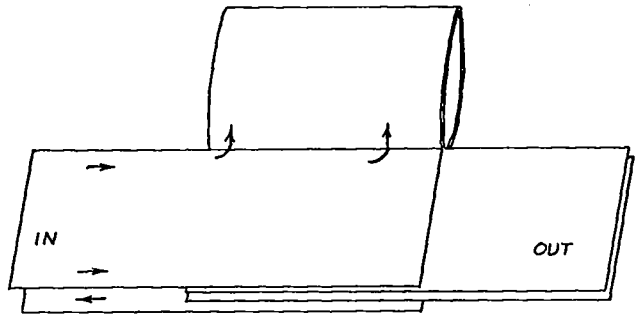

1. Schematic drawing of a 1 turn skin-effect pulse transformer.

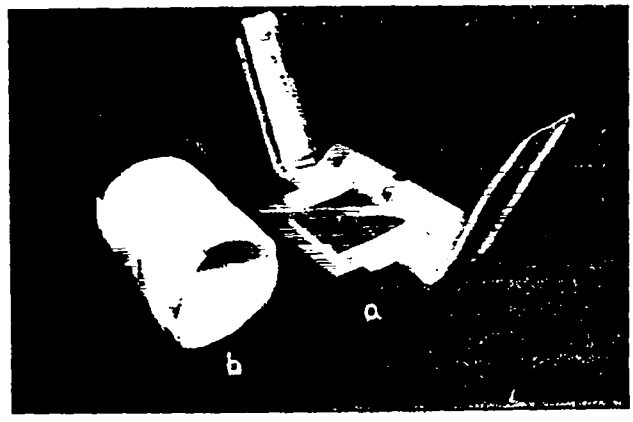

2. High-voltage isolation transformers: a) 1 turn, 1 input, 2 output transformer b) 5 turn 1:1 transformer.

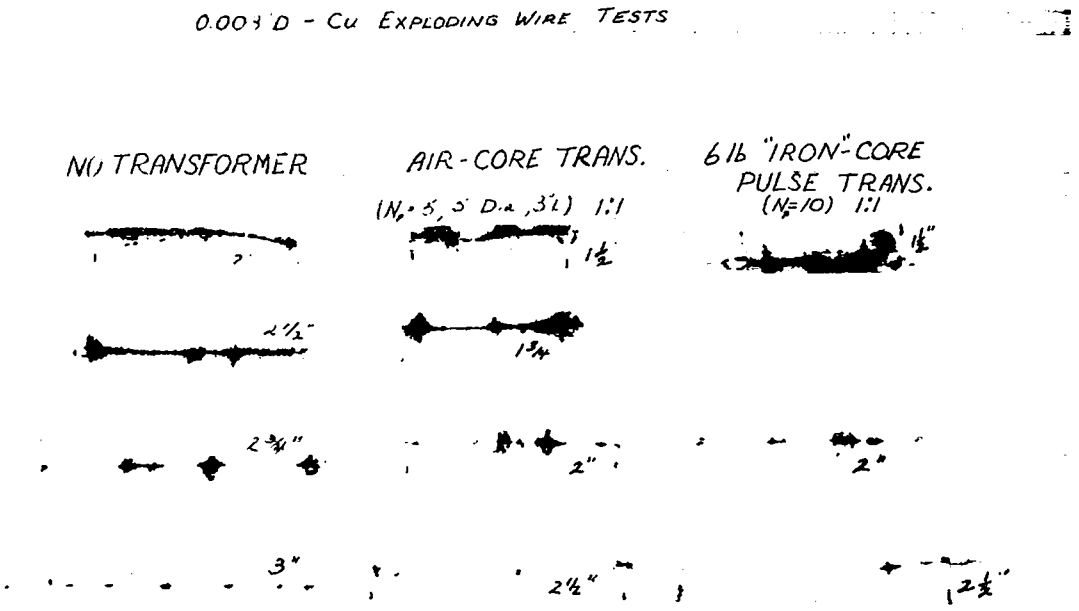

3. Exploding wire dielectric test. Equivalent results are compared as to wire length.

A HIGH PERFORMANCE, PROGRAMMABLE 25-kV, 2-A POWER SUPPLY*

A. F. Waugh
Lawrence Radiation Laboratory
University of California
Livermore, California

ABSTRACT

This paper describes the performance, circuit and construction features of a 50-kW, HV, precision programmable voltage-regulated, dc power. supply. This system is used as a HV power supply for an ion source Its high voltage output is applied across the extraction apertures of the ion source to create the high field gradient required to extract an ion beam from the source plasma discharge chamber.

The output voltage is adjustable from 200 V to 25 kV. The maximum continuous load current is 2 A. The output voltage is regulated to within ±0.05% for ±5% line and ±10% load changes. The peak-to-peak output ripple and noise do not exceed 5 V. An adjustable current limit feature causes the regulator system to instantaneously change from voltage regulating mode to current limiting mode at the current limit set point.

It is possible to modulate or program the output HV from a low-level input signal with a gain of 1000. The output may be modulated to a peak-to-peak amplitude of 20 kV at up to 100 Hz and for linearly decreasing amplitude vs. frequency down to 100 V at 10 kHz.

All of the regulation and control is done by a single water-cooled power-tetrode series pass tube in the HV output line. The remainder of the control circuitry consists of pc-board-mounted solid-state components and discrete circuit elements. The grid of the HV regulator tube is driven by a single power transistor.

A key component in the regulator loop is a photon-coupled isolator. This wide-bandwidth, signal-coupling element consists of a gallium arsenide electroluminescent diode infrared source and a silicon PIN photodetector. This device is used to couple the output of the ground potential regulator amplifier up to the series pass-tube control circuit which is floating at the output high voltage.

INTRODUCTION

A rugged, versatile, high-performance, high-voltage power supply has been needed by the Ion Source Development effort in support of the Alice Machine Program at Livermore. We believe we now have such a supply. This paper briefly describes it.

Such a power supply, in the 5-kV to 30-kV, 1- to 2-A range, is required to provide the accelerating high-voltage extraction potential in the high beam current hydrogen or deuterium ion source systems. The reasons why an outstanding high voltage supply is required are mainly two-fold.

First, the LRL calutron-type ion source requires an accelerator high-voltage supply, voltage regulated to about 0.05% of the nominal output. This is because immediately after extraction, the ion beam is bent through a 90° arc by a transverse magnetic field and then sent down a long, collimated beam tube. The beam trajectory is critically dependent on maintaining precise, matched values of accelerator voltage and bending magnet field strength.

Second, the calutron, duo-plasmatron, Von Ardenne, RF ion sources and variations of them all present a peculiar, troublesome load charac-

*Work performed under the auspices of the U. S. Atomic Energy Commission.

teristic to their high-voltage power supplies. The output of the high-voltage supply is applied across two exit orifice extraction electrodes of the ion source, one of which is grounded. The high-voltage gradient thus produced across the exit orifice gap extracts the beam of possitive ions from the source gaseous discharge chamber. Due to gas impurities, surface outgassing and other unknown causes, the extraction gap does break down randomly and repeatedly at an average repetition rate of 2 to 5 per second. Only if the initial fault currents can be instantaneously limited are these arc-downs self-clearing.

SPECIFICATIONS FOR THE SUPPLY

A search of the industry catalog literature did not turn up any power supply having the needed capabilities. It was decided to write a comprehensive specification requesting all the performance capability and construction features we would want and that the present state-of-the-art could provide. The result of this effort was LRL specification LES-21240, a 34-page volume.

A philosophy adopted early in the specification writing effort was that we would ask for only that performance which could be verified by relatively simple, direct tests at the vendor's plant. A full schedule of tests was written into the specification as an integral part of it. The value of this approach was subsequently well proven. Had we accepted the finished power supply on the basis of initial superficial operation, it would have been shipped to us with several serious deficiencies. Instead, all deficiencies revealed by the tests were corrected by the manufacturer, and the delivered supply met or exceeded all the requirements of the specification.

The following is a much abbreviated description of the power supply as per the specification:

Output Requirements

Adjustable from 3-kV to 25-kV, with a manual output control resolution of 0.05% or better of maximum output.

Positive output, negative grounded. Maximum continuous current, 2 A.

Input Power

480 V, 3 ϕ, 60 Hz.

Voltage Regulation

Against line change:	±0.05% of nominal output ±5 V.
Against load change:	±50 V for NL to FL, ±5 V for ±0.2-A load change.
Ripple and noise:	±5 V maximum peak-to-peak for any rated output.
Transient response:	1 msec for step charge of load current of 0.5 A.
Short-term stability:	±0.05% of any nominal output for fixed operating conditions during any 10-minute period after a 30-minute warm-up.

Table 1 shows a tabulation of the specified regulator performance, and some actual test measured values.

Provision for Output Current-Limiting

Provisions were made for setting an adjustable output current limit ($I_{c\ell}$) over the range of 0.2 to 4 A. Current-limiting is effective within 1 msec after the onset of a load fault, and a load short-circuit current (I_{sc}) is limited to $1.2 \times I_{c\ell}$ (see Fig. 1).

Provision for Remote Voltage Programming

Provisions were made for modulating the output high voltage by a low-level, single-ended, dc-coupled, input signal with a ratio of 1000 V/V. The effect of the external reference signal is additive with the internal manual output adjustment. The output amplitude-vs.-frequency response to external sinusoidal modulation is as follows: 10 kV peak from dc to 50 Hz, then the output falls off at 6 dB per octave for all higher frequencies (see Fig. 2).

Output Voltage Monitor Signal

On the remote control chassis there is a BNC-type coaxial connector, at which a signal equal to 1 V/kV of the input high voltage is available.

Provision for Remote Control

A removable control chassis is provided

which contains the minimum, essential operator controls, indicators, and meters for operating the supply from up to 200-ft cable length from the main supply enclosure.

Manually Operated 480-V Input Power Circuit Breaker

A manually operated input power circuit breaker is provided on the supply which has an undervoltage trip device wired in series with all the enclosure door interlocks such that if any enclosure access door is opened the circuit breaker will trip open. All control and auxiliary power is derived from the 480-V input power.

Construction

All components of the power supply and regulator are housed in a substantial metal frame enclosure covered by metal panels and doors, dead front and read, floor mounted and free standing.

The supply is portable, caster-mounted, and has provisions for forklift and crane handling.

ACTUAL POWER SUPPLY OBTAINED

Figure 3 is a simplified schematic diagram of the power supply as built to our specifications.

You will note the input power circuit breaker, with the cabinet door interlocked by the undervoltage trip coil, and that all the supply power is derived from this one source.

The high-voltage transformer feeds a solid-state, 3-phase, full-wave bridge rectifier circuit with a single section LC filter on its output. A single, high-power, water-cooled tetrode series pass tube does all the output voltage regulating and current limiting. A special high-voltage isolation transformer with three separate secondary windings provides power for the +500 V dc screen bias supply, the -400 V dc control grid bias supply and the driver amplifier, all of which float at high voltage.

All of the low-level, ground potential regulator circuitry is ±15 V operated, plug-in, PC-board-type hardware with plug-in operational amplifiers and their associated input and output circuits.

The important link that couples the ground potential regulator control signal up to the driver amplifier at high voltage is a photon-coupled isolator. This device is rated to hold off up to 50 kV between the gallium arsenide electroluminescent diode infrared source and the silicon PIN photodetector diode. It has a bandwidth of up to 5 MHz.

Figure 4 is a photograph showing a front view of the supply cabinet. There are identical access doors on the rear side of the enclosure. Figure 5 is a view of the interior of the brute force dc supply and control section. Figure 6 shows the inside of the high-voltage regulator section.

Figure 7 is an oscilloscope trace of the output high-voltage response to a 2-V, 1-cycle, square-wave input signal from a Hewlett-Packard Model 3300 function generator. The supply was operating into a dummy resistance load at 20 kV, 1 A at the time. The settling time following rise and fall is about 200 μsec. The initial overshoot on the rise is 200 V, 1% of the dc level, and the initial undershoot on the fall is about 700 V or 3.5% of the dc level. All these values are well within the requirements of the specification.

The value of a clear, comprehensive specification was well demonstrated on this acquisition. The manufacturer appreciated the thorough guidance the specification provided. No misunderstandings or disagreements arose during the design, fabrication or testing periods.

The cost of this power supply, which was purchased on a "one only" basis was $38,400 or about $770 per rated kilowatt output. Had we been able to order a quantity of 3 units the price would have been approximately $27,500 per each unit or $550 per kilowatt.

Table 1. Regulator Performance

Nom. Output Voltage (kV)	±0.05% of Nom. Output (V)	Regulation Against ±5% Line Change Spec.: ±0.05% ±5 V			Ripple & Noise Spec.: 5 V p-p		Regulation Against Load Changes			Short-Term Stability (10 min) ±0.05% of Nom. Output
							NL-FL ±50 V	For ΔI_0 = ±0.2 A $\Delta V_0 \leq$ ±5 V		
		±0.05% ±5 V % of Nom.	±0.05% ±5 V	Act. Perf.	% of Nom.	Act. Perf.	NL-FL Act. Perf.	% of Nom.	Act. Perf.	Act. Perf.
25	±12.5	±0.07	±17.5 V	±5 V	0.02	8 V		±0.02		
20	±10.0	± .075	±15.0 V		.025	3 V	30 V	± .025	±2 V	ΔV = -10 V
15	± 7.5	± .083	±12.5 V	±3 V	.033	3 V		± .033		
10	± 5.0	± .10	±10.0 V	±3 V	.05	3 V	32 V	± .05	±1 V	
5	± 2.5	± .15	± 7.5 V		.10			± .10		
3	± 1.5	±0.217	± 6.5 V	±4 V	0.167	2.5 V	32 V	±0.166		ΔV = 3 V

Act. Perf. = Actual test measured performance.

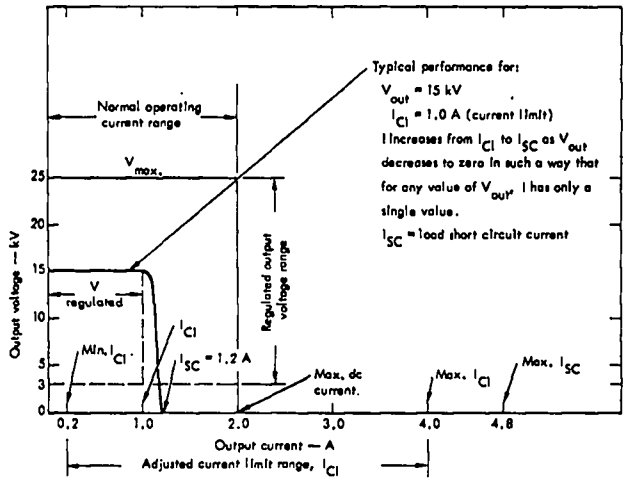

Fig. 1. Regulation and current limit range diagram.

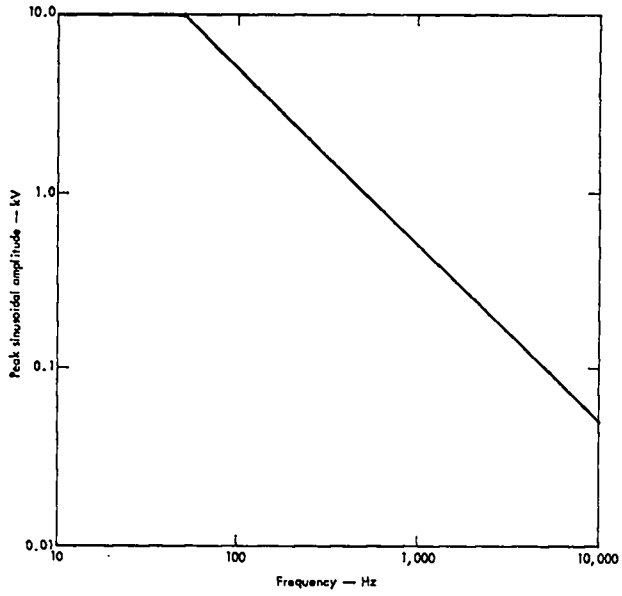

Fig. 2. Peak sinusoidal amplitude vs. frequency.

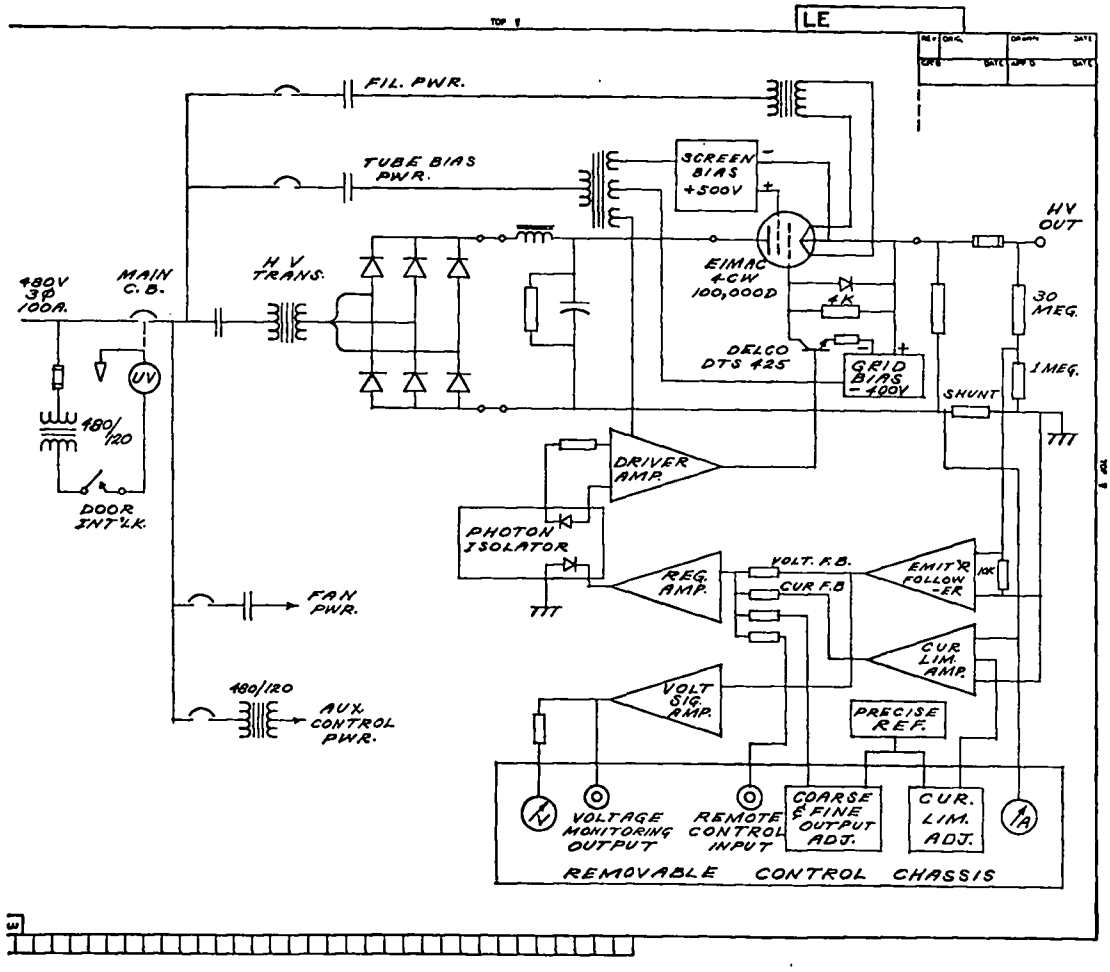

Fig. 3. Simplified schematic diagram.

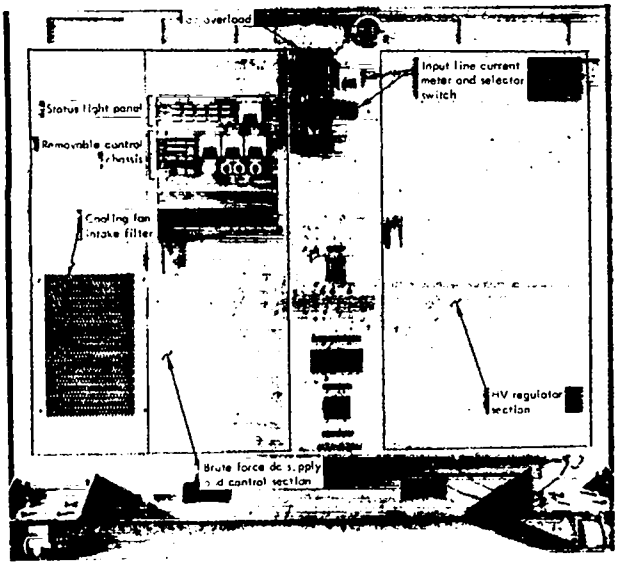

Fig. 4. Front view of power supply.

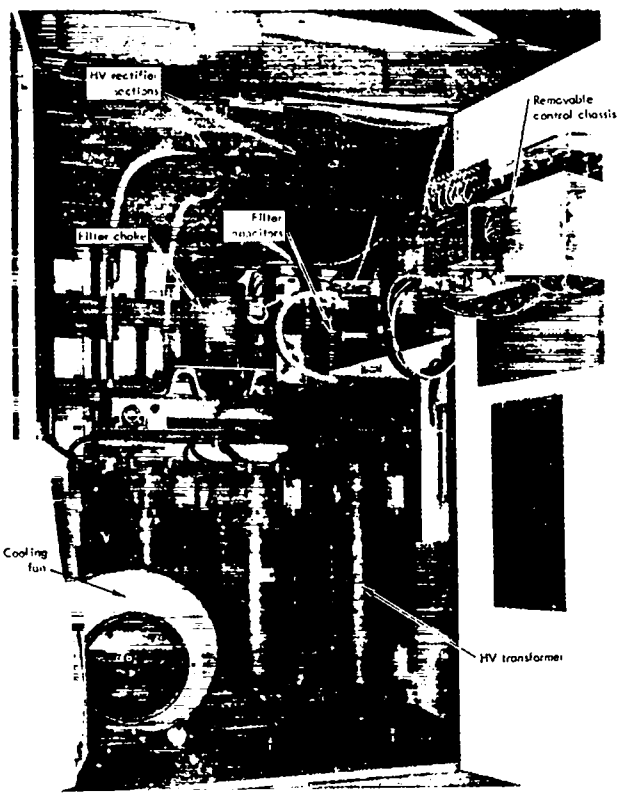

Fig. 5. Interior of brute force dc supply and control section.

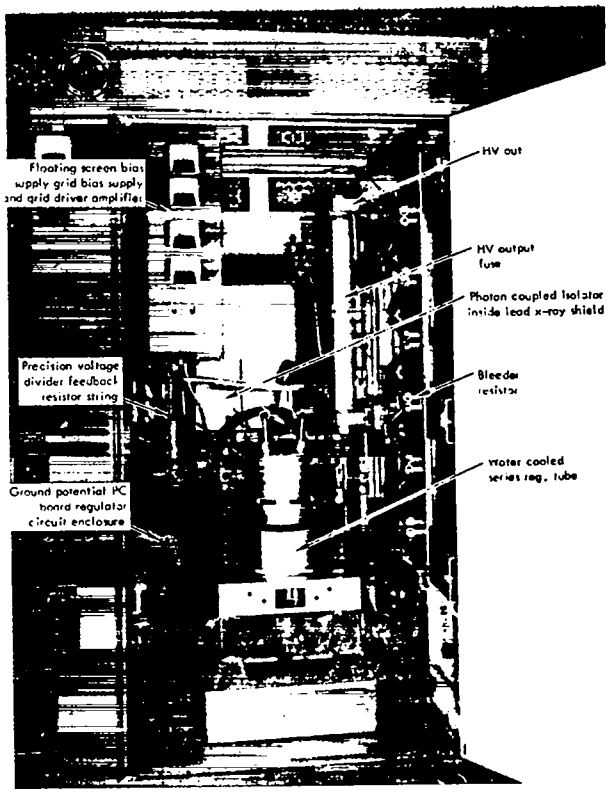

Fig. 6. Interior of high-voltage regulator section.

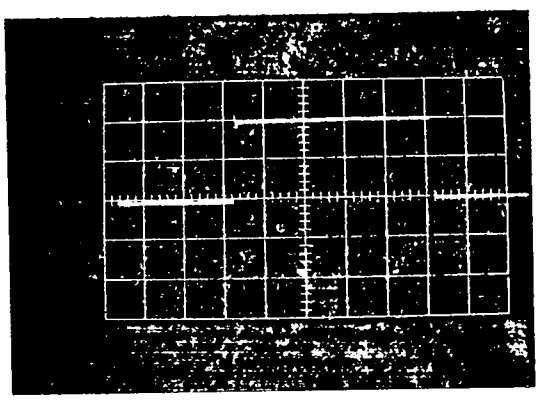

Vertical: 1 kV/cm

Horizontal: 1 msec/cm

Fig. 7. Output response to square-wave input modulation.

PRECISE REGULATION OF A 500 KW D. C. GENERATOR WITH A 2500 AMPERE SERIES-PASS TRANSISTOR BANK *

by

John McLeod and John Langdon Rand
Los Alamos Scientific Laboratory, University of California
Los Alamos, New Mexico

ABSTRACT

Design, construction, and testing of a transistor regulator and control system for ± .01% regulation of a magnet power supply is described. By placing a fast electronic regulator in series with the generator the problems inherent in quickly changing the generator output by forcing current into the field winding are avoided. Generator field control is used to maintain the average potential drop across the transistor regulator at its optimum value of 7 volts.

Two closed loops are used to control load voltage and current. Changes in load voltage or current will affect the drive to the series-pass transistor element. The voltage feedback is balanced against a voltage developed by integrating the difference between the measured current to the magnet and the reference. Thus, the current feedback loop with a response time of 50 milliseconds contains the voltage feedback loop with a response time of 1 millisecond as a nested element. The current loop response time of 50 milliseconds is adequate since its principal purpose is to correct for the effect of changes in magnet temperature. The voltage loop corrects for changes in generator output due to transients and armature asymmetry up to about 160 Hertz. Faster changes do not affect the magnetic field, and can be allowed to appear across the load.

The load and transistor regulator are water cooled by a closed-loop water to air heat exchanger. Protective circuits are provided to prevent transistor burn-out with alarm and automatic shut-down in case of various equipment failures.

Field stability of ± 0.5 gauss at 3.5 kilogauss has been achieved. Current stability of ± .01% of operating point appears to be limited by stability of the reference source.

Introduction

Our basic experimental research program depends heavily on electron cyclotron resonance both for heating and for diagnostic purposes. As a result, exceptional stability and reproducibility is required of the magnetic field produced by our air core solenoids and hence of the current supplied to them. By installing a bank of transistors in series with the armature of our 500 kilowatt (2000 amperes at 250 volts) motor generator set, a feedback loop has been constructed with the capability of suppressing injected noise to a residual level of .01% of the operating current over a wide range of currents. Previous attempts at regulation using the more customary technique of controlling the generator field current failed to accomplish such a high degree of regulation due to the extremely narrow band width which can be achieved in this way. The transistor bank included in the new system provides a much faster means to suppress the effects of changes in the generator shaft speed. The use of a synchronous motor does not insure the constancy required in the shaft speed both because of changes in the line frequency and because the armature phase angle can change in response to a change in line voltage and will then ring at a frequency of one to a few Hertz. Such changes have been observed to amount to a few tenths of one percent. The transistor bank is also being used to suppress noise injected from many other sources, in particular, the exciter generator and its driver amplifier, precise regulation of which by other means would be almost as difficult as building the main pass bank.

A simplified block diagram of the system is shown in Fig. 1. A 200 micro-ohm (500 millivolt at 2500 amperes) water cooled shunt is the basic measuring tool whose output is compared with a current set point reference source. No attempt is

made, however, to realize the bandwidth capability of the transistors using this current measurement since its bandwidth is limited by the inductance of the load. Instead, the current error is integrated electronically and the integral becomes a new set point for a fast load voltage control loop which senses the magnet voltage and which must operate to keep the current error zero or its own set point will change. This scheme provides a voltage set point which automatically changes to compensate for changes in the resistance of the magnet as its temperature changes.

Since the transistors used in the series-pass regulator can not withstand the full output voltage of the generator it is necessary to provide automatic protective circuits and to maintain the average generator output voltage seven volts greater than load demand. This is accomplished by measuring the collector to emitter drop across the series-pass transistors and providing control of the generator field to maintain the necessary generator output.

Series-Pass Transistor Bank

The series-pass transistor bank uses 270 type 2N2152A transistors in parallel. Water cooled aluminum plates are used to mount the transistors and other hardware in groups of 30 each. The transistors were matched before assembly by measuring beta at the expected full load current of 9.3 amperes per transistor and assembling 30 matching betas per heat sink. Current distribution among the 30 transistors on each heat sink is aided by a 0.025 ohm resistor in each emitter lead, and a 5.6 ohm resistor in each base lead.

Base drive for each group of 30 transistors is provided by one type 2N3773 transistor. The physical arrangement is shown on Fig. 2.

Division of current among the 9 banks of 30 transistors is accomplished by a variable resistor in the base circuit of each 2N3773 driver. This resistor is initially adjusted to produce a nominal current of 100 amperes per heat sink when the voltage applied to the driver transistor's base emitter circuit is one volt, and can be readjusted to produce equal currents or equal heat sink temperatures at full load.

Figure 3 shows the arrangement of heat sinks for the complete bank of 270 transistors. The terminal strips at the bottom provide the common points needed to connect the nine driver base circuits together, and to connect power sources for the monitor circuit board and other protective devices.

Transistor Protection

The 2N2152A transistors have a V_{CE} limit of 30 volts and a maximum power dissipation capability of 170 watts. To prevent exceeding the V_{CE} rating, output of the generator is controlled by the average collector to emitter voltage, action of the drive current control system is limited, and a protective circuit triggered at V_{CE} = 25 volts is incorporated on each heat sink. Cooling water temperature and volume has been designed to keep the transistor case temperatures below 65° C.

Control voltage limiting is necessary to prevent the control system from cutting off drive to the series-pass transistors in response to a demand for less load current. If base drive current should go to zero the transistors would try to stop current flow in the load circuit and whatever generator voltage is available would appear from collector to emitter. A limiter is incorporated to supply drive current when V_{CE} reaches 12 volts. A limiter is also available to prevent driving the series-pass transistors into saturation.

A last ditch protective circuit has been included on each heat sink. See Fig. 4. It consists of a silicon controlled rectifier and 1.5 ohm resistor connected from the common base bus to the common collector plate. By means of an auxiliary trigger circuit the SCR on each of the 9 heat sinks will be triggered into conduction when V_{CE} exceeds 25 volts. This action connects 1.5 ohms from the collector to the base bus for each group of 30 transistors which will supply sufficient base drive to limit V_{CE} to about 10 volts. It is necessary to reduce generator output to zero to unlatch this circuit once the SCR's have fired.

The transistor bank is protected against induced voltage from the collapsing field of a magnet by the diode connected from collector to emitter. If the collector goes negative the SCR circuit previously described will give protection, but it will

not work if the collector goes positive. The diode used is rated at 400 amperes service, 8000 amperes surge.

Protection against loss of cooling is provided by a thermal switch on each heat sink. This switch operates at 95° F and trips the alarm circuit described in the next section.

Monitor and Alarm Circuits

A circuit designed to continuously check the condition of each transistor is shown on Fig. 5. The voltage drop across each 0.025 ohm emitter resistor on a heat sink, that is 30 each, is diode coupled to the monitor circuit board mounted on the heat sink. If a transistor fails and short circuits itself approximately minus 6 volts will appear at the emitter, the 0.025 ohm resistor will burn out, and the transistor will be disconnected from the load circuit. This minus 6 volt signal unbalances the integrated circuit operational amplifier and causes a positive output voltage to trigger the triac and turn on the alarm lamp. Current supply for the 9 alarm lamps is through a meter-relay located on the series-pass transistor bank frame assembly (see Fig. 3). Contacts of this meter-relay shut down the generator.

The monitor circuit also provides an alarm if one transistor fails and open circuits itself. This is accomplished by balancing the average voltage drop across 15 emitter resistors against the average drop across the other 15 emitter resistors on each heat sink. At 5 amperes per transistor a voltage of 0.125 volts is expected across each emitter resistor. If one voltage out of 15 goes to zero a differential voltage of about 8 millivolts will be produced between the two busses. The integrated circuit differential amplifier responds to this unbalance and provides enough output to trigger the triac and subsequent alarms. Experience to date has produced no open transistors, and the unbalance detector will probably be eliminated in favor of a circuit responding only to the minus 6 volt signal from a shorted transistor on future production.

Control Circuit Theory

A complete control circuit diagram is shown in Fig. 6. In order to suppress transients occurring at about 5 Hertz by a significant factor, a voltage loop gain-bandwidth product of about 200 Hertz is required. The main transistor amplifier is an element of this loop and must, therefore, have a bandwidth in excess of 200 Hertz. At first glance, this would seem easy, since the bandwidth of a 2N2152A as a current amplifier is about 2 kilohertz. Difficulty arises from the fact that four stages of current gain are required in cascade to produce the required magnet current from a tractable control signal. The small signal transfer impedance of this device, i.e., the ratio between a change in collector voltage and the change in input current required to produce it, varies by a factor approaching a thousand with changes in operating point. If the other components of the loop are adjusted so that a gain bandwidth product of 200 Hertz is maintained at high current and low collector voltage, then the low frequency gain bandwidth product is about 100 kilohertz at the opposite extreme. With four lag elements, each with a bandwidth of a few kilohertz, this loop ought to oscillate,and oscillate it did! In order to obtain satisfactory operation, the transistors in the first two stages were replaced by RF transistors with bandwidths of one megahertz or more and the last two, for which this replacement is not feasible, were compensated at a low power level. The acquisition of adequate data on which to base the design of this compensation has proved most time consuming due to the necessity of testing at a large number of operating points with various collector voltages as well as currents. Bode plots of the amplifier and compensation transfer functions are shown in Fig. 7.

Since the current control loop includes the voltage control loop, the current control loop need not have the bandwidth to suppress generator noise. Its active role is suppression of the electrical effects of changes in the magnet cooling water temperature, which is difficult to regulate because of the huge transport delays in the plumbing to and from the cooling tower. Since the magnet resistance is unlikely to change as rapidly as 1%/min, a 3 Hertz bandwidth is adequate for the current loop. The integrator used to reduce the steady state error is compensated so as to transfer the integrating action to the magnet inductance for frequencies above its break frequency. Several compensation networks are provided together with a selector

switch to facilitate use with various magnets. The same integrator also holds the set point voltage for the voltage loop.

The exciter generator has its own local feedback loop which includes its driver amplifier consisting of 30 beam power pentodes (Type 5881) in parallel. The purpose of this loop is to suppress the injection of low frequency noise from the non-synchronous motor driving the exciter shaft and the unregulated power supply driving its field. The resulting exciter amplifier is an element in the generator control loop which senses the collector to emitter drop in the series-pass transistor bank and strives to hold it constant; but is only capable of holding the time average constant due to the slow response of the generator field winding. The integrator used in this loop is compensated for the break frequency of the generator field winding. It has proved necessary to insert two nonlinear elements in this loop. One compensates for the saturation of the generator field iron at high output voltages. The other accelerates run-up and run-down and comes into play if the collector voltage drop remains near one of its limits for an appreciable time.

*Work performed under the auspices of the U.S. Atomic Energy Commission.

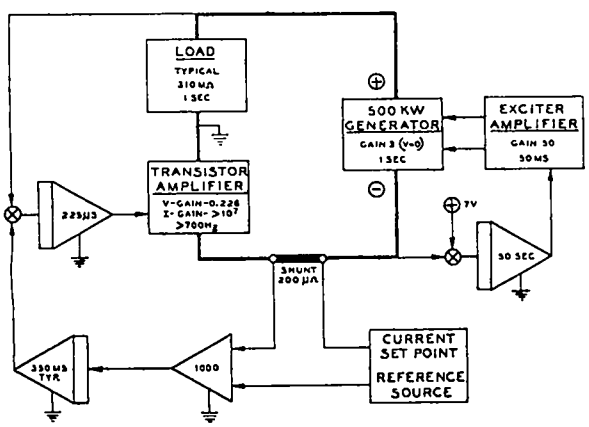

Fig. 1 Control System Block Diagram

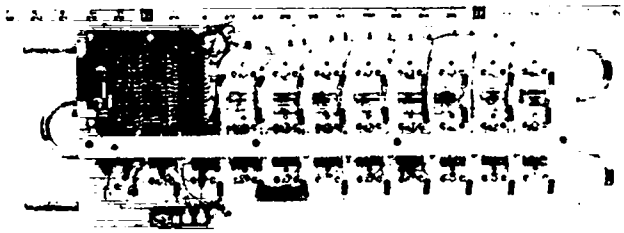

Fig. 2 Basic Regulator Element

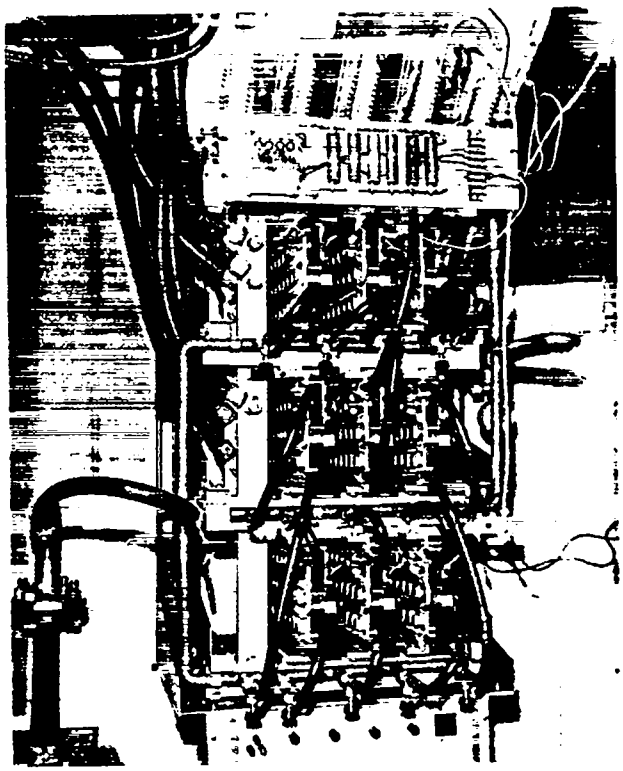

Fig. 3 Complete Regulator Assembly

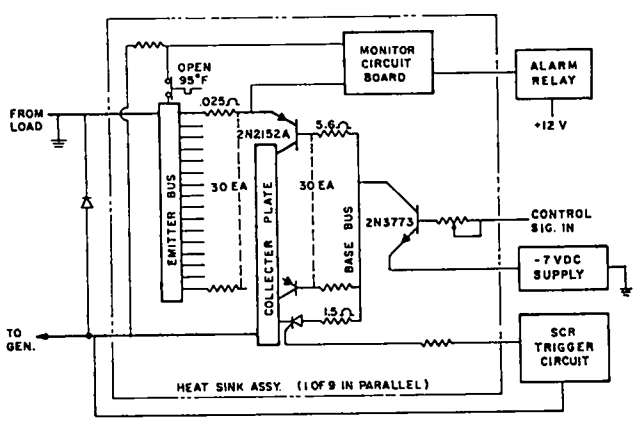

Fig. 4 Regulator Schematic

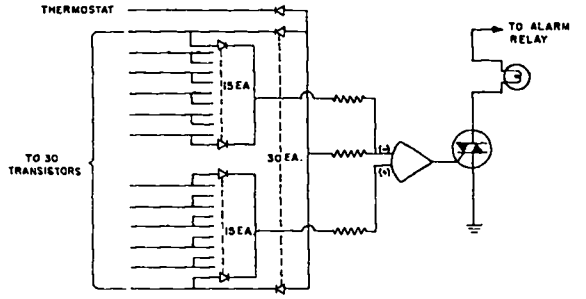

Fig. 5 Monitor and Alarm Schematic

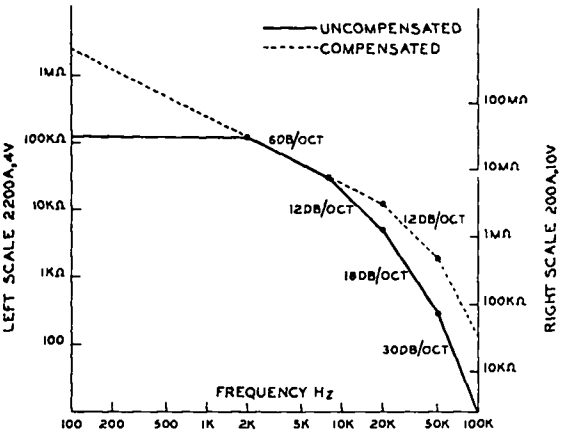

Fig. 7 Frequency Response of Regulator

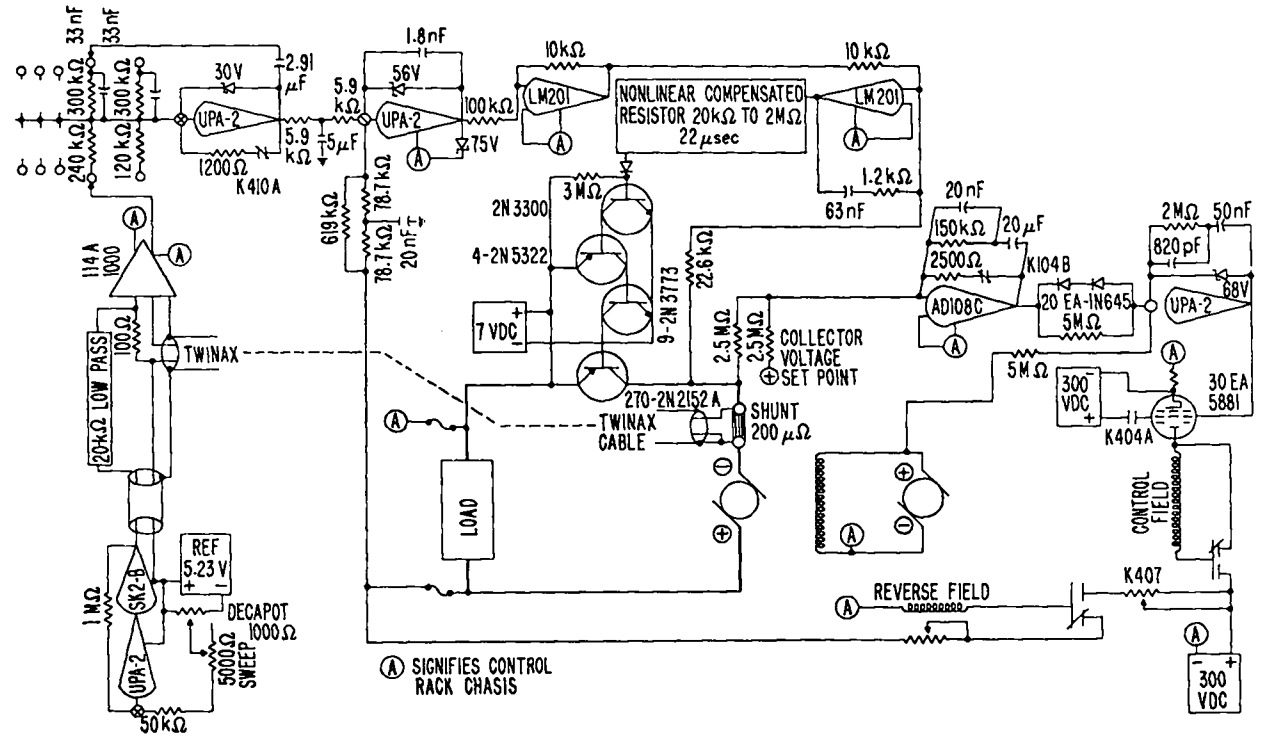

Fig. 6 Detailed Control System Schematic

VARIABLE-VOLTAGE, DIRECT-CURRENT POWER SUPPLIES FOR ENERGIZING CRYOGENICALLY COOLED AND SUPERCONDUCTIVE ELECTROMAGNETS

by J. C. Laurence, E. H. Meyn, and R. J. Jirberg
National Aeronautics and Space Administration
Lewis Research Center
Cleveland, Ohio 44135

ABSTRACT

Power supplies for energizing electromagnets, cryogenically cooled and superconductive, and their control circuitry are described in this paper. The first is a dc generator of the homopolar type with a continuous rating of 0 to 60,000 amperes at 38 volts. Overloads of up to three times the continuous current output are available for a duty cycle of 2 minutes. Control circuitry provides for complete reversal of the output voltage by reversing the direction of exciter field. This feature is useful for discharging an electromagnet in the shortest possible time. The second of these converts three phase, 440 volt, 60 hertz power into a variable voltage (0 to 45 volts), direct current (0 to 15,000 amperes) continuous rating with a 200% overload rating for a duty cycle of 2 minutes. The fundamental ripple frequency is 360 hertz and its peak-to-peak amplitude is less than 18% of the dc output voltage. Variations in the preset dc output voltage under continuous load are limited to ±1% when the ac input power variations are regulated to ±5%.

INTRODUCTION

The Lewis Research Center has primary NASA responsibility for research on advanced concepts of power generation and propulsion. Some of these concepts require intense, large-volume, magnetic fields, generated by lightweight equipment with low power consumption. Electric propulsion, magnetohydrodynamic power generation, thermonuclear power and propulsion, space radiation shielding, and reentry of spacecraft into the Earth's atmosphere are some of the concepts for which such magnetic fields may be required. In addition, the development of intense magnetic fields is of importance for studies in a variety of disciplines, such as elementary particle physics (accelerators, bubble chambers), solid-state physics, and plasma physics.

When the program to provide large-volume, intense magnetic fields was initiated at the Lewis Research Center, many different means of producing these fields were investigated.[1] To reduce structural problems and simplify magnet construction and operation, it was decided to use low-impedance, high-current design. This design criterion was applied first to the copper water-cooled coils, and later to the aluminum cryogenically cooled coils. The power sources which resulted from this program are described in this report.

HOMOPOLAR GENERATOR

A large homopolar generator[2] was selected as the best power source for the low-impedance electromagnets to be constructed. In this machine a cylinder 30.5 cm in diameter and 61 cm long is rotated at high speed (7000 rpm) in the magnetic field produced by the field windings. These windings are powered by a separate motor generator set with a controllable output. Charges are induced on the rotating cylinder as a result of the rotation in the field and are collected by two flowing streams of a sodium-potassium alloy (NaK). The currents resulting are transferred to copper, water-cooled, bus bars which carry the current to the load. Figure 1 is a photograph of the homopolar installation. The motor switch gear, the

exciter set, the generator, the NaK pumps, and the speed increaser are shown in this photograph.

The operating range of the generator and its associated equipment and a response curve are shown in figure 2 up to the 1-minute limit. The continuous rating, however, is 60 000 amperes at 1.8 megawatts. The upper current limit is determined by the current capacity of the steel rotor so as to avoid overheating, which would destroy the insulation on the rotor.

The output potential (fig. 2(a)) of the generator is a function of the rotational speed and the field power. The constant rotational speed limits the maximum voltage to 38 volts because of the generator field windings, the associated iron saturation, and the maximum output of the exciter. The electromotive force of the homopolar generator is controlled through the control of the exciter set. The machine can be operated in two modes. Since the internal resistance of the generator is only a few microhms, one mode of operation provides a constant-voltage or zero-impedance characteristic whereby the system current is determined by the load resistance. In the other mode, the current regulation is independent of load resistance and thus constitutes a constant-current system.

Since the time constant of the generator circuit is large (about 2.5 sec) compared with the desired current rise time in magnet applications, the automatic control circuit uses a forcing technique to raise the output to 90 percent of the preselected value (fig. 2(b)) in about 1 second.

The controller system (fig. 3) is a closed-loop control. The controller unit generates fixed voltages or variable-slope ramps which terminate at a predetermined fixed voltage. The voltage generated by the controller is an analog of the desired output current from the homopolar generator. Amplifier A-2 compares this voltage with the amplified signal from the shunt which provides a voltage proportional to the output current. The error is amplified by amplifier A-3 and the exciter. This signal drives the output of the homopolar generator through its field to bring the net error to zero and thus bring the output current to the value set by the controller.

The shunt is composed of three 20 000-ampere, 50-millivolt shunts in parallel, which are water cooled for efficient operation up to the generator maximum current of 200 000 amperes (see fig. 4).

Manual control is accomplished by connecting the controller output into amplifier A-3 without comparison with the current in amplifier A-2.

The two reversing relays allow for reversal of the exciter field for the purpose of quickly driving the current to zero in an inductive load. This field-forcing feature is most valuable when the generator is used, as it is at Lewis, to power an electromagnet of high inductance, long time constant, high energy storage, and limited capacity of cryogenic coolant.

ELECTRONIC RAMP-AND-HOLD FUNCTION GENERATOR AS CHARGING CONTROL FOR ELECTROMAGNETS

In the control of many electrical or mechanical systems it is often desirable to operate the system between preset points and to accomplish the change between these points in a linear fashion with time. This mode of control is frequently referred to as the "ramp-and-hold" operation. A typical situation in which this type of control is sought is the energizing of an electromagnet to a preselected magnet field level at a fixed rate so as to maintain a constant charging voltage during the field sweep.

Basically, a voltage ramp function may be generated in a number of ways. Two readily obtained methods utilize (1) the voltage appearing across a capacitor charging from a constant current source, and (2) the voltage at the slidewire of a motor-driven potentiometer fed from a constant voltage source. The first of these methods has been applied to the water-cooled and neon-cooled electromagnets and the second is chosen for the controller of a 14-tesla superconductive magnet described in reference 1.

The ramp voltage appears at the output of an operational amplifier integrator, the input of which is a constant voltage. The fundamental integrator circuit is shown in figure 5. The ramp

is dependent both on the time constant determined by the resistance R and the capacitance C and on the magnitude of the input voltage e_i. Removal of the constant voltage input after a period of integration establishes a "hold" condition.

The complete circuit diagram of the function generator is shown in figure 6. The voltage ramp is produced by the operational amplifier 1 (OA-1) stage comprised of the 2-megohm input resistor, a series of feedback capacitors so chosen as to permit integrating time constants between 0.1 and 10 seconds, and a voltage source (the output of OA-3). The OA-3 stage functions as a bipolar switch with a graded null, the characteristics of which are shown in figure 7. During periods when OA-2 drives the input of OA-3 away from zero, the integrator is presented with an essentially constant voltage of approximately 0.6 volt to integrate and produce the ramp output. When the output of OA-2 is zero the input voltage to the integrator is reduced to zero, and a hold condition results.

The OA-2 stage functions as a voltage comparator which senses the difference in the magnitude of the ramp output to that of the "limit" voltage set by the 10-turn potentiometer. This potentiometer serves as a variable reference and produces an output which switches between nearly constant levels in a manner identical to the action of OA-3. The polarity of the output indicates the sense of the error of the ramp away from the selected limit voltage. Hence, under conditions during which the magnitude of the ramp output is not equal to that of the set limit voltage, a fixed-level voltage appears at the input to the integrator and is phased so as to drive the ramp output to the point set by the "limit" control.

Under this closed-loop mode of control the stability of the hold is determined solely by the stability of the voltage reference. The reference incorporated into the circuit of figure 6 derives its stability from a Zener diode carrying a nearly constant current.

The rate at which the output voltage ramps toward the set point is made adjustable by choice of the integrating time constant (a range adjustment), and by scaling the voltage presented to the integrator with the potentiometer at the output of OA-3 (a fine adjustment).

The 1-megohm feedback resistors around OA-2 and OA-3 are included to ensure graded nulls and gains not to exceed 10 and 100, respectively. The use of four diode pairs as nonlinear feedback and load elements for OA-2 and OA-3 serves to provide an essentially constant input voltage to the integrator regardless of the magnitude of the error between output and reference.

If it is necessary to interrupt the ramp momentarily during a sweep, a pushbutton (S-2 in fig. 6) is provided to remove the voltage to the integrator and thus produce a hold. This hold condition is, of course, subject to drift; the drift can be minimized by careful adjustment of the offset voltage of OA-1.

Additional controls include a selector switch S-4 for selection of either positive or negative output polarities or the zero potential reference, and a reset switch S-1 to disable the integrator and clamp its output to zero when selecting integrating capacitors or for instantaneous return to zero output.

Before a ramp-and-hold operation, switch S-1 is placed in the "reset" position, switch S-4 is placed in the "0" position, an appropriate time constant is selected with switch S-3, and the limit point is set as indicated on the 10-turn potentiometer. The ramp-and-hold operation is then executed by switching S-1 to "active" and S-4 to either "+" or "-", depending on the desired output polarity.

The homopolar generator and control system has proved to be an excellent magnet power supply. The ripple in the supply voltage is for practical purposes nonexistent (<1 mV at full rated current). The maintenance problems have been concerned primarily with supplying the NaK system with a continuous dry cover gas, such as nitrogen or argon, and limiting the very high current runs so that the rotor insulation is not damaged by overheating.

TRANSFORMER-RECTIFIER SYSTEM

In addition to the homopolar generator a

transformer-rectifier power supply is used to power some of the electromagnets. This system is a three-phase, full-wave rectifier supplied from variable-voltage transformers.

In figure 8, which shows one phase of the rectifier power supply, the 440-volt, 60-hertz input is regulated to compensate for line voltage variations. This voltage is then applied to a pair of variable transformers (fig. 4). The movable contact wipers of this variable set of transformers (T-1 and T-2) travel in opposite directions. When both wipers tap equal potential points, zero voltage is supplied to the primary of transformer T-3; its secondary has no voltage drop across it. The voltage drop across the primary of transformer T-4 is then 440 volts. However, when the voltage taps of T-1 and T-2 are at opposite ends of the tapped windings, 440 volts will be supplied to the primary of T-3. The one-to-one winding ratio of T-3 will, therefore, produce 440 volts across the secondary of T-3. If the phase of this voltage, which is in series with the 440-volt line, is subtractive, then the voltages will cancel and apply zero volts to T-4. Conversely, the opposite extremes of T-1 and T-2 will yield 440 volts of the opposite polarity across the secondary of T-3, which is additive, and T-4 will be energized with 880 volts on its primary.

This variation, to 880 volts, presented to the rectifiers (fig. 10) connected in a three-phase bridge circuit from the three-phase, step-down rectifier-transformer controls the output of the supply from 0 to 45 volts dc. This power source is capable of supplying 15 000 amperes continuously or 30 000 amperes for 2 minutes.

A picture of the complete installation is shown in figure 11.

CONCLUDING REMARKS

The power supplies and their control circuits described in this report are being used to power magnets for experiments in solid state and plasma physics research. Their performance has been satisfactory.

REFERENCES

1. Laurence, James C.: High-Field Electromagnets at NASA Lewis Research Center. NASA TN D-4910, 1968.
2. Fakan, John C.: The Homopolar Generator as an Electromagnet Power Supply. High Magnetic Fields. Henry Kolm, Benjamin Lax, Francis Bitter and Robert Mills, eds., M.I.T. Press and John Wiley & Sons, Inc., 1962, pp. 211-216.

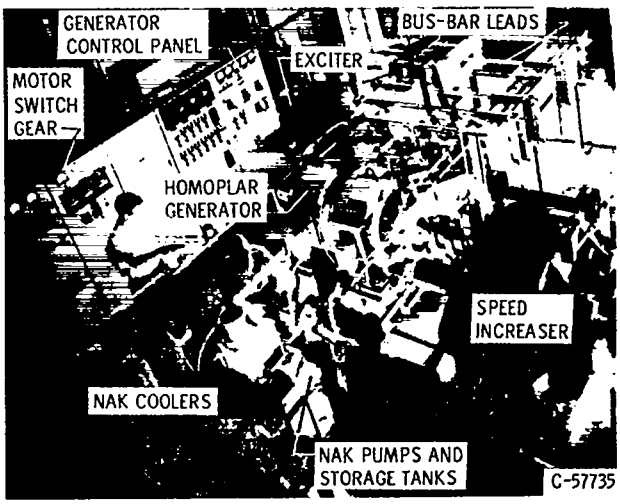

Figure 1. - Homoplar generator installation. (Drive motor is off picture to right.)

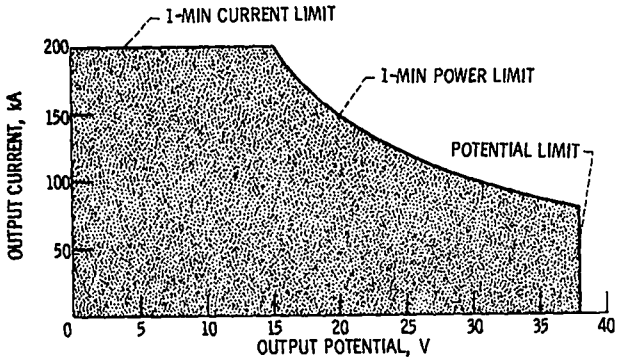

(a) Range of operation.

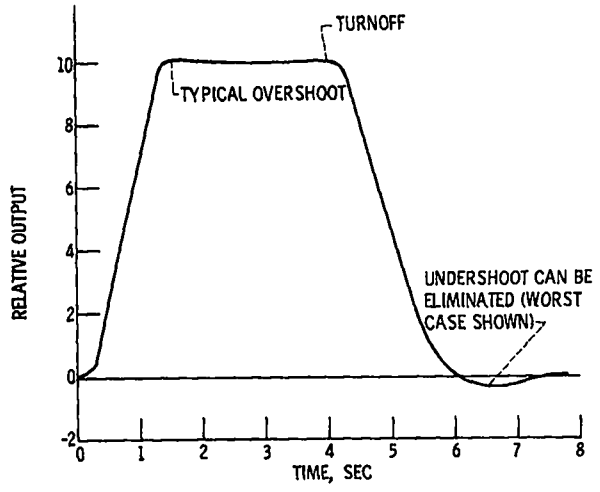

(b) Typical response curve.

Figure 2. - Operational characteristics and typical response curve of the homopolar generator.

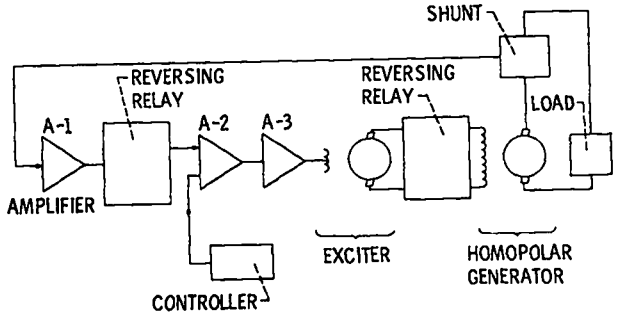

Figure 3. - Control circuit for homopolar generator.

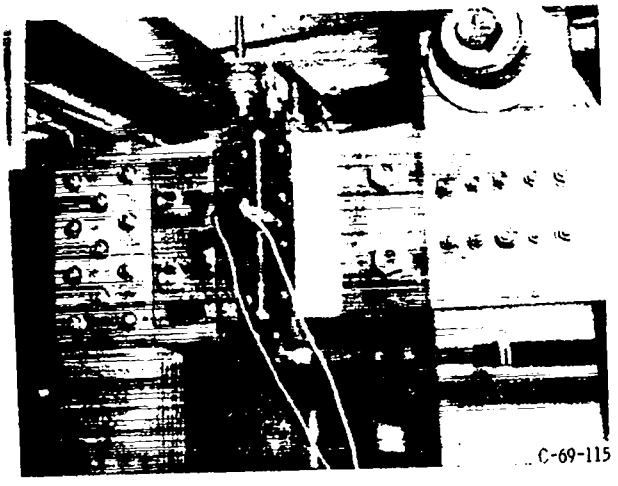

(a) Single water cooled 60 000 amp. shunt.

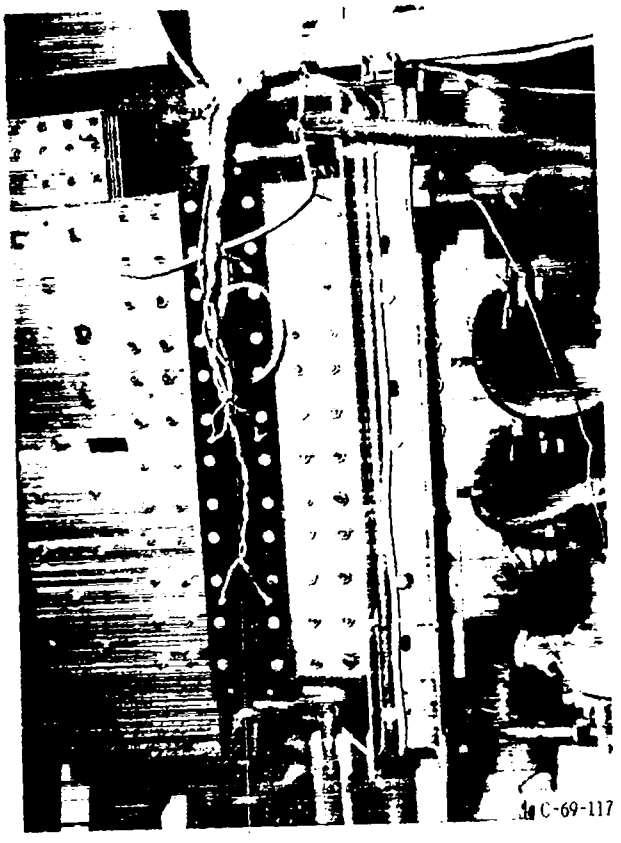

(b) Three paralleled water cooled shunts.

Figure 4. - Current measuring shunts.

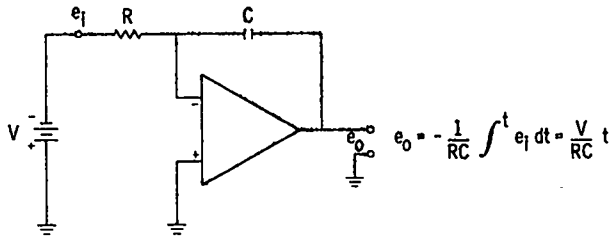

Figure 5. - Integrator circuit.

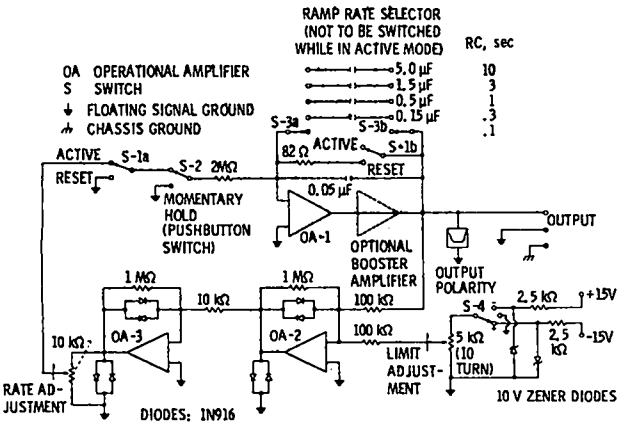

Figure 6. - Electromagnet controller circuit.

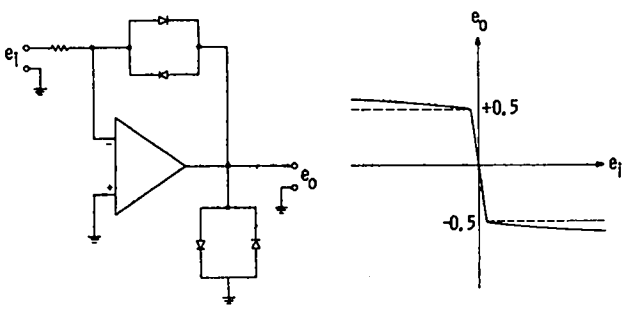

Figure 7. - Characteristics of bipolar switch stage of controller.

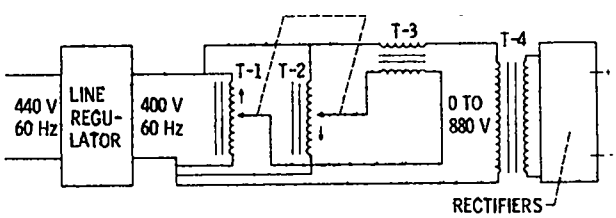

Figure 8. - Schematic diagram of rectifier power supply.

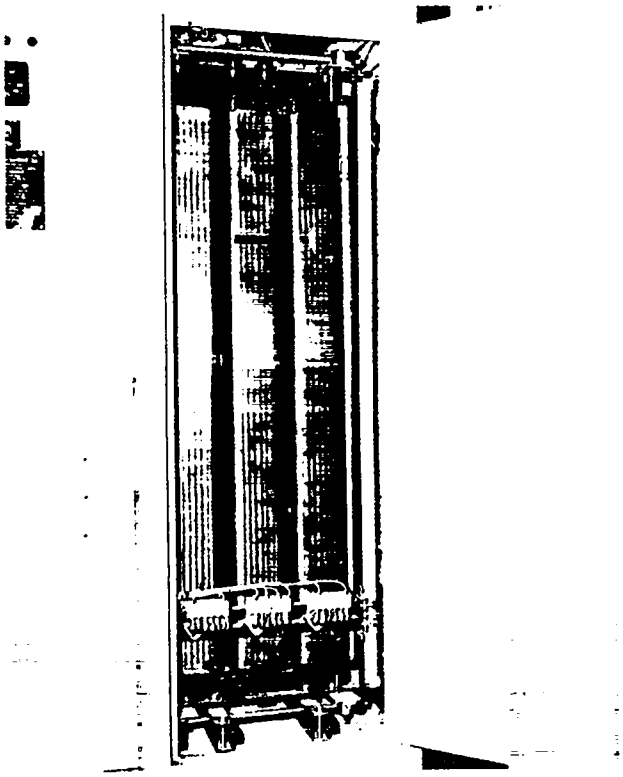

Fig. 9. Variable transformer section.

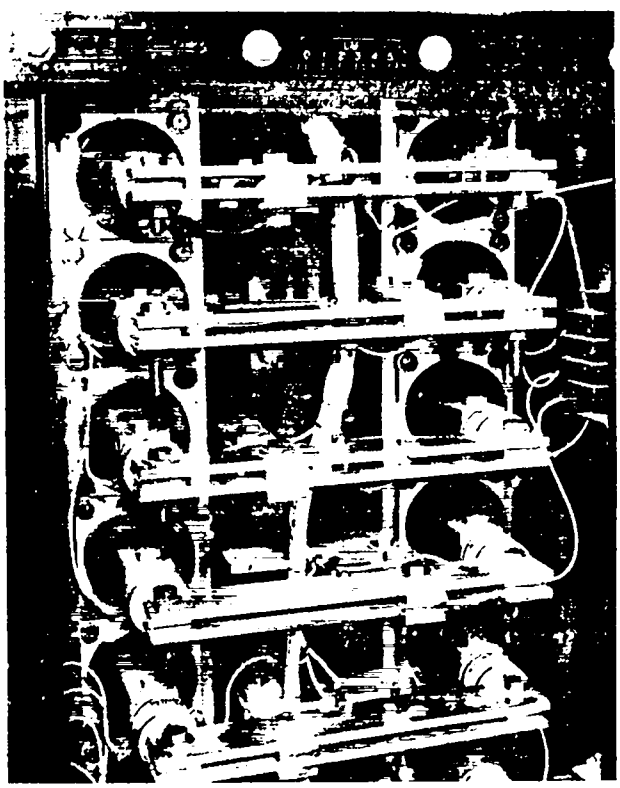

Fig. 10. A part of rectifier section.

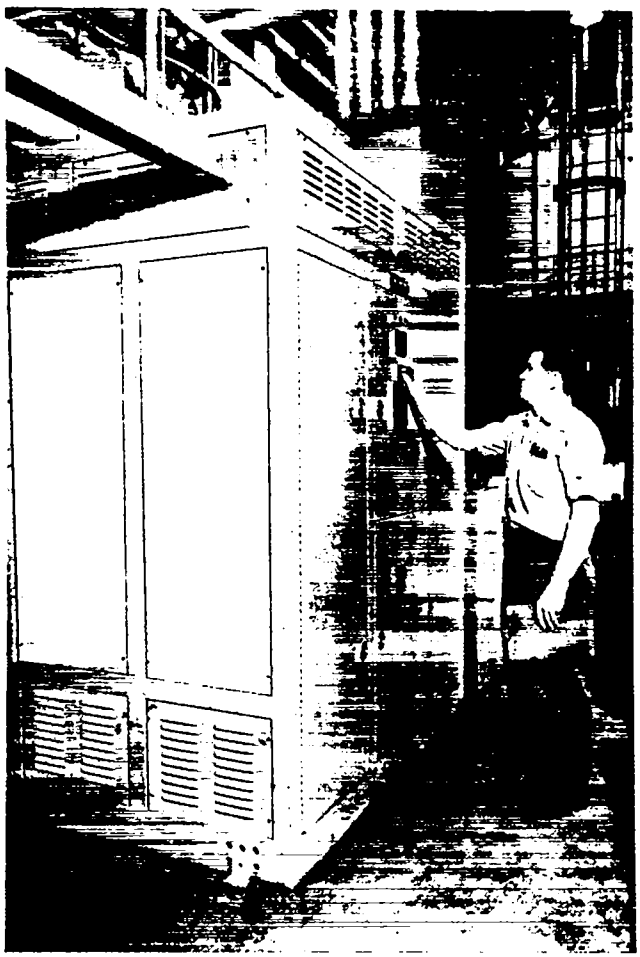

Fig. 11. Power supply installation.

HIGH POWER TECHNOLOGY ASSOCIATED WITH DENSE PLASMA FOCUS RESEARCH[1]

by

K. D. Ware, J. P. Carpenter, P. J. Bottoms,
A. H. Williams, and J. W. Mather

Los Alamos Scientific Laboratory
University of California
Los Alamos, New Mexico

ABSTRACT

The technology of a fast, 120 kJ - 50 kV capacitor bank used with the dense plasma focus experiments (DPF-V) which has the capability of delivering ~ 5 MA into a shorted load is discussed. The capacitor bank has 12, 10 kJ - 50 kV modules which fire simultaneously to within ± 10 nsec. Each module consists of 4, 2 μF - 50 kV capacitors parallel connected by a closed coaxial header to a single vacuum switch. The capacitor-switch module is triggered by a coaxial spark plug with a fast rising transformer isolated pulse, 1.3×10^{12} V/sec up to 60 kV, and has an output voltage rise rate of 1.5×10^{12} V/sec. The vacuum switch has discharged the 10 kJ of energy while repeatedly passing currents of 0.4 MA for over a thousand shots.

The engineering and technology pertaining to the operation of a fast, 120 kJ - 50 kV capacitor bank associated with dense plasma focus research (DPF-V) is described in limited detail. Various photographic views of the equipment are presented with discussion on the construction and operation of the more unusual hardware components. Special handling of high voltage insulating materials associated with the capacitor bank is briefly considered. A major part of the paper is devoted to detail of the basic unit of this capacitor bank which is a 10 kJ - 50 kV vacuum switch module and its operation.

Figure 1 shows a cross sectional view of the coaxial accelerator used to produce the dense plasma focus. This shows the basic arrangement of the discharge, and the requirements of the capacitor bank and the vacuum system. The technology used to meet these requirements is the main subject of this paper.

The coaxial discharge electrodes with inner and outer diameters of four and six inches respectively are typical with a center electrode length of nine inches. Upon application of a fast rising, high voltage signal to the breech of the accelerator the gas breaks down and begins conducting current along the surface of the insulator. While the current is increasing, the sheath moves out and down the accelerator as predicted by the classical "snow plow" theory at a velocity of $\sim 10^7$ cm/sec. By adjustment of the voltage, gas pressure, and inner electrode length, the sheath is made to arrive at the end of the center electrode at peak current or approximately the quarter period of the electrical circuit. As indicated in Fig. 1, the magnetic pressure $B^2/8\pi$ collapses the current sheath in a symmetrical two-dimensional pinch and forms a high temperature (2 to 5 keV) and dense ($\sim 10^{19}$ particles/cc) plasma which remains stable for about 1 to 2×10^{-7} sec. The current is of the order of a

few MA with a quarter period of about 1.5 to 2 μsec.

Figure 2 is a plan view of the DPF-V system. The coaxial accelerator is situated with a vertical axis within the copper vacuum chamber. The 50 kV-120 kJ capacitor bank consists of 12 - 8 μF modules which are connected to the coaxial header by 96 - 9 foot lengths of Belden YK-198 coaxial cable. Maximum current under short circuit conditions is ~ 5 MA.

At the top of Fig. 2 is the vacuum equipment for the discharge chamber and the 12 vacuum spark gaps. The vacuum requirements for the discharge are not extreme although a fast pump-down for recycling the fill gas is desired. Under normal operating conditions the working gas in the discharge is pumped below 10^{-5} torr and is then statically filled to a few torr of D_2 or H gas every 5 to 10 minutes. In order to pump this relatively high pressure rapidly, liquid nitrogen cooled cryosorb pumps are used to evacuate the system to a few mtorr in 1 to 2 minutes. The 6-inch-diffusion pump and liquid nitrogen trap is then automatically cycled to complete the evacuation to $< 10^{-5}$ torr. With this system, approximately 3 minutes are required to cycle the fill gas. The gas pressure is monitored by a Wallace Tierman pressure gauge which is also part of the safety interlock circuit. This circuit prevents recharging of the capacitor bank without the proper gas pressure.

The spark gaps are back-filled to a few mtorr of krypton or dry nitrogen while being mechanically pumped through a liquid nitrogen trap. The vacuum pumping line is ~ 12 feet of 1/2 inch polyethylene tubing and connects to the high voltage terminal of the spark gap. A non-electrical conducting vacuum pinch-off valve shown in Fig. 3 inserted in these vacuum pump lines prevents high voltage flashover to ground for voltages > 30 kV. A pneumatic valve operates the winged-hinge which pinches a soft rubber tubing vacuum section and effectively opens circuits to the vacuum lines. This valve has been tested up to 55 kV and is sequentially operated during the charge-to-firing stages of the capacitor bank.

Figure 4 shows the charging network for the capacitor bank which consists of the power supply, charging resistors and master trigger unit. The 60 kV - 3 A constant current power supply built by Hill-Magnetics, Inc., reaches peak charging current in less than one second; after full charge, the amount drops to zero by automatically opening the 480 V, 3Ø contactor. The charging current is delivered to the 12 module capacitor bank through $CuSO_4$ resistors shown in Fig. 4. Ordinary wire-wound high voltage resistors were found unsatisfactory because of their low wattage rating. However, the wattage rating of these liquid resistors is very high. For example, dumping the entire stored energy of 120 kJ into these resistors would produce only a 3° rise in their temperature. It should be noted that a saturated solution of $CuSO_4$ in these tubes is ~ 200 Ω and with an addition of 3% by volume of sulfuric acid it is reduced to ~ 20 Ω. Similar isolation and charging resistors have been used with another DPF device for the past seven months with no problems. Because of the fast charging capabilities of the power supply, a parallel arrangement of shorting switches and high voltage metering circuits are included. These shorting circuits are fully interlocked for safety. At the right hand side of Fig. 4 is a hydrogen thyratron master trigger used to trigger the vacuum spark gaps. The trigger signals are discussed later.

In Fig. 5 is the capacitor-vacuum-switch modules which consist of 4, 2 μF capacitors parallel connected to a single graded vacuum switch. The module stores 10 kJ at 50 kV and is charged through the lead entering the side of the solid ground plate. The vacuum switch is located in the lower 3 inches of the 12 inch output chimney terminal which connects the module to the coaxial accelerator header through the 8-coaxial cables. The figure shows the construction within the closed ground system with some of the polyethylene sheets cut away in order to expose the high voltage terminal plate. The lower plate is O-ringed to each capacitor, outside the bolt circle. Insulation is provided, in addition to the sheets of polyethylene above and below the high voltage plate, by a technique of polyethylene coating of the metal surfaces. This makes a continuously insulated path without expensive molding or insulator machining. After closing the top plate the header is filled with transmission oil by vacuum "drawing" the oil. The oil is the only insulation between the high voltage boss and the ground plate, which is about 1-1/2 inches path length.

A cross-sectional view of the vacuum switch is shown in Fig. 6. The lower terminal is at high voltage and the upper one is dc grounded through the 8-coaxial cables and a shunt inductance across the discharge header. The nylon bushing compresses the two main electrodes, the three 1/4-inch glass discs (with 1-1/2 to 2-1/8 inch holes), and two 1/8 inch brass discs electrodes (with 1/2 to 5/8 inch holes), to form the graded switch. The region outside the glass discs and floating electrodes is pressurized to ~ 35 psi of SF_6 in order to prevent voltage breakdown in this outer region.

The coaxial spark plug (not shown in Fig. 6) is axially located on the upper electrode. The construction consists of a 1-1/2 inch length of Al_2O_3 tubing with 3/16 inch outer diameter is used to insulate the central tungsten rod and outer brass sleeve of the spark plug. This alumina tube must withstand rather severe treatment from the spark gap discharge and much care has gone into the quality control to prevent chipping and cracking. To insure quality control, radiography and fluorescence penetrants are used to reveal cracks or other flaws in the ceramics body.

The vacuum switches are initiated from a fast hydrogen thyratron master trigger unit. However, the thyratron voltage pulse is not used directly to trigger the spark plugs but is stepped up to about 60 kV using a 3:13 turn ratio laminated iron core. In addition to increasing the voltage pulse to about 1.3×10^{12} V/sec the transformer provides high voltage isolation. The spark plugs fire at about 16 kV and the fast voltage pulse triggers all the plugs within a few nsec of each other.

The vacuum switch components are all thoroughly cleaned and assembled with utmost care in order to prevent the presence of any organic materials inside the gap. The gap is then evacuated to a vacuum of $\lesssim 0.3$ mtorr and "conditioned" by passing energies > 1000 J through the switch while maintaining vacuum. Except for outgassing the surfaces, the initial conditioning process involves scoring of the side walls of the Pyrex insulators by the discharge. The fine cracks of this "crazing" process form the nucleations for subsequent copper crystal growth. These copper growths grade the gap voltage and prevent buildup. When conditioned the gap can be triggered over a large voltage range from ~ 100 V to 55 kV.

Figure 7 shows several typical output voltage traces. The oscillographs on the left are for the vacuum condition (< 0.2 mtorr) and those on the right are with ~ 4 mtorr of backfilled krypton. Notice there is little improvement at these voltages in the rate of voltage output rise with or without the backfilling gas. At lower voltages the rise is better with the fill gas, but primarily the krypton filled gap has much better firing statistics as seen in the lower two oscillographs. The jitter of gap firing without backfilling gas is shown by five consecutive discharges. Similar traces, with 13 mtorr of krypton gas, at faster sweep speed show a spread of only 3.5 nsec for five discharges. A typical rate of rise of the output voltage is a 1.5×10^{12} V/sec.

The 9 MHz frequency inherent in the traces in Fig. 7 is parasitic and is due to reflections at the end of the shorted load test cables. Similar oscillations of a more troublesome nature occur with the 9-foot cables delivering the high power to the discharge header. Voltage doubling and cable damage usually result without some impedance matching termination. Figure 8 is a view of the input side of the discharge header. The inner plate is the high voltage feed which connects to the center electrode shown. Forth-eight terminators of 8 - 1 watt carbon resistors with a resistance of 37 Ω per string are used to minimize impedance mismatch. These terminators are quite adequate for the 96 - 16 Ω discharge cables and only take about 66 kA at 50 kV or roughly ~ 2% of the available current. One watt Allen-Bradley resistors have very good pulsed high voltage integrity up to ~ 15 kV.

Each capacitor module has a $\dot{B}$ probe monitoring the output current signal. These signals are used to monitor the individual vacuum switch behavior and for the twelve channel ± 10 nsec coincidence circuit. The signal is also used with a twelve channel non-coincidence circuit to give a positive indication that a gap has fired. This latter circuit is very helpful in locating gap prefiring.

Another monitoring circuit being developed consists of an acoustical crystal sensor mounted on each module with individual integrated meter readouts. Often when a capacitor is faulty in

construction the high current capacitor tabs will make and break producing in acoustical noise. The audio detector has been very successful in locating the faulty capacitors. The faulty capacitor also creates sufficient rf noise to prefire the vacuum gap.

Of course, there are many problems associated with the physics of dense plasma focus research, but this paper attempted to emphasize only some of the problems and their solutions pertaining to the operation of high power capacitor banks and their energy transfer.

References

1. Work performed under the auspices of the U.S. Atomic Energy Commission and Defense Atomic Support Agency.

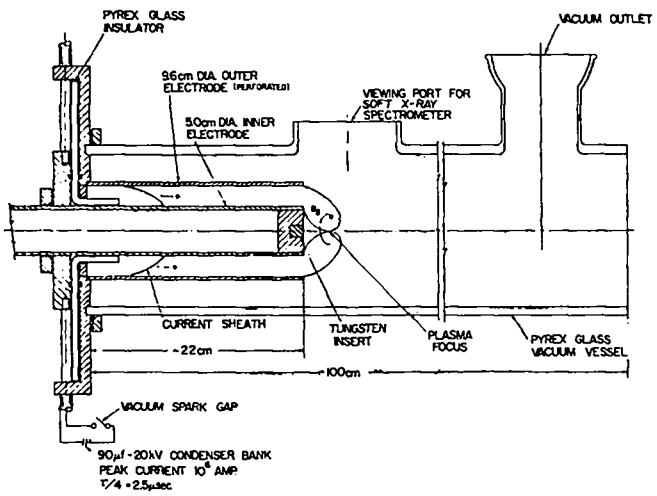

1. Cross-sectional view of a dense plasma focus coaxial accelerator.

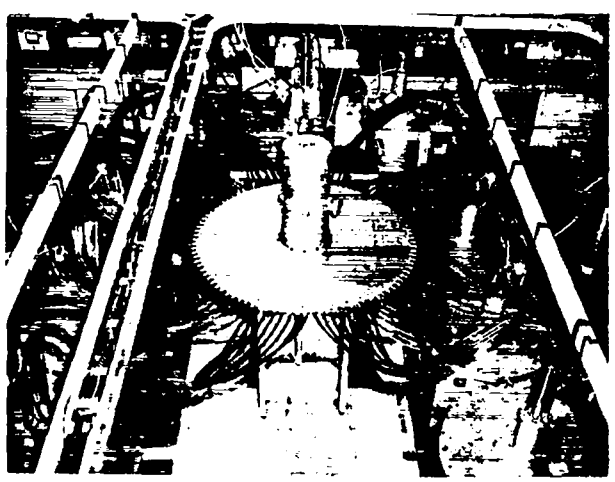

2. Overhead view of the DPF-V system.

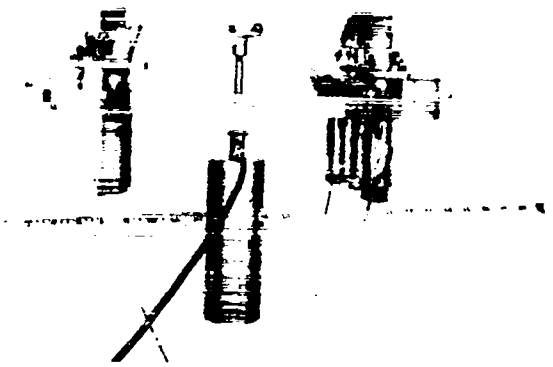

3. An 8-line vacuum pinch-off valve.

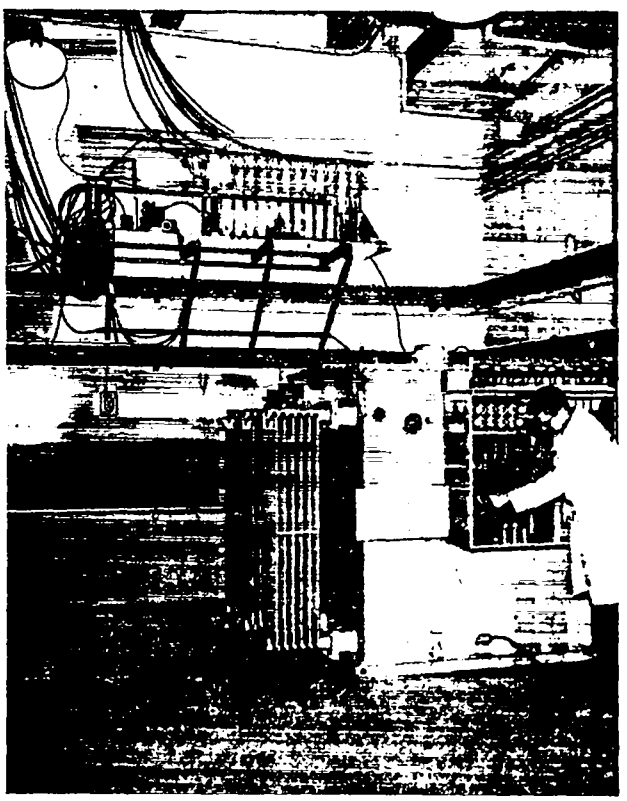

4. 60 kV - 3 A power supply and charging network for the 120 kJ - 50 kV capacitor bank.

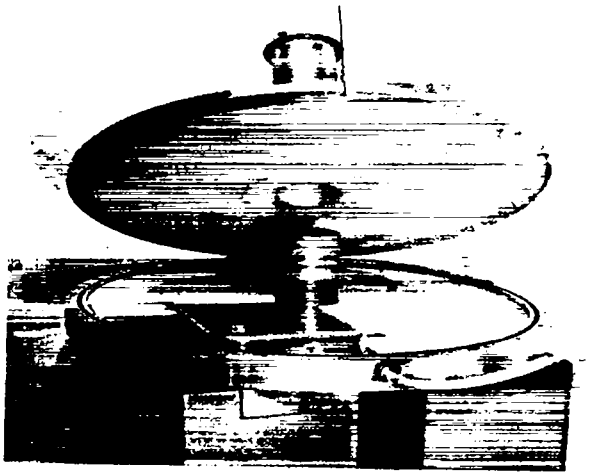

5. A 50 kV - 10 kJ capacitor module and vacuum switch.

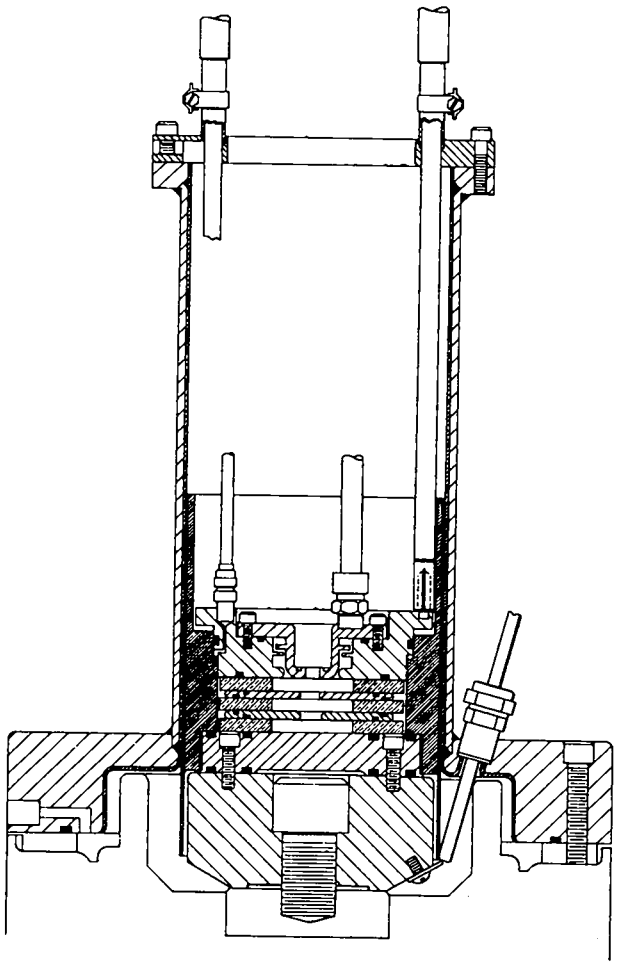

6. The 50 kV vacuum spark gap mounted on a 2 μF capacitor.

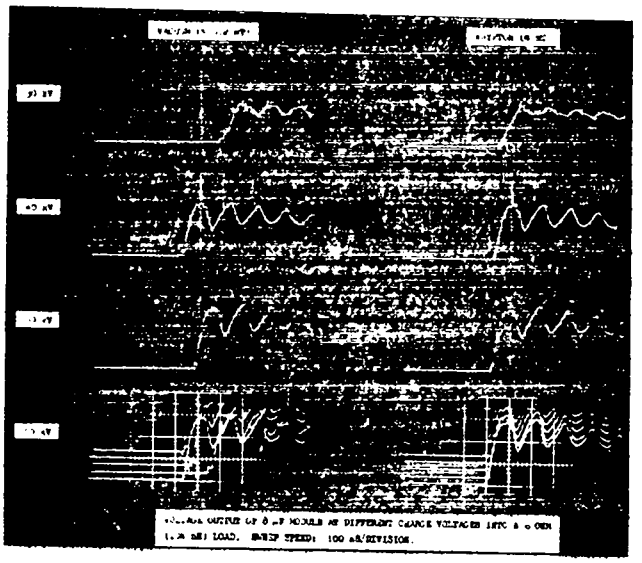

7. Several voltage output traces of a 50 kV - 10 kJ capacitor switch module.

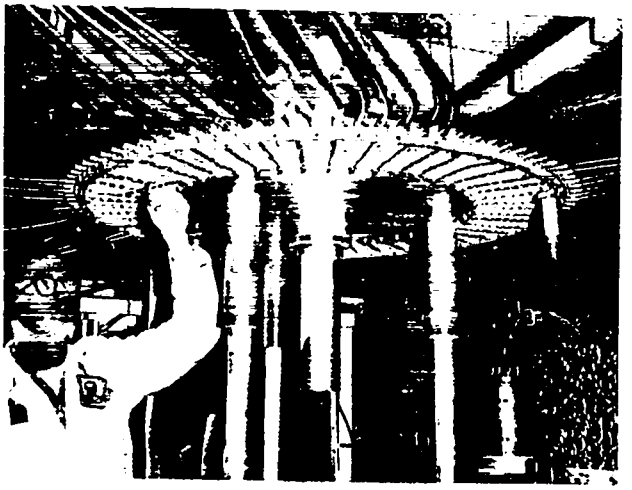

8. The input header for DPF-V, showing the carbon resistor, coaxial cable terminators.

IMPEDANCE MATCHING THE PLASMA FOCUS DEVICE†

by

J. P. Carpenter, K. D. Ware, P. J. Bottoms,
A. H. Williams, and J. W. Mather

Los Alamos Scientific Laboratory
University of California
Los Alamos, New Mexico

ABSTRACT

The electrical circuit for a dense plasma focus discharge is analyzed and the important parameters for optimizing the current to the discharge are obtained. Electrical and geometrical means for increasing the available current to the discharge are investigated. Optimization of the magnetic energy in the system is discussed.

Increasing the available current to a dense plasma focus (DPF) device increases the plasma temperature and/or density as shown by the relationship $I^2 \propto nkT$.

Circuit Analysis

Circuit analysis of the DPF machine which exhibits a varying load inductance can reveal the important parameters for optimizing the available current in this LC circuit. The electrical circuit of the DPF device is shown in Fig. 1. The capacitor bank C_o which is charged to a voltage V_o is discharged through a constant external circuit inductance L_e in series with the linearly varying inductance L_D of the plasma. The circuit equation is

$$(L_e + \dot{L}t)\,\dot{I} + I(R + \dot{L}) + \int_o^t I/C_o\, dt = V_o$$

The small external resistance R_e is neglected in this analysis. From experimental evidence[1] $L_D \cong \dot{L}t$.

Solution

As seen from the solution[2] of this circuit equation on Fig. 2, the time dependent current ratio $I(t)/I_m$ is a function of the dimensionless parameter $\beta \equiv \dot{L}/R_c$. The maximum current I_m is

$$I_m \equiv V_o \sqrt{C_o/L_e}$$

and the critical surge impedance R_c of the external circuit is

$$R_c \equiv 2\sqrt{L_e/C_o}$$

Current Enhancement

It can be seen that I(t) is enhanced when R_c is increased or $\dot{L}$ is decreased, i.e., when $\beta \to 0$. $\dot{L}$ is related to the finite work done on the plasma during the acceleration phase. Electrically I(t) can be increased by using a low capacitance high voltage system. Lowering the capacitance serves to increase the critical surge impedance R_c which results in a lower β. However, the applied voltage V_o must be increased to account for the resulting reduction of the maximum current. I(t) also can be increased geometrically by using larger electrodes while maintaining a constant electrode spacing. This reduces the aspect ratio r_o/r_i of the accelerator, which, in effect, reduces $\dot{L}$ since for a straight coaxial geometry $\dot{L}$ is defined as

$$\dot{L} = \frac{\mu_o}{2\pi} v \ln r_o/r_i$$

where v is the sheath velocity ($\sim 10^5$ m/sec) and r_o and r_i are the radii of the outer and inner electrodes, respectively. Thus, β can be affected by the term $\ln r_o/r_i$.

AN INTERCHANGEABLE THETA-PINCH PLASMA FOCUS MACHINE

by

Charles P. Wolfe
High Altitude Observatory
National Center for Atmospheric Research
Boulder, Colorado

ABSTRACT

A 224 uf 17 kV capacitor bank capable of interchangeably driving either a single turn theta-pinch coil or a high density plasma focus gun has been constructed at the High Altitude Observatory. This device is used as a spectroscopic light source for the study of atomic spectra of astrophysical interest in the soft x-ray and vacuum ultraviolet regions of the spectrum. When deuterium is used in each of the configurations, no detectable neutrons are generated in the theta-pinch, but a copious amount of neutrons are observed with the focus arrangement. Design criteria and operational characteristics of the machine will be described.

INTRODUCTION

At the High Altitude Observatory,* a high temperature plasma physics laboratory has been constructed. The purpose of this program is to provide laboratory identifications of spectra of highly ionized elements observed in the Sun. These identifications would allow a better understanding of the temperature and density structure and the chemical composition of the solar atmosphere. Two plasma devices, a theta-pinch and a plasma focus have, therefore, been built to serve as spectroscopic light sources. Conversion between the two systems is accomplished through the use of an interchangeable theta pinch coil and plasma focus gun. The same basic capacitor bank drives both systems.

In this paper we discuss some of the operational and design problems associated with this project with particular emphasis on capacitor and switching problems encountered. Preliminary measurements of neutron yields and electron temperature that have been made in each configuration are briefly reported.

* A division of the National Center for Atmospheric Research with primary laboratories located at Boulder, Colorado and operated for the University Corporation for Atmospheric Research, a 27 member university organization.

THE THETA-PINCH CONFIGURATION

The initial design of the theta-pinch (See Fig. 1) consisted of a main bank (BZ) of 16, 14μf, 20 kV capacitors - each with a low inductance folded return ignitron switch assembly.[1] Ninety-six 20P2 BICC cables (6 per switch), each 2' long, were attached to three sides of a pair of 4' square collector plates. These plates have an interchangeable tapered section on the fourth side feeding into a coil of adjustable length. The coil most often used was 6" long (26 nh) with a 1.16 mirror ratio and a 2-1/2" O.D. ceramic or pyrex discharge tube was inserted into it. The total inductance of the system was ~ 31.7 nh when using the 6" mirror coil which provided an initial voltage transfer from the capacitor bank to the coil of 82 percent.

Since second-cycle operation, hence a cooler plasma, was considered to be adequate for our preliminary work, only an initial RF pre-ionization was used while the first half-cycle of the BZ discharge was allowed to complete the ionization.

Thus, the spectra studied were generated during the second compression. The RF pre-ionization was obtained with a one kilowatt pulsed CW 27 MC transmitter turned on two seconds prior to, and off one second after, the discharge of the main bank.

The main bank capacitor failure rate was high, approximately one every 25-50 discharges. This problem was thought to be due to the short length of cable not providing adequate inductive isolation between the capacitors. The jitter time of the ignitron switches was sometimes as long as one microsecond. The possibility was considered that some of the switches firing early placed a near equal potential across the ignitrons that had not yet fired. This would cause some of the ignitrons not to switch on until the second half-cycle. This situation, creating an over-volting condition on the capacitor, possibly contributed to the failure rate.

The BZ cable length was extended to 10' in an attempt to reduce capacitor failure, however, an improvement was not noticed. The total circuit inductance increased to ~ 34.2 nh, while the voltage transfer efficiency dropped to 76 percent. Although usable spectra was being taken during this time, it became evident that a hotter source was desirable and a pre-ionization bank was added to move the operation to the first half-cycle. The pre-ionization bank (PI) consisted of two 1μf, 50 kV capacitors with switches and 10' cables identical to those used with the BZ bank. Nominal initial charge voltage was 18 kV. The circuit oscillated at 400 KC.

After addition of the PI bank, the prefire rate of the BZ bank increased sharply. The ignitrons apparently were incapable of holding off the ringing PI bank voltage until the desired time to fire the main bank.

The ignitrons had previously been cooled with continuously flowing tap water (45°F), but after the increased prefire rate, a refrigeration system was installed to circulate much cooler water (20°F). The prefire conditions remained about the same and the ignitron jitter became considerably worse. Next, 50-watt lights with aluminized reflectors were placed on the anode in an attempt to keep the top part of the ignitron hot so that the mercury would flow more easily into the reservoir at the base of the ignitron. A range of water cooling temperatures at the base of the ignitrons were tried at the same time the anodes were being heated. Satisfactory operation was not obtained. The jitter remained too large and the voltage hold-off capabilities inadequate.

Meanwhile, E. L. Kemp et al.[2] of the Los Alamos Scientific Laboratory developed a three element spark gap for the Scyllacita experiment. They most generously offered to share the new low inductance switch design with us. Since several of the major parts of the respective switches were interchangeable, with minor expense and time, a conversion was made to the folded return spark gap configuration. The spark gap switch vastly improved operation over the ignitron switches. The PI bank could now be fired without causing the BZ bank to prefire and the firing jitter between switches was reduced.

Although the spark gap proved to be a considerable improvement over the ignitron switch, an effort was made to modify the switch so that an increased number of shots could be obtained before switch maintenance was required (See Fig. 2). In addition, an attempt was made to further decrease the jitter. This was done by taking the cue from W. H. Lupton[3] of the Naval Research Laboratory. To accomplish this, the insulator around the trigger element was increased in diameter so that the discharge jumped from the trigger element to the bottom electrode, rather than to the top electrode. This mode of breakdown (mode I) serves to rapdily ionize the gap between the cathode and anode of each switch which reduces the jitter time. Mode 2 operation, with breakdown occurring between the trigger element and the top electrode, requires that the ionized particles diffuse outward from the anode toward the cathode. When the ionized cloud comes close enough to the cathode to arc over, the switch fires. Since each ionized cloud does not necessarily propagate with the same velocity nor have the same density, a slightly different firing time for each switch is

possible. A Mullite insulator of 5/16" diameter with a 3/32" bore into which a 3/32" pure tungsten welding rod is inserted serves as the trigger insulator and electrode.

Several different electrode surface configurations were tried. The arrangement finally adopted was a 5/8" wide flat surface that was machined on the end of each hemisphere and then radiused to blend into the hemisphere. The gap between the top and bottom electrodes is typically set at 0.400". This is sufficient to hold off PI ringing voltages of 18 kV without prefiring, when the BZ bank is charged to 17 kV. The jitter time of these switches does not exceed 50 ns. The switches have been fired in excess of 4000 times with only minor maintenance. Although conversion to the spark gap switch provided a more reliable operation, the capacitor failures still occurred at a high rate.

It was obvious that the capacitor failure was not determined by switch problems and we could find no appreciable transients in the system. We then began to open capacitors that had failed and examine them. To the best of my knowledge, the engineering techniques applied to the design of these units was sound. The failures all appeared to occur because of improperly applied solder connections between the tabs and the individual capacitor sections or the collector.

A possible explanation is related magnetic forces exerted on the poorly soldered tabs which cause them to work apart. Since the current is traveling in the same direction through areas separated by small voids, the magnetic pressure first constricts the loose section. When the current passes through its peak and starts towards zero current again, the constricted force is gradually released. The momentum of the loose section, as the current goes through zero, is sufficient to tear loose an additional area of the tab or the collector, depending upon where the void occurs. Repeated discharges enhance the problem and internal arcing then begins to occur. This causes small pieces of loosened material and chared oil to permeate the capacitor until they bridge the area between the charged portion of the unit and the grounded case. Later evidence presented in the discussion of the plasma focus, strengthens the above argument. An excellent argument for the necessity of building high energy capacitors very rugged and solid appears in a book by F. B. A. Früngel.[4]

With deuterium added, no neutrons were generated while using any or all of the configurations described above. Also, no noticeable deterioration of the Al_2O_3 discharge tube under the coil was observed after many thousands of discharges as has been reported in other experiments.[5] This suggests that it is the hot ions that do the work of destroying the area of the discharge tube under the coil when neutrons are produced. The electron temperature in our machine and others where neutrons are produced, are very similar (~300-350 eV).

THE PLASMA FOCUS ATTACHMENT

With the knowledge available of some of the effects of the circuit parameters, a plasma focus type attachment (See Fig. 3) was considered for producing higher electron temperatures to further extend our studies of atomic spectra. (Smaller plasma focus configurations[6] have been used for several years in our shock tube laboratory. In this laboratory, one of the studies involved the investigation of the effects of circuitry producing the limiting current phenomena[7]. The reader is referred to references 6 and 7 for details).

Because we had planned to use both the theta-pinch and the plasma focus attachments, depending upon the conditions required during the specific data taking period, it was desirable to be able to change configurations with the minimum overall effort. Another constraint was placed on the system by requiring the theta-pinch and plasma focus diagonostic axes to be the same. This resulted in a system having an asymmetric current feed. Approximately six man-hours are required to convert from one configuration to the other.

The inner diameter of the accelerator is 2 3/8", while the inner diameter of the outer conductor is 3 7/8". The length is 18" from the

current characteristics of the plasma focus configuration, the capacitor life was extended over that found when the bank was used as a theta-pinch. Large voltage transients in the system have thus far had no significant effect.

ACKNOWLEDGEMENTS

During the design and construction phase of the theta-pinch machine, many people in the Los Alamos Sherwood Project have shared their knowledge with us, to whom we are most grateful. Particular appreciation is expressed for the assistance provided by F. C. Jahoda, E. L. Kemp, G. A. Sawyer, and W. E. Quinn. Appreciation is also due to R. J. Wolf who provided valuable suggestions while the plasma focus attachment was being designed. Finally, my appreciation to L. L. House who has directed the project and has contributed invaluable assistance in preparing this paper.

REFERENCES

1. R. S. Dike and E. L. Kemp, The Design of a Capacitor and Switch Assembly for Low Inductance, LA-2957, October 14, 1963.
2. E. L. Kemp, E. M. Dolnick, R. S. Dike, G. A. Sawyer, and J. L. Tuck, Scyllacita-Compact High Voltage Theta-Pinch Machine, Rev. Sci. Instru., 37, 1065-1068, 1966.
3. W. H. Lupton, Fast Triggered Spark Switches for a Two Megajoule Capacitor Bank, Proceedings of the Fifth International Conference on Ionization Phenomena in Gases, Munich, 1961, (North Holland Pub. Co.).
4. F. B. A. Früngel, High Speed Pulse Technology, 1, 41-44, 1965, (Academic Press).
5. K. Boyer, W. C. Elmore, E. M. Little, W. E. Quinn, and J. L. Tuck, Studies of Plasma Heated in a Fast-Rising Axial Magnetic Field (Scylla), Phys. Rev. 119, 831-843, 1960.
6. R. J. Wolf and Y. Nakagawa, Plane Blast Wave Produced by "Dense Plasma Focus", to be published.
7. Y. Nakagawa, R. J. Wolf, and F. Y. Sorrell, On Limiting Speed of Current Sheet in Plasma Accelerators, to be published.
8. R. L. Blake, Plane Crystal Measurements in the Ultrasoft X-Ray Region With Application to Solar Physics, Thesis, Ph.D., Univ. of Colorado, 1968.

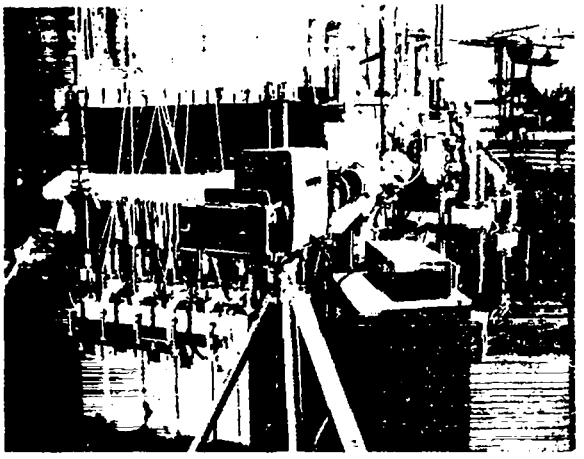

Fig. 1 General view of the initial design of the theta pinch.

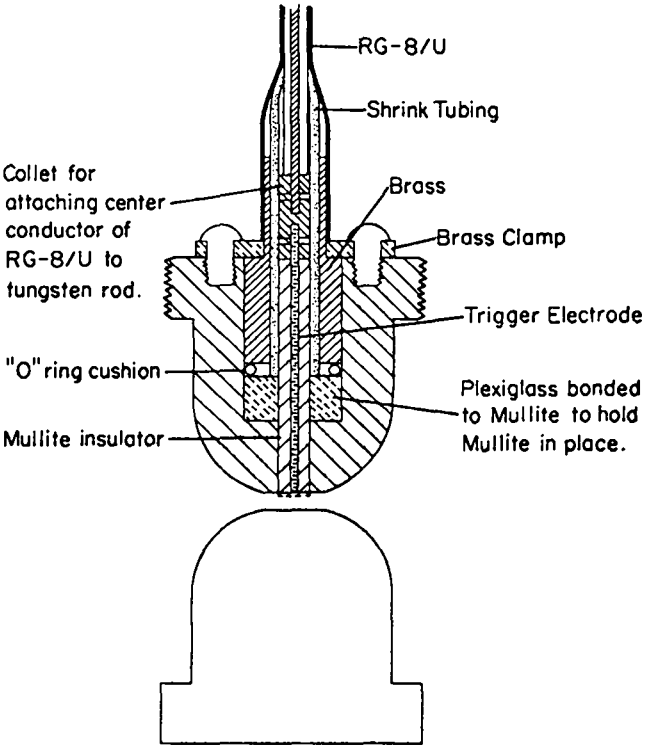

Fig. 2 Cut away view of the part of the low inductance three element spark gap switch showing the modified configuration. (See Ref. 2 for details)

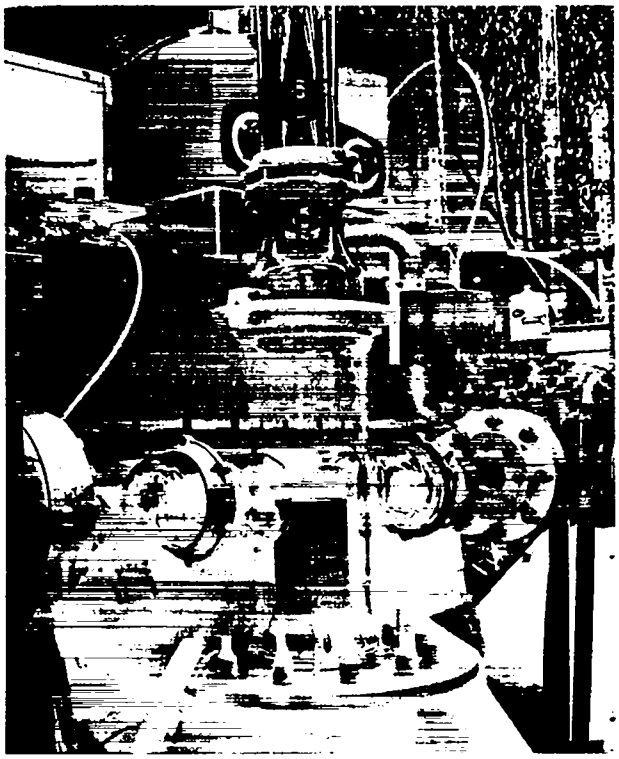

Fig. 3 The plasma focus attachment mounted in a vertical position so that the plasma formation is on the same diagnostic axis as the theta pinch plasma. The return current path extension is removed.

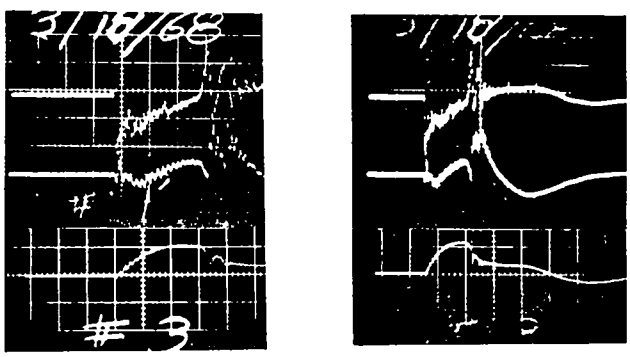

450μ Xe; 4370μ H₂, 1μs/cm; 10 capacitors

450μ Xe; 4320μ H₂, 2μs/cm; 10 capacitors

Ch 40 kV probe pickup at base of gun; 5 V/cm

Ch sum of Rogowsky loops - one on each capacitor; 1 V/cm

Ch current waveform from loop in lower collector plate; 0.5 V/cm

Fig. 4 Two sets of pictures showing the high voltage - fast transient signals associated with the plasma focus collapse. Also, note the damped signal and extended period after the collapse occurs.

APPLICATION OF THE NET-1 NETWORK ANALYSIS PROGRAM TO DISTRIBUTED CIRCUITS*

by

Grenfell P. Boicourt

Los Alamos Scientific Laboratory, University of California
Los Alamos, New Mexico

ABSTRACT

The NET-1 Network Analysis program is an engineering-oriented computer program which calculates the voltages and currents in an electrical network as functions of time. This paper describes the program briefly and discusses the modeling procedures for capacitors, cables, inductors, and switches, as well as large scale capacitor discharge circuits. Several examples are given which illustrate the exceptional capabilities of the program.

I. INTRODUCTION

NET-1 is a generalized network analysis program developed at the Los Alamos Scientific Laboratory by Malmberg and Cornwell.[1,2] The program performs a non-linear analysis of systems which can be modeled as lumped constant networks. While NET-1 is specifically designed for the analysis of transistorized electronic networks, it is capable of solving any mathematical system which can be treated as a fixed network. Kron[3,4] has shown that a surprisingly large group of mathematical structures can be treated exactly as fixed networks.

NET-1 calculates the voltages at each node of the circuit and the current through each inductor diode and transistor as a function of time. By use of the solution output program described in Refs. 1 and 2 it is possible to perform integration of one function with respect to another as well as form algebraic expressions involving the variable and time. The NET-1 program contains an internal library of transistor and diode characteristics and will print out warnings if the maximum ratings of such components are exceeded. Examples of steady-state and transient analysis are given in Refs. 1, 2, and 5. The computational methods are described in Ref. 6.

The original program was written for the MANIAC II computer and this version is described in LA-2853.[1] A second version has been written for the IBM 7090/94 and this is described in LA-3119.[2]

II. MODELING

In order to compute the action of a given circuit it is necessary to assign to each physical circuit component a network model, i.e., an equivalent circuit, made up of resistors, capacitors, inductors, power sources, etc. This model should describe the electrical properties of the component with sufficient accuracy that when the component model is used in the overall circuit model, the resulting solution approximates the actual solution to within whatever limits are required. It is possible to use quite elaborate models even for what could be considered simple components.

There are a number of things to be considered when choosing component models for NET-1. These

include, among others, the size of the final circuit, the type of solution desired, and how much time can be spent in computing the solution. The memory size of the computer on which the problem is to be run limits the total number of resistors, capacitors, and inductors which can be used in the overall circuit model. Thus it may be necessary to choose simple equivalent circuits for the components if the overall circuit is large. The situation which arises concerning the type of solution can best be illustrated by an example. Suppose one wishes to model a capacitor discharge circuit and the desired solution is the voltage and current profile at the load. In this case the capacitive components can usually be modeled as pure capacitors or as a simple series connection of a pure capacity, a pure resistance, and a pure inductance. However, if one wants to know what voltages and currents may occur during discharge inside the capacitive components themselves, such models would not be suitable. The time required to solve a problem increases with the number of circuit elements so time and cost limitations may dictate the use of simpler equivalent circuits and the acceptance of less detailed information about the circuit.

Generally we have found that the simpler models are adequate. A resistor is modeled by a pure resistance. An inductor is modeled by a pure inductance in series with a resistor. Since NET-1 requires that a resistance accompany any inductor this model is the simplest inductance model allowed. If a resistive value does not accompany the inductive value on the input list the program will supply a value of 10^{-7} ohms. A capacitor is usually described by a pure capacity in series with an inductance and resistance. Coaxial cables can be modeled as ladder networks of series inductors and parallel capacitors. The cable resistance is included as the resistance associated with the inductors.

In NET-1, switching is handled by specifying the conditions in the circuit at the instant the switch is closed and starting a transient analysis at that time. Thus at turn-on time in a capacitor discharge circuit, capacitors are charged and no current is flowing. The switch then appears in the circuit usually only as a passive element with inductance and resistance. If it is desired to simulate the firing of a spark gap, it is possible to specify a voltage source which is connected bucking the capacator voltage and which decays exponentially with a specified time constant. This is equivalent to assuming an exponentially decaying arc drop in the gap. An extension of NET-1, NET-2, will have a number of features which are not present in NET-1. One of these features will be a much greater capability in handling switched circuits.[7]

III. EXAMPLES

Figure 1 shows the network analog of a test circuit used for testing capacitors and cable cartridges. C1 is the source capacitor, L1 is the internal inductance of the capacitor, L2 is the inductance of the capacitor header, and L3 represents the inductance of the spark gap switch. L101 through L116 and C101 through C116 form a ladder network which simulates six parallel coaxial cables. L117 represents the inductance associated with the cable cartridge and C200 is the capacity of the collector plate holding the cartridge. L200 simulates an inductive load which in this case is a 16-inch diameter copper loop. Each node to which components are connected or at which the voltage is desired is numbered. The common node at the bottom which would normally be grounded is assigned the node number 0.

The input list requirements for NET-1 are described in detail in Refs. 1 and 2. Figure 2 shows the input list for the network of Fig. 1. The first column gives the program designation for each component. The second and third columns give the nodes to which the component is connected. The fourth column specifies the value of the component. The fifth column specifies the value of resistance to be associated with the inductors. The units used in the NET-1 program are picofarads, microhenries, kilohms, milliamperes, nanoseconds, and volts; however, any other consistent set of units may be used. The initial conditions on each circuit component are specified individually under the obvious heading. The voltage is specified for a capacitor and the current for an inductor. If the name of a component does not appear in the initial conditions list, the appropriate value is assumed to be zero by the program.

Let us return to the circuit shown in Fig. 1. If the source capacitor C1 is initially charged to 60 kV and C200 is small, it is possible to observe

the effect of terminating the cables in a large inductive load. The impedance mismatch leads to voltage enhancement at the load which is then reflected back toward the source capacitor. This reflection is illustrated in Fig. 3 which shows the voltage-distance-time surface for the cable in the circuit of Fig. 1 during the first 110 nsec of the discharge as computed by NET-1. As we go from node 18 toward node 1, we see the voltage rising toward 60 kV at later times. At approximately 42 nsec, the voltage at node 1 passes above 60 kV and the voltage reflection back toward the source capacitor. The ability to follow a pulse, as just illustrated, is one of the remarkable properties of the NET-1 program. After a little practice one finds it easy to follow reflected pulses for quite large distances and times even in more complicated circuits merely by scanning the print-out. This gives an intuitive understanding of the action of the circuit probably not obtainable in any other way. This understanding allows one to pinpoint areas where large overvoltages may occur and to provide for the proper insulation at these points in the physical circuit.

An example where the cables are terminated in a capacitive load is shown in Fig. 4. In this case C2 is much smaller than the source capacitor C1, but the combination of C2 in parallel with the cables to the bottom left and to the right of it presents an almost capacitive termination. This is a model of the pulse test used to evaluate coaxial cable and capacitors. The cable to be evaluated constitutes the ladder network running to the bottom left. The action of the circuit is essentially that of a capacitive doubling circuit. That is, in the absence of the cable to the right and the inductor L2, the capacitor C2 would discharge to approximately

$$V_{c2} \approx \frac{2\,V_{oc1}}{1 + C2/C1}\,.$$

L2 represents the inductance of C2. The cable on the right, which represents a high impedance, is used to drain off the charge. The test cables follow the voltage on C2 except that some transients are induced which result in further overvoltage to the test cables.

During the preliminary design work for Scyllac it was felt that it would be desirable to be able to disconnect the cables at the end of each capacitor rack. This was to have been accomplished by making a plug-in splice in each cable. A metal splice tube was designed which was 15 inches long with polyethylene insulation inside to separate the center conductor of the cable from the coaxial return of the tube. The cable was then to be cut and plugged in each end of the tube with suitable hardware. The tube was designed for use in air.

The model in Fig. 4 was used to estimate the voltage appearing at the mismatch which the tube introduced. Capacitors C36 and C37 and inductor L36 were changed to the capacitance and inductance values calculated for the tube. Figure 5 shows the voltage at node 26 calculated by NET-1 as well as the voltage at node 2. An actual test was made with 6 tubes, one on each of the cables in the test, inserted at the position of L36. Five of the six tubes arced on the first shot. These arcs occurred across 7 inches of polyethylene insulation parallel to the axis of the cable. Since the E-field must be predominantly radial in this configuration, it indicates what a sizable voltage must have been present to cause the arcing. From the figure we see that NET-1 calculated this voltage to be approximately 118 kV. It will be noted that the voltage at node 26 follows grossly the voltage at node 2 but at a higher level and with a time delay of about 20 nanoseconds.

Figure 6 shows the NET-1 model for an entire cartridge-fed theta-pinch machine. The nodes along the top horizontal line correspond to cable cartridge rows, the inductors between them represent the inductance of the collector plates between the rows. The main bank consists of capacitors C1 through C14, the ladder networks between the capacitors and the cable cartridge nodes represent cables. The capacitors directly below the cartridge nodes represent the collector plate capacity. Observation shows that there is some high frequency ringing between the load inductance, L500, and the collector plate capacity which does not seem to involve the main bank or cables. Since the resistance which the collector plate presents to this oscillation is considerably higher than the resistance presented to the primary oscillation, resistors having the values calculated for the higher frequency are introduced in series with the capacitors which represent the collector plate capacitance.

It is believed that this circuit is the largest ever run on NET-1. The circuit has 170 nodes, 153 capacitors, and 154 inductor-resistor combinations. The problem was run on MANIAC II which at the time had a memory of 80 K decimal. A check at the time showed that it would be possible to increase the size of the circuit by about 15 nodes. With this size circuit computing time becomes critical. The computing rate was about 50 nanoseconds circuit time per hour of real time.

IV. SUMMARY

In summary, the NET-1 program provides a useful means for analyzing capacitor discharge systems in particular, and any network system in general. The use of NET-1 can lead to better understanding of the transient phenomena associated with such circuits. It is an aid in explaining high-voltage system failures and can be used to establish better design criteria for the components used in such systems.

ACKNOWLEDGEMENTS

The author would like to thank F. L. Cornwell, K. W. Hanks, E. L. Kemp, A. F. Malmberg, and C. L. Wilson for their help and encouragement.

REFERENCES

* Work performed under the auspices of the U. S. Atomic Energy Commission.

1. A. F. Malmberg and F. L. Cornwell, "NET-1 Network Analysis Program", Los Alamos Scientific Laboratory Report LA-2853 (1963).
2. A. F. Malmberg, F. L. Cornwell, and F. N. Hofer, "NET-1 Network Analysis Program, 7090/94 Version", Los Alamos Scientific Laboratory Report LA-3119 (1964).
3. G. Kron, "Diakoptics, The Piecewise Solution of Large-Scale Systems", MacDonald and Company, Ltd., London (1963).
4. G. Kron, "Tensor Analysis of Networks", MacDonald and Company, Ltd., London (1965).
5. A. F. Malmberg, "NET-1 Gets 'A' for Accuracy", Electronics 40, No. 3, p. 76 (1967).
6. A. F. Malmberg, "Computational Methods in the NET-1 Network Analysis Program", Los Alamos Scientific Laboratory Report, LA-DC-8921 (1966).
7. A. F. Malmberg, "NET-2 Extensions and Differences with NET-1", Los Alamos Scientific Laboratory Report, LA-DC-8787 (1967).

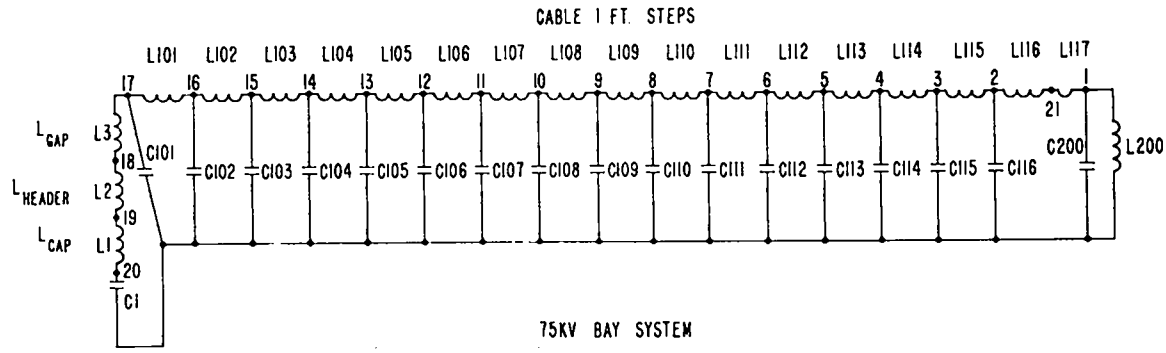

Fig. 1. NET-1 model capacitor discharge through cables into inductive load.

```
"75KV BAY SYSTEM BOICOURT"
c1     20     0        1.85+6
c101   17     0     456.
c102   16     0     456.
c103   15     0     456.
c104   14     0     456.
c105   13     0     456.
c106   12     0     456.
c107   11     0     456.
c108   10     0     456.
c109    9     0     456.
c110    8     0     456.
c111    7     0     456.
c112    6     0     456.
c113    5     0     456.
c114    4     0     456.
c115    3     0     456.
c116    2     0     456.
c200    1     0     432.
l1     20    19       6.-3        .87-6
l2     19    18      14.-3       2.03-6
l3     18    17      50.-3      12.1-6
l101   17    16       7.167-3     .1833-6
l102   16    15       7.167-3     .1833-6
l103   15    14       7.167-3     .1833-6
l104   14    13       7.167-3     .1833-6
l105   13    12       7.167-3     .1833-6
l106   12    11       7.167-3     .1833-6
l107   11    10       7.167-3     .1833-6
l108   10     9       7.167-3     .1833-6
l109    9     8       7.167-3     .1833-6
l110    8     7       7.167-3     .1833-6
l111    7     6       7.167-3     .1833-6
l112    6     5       7.167-3     .1833-6
l113    5     4       7.167-3     .1833-6
l114    4     3       7.167-3     .1833-6
l115    3     2       7.167-3     .1833-6
l116    2    21       7.167-3     .1833-6
l117   21     1       5.330-3    1.-8
l200    1     0       1.        14.4-8
interrupt    16.+3
print  2.
resolution     .5
initial conditions
       c1    -6.+4
       time 00.0
end
```

Fig. 2. Typical input list for a NET-1 problem.

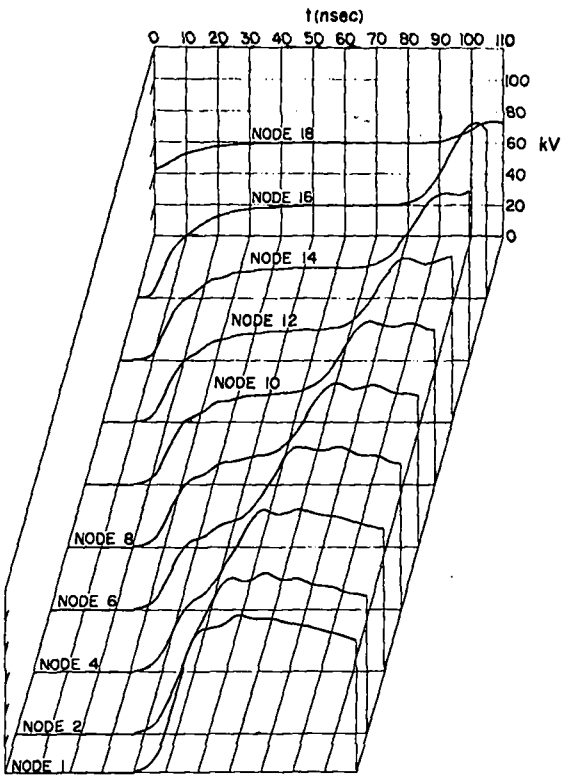

Fig. 3. Voltage-time-distance surface showing reflections of pulse by an inductive load.

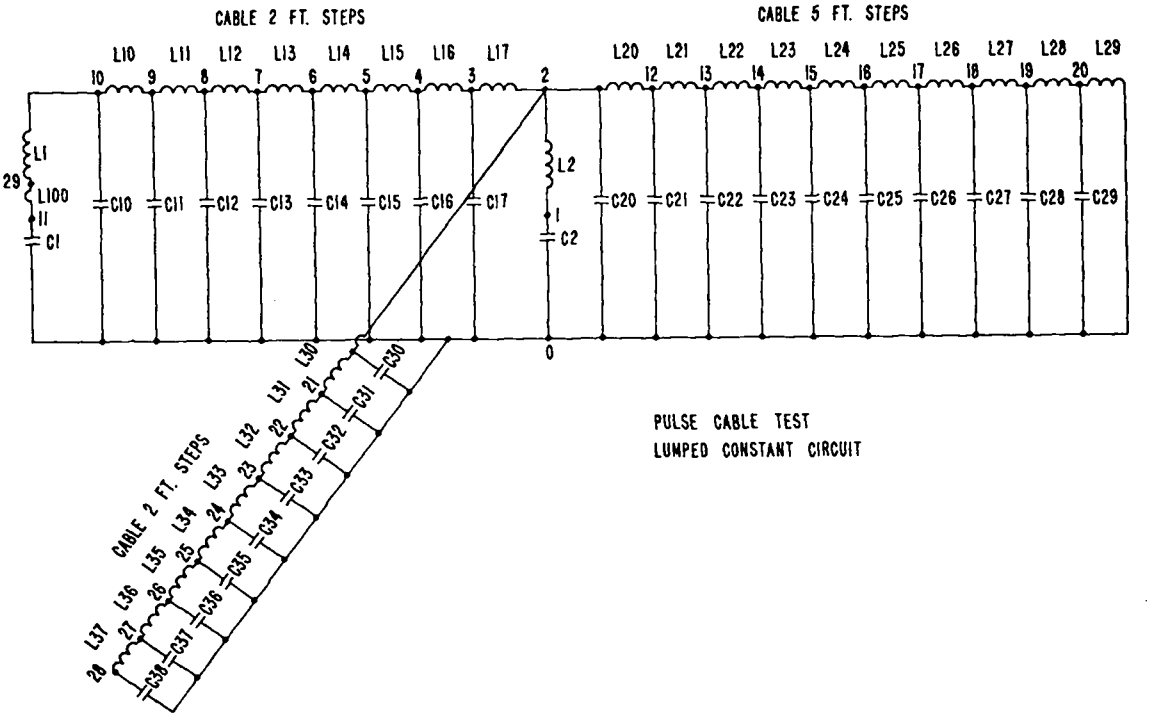

Fig. 4. NET-1 model of pulse cable test.

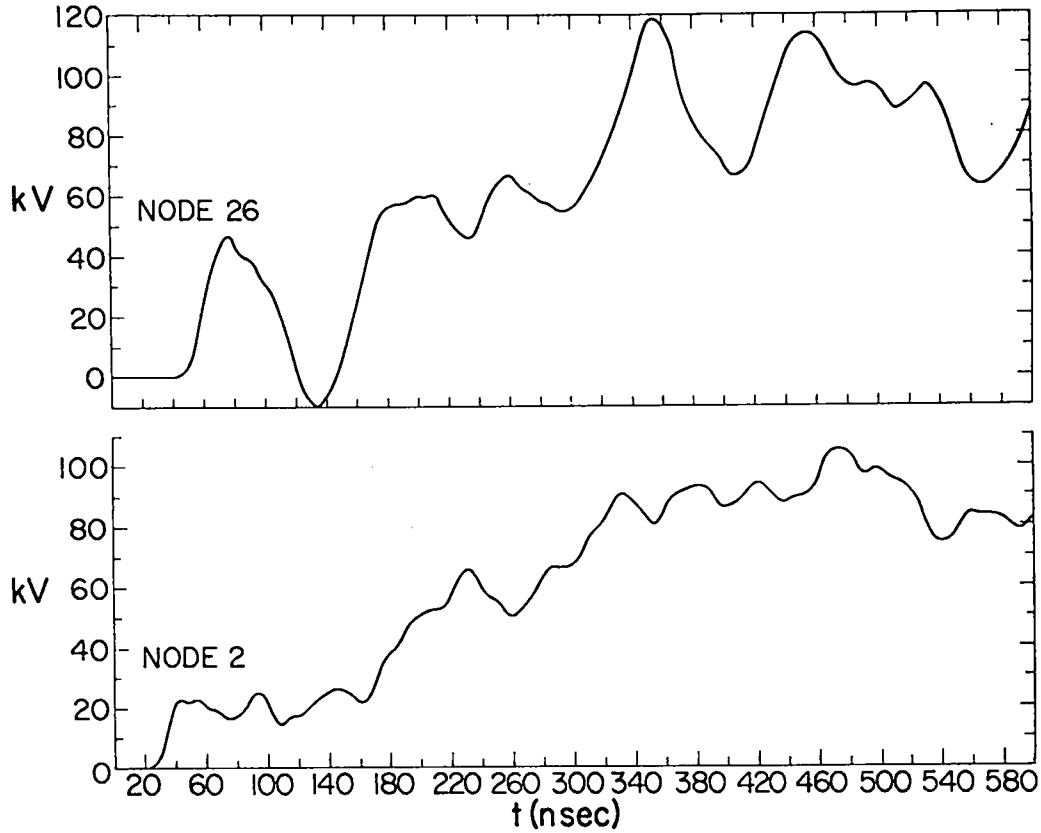

Fig. 5. Computed voltage traces for nodes 2 and 26 in circuit of Fig. 4.

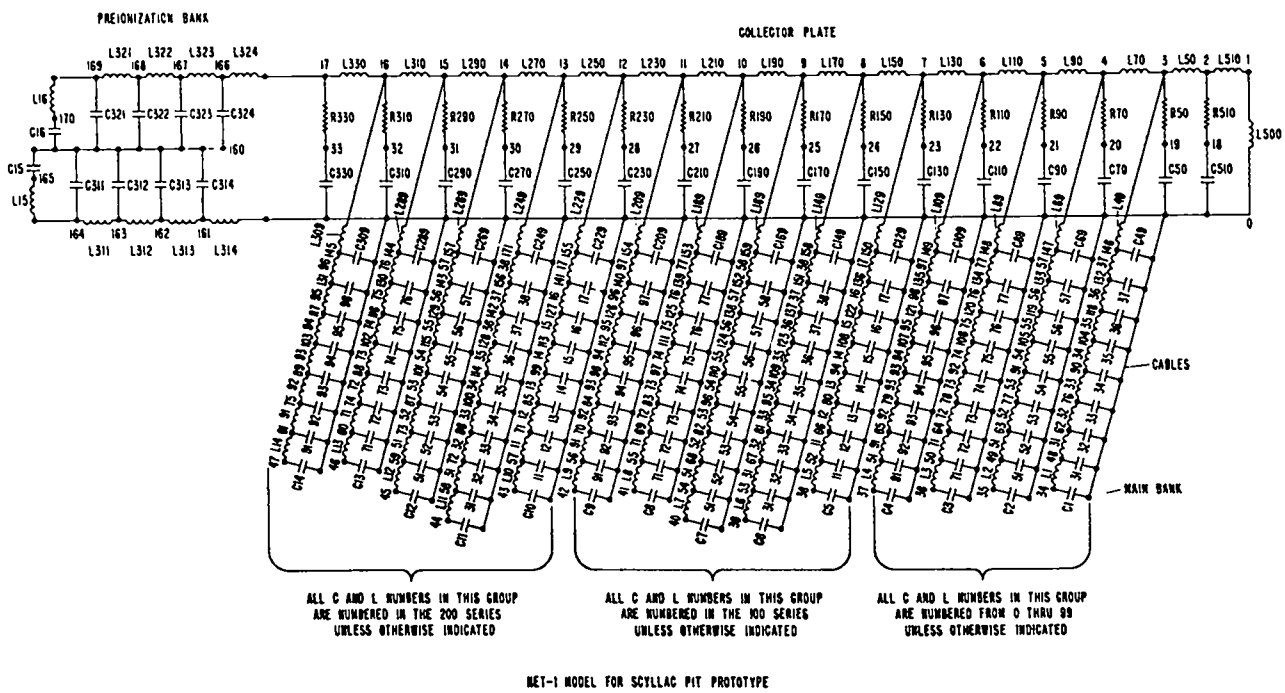

Fig. 6. NET-1 model for a complete theta-pinch machine.

HIGH CURRENT COAXIAL DC BUS SYSTEMS*

by

Charles W. Bushnell
Plasma Physics Laboratory
Princeton University
Princeton, New Jersey

ABSTRACT

Water cooled coaxial DC bus systems, constructed of standard sizes of copper pipe and tube, with current ratings of 500, 5,000 and 20,000 amperes are discussed with regard to the design parameters pertinent in the immediate proximity of a magnetic device.

The attractiveness of a coaxial system is quite obvious when (1) design for normal and fault loading due to self fields, (2) design for loads due to stray fields, and (3) generation of disturbing magnetic fields are considered.

The test results from prototype designs are used to compare and evaluate the coaxial systems with the more standard water and air cooled bus. Parameters considered include: (1) space requirements, (2) power requirements, (3) total system costs, (4) material availability, and (5) design flexibility.

A casual approach toward the problem of bus design in the immediate proximity of an experimental device may result in serious magnetic, structural and financial problems. These problems will be avoided if attention is given to the following eight design considerations:

1. Space availability
2. Normal and fault loading (self field)
3. Loads due to stray fields
4. Generation of disturbing magnetic fields
5. Power requirements
6. Cost
7. Material availability
8. Ease of removal and modification

As a means of evaluating the above factors, three basic designs for a "typical" bus run are shown in Fig. 1. This typical run will also be used to evaluate two other designs.

The design requirements for the run result from the characteristics of a typical power supply available at the laboratory:

Current Steady = 5000 amps
Max. Line Voltage = 800 volts
Max. Fault Current = 50,000 amps
Ground Insulation Test Level = 5000 volts

The first two systems in Fig. 1 represent standard practice presently used at the Plasma Physics Laboratory. The third system, a high current coaxial design, is a significant departure from our standard practice. It should be noted that the relative space requirements for each system would seem to favor the coaxial design.

A test section of the 5000 ampere coaxial design is shown in Fig. 2. The section was designed to be water-cooled utilizing the laboratory 60 psi water system. It was constructed using

*Work performed under auspices of the U. S. Atomic Energy Commission.

readily available sizes of type K and L copper tube and schedule 80 copper pipe.

The interior conductor is a length of 3/4 inch nominal schedule 80 copper pipe with machined fittings brazed in each end that are both water and electrical connections. The assembly is insulated with two layers of heat shrinkable irradiated vinyl tubing.

The exterior conductor is itself a coaxial pair, fabricated using two lengths of copper tube. The outside tube is 1-1/2 inch type L and the inside tube is a length of 1-1/4 inch type K. These are brazed into machined end blocks which form the water and electrical connectors. Section to section connections, both straight and right angle, are made using lengths of 1/2 inch thick copper bar stock. An insulation system of mylar and glass-epoxy will be used on the exterior conductor.

As a further means of evaluating the three designs, Fig. 3 summarizes basic engineering data and the costs involved in each. With Fig. 3 in mind, let us consider the remainder of the basic design considerations:

Normal and Fault Loading (Self Field) - The first two designs have been braced for this, resulting in higher costs. The coaxial system presents no problem and the costs reflect only the interconnecting bolts.

Load Due to Stray Fields - Obviously, the coaxial system is free from this effect and the costs of the other system do not reflect this problem as it is hard to establish a realistic value in an analysis of this nature.

Generation of Disturbing Magnetic Fields - The coaxial system not only solves the problem, but it avoids such things as the cost and time of computer studies to evaluate the effects of the first two systems.

Power Requirements - The air cooled system is superior, however, the requirements of the other two systems represent a loss of less than 0.5% of the total available from the supply.

Cost - The figures speak for themselves, however, they are only material costs. Fabrication of the coaxial system would obviously be higher due to the more complicated nature of the end connections. The latter would be compensated for, to some degree, by cost of extra bracing required for stray field loads on the first two systems. If an increase in resistance of approximately 30% can be tolerated, standard water tube and pipe can be used in the coaxial design resulting in a cost-per-foot reduction of about 10 to 15%. It should also be noted that minimum order requirements in extruded copper are usually in the 1000 to 5000 pound range and for small jobs this can greatly affect the actual cost of the standard water-cooled design.

Material Availability - The material (ETP Copper) for the air-cooled design and the connectors in both the water-cooled and coaxial design is readily available. Purchase of special extrusions required for the standard water-cooled design is involved with not only minimum requirement clauses but also long (10-15 week) delivery schedules. High conductivity tube and pipe are available in 3 to 4 weeks and standard water tube and pipe are usually off the shelf items in any quantity.

Ease of Removal and Modification - It would appear that all three systems are about equal in this regard.

Two other coaxial systems are listed in Fig. 3. A test section of the 500 ampere design is shown in Fig. 4. This design uses 1/2 inch type L tube as the interior conductor and single cooling path. This conductor is insulated with a single layer of heat shrinkable irradiated vinyl tubing and then potted in place within the exterior conductor with RTV-11 Silicone rubber. This electrical insulation is also used as the thermal

conductor from the exterior electrical conductor to the central cooling path. The exterior conductor is a 3/4 inch type L tube (5/8 O.D.). Straight and right angle connectors are made using 1/8 inch thick copper bar stock. Tests of the prototype design, shown in Fig. 4 have produced values of thermal conductivity of the combined RTV-vinyl system of 0.0064 watts/in-^{o}C (Were both interior and exterior conductors to be changed to type K of the same respective sizes, the rating of this design could easily be doubled.) The other design features of this system are generally similar to the 5000 ampere system.

The last column in Fig. 3 represents scaling of the 5000 ampere coaxial system to a D.C. current rating of 20,000 amperes. In this design the exterior conductor is again a pair of coaxial tubes. The exterior is a 3-1/2 inch type K tube and the interior is size 3 inch type K tube. The interior conductor is a length of 2 inch schedule 160 pipe. Straight and right angle connectors are made using 1 inch thick copper bar stock. Materials for this design are available in high conductivity copper on a 3-5 week delivery basis. The power requirements for the "typical" design run seem high, however, they are actually only 1-1/4 % of the capability of the anticipated power supply.

Costs of terminal fabrication may make the coaxial design more expensive than conventional bus systems. This cost, however, is frequently justified when consideration is given to all requirements which must be considered in the neighborhood of a magnetic device.

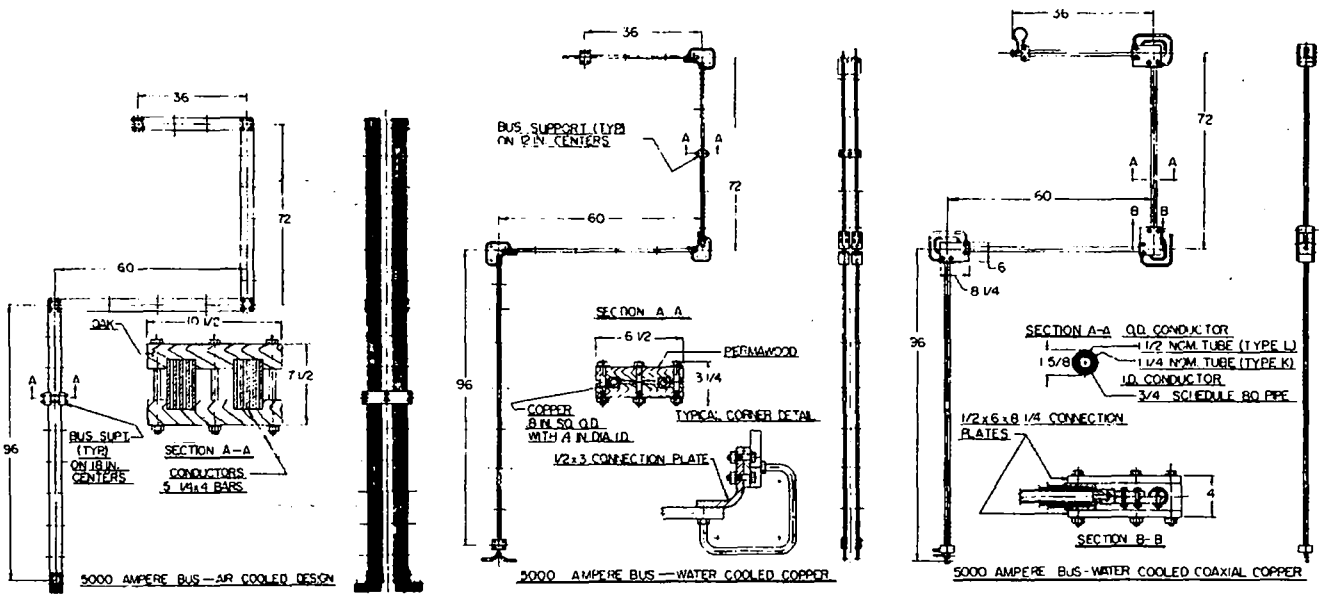

Fig. 1. A typical bus run for three designs.

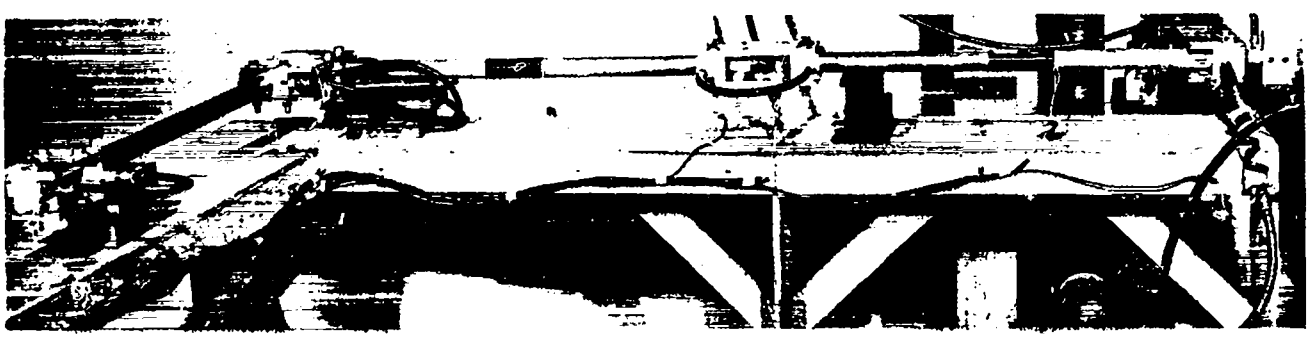

Fig. 2. Test setup for the prototype 5000 ampere water cooled coaxial bus system.

(1)

ENGINEERING DATA AND COST COMPARISONS FOR SEVERAL BUS SYSTEMS

	Air Cooled	Water Cooled	W/C Coax	W/C Coax	W/C Coax
Design Rated Current - Amps.	5000	5000	5000	500	20000
R/Loop Foot (at 20°C)-Ohms x10^{-6}	3.3	33	33	180	6.5
Current Density - Amps/$in.^2$	1000	10000	10000	5200	8000
Total Voltage Drop - Volts	0.42	3.5	3.5	2.1	2.8
Total Power Loss - kW	2.1	18	18	1.1	56
COSTS:					
Conductors	$ 720	$ 152	$178	$ 31	$ 889
Supports, Bolts, Etc.	159	37	15	6	57
Insulation	--	17	28	25	42
Water Cooling	--	24	21	12	39
TOTAL	$ 879	$ 230	$242	$ 74	$ 1027
COST PER LOOP FOOT	$ 40	$ 10	$ 11	$ 3	$ 47

(1) Based on design shown in fig. 1 and using 100% I.A.C.S. copper

Fig. 3. Engineering data and cost comparisons for several bus systems.

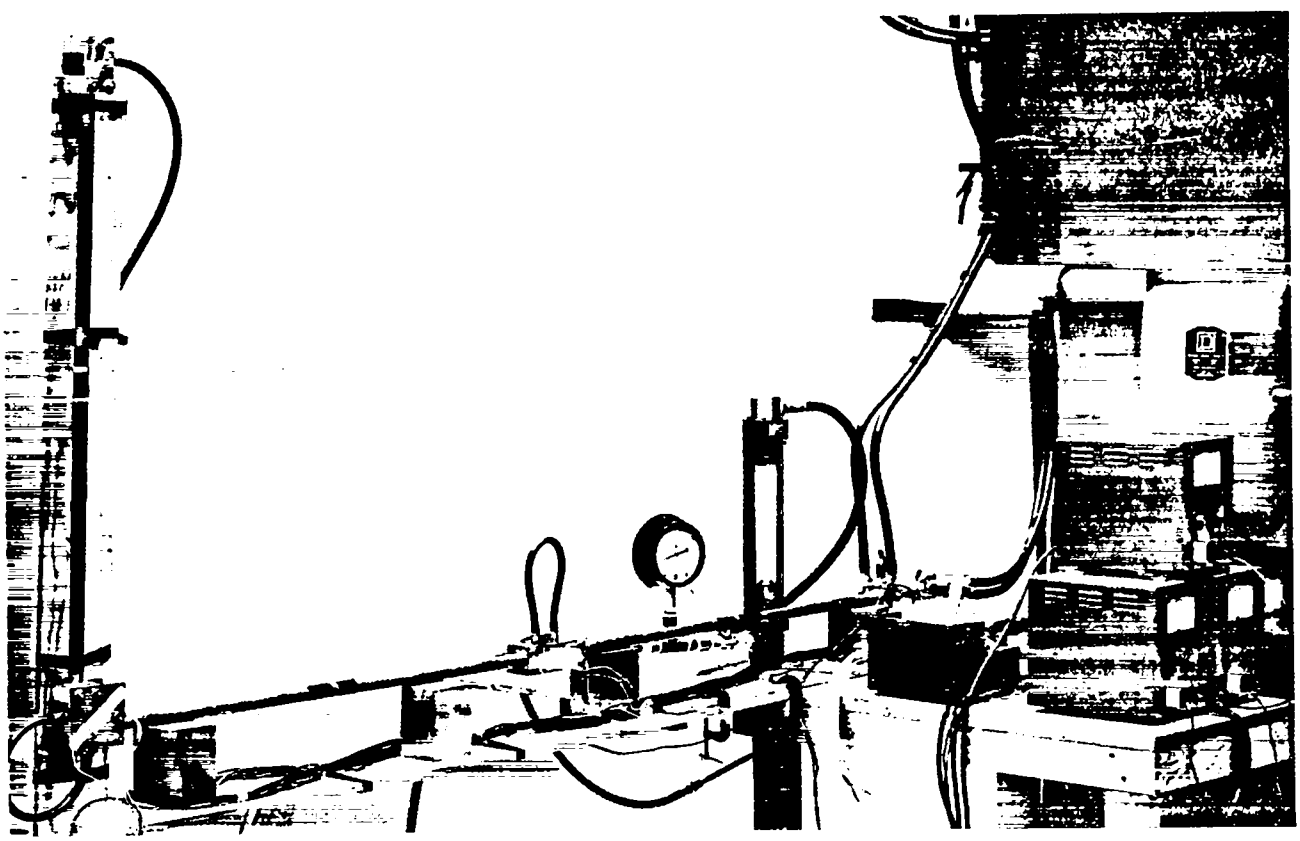

Fig. 4. Test setup for the prototype 5000 ampere water cooled coaxial bus system.

HIGH-CURRENT JOINT TECHNIQUES*

by

R. S. Dike and W. H. Borkenhagen

Los Alamos Scientific Laboratory, University of California
Los Alamos, New Mexico

ABSTRACT

This report discusses various methods of transferring high-current pulses in the range of 5 - 100 kA/cm through mechanically-made joints of a type that can be easily disassembled. The examples cited and the techniques involved are taken from devices actually in successful operation. Several different joint designs have been developed and those presented are divided into the following categories: (1) joints for flat plates; (2) joints for round bars; and (3) joints for cable terminations.

Joints for Flat Plates

In the design of flat plate transmission lines to energize theta-pinch coils, the plates are often of a nature and/or size that necessitates their being made in sections and then secured together in a suitable fashion for efficient transfer of the current in an unrestricted manner. The theta coil itself must also be attached to the transmission line. The methods used to physically join the pieces together in a non-sparking manner have been of major concern to our designers.

Figure 1 shows a typical flat plate joint of the butted variety and one that is quite common in the theta-pinch business. This type of joint is now in use on the Scylla IV device. A soft annealed copper gasket is between the sections being joined, and the joint is pulled together by a bolt and barrel nut arrangement. Such a joint may be made as long as desired to accommodate any plate width, provided the bolt loading and spacing is adequate per unit area. This joint, currently in use, is transferring approximately 25 MA or about 54 kA per cm, with little or no sparking.

* Work performed under the auspices of the U. S. Atomic Energy Commission.

Figure 2 shows another type of flat plate joints. This one differs only in one respect and involves the position of the gasket. Here it is placed horizontally as opposed to the vertical butted type shown in Fig. 1. By extending a few sheets of insulation material into the vertical crack, one can prevent the current from jumping across the gap. Even though the current is forced to transfer in a seemingly undesirable manner, this joint is in some respects superior to other flat plate joints. The bolt loading and spacing are essentially the same as in other joints, but an advantage in using this type is the deletion of the bored holes necessary for the barrel nut arrangement, allowing one to maintain consistent plate strength throughout. One possible disadvantage, however, is some added inductance in the system due to the small loop the current must make at the transfer point.

A third type of joint is shown in Fig. 3. This is a welded flange type, used with only marginal success due to the inefficiency of the bolting method. Adequate bolt loading is difficult to realize at the current transfer point since the maximum bolt-load pressure is too far removed from where it should be to assure a non-sparking contact. This type is

recommended only where current densities are less than about 50 kA per cm.

Bolt load calculations for these joints may be performed to determine bolt size and preload torque in the following manner:

$W = \pi b\, gy$* (for cylinder configurations)

$W = bly$ (for linear configurations)

where W = bolt load (pounds)

b = seating value (see ref.)

g = mean gasket diameter

y = minimum design seating stress

l = length of gasket

*Pressure Vessel Code 1962 (UA-49.2)

This formula, used primarily in pressure vessel applications in gasket pre-load requirements, has worked quite well for the high-current joints under discussion here. Figure 4(a) shows the suggested use. The bolt-load value, "W", thus obtained, may be divided by any number of bolts desired, but several small bolts will be better than a few large ones since they can assure a more uniform gasket pressure over the area involved.

Machined steps, either in the gasket or in the plate material, have been found to be desirable since the contact area is thus reduced allowing the bolt load requirement to be much less. Figure 4(b) shows such an arrangement. Here "n" width of gasket refers only to the material actually making contact with the two plates.

Bolts should be carefully torqued to the value indicated by the gasket seating pressure requirement. However, there may be instances when the magnetic field pressure between the plates is large enough to affect significantly the gasket pre-load value and loosen the joint. When this is the case, the torque per bolt should be increased accordingly.

Joints for Round Bars

High-current transfers from round bars presents rather a challenging problem. In the design of the Quadrupole Device for Cross-Field Injection, for instance, one is confronted with the design of a single coax conductor capable of carrying in the order of 750 kA or a current density of 100 kA/cm at close to a 1-millisecond period. Figure 5 shows one solution to the problem. In use here as the transfer method is a kind of collet device similar in some respects to the type used in machine lathes for holding stock while it is turning. The mechanical advantage gained by using a collet is well known. Considerable frictional resistance can be obtained through the use of the taper. For instance, the taper-shanked drill, when forced only hand-tight in a tapered socket, can resist very high turning forces when drilling a hole in some material. These forces prevent the drill from twisting in the socket, and their magnitude, normal to the tapered surfaces, is many times higher than that required to simply initiate the seat. It is this taper principle, then, that when applied to current joints of the round bar variety, can achieve a highly effective means of accomplishing an efficient, non-sparking interface.

The collets used in this instance are machined with a 5° taper angle. Care must be taken to assure that the contact surfaces are smooth, preferably polished, and with no tool marks. Diameter of collet hole and shaft diameter are made to the same size and toleranced very closely so that when the collet is tightened, the surfaces of the collet hole and shaft are parallel.

If one realizes the above conditions, the tightened collet around the shaft approximates a cold weld joint. Such was the condition of a test sample. Figure 6 is a photograph showing collet, shaft, and collet seat after having passed 750 kA for some 200 shots. It will be observed that very little, if any, burning can be detected; and in view of the current densities, i.e., 100 kA/cm and 70 kA/cm, these joints have passed, we consider this method to be extremely satisfactory.

Another example of the taper joint connection in use on the Quadrupole Device is shown in Fig. 7. The object is to transfer current from the outer turn of the coil to a round conductor of dissimilar material. Space within the coil geometry precludes the use of a collet here, but the taper principle is still being applied though in a slightly different manner. The conductor in this instance has been tapered at both ends, at 6° on the side. The seat at each end, however, is tapered at 5° on a side. In the enlarged portion of Fig. 7 the results can be observed. The seating of the two different tapers results in a line contact when lightly assembled by hand. After the draw bolt is tightened, however, and the dissimilar tapers are forced together, the line contact has been greatly enhanced by a deformation of the seating edge

as it tries to conform to the shape being pushed or drawn into it. Obviously when any deformation occurs, there must be sizable forces present creating it. Here again it is these forces upon which one is dependent for the reliable current transfer from piece to piece.

A fourth kind of connection for round bars is achieved by the shrink-fit method employed as a means of tightly joining machine elements together. In this process the contraction or shrinkage of a round bar may be achieved by immersion of the part in liquid nitrogen. Conversely, the part containing the hole may be heated to cause expansion or an enlargement of the hole. When the two parts are brought together and allowed to return to ambient temperature, fairly high tensile stresses are developed as a result of the deformation of the interfaces. This method has been successfully used, for instance, in securing tungsten inserts within spark gap electrodes. Figure 8 illustrates such an application, and in this particular geometry the current being passed is in the order of 10 kA per cm and no detectable sparking has ever been observed. This, however, is a rather modest current density, and higher service conditions are possible to about 50 kA per cm, with the same degree of success. The objections to this type of fit are many, one of which is the fact that the degree of tightness that can be realized is restricted by the amount of contraction and/or expansion of the parts due to the temperature differential between them. In other words, there is a limit as to the amount of interference that is possible and have one still be able to physically assemble the parts. If the interference is limited, the resulting deformation is also limited, which in turn limits the magnitude of tensile stresses developed at the interfaces. Another objection is the degree of care one must use in the assembly process. Also, this type of joint is quite permanent and disassembly becomes almost out of the question.

A fifth and final round bar type joint is shown in Fig. 9. In this instance, the current is being transferred from the bolt to the cable high-voltage plate by means of a crushable copper O-ring. The O-ring is made by forming standard copper tubing with a squared off, butt joint. The application is presently being used successfully on the Scylla IA device, where the current density per joint is in the order of 15 to 20 kA per cm. This is a very satisfactory type of joint, it is easy and economical to make, and reliable for use with currents as high as 45 - 50 kA per cm. Higher densities than this would be questionable since the tightness achieved is controlled and limited by the amount of deformation the crushed ring can experience within the confines of the geometry.

Some comment should be made regarding what we term slit-finger joints. These are of a type that are pushed together by hand, and consist essentially of a solid plug pushed into a serrated socket. There have been a few instances where such a joint was desirable, as shown in Fig. 10. Here the application is used on an early cartridge design and, as will be noted, the current is being transferred from the upper cable plate to the center, rod-like conductor by means of a slit-finger connection. A more simple rendering of this connector method is shown schematically in Fig. 11. If the current densities are not higher than about 8 to 10 kA per cm, this joint will work. Any slight misalignment of the common axis at assembly, however, tends to distort the fingers, and then severe sparking will occur.

Joints for Cable Terminations

Because of the extensive use of coaxial cables for efficient current transmission in the CTR business, economical and reliable cable terminations have become increasingly necessary. The expense of preparing cable ends for use in a system such as the Scyllac device, which will use more than 60,000 of them, becomes significant. The whole cable termination problem has been rather extensively examined, and the discussion which follows presents some of our conclusions.

Any type of termination or connector installed on a cable must, of course, be preceded by the usual cable dressing procedure, including jacket and conductor trimming to suit the particular geometry and voltage requirement.

Figure 12 shows a typical example of a cable header installation. In this design the ground braid of the cable is simply clamped to a pipe adapter by means of a standard hose clamp. The pipe adapter, having a tapered thread, makes an extremely good electrical connection in the ground plate by the kind of galling effect found in pipe joints. The center

conductor with its insulation continues through the pipe adapter, where it makes connection with the high-voltage plate. Here the center braid has been soft-soldered into a brass slug, and the connection is achieved by a set screw. This satisfactory termination is quite simple to prepare and has been used successfully for densities as high as 6 to 7 kA per cm. By varying the pipe adapter and slug size, practically any size cable can be accommodated.

Though the above type of connection looks simple, it is nevertheless expensive. Most of the cost is in the soldering operation of the center conductor. In addition, the time involved in actually making the connections is another drawback since, in our experience, the assembly procedure must be altered drastically many times in order to provide access to the center conductor set screws. The twin problems of expensive soldering and getting at the set screws has led us to a new design concept of "plug-in" connectors.

Tests showed that certain types of "banana-plug" joints would work for cable terminations of various sizes provided that the pulse periods were relatively fast and current densities not excessive. Obviously, the center conductor termination would determine the design criteria since its size, being the smaller of the two conductors, had to be limited to a current density not exceeding say 3 or 4 kA per cm. Naturally, if this density could be successfully carried by this size conductor, there certainly would be no sparking problem with the larger outer conductor since its density would always be much less.

Figure 13 shows one approach employing "plug-in" features. The attempt here was aimed at the use of mechanically-made joints, thereby eliminating the costly solder operation employed in previous designs. During the course of design study associated with the Type 17/14 cable, we observed that the amount of clearance between two standard copper couplings enabled us to force them together with the outer braid between them, thus providing a desired "plug-in" capability. By slotting the end of the smaller coupling in a slit-fingered manner, and pushing it into a properly-sized hole, we could use this combination quite nicely as the ground braid connection. The center conductor fitting, essentially a screw-machine-made item, was also slotted for like plug-in characteristics. Its attachment to the inner braid was accomplished by a kind of swaging operation, which, in effect, provided a strong clamping force on the braid between the fitting and a soft copper ring. The swaging was done either mechanically, by a specially-designed crimping device, or electrically through the use of magnetic-forming techniques. In either case, the procedures that were followed in implementing this design of "plug-in" capability for cable ends, now appears to be a very economical course to follow. Furthermore, this design provides the experimenter with increased freedom in assembly methods, ease of cable replacement, and, if desired, more cables per unit area because of the closer center distances possible. While the main emphasis here was the development of fittings for the Type 17/14 cable, other cable sizes can be accommodated in a similar manner. Caution must be taken, however, to avoid making the center conductor fitting too small when designing for the smaller cable. Avoid having anything smaller than about 1/4" diameter.

There are, to be sure, other types of cable terminations that could be considered. Some of them might be of a more sophisticated variety than those presented here, as well as some of a more elementary nature which probably could be made to work. However, the few suggested here have been found, in our own experience, to be reliable and economical solutions to the cable termination problem.

Conclusion

The foregoing presentation of various types of high-current joints has been restricted solely to those that can be disassembled and put back together again with comparative ease. If it is possible, however, during the course of a design study, to incorporate permanent joints either by welding or soldering, or to eliminate joints entirely, then do so. Any of the solutions described here are workable with a few limitations. To transfer current efficiently with a minimum of sparking, the following points should be considered by the designer.

In general, the best, non-sparking joint will always be the tightest one. This is not to imply, however, that the tighter the joint the more current it can carry. The higher current densities are successfully carried not only by tighter interfaces but also by much more careful joint preparation. Surface

finishes become extremely important, and the flatness and parallelism of parts to be joined should be held to very close tolerances. Additional benefits may also be gained by a light silver plating, which has in a few instances reduced contact or surface resistance. Polishing and lapping of contact surfaces might also be considered, particularly in the use of round bar conductor applications where current densities are in the order of 100 kA per cm.

Figures 14 and 15 are curves which may be found useful in the designing of flat plate joints. Figure 14 shows the seating value of "b", used in the bolt-load formula, as a function of gasket width. Figure 15 shows the gasket load in pounds per linear inch as a function of gasket width, and may be used in lieu of the bolt-load formula if desired.

Acknowledgements

The authors wish to express their appreciation to the following colleagues for their assistance in the preparation of this report: K. W. Hanks, G. P. Boicourt, J. E. Hammel, C. G. Charlton, and R. F. Berglund.

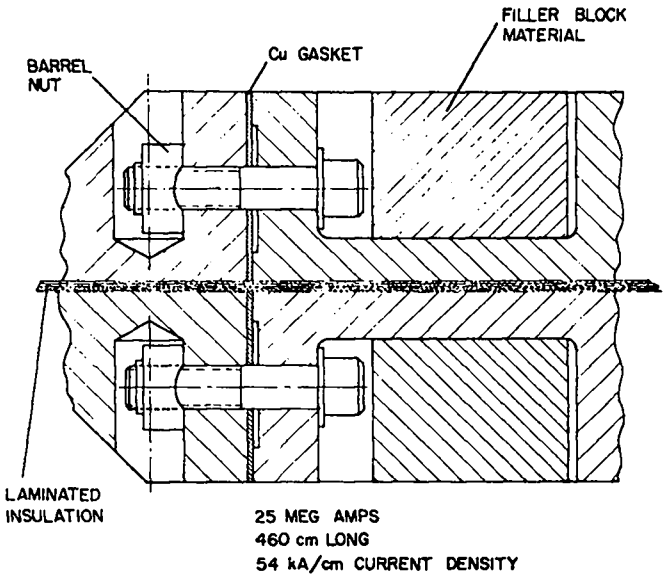

Fig. 1. Scylla IV collector plate joint.

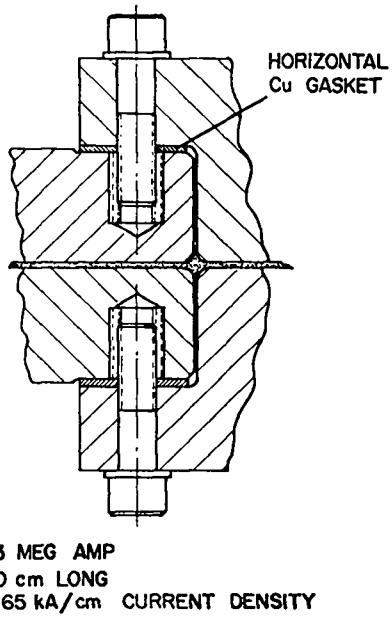

Fig. 2. Scylla IA theta coil to collector plate joint.

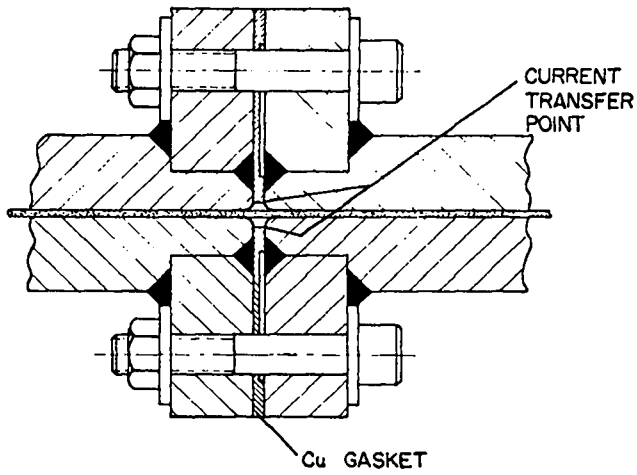

Fig. 3. Z-pinch device collector plate joint.

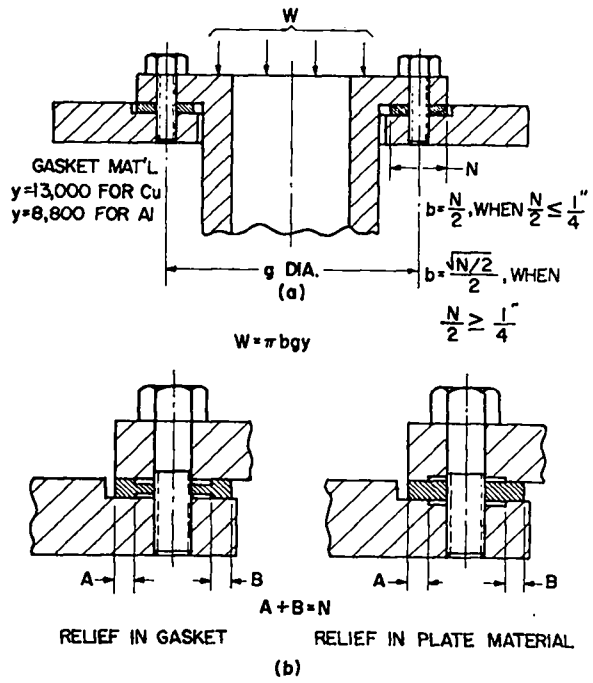

Fig. 4. (a) Bolt load formula as applied to current joints. (b) Gasket or plate reliev to reduce contact area.

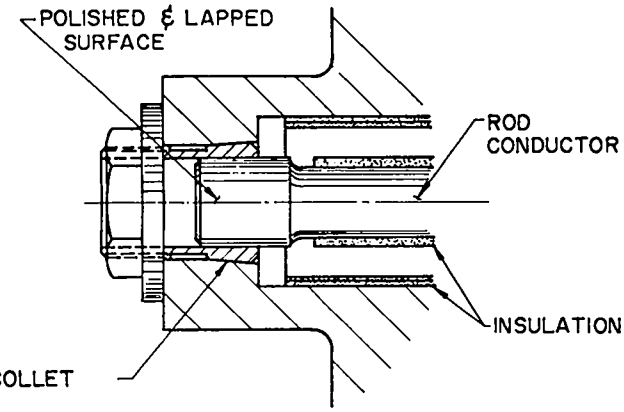

Fig. 5. Quadrupole device collet connection to rod-like conductor.

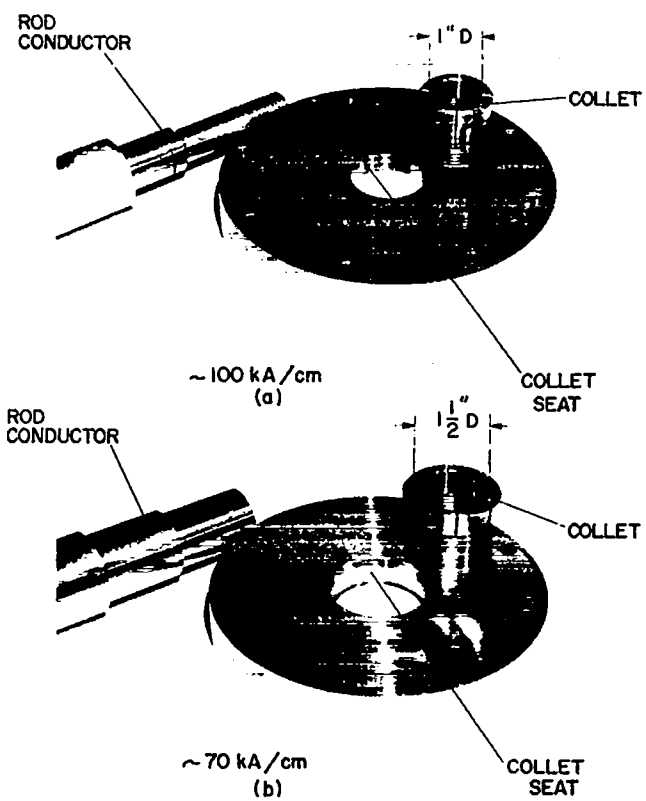

Fig. 6. (a) and (b) Photograph of test elements after passing 750 kA for 200 shots.

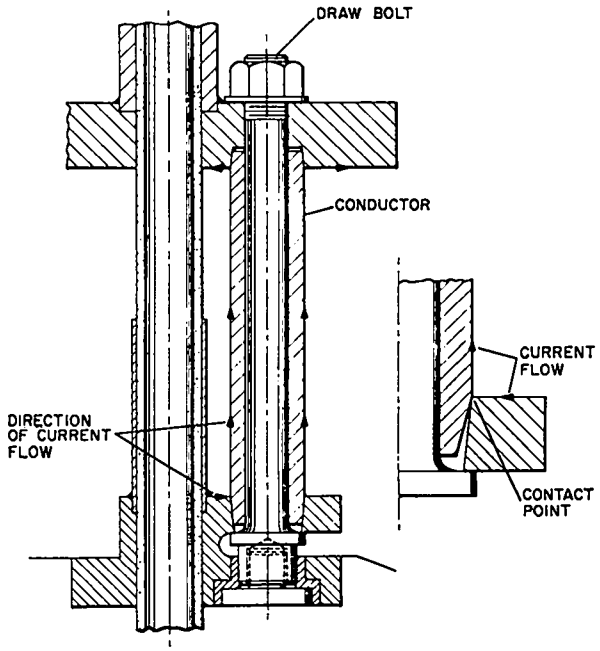

Fig. 7. Quadrupole device dissimilar taper joint.

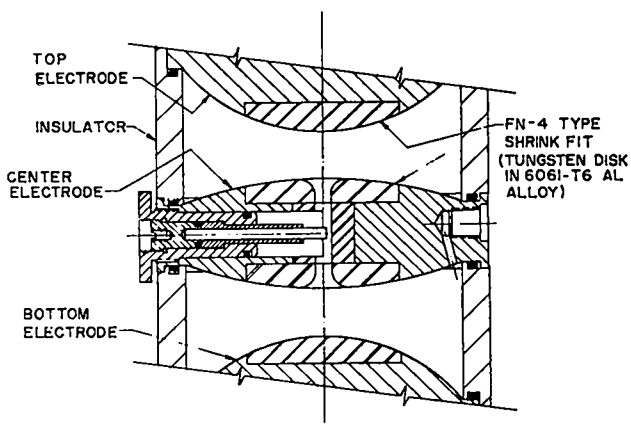

Fig. 8. 60-kV spark gap electrodes showing shrink-fitted tungsten alloy inserts.

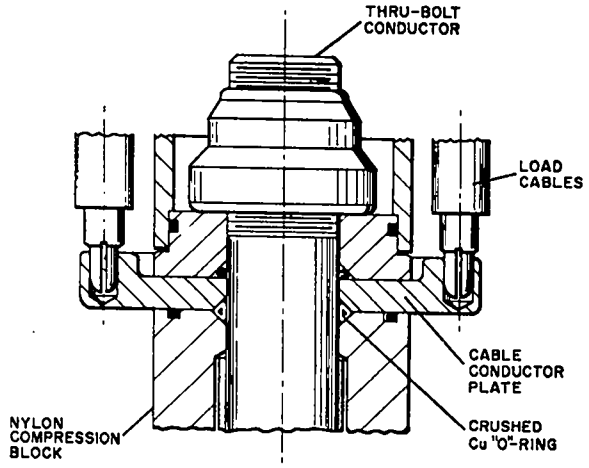

Fig. 9. Scylla IA cable cartridge showing crushed O-ring connection from through-bolt conductor to cable conductor plate.

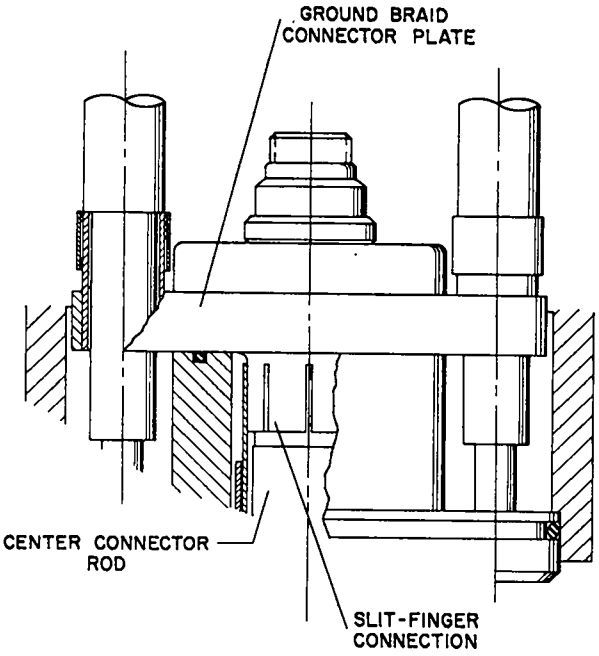

Fig. 10. Early cable cartridge design using slit-finger connection.

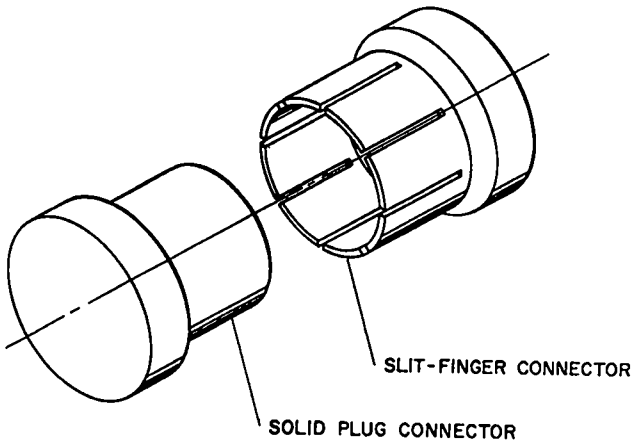

Fig. 11. Slit-finger principle, schematic.

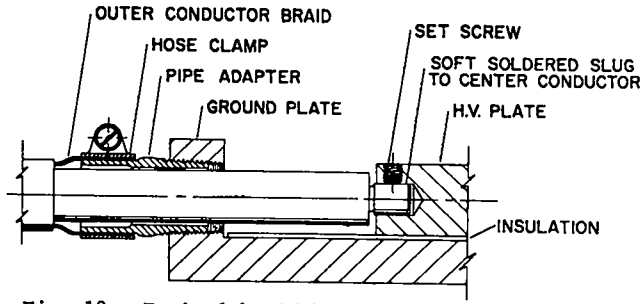

Fig. 12. Typical braid header application showing inner and outer cable braid terminations.

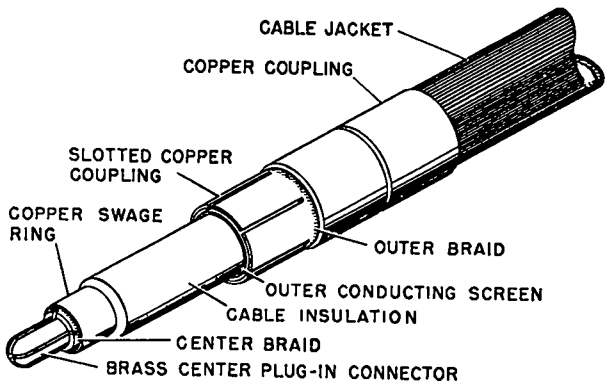

Fig. 13. New "push-in" cable termination showing swaged copper couplings and slotted center conductor.

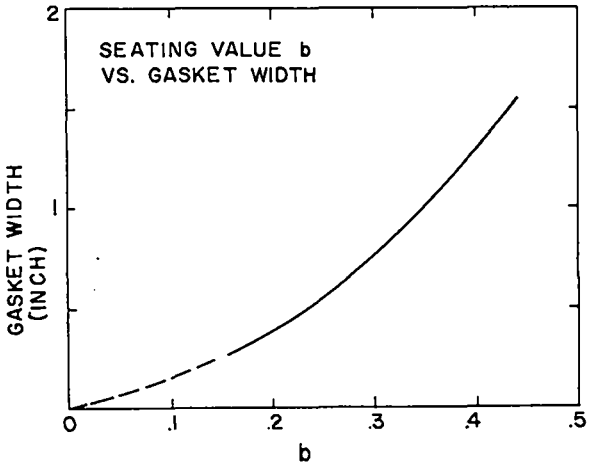

Fig. 14. Curve showing seating value "b" as a function of gasket width.

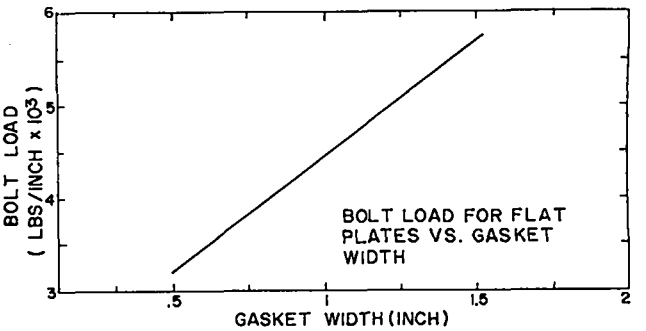

Fig. 15. Curve showing bolt load in pounds per inch of length as a function of gasket width.

THE FINAL DESIGN OF SCYLLAC*

by

Edwin L. Kemp

Los Alamos Scientific Laboratory, University of California
Los Alamos, New Mexico

ABSTRACT

Scyllac is a theta-pinch machine 15-m long with a 10-cm coil diameter. Two versions will be built, a 10-meter linear model and a 5-meter curved sector and later, a 15-meter circumference toroidal model. The same capacitor bank and collector plates will be used for both versions. The machine will be divided into 15 coil, collector plate sections. The 720-kJ Primary bank for each section will consist of 216 capacitors, each capacitor having a spark gap and 6 low-inductance coaxial output cables. The cables from each pair of capacitors will terminate at the collector plate in a low-inductance cable cartridge termination. Each collector plate will also have a high frequency B_z preionization system and a reverse, B_θ system. The toroidal system will also include static and dynamic stabilization systems.

The design of Scyllac is proceeding in three phases: component development, system development, and system design. The main components being developed are: a 1.85-μF, 60-kV capacitor; reliable, low-inductance coaxial cable; a low jitter, 60-kV "start" spark gap that also incorporates a "crowbar" spark gap; a low-inductance, cable cartridge termination; plug-in connectors, and miscellaneous hardware. After the components have been approved by the development laboratory they are installed in substantial quantites in a prototype system and tested. The components that qualify in the prototype system are used in the Scyllac system design. This paper describes the component developments, the prototype system testing program, and the final design of the complete Scyllac system

I. INTRODUCTION

The theta-pinch program at the Los Alamos Scientific Laboratory began in 1957 with a 30-kJ machine, Scylla I.[1] It has grown to the present 550-kJ machine, Scylla IV.[2] All these theta-pinch experiments have certain common characteristics; the coil I. D. is about 10 cm, about 40 kV is applied to the terminals of the coil producing an E_θ of about 1000 volts per cm; the current rises in less than 4 μsec producing a peak magnetic field of 5 to 10 teslas. The deuterium pressure in the discharge tube is usually 10 to 100 mTorr. The gas is first preionized, then the E_θ shock-heats the gas to 1 to 2 keV, and then adiabatically compresses it by a fast-rising magnetic field. Neutrons are produced near the peak of the magnetic field. The early machines lost the plasma by end losses due to the short coils which were 15 to 30 cm long. The Scylla IV machine has a 1-meter coil but when it was power-crowbarred to extend the time of the magnetic field to over 40 μsec, the plasma still escaped in less than 10 μsec, even though the plasma was radially stable. The thermonuclear quality of this theta-pinch plasma and

*Work performed under the auspices of the U. S. Atomic Energy Commission.

its apparent stability were the main motivating factors for the proposal of a 15-meter circumference toroidal machine called Scyllac, for "Scylla closed".

The Scyllac proposal[3] was thoroughly examined by a highly-qualified committee and was approved[4] with the stipulation that a linear machine be built first. The U. S. Congress appropriated $8.5 million for the Scyllac project in 1968.

II. GENERAL SYSTEM

Figure 1 shows the first version of the system. The experimental area to house the capacitor banks and the machine is 100 feet by 100 feet with a crane hook clearance height of 40 feet. There is a three-story office and laboratory wing adjacent to the experimental area.

Figure 1 shows the layout of the initial version. The linear machine will contain 10 sectors, each sector being driven by 720 kJ at 60 kV. The racks are separated to allow access to the capacitors and this requires the collector plates to alternate left and right. Since the current must flow in the same direction in both the left and right coils, the current must enter the top of the left collector plates and the bottom of the right plates. This requirement complicates the feed system of the collector plates and will be discussed in more detail later. The 5-m curved sector is one-third of torus and will be installed and left in its original position when the entire system is converted into a torus.

Figure 2 shows the toroidal Scyllac. The same capacitor racks and collector plates will be used but relocated into a toroidal geometry. The control, charging, and triggering systems will be similar to the initial version.

Three capacitor banks will be used on a typical shot in the linear machine. A 10-kV B_o bias bank will provide a modest reverse bias field. When this long period field reaches maximum, a 75-kV preionization (P.I.) bank will be fired into the coil. This bank will oscillate and ring out, fully ionizing the gas. This capacitor bank will subsequently be pulse-charged to 120 kV by the Primary bank so the P.I. capacitors must be rated at 120 kV. When the preionized plasma has become quiescent, the 60-kV Primary bank will be fired. At maximum current the Primary bank is crowbarred. The "start" spark gaps in the Primary bank will incorporate a crowbar spark gap that is designed to fire at the quarter period time when the voltage across the gap is very low. The crowbarred current will decay with an L/R time of approximately 150 microseconds. The toroidal version will also use a solid dielectric crowbar switch to relieve the spark gap crowbar switches and extend the decay time to over 500 microseconds. The toroidal Scyllac will also have a 60-kV Static Stabilization bank and a 60-kV Dynamic Stabilization bank.

III. COMPONENT DEVELOPMENT

The engineering of Scyllac is divided into three phases: component development, prototype system development, and system design. As new components are developed in the laboratory, they are installed in statistically significant numbers into a prototype system. When the new components have operated satisfactorily in the prototype, they are qualified for use in the Scyllac system.

Each Primary bank 60-kV capacitor will have a spark gap mounted on it and 6 output cables. The cables terminate at the collector plate in a 12-cable cartridge that incorporates a bolt to contain the magnetic forces between the two plates. These items and several others are being developed especially for Scyllac. The new components are a 1.85-μF, 60-kV energy storage capacitor; 60-kV, low-inductance coaxial cable; start and crowbar spark gaps; a solid dielectric, metal contact crowbar switch; low-inductance cable cartridges; reliable cable terminations; and an electrolytic resistor.

1. 1.85-μF, 60-kV Capacitor. The capacitor required for Scyllac is a 1.85-μF, 60-kV, 25-nH capacitor with a minimum life of 30,000 shots. Six capacitor companies were selected to develop this capacitor. A specification was written and sample units ordered from each company. When received, each capacitor was tested in a ringing circuit similar to the application without crowbarring. After three years, five companies have manufactured satisfactory sample capacitors and several companies can now produce them in production quantities.

Figure 3 shows the construction of the capacitor. It has a low-profile, low-inductance header; there are an appropriate number of packs connected in parallel to an internal current collector. Each pack has 8 series sections with a pad dielectric stress of less than 2100 volts per mil. This capacitor has 24-nH internal inductance and an average life of 45,000 shots ringing with 85% reversal.

2. Low-Inductance, 60-kV Coaxial Cable. Scyllac will contain over 750,000 feet of coax cable so it is imperative to have reliable cable. In early 1965, a cable specification was written and sent to the cable industry. Three companies were selected and orders given for sample quantities. When received, the cable was tested in an application similar to Scyllac. The cable construction is shown in Fig. 4. The center core is foamed polyethylene. Two layers of braid form the center conductor. The inner screen is a thin extrusion of conducting polyethylene. The active polyethylene dielectric is extruded over this and a thin screen of conductive poly-vinylchloride is extruded over the active P/E. The two conducting screens protect the active dielectric by grading the stress at the ends of any broken braid wires. The outer conductor is braided over the outer screen and covered with a protective jacket. This cable inductance is 45 nH per foot. The life exceeds 100,000 shots in the Scyllac test system. Three companies have produced reliable cable in production quantities.

3. Switches. The Primary bank will contain 3240 individual spark gaps. Each gap will perform two functions: the "start" gaps will hold off the charge voltage, then fire with low jitter. The "crowbar" spark gap closes at peak current and prevents the coil current from recharging the capacitor. Since one electrode of the crowbar gap is common with the start gap, both gaps can be conveniently incorporated into one assembly having a start gap and a piggyback crowbar gap.

Figure 5 shows the two gap assembly. The bottom electrode of the start gap mounts directly to the capacitor. The center electrode contains the spark plug which is the fourth electrode for illuminating this 4-element gap. A low-inductance capacitor for fast triggering is formed by the annular ring around the center electrode and the outer housing. The top electrode completes this gap. The load cables and the trigger cable use plug-in connectors. The top spacing is one-half the bottom spacing. The insulators are nylon, the electrodes are aluminum with tungsten alloy inserts for carrying the arc. This gap is pressurized to about 0.6 atm and is flushed after each firing. The annulus between the outer housing and the electrodes is filled with insulating oil. The capacitor is charged negative and the gap triggered with a positive 150-kV pulse having a rise time of 100 nsec. Operating between 50 kV and 60 kV the delay is 20 nsec with an RMS jitter of 10 nsec. The peak current is about 60 kA rising in about 4 μsec.

The crowbar spark gap bottom electrode is attached directly to the start gap top electrode, hence the name "piggyback". The crowbar top electrode is attached to the gap lid via a coaxial cylinder. The annulus in the coax is filled with ferrite toroidal cylinders. A spark plug is installed in the top electrode.

The crowbar gap is fired in the following manner. A 75-kV capacitor, charged negative, is connected through a spark gap and a coax cable to the crowbar spark plug. This piggyback trigger gap is fired shortly after the start gap fires. The trigger current flows up and down the coax cylinder driving the ferrite far into saturation. The trigger voltage breaks down the spark plug and creates a plasma but since the polarity is the same as the start gap top electrode at this time, the crowbar gap does not break down. The period of the spark plug is about 2 μsec and the crowbar trigger gap is fired so the spark plug trigger current passes through zero at the same time the start gap reaches maximum current. When the spark plug current passes through zero the ferrite swings out of saturation presenting a momentary high impedance to the crowbar trigger capacitor. The trigger capacitor which has reversed polarity at this time imposes a large positive voltage on the crowbar top electrode and drives the spark plug plasma across the gap closing the crowbar switch.

The crowbar gap operates with small positive pressure to hold off the initial start gap voltage. Both gaps will run over 2000 shots without maintenance. The crowbar jitter is less than 0.5 μsec and is adequate for Scyllac which has a rise time of about 4 μsec. This crowbar L/R time is about 300 μsec requiring the gap to conduct about 18 coulombs. One 75-kV trigger gap is used to trigger 18 piggyback gaps.

The field L/R in the torus must be over 500 μsec so spark gap crowbar switches are not sufficient. Two solid dielectric, metal contact crowbar switches will be installed in the transition section of each collector plate to crowbar each meter of coil essentially at its terminals. The principles of the

switch are shown in Fig. 6. A copper foil, 6" long, 0.5" wide, by 0.003" thick is insulated and tightly compressed between two expendable Al plates. The foil is exploded with 4000 joules, the current rising in about 2 μsec. The high pressure generated by the exploded foil drives the transfer plate into the contact slot with a closing time of 9 μsec and an RMS jitter of 0.5 μsec. The contact resistance of the closed switch is 10 μΩ. Each switch conducts 5-MA peak current and carries about 2500 coulombs.

4. Cartridges. In the linear machine the current must enter the top of the right-hand collector plates and the bottom of the left-hand plates. The cartridge termination for the right-hand collector plates is shown in Fig. 7. The current from the center of the 12 cables enters the terminating plate and flows to the top collector plate over the soft copper washer current joint. The current then goes to the coil and returns on the bottom plate. It flows across the bottom soft copper washer, not labeled in the figure, to the 1.5" O.D. steel bolt. It then flows up the surface of the bolt to the copper tubing high-current joint, where it contacts the outer braid collector plate and returns to the capacitor. The copper tubing ring is made by winding a helix to the approximate diameter, cutting it into one-turn coils and then cutting out an appropriate amount until the two ends almost touch when installed in the cartridge. The beveled edges of the containing parts force the circular cross-section into a triangular cross-section. The cartridge carries a peak current of approximately 120 kA. The cable area is filled with oil to minimize the cable terminating length. The inner chamber between the plates is pressurized with SF_6. The measured inductance of this cartridge is 22 nH, using 2" thick plates. Incidentally, the copper tubing joint in the above dimensions has been successfully tested to over 400 kA ringing with a period of 200 μsec with 50% reversal.

The left-hand plates use a similar cartridge but it reaches through the top plate to connect the cable centers to the bottom plate. The current returns on the top plate to the cable braid. Each collector plate terminates over 1300 cables. If all cartridges were installed on the top plate the cable congestion would make maintenance very difficult. Therefore, two other types of cartridges were designed to be installed on the bottom of the collector plates. Approximately half the cables are installed in the bottom cartridge.

5. Connectors. The design of the spark gaps and cartridge requires plug-in cable terminations. The termination developed for this application is shown in Fig. 8. The back end of the center connector is hollow and slips over the cable center core. The cable inner braid is clamped between the connector and a copper swage ring that is magnetically swaged. The end of the connector is segmented into quarters. This connector can be installed and removed many times and still operate satisfactorily carrying 10-kA peak current.

The outer braid connector is made from two copper fittings used in the plumbing trade. The outer coupling is slipped over the outer cable braid, a ridge retains it against the cable jacket. The inner coupling is pressed under the cable braid, clamping the braid tightly between the two couplings. The assembly is made with a simple jig. The outer connection carries 10 kA easily without sparking. Using these two connectors the Scyllac cables can be cut and dressed reliably and economically.

6. Electrolytic Resistor. Each meter of Scyllac will be driven by 216 capacitors which are all charged from one power supply. The original charging circuit is shown in Fig. 9. Each group of six capacitors was connected to a power supply through an isolation resistor and a 60-kV fuse. In concept, when one capacitor in a 6-capacitor module failed while charging, the fuse would prevent all adjacent modules from discharging into the failed capacitor. The concept was good but the fuse proved unreliable. It was found during tests that the fuse would open but not before the isolation resistor had also failed. Another more serious problem was prefiring spark gaps. When one gap in a module prefired, it would not trigger any other gaps. To the charge system then a prefire appeared as a shorted capacitor and all the other capacitors would try to discharge through the prefired module and would immediately clear the fuse. This meant that each prefire would clear a $50.00 fuse, a situation that is clearly intolerable.

The solution used in Scyllac is to install an isolation resistor with an energy capacity sufficient to dissipate all the energy, 720 kJ, from the

adjacent capacitors. The 2000-ohm electrolytic resistor shown in Fig. 10 was designed to accept three consecutive prefires before the temperature of the copper sulfate electrolyte reaches the boiling point. This resistor operated successfully in simulated prefiring systems.

IV. PROTOTYPE SYSTEM

The function of the prototype is to evaluate all components and circuits in a system that is a one-third scale model of one meter of Scyllac. It is large enough to provide meaningful system data but can be modified to incorporate new concepts and improved components.

The prototype is shown in Fig. 11. The collector plate was originally designed with deep skirts on each side of the collector plate. Later concepts changed the plate geometry so the outer half of the skirt was removed, eliminating the skirts from the system. The system shown consists of seventy-two 60-kV capacitors and start gaps, 432 cables, and 36 cartridges. The peak current produces the same peak magnetic force between the plates that will be produced between the Scyllac plates. Another coil is used to produce the peak voltages that will occur in the Scyllac system. The prototype includes charging and triggering circuits, and many other special circuits and components.

The prototype is operational without a crowbar system. The two crowbars will be added when the capacitors, cables, cartridges, and other items have performed satisfactorily. The prototype has been very useful in identifying system assembly problems. It has also located several deficiencies in some of the components when they are operated in a system. As the problems are identified, they are corrected and re-evaluated in the prototype, the cycle repeating until the problems are eliminated.

V. SYSTEM DESIGN

The Scyllac system is being designed in two parts, the capacitor bank and the machine. The bank design consists of the structural hardware, racks and support systems; and the electrical system that includes the charging system, the control system, and the trigger system. The machine design incorporates the collector plates, the load coil, and the vacuum system.

The racks are designed as 2-shelf modules, each module to be loaded with capacitors, transported to the Scyllac building, and erected with the aid of a 25-ton bridge crane. The racks can also be disassembled with relative ease. The components are designed for economical manufacture and reliable assembly.

The charging system uses monocyclic networks for constant-current charging. The entire system can be charged in 30 seconds. Each power supply can be started independently so that all banks reach full charge at the same time. The control system uses mechanical relay logic circuits. Transistor circuits are avoided because of their susceptibility to damage from transients which are occasionally produced by misfires and arcs. The control system will include a digital computer which will mainly be used to accumulate and reduce the plasma data. The computer will also be used to monitor the bank operation for each shot. Each spark gap will be monitored and the data fed into the computer. Prefire and jitter data for each spark gap is immediately available on demand.

The trigger system uses a 10-MHz electronic clock that is scaled down. There are 36 output channels, each channel can be set to any delay time with 10-nsec resolution. The Primary bank has one master trigger, it fires 60 sub-master triggers, each sub-master firing 54 gaps. The trigger capacitors are cables, pulse-charged by a Marx bank. The trigger spark gaps are 4-element, pressurized gaps, designed for minimum inductance.

The reliability of each component is one of the most serious concerns of the entire system. A procedure has been established to test all of the commercially-manufactured components before installation. When a capacitor arrives it will be fitted with a spark gap and the two units fired 1500 shots at rated voltage before installation into a rack module. As the 25,000 dressed cables are received, each one will be tested to 1500 shots before installation. A special test facility has been set up to conduct this essential testing.

The machine consists of 15 collector plates, Fig. 12 shows a typical plate. It has 123 cartridges to accommodate the B_o, the P.I., and the Primary banks. The shallow skirts along the tapered edges lower the inductance of the plate. Each plate is 2" Al, the insulation between the plates is 0.090" of Mylar. All plates are designed to accept any of

the four types of cartridge. The solid dielectric switch will be incorporated in the transition plates which will be changed for the toroidal coil.

The inductance of the various components and the energy transfer efficiency are essential to predict the performance of the system. The inductance of the capacitor, spark gap, and cable have been accurately measured. The layout of the collector plate and the cartridges precludes a simple model for calculating the collector plate inductance. Current flowing from the back must flow around the forward cartridges. A fluid mapping model was used to show the current flow pattern around the cartridges and establish an effective inductance for incoming current. A resistance paper model was used to determine the effectiveness of the skirts and also predict the inductance of the entire collector plate. A NET II code was also used with the MANIAC II LASL digital computer to calculate the inductance of the collector plate and the system.

The prototype system was used to evaluate the methods of calculation. The prototype system inductance was measured and this measurement compared with the resistance paper model and with the NET calculations. The initial predictions were within 10% of the measured value. Applying suitable constants for current flow patterns, it is believed that the performance of Scyllac can be predicted to a reasonable accuracy.

The Scyllac bank characteristics for a 1.0-meter coil are shown in Table I.

VI. SCHEDULE

The Scyllac building which is under construction will be completed in early 1970. A five-meter sector of the toroidal machine is scheduled to begin physics experiments in the spring of 1971. The 10-m linear system is scheduled to become operational in early 1972.

TABLE I

Scyllac Bank Characteristics for 1.0-Meter Coil

	Units	B_o	PI	Primary
W	kJ	102	28	720
V_{cap}	kV	10	75	60
C_{cap}	μF	170	1.0	1.85
C_{Total}	μF	2040	10	400
I_{Max}	kA	425	1227	8970
τ	μsec	248	3.74	16.25
B_{Max}	Teslas	0.628	1.53	11
$E_{0\ Max}$ at coil terminals	V/cm	5.7	480	1245
L (cap. + sw.)	nH	140	75	67
L_{cables}	nH/M	205	141	141
$L_{coil\ (Linear)}$	nH	11.25	11.25	11.25
Trans. Eff. (Linear)	%	1.4	30.4	71.7
L/R (Linear)	μsec	-	-	300
No. of Capacitors	Total	12	10	216
No. of Switches	Total	8	10	216
No. of Cables	Total	12	120	1296
Average Cable Length	ft.	100	20	28

ACKNOWLEDGEMENTS

The engineering of Scyllac is the accomplishment of a large number of engineers and physicists. The author would like to particularly recognize the contributions of the following people: G. P. Boicourt, W. H. Borkenhagen, D. L. Call, R. S. Dike, R. F. Gribble, C. F. Hammer, K. W. Hanks, and W. A. Bradley an and his team of fine design engineers.

REFERENCES

1. K. Boyer, W. C. Elmore, E. M. Little, and W. E. Quinn, Proceedings of the Second International Conference on the Peaceful Uses of Atomic Energy (United Nations, Geneva, 1958) 32, p. 337.

2. E. L. Kemp, T. M. Putnam, W. E. Quinn, and F. L. Ribe, Los Alamos Scientific Laboratory Report, LAMS-2609 (1961).

3. Project Sherwood Personnel, Los Alamos Scientific Laboratory Report, LA-3487-MS (1966).

4. H. Griem, H. Grad, D. Grove, C. Hartman, R. Kilb, N. Lazar, and F. Ribe, Report TID-23705 (1966).

5. G. P. Boicourt, "Capacitor Development for Scyllac", Paper CI-1, this Symposium.

6. G. P. Boicourt and E. L. Kemp, "Development of Reliable, High-Voltage, Low-Inductance Coaxial Cable for Scyllac", Paper CI-2, this Symposium.

7. C. F. Hammer and R. F. Gribble, "Scyllac Spark Gap and Trigger System Development", Paper CI-4, this Symposium.

8. R. F. Gribble, "A Ferrite Loaded Piggyback Crowbar Gap", Paper DI-5, this Symposium.

9. K. W. Hanks and G. P. Boicourt, "The Design and Development of Cable Cartridges for Scyllac", Paper CI-3, this Symposium.

10. R. A. Haarman, "Liquid Resistor Development", Paper DII-9, this Symposium.

11. A. Malmberg and F. Cornwell, Los Alamos Scientific Laboratory Report, LA-2853 (1963).

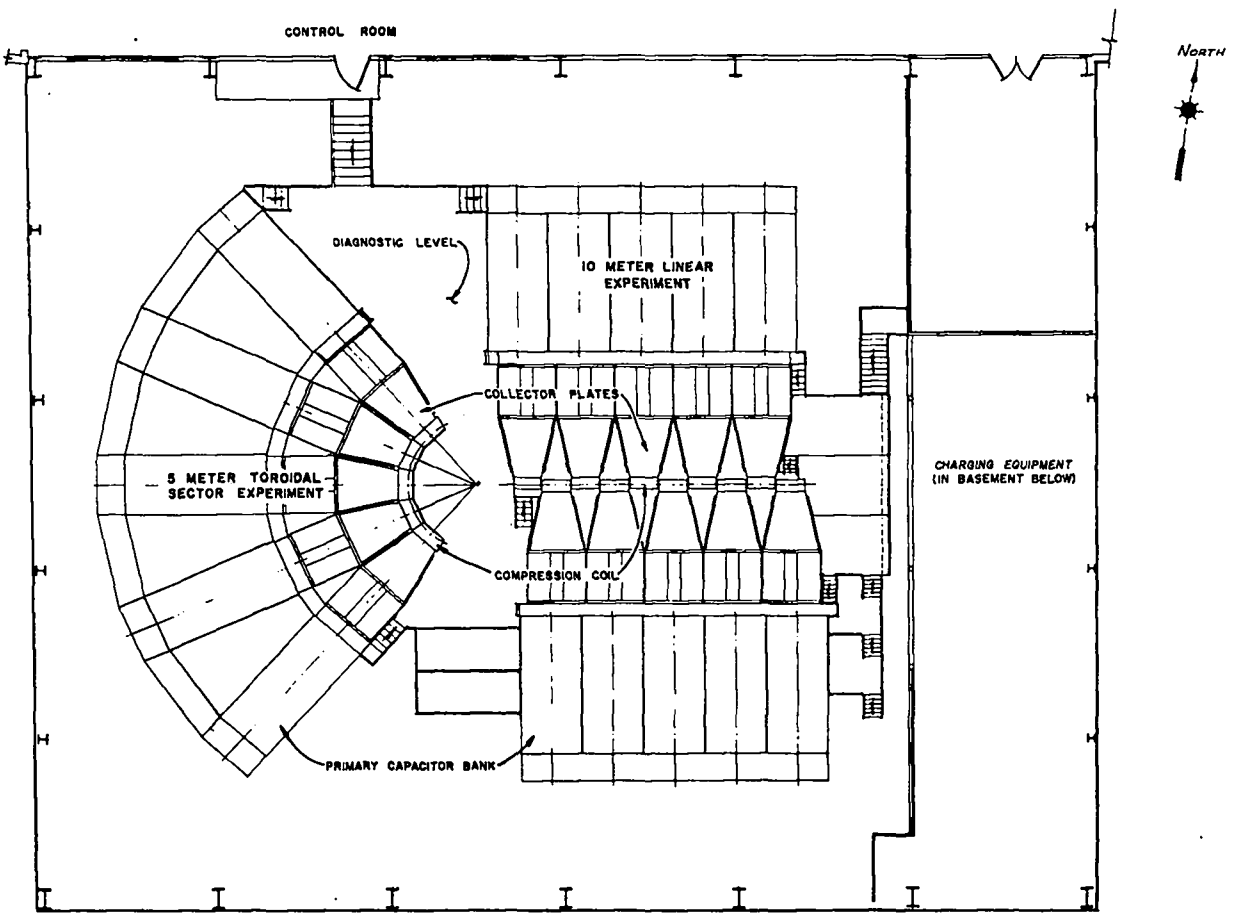

Fig. 1. Layout of initial Scyllac system.

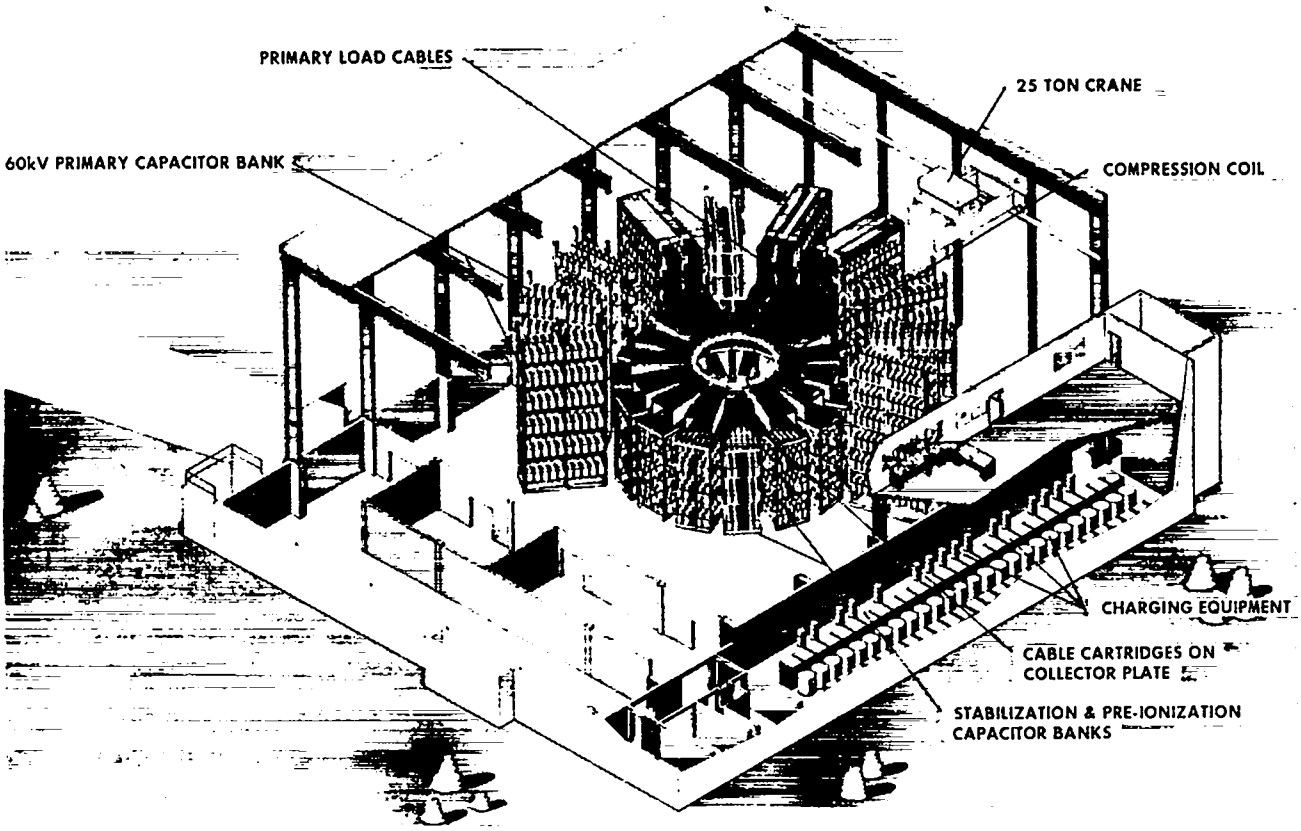

Fig. 2. Layout of toroidal Scyllac system.

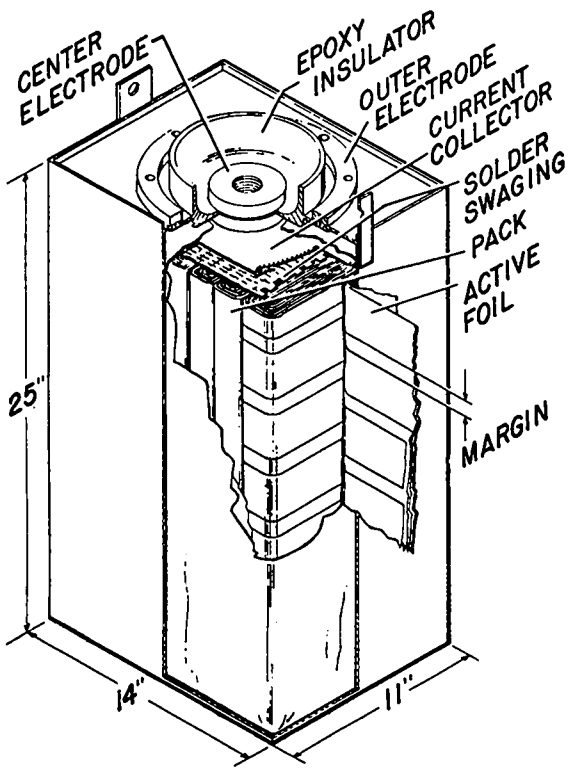

Fig. 3. 1.85-μF, 60-kV capacitor cross-section.

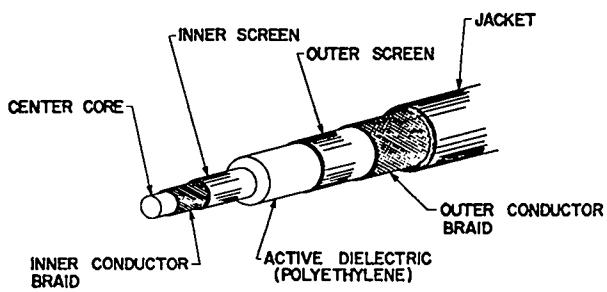

Fig. 4. Scyllac low-inductance load cable.

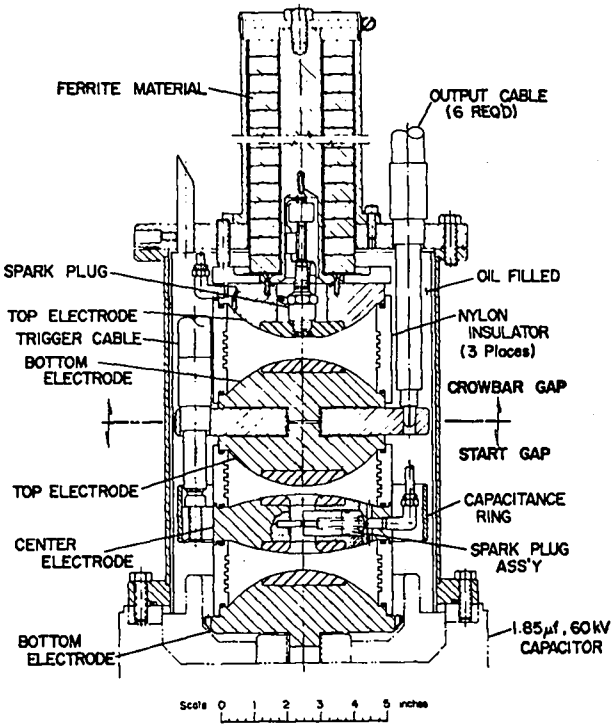

Fig. 5. Scyllac start and piggyback crowbar spark gap.

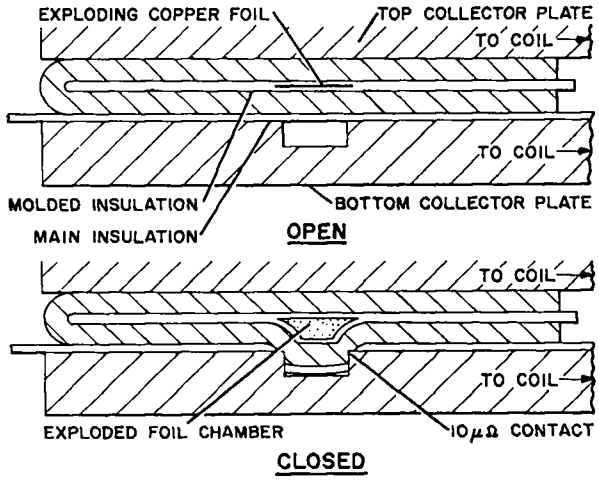

Fig. 6. Solid dielectric metal contact crowbar switch.

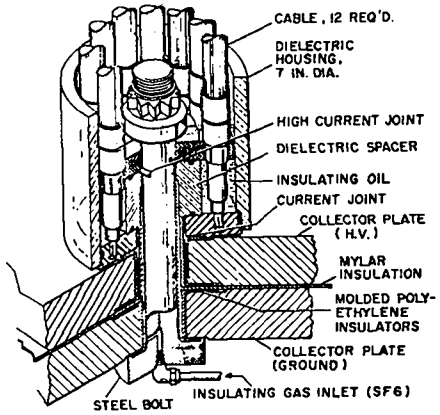

Fig. 7. Top surface cartridge.

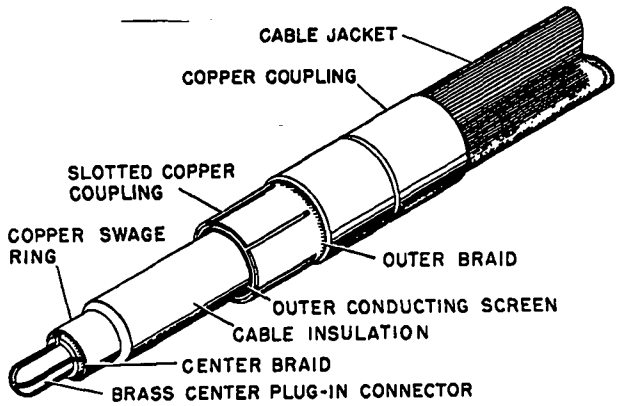

Fig. 8. Cable terminations.

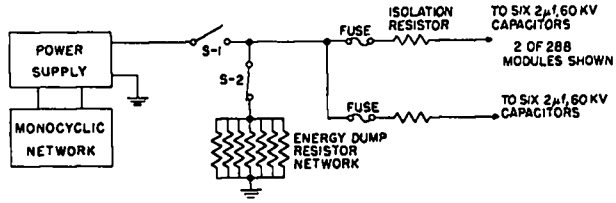

Fig. 9. Original charging circuit.

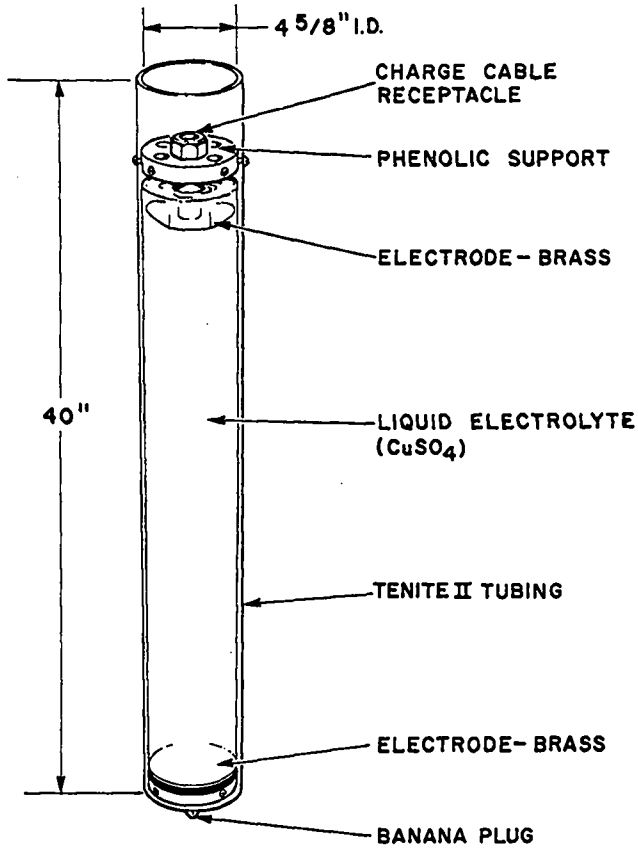

SCYLLAC LIQUID RESISTOR

Fig. 10. Electrolytic resistor.

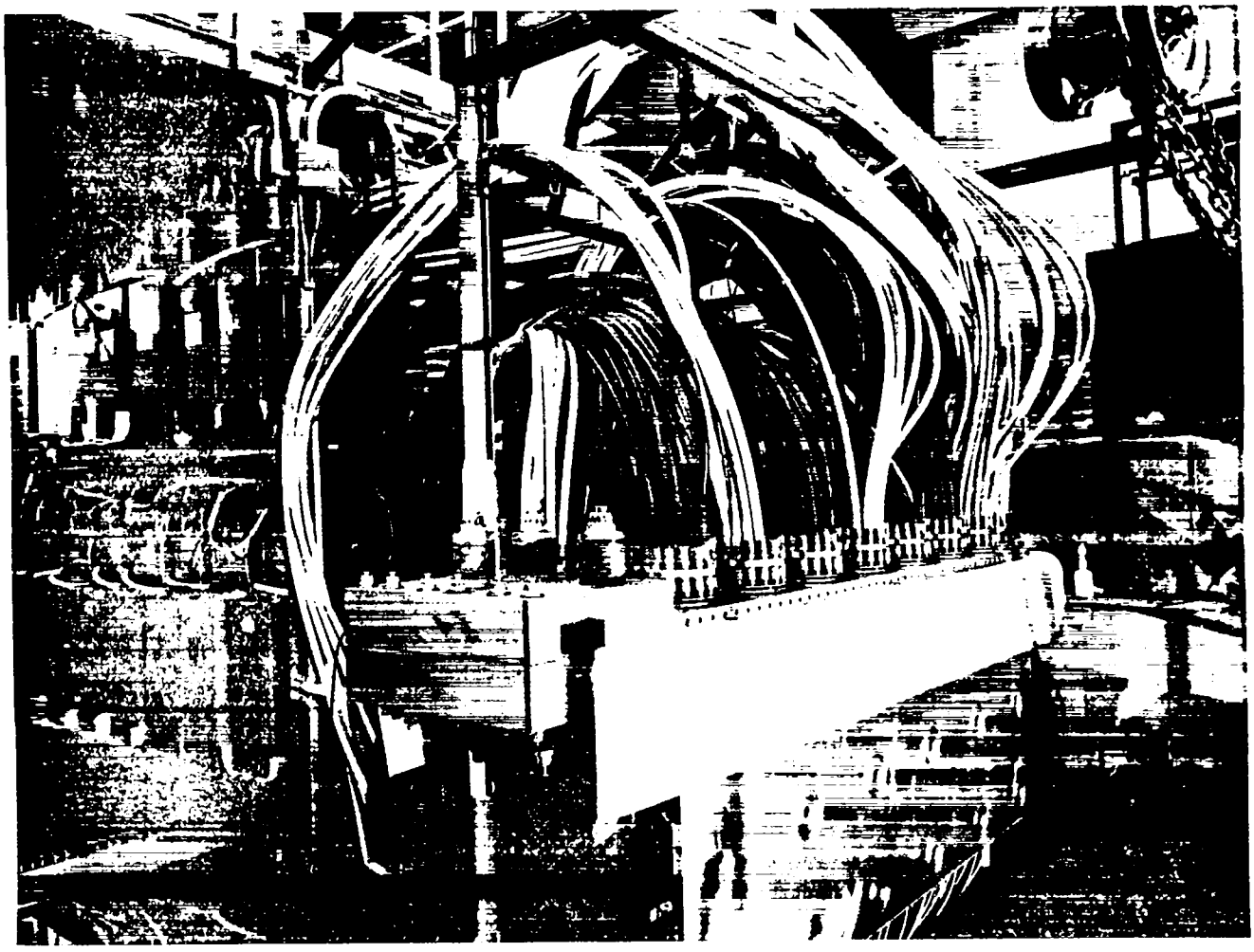

Fig. 11. Prototype collector plate and capacitor bank.

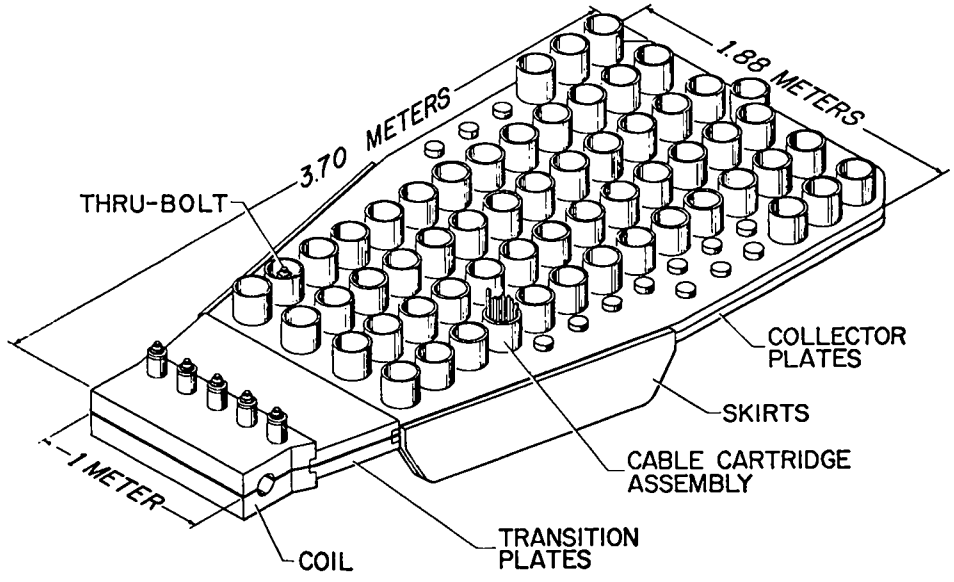

Fig. 12. Scyllac collector plate.

THE STABILITY OF MULTIFILAMENT SUPERCONDUCTORS*

Carl D. Henning
Lawrence Radiation Laboratory
University of California
Livermore, California

ABSTRACT

The need for higher current density magnets has lead to the development of superconductors with inherent stability, i.e., conductors in which flux jump instabilities have been reduced sufficiently to permit magnet operation beyond the nucleate boiling stability limit. One method of producing inherent stability is to reduce the diameter and increase the number of niobium-titanium filaments in a composite conductor. This report presents experimental data to confirm the stabilizing effect of such multifilamentation. Short-sample tests are compared to magnet operation and a correlation drawn between filament size and stability as a function of magnetic field.

INTRODUCTION

The instabilities in superconducting magnets have been described by Kim[1] as being thermal in nature and resulting from the penetration of the magnetic field into the superconductor. A flow of magnetic flux past the supercurrent produces a voltage, a corresponding power dissipation, and a heating of the superconductor above its transition temperature. To counteract this fundamental instability, Kantrowitz and Stekly[2] proposed the liberal use of a normal conductor, such as copper, to cryogenically stabilize a superconductor. Since then, this technique has been successfully utilized in several large magnets.[3-5] However, the large amounts of copper paralleling the superconductor not only greatly decreased the useful current density but increased both the size and the weight of the magnet.

In 1967, Chester[6] suggested that inherent stability of superconductors could be attained by coextruding fine filaments of Nb-Ti with copper to form a composite conductor. By reducing the size of the filaments, the surface-to-volume ratio would be increased to conduct away the heat dissipated by flux motion. Unfortunately, the filament sizes recommended were quite small and inconvenient to manufacture; therefore, a method was needed to determine a maximum usable size for a given application.

As a criteria of inherent stability, Gauster at ORNL[7] proposed that a short length of conductor which could share current between the super and normal materials would be inherently stable in a magnet. Several analyses ensued to describe the thermal nature of this current-sharing process and the requirements for inherent stability. It is the purpose of this report to experimentally relate magnet performance to conductors with inherent current-sharing stability. In addition, a correlation is given for a maximum Nb-Ti filament size as a function of a magnetic field.

ANALYSIS

The data in Fig. 1 collected by ORNL[8] exhibit two types of current-sharing: (1) reversible and (2) discontinuous. As the critical current in a short length of conductor is exceeded, some current passes into the copper. A voltage gradient is produced, and power is dissipated along both the super and normal conductors. At magnetic fields above 60 kG, the voltage appears and disappears along the same line and may be termed reversible (see Fig. 1). Between 25 and 60 kG the current-sharing is discontinuous; while below 20 kG all the current transfers to the copper whenever the

*Work performed under the auspices of the U. S. Atomic Energy Commission.

critical current is exceeded.

Fairbanks[8] analyzed the current-sharing process and derived a stability relation,

$$\frac{n}{\alpha} > I_0^2 R, \tag{1}$$

where n is the number of Nb-Ti filaments in a composite conductor, I_0 is the critical current, R is the copper resistance, and α is an experimentally determined constant related to the power dissipation. When the above equation is satisfied, Fairbanks predicts reversible current-sharing.

By a simple manipulation of Eq. (1), the maximum filament diameter, d, may be found as a function of magnetic field, B. The copper-to-superconductor area ratio is assumed constant, and the variation of critical current is taken to be

$$I_0 = J_c n \frac{\pi}{4} d^2 e^{-B/40}. \tag{2}$$

By substituting into Eq. (1), the following relation is derived:

$$d = Ce^{B/120}. \tag{3}$$

The constant C is evaluated from the data of Fig. 1 corresponding to the 60-kG field at which the 0.015-in.- diam filaments begin to current-share reversibly, so that

$$d = 0.00925e^{B/120} \tag{4}$$

where B is the magnetic field in kilogauss and d is the filament diameter in inches.

El Bindari and Bernert[9] have derived a stability parameter, θ, which predicts reversible current-sharing when θ is less than unity:

$$\theta = \frac{kR_n I_0^3}{hP(T_c - T_b)} \tag{5}$$

Here h is the heat transfer coefficient, I_0 is the critical current, k is a material constant, P is the perimeter of the filament, R_n is the normal resistance, and T_c and T_b are the critical and bath temperatures, respectively. The material constant, k, is generally unknown so that stability cannot be predicted. However, by again using the 60-kG transition for a 0.015-in.-diam filament, Eq. (5) can be modified to give a maximum filament diameter for a given magnetic field. The same proportionality in Eq. (2) for critical current is used, and the appropriate expressions for the normal resistivity and perimeter are inserted. The copper-to-superconductor area ratio is assumed constant to give

$$d < 0.0035e^{B/40} \tag{6}$$

where d is in inches, and B is in kilogauss.

This expression differs from Eq. (4) because of the model for flux-flow resistivity. Fairbanks'[8] analysis assumes a flux-flow resistivity, ρ_f, of the type given by Strnad, Hempstead, and Kim,[10]

$$\rho_f = \rho_n \frac{B}{H_c} \tag{7}$$

where ρ_n is the normal resistivity, B is the applied magnetic field, and H_c is the upper critical field. This model corresponds to a linear voltage increase when the critical current is exceeded during current-sharing. However, El Bindari and Bernert[9] accounted for a nonlinear onset of voltage of the type seen in Fig. 2. At a voltage gradient of 10 μV/cm, the flux-flow resistivity of the Nb-Ti would be more than an order of magnitude less than that of the stabilizing copper. Kim has reported a similar nonlinear flux-flow resistivity in samples of Nb-Ta and Pb-In below voltage gradients less than 100 μV/cm.[10] It appears that this initial behavior of the flux-flow resistivity could be quite important to inherent stability.

In Fig. 3 note that Eq. (6) adequately predicts the maximum filament size for reversible current-sharing. The data shown are for Nb-Ti alloys from various manufacturers and with copper-to-superconductor ratios between 2:1 and 7:1. This surprisingly good agreement suggests that the common Nb-Ti alloys obey Eq. (2) reasonably well, and that the amount of copper has little importance during incipient current-sharing. When the power dissipated is small, each Nb-Ti filament is surrounded by a nearly infinite heat sink, which satisfies one of the assumptions used in the derivation of Eq. (6).

The upper line in Fig. 3 distinguishes the discontinuous current-sharing region. Not all Nb-Ti alloys exhibit this behavior, but it is commonly found in the T48B alloy* for which these data are given.

An alternate to Eq. (6) can be derived by combining Eq. (6), Eq. (2), and the data in Fig. 1 to give

$$J_c d < 3000 \tag{8}$$

where J_c is the critical current density in A/cm^2 and d is the filament diameter in centimeters. Hancox[12] has derived a similar expression for the elimination of flux jumps in superconductors which indicates that reversible current-sharing and flux jumping are related phenomena.

SOLENOID TESTS

Several experimental solenoids of the type shown in Fig. 4 were used to relate current-sharing to inherent stability. Complete details are given in Ref. 13, but some representive results are given in Fig. 5 where the critical currents for conductors A and B are plotted against magnetic field. Conductor A did not exhibit any current-sharing below 65 kG, and the corresponding solenoid did not reach the critical current. Instead it quenched when the Stekly number, α_s, equaled unity[14]

$$\alpha_s = \frac{I^2 R}{hP(T_c - T_b)} \tag{9}$$

That is, when the heat generated in the copper could no longer be removed by nucleate boiling of liquid helium, the transition to film boiling raised the superconductor above its transition temperature and precipitated a quench. The peak heat flux was $0.4\ W/cm^2$, which is consistent with the measurements by Whetstone and Boom[15] within the magnet insulation passages. The solenoid current increased at low field only because of decreasing magneto-resistance of the OFHC copper, which obeyed the relation for resistivity:

$$\rho = \rho_{4.2^\circ K} + 4 \times 10^{-10} B \tag{10}$$

where the magnetic field, B, is in kilogauss and the resistivity, ρ, is in ohm-cm.

Contrast the performance of solenoid A with that of solenoid B in Fig. 5. Conductor B, which exhibited only marginally reversible current-sharing at 60 kG, operated in a solenoid to the critical current. Even at lower magnetic fields where only discontinuous current-sharing was observed, the solenoid reached a Stekly number, α_s, equal to 1.4. This meant that the conductor was inherently stable beyond the ability of the copper to carry the full magnet current.

CONCLUSIONS

The data are far from complete, but these experiments strongly indicate that superconductors which current-share in short-sample tests can be operated in solenoids beyond the nucleate boiling stability limit (i.e., a Stekly number greater than unity). For reversible current-sharing, the maximum filament diameter in inches is given by $d < 0.0035e^{B/40}$ or alternately by the expression $J_c d < 3000$, where d is in centimeters and J_c is in A/cm^2. The smallest practical filament will produce the greatest inherent stability, but filaments smaller than 0.0035-in. should be unnecessary even in low magnetic fields. Larger filaments may be used if the conductor will at least discontinuously current-share at the operating field.

The experimental results in this report agree with analytical predictions based on the assumption that the Nb-Ti filaments in a composite behave independently. However, P. F. Smith, et al.[16] have shown that magnetic shielding currents will pass between filaments unless the composite is twisted or a poor electrical conductor is used in place of the copper. It may be possible that the diffusion of copper into the Nb-Ti filaments during their manufacture produces a poorly conducting layer to insulate the filaments, satisfying the conditions by Smith.

*Made by Supercon Division of Norton Co., Natick, Mass.

REFERENCES

1. Y. B. Kim, Phys. Today, Sept. 1964.
2. A. R. Kantrowitz and Z. J. J. Stekly, Appl. Phys. Letters 6, 56 (1965).
3. Z. J. J. Stekly, et al., "A Large Experimental Superconducting Magnet for MHD Power Generation," presented at the International Institute of Refrigeration Commission I Meeting, Boulder, Colorado, 1966.
4. J. R. Purcell, "Argonne National Laboratory 12-ft. Hydrogen Bubble Chamber Superconducting Magnet," presented at the International Colloqium of the National Center of Scientific Research, Grenoble, France, 1967.
5. C. E. Taylor, R. L. Nelson, C. D. Henning, A. R. Taylor and A. R. Harvey, "A Lightweight, 1-Meter-Diameter, 11-kG Superconducting Magnet for a Balloon-Carried Cosmic Ray Experiment," presented at 2nd International Conference on Magnet Technology, Oxford, England, July 1967.
6. P. F. Chester, "Materials for Superconducting Magnets," in Proc. First International Cryogenic Engineering Conference, Kyoto, Japan, April 1967, pp. 147-149.
7. W. F. Gauster, "On the Stability of Superconducting Magnets," in Proceeding of Engineering Problems of Controlled Thermonuclear Reactors (1966), pp. 123-126.
8. D. F. Fairbanks, "The Transition to Current-Sharing on Composite Conductors," presented at the 1968 Cryogenic Engineering Conference, Cleveland, Ohio.
9. A. El Bindari and R. Bernert, "Improved Stabilized Superconductors," Research Report 291, AVCO Everetty Research Laboratory, March 1968.
10. A. R. Strnad, C. F. Hempstead, and Y. B. Kim, Phys. Rev. Letters, 13, 794 (1964).
11. D. L. Coffey, "Superconducting Magnets for IMP," presented at the Summer Study on Superconducting Devices and Accelerators, Brookhaven National Laboratory, July 1968.
12. R. Hancox, Phys. Rev. Letters 16, 208 (1965).
13. R. L. Nelson and C. D. Henning, "Testing Composite Superconductors for the LRL Baseball Magnet," presented at the 1968 Cryogenic Engineering Conference, Cleveland, Ohio.
14. Z. S. S. Stekly and J. L. Zar, "Superconducting Coils," IEEE Trans. Nucl. Sci. NS-12, 367 (1965).
15. C. N. Whetstone and R. W. Boom, "Nucleate Cooling Stability for Superconductor—Normal Metal Composite Conductors in Liquid Helium," Advan. Cryog. Eng. 13, 68 (1967).
16. P. F. Smith, M. N. Wilson, C. R. Walters, J. C. Lewin, "Intrinsically Stable Conductors," presented at the Summer Study on Superconducting Devices and Accelerators, Brookhaven National Laboratory, July 1968.

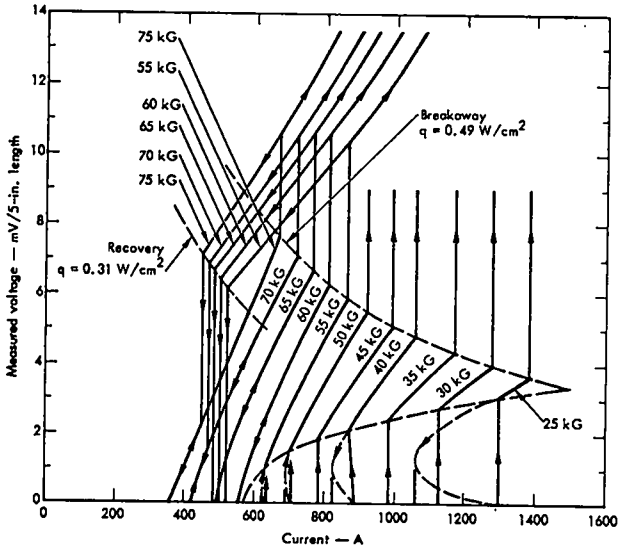

Fig. 1. Current-sharing in an 0.080-in. square composite conductor with six 0.015-in.-diam. Nb-Ti filaments.

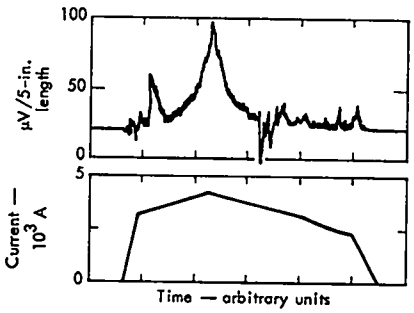

Fig. 2. Reversible current-sharing in a 0.25-in. square composite conductor with seven hundred 0.0046-in.-diam. Nb-Ti filaments.

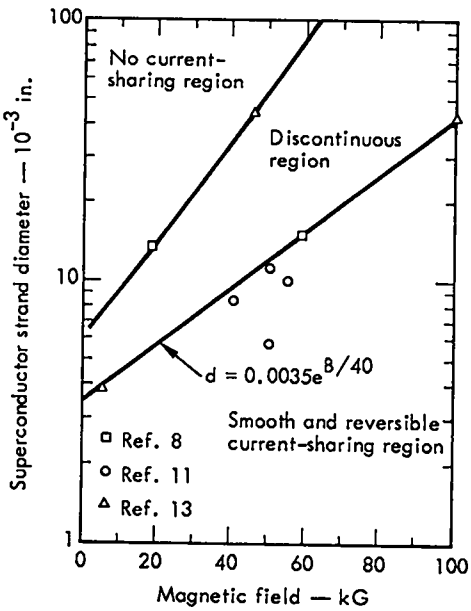

Fig. 3. Transition to current-sharing in Nb-Ti composite conductors.

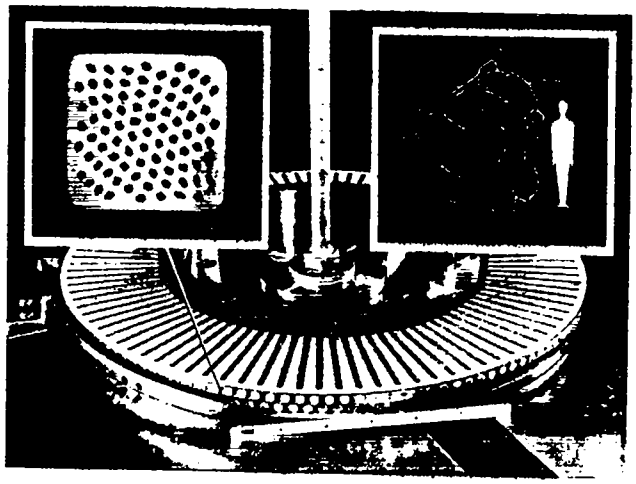

Fig. 4. Superconducting solenoid. Sample conductor was made by Air Reduction Company.

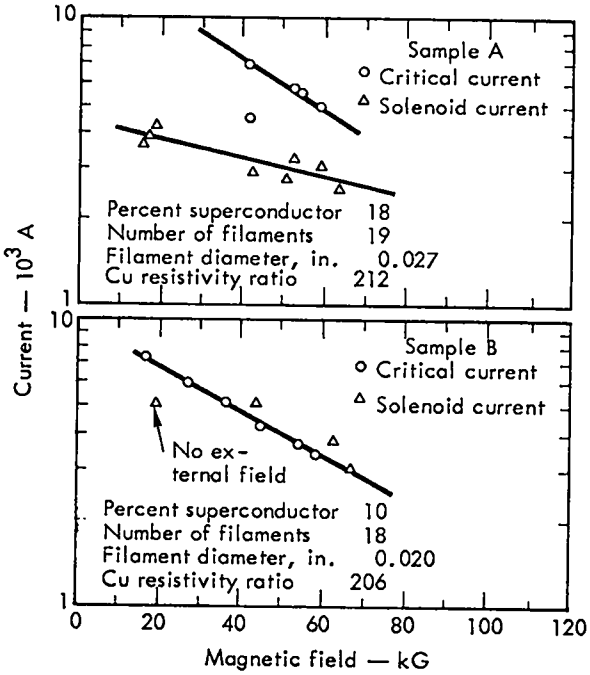

Fig. 5. Critical current and solenoid performance for samples A and B.

BASEBALL II COIL FORM GEOMETRY AND FABRICATION*

Manuel O. Calderon
Lawrence Radiation Laboratory
University of California
Livermore, California

ABSTRACT

The Alice Baseball II superconducting magnet presented unique problems in the choice of geometry and in the design of a coil structure that would enclose the conductor in a helium environment and resist the large distortion forces. The geometry and the relative size of the coil form in component and assembled state is illustrated and explained. Also discussed are some of the requirements and solutions involved in the selection of fabrication methods and in the choice of materials. Additionally presented are problems that were encountered during the actual production of this large coil form. Closing comments describe the present status of the construction.

INTRODUCTION

The liquid-helium-cooled Alice Baseball II superconducting coil has a 20-kG central field. When wound it will weigh 23,000 lb and will occupy a spherical space roughly $6\frac{1}{2}$ ft in diameter. The support structure, its geometry, and its fabrication is the subject of this presentation.

The geometry of the baseball coil is basically two sets of arcs joined at right angles to each other. The top half of Fig. 1 shows this. But to obtain the desired magnetic field characteristics, the lobe angle α was required to be 10 deg. With this geometry we find that the center line is continuous except for a slight misalignment at the junction of the arcs. However, for a square conductor cross-section, the corners do not meet (Fig. 2). To overcome this, a section of about 3-in. on either side of the center line was replaced with plane surfaces that allowed an acceptable transition between arcs without compound curves.

Figure 3 shows the coil housing in basic cross-section. The primary components include the inner shell, which also serves as the winding form, and the outer shell which is composed of four half-circle pieces. The conductor space is a square, 14.17-in. on a side, formed by walls $1\frac{1}{2}$-in. thick for the inner shell and $2\frac{1}{2}$-in. thick for the outer shells. These thick sections are necessary to resist the large magnetic forces of 1,000,000 lb in tension and the varying pressure of 500-4000 psi in an outward radial direction.

Originally, thought was given to casting this structure, but owing to strength considerations and the presence of ferrites after cooling, casting was rejected. Forging was also rejected when it was found that for other than simple shapes, expensive tooling was required; the cost was not feasible for this one-shot operation. These considerations then led us to decide that a welded plate assembly would be preferable.

Figure 4 is a picture of a quarter-scale model that was constructed prior to actual fabrication for use as a visual aid. Shown at the corners are the splice plates which join the outer shells. The members across the lobes are the tie-bars needed to resist the large lobe-spreading forces. These bars were placed so as to balance the bending moments at the lobes and at the splice joints.

Material was chosen on the basis of high strength, low magnetic permeability, ductility, and weldability. The 300-series stainless steels were not acceptable because of their low yield strengths, and because their permeability rises with the repeated cold cycling which would be encountered.

*Work performed under the auspices of the U. S. Atomic Energy Commission.

The material selected was Armco 21-6-9, which is nominally 21% chromium, 6% nickel and 9% manganese. At 4° K it has a yield strength of 196,000 psi and an ultimate strength of 245,000 psi. Its ductility and toughness are acceptable, as is its magnetic permeability which is less than 1.005. Further, welding may be accomplished with the usual techniques required for vacuum service using an Inconel-182 filler-rod which results in a fully austenitic high-strength weld at liquid helium temperature. Post-annealing is required to eliminate the ferrites in the heat-affected zone.

All materials used for the housing, including the bolting, are Armco 21-6-9. Bolting consists of 1-in. diam bolts that tie the inner and outer shells together, 1-in. diam bolts that hold the tie-bars, and 2-in. diam shoulder bolts which make up the joint at the splice plates. Each tie-bar is actually a lamination of four 2-in. thick plates. This was done to keep the number of different plate thicknesses low.

In a steady-state coil operation, liquid helium is circulated through the coil housing by natural convection, and, accordingly, piping holes have been located with attention to equalizing path lengths, avoiding gas pockets, and providing for power-lead access. Four power-lead tubes at the top of the housing exit the leads through a cold helium gas environment. Additional helium cooling is needed for the tie-bars because thermal conduction between housing and bars would only be through contact in the area of the bolts.

Our needs for plate, both in quantity and sizes, required a mill run. The plate was ordered cut to size for each part, and the order was subsequently delivered directly to the fabricator with a resulting time-saving of about three months.

When the design had been completed, we felt that we had a complex fabricating job. This was confirmed by the single bid that we received from the 18 requests originally sent out. To meet the due date and to preclude castastrophic errors requiring replacement material with its attendant time delay, it was felt that close supervision during fabrication would be needed not only for inspection but also for guidance on a continuous basis. The fabrication of the coil housing took considerably longer than our original estimate of six months. It was actually 13 months before it was finally received.

Fabrication began with the layout of templates that defined outline and forming operations. The various parts were then plasma-arc cut using a template tracer arrangement. A 600-ton hydraulic break was used to do the forming; in Fig. 5 we see one of the outer shell plates being formed. This plate is 4-in. thick as shown but was eventually reduced to $2\frac{1}{2}$-in. thick except in the area of the splice plates. It was necessary to anneal these plates in order to complete the forming because of work-hardening.

Because of their symmetry, quarter units of both the inner and outer shells were first built and then all were assembled to perform the welding of the inner form. Figures 6 and 7 show typical quarter units of the inner and outer shells respectively. All welds were fully radiographed and in addition were inspected with a fluorescent dye penetrant. The inner coil form is shown in Fig. 8 with all but one outer shell removed.

At this point the external machining is still to be done for the splice plates, the tie-bars, the shell-to-shell bolting, the helium piping, and the three points of support. Figure 9 shows the machining of the splice plate holes. There are eight plates, each held with twelve 2-in. diam shoulder bolts for a total of 96. The final assembly is pictured in Fig. 10 with a man shown for relative size comparison.

Winding of the conductor will now be done in-house. When this has been completed, the last operation of vacuum sealing all the shell-to-shell joints and the areas around the splice plates will be done. The coil is located in high vacuum and these sealing pieces are designed to withstand an expected pressure of 40 psi which occurs during the cool-down phase.

The projected date for coil startup is late this year.

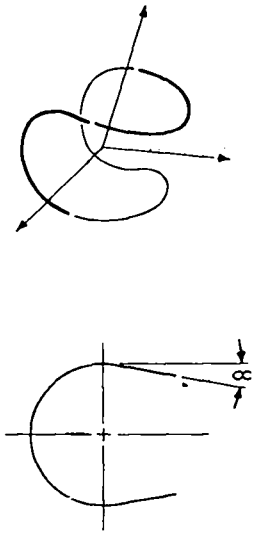

Fig. 1. The geometry of the baseball coil.

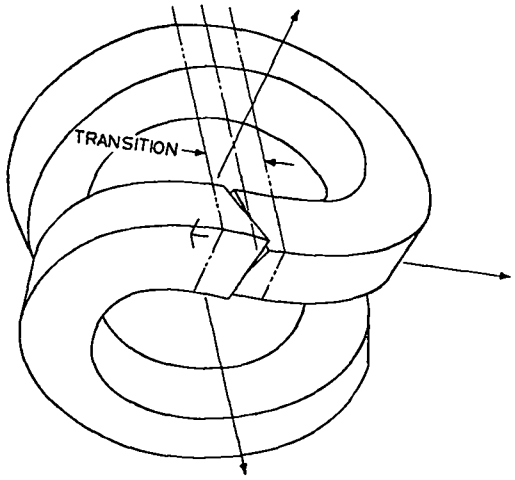

Fig. 2. Conductor corner misalignment.

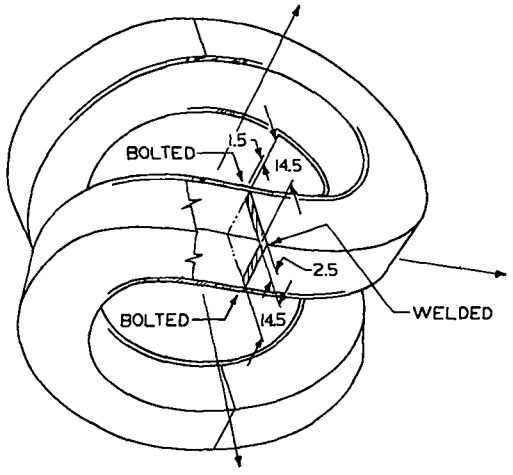

Fig. 3. Basic cross-section and components.

Fig. 4. Quarter-scale model.

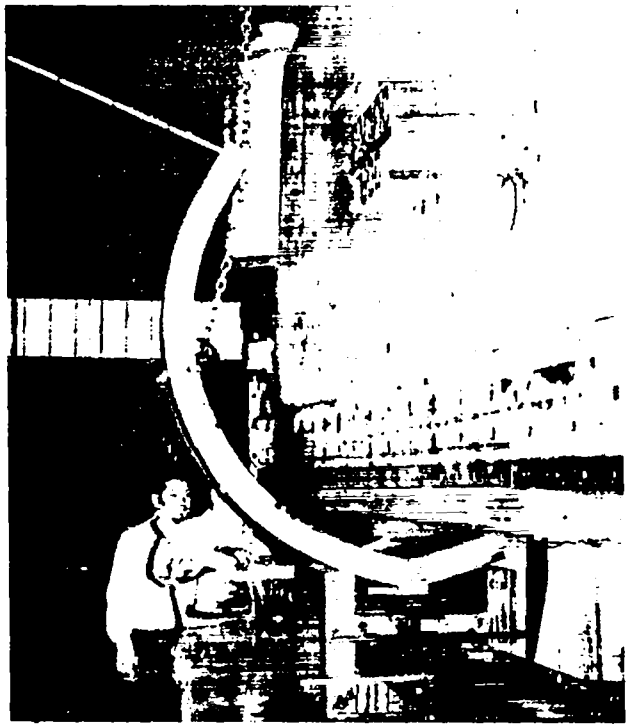

Fig. 5. Forming one of the outer shell plates.

Fig. 6. Typical inner quarter unit.

Fig. 7. Typical outer quarter unit.

Fig. 8. Welded inner form.

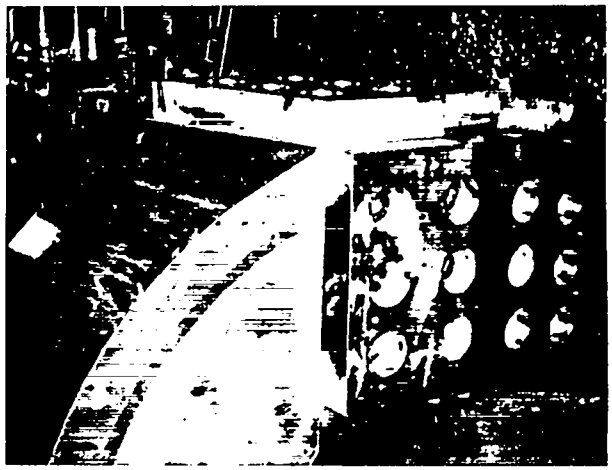

Fig. 9. Machining of splice plates.

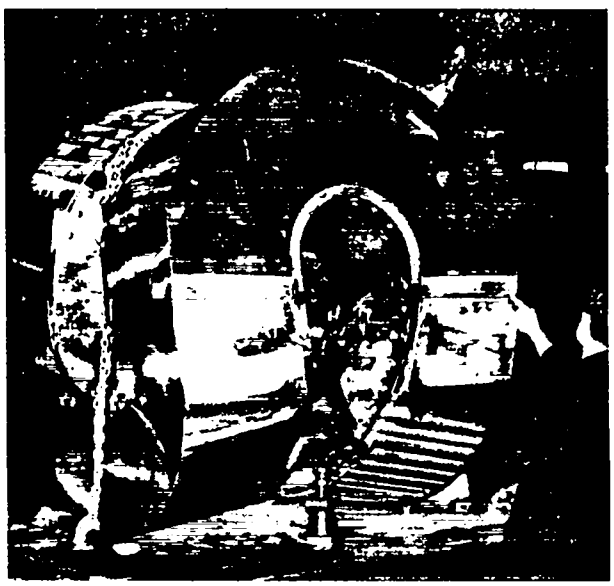

Fig. 10. Assembled coil housing.

CRYOGENIC ASPECTS OF BASEBALL II*

Robert L. Nelson
Lawrence Radiation Laboratory
University of California
Livermore, California 94550

ABSTRACT

This report covers the design of the cryogenic system required for operation of the superconducting baseball magnet now under construction at LRL. It includes a detailed analysis of the heat leak into the system as well as discussion of the shielding and magnet support techniques used to minimize this heat leak. Other problems considered are the magnet cooldown and thermal stresses encountered during the cooldown operation. Schematics of the closed helium cycle and the associated refrigerator and helium recovery system are also included.

INTRODUCTION

A 1.2-m diameter superconducting baseball coil for the Alice experiment is now under construction at LRL and should be completed by the fall of 1969. Details on magnet parameters, superconductor performance and construction techniques are available in other reports.[1,2,3] This report will describe a cryogenic system for the cooldown and operation of the baseball magnet. The system includes the following components: a helium liquefier capable of producing 60 liters/hr of liquid helium (LHe) as well as the necessary refrigeration for magnet cooldown, an LHe storage Dewar vessel of 10,000-liter capacity to act as a thermal ballast in the system, and a gas storage, recovery and purification facility. The magnet, consisting of 10,000 lb of composite superconductor and 14,000 lb of stainless steel structure can be cooled from room temperature either by operating the liquefier as a refrigerator or by the direct transfer of liquid from the 10,000-liter Dewar.

HEAT LOADS

Heat leak into the cryogenic environment of the baseball magnet is a combination of joule heating in the current leads, radiation, conduction, and heat generated in the normal joints of the superconducting wire. Early in the design phase of the project, heat loads were calculated primarily to size the helium liquefier. The long lead time required for the purchase and installation of such an item made these preliminary estimates necessary. Later, as the design progressed, some changes in heat load were made. Figure 1 is a schematic of the baseball coil showing the leads, supports, and heat shields. The theoretical heat loads on the system are tabulated in Table I.

The electrical leads which carry the large currents into the LHe Dewar, are a major heat leak on the system and must operate continuously. That is, the coil is never disconnected from its power supply. It was found that this scheme simplified the coil protection circuitry. Several different designs of cryogenic current leads are now undergoing tests at the LRL cryogenic laboratory in an effort to build an optimum 2400A lead. Basically the designs are quite similar in that the joule heat generated in the copper lead is transferred to the helium boil-off gas leaving the Dewar. Typically a pair of optimum 2400A leads will consume 8 liter/hr of LHe.[4]

Radiation from the liquid nitrogen (LN_2) heat shields to the coil is a significant factor since the exposed area is large and some of the shielding surfaces will have high emissivity. This high emissivity is caused by the titanium getter that is deposited on surfaces to maintain the ultrahigh

*Work performed under the auspices of the U.S. Atomic Energy Commission.

vacuum required for the experiment. Surfaces exposed to the getter will very soon lose their low emissivity and increase the radiant heat load. To minimize this loss, two heat shields are used. A primary shield, spaced 2 cm from the coil face, completely surrounds the coil and follows all of the coil contours. It is supported by low conductivity thermal insulators from the coil surface. Since the inside face of this primary heat shield is not exposed to the titanium getter, it will not increase in emissivity. A second shield, LN_2-cooled, will line the inside of the vacuum vessel and will be partially blackened by the titanium getter. When thermal equilibrium is reached with this method of shielding, the primary shield will float at 70°K. With these conditions, the radiant heat load on the coil is limited to 5 W.

Heat transfer to the coil by conduction is controlled by thermally shorting all heat paths to LN_2 temperature and maintaining long heat paths of small cross-sectional area. Fortunately most austenitic materials are poor thermal conductors, particularly at temperatures below that of LN_2, and also exhibit improved mechanical properties at these low temperatures. For example, the material used for the support tubes on the baseball magnet is Inconel 750 with a room temperature strength of 170,000 psi and a mean thermal conductivity of 80 mW/cm°K. Support of the primary heat shield, however, is more difficult. In this case the heat path is short and the temperature difference will always be about 65°C because of the high emissivity of the primary shield outside surface. Of necessity these supports are made of a plastic material and are tapered to deter conduction of heat. This technique limits the loss due to conduction through the primary shield supports to 3 W.

The superconductor designed for the baseball magnet is 0.25 in. square and is a composite of Nb-Ti and high conductivity copper. A total of 44,000 ft of conductor is required to wind the magnet, and, since the material cannot be produced in lengths greater than 1200 ft, many joints are necessary. To date, there is no practical way to make a joint in a superconductor that will be superconducting in a high magnetic field. The joints within the magnet must then be normal and will generate heat. In the case of the baseball magnet, the joints must also be strong to withstand the high magnetic loads. Development of a suitable lap joint is now in progress at the LRL cryogenic laboratory. The lap joints will generate less than 0.1 W each (about 4 W for the entire coil) and have at least 100% mechanical efficiency.

HELIUM SYSTEM

Liquid helium production and refrigeration for coil cooldown is provided by an Airco 60-liter/hr helium liquefier/refrigerator (shown schematically in Fig. 2), with the design specifications given in Table II. The unit operates on the Claude cycle employing LN_2 for precooling, a single expander, and a Joule-Thompson expansion valve. A small radial inflow turbine with gas-lubricated bearings removes energy from the system during gas expansion. A gas brake, essentially an inefficient compressor driven at turbine speed, converts the turbine output into heat which is removed in a water-cooled heat exchanger. Turbine speed is controlled by varying the pressure and therefore the density of the brake gas. A nonlubricated two-stage compressor manufactured by Rix Industries compresses the 650 ft^3/min of helium gas to 11 atmospheres for the liquefier operation. The Airco unit is the most complex part of the complete helium system (Fig. 3). Boil-off gas from the magnet and storage Dewar is collected in the 8000-ft^3 gas bag. If this gas is clean, i.e., Grade A helium or better, it can be compressed with the high-pressure dry compressor and stored in clean gas storage at pressures up to 1800 psi. If the helium has become contaminated with air or other impurities, it can either be stored as dirty gas or purified before storage. A gas analyzer is a permanent part of the helium recovery system to monitor gas purity. The total storage capacity (clean and dirty helium) is 400,000 std. ft^3 at 1800 psig.

MAGNET COOLDOWN

Before cooldown, the magnet and its Dewar must be filled with clean helium. Normally the liquefier will be operated as a refrigerator to cool the 24,000 lb of superconductor and stainless steel from ambient temperature to LHe temperature.

However, in the event of refrigerator failure, or if additional cooling is required, LHe can be transferred from the 10,000-liter Dewar directly into the magnet Dewar. Under optimum conditions, using only the refrigerator, cooldown will take about 25 hr (Fig. 4). When cooling with the refrigerator from room temperature, the Joule-Thompson valve on the magnet Dewar is fully opened to allow unrestricted flow of helium gas through the magnet. The LN_2 is turned on in the cold box and the compressor is started. Helium gas is cooled in the LN_3 boiler and circulated through the coil, then back to the compressor (Fig. 2). When the magnet temperature reaches 80°K, the turbine is started to remove energy, and the system then begins to cool below LN_2 temperature. When the turbine inlet temperature is reduced to 15°K, Joule-Thompson throttling becomes effective and will bring the magnet down to its steady-state operating temperature of 4.4°K. Under these conditions the magnet will be flooded with LHe.

REFERENCES

1. C. D. Henning, R. L. Nelson, M. O. Calderon, A. K. Chargin, and A. R. Harvey, "Large Superconducting Baseball Magnet - Part I," Presented at Cryogenic Engr. Conf., Cleveland, Ohio, Aug. 1968 [Lawrence Radiation Laboratory, Livermore, Rept. UCRL-71010 (1968)].

2. R. L. Nelson and C. D. Henning, "A 75-kG Superconducting Test Facility," presented at Cryogenic Engr. Conf., Cleveland, Ohio, Aug. 1968 [Lawrence Radiation Laboratory, Livermore, Rept. UCRL-71022 (1968)].

3. M. O. Calderon, "Baseball II Coil Form Geometry and Fabrication," to be presented at this Symposium [Lawrence Radiation Laboratory, Livermore, Rept. UCRL-71534 (1969)].

4. C. D. Henning, "Cryogenic Leads," prepared for the Proceedings of the Symposium on Superconducting Devices and Accelerators, Upton, New York, 1968 [Lawrence Radiation Laboratory, Livermore, Rept. UCRL-71150 (1968)].

Table I. Heat load on the Baseball experiment.

Source	Watts
Radiation	5
Conduction	
Coil and Dewar supports	2
Primary shield supports	3
Instrumentation leads	1
Cryogenic leads	6
Joule heating at superconducting joints	4
Total	21*

*30 liters LHe/hr.

Table II. Design specifications for Airco liquefier.

LHe production	
(liter/hr in either Dewar at 2 psig)	60
Cycle type	Claude with LN_2 precooling
Cycle pressure ratio (nominal)	9:21:1
Cycle maximum pressure (atm)	11.0
Compressor	
Manufacturer	Rix Industries
Type	DBG 1050 reciprocating, nonlubricated, vertical
Number of stages	2
Flow rate (std. ft^3/min)	650
Power consumed (H.P.)	200
Expander	
Type	radial inflow turbine
Model	185H
Speed (rev/sec)	4000
Bearing type	hydrostatic-gas-lubricated
Operating characteristics	
Inlet temperature (°K)	18
Flow rate (std. ft^3/min)	465
Isentropic efficiency (%)	65
Refrigeration produced (W)	1220
Heat exchangers	
Type	extended surface
Material	brazed aluminum
Precooling and heat shielding	
LN_2 consumption for steady-state operation as liquefier (liter/hr)	45
Cooldown performance	
Helium flow rate available at approximately 80°K (std. ft^3/min)	625
Refrigeration available at 80°K (W)	1700
Refrigeration available at 40°K (W)	1400
Refrigeration available 5°K (W)	200

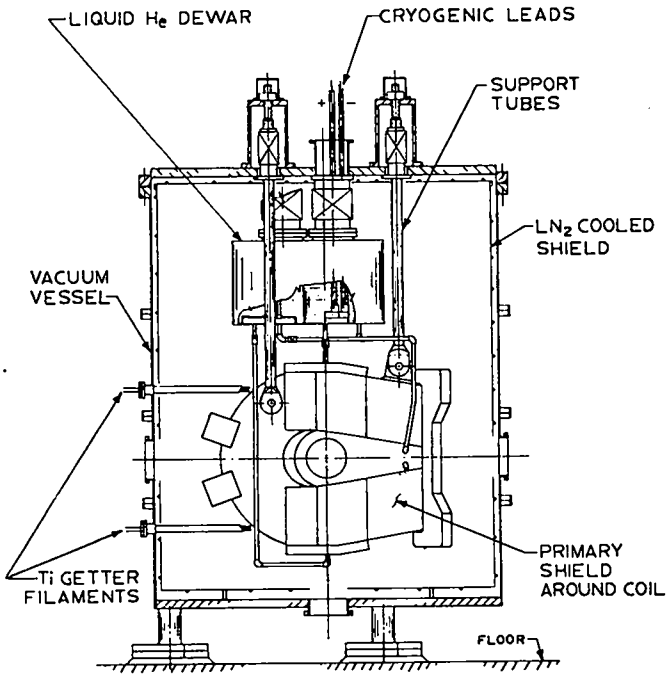

Fig. 1. Baseball magnet.

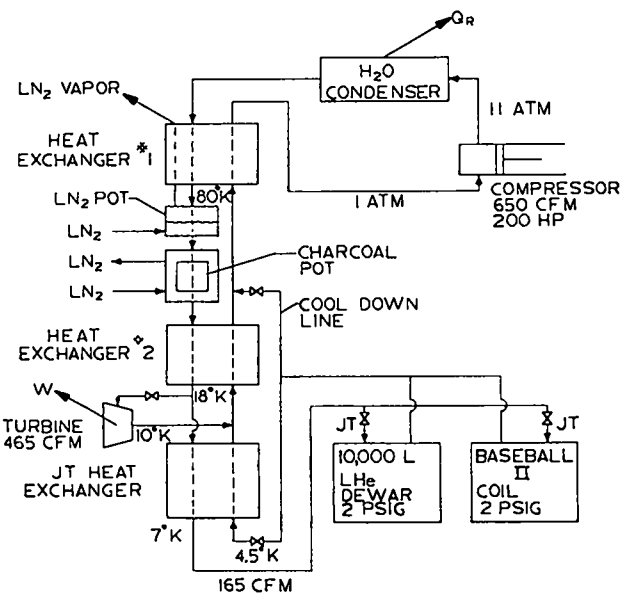

Fig. 2. The helium system of the Baseball experiment.

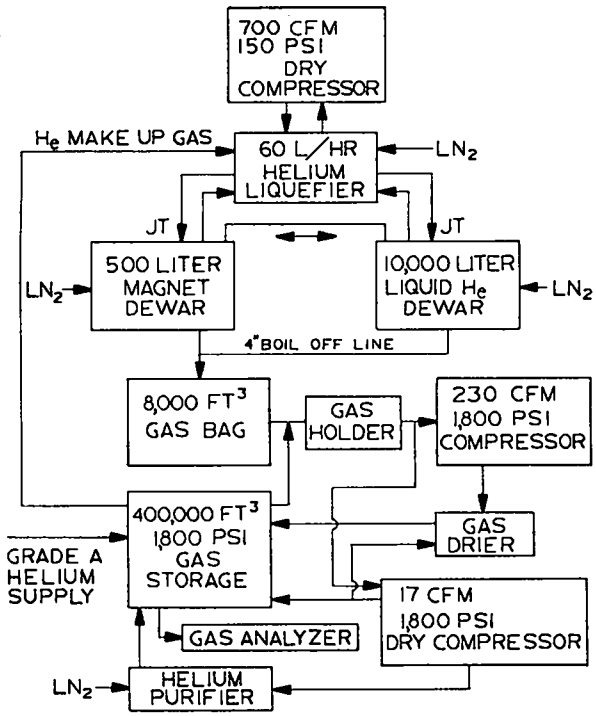

Fig. 3. Schematic showing the entire helium system.

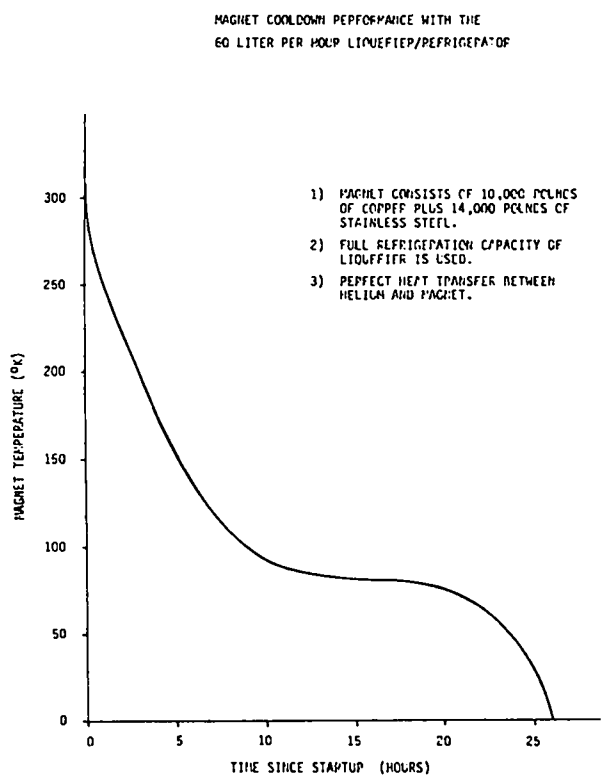

Fig. 4. Cooldown curve.

MAGNETIC FIELD AND FORCE BY FINITE ELEMENT TECHNIQUES*

Anthony K. Chargin and Carl D. Henning
Lawrence Radiation Laboratory
University of California
Livermore, California

ABSTRACT

In the design of modern superconducting magnets a detailed knowledge of magnetic fields and forces within the conductor bundle is essential for predicting successful magnet operation. The classic equations of electricity and magnetism cannot be practically employed to calculate magnetic field strength and force magnitudes for a conductor bundle of an arbitrary shape. Any magnet configuration can be approximated with a finite number of several fundamental elements. A computer program is used to sum the electric and magnetic effects of all the elements.

The technique of selecting the type of element and the number of each is extremely important in obtaining correct results. Errors on the order of 200% are possible with incorrect selection of finite elements. This paper presents the parameters to consider in numerically approximating a conductor bundle. Relationships of these parameters are developed to aid in optimizing the selection of the type and number of fundamental elements for the desired accuracy. The correlation between the numerical approximation and the experimentally measured magnetic fields in several test magnet configurations has been excellent.

Introduction

Recent plasma physics and controlled thermonuclear fusion experiments at Lawrence Radiation Laboratory involved the design of superconducting magnets of unusual shapes. The High Altitude Plasma Physics Experiment (HAPPE) magnet[1] (Fig. 1) has a saddle-like shape, while Baseball II[2] (Fig. 2), a magnet in the ALICE series of experiments, has the shape of a baseball seam. Two important parameters in the design of such magnets are the field at the conductor and magnetic force induced in the conductor bundle. The classic equations of electricity and magnetism can be conveniently used to calculate fields and forces in simple two-dimensional or axisymmetric current paths. Very good tables and graphs exist[3] to aid in optimizing solenoid design. However for nonaxisymmetric, three-dimensional magnets such as Baseball II or HAPPE no ready-made solutions exist. This paper presents a modeling scheme to obtain valid answers for three-dimensional shapes from existing computer programs.

Finite Element Method

In the finite element method, magnetic quantities are calculated for current elements of infinitesimal cross section, such as circular loops, circular arcs, helices, and straight lines. Then a magnet system with distributed currents is approximated by a number of such elements, and the corresponding input is supplied to computer programs such as MAFCO[4] and FORCE.[5] When the point at which the magnetic field is to be calculated is relatively far from the conductor bundle, the scheme for modeling the physical system by finite elements is not critical. However, as the point of interest gets closer to the winding or even within it, the modeling procedure is extremely important. For example, in modeling a 12 × 12 cm cross-section solenoid of 100 cm radius, one finite element, a 100-cm-radius loop, would yield the correct central field. However, to obtain the correct maximum field within the cross section, 16 loops (each representing a 3 × 3 cm area) are required, as will be demonstrated.

*Work performed under the auspices of the U. S. Atomic Energy Commission.

Self Field in Short Line Elements

The simplest form of conductor for which the finite element method can be compared to the analytical solution is an infinitely long straight wire. The self field at the surface of such a conductor of circular cross section can be easily found from Ampere's work:

$$\oint B \cdot ds = \mu I,$$

and therefore

$$B_{self} = 0.4 \frac{I}{d} . \quad (1)$$

To find the self field of a square conductor by classical means is more difficult. Interestingly, a very close approximation can be obtained by relating the side of a square to the radius of a circle of equal area and substituting into Eq. (1):

$$B_{self} = 0.354 \frac{I}{w} . \quad (2)$$

With finite element computer analysis B_{self} is quickly found to be 0.353 I/w by increasing the number of elements per square cross section. For less-than-infinite-length square conductors, Fig. 3 shows the self field that can now be used as a fundamental building block.

Field in Thin Loops

A loop is another fundamental element that would be useful in modeling a physical system such as a solenoid. In the FORCE computer program a loop is represented by an infinitesimally thin circular line, so that the field at the loop would theoretically approach infinity. However, the corresponding infinite current density is a physical impossibility. To avoid this computational problem, a cut of several degrees is made in the loop and a straight line is substituted along the chord for the cut arc. FORCE is designed to calculate magnetic fields and forces in the middle of each such straight-line element by excluding it temporarily from calculations while considering all other elements supplied in the input. In this manner the computational difficulty of dealing with infinity is avoided.

For example, given a 100-cm mean radius loop 8.7 × 8.7 cm in cross section, obtain the magnetic field at the conductor, B_{max}. This loop may be inputted into FORCE as a 350° circular arc element with 100 cm radius, plus a line element corresponding to the chord for the remaining 10° arc. FORCE gives a value of 8.9 G/kA at the center of the chord, which has been excluded from the calculation. From Fig. 3, corresponding to a chord length l = 17.4 cm and width w = 8.7 cm, B_{self} of the excluded chord is 35.9 G. Now B_{max} is 8.9 + 35.9 = 44.8 G. From published tables[3] the correct B_{max} is 44.9 G. This excellent correlation is not accidental. The l/w ratio corresponding to a given range of degree of cut in the loop, θ, determines the accuracy of the results.

Table I shows the errors incurred for a reasonable range of l/w ratios and degrees of cut. Although intuitively one might want to decrease the chord length to improve accuracy, this could produce large errors. Instead, the length-to-width ratio of the element must be controlled. Table II shows the error band width for the combinations of l/w and θ shown in Table I. For an error range of ±5% the l/w ratio may vary between approximately 1 and 5. However, for best accuracy the following rule of thumb should be used:

$$\frac{l}{w} = 1.7 \quad \text{for } 3° < \theta < 10° . \quad (3)$$

Since $l = r\theta$ for small angles, an alternate expression can be used, where θ is given in degrees:

$$\frac{r\theta}{w} = 100 \quad \text{for } 3° < \theta < 10° . \quad (4)$$

Field in Thick Coils

The fundamental finite elements developed above can now be used as building blocks to model any three-dimensional coil. Countless possibilities exist in choosing proper types of elements and their respective numbers. Usually an auxiliary computer program is used to generate the elements, and any type of symmetry eases the calculations. For example, consider a thick solenoid for which a plot of the magnetic field is needed throughout the cross section. The dimensions may be r_i = 100 cm, r_o = 150 cm, and W = 50 cm. Using Eq. (4), θ = 7°, and $r = r_i$, w ≈ 7 cm for the first loop at the inner radius. Keeping θ and w constant throughout the solenoid, the model would consist of a 7 × 7 square array of circular arcs, 353° each, and a corresponding array of lines along the 7° chord for each arc. The l/w ratio increases from 1.7 at inner surface to 2.6 at outer surface. The corresponding

error increases from 0 to 2% at each midchord, considering only the field due to its associated loop. Due to the uniform current distribution, each loop contributes about 10% to the field at its own midchord, and 90% is due to the remaining 48 elements around it. Now the maximum error at the outer surface becomes 2% of 10%, or 0.2%. At the inner surface where the l/w ratio is correct, the error between calculations by the published tables and FORCE is not observable. It should be pointed out that straight-line elements need be inserted in loops only where field mangitudes are desired.

A pair of superconducting coils wound as solenoids were designed by using FORCE. It was necessary to plot the maximum field at the conductor and the central field as a function of distance between the coils. The central field was calculated by placing the midpoint of a fictitious straight-line element with zero current at the center of the coil system. (The fictitious-line-element technique may be used to calculate fields at any other point away from the conductor.) For the designed pair of coils it was impossible to measure experimentally the difference between the calculated field magnitudes and the test results.

Force Calculations

In the FORCE computer program the magnetic force is calculated by the relation

$$\overline{F}_i = \overline{I}_i \, (\overline{l}_i \times \overline{B}_i) \, , \tag{5}$$

where $\overline{B}_i$ is calculated at midpoint of each line element specified and $\overline{I}_i$ corresponds to the magnitude and direction of that line element. The line element i is excluded in calculating $\overline{B}_i$ but not in computing $\overline{B}_{i-1}$ or $\overline{B}_{i+1}$, for which line elements i-1 and i+1 are excluded, respectively. By this technique the danger of dealing with infinite theoretical magnetic fields at the infinitesimal-cross-section conductor is eliminated.

Force on Thin Loop

In using Eq. (5) to calculate magnetic forces in a loop due to its own field, the assumption is made that B_i is the correct average field within the loop, even though a chordal length has been excluded from the calculation. By making the energy-balance calculation it will be shown that this assumption is true, if the rule specified in Eq. (3) or (4) is followed. During an infinitesimal expansion of a current loop the change in mechanical strain energy can be equated to the change in magnetic energy at constant current:[6]

$$F = \frac{I^2}{4\pi} \frac{dL}{dr} \, . \tag{6}$$

Inductance in a loop of wire is given by:[7]

$$L = r \left[\mu \left(\ln \frac{8r}{a} - 2 \right) + \frac{1}{4} \mu' \right] \, . \tag{7}$$

Assuming that $\mu = \mu'$ and substituting Eq. (7) into (6) gives:

$$F = \frac{I^2 \mu}{40\pi} \left(\ln \frac{8r}{a} - \frac{3}{4} \right) . \tag{8}$$

Since the tensile force F, the outward radial force P, and average magnetic field B are related by Eq. (5), and since $P = B^2/8\pi$ and $F = Pr$, the following relation holds:

$$B = \frac{I\mu}{4\pi r} \left(\ln \frac{8r}{a} - \frac{3}{4} \right) \, . \tag{9}$$

By using Eqs. (1) and (2) to relate the self field in circular and rectangular cross sections, the average magnetic field for a current-carrying loop of rectangular cross sections is found:

$$B = \frac{I\mu}{4\pi r} \left(\ln \frac{8\sqrt{\pi} r}{w} - \frac{3}{4} \right) \, . \tag{10}$$

The above formula gives the relationships among B, w, and r to obtain the correct loop force.

In the FORCE code B_i is obtained at midchord, which for a given r immediately determines the correct w, by Eq. (10), to yield accurate force. As previously discussed, B_i is distinctly dependent upon the l/w ratio. Since field and force are directly related by Eq. (5), Table II also corresponds to the approximate error band for forces as a function of l/w.

Force in Thick Coils

As well as being able to calculate magnetic fields within thick coils by using several types of fundamental finite elements, it is now possible by the same procedure to calculate forces. For example, when FORCE is used to calculate magnetic forces on each finite element used to model a long solenoid and the sum is compared with $B^2/8\pi$, the magnetic pressure formula, the results are very close.

The real advantage of FORCE is that any complex system can be modeled, since there are no limitations on geometry. Consider, for example, the Baseball II coil, for which the preliminary design was done by using 44 straight lines along the baseball seam centerline corresponding to $l/w = 0.208$. The central field thus obtained was very close to the right magnitude, as shown in Fig. 4, since the center point was quite distant from the conductor. However, when the point of interest was within the current bundle, more finite elements per cross section had to be used. Figure 4 shows the convergence of the maximum field at the conductor with improving l/w ratio. Even when l/w was quite small—corresponding to a series of straight lines only along the centerline of cross section—the maximum field at the conductor was in error by only 13% from the improved model. Of course, the maximum field estimates include the self-field correction for the straight line at the point of interest.

The convergence of calculated magnetic forces with improving l/w ratio is shown in Fig. 4. When only the centerline is used to model the conductor bundle ($l/w = 0.208$), the force is incorrect by 238%. However, even a slight improvement in l/w to 0.6, still quite below the recommended 1.7, reduces the error to 9%. It is estimated that the final numbers used are within 1% of true force magnitudes.

Conclusion

The finite element technique is readily applicable to the magnetic field and force calculations of complex systems. The fundamental finite elements consist of straight lines, circular loops, and circular arcs, which are assumed to have a definite cross sectional size. This assumption is valid when the length-to-width ratio of straight-line elements is approximately 1.7 for arc angles between 3° and 10°. The circular finite elements necessarily have cross sections similar to the straight lines in close proximity. MAFCO is used to calculate only the magnetic fields at a grid of points away from conductor. However, FORCE may be used to calculate the field within the conductor bundle and the force due to the field. The geometry of the magnet is not restricted in any way, since the fundamental elements described here may be used to model any three-dimensional magnet system.

Nomenclature

a	radius of wire, cm
B	magnetic field, gauss (G)
d	cross-sectional diameter of wire, cm
F	force, dynes
I	current, amperes (A)
L	inductance, henrys
l	length of straight line, cm
P	pressure, dynes/cm^2
r	radius of circular arc, cm
W	solenoid length, cm
w	width of finite element, cm
θ	arc angle, radians or degrees
μ	permeability of space, 0.4π
μ'	permeability of wire

References

1. C. E. Taylor, R. L. Nelson, C. D. Henning, A. R. Taylor, and A. R. Harvey, "A Lightweight, 1 Meter-Diameter, 11 kG Superconducting Magnet for a Baloon-Carried Cosmic Ray Experiment," presented at 2nd Internat. Conf. on Magnet Technology, Oxford, England, July 1967.
2. C. D. Henning, R. L. Nelson, M. O. Calderon, A. K. Chargin, and A. R. Harvey, Large Superconducting Baseball Magnet - Part 1, Lawrence Radiation Laboratory, Livermore, Rept. UCRL-71010-Rev. I (1968).
3. M. W. Garrett, Table of the Ratio B_0/B_{max} from Magnetic Coils with Rectangular Cross-Section and Uniform Current Density, USAEC Rept. ORNL-3972 (1966).
4. W. A. Perkins and T. C. Brown, MAFCO - A Magnetic Field Code for Handling General Current Elements in Three Dimensions, Lawrence Radiation Laboratory, Livermore, Rept. UCRL-7744-Rev. II (1966).
5. C. D. Henning, FORCE: A Computer Program for Calculating Magnetic Forces Developed in Electromagnets, Lawrence Radiation Laboratory, Livermore, Rept. UCRL-14917 (1966).
6. W. K. H. Panofsky and M. Phillips, Classical Electricity and Magnetism (Addison-Wesley, Reading, Mass., 1962), 2nd ed.

7. W. R. Smythe, Static and Dynamic Electricity, (McGraw-Hill, New York, 1950).

Table I. Percent error in single-finite-element calculations for a range of length-to-width ratios in the interval $1° \leq \theta \leq 15°$.

θ (deg) \ l/w	0.2	0.5	1	2	5	10
1	22.0	12.2	0.1	-5.3	-9.4	-18.5
3	20.5	17.4	4.4	-4.0	-7.5	-22.0
5	20.3	17.1	6.6	-2.6	-6.5	- 5.7
7	20.2	16.4	6.7	-1.4	-4.1	- 6.1
10	21.4	15.4	5.9	-0.1	-5.0	- 6.2
15	NA	14.9	5.3	-0.9	-3.8	- 5.2

Table II. Tabulation of length-to-width ratios for error band of ±5% in the interval $1° < \theta < 15°$ for single finite element.

θ (deg) \ Error (%)	+5	+3	+1	0	-1	-3	-5
1	0.7	0.8	0.9	1.0	1.1	1.4	1.9
3	1.0	1.1	1.3	1.4	1.5	1.8	2.4
5	1.2	1.3	1.4	1.6	1.7	2.1	3.1
7	1.2	1.3	1.5	1.7	1.9	3.3	6.4
10	1.1	1.3	1.7	2.0	2.3	3.2	5.0
15	1.0	1.2	1.5	1.7	2.0	3.8	7.8

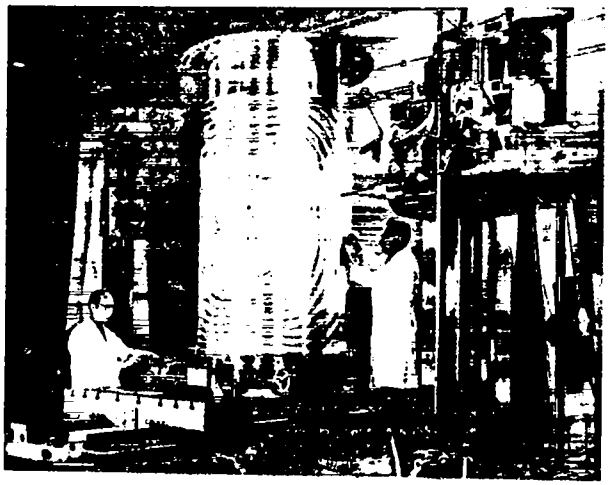

Fig. 1. Winding form for the HAPPE magnet.

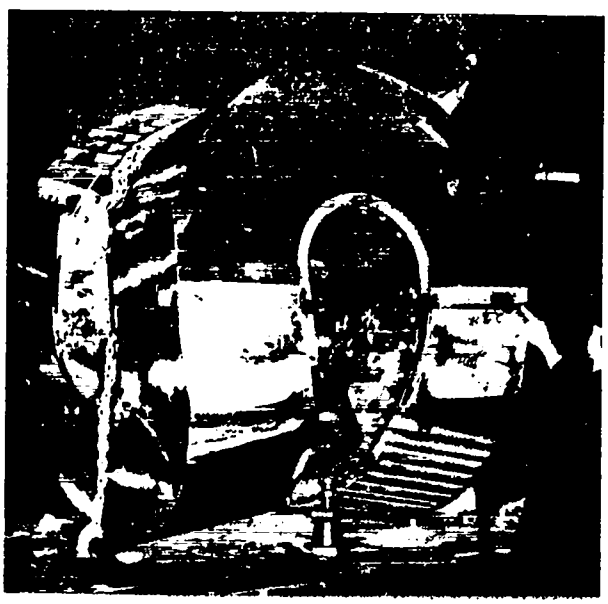

Fig. 2. Coil form for the Baseball II magnet.

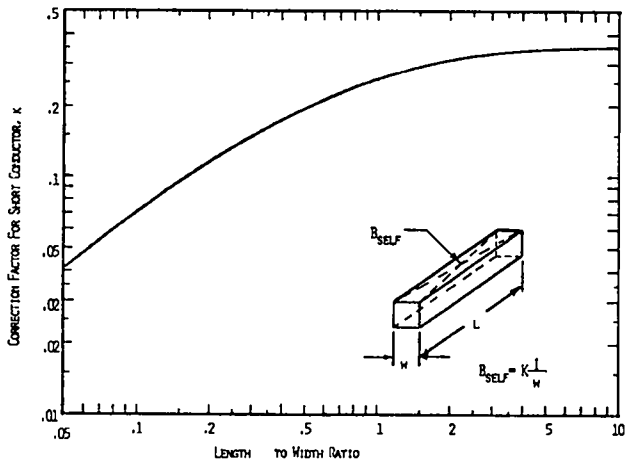

Fig. 3. Self magnetic field of a finite-length-and-width square conductor.

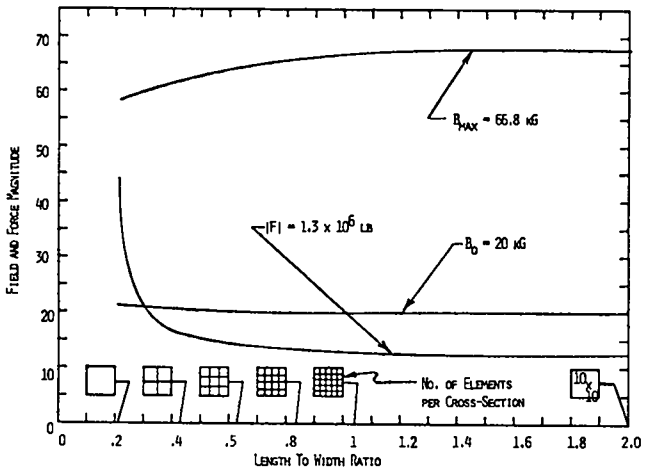

Fig. 4. Convergence of magnetic field and force in Baseball II coil with improving length-to-width ratio of finite element.

SUPERCONDUCTOR EVALUATION TESTS FOR IMP*

D. L. Coffey†
W. F. Gauster
Oak Ridge National Laboratory
Oak Ridge, Tennessee

ABSTRACT

Physically similar quadrupole magnet systems, using NbTi and Nb_3Sn, have been considered for IMP. State-of-the-art techniques for the two types of magnet systems are compared for volume requirements, conductor price, stability, current density, and mechanical rigidity.

The results of an extensive material testing program are reviewed in an attempt to correlate short sample and coil performance, and to empirically define the conductor conditions leading to electrical stability.

The magnet system for the IMP (Injection into Microwave Plasma) experimental facility is to be a superconducting mirror-quadrupole system (Fig. 1). It will produce a central field of 20 kilogauss, an axial mirror ratio of 2 (i.e. B_{max} = 40 KG, and in any direction a minimum mirror ratio of 1.3. Peak magnetic fields of 66 and 80 kilogauss will be generated in the mirror and quadrupole coils respectively. Note that the coils have been designed to accommodate simple layer windings and planar pancake windings.

The mirror coils are layer round of multicore composite NbTi in copper manufactured by Supercon Division of the Norton Company (Fig. 2). They have been tested to short sample operation producing B_{max} = 60 kilogauss at 10,000 amp/cm^2, and will be operated at 6700 amp/cm^2 in order to produce the desired B_{max} = 40 kilogauss.

The quadrupole coils are to be pancake wound of Nb_3Sn ribbon (Fig. 2) (manufactured by General Electric Company) which are laminated with copper for stability and with stainless steel for structural strength.

A midplane section view of the magnet system (Fig. 3) compares NbTi and Nb_3Sn quadrupole magnets and shows that the magnetically equivalent NbTi quadrupole is some 30 percent larger dimensionally than the Nb_3Sn quadrupole. This assumes reasonable operating current densities of 8400 amp/cm^2 in the NbTi system and 13,500 A/cm^2 in the Nb_3Sn system. The Nb_3Sn conductor volume is about one-half that of the NbTi system; however, the required quantity of Nb_3Sn is almost twice as expensive as the NbTi.

Consideration of the electromagnetic "breathing" motion of the quadrupole windings has led to a greater level of confidence in the pancake windings of the Nb_3Sn ribbon than in the less rigid layer windings of the NbTi system.

Electrical stability of the superconductor winding materials (NbTi for the mirror and Nb_3Sn for the quadrupole coils) has been principally evaluated by the "cusp coil" test[1]. The test subjects about 1000 foot conductor samples to the extreme conditions of the actual magnet winding; i.e. forces, fields, current densities, and cooling conditions approximate those of the full size magnet. By applying 0 to 60 kilogauss background fields, it has been possible to evaluate the conductors over a range of peak magnetic fields (i.e. background plus self field) up to about 80 kilogauss. Figure 4 shows the results of a number of tests on five NbTi superconductors. To understand the data, consider first the top sample. It is a conductor 0.057 in. x 0.114 in. by Supercon, consisting of 18 strands of NbTi, each 0.0116 in. diameter, in a copper matrix. The ratio of copper-to-superconductor is 2.4. Bare short sample performance of this conductor in unrestricted helium flow is shown

*Research sponsored by the U. S. Atomic Energy Commission under contract with Union Carbide Corporation.

†Denotes Speaker.

in the upper right graph. The data show V-I performance in a background magnetic field as the current is increased into the resistive state, and again as the current is decreased until the full current returns to the superconductor (shown at 70, 60, and 50 kilogauss). The upper center graph shows the same conductor as it performs in the cusp coil. Since several background fields are used (0, 15, 30, 45, and 60 kilogauss), load lines are shown for the performance data at each background field. The effect of rapid (10 amp/second) and slow (0.2 amp/second) charging rates is indicated and compared to the short sample critical current curve (SS). Each of the other four samples were measured in an identical fashion.

The obvious correlation in the data shown is that those conductors which exhibited a smooth transition into the current sharing (resistive) state, notably the Supercon 15 and Avco 252 samples, also performed best in the cusp coil test. This correlation has led to the following explanation of the source of degradation. Though the calculations used are only very approximate, they seem to relate closely to experimental results.

Energy stored in diamagnetic current loops between superconducting cores of multicore composite conductors is examined as a source of degradation in superconducting magnets using these materials.

Consider a conductor such as in the IMP mirror coils (Fig. 2) simplified to two cores separated by d = 0.05 in. center to center.

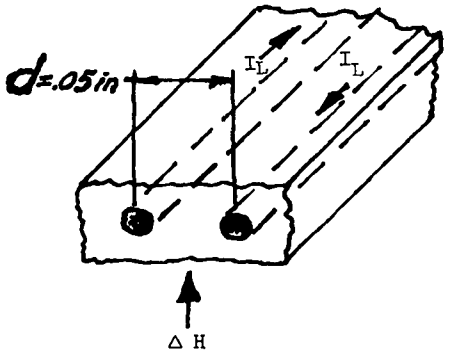

With a 4 in. length of conductor sample ($\ell \simeq 10$ cm) the inductance between the two cores with opposite currents I_{loop} is[2]

$$L = 2 \times 10^{-9} \ \ell \left[\ln \frac{2\ell}{d} - 1 + \frac{d}{\ell} - \frac{1}{4} \frac{d^2}{\ell^2} + \ldots \right] = 8 \times 10^{-8} \text{ H} \quad (\ell \text{ and d in cm.})$$

The approximate resistance experienced by the current I_{loop} is (assuming 5 kilogauss in the critical region)

$$R = \frac{\rho \ell}{A} \sim \frac{1.2 \times 10^{-8} \times 2 \times .05 \times 2.54}{.057 \times 2.54 \times 5} = 4 \times 10^{-9} \text{ ohm}$$

Therefore, the time constant is

$$\tau = \frac{L}{R} = \frac{8 \times 10^{-8}}{4 \times 10^{-9}} = 20 \text{ seconds.}$$

Experimentally the time constant was found to be approximately 13 seconds for these conditions.

The magnetic energy of the current loop in the short sample is $1/2 \ LI^2$. Assume that this energy is quickly released and adiabatically absorbed by the copper substrate. The 10 cm sample weighs 3.6 gram (principally copper). To raise this mass by 5°K (to the critical temperature of about 9.2°K) would require 1.6×10^{-3} joules. Therefore, a loop current change of

$$\Delta I_{loop} = \sqrt{\frac{2w}{L}} = \sqrt{\frac{3.2 \times 10^{-3}}{8 \times 10^{-8}}} = 200 \text{ amps}$$

would be sufficient to heat the superconductor to its critical temperature.

One possible cause for the release of energy can be understood as follows: In one core the transport current I_{transp} and the loop current I_{loop} are additive, in the other core the current difference Itransp - I_{loop} is flowing. If the sum

of transport and loop currents exceeds the critical current I_c of one core, a transition to the normal state or to the flux flow state will occur. In the first case, stored loop energy will be quickly released.

The mentioned condition is not a necessary condition, i.e. energy release can occur without satisfying this condition, e.g. by a flux jump in one of the cores. However, if flux jumps, below I_c, were responsible for the degradation, they would seem to be equally probable in any of the indicated materials. Alternatively, if $I_{transp.} + I_{loop} > I_c$ conditions are responsible, then those conductors which exhibit smooth current sharing would be expected to be more stable; and this was found to be the result observed experimentally.

A local transition to the normal state may not be sufficient to produce a propagating normal zone. The transport current and the surface cooling conditions determine whether the normal section recovers ($I_{transport}$ < minimum propagating current) or continues to warm ($I_{transport}$ > minimum propagating current.)

There are at least two possibilities of preventing the degradation described here. The first avoids charging the current loops, and the second does not allow the stored energy to be released.

If the superconducting cores are twisted (or better transposed) as suggested by Smith,[3] then the increasing field penetrates very rapidly without causing the cores to charge to I_c. The penetration time constant, measured by Iwasa[4] is

$$\tau = \frac{27}{n^2} \text{ seconds (n = twists per foot.)}$$

The short sample of 4 in. length without a twist corresponds to a twisted sample with a transposition cycle distance of 8 inches which suggests a time constant of 12 seconds (by Iwasa) as compared with the measured 13 seconds. In energizing a magnet with twisted core conductor, it is possible to maintain $\frac{dH}{dt}$ sufficiently low that field penetration occurs without generating a significant diamagnetic loop current. Since the loop current without a driving magnetomotive force dissipates as $\frac{dI}{dt} = -\frac{IR}{L}$; and the loop current builds up as $\frac{dI}{dt} = \frac{1}{L}\frac{d\phi}{dt}$ due to an increasing external field, then the equilibrium point is

$$\frac{d\phi}{dt} = I_{loop}\ R_{loop}.$$

A greater $\frac{d\phi}{dt}$ leads toward I_c, and a lesser $\frac{d\phi}{dt}$ allows the loop current to dissipate. Generally, the $\frac{d\phi}{dt}$ of large magnets is such that only a slight twist (perhaps two per foot) might be sufficient to eliminate large diamagnetic currents.

The second means of elimihating diamagnetic degradation is to fabricate untwisted conductors in such a way that when the loop current (plus the transport current) reaches I_c, any additional energy is smoothly dissipated as ohmic power through the flux flow resistance of the conductor and the resistance of the substrate. This technique requires conductor conditions which prevent appreciable transients or jumps as the conductor current begins to share between the superconductor and copper, because any small disturbance might release the energy of the fully charged loop current. If the special wire conditions allow smooth current sharing, as seems to be the case with the two samples Supercon 15 and Avco 252, then the excess charging energy may be steadily dissipated to the helium bath and premature quenching will not occur. An insight into current sharing in composite conductors with $I > I_c$ is given in another paper.[5]

A number of short sample and cusp coil tests in addition to those performed with NbTi materials were conducted with both vapor deposited and diffusion formed Nb_3Sn conductors. With slow charging rates, these tests showed that either material performs very stably (i.e. achieves short sample performance) in the self field of the cusp coil; however, with an externally superimposed field of even only 10 kilogauss the vapor deposited conductor became unstable. The diffusion formed conductor remained stable at all external fields available up to 60 kilogauss corresponding to a total field of 78 kilogauss. The maximum current density stably achieved in the cusp coil test was more than 20,000 amperes/cm^2. Since the IMP

quadrupoles operate in the field of the mirror coils, the choice of the latter conductor was required. Short sample critical currents of 600 amps + 15 percent, - 10 percent at the rated field of 80 kilogauss were specified to avoid instabilities caused by excessively high critical current capacities which were observed in some conductor samples.

Finally, it is important to report some preliminary examinations which are underway at ORNL to determine the extent of liquid helium loss in charging or discharging "shorted" Nb_3Sn coils, i.e. coils employing only stainless steel as turn-to-turn insulation. Appropriately scaling experimental values from small coils indicates that probably more than 1000 liters of helium would be expended in either charging or discharging the quadrupole coil system. By adding a partially resistive surface cover for increasing the turn-to-turn resistance, we anticipate that this charge loss figure can be reduced by 1 or 2 orders of magnitude.

---

[1]D. L. Coffey and W. F. Gauster, 1968 Summer Study on Superconducting Devices and Accelerators, Brookhaven National Laboratory (June 10 - July 19, 1968) UAC-15655 to be published.

[2]Frederick W. Grover, Inductance Calculations, Dover, 1962.

[3]P. F. Smith, et al., 1968 Summer Study on Superconducting Devices and Accelerators, Brookhaven National Laboratory (June 10 - July 19, 1968) UAC-15655 to be published.

[4]Y. Iwasa, Magnetization of Single-Core, Multi-Strand and Twisted Multi-Strand Superconducting Composite Wires, Appl. Phys. Letters, to be published.

[5]W. F. Gauster, Steady State Performances of of Multi-Strand Superconducting Compound Conductors, Journal of Applied Physics (April, 1969).

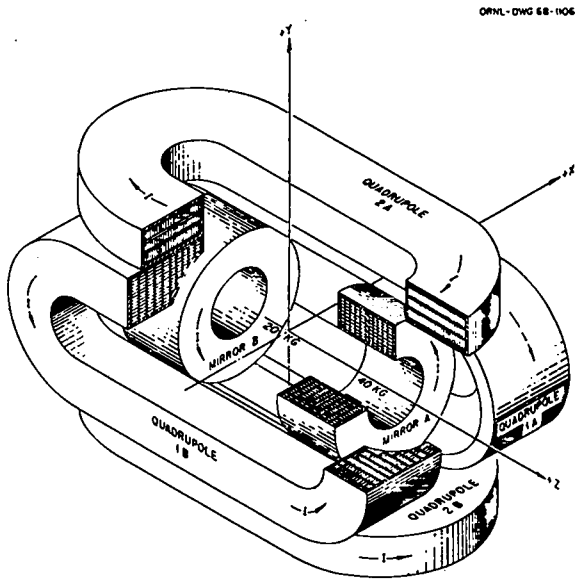

1. Mirror - Quadrupole Magnet System for IMP.

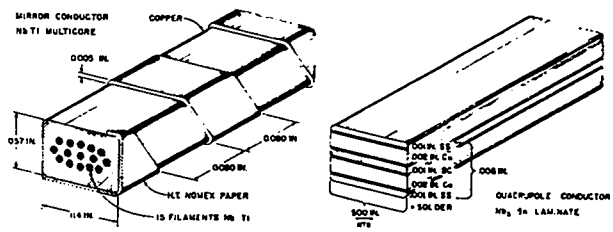

2. IMP Superconductor.

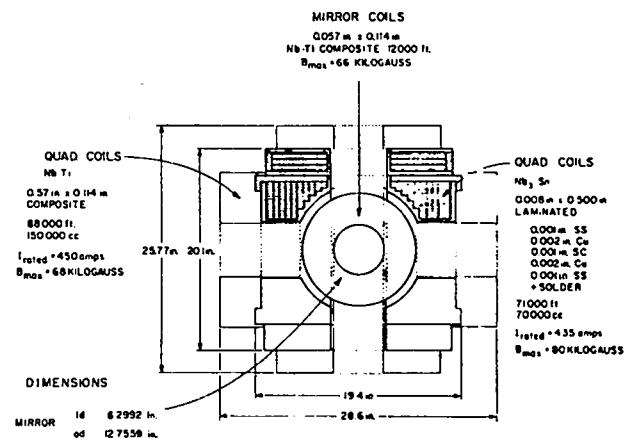

3. NbTi vs. Nb_3Sn Mid-Plane Section of IMP.

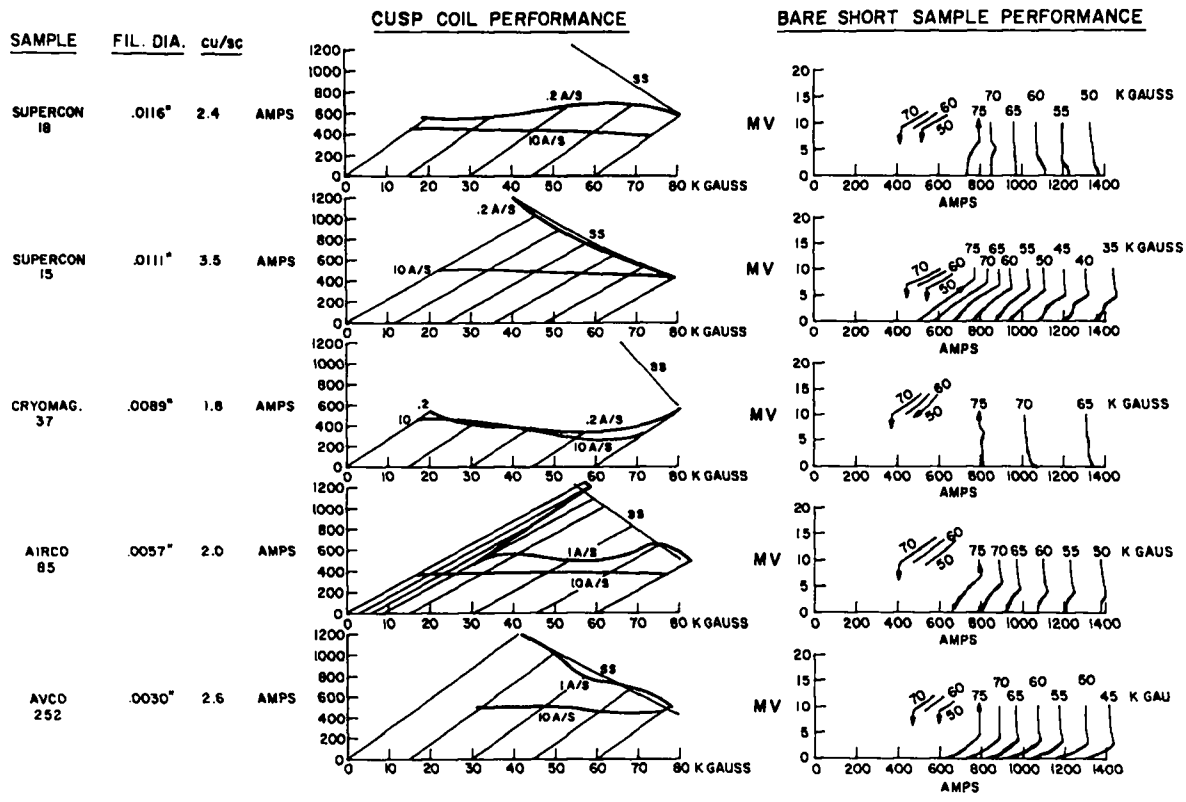

4. Comparative Cusp Coil and Short Sample Tests with .057 in. x .114 in. Composite NbTi-Copper Conductors.

WINDING TECHNIQUES FOR SUPERCONDUCTING MAGNETS*

R. L. Brown
Oak Ridge National Laboratory
Oak Ridge, Tennessee

ABSTRACT

Several new techniques have been developed for winding axisymmetrical and nonaxisymmetrical superconducting magnets. These methods make possible magnets with improved mechanical rigidity and with more reliable interconnections between coil sections (layers or pancakes).

It is very important that the windings of a magnet not be allowed to move, since any motion tends to damage insulation and may lead to superconducting coil degradation. This suggests that the magnet must be wound tightly and must be free of void spaces. Techniques to make fitted void filler pieces for layer wound coils are described. These filler pieces are especially important for making interlayer transitions. Furthermore, a new method is shown for making splice free transitions between pancake sections. In pancake wound coils, such as with Nb_3Sn ribbon, splices are avoided by spiraling the conductor around tilted pins appropriately arranged.

Prototype coil winding tests have shown a clear advantage in using a slight curvature on the "straight" sections of quadrupole magnets. Tests show that the curvature eliminates winding looseness which usually occurs in these parts.

The electromagnetic forces generated in magnet windings produces stresses in the conductors which must ultimately be transmitted to other coil support structures. Unfortunately, the soft OFHC copper, which is used in composite superconductors, is a very ductile material capable of withstanding only moderate stresses. Ventilated magnet construction, using conductors with spiral wrapped insulation[1,2], increases the local stresses since the partial covering makes the load bearing surfaces smaller.

In layer wound magnets specially fabricated filler pieces are required in two places. In making the interlayer transition, it is important that the conductor at the end of one layer not be allowed to simply ride radially outward to the next layer without spacers; such construction causes a scissors action between conductors which damages both insulation and conductors. Rather, the final turn of one layer must rest on a ramp (or wedge) shaped filler piece which guides it to the radial position of the next layer (Fig. 1). Secondly, since the number of turns per layer seldom exactly fills the layer, a filler piece is necessary to eliminate the resulting circumferential void. This piece is always less than one conductor width. It generally must be hand fitted to exactly fill the void space. It is convenient to install the circumferential filler piece between the last and the next-to-the last turn (Fig. 1) of the layer. The effect of these filler pieces is to distribute very evenly the forces on the superconducting wire in the critical layer transition area. They greatly reduce the motion of windings subjected to electromagnetic forces and eliminate the "scissors" insulation damage.

The filler pieces must be fabricated of material which is (1) an insulator, (2) mechanically strong, but not brittle at liquid helium temperatures and (3) readily machined and formed. A compression test of thermoplastic polycarbonate (Lexan) indicated a yield strength of 3.1×10^4 psi at 77°K (about twice that of soft copper.) Though no data are available on the properties of

*Research sponsored by the U. S. Atomic Energy Commission under contract with Union Carbide Corporation.

this plastic at lower temperatures, judging from the properties of similar plastics, we expect even greater strength at liquid helium temperature. The thermoplastic property of polycarbonate makes it possible by heat treating the filler pieces at 150°C for forty-five minutes to form them to the curvature of the magnet winding (Fig. 2). From a sheet of polycarbonate, the filler pieces are cut to a width slightly greater than the conductor width. These strips are ground to close tolerance on a rotary grinding wheel (Fig. 3). The grinding operation should be fast since the filler pieces must be custom fitted at the end of each layer. The wedge shaped filler pieces are fabricated in advance on a manually operated air grinder (Fig. 4). It has been found that the wedge shaped filler piece must provide both a radial ramp and an axial ramp. This requires that the filler piece have a ramp at each end with one rotated 90° with respect to the other.

Model winding studies, in connection with the development of IMP magnets, have led to several interesting improvements in the winding technique for layer wound coils. Uniform conductor winding tension has been maintained by a brake wheel in which the conductor rides on a neoprene disc (Fig. 5). The tension is read and maintained by a torque wrench and clutch arrangement. The entire brake assembly is motor driven to move axially so that the conductor is kept in proper alignment with the coil.

Racetrack shaped coils, for quadrupole magnets, presented another problem. In the straight sections, the windings become very loose since there is no radial force to keep the layers compressed. Attempts to use clamps during winding still did not produce a tightly wound section. It was finally necessary to allow a slight curvature in the "straight section" to maintain radial compression. Several coils with sections of various curvatures were wound to examine the influence of curvature on tightness (Fig. 6). A technique was developed to measure relative tightness by compressing the coil surface with 100 pounds on a one inch square surface and recording the resulting deflection. As can be seen in Fig. 7, with a rise of 0.394 in. at the center of a section with a length of 25 in., the deflection leveled off to approximately 0.0045 in. after about 12 layers of .057 in. x .114 in. composite conductor were wound.

Where splices of the composite conductor were required, they were made by soft soldering the narrow edges of the two conductors over a length which is 1/8 in. less than one turn (Fig. 1). This sacrifices one turn but provides a joint which is electrically and mechanically good.

When the decision was made to use Nb_3Sn ribbon[3,4] in the quadrupoles of IMP, it became necessary to find an improved method of making transitions between pancake sections. The transition area is often the location of faults in pancake coils. An added difficulty arose in trying to make reliable transitions between pancakes with different inside radii (Fig. 8). A satisfactory solution seems to be the use of a tilted pin, about which the ribbon conductor spirals to move from one pancake plane to the next. It can be seen in Fig. 9 that the angle of the pin tilt is proportional to the conductor width and pin diameter. Details of this technique are given elsewhere.[5]

---

[1]Thermonuclear Div. Semiann. Prog. Rept. April 30, ORNL-4150, pp. 142-147.

[2]Thermonuclear Div. Semiann. Prog. Rept. Oct. 31, 1967, ORNL-4238, pp. 143-147.

[3]C. D. Graham, Jr. and H. R. Hart, Jr., "Design and Construction of Tape Wound High Field Superconducting Solenoids", a rept. by G.E. Research and Development Center, Schenectady, N. Y.

[4]E. R. Schrader, "Design and Construction of Nb_3Sn Superconductive Magnets", a rept. by RCA, Harrison, N. J.

[5]R. L. Brown, "Novel Techniques for Winding Superconducting Tapes", ORNL-TM-2450 (Jan. 1969).

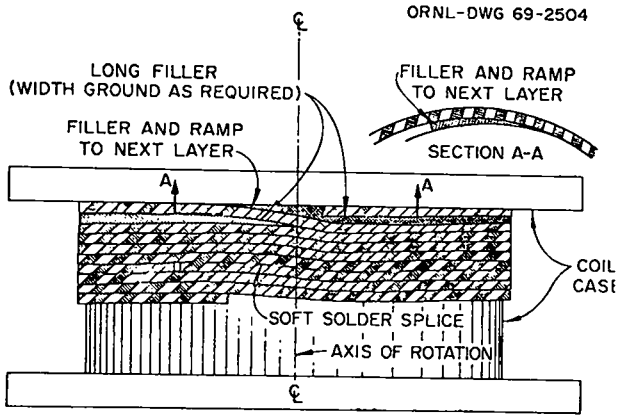

Fig. 1. Magnet Coil Fillers and Splices.

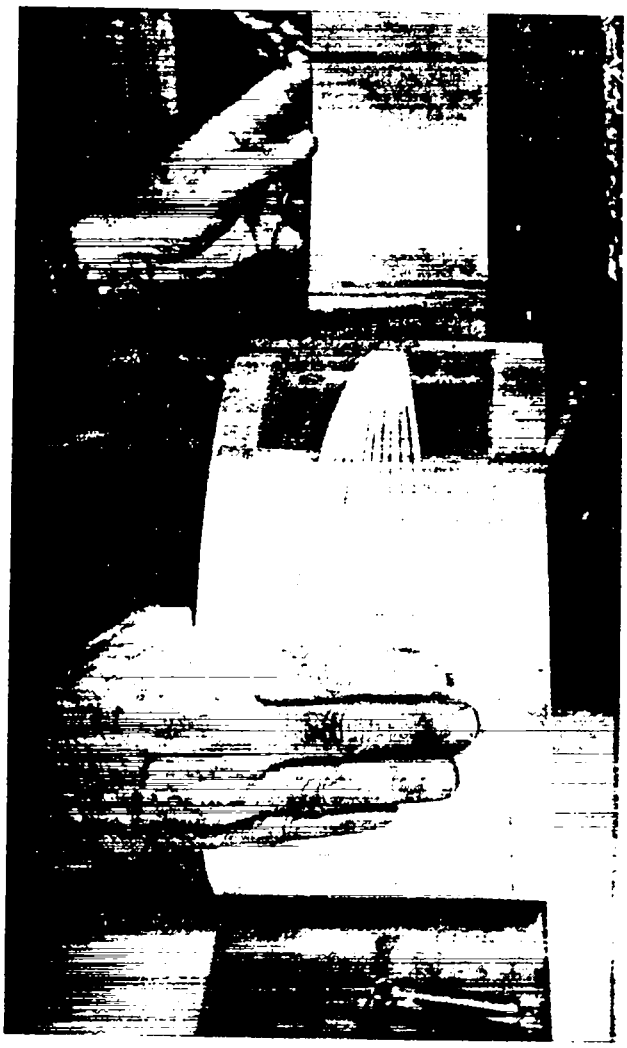

Fig. 2. Forming Curved Fillers.

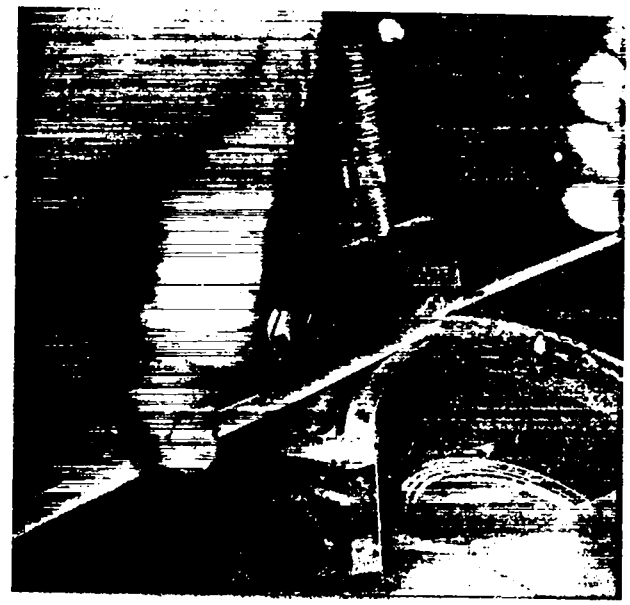

Fig. 3. Grinding Straight Rectangular Fillers.

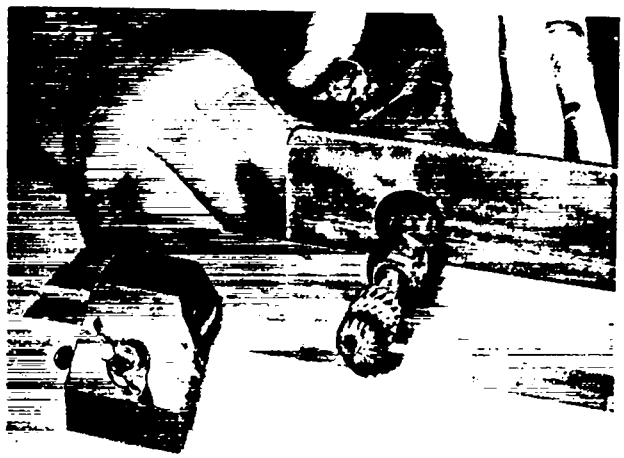

Fig. 4. Grinding Wedge Shape Fillers.

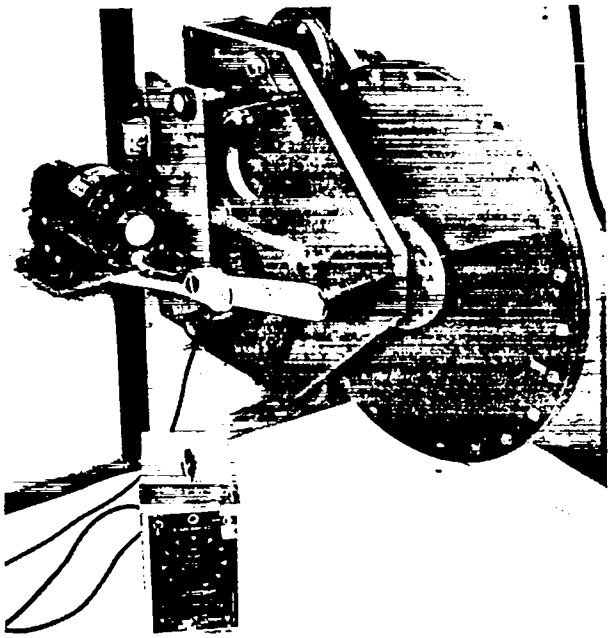

Fig. 5. Brake for Conductor Winding Tension.

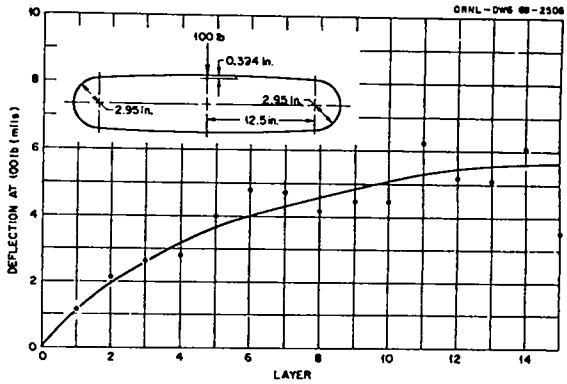

Fig. 7. Winding Tightness Test (deflection vs layers).

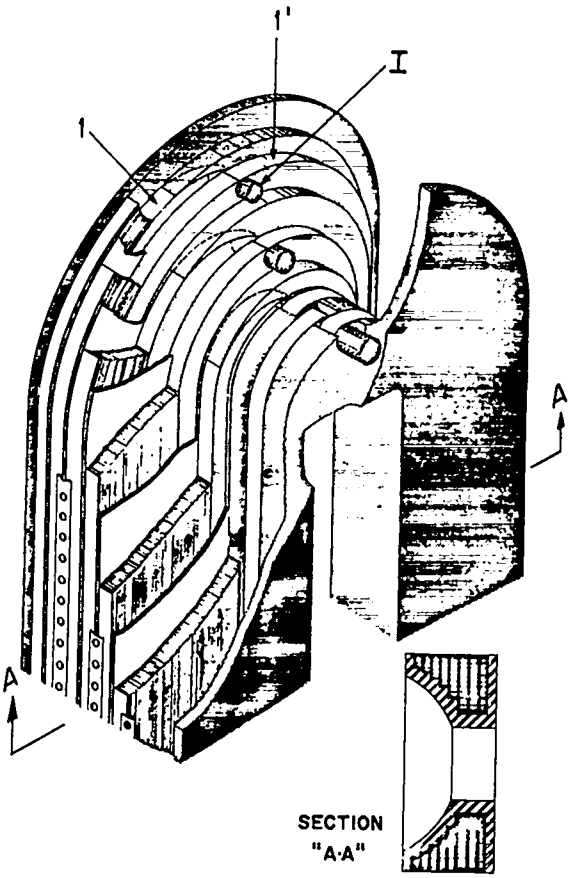

Fig. 8. Transition Pins in IMP Quadrupole Coils.

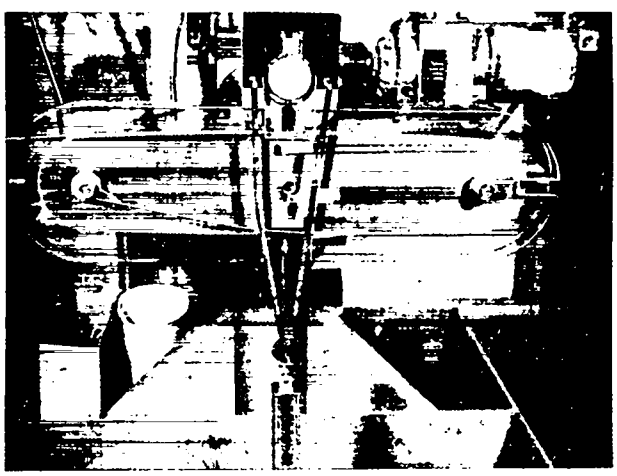

Fig. 6. Winding Tightness Test.

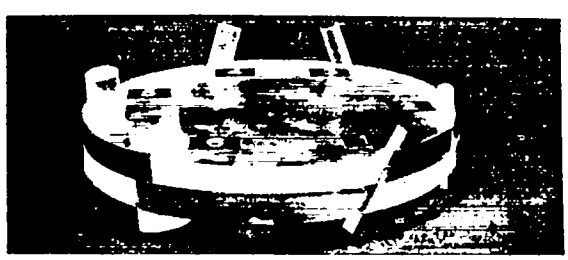

Fig. 9. Model Demonstrating Tilt vs. Pin Diameter.

HIGH-FIELD CRYOGENIC MAGNETS WITH PURE ALUMINUM CONDUCTOR

by Gerald V. Brown
National Aeronautics and Space Administration
Lewis Research Center
Cleveland, Ohio 44135

ABSTRACT

The use of very pure aluminum conductor in high-current-density cryogenic magnets is considered. The need to limit the strain in the aluminum by appropriate structure strength is analyzed. The conclusion is that aluminum with a resistivity ratio above 10,000 could be effectively used if the strain is limited to a few tenths of a percent. Magnetoresistance is a more serious problem at high fields than is strain resistivity. It is shown that average current densities needed to produce fields of 300 KG and over could be obtained even though large amounts of structure are needed to keep the strain low. An examination of the forces in a tape-wound solenoid shows that the problem of the low yield stress of pure aluminum can be solved by making the conductor thin and thus preventing excessive accumulation of force within the conductor. The amount of structure needed in a tape-wound coil is analyzed in terms of a non-dimensional parameter containing the conductor current density and the Young's modulus of the structure. The advantage of a high modulus structure is emphasized.

I. INTRODUCTION

Recent improvements in the residual resistivity ratio (RRR) of Al have increased interest in cryogenic aluminum solenoids. Two serious problems in using very pure Al in high field coils are its softness and its strain resistivity. This paper analyzes these problems and presents one method of solving them for tape-wound solenoids.

II. STRAIN RESISTIVITY

Strain in the plastic region can increase the resistivity, ρ, of Al substantially. Increases near a factor of ten for RRR = 2350 occur for a stress of 15,000 psi (1.0×10^8 N/m^2).[1] But this stress corresponds to a few percent strain. (See stress-strain curves in Ref. 2.) In a magnet, structure can limit strain to tenths of a percent. For 0.3% strain the 2350 RRR sample ρ increases 30% or less. At that strain, the stress in steel is 90,000 psi (6.2×10^8 N/m^2); the structure stress clearly need not be low to give reasonable strain values.

Aluminum with 10,000 RRR is now commercially available. New refining methods yield RRR $\approx$ 50,000.[2] For very high fields, RRR above about 10,000 offers little advantage because magnetoresistance (MR) dominates.

The increase $\Delta\rho(\epsilon)$ of ρ with strain ϵ is usually fitted by a power law, $\Delta\rho(\epsilon) = A\epsilon^n$, where A varies widely, but n is usually between 1.0 and 1.5.

Figure 1 contains data on strain resistivity at 4.2 K. The curve from Arp, et al[2] is an empirical data fit:

$$\Delta\rho(\epsilon) = 110\epsilon^{1.19}(10^{-9}\Omega\ \text{cm}) \qquad (1)$$

Data from Ref. 1 were converted to $\Delta\rho(\epsilon)$ data by using the lowest 2000 RRR stress-strain data of Ref. 2. Two points from Cheever, et al,[3] in the strain range of interest, are shown. Some single crystal data[4] are very close to Eq. (1). Because of the data spread, a "best" and a "worst" case will be considered. The spread is

less important when MR is included for high fields. Equation (1) is used as the best case. The worst case is taken to be a line of slope 1.0 above all the data. The $\Delta\rho(\epsilon)$ are assumed to be independent of RRR. Thus the strained resistivity ρ_s in zero field equals the residual resistance, ρ_o, plus $\Delta\rho(\epsilon)$. Adding the MR, $\Delta\rho_H$, gives $\rho(\epsilon, H) = \rho_o + \Delta\rho(\epsilon) + \Delta\rho_H$. The Corruccini empirical relation,[5] will be used for the MR, with ρ_s put in for the zero field resistivity:

$$\frac{\Delta\rho_H}{\rho_s} = \frac{H_*^2(1 + 0.00177\ H_*)}{1.8 + 1.6\ H_* + 0.53\ H_*^2} \qquad (2)$$

where $H_* = H \times \rho_{RT}/\rho_s$ (in megagauss (100T)).

Figure 2 shows the "best-case" $\rho(\epsilon, H)$ for several strains. The "worst-case" $\rho(\epsilon, H)$ are obtained by adding 0.31, 0.90, and 1.42×10^{-9} Ωcm for 0.1, 0.3, and 0.5% strain, respectively, to the values shown. This is valid because the field range in Fig. 2 is in the linear, or so-called "saturated", region of the MR for all the RRR's shown. The curves, extrapolated far beyond the range of the data underlying Eq. (2), are sensitive to the slope of the linear region.

For any RRR, $\rho(0.5\%, H) - \rho(0.1\%, H) = 0.5\times10^{-9}$ Ω cm for the best case, but is equal to 1.6×10^{-9} Ω cm for the worst case. So for the best-case there is not much benefit in keeping the strain low (which requires more structure), except for the highest RRR and well below 10 T. If the worst case applies, there is a greater benefit in low strain.

At 10 T, increasing the RRR has a diminishing return above 20,000; for 0.3% strain only a 20% reduction in $\rho(\epsilon, H)$ is obtained by going from 20,000 to 50,000. At 30 T the use of RRR > 10,000 would be unrewarding; at 0.3% strain there is only a 10% reduction in $\rho(\epsilon, H)$ from 10,000 to 20,000 RRR and only 20% from 10,000 to 50,000.

Because H and ϵ vary with position in a coil, ρ will, also. The average ρ then lies between the extremes that occur inside and outside.

Strains of 0.1% or lower may be difficult to achieve because the differential thermal contraction between steel and aluminum is of that order from 293 K to 4 K.

III. LIMITATIONS IMPOSED BY PLASTIC FLOW

Local plastic flow problems can be solved by making the conductor a thin, wide ribbon, backed by a ribbon of structure (steel, etc.). This geometry provides a large bearing area to transmit force from conductor to structure and limits accumulation of force inside the conductor. The conductor ribbon, structure ribbon, and an insulating film may be wound into a "pancake" or "tape-wound" coil.

Radially Outward Force. This force, largely counteracted by hoop stress in the structure, also produces local radial compression and contributes to the total shear stress in the conductor.

Compression at Outer Radius of Conductor Ribbon. The radial force accumulates in the conductor to a maximum at its outer surface. The compressive stress S_c at that point in a conductor of thickness t_c, carrying current density J_c in an axial field B_z, is $S_c = B_z J_c t_c$. If S_c must be limited to 1000 psi (6.9×10^6 N/m^2), then $t_c \leq 0.03$" (0.77 mm) for B_z = 30 T, and J_c = 30 KA/cm^2. Much higher J_c and B_z or much lower yield stress could pose a conductor flow problem. Tape-wound, edge-cooled Al coils have been made with foils as thin as 0.004" (0.1 mm).[6]

Axial Force on End Turns. The axial force on the end turns is best resisted (for high B and J_c) by shear on the faces of the turns, because the edge of a thin ribbon has very little bearing area.* A new but less severe limit on conductor thickness arises due to the maximum permitted shear stress between the Al and the structure ribbon, provided by friction or bonding.

Ends of Structure Ribbon. To support the conductor, the structure ribbon must be in tension, and the ends must be anchored to resist the tension. This tension force is reduced by decreasing t_c.

*The axial force is assumed to be carried by the structure after it is transferred from the conductor.

IV. STRUCTURE ANALYSIS

It is now shown that enough structure can be provided to hold ϵ below 0.5% and still have enough total current density J_t to reach very high fields. The following analysis can also be applied to superconducting magnets, where the strain must be low to prevent rupturing the superconducting material. Let the structure thickness t_s vary with the local strength requirements. Several factors make this desireable, including hoop force variations, the unwinding problem, and the result that varying λ_s (the structure fraction) allows J_t to be higher at small radius.

Consider the unwinding problem. The hoop force on a turn of radius r, width w, and thickness t_c in an axial field $B_z(r)$ is $2rB_z(r)J_c t_c w$. The fractional strain $\epsilon(r)$ of a supporting hoop of Young's modulus Y is equal to $rB_z(r)J_c t_c/(Yt_s)$. (Ignore the fact that the "hoop" is really a spiral and also neglect the conductor hoop strength.) The increase Δr in the turn radius is $r\epsilon(r)$ or

$$\Delta r = \frac{J_c t_c r^2 B_z(r)}{Y t_s} \qquad (3)$$

Usually Δr is smaller for the inner turns, and they may unwind until they seat against the outer ones. Adhesives, prestressing of turns (by winding tension), and external hoops help prevent unwinding. But these methods cause compressive forces to be passed from turn to turn, which may be troublesome if the conductor is soft.

These problems are avoided if the structure ribbon thickness t_s is proportional to $r^2 B_z(r)$. The resulting variation of the conductor packing fraction λ_c causes J_t to vary, complicating the calculation of $B_z(r)$. The inter-relation of J_t, λ_c, and $B_z(r)$ involve an integral equation.

The Field Distribution Integral Equation

The change in field dH across a radial element dr of an infinite solenoid is $dH = -J_t(r)dr$, in rationalized mks units. Note $J_t(r) = \lambda_c(r)J_c$. The packing fractions are related by $\lambda_c + \lambda_s = 1$. Under load, the structure expands according to Eq. (3). Setting $\Delta r = a_1\epsilon_1$, where a_1 is the coil inner radius and ϵ_1 the fractional strain at a_1, we obtain

$$\lambda_c(r) = \left[1 + \frac{J_c r^2 B(r)}{Y\epsilon_1 a_1}\right]^{-1}$$

To convert to nondimensional variables, let

$$\gamma \equiv \frac{r}{a_1}, \qquad h(\gamma) \equiv \frac{H(\gamma)}{J_c a_1}, \qquad K \equiv \frac{\mu_o J_c^2 a_1^2}{Y\epsilon_1}$$

Then $\lambda_c = [1 + K\gamma^2 h(\gamma)]^{-1}$, and setting $h(1) \equiv h_1$ and integrating dH yields

$$h(\gamma) = h_1 - \int_1^{\gamma} \left[1 + K\gamma'^2 h(\gamma')\right]^{-1} d\gamma' \qquad (4)$$

The integration interval was chosen to make the field in the bore explicit.

A first approximation, $h^1(\gamma)$, to the solution of Eq. (4) is obtained by replacing $h(\gamma)$ in the integrand by h_1:

$$h^1(\gamma) = h_1 - \frac{\tan^{-1}\left(\sqrt{Kh_1}\,\gamma\right) - \tan^{-1}\left(\sqrt{Kh_1}\right)}{\sqrt{Kh_1}}$$

Successive substitutions of new approximations to $h(\gamma)$ into the integrand yield an iterative solution. For $K = 0$ the solution is $h(\gamma) = h_1 + 1 - \gamma$, and for $K = \infty$, $h(\gamma) = h_1$.

Equation (4) has been solved numerically for several values of h_1 and K. The $h(\gamma)$ solutions (Fig. 3) are readily interpreted in conjunction with λ_c and λ_s. The $h(\gamma)$ curves have minimum slope at $\gamma = 1$, where λ_c and J_t are highest. At larger radii, the hoop force increases, requiring more structure. Secondly, $\epsilon(\gamma)$ must decrease as $1/\gamma$ to keep Δr fixed. Hence the working stress in the structure falls as $1/\gamma$, raising λ_s at larger γ. For the larger h_1 and K the curves for $h(\gamma)$ flatten out for large γ, because the increasing λ_s makes J_t approach zero. For lower h_1 and K, there is an inflection point in the curves if the hoop force drops enough to permit λ_s to decrease. Solutions are physically valid only in an interval where $h(\gamma) > 0$, because $\epsilon(\gamma) \propto 1/\gamma$ cannot hold if the hoop force changes sign.

Practicality of Varying t_s

A continuous change of t_s poses a formidable fabrication problem. A simple alternative is a varying number of thin ribbons, approximating a continuous thickness change. The use of thin-rolled ribbons might circumvent the brittleness of the refractory metals, making available the high Young's moduli of molybdenum and tungsten.

V. ACCESSIBLE FIELD RANGE

Within the limits imposed by the properties of very pure aluminum and the structural assumptions, at least 30 T appears attainable.

Consider a coil with $a_1 = 2.65$ cm and outer radius $a_2 = 7.95$ cm. For forced edge-cooling by boiling He, a heat flux of a few W/cm^2, and pancakes 1 cm thick with 50% exposed edge area, the allowed J_c approaches 30 KA/cm^2 for 0.3% strain, 20,000 RRR, and 30 T. Let $J_c = 30$ KA/cm^2, $Y = 30\times10^6$ psi (stainless steel), and $\epsilon_1 = 0.383\%$. Then $K = 0.1$ and $h_1 = 3.0$ for 30 T in the bore. Using Fig. 3, one finds the coil can make 10.6 T and needs a 19.5 T background field to give 30 T total. If the structure were tungsten ($Y = 60\times10^6$ psi), then $K = 0.051$, and the coil would make 14 T. The required 16 T background field is significantly less than the 19.4 T required for the steel structure coil, and is comparable to fields of existing cryogenic magnets. Field strengths of 20 T in a 11.5 cm bore and 14 T in a 29 cm bore have been produced in liquid neon-cooled Al coils.[7] A background coil for the steel structure case above, wound using the methods of the present paper, would be small. For $a_1 = 8.57$ cm, a steel structure, and J_c and a_1 as above, the values $h_1 = 0.6$ and $K = 1.05$ are obtained. Interpolation in Fig. 3 shows that a long background coil 34.2 cm in outside diameter could supply the required 19.4 T.

VI. SUMMARY

It has been shown that strain resistivity in aluminum is not large enough to eradicate the advantage of using aluminum with 10,000 RRR or better in lower field regions of high field coils. In highest fields MR dominates both the residual and strain resistivities, and there may be little reason to go beyond 10,000 in RRR. Conductor strain can readily be held to tenths of a percent by a variable-thickness structural tape wound with the conductor. The changing t_s offers the advantages of (1) preventing accumulated turn-to-turn forces, (2) allowing maximum current density at all points, and (3) producing a current density that varies inversely with radius. An integral equation for the field distribution in such a coil was derived and was solved numerically. The considerable advantage of using a high Young's modulus structure was pointed out from the solutions.

REFERENCES

1. Brooks, J. M., and Purcell, J. R., "Stress Versus Resistivity at Liquid Helium Temperature," Bull. Inst. Int. Froid, Annexe, 521 (1966).
2. Arp, V. D., Kasen, M. B., and Reed, R. P., "Magnetic Energy Storage and Cryogenic Aluminum Magnets," NBS (AFAPL-TR-68-87), Boulder, Colo., Feb., 1969.
3. Cheever, D. L., Howden, D. G., and Monroe, R. E., "A Manufacturing Process for Producing High-Quality Electrical Strip From Ultrahigh-Purity Aluminum for Magnet Applications," Battelle Memorial Inst. (AFML-TR-68-358), Columbus, Ohio, Dec., 1968.
4. Sosin, A., and Koehler, J. S., "Electrical Resistivity Tensor for Aluminum Single Crystal Deformed at Helium Temperature," Phys. Rev. 101, 972 (1956).
5. Corruccini, R. J., "The Electrical Properties of Aluminum for Cryogenic Electromagnets," NBS Tech. Note No. 218, Boulder, Colo., Aug., 1964.
6. Purcell, J. R., and Payne, E. G., "High-Field Liquid H_2-Cooled Aluminum-Wound Magnet," Rev. Sci. Instr. 34, 893 (1963).
7. Brown, G. V., and Coles, W. D., "High-Field Liquid-Neon-Cooled Electromagnets," Advances in Cryogenic Engineering, Vol. 11, Plenum Press, 638 (1966).

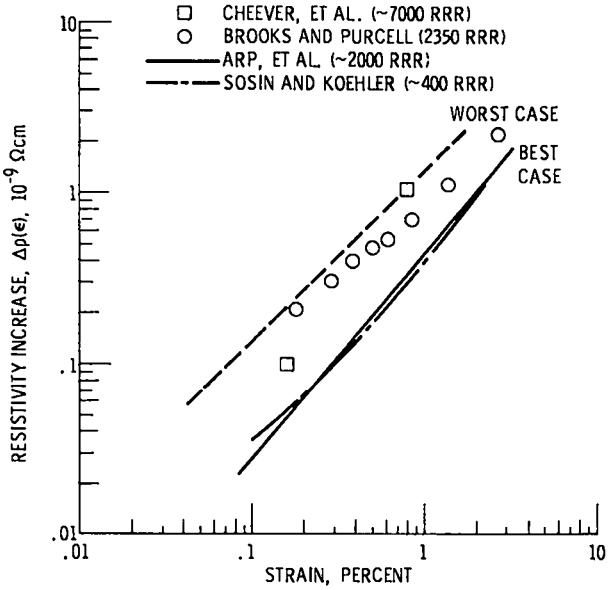

Figure 1. - Strain resistivity for Al.

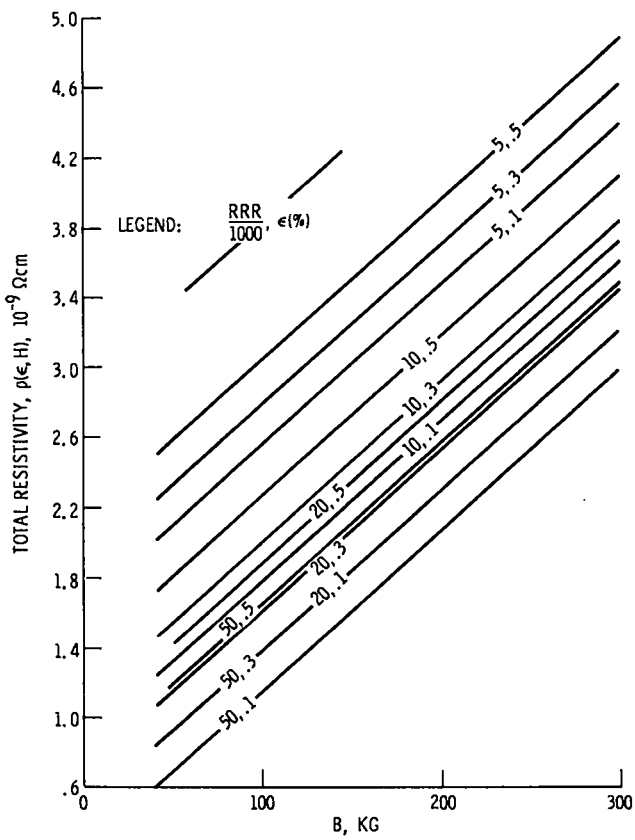

Figure 2. - Total resistivity, strained and in magnetic field.

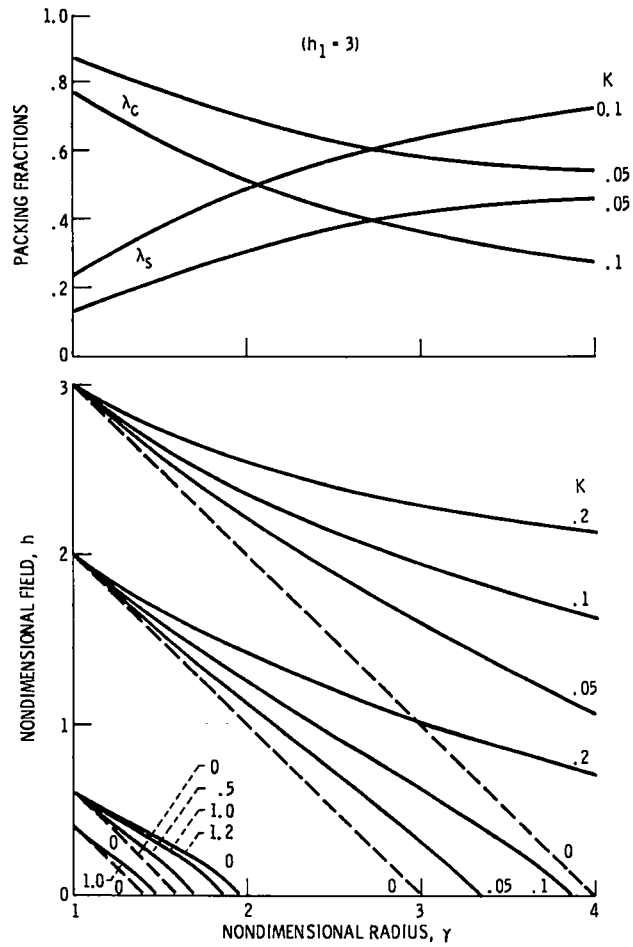

Figure 3. - Nondimensional field and packing factors as functions of nondimensional radius and kappa.

A STUDY OF TOROIDAL AXIALLY SYMMETRIC MAGNETIC FIELD SYSTEMS INCLUDING THE EFFECTS OF FIELD DIFFUSION INTO THE RESISTIVE BOUNDARIES

by

J. Phillpott and T.E. James

U.K.A.E.A. Research Group, Culham Laboratory, Abingdon, Berkshire, England.

ABSTRACT

The paper described the study of field configurations produced by bounded axially symmetric toroidal geometries for infinite and finite conductivity boundary conditions.

1. INTRODUCTION

Magnetic field systems which have toroidal axially symmetric properties (e.g. Multipole and Levitron experiments) have been used to investigate problems associated with plasma containment. In such a system the magnetic field configuration at any time depends on:-

(a) the quantity of flux between the ring conductors and the outer boundary or wall

(b) the shape of the ring conductors and the outer (wall) surface

(c) the varition of flux with time

(d) the rate of field diffusion into the resistive boundaries.

When the time of interest is short compared with the flux penetration, infinite conductivity is assumed, and the flux satisfies Laplace's equation. When the field diffuses into the resistive boundaries, the flux satisfies the Diffusion equation. Computer programs have been written to give various parameters associated with the magnetic field for any point either between or within the metallic boundaries. These parameters may be:-

(e) the magnetic flux plot at any time for any given variations of flux with time

(f) contours of constant magnetic field

(g) total conductor current, surface current densities and contours of constant magnetic scalar potentials

(h) magnetic forces on conductors

(i) line integrals associated with the magnetic field for assessing plasma stability

(j) effective circuit parameters such as inductance, resistance and field decay time constants.

2. PROGRAM OUTLINE

Digital computer programs have been written to solve the field equations using a point successive over-relaxation technique and are shown in block diagram form in Fig.1. There are two user routines which lead to easy modification of input and output information. The region of interest is divided into a series of mesh points and the flux is evaluated at these points for the specified boundary conditions. From these flux values the flux density B may be determined. The overall accuracy of the solution depends on the comparison of distances between mesh points with size of the boundaries. In general, an overall error of less than 5% may be expected, even in regions of high field gradient. For problems involving diffusion of field, this calculation is repeated for successive time intervals.

3. INPUT

Expressing the boundary shapes in terms of their mathematical equations avoids inputting a vast number of co-ordinates. Complicated boundaries may be formed from a combination of simple shapes.

4. OUTPUT

The values of flux and flux density may be tabulated for each mesh point, together with values of various contour integrals. However, graphical representation of the two matrices is desirable. When drawing flux lines the following integrals may be evaluated:

(1) the value of current $\oint H d\ell$

REFERENCES

1. SPALDING, I.J. et al. Theta-cusp containment; Third Conference on Plasma Physics, USSR, 1968.

2. JAMES, T.E. et al. High β Toroidal Pinch Experiment. Culham Laboratory.

3. PHILLPOTT, J. et al. Design Problems in an Inductively Fed Quadrupole Experiment. 5th Symposium on Fusion Technology, Oxford, 1968.

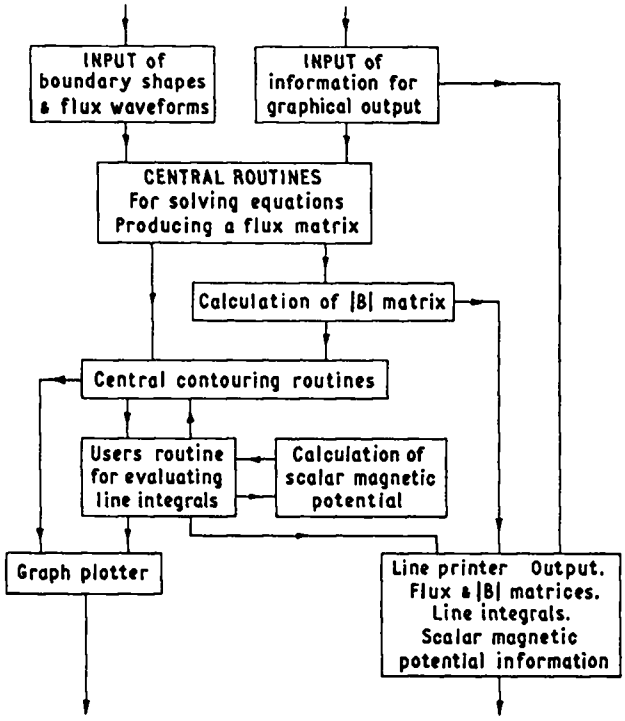

Fig.1 Program Outline

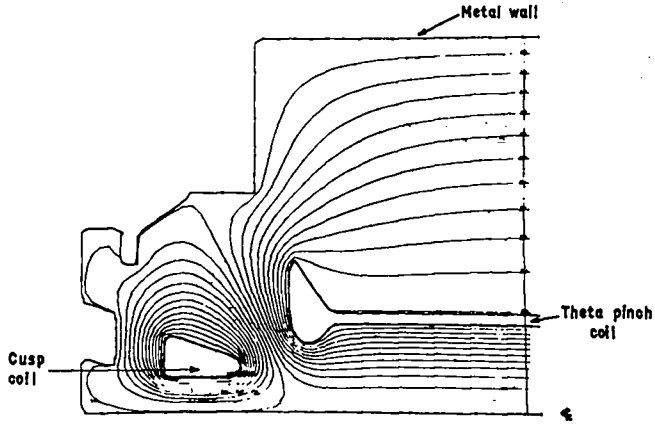

Fig.2 Cusp Ended Theta Pinch Field Plot

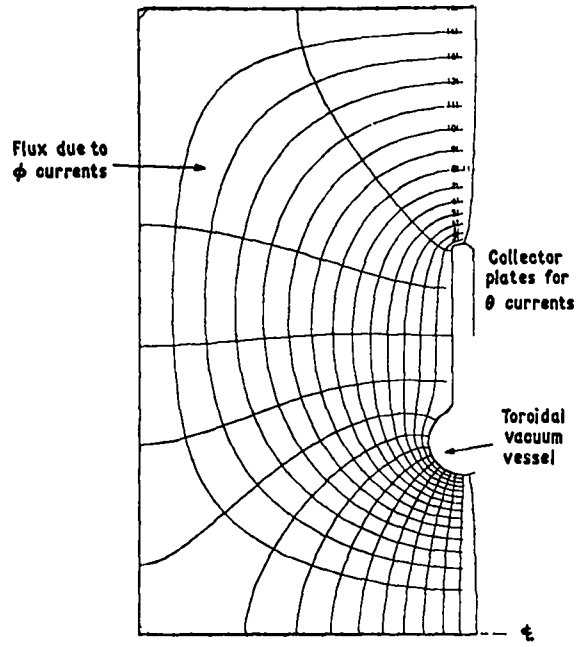

Fig.3 Magnetising Flux Plot of a Toroidal Pinch Experiment

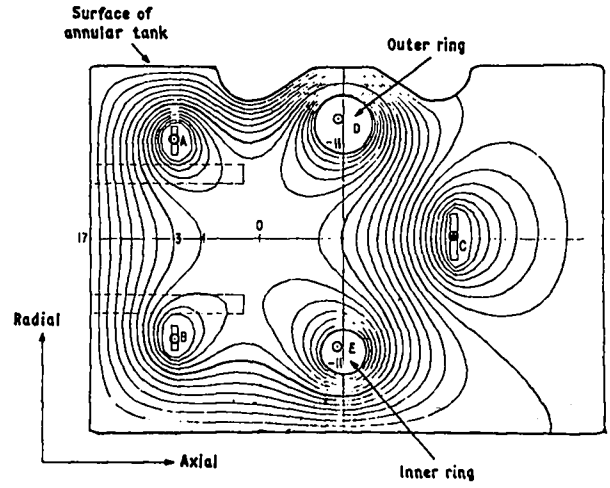

Fig.4 Injection Field Configuration of a Quadrupole

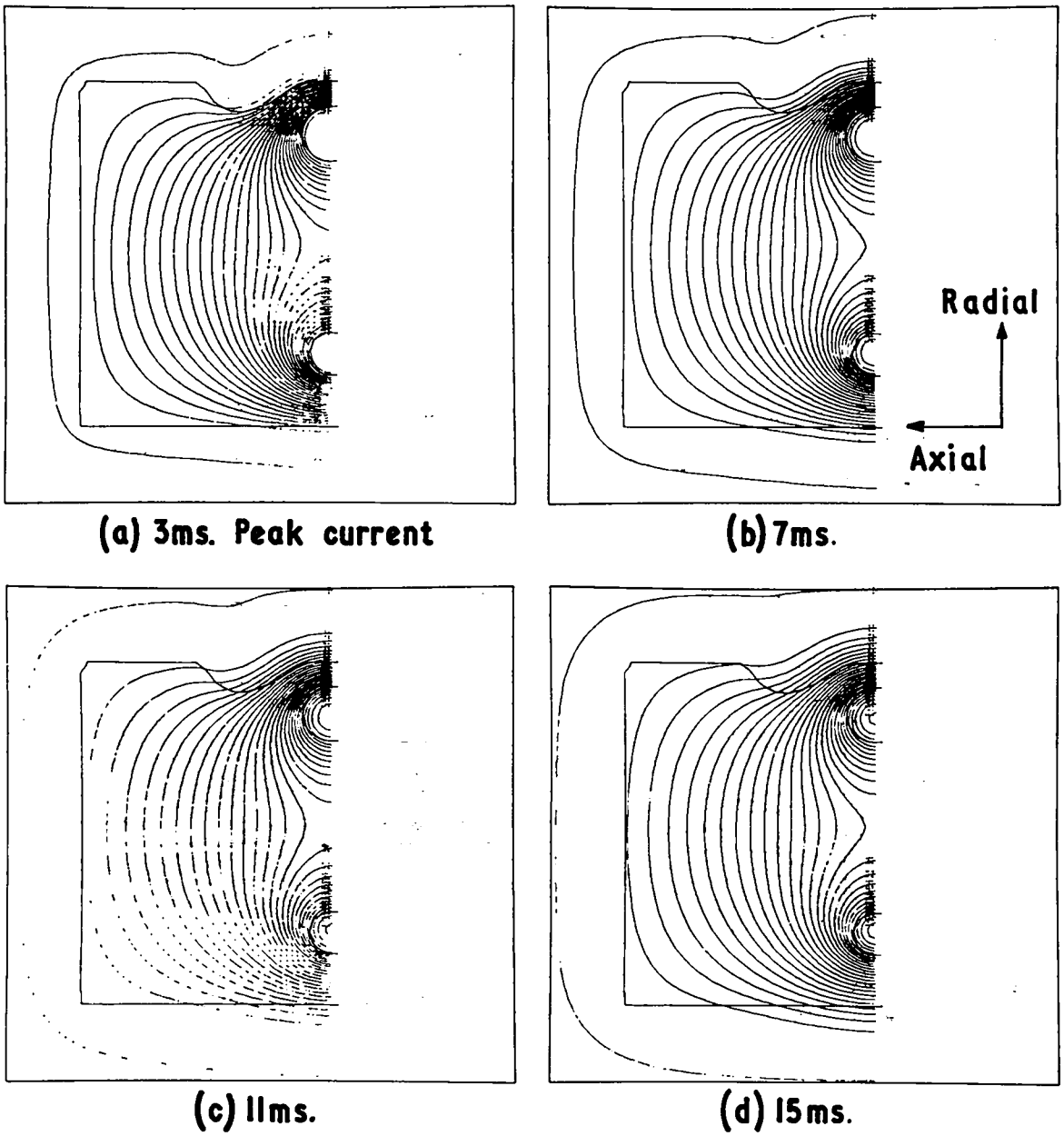

Fig.5 Field Diffusion into Metallic Boundaries of a Quadrupole

DESIGN AND CONSTRUCTION OF AN IMPROVED $\ell = 3$ STABILIZING SYSTEM FOR THE MODEL C STELLARATOR*

J. B. Joyce and G. V. Sheffield

Plasma Physics Laboratory
Princeton University
Princeton, New Jersey

ABSTRACT

The magnetic features of the winding are discussed. The objective of the magnetic design was to obtain high shear and to minimize the island structure of the magnetic surfaces. Methods of adjusting the parameters of the stabilizing winding to give the desired shear, while maintaining the highest degree of magnetic symmetry, are presented. New linear circularizers were adopted that reduce the island structure and allow for adjustment of the magnetic surface quality after the windings are installed. Construction techniques are described with emphasis on new methods as compared to previous windings of this type. A description is given of the use of the vacuum tube as the inner structure for the stabilizing winding. The separate and independent supports for the circularizer windings are discussed. Magnetic, electrical, thermal, and structural specifications are listed.

MAGNETIC DESIGN

The objective of the magnetic design of the SF-3C windings was to obtain a transform of 360 degrees at a radius of 2.5 inches and simultaneously to minimize the island structure of the magnetic surfaces.

Stabilizers

Each stabilizing winding was designed to have 11 field periods over 180 degrees of the U-bend, and the current strength was adjusted to give the required transform. This resulted in a maximum transform per field of about 16.4 degrees, which is well below the limit established by Gibson[1] for the breakup of the magnetic surfaces due to the effect of curvature. (See Fig. 1.) The symmetry of the system was increased by making each winding an integer number of field periods and by having both windings identical. This higher degree of symmetry reduces the size of the island structure.

Circularizers

An earlier study by Sheffield[2] showed that circularizers are one of the major perturbations that enlarge the island structure of the surfaces. For this reason a study was undertaken to determine if a circularizer configuration could be selected that would reduce this effect.

The evaluation was done by determining, through computer calculations, the radial width of the Nth surface island chain, where $N = 2\pi/\iota$, and by comparing this value for the various circularizer configurations.

The two main types of circularizers, helical and linear, are shown in Fig. 2 along with the expressions relating their parameters. The results of the computer runs are also given. It can be seen that compared to the helical type, the linear type reduces the island size significantly and that the second set of linear parameters gives the best results. This second linear

*Work performed under the auspices of the U.S. Atomic Energy Commission.

configuration was adopted for use in the SF-3C windings.

An interesting computer experiment was carried out using this final circularizer design. Up to this point the circularizer had been positioned adjacent to the end of the stabilizing winding. In this experiment the circularizer was mathematically displaced over a range both away from and overlapping the end of the stabilizing winding. The resulting N = 2 island widths measured as a function of the displacement are shown in Fig. 3. The displacement is positive for translation away from the end of the stabilizing winding, and a negative island width indicates a change in the phase of the island chain (a center of an island occurs where a stagnation point between islands occured previously). This plot shows that the phase of the island chain reverses when the displacement is zero, which accounts for the disappearance of the island chain at this point. As a result of this experiment, translational adjustment has been built into the SF-3C circularizers that may be used to further minimize the island structure after the windings have been installed on the C stellarator.

A computer study of the final SF-3C design in a simulation of the C stellarator racetrack shows that the flux lines of the N = 1 surface are contained in the machine and form an island chain whose radial width is of the order of 0.1 inch. As a comparison, when this study was made for the two stabilizing windings now on the C stellarator (SF-3A and SF-3B), the first group of contained flux lines which form an island chain of comparable radial width are on the N = 4 surface. This result shows that the new SF-3C windings are magnetically a substantial improvement over the existing stabilizing windings, since they give four times the transform on surface island chains of comparable radial width.

MECHANICAL DESIGN AND CONSTRUCTION

Stabilizer Windings

With the required features of the windings established by magnetic parameters, the next step was to design, manufacture, and assemble the actual components. The first dimension to be set was the minor diameter of the stabilizer conductors. Implied in this diameter are the conductor size and the number of conductors per bundle. Every effort was made to position the conductors as close to the magnetic centerline as possible.

The first step in this direction was positioning of the conductors directly on the vacuum tube. Previous windings of this type for Model C used structural support systems that were independent of the vacuum tube. To utilize the vacuum tube as the inner structure required a tube with a wall thickness capable of supporting the inward forces. At the same time the wall thickness could not be allowed to dictate a position for the conductors beyond the desired radial location. Some additional space was obtained by decreasing the vacuum tube inside diameter from 8 to 7.8 inches. Analysis of the tube, loaded by three equally spaced, uniformly distributed forces, indicated excessive wall thicknesses. Additional support for the inner tube was required. Stiff outer rings were used to restrict the outward deflection of the vacuum tube in the non-loaded span and thereby reduce the moments in the loaded portion. With this design, a wall thickness of 0.25 inch was found to be sufficient.

The vacuum vessel was formed from an extruded 304 stainless steel tube with a 7.8-inch inside diameter and 0.625-inch wall thickness. After bending the tube to the desired major radius the outside surface was machined to give the 0.25-inch wall thickness. Tolerance on the total indicated reading of the tube outer surface was ± 0.01 inch.

Forming of the conductors was done on a carbon steel mandrel. Contoured strips were bolted to the mandrel to produce the helical pattern. Insulation of the conductors was done before forming. After the conductors were formed and cut to proper length, a turnaround block was brazed between appropriate conductors. A cooling tube was brazed in this block connecting the cooling paths of the two conductors.

With the winding completely formed and connected, it was shifted from the mandrel onto the vacuum tube. The exact position for the conductor bundles was established with a protractor head. The outer bands of glass epoxy were then applied. A steel band was pressed over the turnarounds at each end of the winding and a split steel band clamped over the electrical lead crossovers. These steel bands were necessary to carry the increased load in the transition areas. The end bands also served as bearing surfaces for the circularizer support cylinders.

Cooling is provided by deionized water with a pressure drop across each cooling path of sixty pounds per square inch. Water is supplied at each end of the winding and exhausted at the center, resulting in a path length of approximately 90 inches. The hole size in the conductor is 0.25-inch diameter. Formed conductors for one of the stabilizer windings is shown in Fig. 4.

Circularizer Windings

The circularizer windings represent a complete departure from previous design. In an effort to provide increased flexibility, as well as incorporate the linear conductor positionings, the circularizer portion of the system was made as separate coils. This provides the ability to rotate, translate, and adjust the current of the circularizer windings relative to the stabilizer winding.

In order for the circularizer turnarounds to be in the same plane as the turnarounds of the stabilizer windings, the circularizer conductors were formed at a diameter that could be passed over the end steel bands. This larger diameter also permits translation of the circularizers, giving the phase shift of island structure shown in Fig. 3. The larger diameter also required four conductors per bundle to accomplish the circularizing. These were arranged in two layers making the bundles two conductors wide and two high. Formed conductors for the circularizer windings are shown in Fig. 5.

Cooling is provided for the circularizer windings from the same source described for the stabilizers. The path length is approximately 80 inches through a 0.25-inch hole.

Table I. SF-3C Characteristics

	Stabilizer	Circularizer
Helical Pitch (radians per centerline inch)	0.170543	-
Field Periods	11	-
Number of Bundles	6	6
Number of Conductors per Bundle	4	4
Continuous Current (amperes)	20, 000	20, 000
Pulse Current (amperes)	40, 000	40, 000
Conductor Area (square inches)	0.560	0.437
Conductor Length (inches)	173.5	79.0
Resistance at 20°C (milliohms)	5.03	0.49
Water Flow (gallons per minute per path)	2.6	2.7

References

1. A. Gibson, Culham Laboratory Report, CLM-P-129 (1967).
2. G. V. Sheffield, Princeton Plasma Physics Laboratory MATT-Q-24 (1966) pp. 335-343.

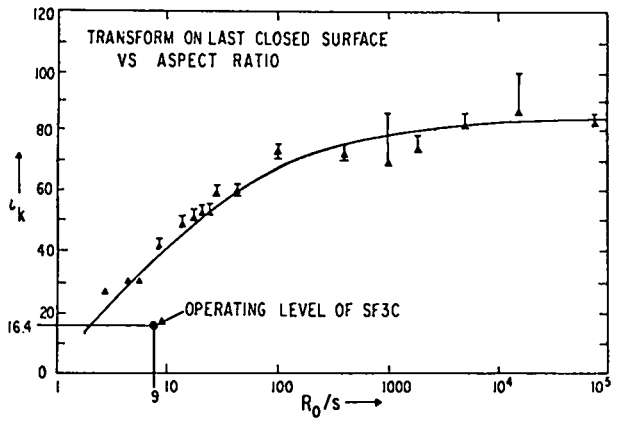

Fig. 1. Transform on last closed surface.

	HELICAL			LINEAR			
GEOMETRY	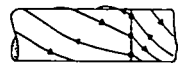						
PARAMETER RELATIONS	$\frac{I_s k_c}{I_c k_s} = 2$			$\frac{I_s}{I_c L_c k_s} = 3$			
LENGTH OF CIRCULARIZERS	$L_c = \pi / 3 k_c$						
	I_c/I_s	k_c/k_s	$\frac{\Delta}{\ell} N=2$	I_c/I_s	L_c	$\frac{\Delta}{\ell} N=2$	$\frac{\Delta}{\ell} N=1$
	$\frac{2}{3}$	$\frac{4}{3}$	0.034	$\frac{1}{2\pi}$	$\frac{2\pi}{3k_s}$	0	0.011
	$\frac{1}{2}$	1	0.034	$\frac{1}{\pi}$	$\frac{\pi}{3k_s}$	0	0.004

Fig. 2. Circularizer variations.

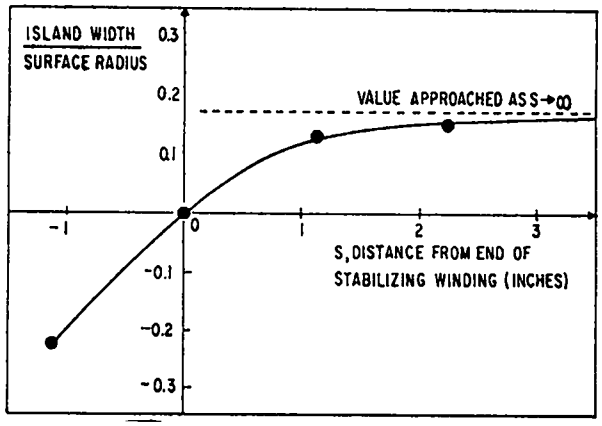

Fig. 3. Island phase shift.

Fig. 4. SF-3C stabilizer conductors.

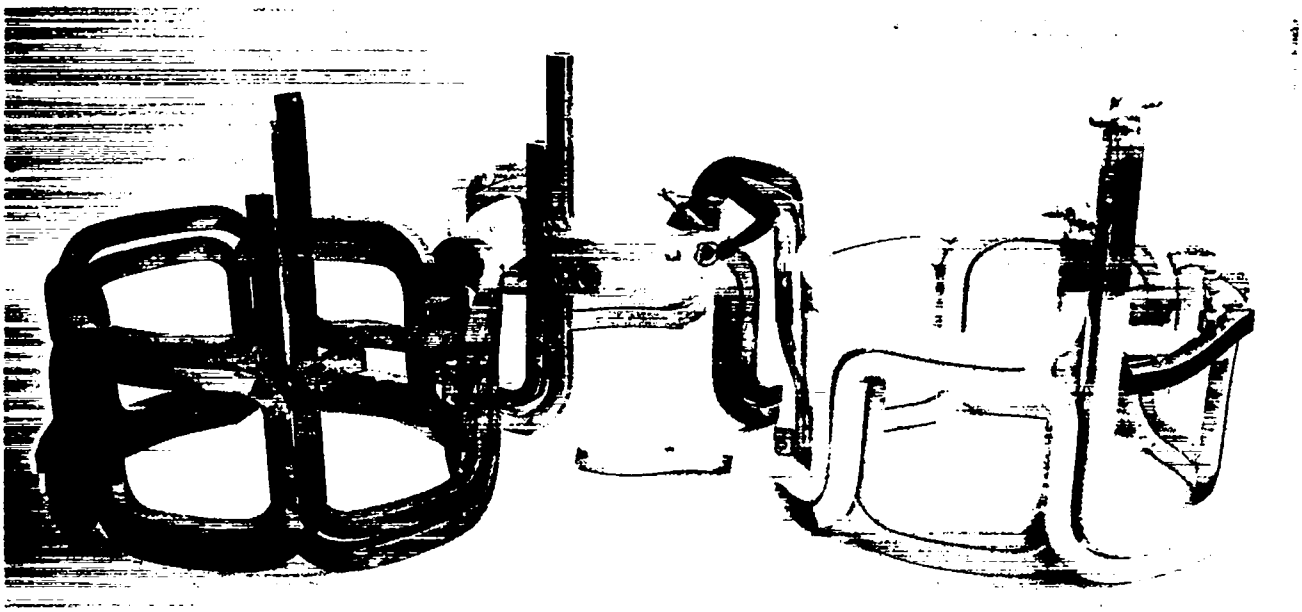

Fig. 5. SF-3C circularizer conductors.

FABRICATION TECHNIQUES FOR RECENT COMPLEX MAGNET SYSTEMS*

Arthur R. Harvey
Lawrence Radiation Laboratory
University of California
Livermore, California

ABSTRACT

Within recent years magnetic field requirements have fostered magnet systems of ever increasing complexity. Large superconducting magnets with nonconventional geometries, lumped solenoids that produce fields of high uniformity, and solenoids requiring greater heat dissipation properties present fabrication problems heretofore unencountered.

Magnets of this type or their prototypes are currently being constructed in our magnet fabrication facility at Lawrence Radiation Laboratory, Livermore.

This is a report on some of the difficulties encountered and the techniques we have developed for the design and fabrication of a single magnet system.

INTRODUCTION

Magnet systems which exist in our present experiments are no longer a collection of simple solenoids which may be purchased with minimum consideration of design and economy. To cite a few examples, the present Astron, superconducting HAPPE, and the forthcoming superconducting Alice Baseball II magnets fall within this category. To attempt to describe them all in this report would do justice to none. Therefore, the design and fabrication techniques developed for the Astron 1.4-meter magnet system will be discussed in detail here, with particular emphasis placed on its uniqueness, precision, and economy.

HISTORY

The former magnet system, in brief, consisted of a single layered solenoid (Fig. 1) with electrical and water connections at every 12 turns. Diagnostic entries were provided at locations originally deemed necessary.

Difficulties encountered with this system were:

a) Maintenance of concentricity, alignment, and roundness primarily affected by the independent magnet and vacuum tank support.
b) Field perturbations induced by the single layer winding and terminal arrangements.
c) A satisfactory method for providing additional diagnostic entries. This is evident in Fig. 2, in which case the conductor bypasses were field-installed, with subsequent charring of insulation.

PHYSICS REQUIREMENTS FOR 1.4-METER MAGNETS**

Requirements for the present 1.4-meter magnet system were as follows:

a) Maximum diagnostic access.
b) Cancellation of net axial current flow.
c) Minimum lead induced field perturbations.
d) Maximum field uniformity.
e) Optimization of magnet modules to existing 30-kW power supplies.

BASIC ENGINEERING APPROACH

To provide maximum diagnostic access, lumped solenoids were clearly the solution. To minimize net axial current flow, conductor layers in multiples of two were required, so that odd-numbered layers impart an axial current flow in one direction cancelled by reverse flow in the

*Work performed under the auspices of the U. S. Atomic Energy Commission.

**Detailed physics design as well as magnitude of field errors introduced by magnet geometry may be found in Ref. 1.

even-numbered layers. To further cancel this net flow, adjacent modules wound in opposite sense impart divergent current flow in layers of equal radii.

To minimize field perturbations induced by the leads, a coaxial arrangement was required. Maximum field uniformity required uniform magnet diameters in addition to precise concentricity, axial alignment, and module spacing.[1]

Optimization of magnet modules with respect to existing power supplies was accomplished by a computer program entitled "INFSOL." This program selectively alters the parameters of number of turns, conductor size, and length and diameter of water passage to provide the maximum field obtainable within a given geometric confinement.

The system was now basically set to provide 90 ft of lumped solenoids spaced on 9.6-in. centers. One hundred sixteen solenoids were required, four of which were spares.

DETAILED ENGINEERING DESIGN

Magnet Support and Alignment

As shown by its dimensions a single module of the magnet system (Fig. 3) is a rather large thin cylinder. A conventional method for maintaining roundness would be to fabricate precisely machined coil forms with stiffening rings. However, taking advantage of the accurately machined o.d. of the heavy walled vacuum tanks, our approach was to use the tanks as the means of support.

To maintain proper roundness and accurate module spacing, we had to provide cores (Fig. 4) with accurately machined parallel edges and inside diameters capable of being held to tight tolerances. The conventional approach would require complicated and expensive machining of cylinders. Since the cylinders are thin, our approach was to maintain an accurate circumference by the following method. The plate for the cores was first planed for width and circumferential length, next, it was rolled and placed on an accurately machined mandrel which assures proper width and parallel edges. The closing edges were then drawn together by banding to the proper diameter. The circumference was then measured and, if within tolerance, the closing weld was made. This technique proved very successful; on nine trial cylinders the inside diameter ranged from nominal to less than +0.020-in. based on circumferential measurements. The cost of $89.00 each was a gross saving over the alternate method.

The coils are supported (Fig. 5) on the tank by expandable rubber blocks, which permitted a high degree of concentricity and roundness. Proper spacing between modules is maintained by accurately machined interlocking bars. The combination of the blocks and bars maintains axial alignment.

An added bonus to this method of support is the additional diagnostic entry space given by eliminating the stiffening rings.

Coaxial Leads

Coaxial leads present a very difficult problem because the return lead terminal block cannot be soldered to the conductor while in place without destroying the magnet insulation. The method shown in Fig. 6 was selected to provide the water-cooled coaxial power leads. The inner lead rod is electrically isolated from the outer terminal block by an epoxy-fiberglas layup on the rod. Insulation between the inner and outer terminal blocks is a 1/32-in.-thick epoxy glass laminate sheet. The low conductivity water seal is an O-ring between the rod and the outer terminal. The rod is screwed to block 'A'. This allows the rod to be removed and the seal to be replaced without removing the coil from the tank. This arrangement also requires precision alignment of the rod to effect the seal and to intercept the inner rod screw. The seemingly redundant block 'A' makes this possible. Prior to placing the outer terminal block over the inner block, the screw hole for the rod is left undrilled. The coil fabricator may then place and clamp the outer block in place within reasonable coil-winding tolerance. Using a special punch he may then precisely locate the screw hole center. Block 'A' may then be removed, drilled, and replaced to complete the rod assembly.

Guaranteed Coil Tolerances

For uniform current density, conductors throughout the coil must be evenly spaced as shown by coil sections from different locations (Fig. 7).

To insure the same degree of accuracy for a coil as applied to its core, we designed and constructed two mandrels which held the cores round during winding and prevented the coil lengths from exceeding the core lengths. Helical ramps were incorporated to properly shape the lower layer. Retractable blocks of proper length, when engaged, imparted the return helix. Using this method of fabrication, the coil-winding tolerances are guaranteed.

CONSTRUCTION

The Prototype Coil

To obtain rapid delivery and effect further economy, we attempted throughout our design to select materials and techniques which would assure the construction of a single module within a normal working shift.

To verify this goal, a prototype coil (Fig. 8) was constructed in our shop. The webbing terminated by two holes (our original concept for coil handling) proved two costly and time consuming. The terminal arrangement (Fig. 9) caused clamping difficulties. Also, removal of the coil from the mandrel was difficult due to the orientation of the water leads.

The Final Magnet System

The modules were redesigned to eliminate these and other problems encountered during construction of the prototype. Figure 10 shows one of the purchased modules. The previous method of coil handling was replaced by clamp-positioning holes in the core at a saving of $23 per coil. The revised terminal arrangement (Fig. 11) provides sufficient clamping holes and slots, which may be utilized to mechanically bolt the terminals together if required.

The water-cooling circuit may be seen in Fig. 12, which is a view of the partially assembled machine. Water enters through the hoses into the fittings opposite the terminals. Parallel flow then occurs in the top and bottom layers. Flow from the top layer directly enters the coaxial cavity, while water from the bottom layer discharges through the tube in the lower terminal. Flow is recombined through a nonconductive fitting so that all of the water flows up the coaxial leads where it discharges.

SUMMARY

The 1.4-meter magnet system recently developed at LRL, Livermore, is unique in its fast construction, methods of assembly, and reduced costs. Manually wound solenoids were constructed with high uniformity and machined-level precision. Parts most prone to failure can be easily and economically replaced. The method of magnet support and spacing is simple but highly reliable.

An average solenoid system would cost from $3-$4 per lb. A precision solenoid system of this nature could conceivably cost $6 per lb or more. Our solenoids cost about $738 each or less than $2.90 per lb. including tooling. This economy could not be achieved by using a more conventional approach.

REFERENCE

1. Jack W. Beal, "Coil System Design for a Proposed Astron Device," Lawrence Radiation Laboratory, Livermore, Calif., Report UCRL-50136, 1966.

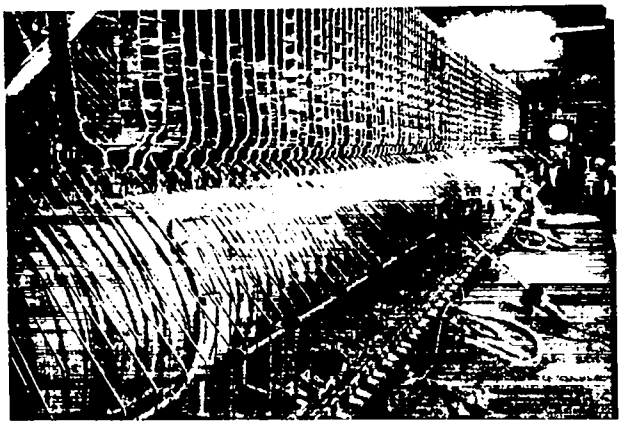

Fig. 1. Former main magnet system.

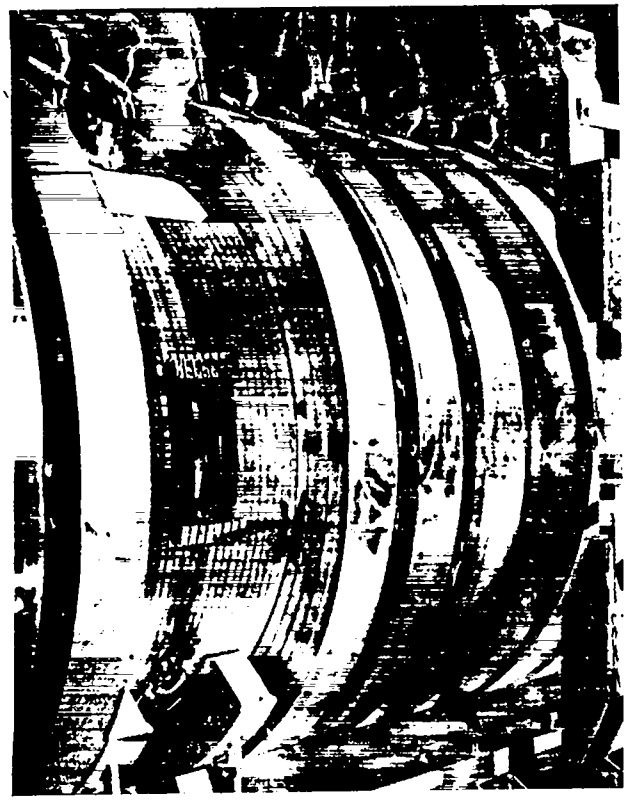

Fig. 2. Field penetration of magnet.

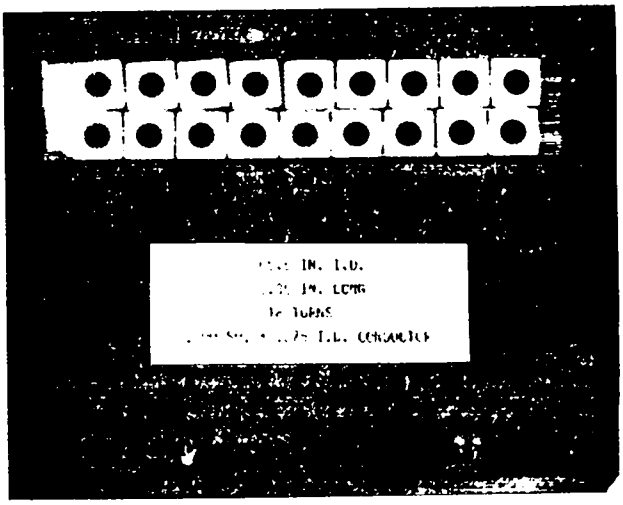

Fig. 3. Basic conductor array.

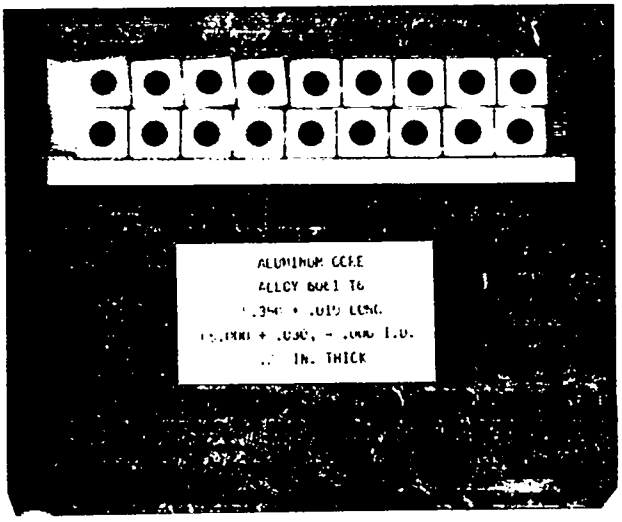

Fig. 4. Aluminum core.

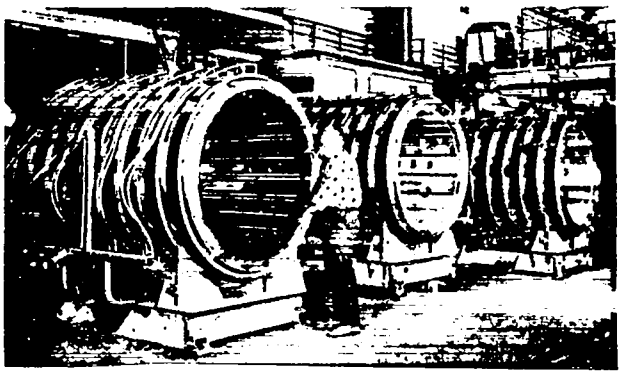

Fig. 5. Method of coil support.

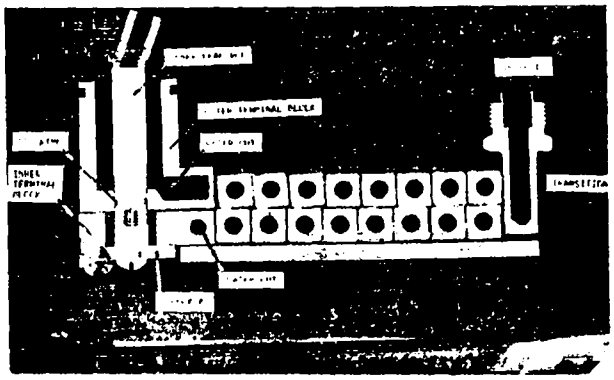

Fig. 6. Coil section, terminal area.

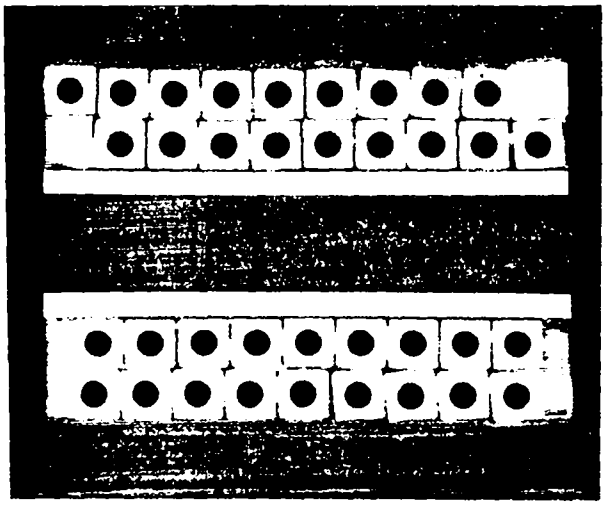

Fig. 7. Helical nature of winding.

Fig. 8. Prototype coil.

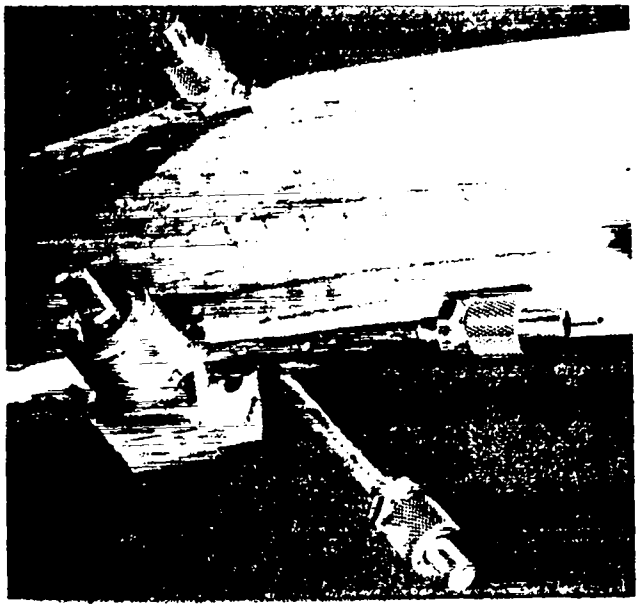

Fig. 9. Prototype terminal area.

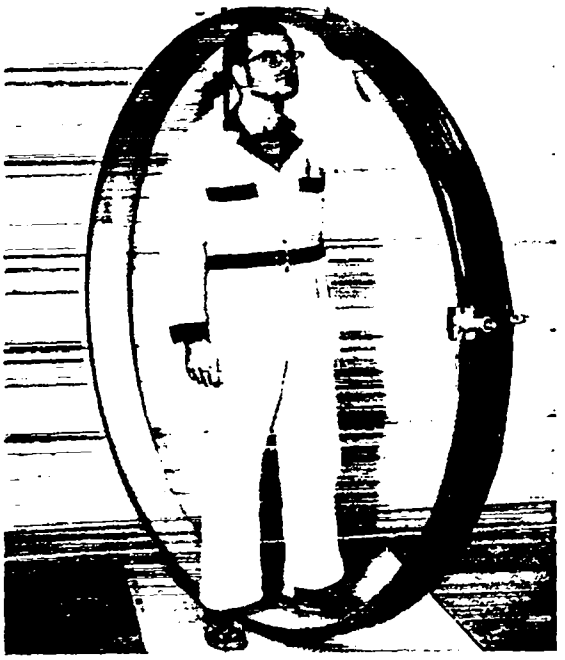

Fig. 10. Fabricated coil.

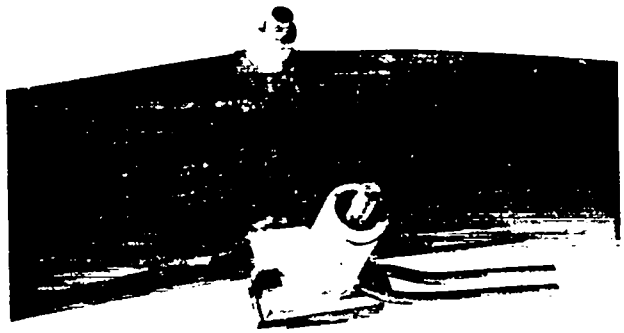

Fig. 11. Final terminal arrangement.

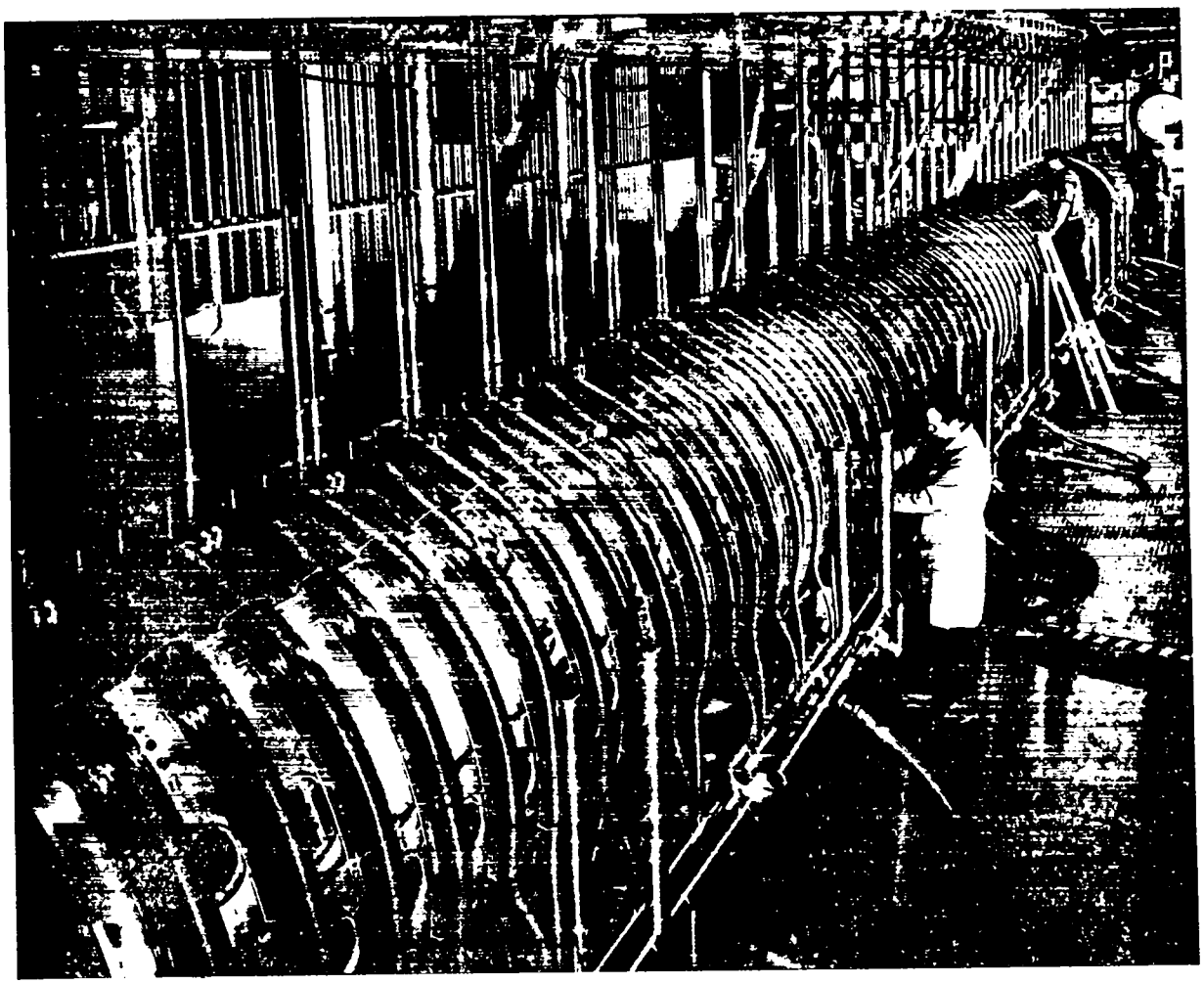

Fig. 12. Overall view of redesigned magnet system.

MINIMUM-B CONFIGURATION IN THE INTEREM FACILITY*

R. C. Davis, J. N. Luton, Jr., O. D. Matlock,** and W. L. Wright
Oak Ridge National Laboratory
Oak Ridge, Tennessee

ABSTRACT

The INTEREM facility has been modified by the addition of a pair of coils arranged to superimpose a quadrupole magnetic field on the existing mirror configuration. The coils, made of 42 turns of 0.565" x 0.565" hollow, water-cooled copper conductors, designed to carry ~ 5000 amperes, were cast in epoxy and mounted around a perforated copper cavity which confines the ~ 20 kW of applied microwave power. The coil and cavity assembly is then inserted as a unit into the INTEREM vacuum tank. The vacuum feed through seal for the current and water leads to the coils was also cast of epoxy and has been found to be reliable over many pump-down cycles. The arrangement used to restrain the coils against the magnetic forces will be described.

For some years we have been producing hot electron plasmas in a steady state by electron cyclotron resonance with high power, CW, microwave radiation fed into a high-mode reflecting cavity. The electron densities run between 10^{11} and 10^{12} electrons/cm^3 with mean energies that range around 100 keV, with some electrons as high as several MeV. Plasma volumes are usually ~ 1 - 10 liters. In INTEREM the microwave power available originally ranged up to 40 kW at a frequency of 10.6 GHz which is resonant with electron cyclotron frequency at a field of 3780 gauss. During these years of operation, many modifications have been made. We will look at the machine and review the major changes.

Figure 1 shows the machine in April 1967. The lead walls, made up of 4' x 3' sections, make a room 16' x 28'. The lead in the lower panels is three inches thick, the top row is two inches thick. Additional shielding can be seen at the operating area, on top of the tank, and at the ends. Also many tons of lead brick are also used. The total weight of the lead as seen is 191,000 lbs. The reason for so much lead? Radiation at the tank wall can exceed 150 R/Hr. Holding up all this weight would normally be a problem, but we are fortunately in an area that originally was built for an alpha calutron track. The live load floor weight of 250 lbs/sq. ft. and massive pillars on close centers make it possible to hold most any load.

The round cage at the top of the tank houses a duoplasmatron ion source and neutralizer. The beam system can produce a beam of neutral atoms ~ 100 mA equivalent at 20 keV. The source pumps and manifold are at the left. The source power supplies are in the square cage at the right. Hidden under the steps at the left is the 40 kW microwave power supply.

Electron cyclotron heating experiments started in INTEREM with simple mirror coils arranged with a 3:1 mirror ratio and a single microwave cavity (Fig. 2). Later, coils with a 2:1 mirror ratio were installed. Then two additional cavities with outboard coils and spool pieces were added, making a vacuum system 1.25 x 1.25 meters square and 3.7 meters long. Pumping was done originally with four 20" oil diffusion pumps with water cooled baffles. The base pressure was ~ 10^{-6} torr with considerable oil vapor often found condensed on the water-cooled cavity surfaces. In this configuration, microwave power was fed into the three cavity sections.

The system was then modified for a minimum-B

* Research sponsored by the U.S. Atomic Energy Commission under contract with the Union Carbide Corporation.
** Denotes speaker.

mirror-quadrupole magnetic field. At the time that the quadrupole coils were installed, the 20" diffusion pumps and their large volume manifolds were replaced with four 10" diffusion pumps with much smaller manifolding and freon cooled baffles, fundamentally improving the oil feed-back problem which exists with the large pumps.

In Table I, we present the quadrupole coil specifications.

TABLE I

Quadrupole Coil Specifications

42 turns each of 5/8" square hollow copper with 0.300 center hole

Coil mean radius: 25 cm

$B_{\perp}(r = 20 \text{ cm}) = 3000$ gauss (between windings)

Power: 0.5 megawatts (4600 amps, 110 volts)

$\Delta T \cong 20^{\circ}C$

Filler Resin: Peamafil Polyester GE No. 3405

Insulation: Varslot .005 mil bonded on both sides of .001 mil mylar

Wrapping Tape: GE 76504-P semicured polyester treated glass tape

Potting Resin: Maraset No. 124C

Each of the pairs of quadrupole coils, as delivered, had an overall length of 8' by 20" across (Fig. 3). It may be well to point out here that all the epoxy is inside the vacuum. The coils are not canned or isolated.

The cavity (Fig. 4), 15" dia., 44" long, is made up of four alternate solid and perforated 1/16" copper strips welded together in the form of a cylinder. The solid strips go under the epoxy to shield against escaping plasma particles and ultra-violet radiation. Four orthogonal ports are provided. The cavity is water-cooled since all the microwave power is absorbed by the plasma particles which end up on the walls. Especially heavy cooling is needed near the midplane between the coils where most of the particles escape. A bottom view of the assembly at 90% completion is shown in Fig. 5. To the right of the bottom port, an insulated 30 turn copper diamagnetic pick-up coil can just be seen. Also to the left of this port is one of the three pairs of microwave feed points. The locations were chosen so that magnetic field in the wave guides near the windows are either above or below electron resonance for a wide variation in field shape. When resonance is permitted near the window, breakdown usually occurs and the window melts.

Figure 6 shows an angle view of the cavity and coil assembly showing the epoxy end seals and the restraining clamps. The stainless steel bands, joined to the epoxy, provide a slip surface for an "O"-ring seal. The quadrupole coils are anchored to the tank side walls. The center of the 1 3/4" aluminum end plate where the feed-through seal is made has a deflection of 0.120" when the system is pumped down and the slip joint permits this motion.

Figure 7 shows a schematic cut-away of the epoxy end seal. The inlet and outlet water pass through neighboring copper tubing in the seal causing local temperature gradients of $\sim 50^{\circ}C/cm$. The difference in expansion between the hot and cold leads of 0.010" caused the first seals to crack and leak under vacuum. A second mixture of 100 parts Shell Epon 815 and 125 parts of General Mills Versamid 140 used as a hardner resulted in a more pliable material which has been in service many months with no additional problems.

The coil system was tested in place in the machine up to its rated current of 4750 amps. The major difficulty, mechanically, resulted from the spreading forces between the coils at one end (the other end compresses). The coil motion was monitored and a number of different clamp designs were attempted before the motion was finally restricted to 0.010" under the estimated force of 2500 pounds at maximum current. During the early experiments, at somewhat higher fields, we noted an axial motion of the quadrupole coils as a result of inadequate axial clamping. We finally ended up with a yoke and draw bar type restraining system to the side walls, which now restricts all motion to less than 0.010". During the initial vacuum checks, the base pressure fell only to $\sim 10^{-6}$ torr.

A mass analyzer installed in the machine indicated the principal component limiting the pressure, as expected, was water vapor so four liquid nitrogen cooled plates were installed comprising an effective pumping speed for water vapor of $\sim 4 \times 10^{5}$ liters/sec. The added pumping speed reduced the pressure to 10^{-7} torr but when it was shown that most of the outgasing from the epoxy, when the coils

were energized, was also water vapor, it was decided to install seven more cold plates. The total of eleven plates has a combined area of 10^5 cm^2 and the base pressure was reduced to 6×10^{-8} torr. To pump CO and other organic impurities seen, five titanium evaporators were added. The evaporated titanium covers about 1 sq. meter. The base pressure is now 2.8×10^{-8} torr.

Figure 8 shows a schematic arrangement of the entire coil assembly and cavity.

Figure 9 is a view of the west end of the machine showing the quadrupole coil feed-through seals, the electrical connections, the water leads and headers, and the mechanical drives for two movable diagnostic devices. One drives a probe which intercepts the edges of the plasma, requires a motion of 16" into the cavity. The second moves a current detector.

Figure 10 shows the south side of the machine. One sees part of the pump assemblies, the signal leads for the diamagnetic pick-up coil and coils used to compensate for the fluctuations in the magnetic field, a periscope type sight tube, and the water and electrical leads to the titanium evaporators.

Figure 11 is a view of the east end showing the bremsstrahlung detector. It consists of two collimators (4000 lbs. more lead) with shutter assembly and a 3 x 3 NaI(Tℓ) detector. Also shown is another axial current detector which can be scanned in a horizontal plane $\pm 3/8$" across flux lines through the plasma.

Figure 12 is a view outside the east end lead showing our liquid nitrogen storage and distribution system which supplies the eleven cold plates. The system is used only when running; usage is about 120 liters of liquid nitrogen per day amounting to a cost of only $50.00.

Table I Quadrupole Coil Specifications for INTEREM.

Quadrupole Coil (2)

42 Turn each of 5/8" Square Hollow Copper with 0.300" Center Hole

Coil Mean Radius: 25 cm

$B_\perp$ (r = 20 cm) = 3000 Gauss (Between windings)

Power: 0.5 Megawatts (4600 Amps, 110 Volts) $\Delta t \cong 20^\circ$ C

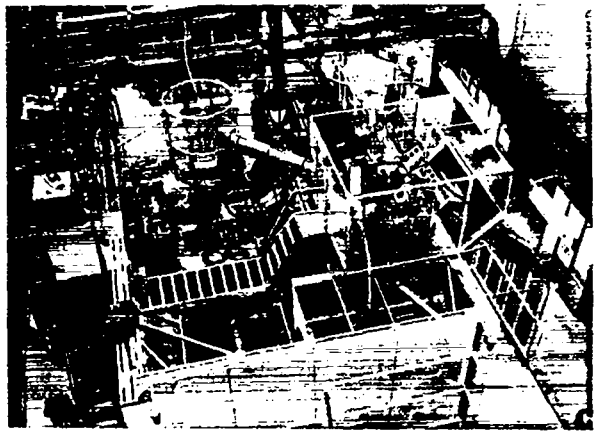

Fig. 1 INTEREM machine and area April 1967.

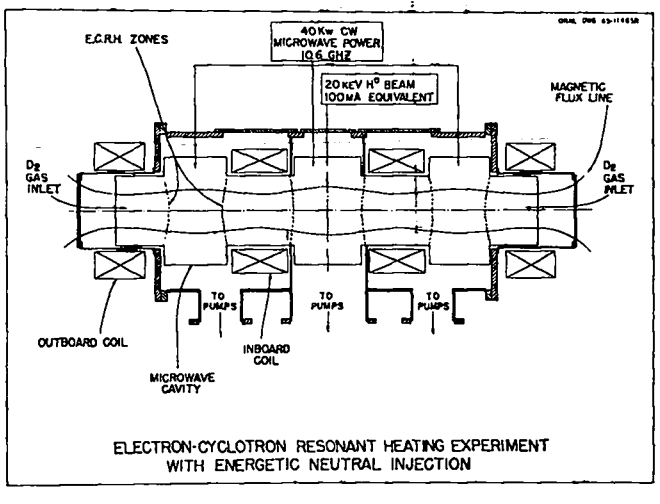

Fig. 2 Schematic INTEREM showing vacuum tank cavities and coils.

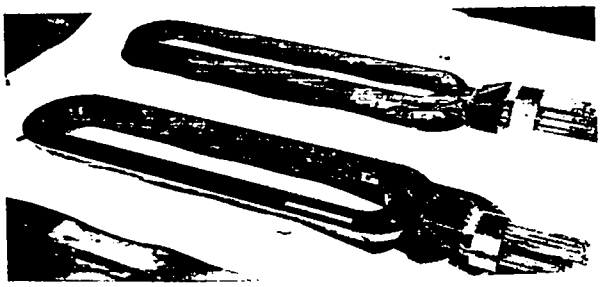

Fig. 3 Each of the pairs of quadrupole coils.

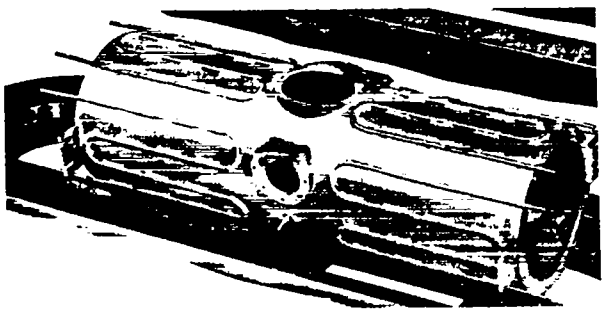

Fig. 4 INTEREM quadrupole cavity.

Fig. 5 Assembly of quadrupole coils and cavity.

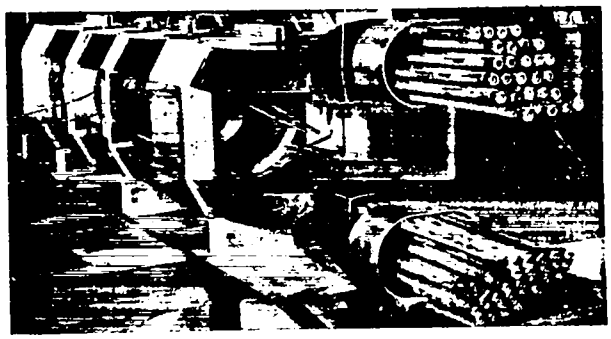

Fig. 6 Quadrupole assembly showing epoxy seals.

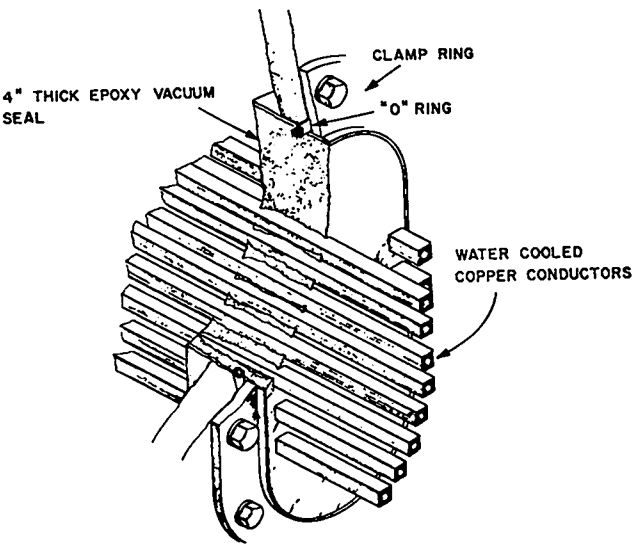

Fig. 7 Schematic cut-away of the epoxy end seals.

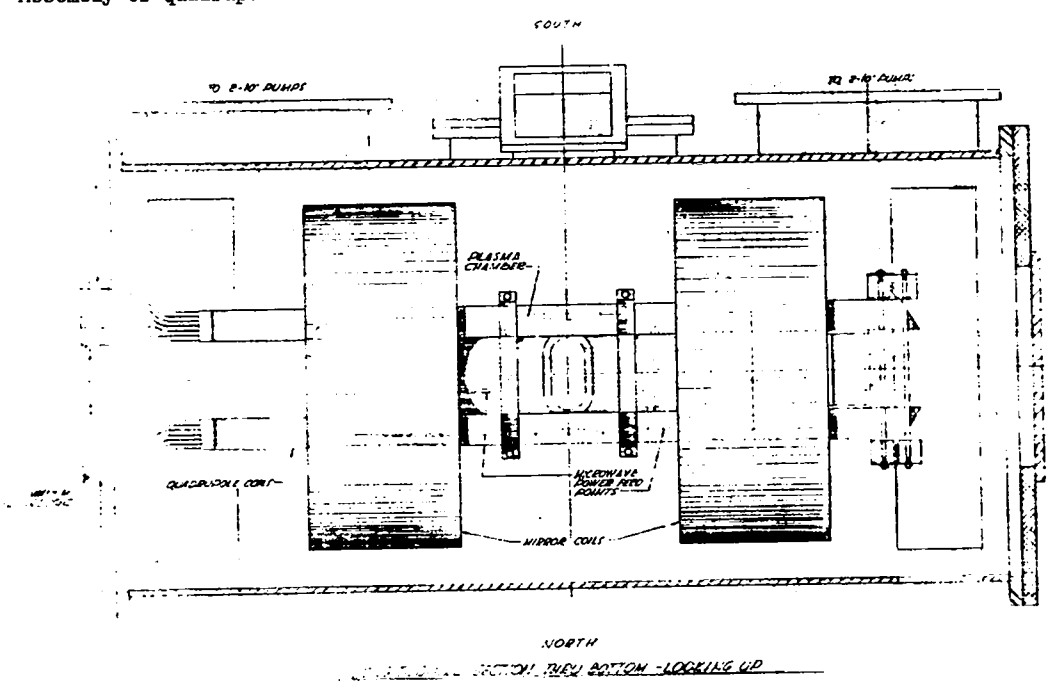

Fig. 8 Schematic of INTEREM vacuum tank with quadrupole shown in position.

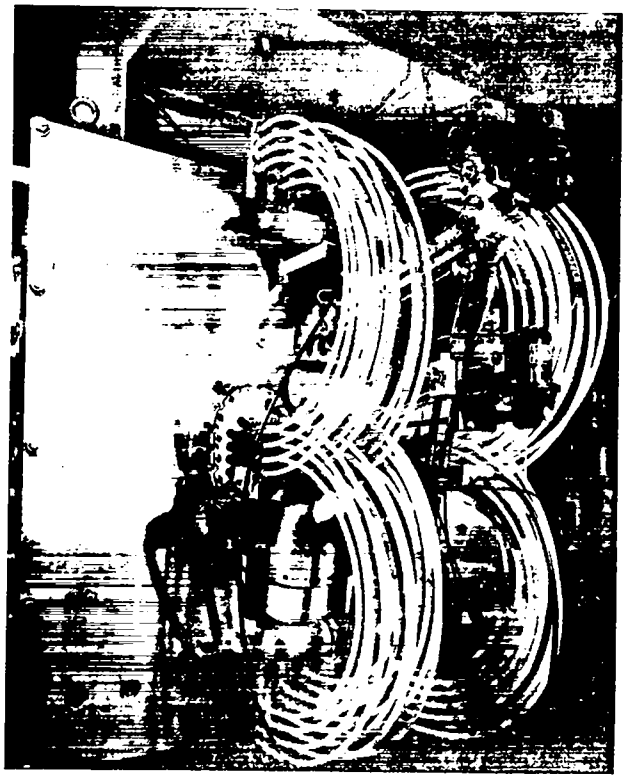

Fig. 9 INTEREM west end.

Fig. 10 INTEREM south side.

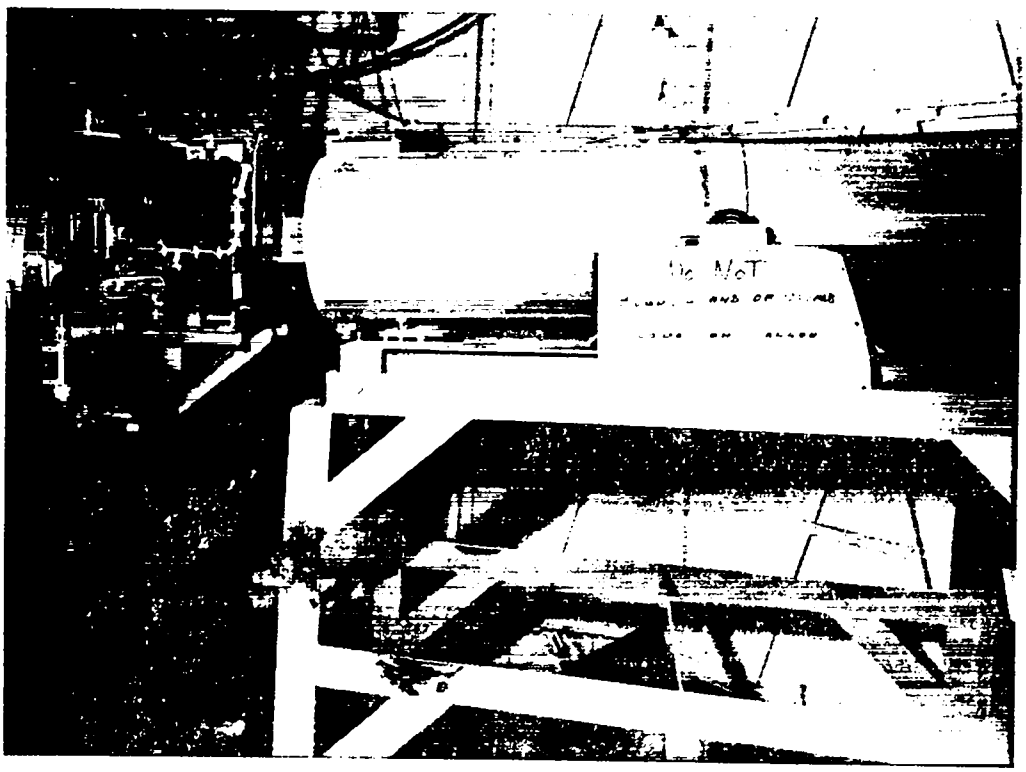

Fig. 11 INTEREM east end.

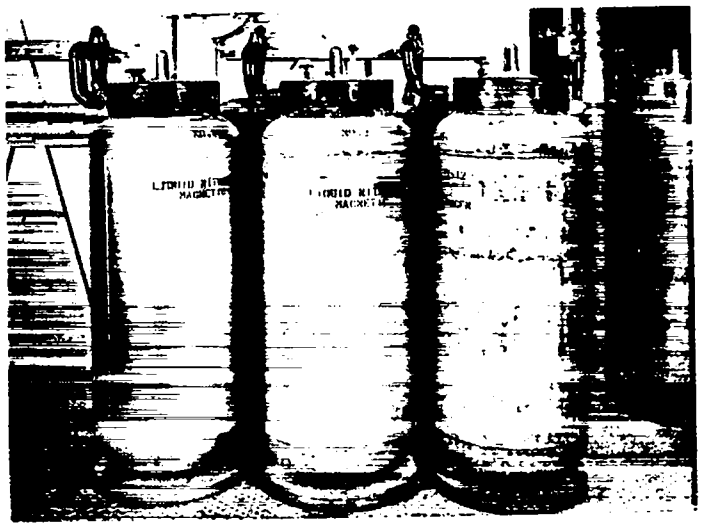

Fig. 12 INTEREM outside lead wall, east end.

CONFERENCE PARTICIPANTS

Aerojet General Corp., San Ramon, California
- David Cummings

Aerospace Corporation, Los Angeles, California
- M. J. Bernstein
- Mitchell Dazey
- John Snyder

Bendix Corporation, Kansas City, Missouri
- Richard Horn
- Vincent L. Willerton

Cornell University, Ithaca, New York
- Michael Ury

Culham Laboratory, England
- John Last
- John Philpott

Kirtland Air Force Weapons Laboratory, Albuquerque, New Mexico
- Arthur Guenther
- Richard Gullickson
- Peter Manly
- Dalton Wirtanen

Lawrence Radiation Laboratory, Berkeley, California
- Donald Hopkins

Lawrence Radiation Laboratory, Livermore, California
- Carl J. Anderson
- R. L. Baty
- Thomas H. Batzer
- Gary G. Berg
- Dale Birdsall
- Eugene T. Bradley
- Richard T. Bulmer
- Manuel O. Calderon
- Henry R. Cavagnolo
- Anthony K. Chargin
- Alan Copeland
- Balwant S. Denhoy
- Thomas J. Duffy
- Frank V. Harshbarger
- Arthur R. Harvey
- Francis B. Headley
- Carl D. Henning
- William C. Hess
- Charles P. Hurley
- R. W. Kuenning
- Miles Loyd
- Blake Myers
- Robert L. Nelson
- Leslie F. Peterson
- Daulton A. Ping
- Glen D. Polzin
- Jerry W. Robinson
- T. L. Rossow
- Harvey Saulter
- Thomas P. Stack
- Clyde E. Taylor
- Alan L. Throop
- George C. Tyler
- Hugh W. Van Ness
- G. E. Vogtlin
- Alfred E. Waugh
- E. P. Westbrook
- Stewart D. Winter

Los Alamos Scientific Laboratory, Los Alamos, New Mexico
- Grenfell P. Boicourt
- Wallace H. Borkenhagen
- Paul J. Bottoms
- David Brown
- Robert S. Caird, Jr.
- Darrell L. Call
- James P. Carpenter
- Robert S. Dike
- Harry Dreicer
- Kenneth J. Ewing
- C. M. Fowler
- W. B. Garn
- R. F. Gribble
- Jay E. Hammel
- Roy A. Haarman
- Charles F. Hammer